Design, Synthesis and Mechanistic Studies of Cationic Antimicrobial Peptides

A Dissertation Submitted to the

Indian Institute of Technology Guwahati

As Partial Fulfillment for the Award of Degree of

Doctor of Philosophy

In Chemistry

Submitted by-

Gopal Pandit

Roll No. 156122018

Supervisor

Dr. Sunanda Chatterjee

Associate Professor

Department of Chemistry

Indian Institute of Technology Guwahati

Guwahati 781039

June 2022

Dedicated to

All of my well wishers

Declaration

I do hereby declare that the matter embodied in this thesis entitled ***''Design, Synthesis and Mechanistic Studies of Cationic Antimicrobial Peptides''*** has been carried out by me under the supervision of Dr. Sunanda Chatterjee, Associate Professor, during the period July 2015 to June 2022, at department of Chemistry, Indian Institute of Technology Guwahati (IITG), India. The work presented here has not been submitted for the award of any other degree or diploma at any other Institution.

In keeping with the general practice of reporting scientific observations, due acknowledgements have been made whenever the work described is based on the findings of the other investigators.

IIT Guwahati
June 2022

Gopal Pandit
156122018

Certificate by the Supervisor

This is to certify that the thesis entitled "***Design, Synthesis and Mechanistic Studies of Cationic Antimicrobial Peptides***" submitted by Mr. Gopal Pandit (Roll No. 156122018) for the award of Ph.D. degree to IIT Guwahati is absolutely based on his own research work under my supervision. This thesis or any part of it has not been submitted for any degree/ diploma or any academic award anywhere before.

Dr. Sunanda Chatterjee
Associate Professor
Department of Chemistry
Indian Institute of Technology Guwahati
Contact: +91 361 258 3310
Fax: +91 361 258 2349
Email: sunanda.c@iitg.ac.in

Acknowledgement

At first, I would like to convey my deepest regards and utmost respect to my supervisor ***Dr. Sunanda Chatterjee***, Associate Professor, Department of Chemistry, IIT Guwahati for her tireless guidance and tenacious motivations and for providing me a conducive ambience for working throughout my research work in the lab. It has been an immense pleasure for me to learn a lot of things by working under her supervision. I would deeply thank her for providing with best of the facilities which was required to carry out my research work. Her suggestions and advice carried me through all the stages of writing my papers and thesis.

I want to extend my sincere thanks to my Doctoral Committee members, Chairperson ***Dr. Kalyan Raidongia***, Associate Professor, Department of Chemistry, IIT Guwahati, ***Dr. Uttam Manna***, Associate Professor, Department of Chemistry, IIT Guwahati and ***Prof. Ramesh Aiyagari***, Professor, Department of Biosciences and Bioengineering, IIT Guwahati for their brilliant comments and suggestions, constant support and encouragement throughout my research work.

I owe my profound gratitude to our collaborator, ***Prof. Anirban Bhunia***, Bose Institute Kolkata, and his group for performing some of the biological experiments in the initial days of my research and giving me the opportunity to train myself in the different techniques related to microbiology and biophysical experiments in his lab.

In addition, a hearty thanks to ***Dr. Priyadarshi Satpati***, Associate Professor, Department of Biosciences and Bioengineering, IIT Guwahati and his group members ***Suvankar Ghosh*** and ***S. R. Vignesh*** for performing the MD simulations reported here in the thesis.

A special thanks to ***Dr. Uttam Manna***, Associate Professor, Department of Chemistry, IIT Guwahati for his motivations and giving me the opportunity to work in his lab. I would also like to acknowledge, ***Prof. Siddhartha S. Ghosh,*** Department of Biosciences and

Bioengineering, IIT Guwahati and his student ***Dr. Anil P. Bidkar*** for MTT assays performed in his lab.

I would like to convey my heartiest gratitude to the ***Prof. Tushar Kanti Chakraborty*** from IISc Bangalore, India and ***Prof. Krishna Kumar*** from Tufts University, USA for evaluating my thesis.

I am also thankful to ***Prof. Debapratim Das***, Professor, Department of Chemistry, IIT Guwahati and my supervisor ***Dr. Sunanda Chatterjee*** for the group meetings that they conducted every week for oral presentations and scientific discussions, which gave me an opportunity to increase my scientific knowledge and confidence level during presenting the scientific work.

A special thanks to my M.Sc Thesis supervisor **Dr. Sanjay Pratihar**, Senior Scientist CSIR-CSMCRI Bhabnagar to teach me about the research methodologies at the initial days of my M.Sc period which helped me a lot to performed the experiments during my Ph.D. period.

I am thankful and fortunate enough to get constant encouragement and support from my friends ***Humaira Ilyas, Sk. Abdul Mohid, Karishma Biswas, Nabarupa Chowdhury, Shruti Mukherjee, Dibakar Sarkar, Ranit Pariary from Bose Institute, Kolkata Tapasi Kalita, Rajatsubhra Giri, Nilotpal Sinha, Bapan Pramanik, Tousif Hussian, Kalicharan Das, Srijita Paul, Krishna Gopal Chattaraj, Rajkumar Gogoi, Jumi Deka, Kundan Saha, Adil Rather, Subrata Mondal, Sujan Kalita, Raman Adil, Angshuman Mahapatra, Bibhas Bhunia da, Soumi Das, Nirmalya Pradhan, Nirban Jana, Kousik Maji Milan Mahadani (TEM Operator)*** from IIT Guwahati.

I would like to gratefully acknowledge Department of Chemistry, IIT Guwahati for providing all the instrumentation facilities for carrying out my research work. I would also like to thank all the staff members of the Department of Chemistry for being there when needed. Special

mentions are ***Dr. Babulal Das*** and ***Mr. Diganta Kumar Hira*** for helping me in learning the instruments.

Also, heartiest thanks to the Central Instruments Facility (CIF), IIT Guwahati for providing facilities like 600 MHz NMR, AFM, FESEM, PXRD, ITC, MALDI, XRD and FETEM experiments.

Words cannot express the love and synergy provided by my lab mates, **Dr. *Karabi Roy, Swapna Debnath, Monikha Chetia, Tanumoy Sarkar*** and ***Maitery Yadav*** who helped me in successfully completing my research work and providing me with all the help needed at different times. In addition, thanks to all the project students who helped a lot in my research work.

A special thanks to the project student ***Subhajit Rom*** for helping a lot during his one year project work in our lab.

I gratefully acknowledge Indian Institute of Technology Guwahati for providing me with all the facilities and financial assistantship for carrying out my work smoothly.

I am thankful and fortunate enough to get constant support and encouragement from my wife Mrs. ***Baisakhi Maity***.

Needless to mention, this thesis could not have been possibly completed successfully without the blessings of my ***Family*** and the ***Almighty*****.**

I thank all for staying there with me through thick and thin.

Gopal Pandit

Abstract

Growing antimicrobial resistance against the conventional commercially available antibiotics, giving rise to the antibiotic resistant superbugs is a matter of imminent concern to the human civilization. Natural defense system of the microbes in combination with several man made reasons have led to the expedited development of antibiotic resistance over the years, which renders most of the existing antibiotics ineffective to treat the infections. In addition, growth of new classes of antibiotics has been very slow over the last few decades. Unless combatted urgently, infections caused by the antibiotic resistant superbugs are predicted to cause a colossal number of deaths in the near future. Hence, there is an urgent need to develop other classes of therapeutics to address the situation.

Antimicrobial peptides (AMPs), isolated from various natural sources have an inherent property to combat microbial infections and act as the first line of defense in the host. AMPs usually have broad-spectrum antimicrobial activity and are effective against several strains of bacteria, viruses, fungi, protozoa etc. The greatest advantage of the AMPs over the conventional antibiotics lies in the fact, that there is a very slow or no development of resistance against them in microbes. Presence of different modes of action in AMPs as opposed to the single intracellular target for the antibiotics leads to the delayed development of resistance against them. AMPs are mostly membrane active, causing membrane deformation, lysis and eventual cell death. Some AMPs traverse the membrane and act on intracellular targets like the genetic material while others are known to have immunomodulatory activities in the host. AMPs are highly variable in their sequences, physicochemical properties and structure. In spite

of having such huge potential, AMPs have limited commercial success so far owing to some drawbacks like long sequence of natural AMPs which make them expensive in terms of time and money, peptide folding issues, salt induced inactivation of antimicrobial potency, pH susceptibility, short systemic half-life owing to protease degradability and cytotoxicity towards mammalian cells. Scientists all over the world are working on developing synthetic AMPs to overcome these shortcomings and create therapeutically better AMPs that may be commercialized.

In this thesis, we have tried to develop small cationic AMPs from *de novo* design with an objective to make them highly potent, non-cytotoxic, salt tolerant and protease resistant. Our research entails design and synthesis of AMPs on one hand and detailed investigations into their structure, modes of action and interactions with the membranes/ membrane mimetics on the other hand. We have used various experimental techniques like biological assays, biophysical, spectroscopic, microscopic, calorimetric techniques in combination with molecular dynamics simulations to perform our investigations.

This thesis has five chapters as mentioned below.

In **Chapter 1** we have introduced the AMPs and the relevance of the studies carried out in the thesis in context to the present scenario. We have described the various classes of AMPs, their advantage over the conventional antibiotics, the disadvantages of the natural peptides and design strategies adopted for development of synthetic peptides. This chapter provides the much needed background for this thesis work.

In **Chapter 2,** we have developed two cationic hepta-peptides P4 and P5 with broad-spectrum antimicrobial activity against various ESKAPE group pathogens and fungi. These AMPs were non-cytotoxic towards mammalian cells and membranolytic in their mode of action. We established that for small cationic AMPs, charge is essential for antimicrobial activity and the

interaction in between the AMPs and the microbial membrane mimetics was primarily of electrostatic origin. We also established that in these small peptides antimicrobial potency was independent of the secondary structure of the peptide.

Chapter 3 described the development of four undecapeptides AMP 21- 24, which were highly potent against a broad-spectrum of fungi and bacteria. Additionally, these peptides were non-cytotoxic towards mammalian cells and primarily membranolytic in their mechanism of action. However, these AMPs might have a secondary intracellular mode of action as well.

Chapter 4: In this chapter the effect of the length and hydrophobicity of the sidechains of hydrophobic amino acid residues on the activity of 14 residue long AMPs with identical positive charge was explored. We established that the longer/ more hydrophobic side chain of leucine in LL-14, led to indiscriminate interaction with both the microbial and mammalian membranes leading to high antimicrobial potency and cytotoxicity. In VV-14, valine with shorter and less hydrophobic side chains gave rise to selective interaction with the microbial membrane generating high activity with low cytotoxicity. These AMPs were unstructured in free state in water and adopted helical conformation upon binding to the microbial membrane mimics (SDS micelles). VV-14 was highly active, non-cytotoxic and membranolytic in action. Further VV-14 was salt tolerant in its antimicrobial activity towards *Salmonella typhi*.

In **Chapter 5,** a salt tolerant and protease resistant AMP, selective towards Gram-negative bacteria *Pseudomonas aeruginosa* was developed. Protease resistance was induced by incorporation of unnatural analogs of Lysine. An optimum side chain length of the charged amino acid residue di-amino butyric acid (Dab) gave rise to the best activity. We established that among similarly charged small cationic peptides, optimum hydrophilic – hydrophobic balance was crucial for best activity. The developed AMP was non- cytotoxic towards mammalian cells and membranolytic in action towards microbial cells.

Contents

Abbreviations

L-Amino Acids with Abbreviations and Single Letter Codes

Amino Acid	Abbreviation	One Letter Code
Leucine	Leu	L
Isoleucine	Ile	I
Alanine	Ala	A
Glycine	Gly	G
Valine	Val	V
Proline	Pro	P
Histidine	His	H
Tyrosine	Tyr	Y
Tryptophan	Trp	W
Phenylalanine	Phe	F
Cysteine	Cys	C
Methionine	Met	M
Threonine	Thr	T
Serine	Ser	S
Arginine	Arg	R
Lysine	Lys	K
Aspartic acid	Asp	D
Glutamic acid	Glu	E
Asparagine	Asn	N
Glutamine	Gln	Q

Unnatural Amino Acids with Abbreviations

Amino Acid	Abbreviation
Norleucine	Nle
Ornithine	Orn
Diamino butyric Acid	Dab
Diamino propanoic Acid	Dap

Abbreviations

AMP: Antimicrobial Peptide

UV: Ultraviolet

SEM: Scanning Electron Microscopy

FESEM: Field Emission Scanning Electron Microscopy

TEM: Transmission Electron Microscope

FTIR: Fourier Transform Infrared Spectroscopy

ESI-MS: Electrospray Ionization Mass Spectrometry

CD: Circular Dichroism

DLS: Dynamic Light Scattering

NMR: Nuclear Magnetic Resonance

NOESY: Nuclear Overhauser Effect Spectroscopy

TOCSY: Total Correlation Spectroscopy

PRE: Paramagnetic Relaxation Enhancement

1D: One Dimensional

2D: Two Dimensional

3D: Three Dimensional

MD: Molecular Dynamics

DFT: Density Functional Theory

SPPS: Solid Phase Peptide Synthesis

HPLC: High Performance Liquid Chromatography

MIC: Minimum Inhibitory Concentration

Boc: Tert-butoxycarbonyl

Fmoc: Fluorenylmethyloxycarbonyl

FITC: Fluorescein Isothiocyanate

HEPES: (4-(2-hydroxyethyl)-1-piperazineethanesulfonic acid

TFA: Trifluoroacetic acid

DNA: Deoxyribonucleic acid

RT: Room Temperature

THF: Tetrahydrofuran

PB: Phosphate Buffer

PBS: Phosphate Buffer Saline

HOBt: Hydroxybenzotriazole

Abbreviations

PyBOP: Benzotriazole-1-yl-oxy-tris-pyrrolidino-phosphonium hexafluorophosphate

DMAP: 4-dimethylaminopyridine

DIC: N, N′-diisopropylcarbodiimide

DIPEA: N, N-diisopropylethylamine

DCM: Dichloromethane

D_2O: Deuterium Oxide

CH_3CN: Acetonitrile

MTT: 3-(4, 5-dimethylthiazol-2-yl)-2, 5-diphenyl tetrazolium bromide

SDS: Sodium Dodecyl Sulfate

DPC: Dodecylphosphocholine

D8PG: Dioctanoylphosphatidylglycerol

DOPE: Dioleoylphosphatidylethanolamine

DOPG: Dioleoylphosphatidylglycerol

POPC: 1-palmitoyl-2-oleoyl-sn-3-glycero-phosphocholine

POPE: 1-palmitoyl-2-oleoyl-sn-3-glycero-phosphoethanolamine

POPG: 1-palmitoyl-2-oleoyl-sn-3-glycero-phosphatidylglycerol

$CHCl_3$: Chloroform

TFE: 2, 2. 2-Trifluoroethanol

DMSO: Dimethyl sulfoxide

PI: Propidium Iodide

NPN: 1-N-phenylnaphthylamine

$DISC_3$: 3, 3′-Dipropylthiadicarbocyanine Iodide

$MnCl_2$: Manganese Chloride

NaCl: Sodium Chloride

$MgCl_2$: Magnesium Chloride

$CaCl_2$: Calcium Chloride

mM: Millimolar

µM: Micromolar

E. coli DH5α: *Escherichia coli DH5α*

P. aeruginosa: *Pseudomonas aeruginosa*

K. pneumoniae: *Klebsiella pneumoniae*

Abbreviations

S. aureus: Staphylococcus aureus

S. typhi TY2: Salmonella enterica

C. albicans: Candida albicans

C. grubii: Cryptococcus neoformans var. grubii.

MRSA*:* Methicillin-resistant *S. aureus*

MDR: Multi-drug resistant

HEK-293: Human normal embryonic kidney

CFU: Colony Forming Unit

DSS: 4, 4-dimethyl-4-silapentane-1-sulfonic acid

LUV: Large Unilamellar Vesicles

DMEM: Dulbecco's modified Eagle's medium

Chapter 1

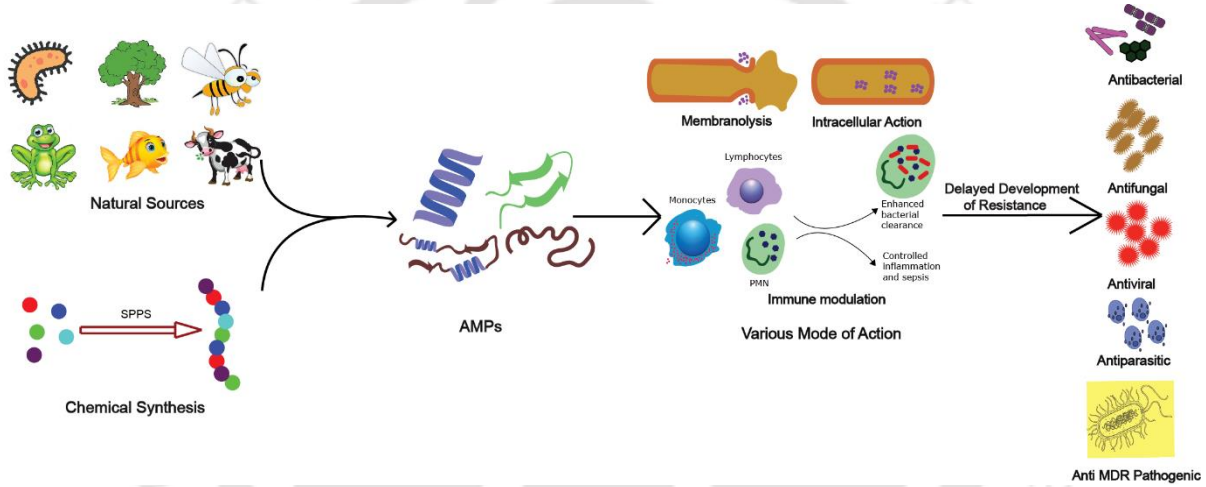

Introduction

1.1. Antibiotic Resistance and Antimicrobial Peptides (AMPs)

1.1.1. Brief History of Antibiotic Resistance:

Accidental discovery of Penicillin in 1928, was the beginning of the golden period for antibiotics (based on natural products, like β-lactams, tetracyclines and aminoglycosides).[1] These were successfully used to treat infectious diseases, and human beings prevailed in the constant battle against bacteria. However, with time the conventional antibiotics are becoming inactive against microbes due to the phenomenon of "antimicrobial resistance (AMR)" (Table 1.1, Figure 1.1).[2-6] Development of antimicrobial resistance is a part of the natural defense mechanism of the microbes[7,8] but it further expedited by the unfinished treatments, improper disposal techniques and excessive use of antimicrobials in raising livestock and fish farming (WHO). Increasing international travel, poor sanitation and hygiene and expulsion of non-metabolized antibiotics through the faeces are also some of the reasons that has led to increased AMP.[9,10] Antibiotic resistance leads to the development of superbugs which are not susceptible to the existing arsenal of antibiotics.[11] Additionally, the discovery of novel classes of antibiotics are extremely slow.[12] The so called discovery void occurred as no major classes of antibiotics have been introduced since the lipopeptide antibiotics (e.g. daptomycin) in the mid1980s.[13,14] The situation is grimmer for Gram-negative bacteria, where no new class of antibiotics drug has been approved in over 50 years.[12] In 2016, the world economic forum announced that multi drug resistance (MDR) is "one of the major health challenges of our time", and without urgent action would cause 10 million deaths worldwide by 2050.[15] Therefore, it is essential to identify and design alternative classes of antimicrobial agents that can prevent resistant bacteria and fungus infection effectively. The world has already witnessed infection in around 30 million people including 6.2 million death globally due to Covid 19.[16]

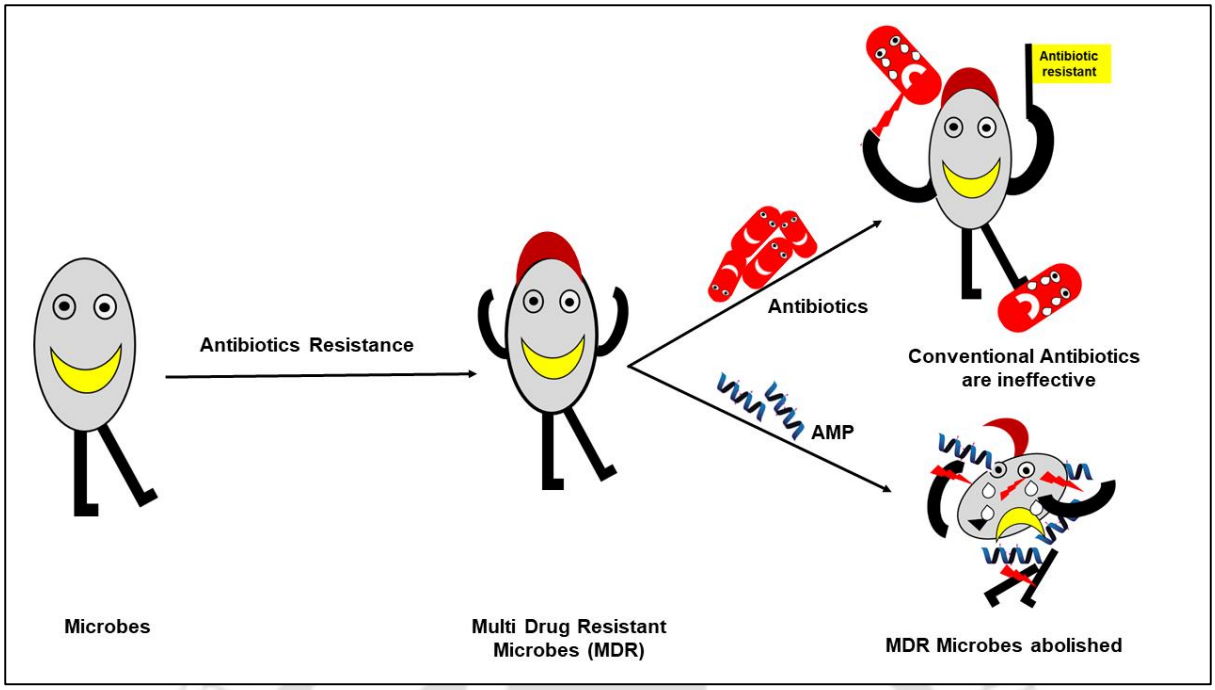

Figure 1.1. Antimicrobial resistance (AMR) or more specifically antibiotic resistance leads to the development of antibiotic resistant (Multiple Drug Resistant (MDR)) bacteria, which cannot be prevented/killed by the conventional antibiotics. Resistance against AMPs do not develop/develop very slowly in microbes due to their multiple modes of action. AMPs are effective against MDR superbugs.

Table 1.1. Different classes of conventional antibiotics against which resistant has been developed in microbes, their targets, initial sources of isolation, time of development of resistance and the mechanism of resistance development. This table has been adopted with permission[17] from Ref. 17. *Copyright 2022, Published by Springer Nature.*

Chemical class	Main microbial target	Antibiotic molecule	Origin	Discovery	1st reported resistance	Main mechanisms of resistance
β-lactam	Peptidoglycan biosynthesis (cell wall)	Penicillin G	*Penicillium notatum*	1928	1940	Hydrolysis, efflux, altered target[18-22]
Sulfonamide	Dihydropteroate synthetase	Prontosil	Synthetic	1932	1942	Efflux, altered target[18,23]
Peptide	Cell membrane	Gramicidin	*Bacillus brevis*	1939	*Gramicidin ?*** 2015: Polymyxin	Altered target, efflux, destruction plasmid-mediated polymyxin resistance gene (*MCR-1*)[24,25]
Aminoglycoside	rRNA (translation)	Streptomycin	*Streptomyces griseus*	1943	1947	Phosphorylation, acetylation, nucleotidylation[18], efflux, altered target[23]
Tetracycline	rRNA (translation)	Chlortetracycline	*Streptomyces aureofaciens*	1945	1953	Monooxygenation, efflux, altered target[18,22,23]
Nitrofuran	citric acid cycle, DNA, RNA, and protein synthesis	Nitrofurantoin	Synthetic	1946	1952	Decreased activation[23,26]

Phenicol	rRNA (translation)	Chloramphenicol	*Streptomyces venezuelae*	1947	1956	Acetylation, efflux, altered target[18,23]
Macrolide	rRNA (translation)	Erythromycin	*Saccharopolyspora erythraea*	1949	1953	Hydrolysis, glycosylation, phosphorylation, efflux, altered target[18,23]
Nitroimidazole	DNA (nucleic acid synthesis)	Metronidazole	Synthetic	1953	1978	Decreased drug uptake, efflux, decreased activation, altered target, increased oxygen scavenging capabilities (SOD/catalase/peroxidase), enhanced activity of DNA repair enzymes[23,27]
Glycopeptide	Peptidoglycan biosynthesis (cell wall)	Vancomycin	*Amycolatopsis orientalis*	1953	1986	Reprogramming peptidoglycan biosynthesis[18,22,23]
Streptogramin	rRNA (translation)	Virginiamycin	*Streptomyces virginiae*	1955	1964	C-O lyase (type B streptogramin), acetylation (type A streptogramin), efflux, altered target[18,28]
Ansamycin	Transcription	Rifamycin	*Streptomyces*	1957	1963	ADP-ribosylation, efflux, altered target[22]

Pyrimidine - antimetabolite antibiotics	Dihydrofolate reductase	trimethoprim	Synthetic	1961	1972	Efflux, altered target[18,23]
Lincosamide	rRNA (translation)	Lincomycin	*Streptomyces lincolnensis*	1962	1979	Nucleotidylation, efflux, altered target[18,23]
Quinolone	DNA replication, Topoisomerase inhibitors	Nalidixic acid	Synthetic	1962	1966	Acetylation, efflux, altered target[18,23]
Oxazolidinone	rRNA (translation)	Linezolid	Synthetic	1978	1999	Efflux, altered target[18,22,23]
Lipopeptide	Cell membrane	Daptomycin	*Streptomyces roseosporus*	1987	2005	Altered target[18,23]

** No report found for a precise year

1.1.2. AMPs: What are they?

AMPs are one of the most promising candidates as a potential alternative to conventional antibiotics to treat antimicrobial infections. AMPs are small molecular weight proteins/peptides with broad-spectrum antimicrobial activity against bacteria,[29-36] viruses,[2,32,37-46] fungi,[37,47-56] parasites etc. They act as the first line of defense[57,58] in host organisms. They were originally isolated from various natural sources like microorganisms, vertebrates,[59] invertebrates,[60,61] plants,[62] amphibians,[63,64] sea creatures,[65,66] insects etc. AMPs vary greatly in their sequence,[67,68] structure and have various modes of action (Figure 1.2).[69-75]

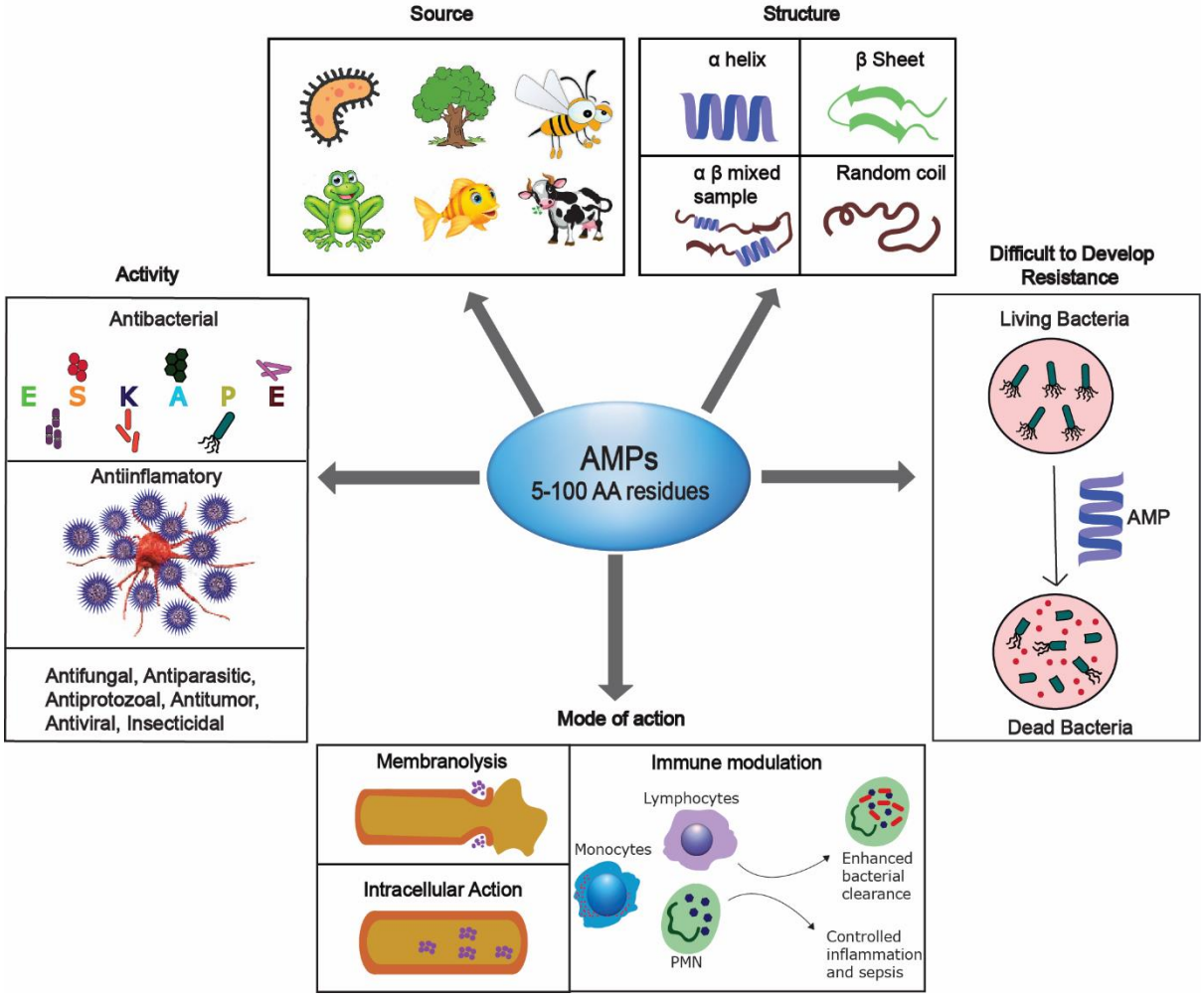

Figure 1.2. A schematic diagram showing different attributes of AMPs. AMPs are short peptides isolated from various natural sources, having a broad-spectrum activity against

bacteria, viruses, fungi, parasites etc. AMPs have variable primary sequences, structure and modes of action. Slow development of resistance against the AMPs make them advantageous over the conventional antibiotics.

1.1.3. AMPs: Their Importance:

AMPs have attracted great attention because they not only possess direct activity against bacteria, fungi, viruses, protozoa, and mutation, but also have indirect immune modulating activity in the host.[76-82] AMPs are also called as host defense peptides (HDPs) and form a part of the innate immune response found among all classes of life. Unlike conventional antibiotics, which function primarily by interacting with specific intracellular targets, AMPs have very diverse modes of action thereby abolishing or reducing the possibility of development of bacterial resistance.[83-86] Additionally, unlike the antibiotics, AMPs are also effective against MDR microbes or superbug. This has led to active research in the field of AMPs[87-89] over the last few decades as potential drugs for the future (Figure 1.3). Presently, more than 3000 AMPs have been isolated and identified from various organisms (e.g., bacteria, plants, animals) and have been documented to possess antibacterial, antifungal, anticancer, and immunomodulatory activities.[90,91] There are several database exist like APD3,[68] CAMP,[92] DrAMP2.0[93] etc. which catalog different types of AMPs which are known to still date.

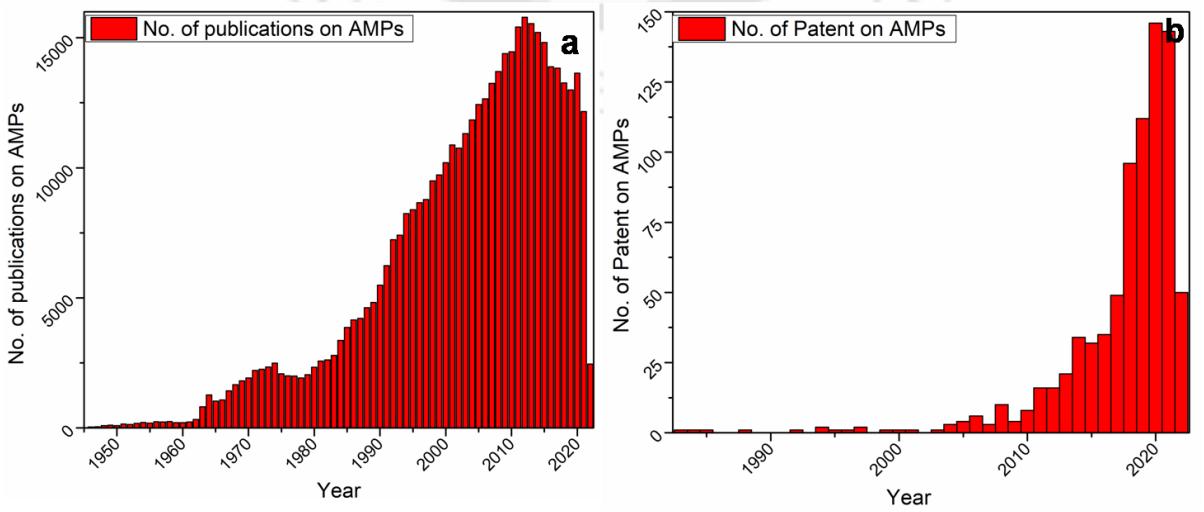

Figure 1.3. The number of publications and patents per year for AMPs. (PubMed, May 2022)

1.1.4. Disadvantages of Naturally Occurring AMPs:

Some AMPs have been commercialized and used to combat antimicrobial infections (Table 1.2).[94] However, in comparison to the number of known AMPs, the number which has been clinically and commercially successful are limited. This is owing to some significant drawbacks of naturally occurring AMPs. High production cost due to long sequence of the natural AMPs, inadequate quantity obtained upon isolation from natural sources, peptide folding issues, salt sensitive antimicrobial potency, short systemic half-life owing to protease degradation and immunogenicity in hosts are some of the disadvantages of natural AMPs (Figure 1.4).[95-97]

Table 1.2. Some representative examples of AMPs.

AMP	Discovery	MW (Da)	Bacterial Strain[a]	Specificity[b]	Structure[c]	Reference
Nisin A	1928	3354.1	G(−) G(+)	*E. coli*, *S. aureus*	Polycyclic CP	98
Gramicidin S	1944	1140.7	G(−) G(+)	*S. aureus*, *E. Coli*	Polycationic CP	99
Polymyxin	1947	1203.5	G(−)	*K. pneumonia*, *A. baumannii*	Polycationic CP	100
Daptomycin	1986	1619.7	G(+)	MRSA, VRE	CP lipopeptide	101
Teixobactin	2015	1242.5	G(+)	MRSA, VISA	CP	102
Melittin	1967	2846.5	G(+)	MRSA	α-helical CAP	103
Magainin	1987	2409.9	G(+)	*E. coli*	α-helical CAP	104
Cathelicidin	1996	4493.3	G(−)	*E. cloacae*, *K.*	α-helical	105

				pneumonia, P aeruginosa,	CAP	
Buforin	1996	2434.9	G(+), G(−)	*E. coli*	α-helical CAP	106

[a]G(+), Gram-positive, G(−), Gram-negative.

[b]MRSA, methicillin-resistant *Staphylococcus aureus*; VISA, vancomycin-intermediate-susceptible *Staphylococcus aureus*; *A. baumannii*, *Acinetobacter baumannii*; VRE, vancomycin-resistant *enterococci*.

[c]CAP, cationic amphipathic peptide; CP, cyclic peptide. This table has been adopted with permission from ref. 94, *Copyright 2019, Published by John Wiley and Sons.*

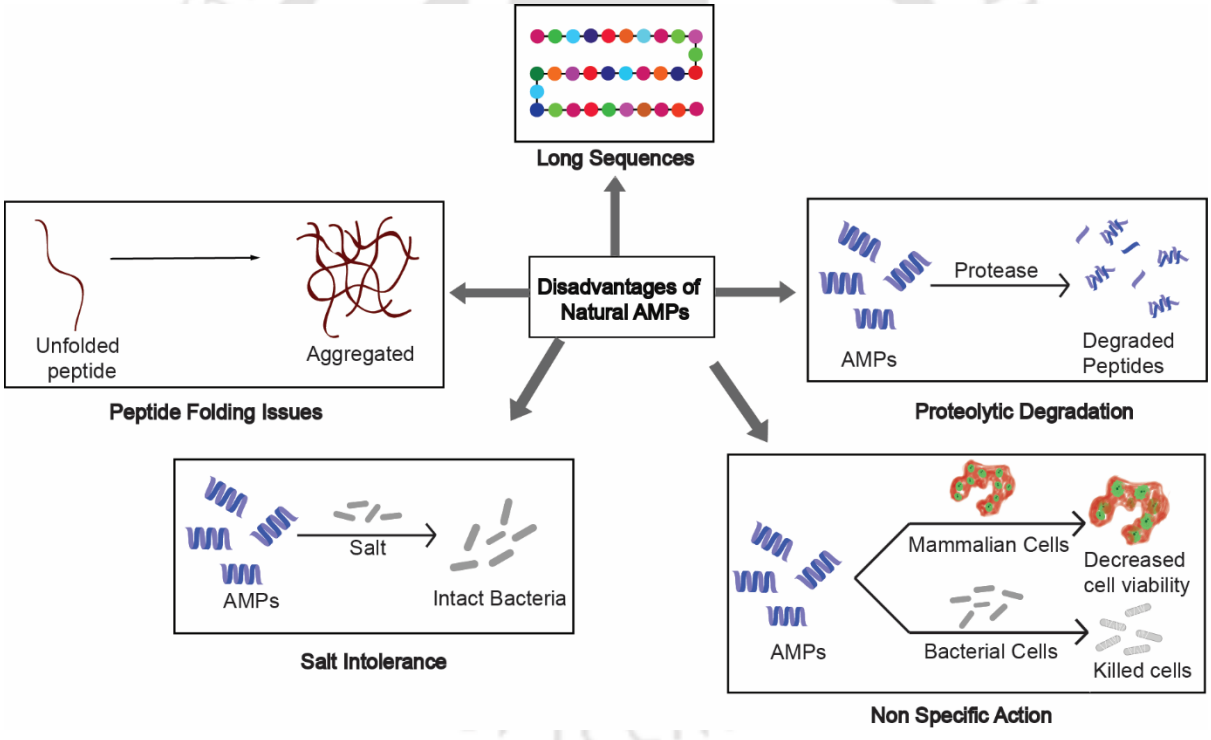

Figure 1.4. A schematic diagram describing the various disadvantages of natural AMPs that limits their use as commercial therapeutic.

1.1.5. Development of Synthetic AMPs: Challenges and Optimism:

To overcome these shortcomings of natural AMPs and generate better therapeutically competent AMPs, research on synthetic AMPs is being carried out globally. Synthetic AMPs

can be generated by modifying and optimizing the natural AMPs/using methods such as sequence truncation,[107-109] residual substitution,[110-113] cyclization,[114-118] use of unnatural amino acids,[107,119-122] use of D amino acids,[123-125] or other peptidomimetics building blocks,[126-135], etc. Synthetic AMPs can also be generated from the *de novo* design of peptide sequences in which only limited types of amino acid residues are involved.[136-140] Unfortunately, generation of synthetic AMPs from the modification of the natural AMPs are largely empirical, making it even harder to decipher common structure−function relationships. More importantly, if the sequences of AMPs are too similar to naturally occurring AMPs, their application may trigger immunogenicity and ultimately compromise the host defense system, causing serious harm to the environment and public health.[141] Therefore, the *de novo* design of peptides with minimal similarity to naturally occurring peptides is an effective way to exploit the safety and effectiveness of AMPs for clinical application. Till date several synthetic AMPs are in different clinical trial phases[94] (Table 1.3), though many technological hurdles still remain to be addressed, such as antimicrobial activity optimization, cell selectivity enhancement, and optimized hemolytic activity.

Rational design of AMP sequences should be done with certain considerations such as positive charge, hydrophobicity, and amphipathicity as these are considered to be vital parameters for AMP activity.[142-147] Although these variables have no stringent relation to antibacterial activity still, a balanced amphipathicity is widely accepted to be critical for maximizing antibacterial activity while minimizing the cytotoxicity of AMPs.[148-150]

Table 1.3. Mechanism and structure of AMPs in clinical trials. This table has been adopted with permission from Ref. 94. *Copyright 2019, Published by John Wiley and Sons.*

Entry	AMP	AMP source	Target[c]	Phase	Company	Admin[d]
1	EA-230	hCG derivative	Sepsis and renal failure protection	II	Exponential Biotherapies	i.v.
2	CZEN-002	α-MSH derivative	Anti-fungal	II[b]	Zengen	top.
3	D2A21	Synthetic	Burn wound infections	III	Demegen	top.
4	XMP-629	BPI derivative	Impetigo and acne rosacea	III[b]	Xoma Ltd.	top.
5	Neuprex (rBPI21)	BPR derivative	Pediatric meningococcemia	III[b]	Xoma Ltd.	i.v.
6	Delmitide (RDP58)	HLA class I derivative	Inflammatory bowel disease	II[a]	Genzyme	top.
7	Ghrelin	Endogenous HDP	Chronic respiratory failure	II[a]	University of Miyazaki; Papworth Hospital	i.v.
8	NVB-302	Lantibiotic	*C. difficile*	I[b]	Novacta	oral
9	hLF1-11	Lactoferricin derivative	MRSA,*K. pneumoniae*, *L. monocytogenes*	I/II	AM-Pharma	i.v.
10	Wap-8294A2 (Lotilibcin)	*Lysobactor* spp.	G(+) bacteria(VRE, MRSA)	I/II	aRigen	top.
11	C16G2	Synthetic	Tooth decay by *Streptococcus mutans*	II	C3 Jian Inc.	Mouth wash
12	SGX942(Dusquetide)	Synthetic	Oral mucositis	III	Soligenix	Oral rinse
13	DPK-060	Kininogen derivative	Acute external otitis	II	ProMore Pharma	Ear drops
14	PXL01	Lactoferrin analog	Postsurgical adhesions	III	ProMore Pharma	top.

15	PAC113	Histatin 5 analog	Oral candidiasis	II[a]	Pacgen Biopharmaceuticals	Mouth rinse
16	POL7080	Protegrin analog	*P. aeruginosa* *K. pneumoniae*	III	Polyphor Ltd.	i.v.
17	LTX-109 (Lytixar)	Synthetic	G(+) MRSA skin infections; impetigo	II[a]	Lytix Biopharma	Nasal top.
18	OP-145	LL-37 derivative	Chronic middle ear infection	II[a]	Dr. Reddy's Research	Ear drops
19	LL-37	Human cathelicidin	Leg ulcer	II[b]	ProMore Pharma	top.
20	Novexatin (NP213)	Cyclic cationic peptide	Fungal nail infection	II[b]	Novabiotics	top.
21	p2TA (AB103)	Synthetic	Necrotizing soft tissue infections	III	Atox Bio Ltd.	i.v.
22	Iseganan (IB-367)	Protegrin analog	Pneumonia, stomatitis	III[b]	IntraBiotics Pharmaceuticals	top.
23	Pexiganan (MSI-78)	Magainin analog	Diabetic foot ulcers	III[b]	Dipexium Pharmaceuticals	top.
24	Omiganan (CLS001)	Indolicidin derivative	Rosacea	III	Cutanea Life Sciences	top.
25	Surotomycin	Cyclic lipopeptide	*C. difficile* (diarrhea)	III[b]	Cubist Pharmaceuticals/Merck	oral
26	Ramoplanin (NTI-851)	Actinoplanes spp	G(+) (VRE, *C. difficile*)	III	Nano-therapeutics	oral
27	Friulimicin B	Cyclic lipopeptide	Pneumonia, MRSA	I[b]	MerLion Pharmaceuticals	i.v.

[a]Completed. [b]Discontinued. [c]G(+), Gram-positive; G(−), Gram-negative; MRSA, methicillin-resistant S. aureus; VRE, vancomycin-resistant Enterococci. [d]top.—topical; i.v. intravenous.

1.2. Classification of AMPs

There are many different ways to classify AMPs based on their biosynthetic pathways (non-ribosomally or ribosomally synthesized), source, secondary structure and physicochemical properties (net charge, primary sequence etc.)

1.2.1. Classification According to the Biosynthetic Pathway:

Natural AMPs are classified into two categories, non-ribosomally synthesized peptides (NRP) (Figure 1.5) and ribosomally synthesized peptides (RP). The former is produced mainly by microorganisms like bacteria and fungi and are not genetically encoded. Their synthesis is catalyzed by large proteins named peptide synthetases.[151,152] Importantly NRPs contain both proteinogenic and non-proteinogenic (unusual) amino acids. Most of the AMPs are ribomally synthesized by a wide range of multicellular organisms.[153] RP's are gene-encoded peptides. Their synthesis involves the transcription of DNA strand into the complementary RNA (mRNA) and its subsequent translation into the corresponding peptide by amino acid polymerization as enumerated in the nucleotide sequence of the mRNA.

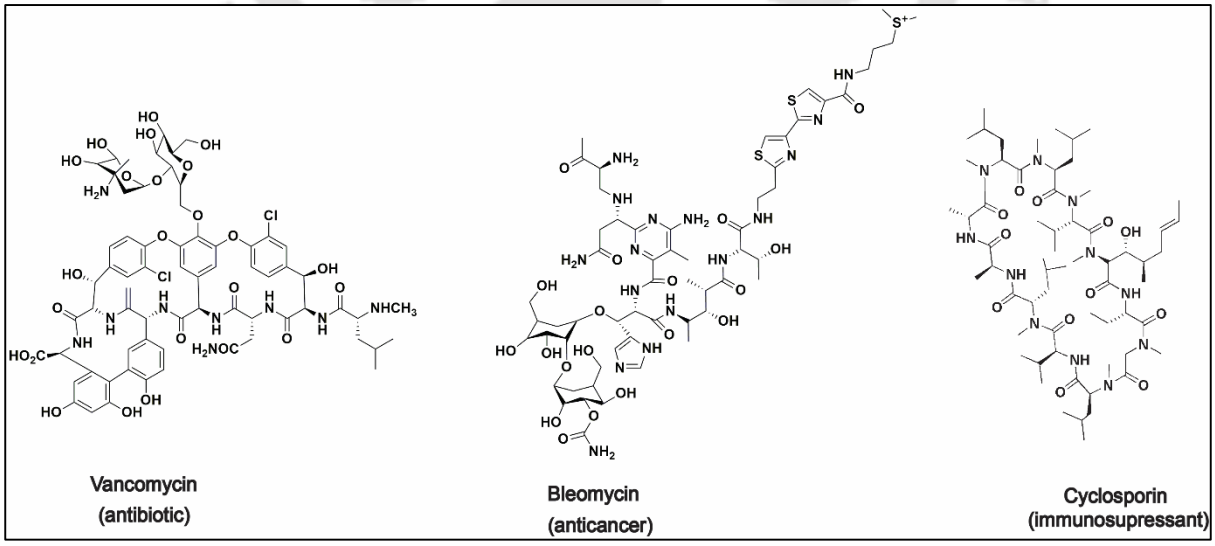

Figure 1.5. Chemical structures of Bioactive non-ribosomally synthesized AMPs.

1.2.2. Classification According to Primary Structure:

1.2.2.1. An Unusual Proportion of Proteinogenic Amino Acids:

A high proportion of certain amino acids in a specific primary structure leads to the folding of the sequences, which is different from regular helices and sheets structure. These types of AMPs are discussed below:

1.2.2.1.1. Defensins:

Defensins are cationic AMP rich in Arg and Cys residues with a β-hairpin structure stabilized by three to four disulfide bonds (Figure 1.6). It binds to the membrane to form pore-like membrane defects that lead to efflux of the intracellular matrix, causing cell death. Plant defensins have antimicrobial, α-amylase,[154] and trypsin inhibitory activities[154] with activity against yeast, oomycetes, and necrotophic pathogens.[155,156] Human defensins are of three types- α, β, θ. There are six subclasses of α defensins containing three conserved disulfide connectivities between Cys $^{I–VI}$, Cys $^{II–IV}$, and Cys $^{III–V}$. [157] β-defensins are longer in sequence than the α defensins and have Cys $^{I–V}$, Cys $^{II–IV}$, Cys $^{III–VI}$ disulfide bond connectivities. There are different subclasses of human β-defensins (hBD). The hBD1 and hBD2 are rendered inactive in the presence of physiological salt concentrations.[158,159] The hBD3 retains its activity against *Staphylococcus aureus* (*S. aureus*) and vancomycin-resistant *Enterococcus faecium* at physiological salt concentrations.[160] Insect defensins are about 29–34 amino acids long, active against gram-positive and gram-negative bacteria.[161] However, the virulence against the gram-positive bacteria (*S. aureus*) is usually more than the gram-negative family.[162]

1.2.2.1.2. Protegrins:

Protegrins are a class of AMPs similar to defensins and contain 16 to 18 amino acid residues. Protegrins are highly active against both Gram-positive and Gram-negative bacteria, chlamydia, mycobacteria and viruses like HIV-1.[169,170]

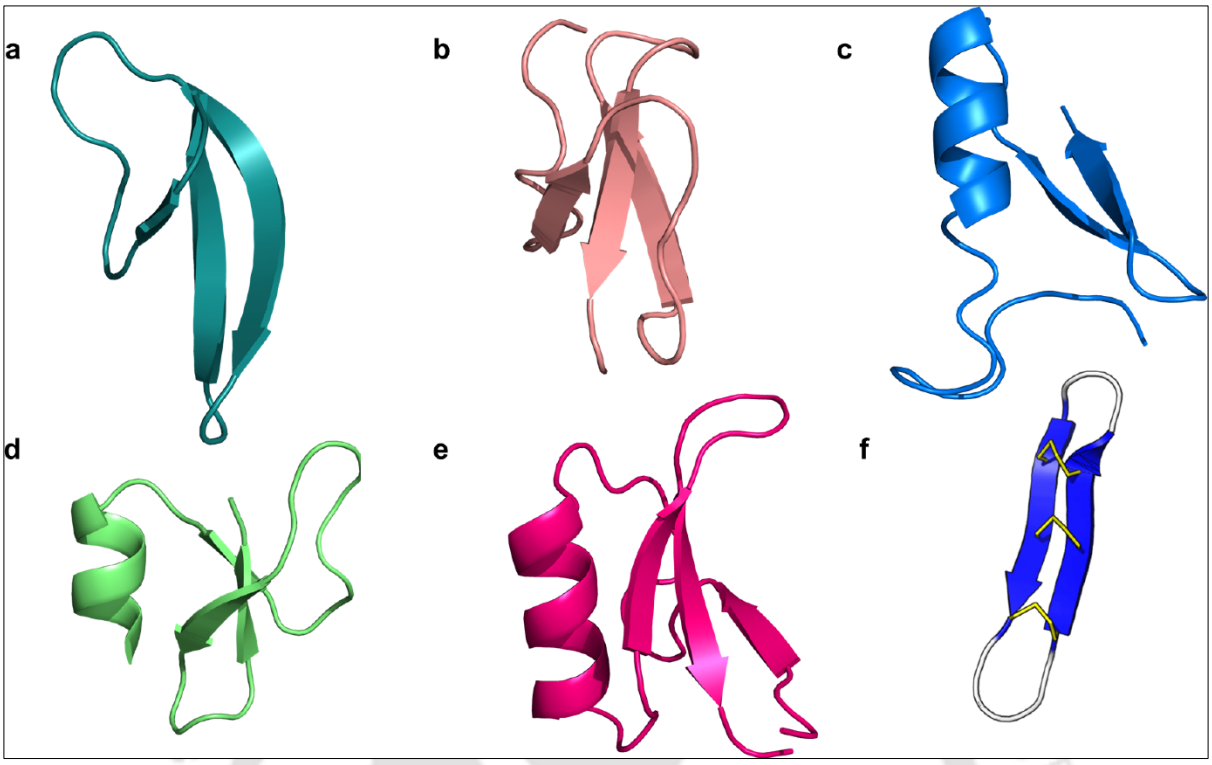

Figure 1.6. Secondary structures of (a) Human α-defensin 1 derivative (2PM5)[163], (b) BNBD-12 bovine neutrophil β-defensin (1BNB)[164], (c) Insect defensin (1ICA)[165], (d) β-defensin HBD-1(1IJV)[166], (e) *Raphanus sativus* Antifungal Protein 1 (Rs-AFP1) plant defensin (1AYJ)[167] and (f) theta-defensin HTD-2 (2LZI)[168]

1.2.2.1.3. Histatins:

Histatins contain a group of neutral and basic His-rich peptides (Figure 1.7) present in secretions of human submandibular and parotid glands and human saliva.[55] The former contains Histatin 5, and the later contains histatin 1 and 3.[171] All three histatins can kill pathogenic yeast *C. albicans*. They are unstructured in aqueous solutions, but they form α helical conformation in the polar protic solvent system. Due to low amphipathicity, histatins are non-cytotoxic compared with other AMPs. Calcitermin C is a 15 residue AMP containing

three His residues at the N-terminal that adopts a helical conformation in the membranes.[172] It is found in human airways and is effective against gram-negative bacteria.

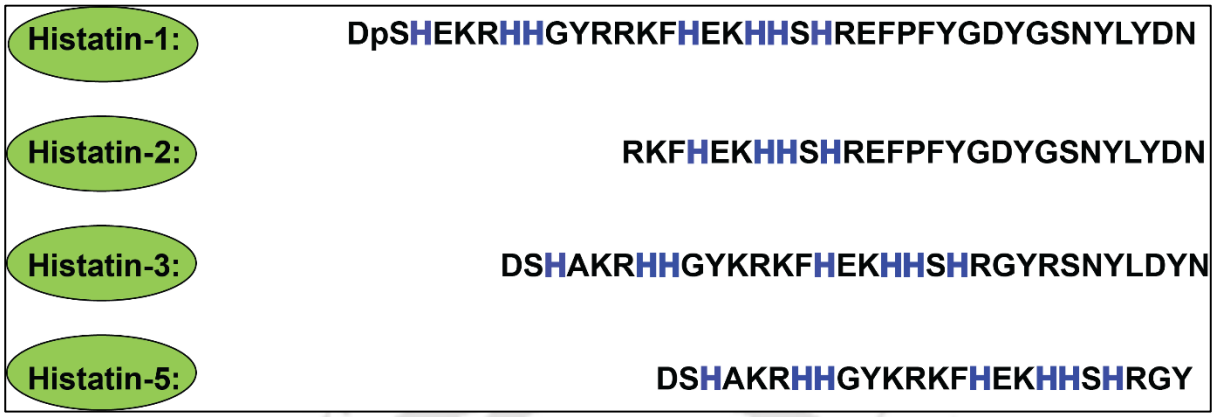

Figure 1.7. Primary sequence for histatin-1, histatin-2, histatin-3, and histatin-5, which are most frequently studied for their antimicrobial activity.

1.2.2.1.4. Cathelicidins:

Cathelicidins are short cationic peptides that belong to the family HDP found in the innate immune system. The mature protein was isolated from the neutrophils, human skin and sweat. Cathelicidins have a 100 amino acid long conserved N-terminal pre-pro region called the cathelin domain (Figure 1.8a).[173] Initially, the cathelin domain was studied for its antimicrobial activity, but nowadays, it is more appreciated for its immunomodulatory functions. The mature cathelicidin peptides vary with both amino acid size and sequences, leading to considerable differences in their 3D structure. Cathelicidins contain α-helices, β-hairpins, extended networks or form cyclic peptides (Figure 1.8b). It is found in nearly all vertebrates. While in some species, like mouse (CRAMP), dog (K9CATH), and humans (LL-37), only one cathelicidin has been identified, multiple cathelicidins are found in chicken, horse, pig, and cattle. The primary source of LL-37 in humans are neutrophils, which store the inactive pro-peptide in their secretory granules and secrete upon activation. However, other cell types, including

macrophages, epithelial cells, lymphocytes, and keratinocytes, also produce Cathelicidins.[174-180]

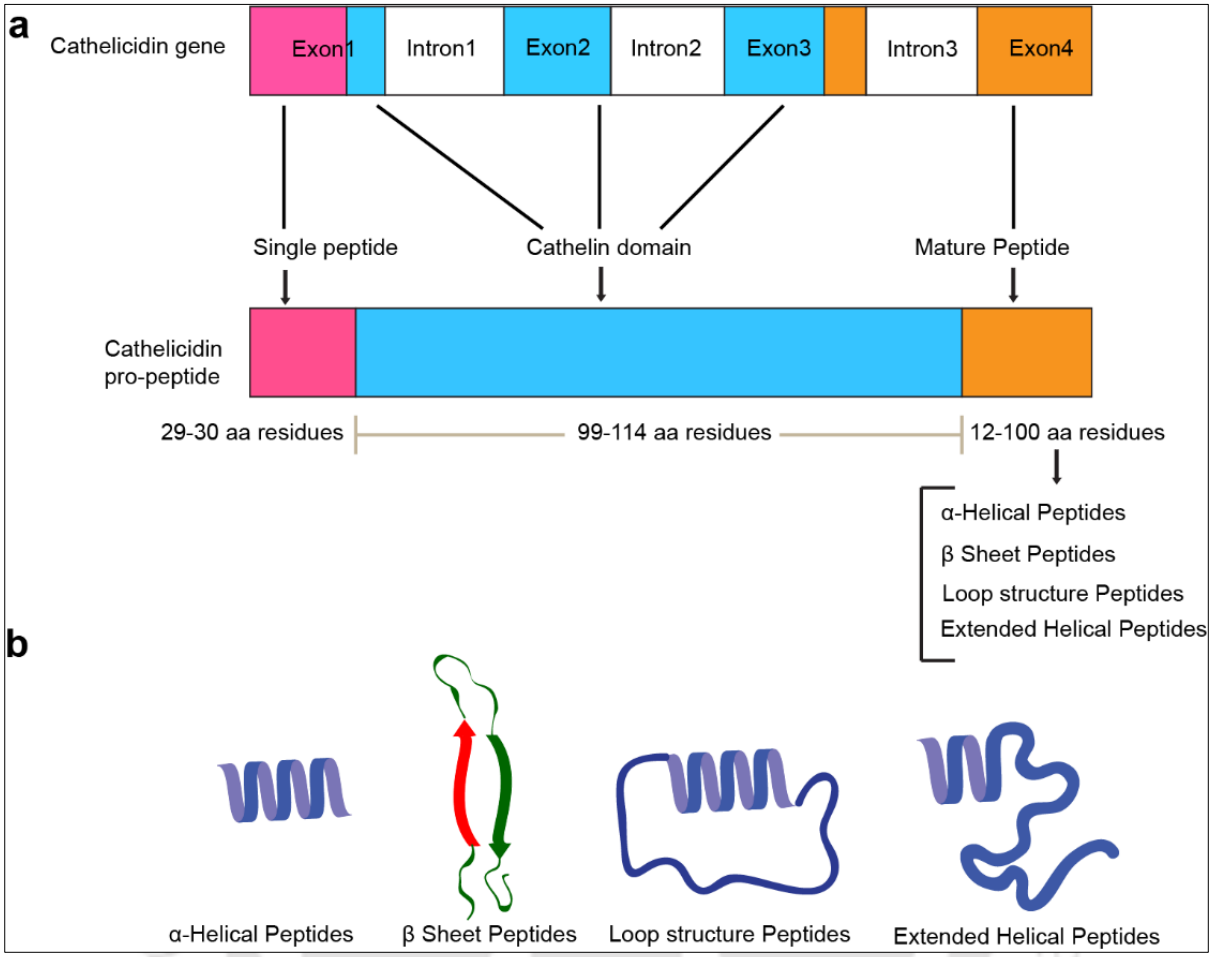

Figure 1.8. (a) Schematic representation of the gene and propeptide of the Cathelicidin in vertebrate.[181-186] Color codes indicate the exons and their corresponding translated peptide fragments. (b) The secondary structure of Cathelicidins include α-helical, β-sheet, extended helical, and loop structure, which were predicted online by the Ressource Parisienne en BioInformatique Structurale web portal.[187] This figure has been adopted from Ref. 173 (open access) with modification.

1.2.2.2. AMPs Containing Uncommon Modified Amino Acid:

These types of peptides are isolated from bacteria and fungi, which are more similar to conventional antibiotics than the AMPs formed in the higher organisms. Lantibiotics and peptaibols are the two classes of peptides considered here.

1.2.2.2.1. Lantibiotics:

They are polypeptide antibiotics containing uncommon modified amino acids with a small ring structure enclosed with a thioether bond. Lantibiotics are ribosomally synthesized and post-translationally modified peptides. These AMPs are well studied due to their commercial uses in the food industries for making dairy products. Lantibiotics are produced by many gram-positive bacteria like *Streptococcus* and *Streptomyces* to attack other gram-positive bacteria. The duramycin family of lantibiotics bind phosphoethanolamine in the membrane of its target cells and disrupts different physiological functions. One peptide of this family is nisin, which binds to lipid II, a cell wall precursor lipid component of target bacteria and disrupts cell wall formation (Figure 1.9a).[188,189] NMR studies reveal that it is flexible in water but forms a β-turn structure upon binding to the micelles. Activity of these AMPs are not related to any regular secondary structures like helices and sheets.[189]

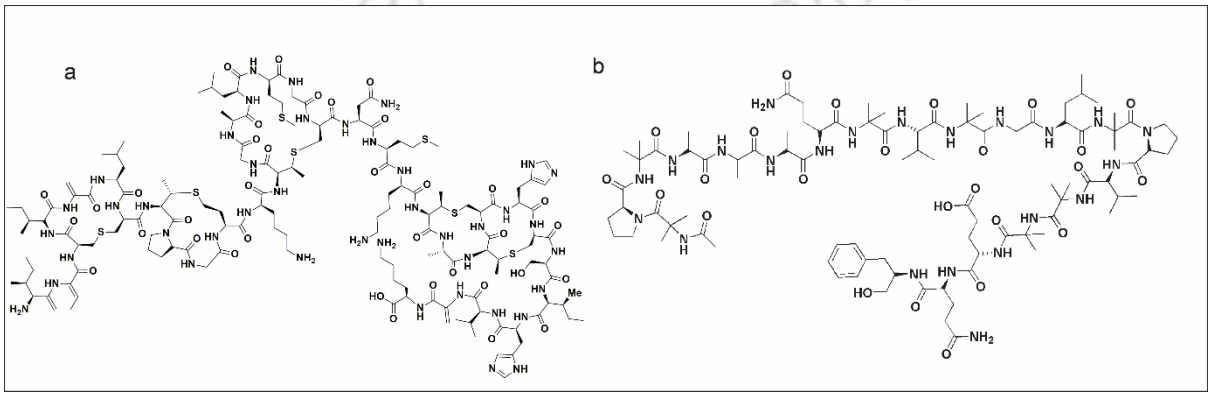

Figure 1.9. (a) Primary structure of nisin. The unusual amino acids present in the primary structure are dehydroalanine (Dha), dehydrobutyrine (Dhb) and L-2-aminobutyric acid (Abu). (b) Primary structure of peptaibol Alamenthicin isolated from *Trichoderma viride* which contains high percentages of unnatural amino acid residue α amino isobutyric acid (Aib).

1.2.2.2.2. Peptaibols:

This is an interesting class of AMPs which contain a large proportion of unnatural amino acid residue α Amino isobutyric acid (Aib). Aib is a conformationally restricted amino acid residue that forms α helical structure. Alamenthicin is a well-known peptaibol containing 20 amino acid residues, isolated from the fungus *Trichoderma viride* (Figure 1.9b). It forms a α-helical conformation in non-aqueous solvent system as well as in lipid membrane bilayers.[190]

1.2.3. Classification of AMPs According to Secondary Structure:

AMPs can be divided into four categories based on their structures including linear α-helical, β-sheet, linear extended structures, and combination of α-helix and β-sheet structures (**Figure 1.10)** Moreover, cyclic peptides and AMPs with more complex topologies (including lasso peptides and thioether bridged structures) are also reported in the literature.[191]

1.2.3.1. α-Helical:

α-helical: Historically, these were the first class of AMPs that were isolated and well-studied in the literature. These types of peptides are unstructured in water; however, they form helical structures in the presence of the microbial mimic lipid membranes. Different classes of these peptides like melittin, ceropins, magainins were isolated from various sources and well-characterized in the literature (Figure 1.11).

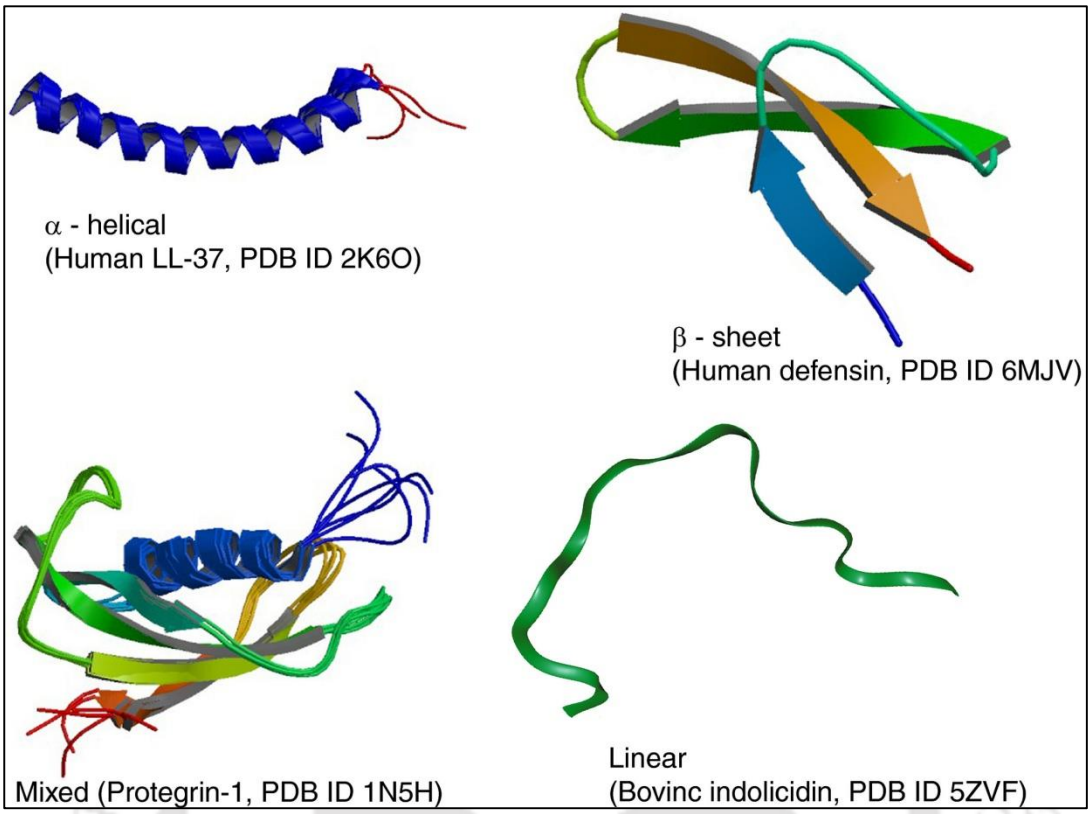

Figure 1.10. Classification of AMPs based on their structure.[85] AMPs can adopt α- helical, β-sheet, linear extended and mixed α-helical and β-sheet like structures. This figure has been adopted with permission from ref. 85. *Copyright 2021, Published by John Wiley and Sons.*

1.2.3.1.1. Melittin:

Melittin is a 26 residue long peptide hormone found in honey bee (*Apis melifera*) venom.[192] It displays broad-spectrum antimicrobial activity[193] and high hemolytic activity.[194] Melittin is also reported to have anti-inflammatory properties[195] and activity against *Xanthomonas oryzae*, a pathogenic bacteria causing destructive bacterial disease in rice.[196] Melittin forms an amphipathic helical structure in the presence of microbial membrane mimics. The Pro residue is responsible for the activity of melittin in its primary sequence.[197] Apoptosis is induced in *C. albicans* by melittin through reactive oxygen species (ROS) mediated mitochondria and caspase pathway.[198] Melittin exhibits strong synergistic effects with the conventional

antibiotics against MDR isolates of *A. baumanni* and *P. aeruginosa*[199] and effective antibacterial activity against MRSA strains.[200]

1.2.3.1.2. Magainins:

Magainins are small Gly rich cationic AMPs isolated from the skin of African clawed frog *Xenopus laevisbbb*. They are highly active against different bacterial and fungal strain and cause osmotic lysis of the protozoa. Magainins form amphipathic α-helical conformations in membrane lipid environments. Esculetins are isolated from frog skin possessing broad-spectrum antimicrobial properties.[201,202] Microbial membranes are the major target for this class of AMPs.[203] Esculentin-2CHa is a 37 residue long cationic antimicrobial peptide isolated from the skin of amphibians like *Lithobates chiricahuensis*. This peptide is predominantly α-helical in structure with broad-spectrum antimicrobial properties.[204]

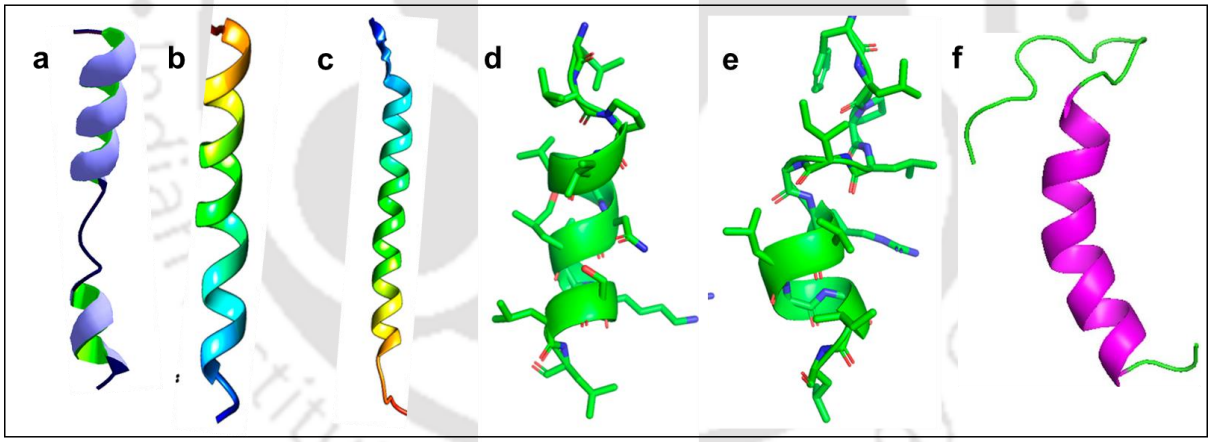

Figure 1.11. α-helical AMPs. (a) Melittin (PDB code:2MW6),[205] (b) Magainin 2 (PDB code:2MAG),[206] (c) LL-37(PDB code: 2K6O),[207] (d) Temporin A (PDB code:2MAA),[208] (e) Temporin B (PDB code:6GIL)[209] and (f) Cecropin-P1(PDB code:2N92).[210]

1.2.3.1.3. Cecropins:

Cecropins are a family (seven subclasses) of small, cationic AMPs isolated from the hemolymph of giant silk moth *Hyalophora cecropia.*[211] They are composed of 31-39 amino

acid residues with broad-spectrum antimicrobial activity. They are widespread throughout the animal kingdom, isolated from different sources. *Eg*. Cecropin P1 is isolated from the pig intestine and cecropin A and B are isolated from the hemolymph of giant silkworm moth (*Hyalaphora cecropia*). They do not show cytotoxic effect against eukaryotic cells, but they are susceptible to protease degradation.[211-213] They form pores in the bacterial membranes causing membrane depolarization and lysis.[214] Bactericidin, lepidopteran, and sarcotoxins are structurally related to cecropins.[215]

1.2.3.1.4. Temporins:

These are another family of tiny α-helical cationic AMPs with a low net positive charge, isolated from frog skin.[216] They are highly potent against bacteria, fungi, viruses, yeasts, and protozoa. Temporins are effective against gram-positive bacterial strains like *MRSA*, vancomycin-resistant *Enterococcus faecium* (*E. faecium*) and *Enterococcus faecalis* (*E. faecalis*).[217] They are non-cytotoxic to mammalian cells and preserve their activity in the presence of serum.[218]

1.2.3.1.5. Buforin II:

It is a 21 residue long cationic AMP, derived from another less active AMP called Buforin I, isolated from Asian toad *Bufobufo garagrizans.*[219] Buforin II has broad-spectrum antimicrobial activity. Buforin II is non-membranolytic and has a very strong affinity for the DNA and the RNA present in the cells.[106] Buforin II has a helix-hinge-helix structure with the hinge at Pro11 residue. The N-terminal helix contains residues 5–10, while the C-terminal helix spans residues 12–21. Systematic structure-activity studies reveal that the α-helical content of the peptide is critical for its antimicrobial potency.[220]

1.2.3.2. β-sheet:

This type of AMPs exhibit antiparallel β-strands in their structure (Figure 1.12). They can be further categorized as a β-sheet structure consisting of (a) three strands (most vertebrate defensins), (b) two strands with a β-hairpin structure, or (c) a hybrid structure that includes both β-sheets and α-helices.

Tachyplesin, is a 17 amino acid residue containing cationic peptide, isolated from the acid extracts of horseshoe crab (*Tachypleus tridentatus*). In water phase, it adopts a two disulfide bond stabilized, rigid antiparallel β-sheet structure with a type I β-turn.[221,222] Protegrins, (PG-1), are cationic peptides which are isolated from porcine leukocytes.[223] It contained four Cys which form two disulfide bridges.[224]

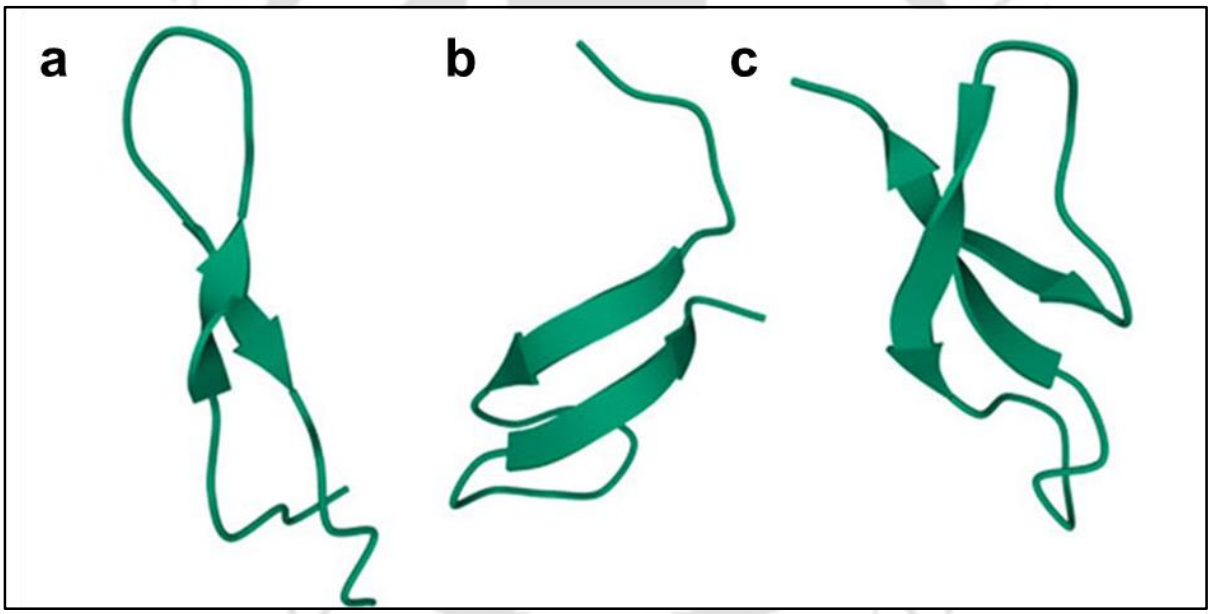

Figure 1.12. β-sheet AMPs: (a) Bovine Lactoferrin (PDB code—1LFC),[225] (b) Hepcidin (PDB code—2KEF),[226] and (c) Rabbit Kidney Defensins (PDB code—1EWS).[227]

1.2.3.3. Cyclic AMPs:

Cyclic AMPs are mostly microbe derived and are produced by non-ribosomal pathways by non-ribosomal protein synthetases (NRPs) containing both proteinogenic and unnatural amino

acid residues (Figure 1.13). The functional diversity of these molecules is enhanced by introducing various chemical modifications, like N-methylation, heterocyclization, and epimerization.[228] A large number of cyclic peptides have been isolated from different natural resources. Cyclic AMPs destroy the target cells by disrupting the membrane or targeting the biosynthesis of components of the microbial cell envelope like chitin, glucan, mannoproteins, and sphingolipids.[229-231] Some cyclic AMPs bind to the membrane and cause membrane lysis, efflux of intracellular materials, and cell death.[232] In contrast, others bind to the membrane, traverse them and act upon specific membrane-bound structures like ion channels, transporters, and receptors.[101] Natural cyclic peptides can be classified depending on the mode of cyclization or their physicochemical properties. Homodetic cyclic AMPs are formed from the cyclization between the terminal amino group and the carboxylic acid group. Argyrin B, guangomide, and valinomycin are representative examples of homodetic cyclic AMPs. Heterodectic cyclic AMPs are formed from the cyclization between the side chains of two amino acid residues or between the chain of one amino acid residue and a terminal amino/carboxylic acid group. Coibamide A, didemnin B, selenamide, and luzopeptin are representative examples of this class. Complex cyclic peptides are formed from the mixture of homodetic and heterodetic linkages and may be bicyclic in nature as in the case of amatoxins, amanitin, phalloidin, and triostin A.[233] Cyclic peptides can be charged as in gramicidine S, polymyxin B and bactenecin, non-polar as in argyrin B, aureobasidin and guanomide A, or of mixed polarities as in kahalilide F, largamide and pseudodesmin A. Some cyclic peptides contain cyclic cysteine knot (CCK) like Kalata B1.[156]

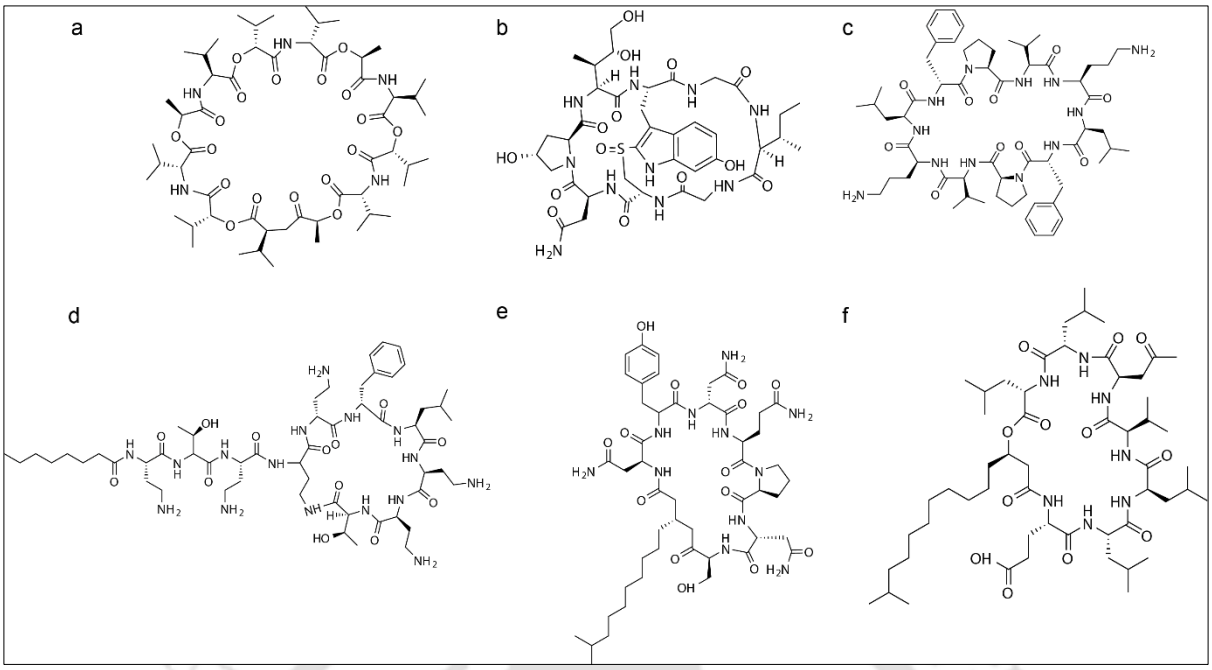

Figure 1.13. Representative example of different classes of cyclic AMPs. (a) Valinomycin, (b) α-Amanitin, (c) Gramicidin S, (d) Polymyxin B, (e) Iturin A and (f) Surfactin C. This figure has been adopted from Ref. 97.

1.2.4. Classification According to the Source:

Naturally occurring AMPs are found across various kingdoms of the living world. Over the last decades, more than 3300 natural AMPs have been isolated from all six kingdoms of life.[68] AMPs are so diversely distributed among the plant and animal kingdoms that it is really difficult to cover all of these in one tabular form. Some of the well-known AMPs isolated from various natural sources are given in Table 1.4.

1.2.5. Classification Depending on the Overall Charge of the AMP:

AMPs can widely vary in their physicochemical property of charge. While a large section of AMPs is cationic in nature, there are several examples of AMPs which are completely hydrophobic or even anionic in charge.

Table 1.4. AMPs isolated from various natural sources[234].

Source of AMPs	AMPs	References
Amphibians	Japonicin-2, Nigrocin-2, Temporin, Dermaseptin, Magainin, Buforin II	234
Insect	Cecropin, Thanatin, Defensin, Drosomycin, Drosocin, Metchnikowin, Apidaecin, Abaecin, Pyrrhocoricin, Melittin	235
Crustaceans	Callinectin, Homarin, Penaeidin, Hyastatin, Arasin	235
Plants	Thionins, Plant Defensins	236
Mammals	Defensin, Histatin, LL-37, Indolicidin, Protegrin, Lactoferricin	237,238
Bacteria	Iturin, Bacillomycin, Syringomycin	239
Fungi	Echinocandins, Aculeacins, Aureobasidin	240
Fishes	Pardaxins, Misgurin, Pleurocidins, Parasin	241
Echinoderms	Strongylocins, Centrocins, Betathymosins	242

1.2.5.1. Cationic AMPs:

A large class of natural AMPs contains a positive charge (+2 to +9) due to the presence of residues like Lys (K), Arg (R), His (H), etc.[67,243-248] (Figure 1.14). Due to the presence of positive charge, cationic peptides can easily interact with a negatively charged microbial membranes. Some cationic AMPs adopt amphipathic secondary structures (helices or β-sheets) in which the positively charged face is separated from the hydrophobic apolar face. Most of the cationic AMPs are membrane disruptive/lytic in nature. Thionins are a class of cationic AMPs present in all crucial plant tissues from endosperms to leaves, which are toxic to microbes. Till date more than 100 individual thionins have been reported from 15 different plants species.[249] Thionins have two antiparallels α helices and an antiparallel double stranded β-sheet with three or four disulfide bridges. Defensins, Magainins, Temporins, Buforin II are the different types of cationic AMPs discussed in details previously. **(section 1.2.2 and 1.2.3)** Nigrocin 1 and 2, isolated from the skin of *Rana nigromaculata*, manifested broad-spectrum antimicrobial activity against various microorganisms through the membranolytic mode of action.[250] It adopted helical conformation in 50% TFE and in SDS individually. Additionally, a Pro hinge was essential for the cell-penetrating ability of the peptide. Mutation of this Pro, converted the peptide into a regular membrane-active AMP. Cathelicidins are a class of human AMPs that are basic and have been discussed earlier in section 1.2.2. Hepcidins are cationic AMPs, 20–25 amino residues long with low positive charge and high content of disulfide bridges. Human Liver expressed AMP LEAP-1 was discovered from human blood filtrate and urine and was named as Hepcidin 25.[251] It is involved in the iron homeostasis in the body.[252]

Figure 1.14. Primary sequence of some representative examples of cationic AMPs.

1.2.5.2. Hydrophobic AMPs:

Few reports available in literature on the AMPs that are completely hydrophobic (Figure 1.15).[253]Alamethicin is a hydrophobic peptide known for its antimicrobial activity.[254] Gramicidin A is another example of a completely hydrophobic antimicrobial peptide.[255]

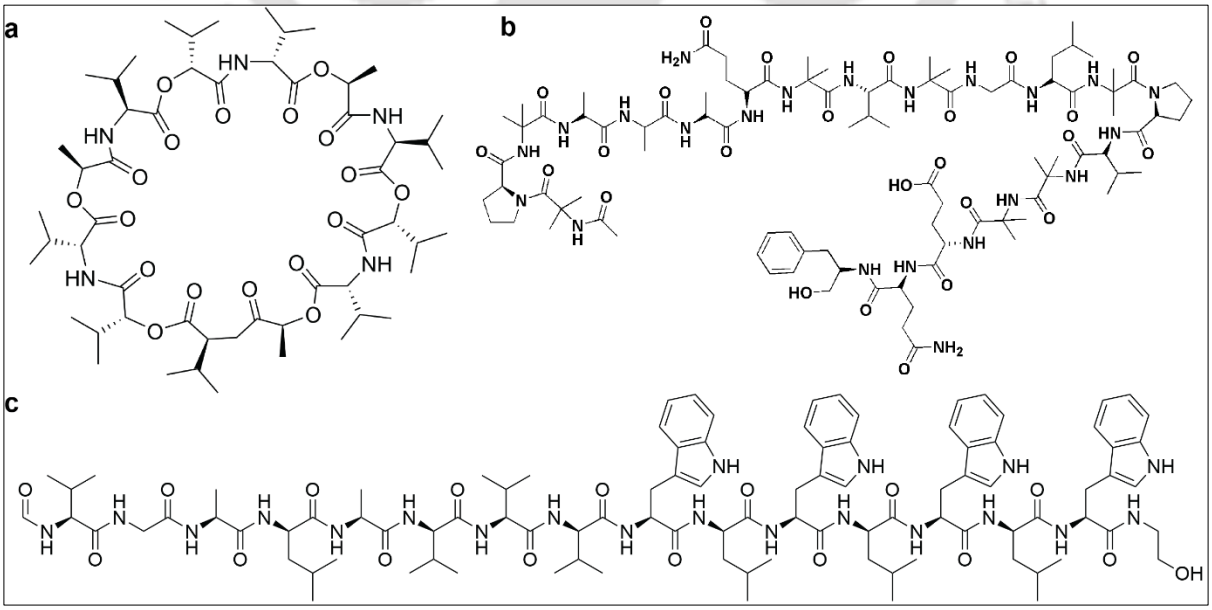

Figure 1.15. Representative examples of hydrophobic AMPs. (a) Valinomycin, (b) Alamenthicin and (c) Gramicidin A.

1.2.5.3. Anionic AMPs:

Although a large section of AMPs are found to carry net positive charges and are predominantly membranolytic in nature, there are exceptions to this general concept (Figure 1.16).[82] Surfactant-associated anionic peptides (SAAPs) were the first report on anionic AMPs.[256] Which were identified from pulmonary secretions of sheep.[257,258] Negatively charged propeptide fragments of ovine trypsinogen activation peptide, and frog (*Xenopus laevis*) PYL activation peptide were found to be active against both Gram-positive and Gram-negative bacterial strains.[259] Maxim H5, a peptide isolated from toad *Bombina maxima* having three aspartate residues and no basic amino acids, and hence carrying a net negative charge was found to be antimicrobial against Gram-positive *Staphylococcus aureus.*[260] Peptide fragment obtained from the proteolytic cleavage of a naturally obtained peptide Dermcidin (secreted by human sweat glands) which carried a net negative was found to be antimicrobial against both Gram-positive and Gram-negative bacteria.[261] Anionic AMPs are known to cause flocculation of intracellular contents.

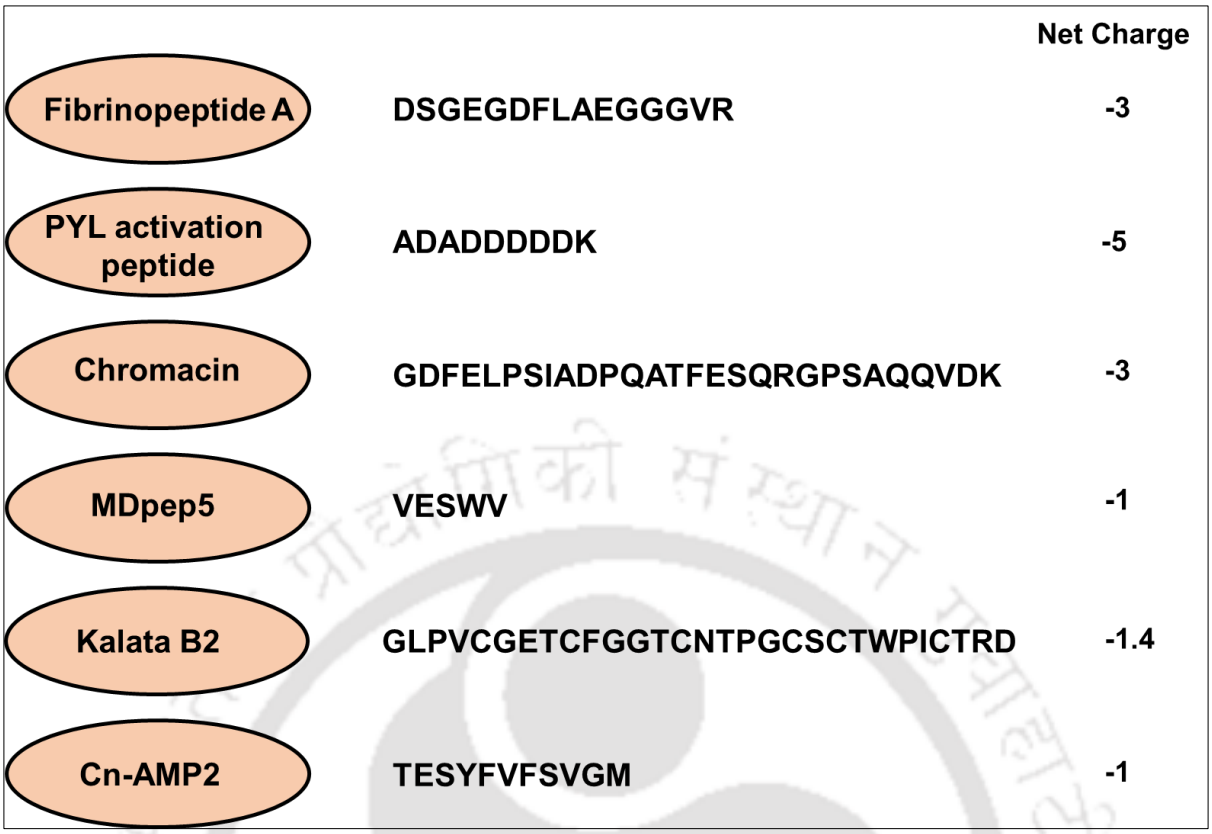

Figure 1.16. Primary sequence of some representative examples of anionic AMPs.

1.3. Effect of Environmental Factors on the Activity of AMPs

1.3.1. Salt:

It is reported in the literature that several AMPs including clavanins, tachyplesin, histatins and defensins lose their activity considerably or completely in the presence of physiological concentrations of salt.[158,262-264] This is of special relevance in the case of cystic fibrosis (CF) caused by the opportunist pathogen *P. aeruginosa*. CF causes chronic infection in the pulmonary mucus which has a typical high concentration of salt. The Cl^- concentration in the trachea and the airway surface liquid (ASL) is much higher than the normal individuals. It is reported that the AMPs are much less effective in the ASL of CF Patient's than in normal individuals.[264,265] Many AMPs are helical in structure and these structures are held together by

hydrogen bonds in between the CO and NH groups of successive turns. The H-bond interactions are dependent on the salt concentration and the pH of the medium. Presence of salts not only affect the structure but also the peptide-lipid interactions. The rate of interaction of AMP magainin with the bacterial membrane mimic bilayers was shown to be slower in the presence of salts.[266,267] Ghosh *et. al.* proved through MD simulations that the initial rate of interaction in between the AMP and the membrane mimetics (SDS micelles) was delayed in the presence of salt.[267] In a separate study, they also established that the dissociated AMP and membrane mimetic systems were selectively more stabilized in the presence of salt, which made the dissociation of AMP: membrane mimetic complex faster in the presence of salts (unpublished results).

Several strategies have been applied to generate synthetic salt tolerant peptides both from natural AMPs as well as *de novo* designed peptides (Figure 1.17). One of the strategies is to modify the natural AMP sequences. For example, truncated 28-mer analog of Dermaseptin S4 was found to have salt tolerant against *E. coli* at high salt concentrations while the 14-mer peptide was inactive.[268] Hybrid peptides designed from combining the insect cecropin and bee mellitin were found to be active in high salt concentrations.[269] Meitzner and coworkers developed *de novo* designed peptides rich in Val and Arg which were salt tolerent in their activity towards *P. aeruginosa* and *S. aureus.*[111,270] Peptidomimetic approaches, like use of D-amino acid residues[271] and bulky unnatural amino acid residues[272] are also reported to improve the salt tolerance of antimicrobial activity.[273,274] Macrocyclization and introduction of di-sulphide bonds were reported as a way of introducing salt tolerance in synthetic peptides.[263,275] Yang and coworkers produced constrained analog of tachyplesin which was active at high salt concentrations.[263] Dimerization of AMPs via the disulphide bond formation or through side chain of Lys was shown to be an effective way to induce salt tolerance of antimicrobial activity.[276,277] As the loss of helical content in presence of salt was considered as a plausible

reason for the loss of activity of the AMPs, introduction of helix stabilizing sequences at the C- and N- termini of the AMPs led to the retention of activity in the presence of high concentrations of salt.[278] Though there are several modifications reported to develop salt sensitivity in the synthetic peptides, unfortunately most of them are peptide or microorganism specific. To develop more general methods to develop salt tolerance, studies are required in greater details to understand the mechanism of inactivation in order to come up with robust design principles.

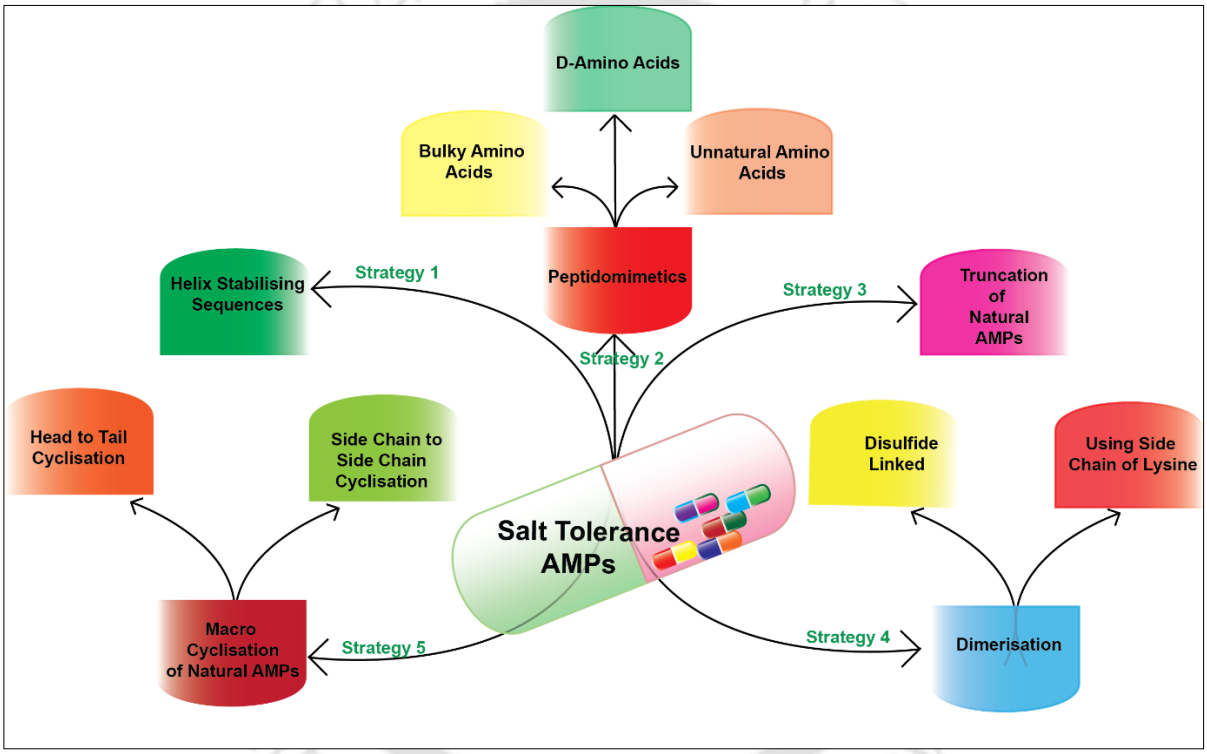

Figure 1.17. Various strategies adopted for generating salt tolerant synthetic AMPs.

1.3.2. pH:

Activity of the AMPs is dependent on the pH of the environment[279] as the pH determines its physicochemical properties and hence its mode of action. The potency of the AMP depends on its therapeutic site as most of the times the local pH may vary from the physiological pH (pH~ 7.4). For example, in the local sites for inflammation like the abscess, the pH is much acidic

owing to the local increase in the concentration of lactic acid and fatty acid by-products formed from the bacterial metabolism.[280,281] In skin the acidic environment (pH = 4-6) inhibits bacterial growth and promotes wound healing.[282,283] pH affects the physicochemical properties of the AMPs i.e., the protonation state of the side chains of charged amino acid residues leading to a change in the overall charge of the peptide. Moreover, pH might also effect the secondary structure of the AMPs, thus varying their activity in the process. Additionally, pH might also vary the nature of the bacterial surface, thereby affecting the AMP membrane binding.[284]

It has been established that the activity of AMPs containing His residue increases at lower pH while it diminishes at the higher pH. At a lower pH, the His residues are mostly protonated (pKa = 6.5), thereby increasing the overall charge of the peptide. On the other hand, at the higher pH, His deprotonates reducing the overall charge of the AMPs and making them less potent against anionic microbial membranes.[262,279,285,286] pH also influences the activity of the anionic AMPs by increasing the overall positive charge at a lower pH.[287,288] Wiey and coworkers established that the activity of AMPs reduced against Gram-negative bacteria in general as opposed to an increase in the activity against Gram-positive bacteria with increasing pH.[289] This was attributed to the change in the charged state of the molecules present in peptidoglycan layer in the Gram-positive bacterial strains at higher pH, such that they did not interfere with the diffusion of the AMPs through the peptidoglycan layer to interact with the inner membrane. Welsh and coworkers demonstrated a decrease in the antimicrobial activity of β-defensin and LL-37 in the acidic pH against *S. aureus* and *P. aeruginosa* and a decrease in the synergistic effect seen in between the two at an acidic pH as well.[289] Alternatively both the peptides showed enhanced activity against *S. aureus* at a basic pH where a reduction in the overall charge might facilitate insertion through the membrane.[290]

1.3.3. Proteases:

One of the major drawbacks of the AMPs in being used as therapeutic molecules to combat bacterial infection, lies in their small half-life. AMPs constituted of all α amino acid residues are susceptible to cleavage by the proteases. Proteases are present in the blood serum and AMPs administered orally or intravenously encounter them. Degradation of the AMPs in the blood circulation even before reaching their therapeutic target reduces their efficiency. Incorporation of D-amino acid residues,[291-293] unnatural analogs of α amino acid residues,[294] N and C terminal protection,[117,295,296] lipidation,[297,298] and cyclization[299] are some of the strategies adopted for conferring protease resistance to synthetic AMPs (Figure 1.18).[300]

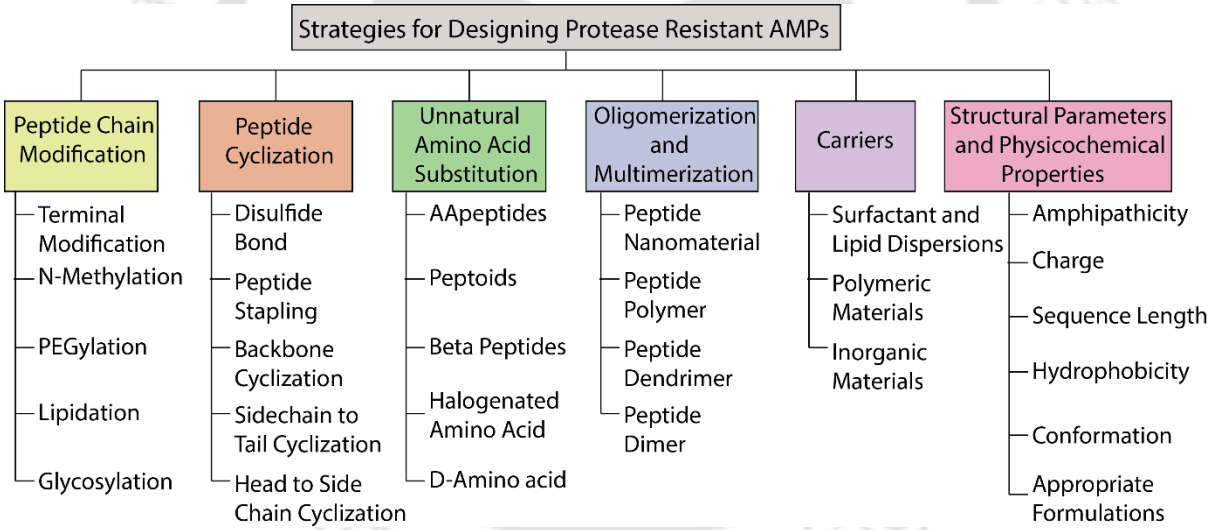

Figure 1.18. Various strategies adopted for generation of protease resistant synthetic peptide.[300]

1.4. Important Considerations while Designing AMPs

In the literature different strategies have been developed and reported to generate highly active non cytotoxic AMPs.

Approach 1: Analysis the sequences of naturally occurring AMPs, determination of the most active region from biophysical experiments and synthesis of its modified analogue by truncation of sequence or mutation/substitution/replacement of specific amino acid residues etc.

Approach 2: Utilization of combinational library to develop helical AMPs.

Approach 3: *De novo* design of AMPs using limited number of amino acid residues.

From the various studies in the literature, it is understood that the activities of the AMPs depend on their various physicochemical properties. Following are the most important attributes of the AMPs which are related to their activity. Thus these factors are always considered during the design of the synthetic peptides.

1.4.1. Secondary Structure:

1.4.1.1. Helicity:

Activity of the AMPs are sometimes related to their ability to adopt helical structures. There are examples of several natural AMPs that are helical as described earlier. Some amino acid residues have high propensity of promoting helical conformation while others are known to be helix breakers.[301] In a study by Sylvie *et. al.*, substitution/ deletion of Gly residue by Leu increased the helicity and in turn resulted in increase the hemolytic activity and antimicrobial activity in Melittin.[302,303] However, substitution of Lys by Gly at position 7 reduced helical propensity which influenced its activity/toxicity. Substituting Gly by helix promoting Ala increased the helicity in the Magainin peptides[304-306] resulted in improved antimicrobial activity. Comparable results were reported for neurotoxin pardaxin where substitution of the helix breaking residue Pro at position 7 by Ala distinctly enhanced helicity along with toxicity.[307] In a another study it was found that incorporation of helix breaker Pro in the N-terminal helix of insect Cecropin A decreased its activity against different strains.[308,309]

Pouny and Shai reported Pardaxin,[310] a α-helix peptide, that showed lytic activity to both microbial and mamalian cells. Incorporation of D-amino acids in its sequence, converted the α-helical conformation to the β- sheet structure, resulting in loss of hemolytic activity but the retention of antimicrobial activity.[311] Replacement of two adjacent amino acid residues by their respective D-isomers produced a stronger disturbance of helix conformation compared with its single amino acid substituted analog.[312, 313] In Magainin exchange of two neighboring residues by their D-isomers decreased its helicity and reduced its permeabilizing activity against neutral and moderately negatively charged lipid vesicles.

However, there are several AMPs in which the activity is not related to their structure. Also there are examples of other classes of AMPs which have β- sheet like structures are those which are completely unstructured.

1.4.2. Charge:

It is believed that the primary interaction between bacterial cell and AMPs are electrostatic in nature. As the microbial cell membranes are negatively charged in nature, presence of positive charge on the AMPs is beneficial for initial electrostatic interaction. Early studies demonstrated a strong correlation between cationicity and antimicrobial activity for α-helical and β-sheets HDPs.[314,315] However such correlation was valid upto a certain range and an intermediate charge of +4 to +6 appeared to be optimal.[316-319] Further increase in charge beyond the optimal range did not necessarily increase the activity.[320,321] In Magainin 2 analogs, excessive charge increased the cytotoxicity instead of activity.[314] Excessive cationicity had direct impact on the disruption of amphipathicity, and reduction of hydrophobicity, which in turn reduced the activity of the AMPs. It was found that in defensins, presence of excessive positive charge led to decrease of its activity. Most the defensins lost their activities at physiological concentration of NaCl, Mg^{2+} or Ca^{2+}. The reason for the salt induced inactivation was of electrostatic

origin.[322-324] Charge density is another important factor that controls the activity of AMPs. Not only the presence of optimal charge but the arrangement or pattern of the charged amino acid residues in the sequence to generate optimal charge density is important for their activity. The activity of Melittin was preserved upon cyclization while cyclic Magainin 2 displayed a reduced activity.[325] This loss or gain of activity was directly related to with the final charge density of the peptides. In cyclic Melittin analogue the charge was accumulated in the small portion of the ring resulting in unchanged activity, while distribution of charge along with the entire structure of Magainin 2 resulting in minimal charge density and reduced activity.[325]

1.4.3. Amphipathicity:

It is the ability of an AMP to arrange the hydrophobic and hydrophilic residues at the different sides of the secondary structure and has a major impact on their activity and toxicity. In several AMPs reported in the literature, attainment of amphipathic helical conformation is considered as advantageous for the gain in activity of the peptides.[316,326,327] The amphipathic helix is a membrane-binding motif present in many proteins and peptides in which one face of the helix is polar while the other face of the helix is hydrophobic in nature. The residues in the primary sequence are arranged in such a way that amino acid residues with polar/charged side chains are alternated with those containing hydrophobic amino acid residues such, that upon folding the peptide attained amphipathic helical conformation. Differently charged faces of the helix help it to optimally interact with the amphipathic membrane. While the hydrophobic part of the AMP interacts with the nonpolar part of the membrane, hydrophilic part of the AMP interacts with the outer negatively charged surface of the membrane. However, perfect amphipathicity is not necessarily important for HDPs for optimal activity and specificity[305,328,329] and it is difficult to quantify the amphipathicity of the AMPs. Eisenberg *et. al*., proposed hydrophobic moment (M_H) as the vectorial sum of the individual amino acid hydrophobicities normalized to an ideal helix which was quantitatively considered as the

measure of the AMP amphipathicity.[330] In many peptides like Melittin hydrophobic and hydrophilic residues are not regularly distributed along the chain. This leads to two regions of distinct hydrophobic moment. Definition of hydrophobic moment comes from hydrophobicity potential considering both the hydrophobic gradient along a peptide sequence and hydrophobic contours around a helix.[331] However, most of the authors prefer to use the conventional term hydrophobic moment to express amphipathicity. Matsuzaki *et al.* reported the absence of a straight forward relationship between hydrophobic moment and lytic activity of the peptides.[332]

In a study Blondelle *et. al.* reported that introduction of Lys into the hydrophobic region of a model peptide enhanced its lytic activity although substitution disturbed the hydrophobic moment. In a separate study it was found that selectivity of a Magainin analogue decreased with increasing the hydrophobicity.[333] This indicated a strong relationship between amphipathicity and the activity. Study with the cationic amphipathic KLAL model peptide confirmed that the amphipathic helix was essential to interact with neutral lipid membrane but less required for the permeabilization of negatively charged bilayers.[327]

1.4.4. Hydrophobicity:

It is the measure of the percentage of hydrophobic residues present in the peptide sequences. Hydrophobicity determines the degree of insertion of the peptides in the membrane bilayers. Increasing hydrophobicity of the AMPs increases the binding affinity towards all types of membranes. Thus while moderate hydrophobicity promotes better activity, too high hydrophobicity results in loss of cell selectivity and increase in the cytotoxicity. Hence optimum hydrophobicity is best for high activity accompanied by low cytotoxicity.[334] There are few literature reports, which claimed that there was no correlation between hydrophobicity and bacterial activity for the different model peptides.[320,335,336]

1.4.5. Presence of Aromatic Residues:

Aromatic amino acid residue like Trp is frequently found in many naturally occurring peptides.[337] Due to the intermediate hydrophobicity of Trp, it has a preference for the interfacial region of lipid bilayers.[338] Due to the presence of negatively charged π electron cloud above and below the ring, Trp has a tendency to interact with positively charged amino acids and choline head group of the lipid through cation π interaction (Figure 1.19).[339] The large hydrophobic indole group can penetrate the acyl chain of the lipid bilayers resulting in insertion of the peptide into the membrane and eventual cell lysis.[338] Changing Trp with other amino acid residues resulted in decrease of the activity of AMPs.[337]

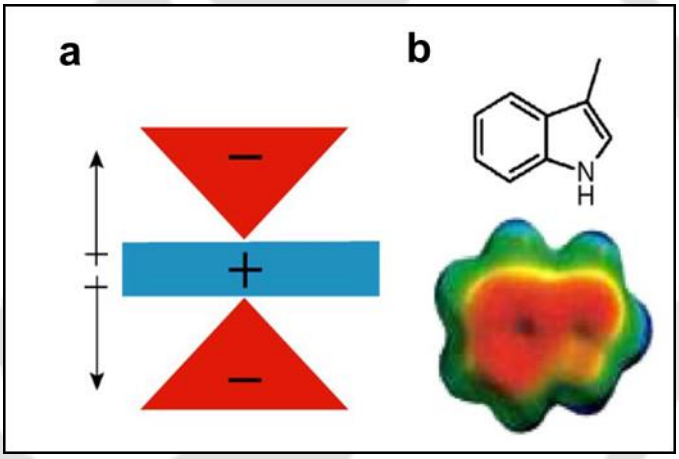

Figure 1.19. (a) Schematic of the dumbbell shaped π-electron clouds above and below the aromatic ring structure of Trp. The arrows on the left indicate dipole moments. (b) Chemical structure of indole side chain of Trp (top) and electrostatic surface of the Trp indole group (bottom). This figure has been adopted with permission from reference 337. *Copyright © 2006 Elsevier B.V. All rights reserved.*

1.5. Design and Synthesis of AMP Based Molecules with Pharmaceutical Potential

Having understood the potential of AMPs as alternative therapeutic molecules to combat microbial infections, significant amount of research has been done on generating synthetic AMPs. As mentioned earlier, synthetic AMPs can be of two types: a. Modification of natural AMPs and b. *de novo* designed AMPs. In the following section, we will discuss about the different classes of synthetic AMPs reported in the literature. As the area is vast, this account below is a representative discussion and not exhaustive in nature.

1.5.1. AMP Peptide Mimetics:

It includes non peptidic molecules like peptoids (Figure 1.20),[108,340,341] β-peptides (Figure 1.21a),[342] oligo-acyl-lysines[341] (Figure 1.21b), arylamides, oligomers like phenylene ethynylenes.[343] These molecules are designed to capture the central physicochemical properties of the natural AMP prototype. It is reported that peptidomimetic oligomers show rapid, non-hemolytic, broad-spectrum bactericidal properties in mice. There is no development of resistance in peptoids. Mojsoska *et. al.* showed that peptoid backbone increased the activity along with minimization of toxicity against human RBC in comparison to its peptide counterpart.[344] Biofilm inhibition is enhanced for peptoid backbone in comparison to its peptide analog. Peptoids are promising in the treatment for pulmonary infections occurring in cystic fibrosis (CF) patients. Oligo- acyl-lysine showed bacteriostatic effect against bacteria via completely a different mode of action that involved leakage of intracellular ATP.[345]

1.5.2. Hybrid Peptides:

Hybrid AMPs are constructed from the active regions of two or more naturally occurring AMPs with an intention of combining the potential benefits of each of the fragments (Figure 1.22). The aim of such design is to increase the antimicrobial activity[346-349] of the AMPs, decrease

the spectrum of their activity[350,351] and reduce the cytotoxic effects on the eukaryotic cells.[352,353] If the different constituent domains have different modes of killing, then the potency of such hybrid AMPs are expected to increase. For example, A3-APO could disintegrate bacterial membranes and inhibit the 70 kDa heat shock protein DnaK.[354,355] Multiple-headed STAMP (MH-STAMP) molecules targeted different bacterial strain which might be utilized to treat different polymicrobial infections or for removal of clusters of constituents.[353]

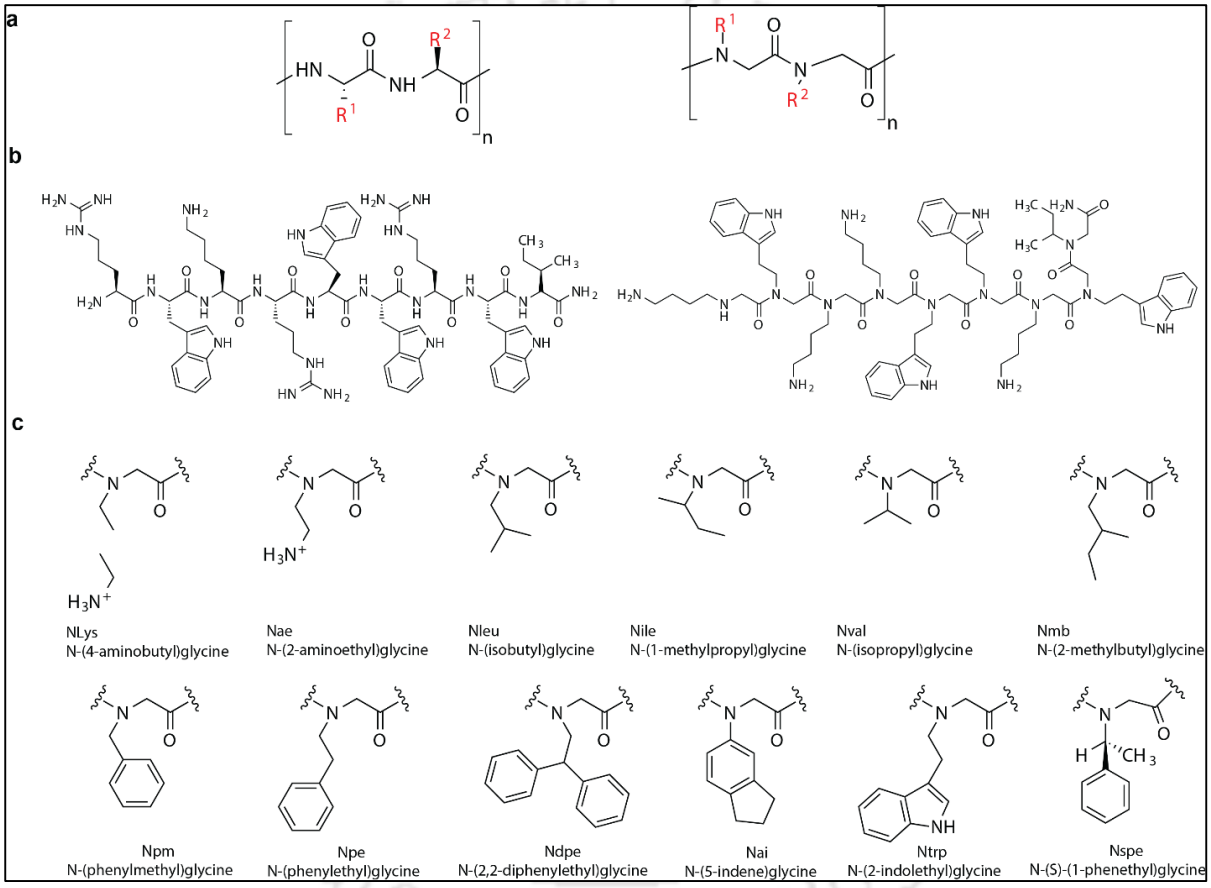

Figure 1.20. Peptoid based AMPs. (a) Chemical structures of peptides (left) and peptoids (right). (b) Chemical structure for studied peptide and peptoids.[340] (c) Chemical structures of peptoid monomers and their abbreviations.[10]

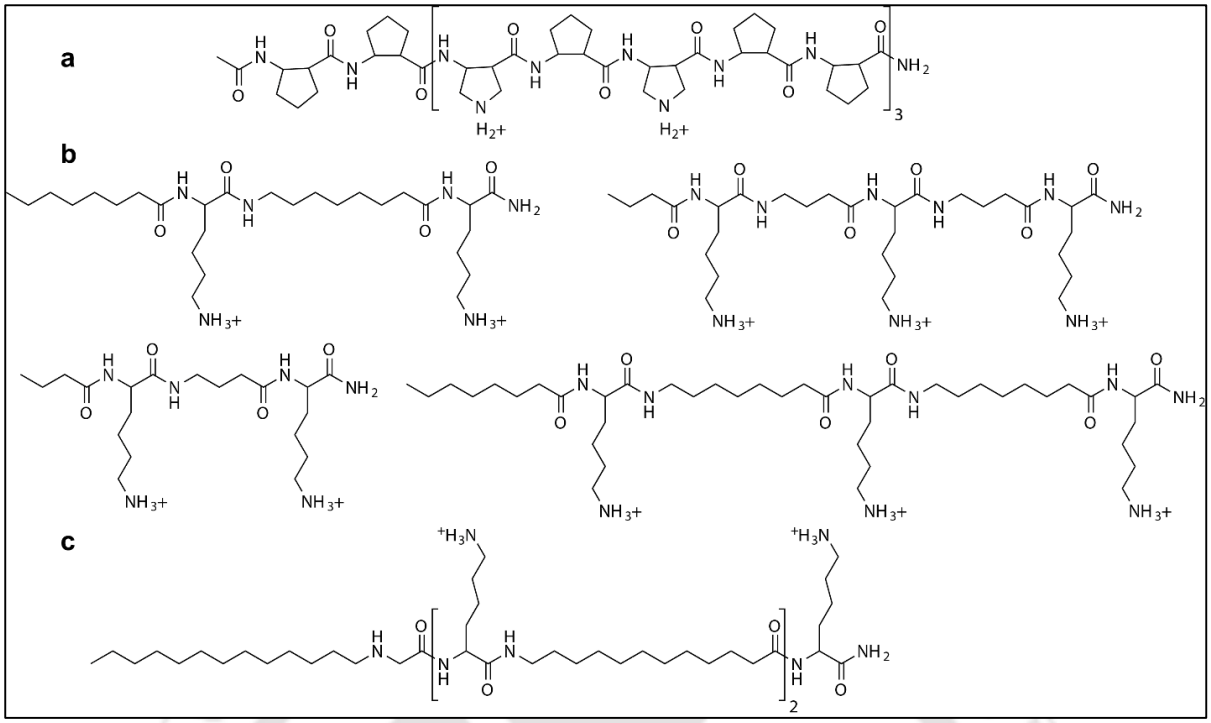

Figure 1.21. (a) β- Peptides[5] and (b) Oligo acyl Urea based peptidomimetics.

Hybrid peptide LLaMA (LL-37 residues 17–29 in combination with wild-type magainin II residues 1–12) and CaLL (cecropin A residues 1–8 followed by LL-37 residues 17–29) showed activity against bacteria.[356] CaLL had antiviral activity as well. However, CaLL was toxic in nature and pegylation at the the N-terminus decreased the toxicity without altering the activity. PEG_2-CaLL and PEG_3-CaLL had two and four fold less toxicity respectively compared with CaLL.[357] FV-LL (Composed of FV7 and LL37) was more potent compared with the natural peptide FV7.[358] A recent study showed that a synthetic hybrid peptide obtained from naturally inspired cathelicidin and aurein peptides, showed broad-spectrum antimicrobial activity especially against clinically isolated *P. aeruginosa* with no toxicity against human RBC and L929 cells.[359] Another recent study reported a hybrid AMP S2 which targeted *S. aureus* and displayed anti-infective activity in a murine model.[360] *In vivo* potency of PA2-GNU7 was greater compared with conventional antibiotics in *in vivo* mouse model against MDR *P. aeruginosa.*[361]

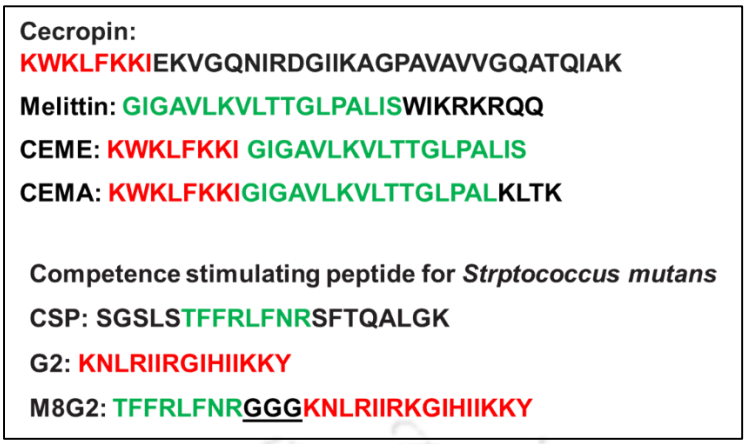

Figure 1.22. Primary sequences of some representative hybrid peptides. CEME and CEMA were constituted by the combination of Cecropin and Mellitin peptides while M8G2 was constituted of AMP CSP and G2.[362]

1.5.3. AMP Congeners:

These are molecules closely related in composition to parent AMPs having similar or antagonistic effects. These are made by relaxing secondary structures, swapping amino acids of the original peptide with new ones to alter the charge or hydrophobicity, systematic truncation of N- or C- terminus to find the shortened and active stretch. Many congeners of defensins,[323,324,363-366] SMAP 29[366-368] have been found using this strategy (Figure 1.23).

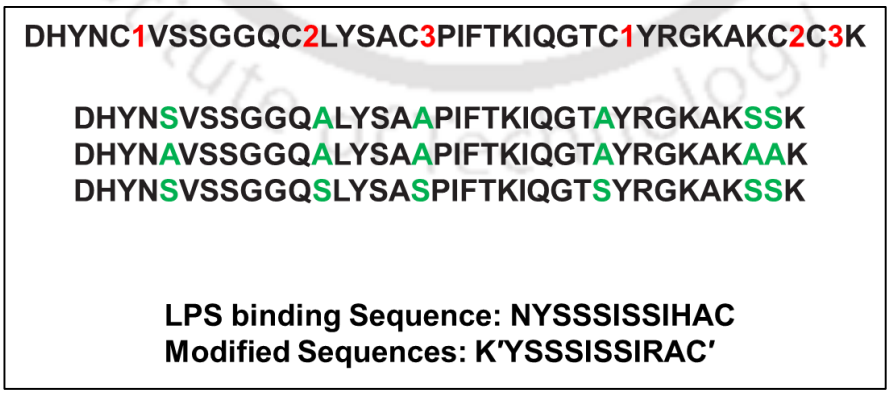

Figure 1.23. Design strategy of some representative AMP Congeners.[369]

1.5.4. Cyclotides:

These are cyclic peptides which have conserved disulphide bridges that form cysteine knots (Figure 1.24). They are have known to possess pharmaceutical activities. Cyclotides are stable owing to their cyclic nature and the cysteine knots. AMPs have been modified and cyclized to enhance their protease resistance.[370,371]

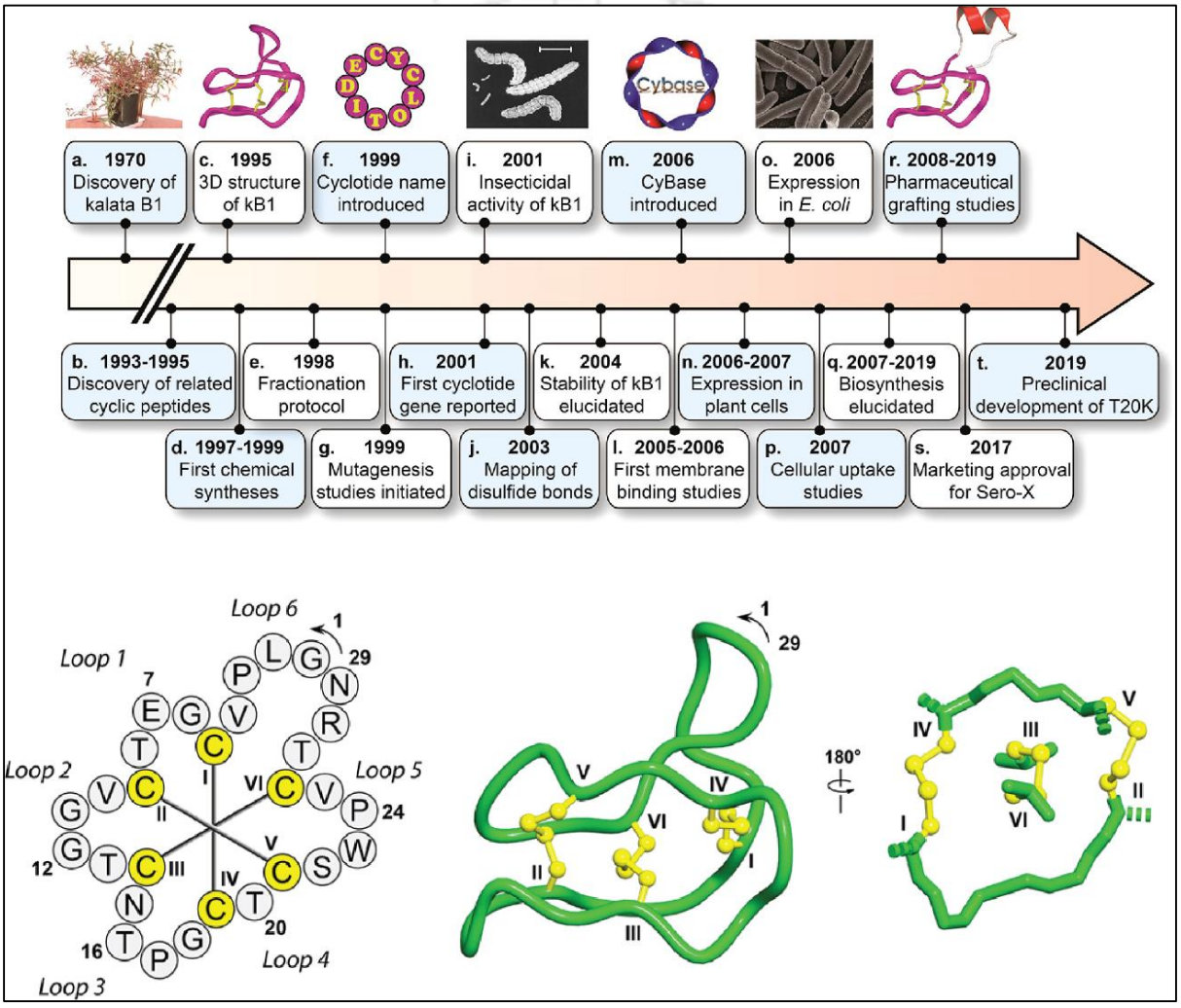

Figure 1.24. Timeline of key milestones in the cyclotide AMP research, sequence and 3D structure of the prototypic cyclotide kalata B1.[372] The figure has been adapted with permission from ref. 372. *Copyright 2019, American Chemical Society.*

1.5.5. AMP conjugates:

Attachment to antibodies or ligands for a receptor on the bacterial pathogen improves targeted delivery, minimum dosage etc.[373] of AMPs. AMP conjugates with fatty acids or steroids have increased antimicrobial activity,[374,375] while those conjugated with micelles equipped with uptake mediating mechanisms efficiently translocates across cell membranes.[376]

1.5.6. *de novo* Small Synthetic AMPs:

1.5.6.1. Leucine-Lysine Containing Peptides:

As discussed earlier, amphipathicity is considered to be an important factor in imparting antimicrobial potency to the AMPs. Amphipathic helical AMP's were developed with Leu and Lys, which had strong helix-forming potential in proteins.[377] Blondelle and Houghten[378] designed a series of model LK peptides composed of leucyl and lysyl residues, varying in length from 8 to 22 residues. Highest antimicrobial activity was found for the 14-mer sequence Ac-KKLLKKLKKLLKKL-NH_2. Similar approach by Beven´ *et. al.*[379] also proposed a 15-residue LK peptide with a strong antimicrobial activity: KLLKLLLKLLLKLLK. Hayne *et. al.* made a series of immobilized peptides attached to resin composed of leucine and lysine, which showed broad-spectrum antimicrobial activity.[380]

1.5.6.2. Tryptophan Containing Peptides:

Tryptophan residues in proteins and peptides often play a crucial role in the membrane interaction[381-384] and stabilization of the helical structure of the membrane-interacting peptides.[381,382,385-387] In addition, some naturally occurring AMPs are particularly rich in Trp.[388,389] Research proved that single tryptophanyl substitution at certain positions of inactive fragments of the amphipathic helical AMPs conferred the antimicrobial activity, without

increasing any significant hemolytic activity.[381,387,390] For example, the D16W substitution in the inactive N-terminal 23-residue fragment (named GGN4N23) of a 37-residue AMP esculentin-2EM (formerly known as gaegurin 4[391]) promoted a full recovery of the antimicrobial activity.[381,390] Peptides with a high content of Trp and Arg residues shows high antimicrobial properties.[392,393] Su-Jin Kang *et. al.* reported two active AMPs ($LKLLKWLLKLLNH_2$ and $LLKLLKWLLKLLK\text{-}NH_2$) composed of a leucine lysine and tryptophan.

1.5.6.3. Lipopeptides:

Lipopeptides are unique among the AMPs in that they are relatively smaller in size as compared to other cationic AMPs, and yet, exhibit excellent antimicrobial activity. Fatty acid acylation of AMPs of bacterial and fungal origin have mostly been limited to non-gene-encoded peptides such as echinocandin,[394] polymyxins,[395] daptomycin,[396] lipopeptaibols[397,398] and syrinomycin, syringotoxin and syringopeptin from Pseudomonas syringae.[399] It has been postulated that fatty acylation of proteins is necessary to increase their membrane association and sorting into specific sub-cellular localizations.[400,401] Consequently, several studies to assess the effect of acylation have revealed that conjugation of fatty acid to cationic peptides enhanced their antimicrobial activity. [402-406] Lipophilic modification at the C-terminus of a peptide based on residues 21–31 of human lactoferrin resulted in enhanced antimicrobial activity against Gram-negative and Gram-positive bacteria.[407] The alkyl chain (6-octanoyl/heptanoyl diaminobutyl group) in the cationic cyclic antimicrobial peptide Polymixin B was shown to be essential for its antimicrobial activity[408]. Removal of 6-octanoyl/heptanoyl diaminobutyl moiety from polymyxin B resulted in the loss of activity.[409] Aliphatic acids could, therefore, be used to increase the hydrophobicity and membrane association of short cationic peptides and consequently improve their antimicrobial activity. In this context Thennarasu *et. al.* made Oct–$OOLLOOLOOL\text{–}NH_2$ (O = Ornithine) with a short helical stretch and an octyl chain at the N-

terminus (Figure 1.25a).[410] Ultra short antimicrobial lipopeptides for broad-spectrum antimicrobial activity were studied by Shai and co-workers.[411] In one of the studies they made lipopeptides with KXXK motif (X = A, L, G, K, E, I) (Figure 1.25d) with various length of fatty acyl chains (C12, C14 and C16) and concluded that C16-KLLK was active only towards the Gram-positive bacteria and fungi tested, whereas C16-KGGK was active toward all types of microbes tested while being non-hemolytic in nature. In lipo-peptides with KXK motif, activity of C16-KKK > C16-KGK > C16-KLK > C16-K*K*>> C16-KAK. Sikorska *et. al.* studied the interaction between several lipopeptides like C16–KK–NH_2, C16–KGK–NH_2 and C16–KKKK–NH_2 and membrane lipids by using ITC, FTIR and MD stimulation studies. Cyclic and acyclic lipopeptides composed of natural and unnatural amino acids are also found in literature.[412] Jian *He et. al*.[413] and Fang *et. al.* [414] synthesized short Arg, Lys and Trp containing lipopeptides and evaluated their antimicrobial activities against a panel of pathogenic microorganisms including *S. aureus*, *E. coli*, and *C.albicans*. In this context Halder *et. al.* established small molecule based lipopeptides and peptoids[415] which inhibited bacterial biofilm formation.[416] Bisht *et. al* reported Orn, based lipopeptides.[417]

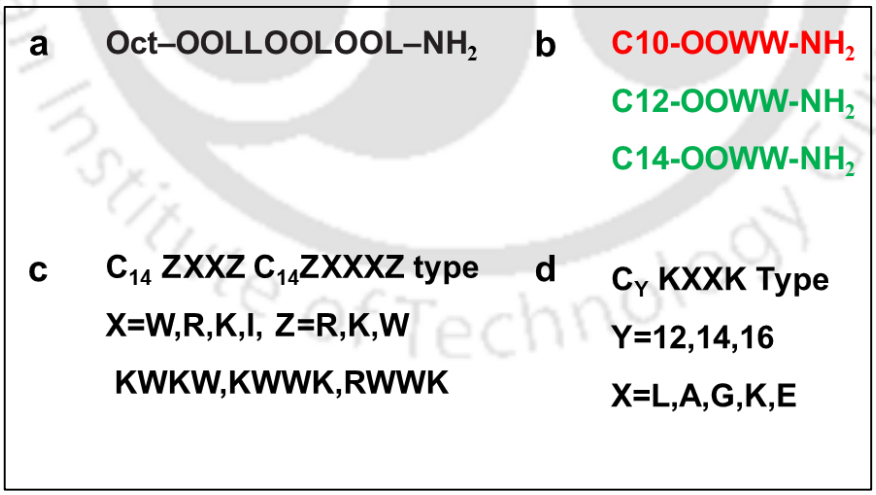

Figure 1.25. Some representative synthetic Lipopeptides.[418-421]

1.5.6.4. Cyclic Lipopeptides:

Cyclic lipopeptide (CLPs) contain a fatty acid tail attached to a cyclic peptide skeleton. They have a broad-spectrum antimicrobial activity towards microbes. In most of the cases, they possess broad-spectrum activity towards bacteria and fungi via membrane integration and pore formation. Syringomycins and syringopeptides derived from *Pseudomonas syringae*, possess strong inhibitory activity against the growth of gram-positive bacteria[422], mycelia[423] and antagonistic property against apple scab causing agent.[424] Lipodepsipeptide Tolaasin D derived from *Pseudomonas tolaasi* prevents growth of *Rhizoctania solani* and gram-positive bacteria *Rhodococcus fascians.*[425] Gram-negative bacteria *Pseudomonas fluorescence* produces several classes of cyclic AMPs. Pseudophomin A and B produced by *Pseudomonas fluorescens* BRG100 significantly inhibits the growth of *Phoma lingam*, *Alternaria brassicae* and *Sclerotinia sclerotiorum* (Figure 1.26).[426]

1.6. Mechanism of Action

AMPs are known to act via different modes of action.

1.6.1. Membrane Interactions:

A major class of AMPs are known to be membrane active molecules. Many AMPs are cationic in nature, being rich in positively charged amino acid residues like Arg or Lys. The membrane active AMPs rely on the nature and the composition of the microbial cell membranes and the host cell membrane to manifest their activity. The mammalian host cell membranes are zwitterionic being composed of zwitterionic lipids like sphingolipids or phosphatidylcholine. On the contrary the microbial cell membranes are negatively charged being composed of negatively charged phospholipids like phosphatidylserine (PS), phosphatidylglycerol (PG) and cardiolipin.[428] In addition the peptidoglycan membrane that surrounds the cell wall of the Gram -positive bacteria contains significant amounts of negatively charged teichoic acid while the

outer membrane of the Gram-negative bacteria is composed of negatively charged lipopolysaccharide (LPS) (Figure 1.27).[429,430]

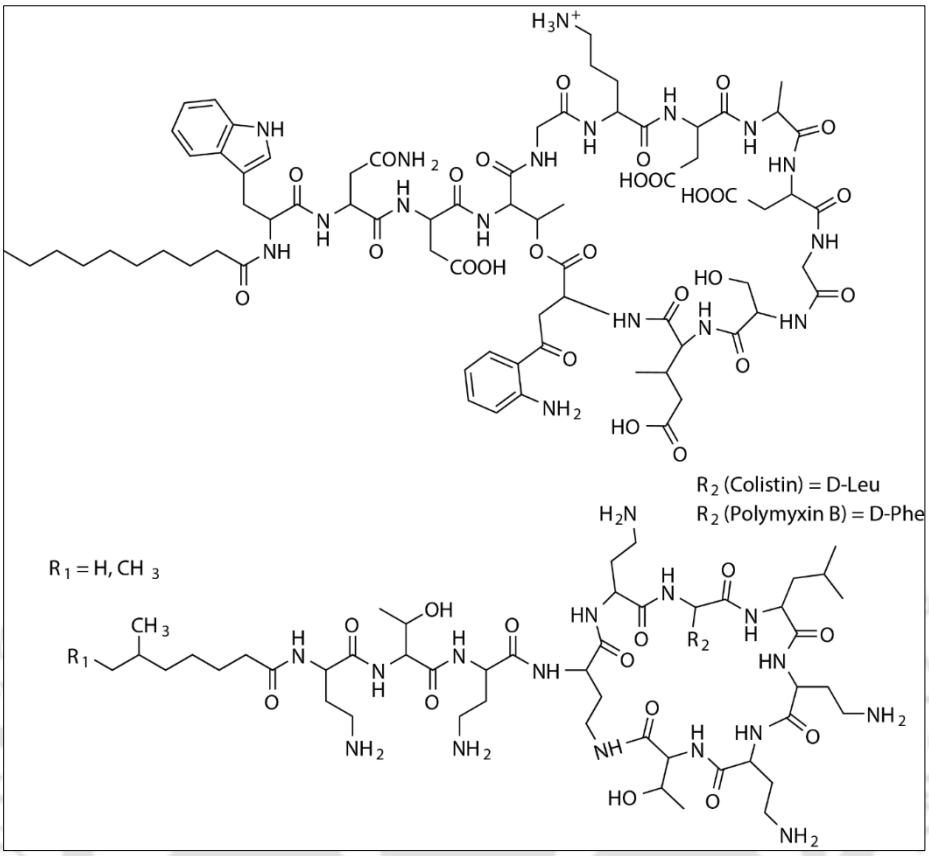

Figure 1.26. Cyclic Lipopeptide Colistin and Polymyxin B.[427]

The positive charge on the AMPs facilitates their interaction with the negatively charged microbial membranes specifically over the zwitterionic mammalian membranes. Though an increase in the positive charge of the AMPs usually increases the antimicrobial potency, it also increases non specificity and cytotoxicity towards mammalian cells. Thus electrostatics play an important role in the AMP-membrane interaction. However, in the case of anionic AMPs, like DCD-1L[288] (with an overall charge of -2), the initial interaction occurs through the positively charged N-terminus of the peptide. The activity of this AMP increases in the presence of Zn^{2+}, Mg^{2+} and Ca^{2+}, most probably due to the stabilization of the anionic parts of the peptide with the anionic head groups of the membrane lipids through salt bridge

interactions, upon interaction with the membrane. Some anionic AMPs completely bypass the membrane binding and are taken up by the cells using transport proteins.[431] However, though the initial binding event of the AMP-membrane seems to be an electrostatic affair, specific AMPs bind to specific parts of the membrane. For example, both nisin and mutacin binds to lipid II which is a precursor of peptidoglycan, while Daptomycin interacts with membrane PG.[432-434] Thus the AMPs are accumulated from the solution on to the surface of the bacterial cells. α-helical AMPs typically adopt helical conformation upon attachment to the microbial surface while the β-sheet AMPs are already folded in solution even before attachment to the microbial cell surface, as in their case the secondary structure is stabilized by the disulphide bridges.[329] As the peptide to lipid ratio on the cell surface increases, the AMPs can bring about disruptive changes to the membrane. This starts with the interaction of the AMPs with the phospholipid head group followed by the insertion of the hydrophobic parts of the AMPs into the membrane.[435]

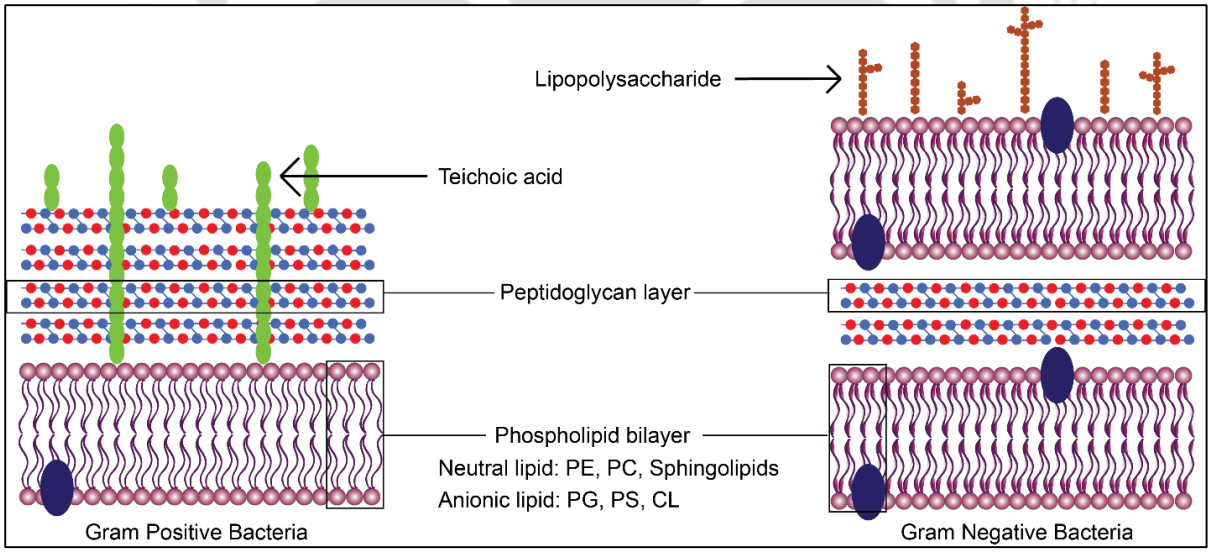

Figure 1.27. Schematic diagram showing the layout of the cell membrane for Gram-positive and Gram-negative bacteria.

Once the AMP has bound to the membrane surface, the membrane-disruptive activity can be asserted in principally three different ways: barrel-stave, toroidal or carpet models (Figure 1.28, Table 1.5). In the barrel-stave model, when the AMP has accumulated on the membrane surface in adequate concentration, it forms bundles which get inserted into the membranes and form pores. The AMP helices are organized in a manner such that the polar side chains point towards the center of the pore and the hydrophobic amino acid residues point towards the lipid bilayer.[32,436] In the toroidal model, the pores are formed, but instead of traversing across the membrane, these peptides bring about local thinning and curvature in the membrane causing membrane disruption.[32,437] In the carpet model, the AMPs cover the surface of the cell membrane that causes disruption of the membrane and its dispersion into pieces, which are sequestered by the AMPs.

There are other less encountered mechanisms of membrane disruption. In one of the mechanisms, AMPs form aggregates that traverse across the membrane to reach the intracellular targets.[438] Some of the AMPs like Buforin II can traverse the membranes to reach intracellular targets without causing membrane permeabilization.[439] In the electroporation model, accumulation of the AMPs on the surface of the membrane builds up such a huge charge that pores are caused across the membranes. However, these pores are not lined by peptides.[440] The means by which membrane disruption causes cell death vary. Membrane disruption ultimately results in dissipation of vital chemical ingredients like protons and metal ions.[439] Change in the ion gradients can cause influx of water into the cell causing osmotic pressure and eventual bursting.

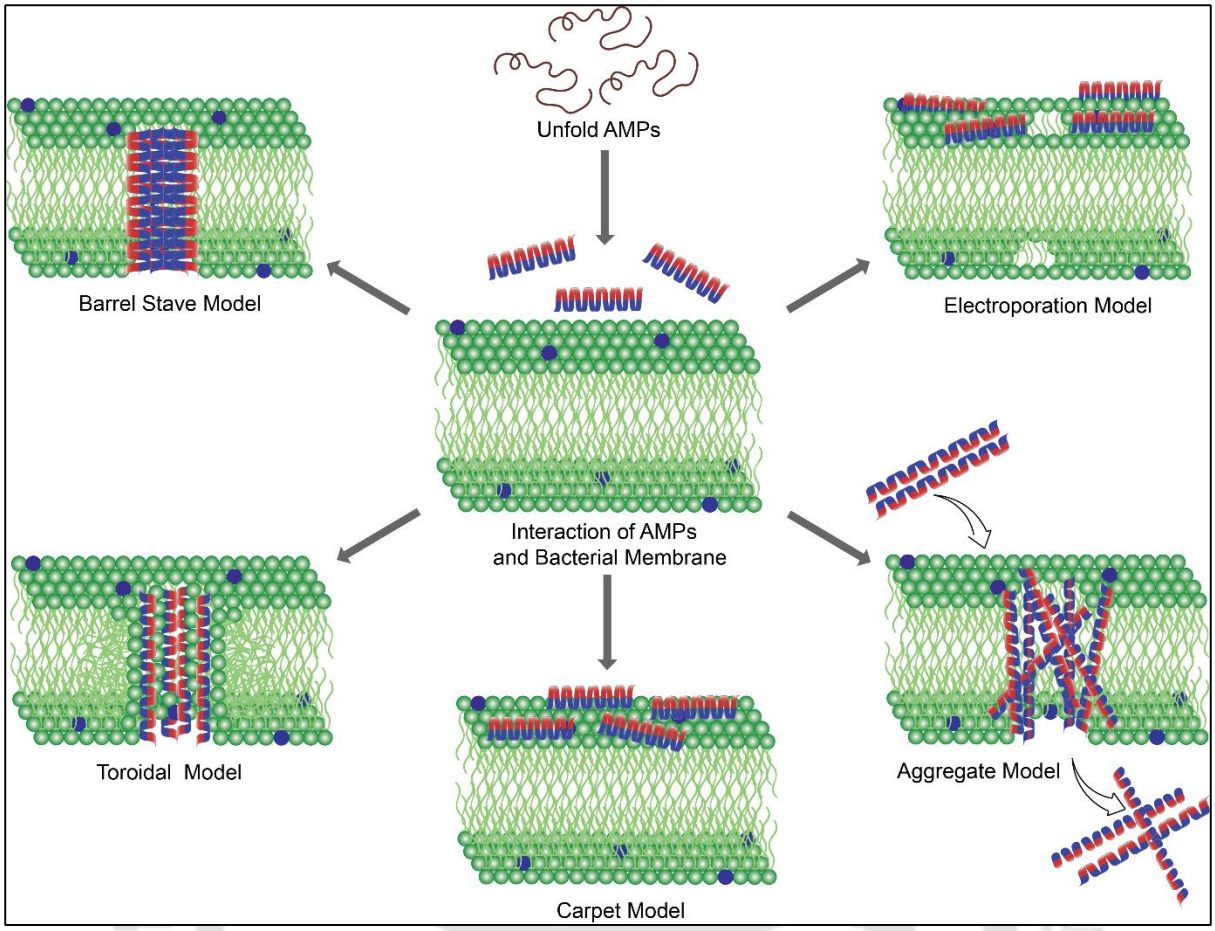

Figure 1.28. Schematic representation of various membrane disruptive pathways for AMPs: (a) Barrel stave model,[254,441-443] (b) Carpet model,[444-447] (c)Toroidal model,[448-450] (d)Aggregate model[431] and (e) Electroporation model.[82]

Table 1.5. Examples of AMPs that adopt various pore forming mechanisms.

Transmembrane pore-forming mechanisms	
Models	Examples of peptides
Toroidal pore	Magainin, protegrin-1, melittin, LL-37 and MSI-78

Carpet	Dermaseptin S, cecropin, melittin, caerin 1.1 and Ovispirin
Barrel stave	Alamethicin (Helical-bundle model)

1.6.2. Intracellular Mode of Action:

The second vital mode of action of the AMPs involve translocation across the membrane and action upon an intracellular target (Table 1.6).[439] Some AMPs like Buforin and Tachyplesin are known to possess nuclease activity against the pathogenic genetic material.[106,451] Anionic AMPs are known to cause flocculation of intracellular contents.[257] AMPs like PR-39, PR-26, Indolicidin and Microcin 25 are known to alter cytoplasmic membrane septum formation.[71-73] Several AMPs are known to inhibit synthesis of intracellular components. For example, Mersacidin inhibits cell-wall synthesis, while Pleurocidin, Dermaseptin, Indolicidin, PR-39, HNP1, 2 etc. are known to inhibit both nucleic acid synthesis and protein synthesis.[452] [453] Histatins, pyrrhocoricin. Drosocin and Apidaecin inhibit enzyme activity.[454,455] AMPs may also act synergistically with other antibiotics by either reducing the barrier to cell entry, thereby facilitating the reach of antibiotic to the target (*eg*. a combination of Collistin and Rifampicin) or by acting as an additional target (*e.g*. in the case of Daptomycin with Ampicillin).[456]

Table 1.6. Modes of intracellular killing in AMPs.

Modes of Intracellular Killing	
Flocculation of intracellular contents	Anionic peptides
Alters cytoplasmic membrane septum formation	PR-39, PR-26, indolicidin and microcin 25.

Inhibits cell-wall synthesis	Mersacidin
Binds nucleic acids	Buforin II and tachyplesin
Inhibits nucleic-acid synthesis	Pleurocidin, dermaseptin, PR-39, HNP-1, -2 and indolicidin
Inhibits protein synthesis	Pleurocidin, dermaseptin, PR-39, HNP-1, -2 and indolicidin
Inhibits enzymatic activity	Histatins, pyrrhocoricin, drosocin and apidaecin

1.6.3. Immunomodulatory Activity:

The third most important mode of action of the AMPs is its immunomodulatory activity of the host. AMPS are a key component of the innate immune system in the multicellular organisms with the ability of elicit anti-inflammatory and immunostimulatory effects. For example, several natural AMPS are known to neutralize LPS-induced inflammation in in vitro and in vivo models of sepsis. AMPs are also able to recruit antigen presenting cells like monocytes and macrophages at the site of infection directly or indirectly through the induction of cytokines. AMPs are also known to suppress the expression of pro-inflammatory cytokines, enhance phagocytosis and pro-inflammatory responses to nucleic acids, induce the expression of anti-inflammatory cytokines, induce the differentiation of dendridic cells and the polarization of T cells, and promote wound healing.[248] Defensins and cathelidins are the most well studied mammalian AMPs with immunomodulatory activities.[248]

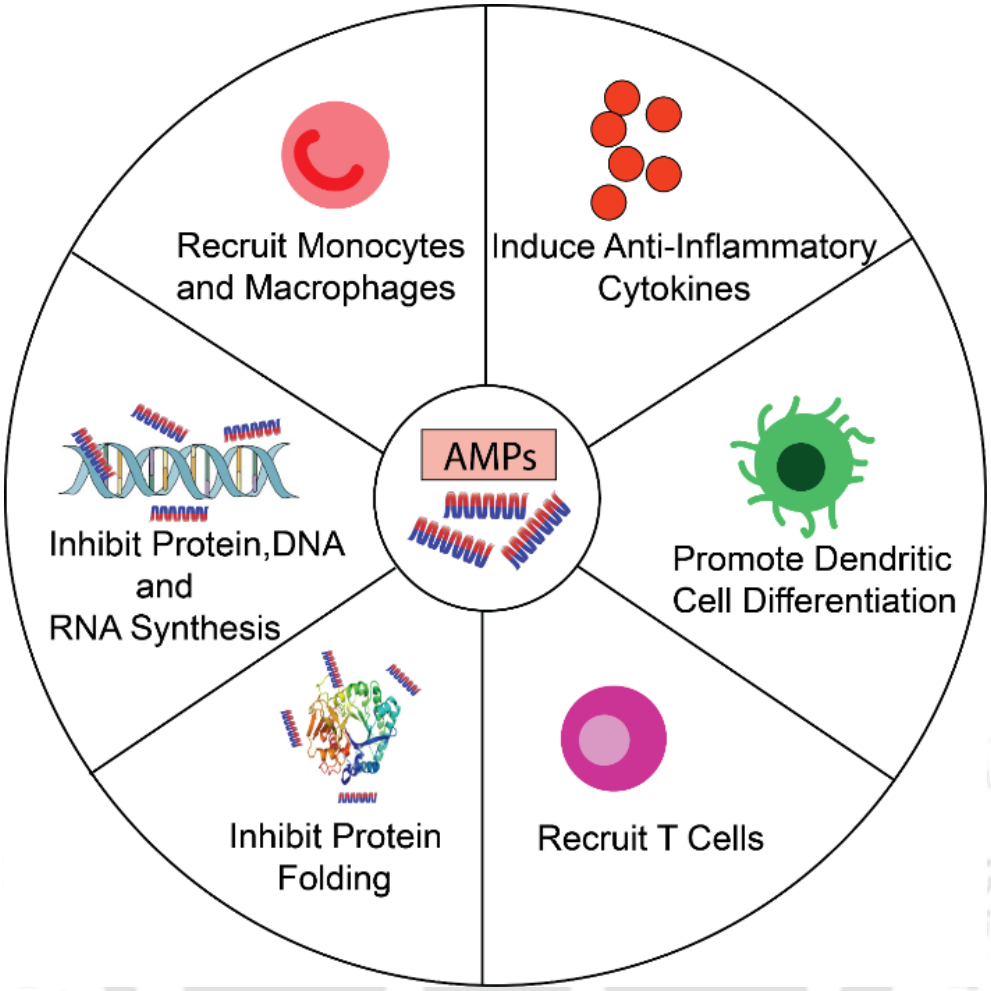

Figure 1.29. Roles of AMPs in modulating the immune system.[82]

The diversity in the mode of action (Figure 1.30)/multi hit strategy of the AMPs forms the basis of the very slow/negligible development of resistance against them. This is the major advantage of the AMPs over the antibiotics that are currently being used extensively. Another important feature of the AMPs against conventional antibiotics is that not only does it kill the metabolically active bacteria but also slow-growing and dormant persistant celles that are present in the biofilms. Due to the existence of one extra barrier in the outer leaflet of Gram - negative bacteria (LPS) it is difficult to kill Gram-negative bacteria by many conventional antibiotics. However, AMPs are highly effective against Gram-negative bacteria. Different

AMPs which penetrate the extra barrier of Gram-negative bacteria are shown in (**Figure 1.27**[435]**).**

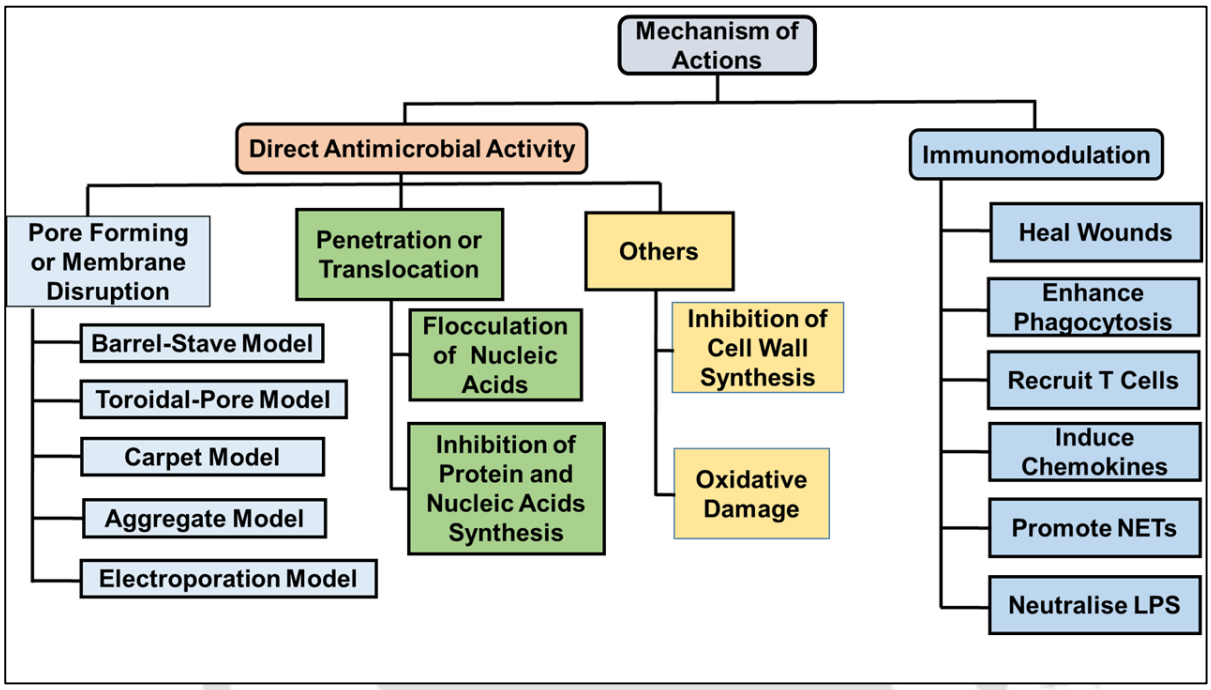

Figure 1.30. Flow chart summarizing the different modes of action for AMPs.[57,94,457]

1.7. Our objective:

In this thesis, we intended to develop synthetic AMPs with better therapeutic attributes, which might be able to overcome the shortcomings of the natural AMPs and the library of synthetic AMPs developed so far. To do this, we have defined our specific objectives as follows:

1.7.1. Design of Short and Economically Viable AMPs: Short AMPs were designed to make them time (manufacture) and cost effective, thus making them more market viable in turn. Secondly, smaller AMPs abolished the problems related to protein folding.

1.7.2. Cationic AMPs: Cationic AMPs are usually membrane disruptive in their mode of action. The membrane is an indispensable part of the microbe and is very difficult to modify by the microbes. For this reason, it is very difficult for microbes to develop resistance against

the membrane active AMPs. Thus our objective was to generate membrane active cationic AMPs.

1.7.3. Highly Potent and Salt-Tolerant AMPs: Our objective was to design AMPs with high potency against various broad-spectrum of microbes. We wanted to induce salt tolerance in the antimicrobial activity of the AMPs which would make them effective even in the physiological context.

1.7.4. Non-Toxic AMPs: As non-toxicity towards the mammalian cells is one of the most essential criteria for any therapeutic application, our objective was to develop non-cytotoxic AMPs.

1.7.5. Protease Resistant AMPs: To overcome one of the gravest shortcomings of the natural AMPs, we wanted to increase their systemic half-life by conferring protease resistance to them.

1.8. Methodology

For achieving our afore said objectives we have adopted a methodology with the following salient features:

1.8.1. De-novo Design of AMP Sequences: We have designed our short AMPs based on *de novo* approach using a library of selected amino acid residues. The sequences were designed by careful survey of the existing literature in the field and keeping in mind the most important attributes that are important for the activity of the AMPs.

1.8.2. Experimental and Computational Approach: In order to study the biological potency of the AMPs, the mechanism of action and the structure-function relation of the designed AMPs we have adopted both experimental and computational approaches. The interactions involved in the AMP: live cell membrane binding were understood clearly by studying AMP: membrane mimic interactions using molecular dynamics simulations. A combined experimental and simulation approach helped us to understand the mechanisms in detail.

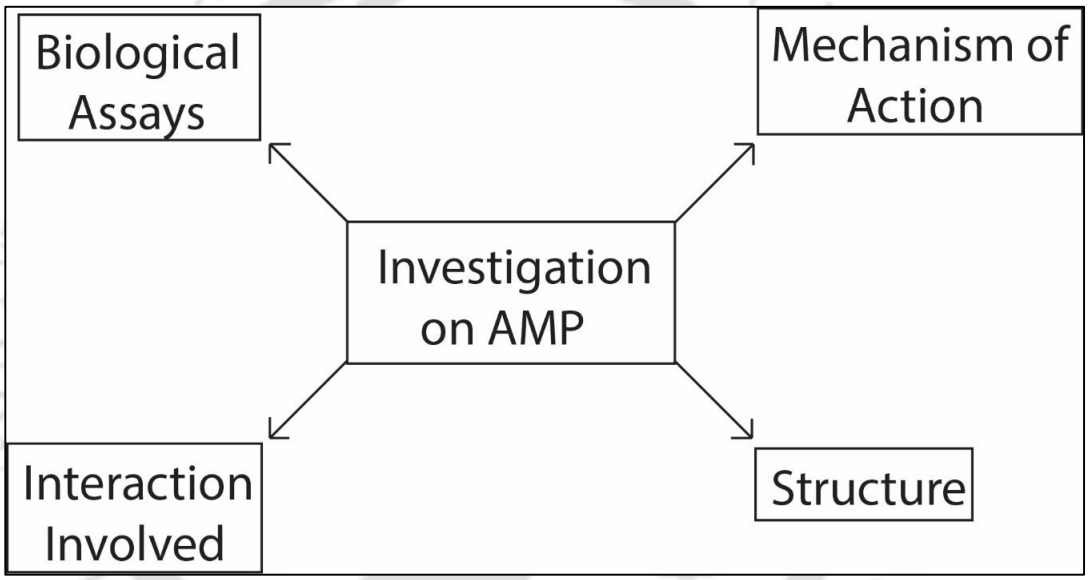

Figure 1.31. Schematic showing the different aspects of investigations on the designed AMPs carried out in this thesis.

1.9. Toolboxes Used to Synthesize, Characterize and Study the AMPs

Studies on the AMPs in the different chapters have been carried out using the similar experimental and computational approaches. In this section, we are presenting a general overview of our investigative strategy.

1.9.1. Peptide Synthesis, Purification and Characterization:

All the peptides studied in this thesis were synthesized by solid phase peptide synthesis (SPPS) strategy on MBHA-rink amide resin or Wang resin using standard Fmoc chemistry (Figure 1.32). PyBop and HOBt were used as coupling reagents (2.5 equiv. each) while DIPEA was used as the base (2.5 equiv.) during each amino acid coupling cycle. Amino acid coupling cycles were repeated to ensure complete coupling. Each coupling step was followed by capping with DMF, acetic anhydride and pyridine mixtures. Fmoc deprotection was performed with 20% piperidine in DMF. After complete assembly, the final peptide was cleaved from the resin using a cleavage cocktail of TFA, TIS and H_2O (96:2.5:1.5). The crude peptide was precipitated in cold diethyl ether and centrifuged down to get the crude solid peptide (Figure 1.32).

Peptide purification and characterization: Post synthesis, the crude peptides were purified using reverse phase semi-preparative HPLC using binary solvent gradient of CH_3CN-H_2O (5-100%) using a dual UV detection at 214 and 254 nm wavelength.

Purity of the peptides was confirmed using Analytical HPLC technique while the peptides were characterized using ESI-MS and ^1H NMR techniques.

The AMPs thus purified and characterized were studied further using several experimental techniques. The studies performed can be broadly classified into the following categories described below.

1.9.2. Biological Assays: The biological potency of the designed and synthesized peptides against microbes and the mammalian cells were determined at first as described below (Figure 1.33).

1.9.2.1. Activity Against Microbes:

Micro broth dilution assay was performed to determine the antimicrobial potency of the peptides against various microbial strains like ESKAPE pathogens (which contain both Gram-positive and Gram-negative bacterial strains) and fungal strains like *C. albicans* and *C. grubii* in the absence and presence of salts. The most potent AMPs among the designed peptides were identified from this basic experiment.[458] **Time kill kinetics** experiment was performed to determine the time required by the potent AMPs to manifest their bactericidal effect. This was performed using **zone inhibition assay.**[459]

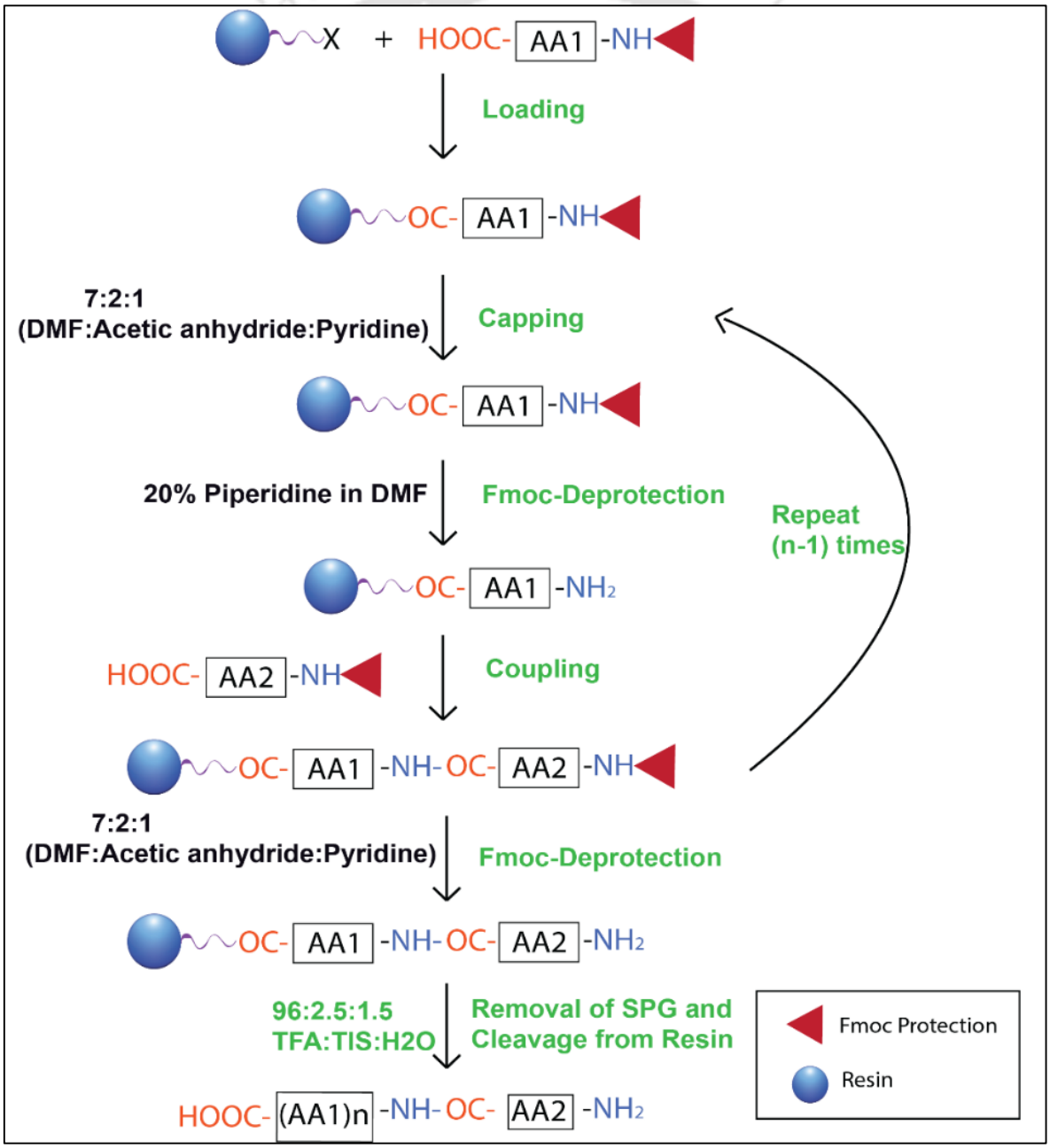

Figure 1.32. Schematic diagram showing the steps in the solid phase peptide synthesis (SPPS) method of synthesizing AMPs.

1.9.2.2. Activity Against Mammalian Cells:

One of the essential attributes for an AMP to become therapeutically competent lies in its being non cytotoxic towards mammalian cells. To investigate this, we have performed MTT assay to determine the effect of our AMPs on various mammalian cell lines as well as on human RBCs.

1.9.3. Mechanism of Action:

After identification of the most potent AMP(s), we have investigated their mode of action in details. For this we have performed various biophysical assays, spectroscopic, microscopic and calorimetric techniques as explained below (Figure 1.33). As all our designed peptides are cationic in nature and cationic peptides are reported in the literature to be membrane active, we performed experiments to look into the membrane activity of our AMPs.

1.9.3.1. Biophysical Assays:

a. **LUV Calcein Dye Leakage Assay:** Stable large unilamellar vesicles (LUV) were prepared from lipids to mimic microbial[460-464] and mammalian cells and calcein was entrapped in these LUVs. Under the normal conditions, entrapped calcein does not fluoresce. However, upon disintegration of the LUVs leading to the leakage of the calcein dye an increase in the fluorescence intensity is observed. The calcein entrapped LUVs are incubated with AMPs and the calcein fluorescence is monitored. Increase in the calcein fluorescence is directly

proportional to the extent of LUV damage and denotes the membranolytic activity of the AMPs.[465]

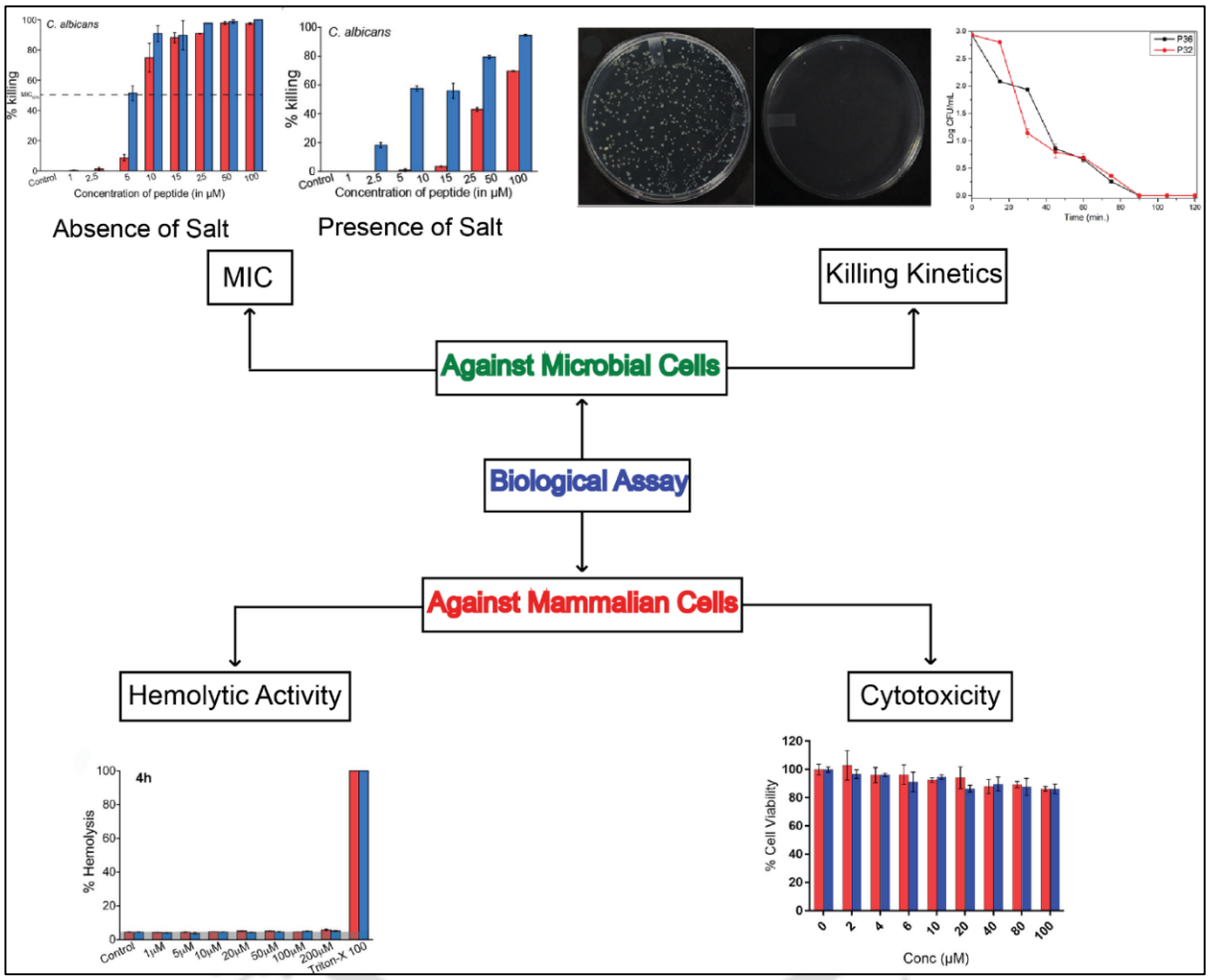

Figure 1.33. Different experiments conducted to determine the biological potency of the designed AMPs against microbial and mammalian cells. MIC = Minimum Inhibitory Concentration.

b. Outer Membrane Permeability Assay: The fluorescent dye NPN enhances its fluorescence intensity upon binding with the membrane lipids. In the normal healthy cells however this interaction is not possible. Upon compromise of the

outer membrane of the microbial cells, NPN can interact with the lipids and result in enhanced fluorescence. Thus an increment of the fluorescence in the presence of live cells is proportional to the outer membrane permeabilization. We have incubated the potent AMPs with live cells in the presence of NPN and monitored its fluorescence to study the outer membrane permeability behavior of our AMPs.

c. **Inner Membrane Permeability Assay:** PI, a fluorescent dye increases in fluorescence upon binding to the generic material. However, PI can only bind the genetic material upon permeabilization of the inner membrane. Thus an increase in PI fluorescence is proportional to the extent of inner membrane permeabilization. We have monitored the PI fluorescence upon incubating the lead AMPs with live microbial cells to get study their inner membrane permeability ability.

Cytoplasmic Depolarization Assay: Fluorescence dye $DiSC_3(5)$ is a cationic voltage sensitive dye that enhances its fluorescence in response to membrane depolarization. AMPs have been incubated with microbial cells in the presence of the dye, when an increase in its fluorescence intensity indicated the membrane depolarization effect of the AMPs.[466]

d. **FESEM/TEM Study:** To visualize the effect of the AMPs on the microbial cell membranes, AMPs were incubated with the live cells and FESEM/TEM was performed. This technique could clearly show the membrane deformation, blebbing, lysis and the cell debri formed from the membrane disruption in case the AMPs were membranolytic in nature.

e. **Live Cell NMR Study:** AMPs were incubated with live cells and ^{1}H NMR was recorded at different time points. Appearance of new NMR signals in the spectra were indicative of presence of metabolites which were refluxed out of the microbial cells. Thus appearance of new NMR lines were indirect proof of the membranolytic mechanism of action of the AMPs.

1.9.3.2. Peptide-Membrane Interactions: In order to be membranolytic AMPs need to bind to the microbial membranes. Also importantly, in order to be highly potent and non-cytotoxic at the same time these peptides need to be able to bind to the microbial membranes selectively over the mammalian membranes. In this section many experiments were performed on membrane mimetic instead of/ in addition to live cells. Negatively charged SDS micelles and zwitterionic DPC micelles are standard microbial and mammalian membrane mimics owing to their right kind of charges.

a. **Fluorescence Techniques:** Most of the AMPs developed in this thesis contain a Trp residue. This residue was incorporated into the design for two reasons: a) Trp is known to help in membrane binding owing to its unique hydrophobicity and b) The intrinsic fluorescence of Trp was used for studying the membrane interaction AMPs.

1. ***Blue Shift Experiment*:** The fluorescence of Trp is dependent on its microenvironment. Upon attachment of the AMP to the membrane mimics/live cells, the microenvironment of Trp became hydrophobic which shifted its fluorescence maxima to lower/blue wavelengths in comparison to the fluorescence emission of Trp in free water. Thus, a blue shift in the fluorescence maxima of Trp of the AMP in the presence of membrane mimics/ live cells was an indication of the AMP: membrane mimic/live cells binding.

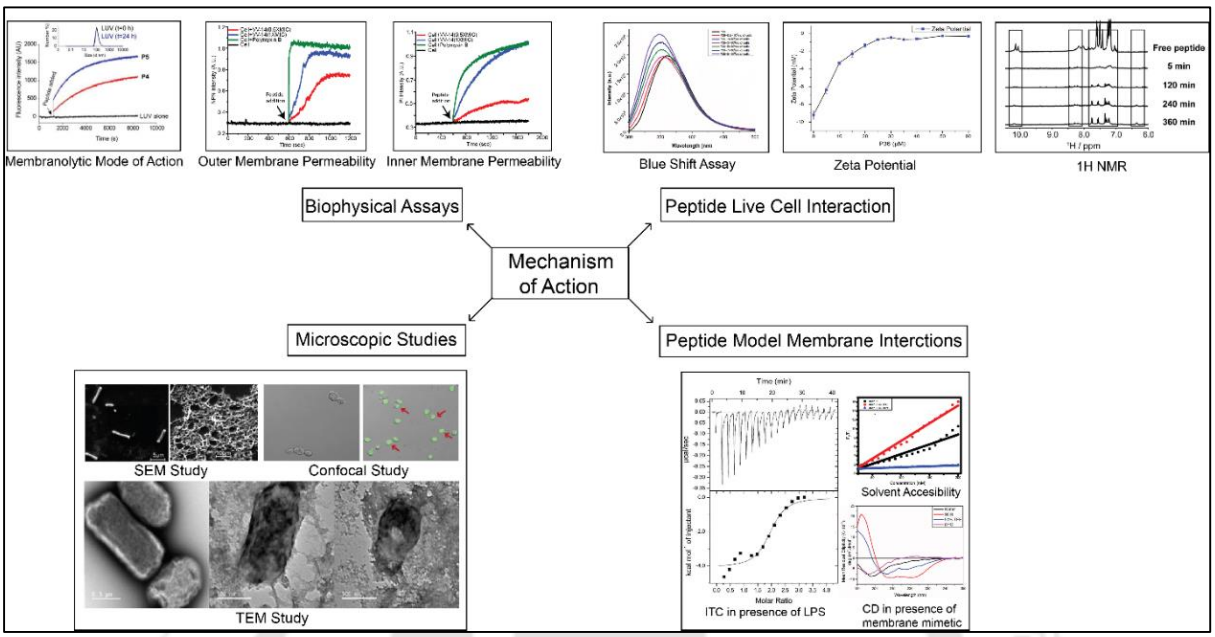

Figure 1.34. Various biophysical, spectroscopic, microscopic and calorimetric techniques that were performed to investigate the mechanism of action of the designed AMPs.

On the other hand, an unchanged fluorescence maxima indicated no interaction in between the AMP and membrane mimic/live cell.

2. ***Solvent Accessibility*:** Bonding of the AMP to the membrane mimic/ live cell led to burial of the Trp side chain in the membrane bilayer. This led to the inaccessibility of the residue to the solvent. Trp fluorescence was quenched in the presence of static fluorescence quencher bisacrylamide. We monitored the fluorescence of Trp in the presence of bisacrylamide and different membrane mimics. A quenched fluorescence indicated no interaction in between the AMP and the membrane mimics while unquenched fluorescence intensity indicated the burial of Trp in the membrane and hence interaction in between the AMP and membrane mimics.

3. ***Anisotropy Experiment*:** Membrane binding leads to anisotropic environment around the Trp residue. Thus study of anisotropy of Trp of the AMPs in the presence of various membrane mimics was undertaken, from which the binding constant of the AMPs to the various membrane mimics (microbial vs mammalian) was calculated.

b. NMR techniques:

1. ***^{1}H NMR in presence of different membrane mimics*:** Interaction in between the AMPs and the membrane mimics led to the broadening of the NMR signals (due to altered relaxation times) of the peptide, often with the shift in the position of the NMR signals. We performed NMR of the AMPs in water (in 10% D_2O) and in the presence of microbial (SDS micelles) and mammalian (DPC) membrane mimetic. In cases where the AMPs were active against Gram-negative bacterial strains, we also performed NMR in the presence of Lipopolysaccharide (LPS), which is present in the outer membrane of the Gram -negative bacterial coat.
2. ***PRE NMR experiment*:** In this experiment $MnCl_2$ was added to the AMP-membrane mimetic solution. The paramagnetic manganese caused the T_2 relaxation of the exposed protons to selectively quench. Upon interaction of the AMP with the membrane mimetics, many of the side chains of the constituent amino acids were buried in the membrane mimetic environment, leading to unchanged NMR signals. On the other hand, absence of interactions in between the AMPs and the membrane mimetics lead to the broadening of the signals. Thus this technique could establish the membrane interactions of the AMPs to residue specific details.

c. CD experiment:

Sometimes interaction of the AMPs with the live cells/membrane mimetics cause changes in their secondary structure. This can be studied with the help of CD spectroscopy. Usually a change of the secondary structure of the AMP in the absence and the presence of live cells/membrane mimetic environments is considered as a clear indication of the absence or presence of interaction respectively in between them.

d. Isothermal Calorimetry:

In order to estimate the thermodynamic parameters related to the binding of the AMP to the membrane mimics, we performed isothermal calorimetry. We were also able to estimate the binding constant of the AMPs for the various membrane mimic systems.

e. Zeta Potential:

The surface of the mammalian cells is negatively charged and hence shows a negative zeta potential. Upon interaction of cationic AMPs with the live cells, the AMPs accumulate at the membrane thereby reducing the charge of the surface which can be monitored by decreasing negative zeta potential value. Hence a decreasing negative zeta potential of the microbial cells in the presence of AMPs denoted interaction in between them.

1.9.4. Structure of the AMPs:

The study on the structure of the AMPs was carried out principally by three techniques

a. CD Spectroscopy was used to investigate the structure of the AMPs in free state in water and in the presence of various membrane mimicking environments like SDS, D8PG, DPC, LPS etc. Any change in structure in the presence of the membrane mimicking environments suggested a binding in between the AMP and the membrane mimic and the interconnection between the structure and the function of the AMPs while an unchanged secondary structure

in the free state and in the presence of membrane mimics suggested either no interaction in between the two or structure independent activity.

b. NMR: Structure of the AMPs in solution in free state and in membrane bound state was determined also using NMR. Membrane binding was usually accompanied by the change in the chemical shifts of the NMR signals and peak broadening. Structure of the AMPs were delineated from the NOEs obtained in the 2D NMR experiments like ROESY or NOESY or it was calculated using CYANA.

c. Molecular Dynamics Simulations: The structure of the AMPs in free and membrane bound state were also computed using MD simulations.

1.9.5. Interactions Leading to Peptide-Membrane Binding: MD simulations that were performed on the AMP in the presence of various membrane mimics (SDS/DPC micelles) either led to the AMP: membrane mimic bound structure or unbound AMP and the membrane mimics at the end of the simulations. The selective binding of the AMPs to the various membrane mimics hinted to the interactions at play. Also from the final AMP: membrane mimic complex, one could delineate the various non-covalent forces at play responsible for the membrane binding. MD simulations enabled the explanation of the properties of the designed AMPs in atomistic details. Such in depth understanding would surely help in the design of AMPs as potential therapeutic molecules in the future (Figure 1.34).[421,465,467-471]

Chapter 2

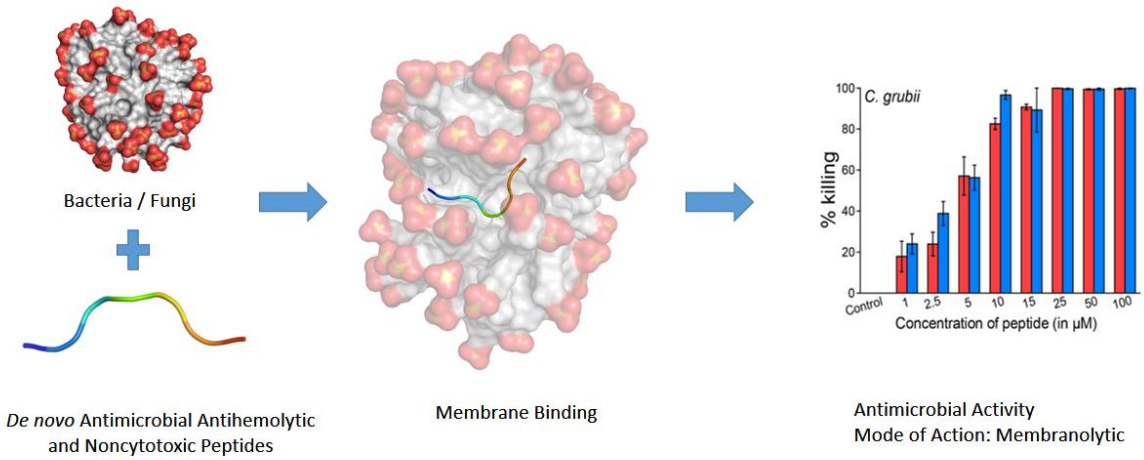

Insights into the Mechanism of Antimicrobial Activity of Seven-Residue Peptides

2.1. Introduction

As discussed in the introduction, naturally occurring peptides composed of Leu and Lys show good antimicrobial activity. But in most studies, attainment of secondary structure and amphipathicity appeared to be the two vital factors for the antimicrobial activity of the LK peptides. Monroc *et. al.* demonstrated that 4-10 residues long linear LK peptides did not show antimicrobial activity, while when cyclized, these peptides showed very high antimicrobial activity due to enhanced hydrophobicity.[472] Cyclization of the peptides, is known to increase structural rigidity, leads to increased binding due to diminished entropic penalty. In a separate study, Doele and co-workers demonstrated that simple synthetic LK peptides immobilized on solid phase resins functioned as antimicrobial agents against various strains, while their soluble counterparts were completely inactive.[473]

Several naturally occurring AMPs are also rich in Trp.[253,474] Researches have proved that a single Trp substitution at certain positions of inactive fragments of the amphipathic helical AMPs could confer them with antimicrobial activity, without significantly increasing the hemolytic activity.[475] There are reports on synthetic peptides composed of Leu, Lys and Trp of varying length with antimicrobial activity and different extent of hemolytic activity.[476-478] In most of the studies, 11-mer LxKyW (x = 5, y =5) peptides were found to be the most active ones.

To circumvent the problem of high production cost[479-481] associated with large-scale synthesis of AMPs to be used as therapeutic molecules, we are interested in designing short AMPs, which would economize the cost and time of synthesis. In this present study, we have designed an array of five peptides P2-P6, (Figure 2.2 and Table 2.1), out of which P4 and P5 were effective against bacterial strains like *E. coli* DH5α, *P. aeruginosa, K. pneumoniae, S. typhi, and S. aureus* as well as fungal strains like *C. albicans* and *C. neoformans var. grubii*. These were

obtained by modification of the peptide P1 studied earlier by Doele *et. al*.[473] and was reported to be a moderate antimicrobial agent when immobilized on solid phase resin while being completely inactive in its soluble form. Positively charged residue i.e. Lys in P1 was modified to Arg and His in P2 and P3, respectively, to see if the change in the positive side chain would have any effect on the activity of the peptides. Keeping in mind the role of C-terminal amidation on the activity of AMPs and the prevalence of Trp residues in several natural and synthetic AMPs, peptides P4, P5, P6 were designed from peptides P1, P2, and P3, respectively by mutation of L3 to Trp residue and C-terminal amidation (Table 2.1).

The peptides, P4 and P5 were found to be non-hemolytic and non-cytotoxic to human cell lines. We established that these small peptides did not adopt any specific secondary structure in the free or SDS micellar bound state, which proved that secondary structure was not necessary for their antimicrobial activity. In order to get an insight into the orientation of the two active peptides in the membrane, we have performed high-resolution paramagnetic relaxation enhancement (PRE) NMR experiments. Further understanding of the same was obtained from an all-atom MD simulation study. The calculations provide crucial insights into the interaction network between peptides and micelle at the very initial stages of binding. Electrostatic interaction was found to be the most vital factor for interaction of the active peptides, P4 and P5 with the membrane. Also, P4 and P5 most probably adopted membrane deformation and lysis as their mode of action as concluded from both biological experiments and MD simulations. Understanding the mode of action of these AMPs will help in easy design of antimicrobial therapeutics in the future.

2.2. Experimental Section

2.2.1. Peptide Synthesis:

All the peptides were synthesized by standard Fmoc-based solid phase peptide synthesis method on MBHA-Rink amide resin (loading 0.7 mmol/g) and Wang resin (loading 0.7mmol/g). For each amino acid attachment, 2.5 equiv. of Fmoc amino acids, 2.5 equiv. of coupling reagent (PyBOP), 2.5 equiv. of HOBt and 5 equiv. of base (DIPEA) were used. For incomplete reaction, coupling cycles were repeated, followed by capping with 7:2:1 DMF, Acetic anhydride and pyridine. For Wang resin first coupling was done by 2.5 equiv. of DIC, 2.5 equiv. of HOBt in presence of catalytic amount (0.1 equiv.) of DMAP. Fmoc deprotection was performed with 20% piperidine in DMF. The final peptide was cleaved from the resin using a cleavage cocktail (96% TFA, 2.5% TIS and 1.5% H_2O) for 3 h. The crude peptide was precipitated by cold diethyl ether followed by centrifugation to get the crude solid peptide.

2.2.2. Peptide Purification and Characterization:

Crude peptides were purified by RP-HPLC (Thermo scientific dionex ultimate 3000) on a semi-preparative Biobasic 8 column using binary CH_3CN-H_2O (5-100%) solvent system at a flow rate of 5ml/min, using dual UV detection at 214 nm and 254 nm. Purity of the peptides was confirmed using Thermo Scientific Dionex ultimate 3000 analytical HPLC system, using Thermo Scientific BioBasic 18 analytical column. A flow rate of 1ml/min and linear gradient of 5–100% CH_3CN-H_2O was used. The purified peptides were characterized by mass spectrometry on Agilent-Q-TOF 6500 instrument, in ESI positive mode, equipped with Mass hunter work station software. Peptide stock solution was prepared either in water and/or sodium phosphate buffer (pH 7.4) and filter sterilised unless stated otherwise.

2.2.3. Microbial Culture:

For antimicrobial activity assay, *E. coli* DH5α, *P. aeruginosa, K. pneumoniae, and S. aureus* were grown in Nutrient broth and maintained at 310 K under shaking condition while *C. albicans* and *C. grubii* were grown in YPDU broth (1% yeast extract, 1% peptone, 2% dextrose

and 20 µg/ uridine) and maintained at 301K under shaking condition. *S. typhi* TY2 was grown in Nutrient broth containing 50 µg/ streptomycin and maintained at 310 K under shaking condition.

2.2.4. Cell Culture:

Human normal embryonic kidney (HEK-293) cells were purchased from National Center for Cell Science (NCCS), Pune. The cell lines were maintained in DMEM supplemented with 10% (v/v) fetal bovine serum (FBS) and 1% penicillin & streptomycin at 310 K in humidified air containing 5% CO_2.

2.2.5. Micro-broth Dilution Assay:

Standard micro-dilution broth assay as described previously, was used to assay for antimicrobial activity of the peptides.[482] Overnight grown cultures of respective pathogens were used to obtain the mid log phase cultures of *E. coli* DH5α, *P. aeruginosa, K. pneumoniae, S. typhi TY2, S. aureus*, *C. albicans* and *C. grubii*. The cell suspensions were centrifuged at 6000 rpm for 5 min. Cell pellets were washed thrice with 10 mM phosphate buffer of pH 7.4 alone or in presence of 150 mM sodium chloride (NaCl) and re-suspended in the same buffer to obtain a cell suspension containing 10^5 CFU/. The reaction was set in a 96 well plate, 50 µL of the cell suspension was incubated with different concentrations of peptide (ranging from 1 µM to 100 µM) prepared from 1 mM peptide stock in phosphate buffer (pH 7.4) and incubated at their respective temperature (310 K for bacterial and 301K for fungal culture) for 4 h. A negative control containing only cell suspension and a positive control containing 10 µM Polymyxin B with cell suspension were maintained. Next, 150 µL of suitable media was added to each well and incubated overnight with shaking at the respective temperature. Absorbance of the culture was read at 630 nm to monitor microbial growth. The negative control Polymyxin B was used to normalize all other reading. The peptide concentration at which 90% growth

inhibition was observed served as its % (minimum inhibitory concentration at which 90% microbial cells are killed). All experiments were performed in triplicates.

2.2.6. Hemolytic Assay:

Hemolytic activity was assayed using fresh human blood collected in EDTA vial. Erythrocytes pellet, obtained by centrifugation at 8000 × g for 10 min at 277K was washed thrice with PBS (pH 7.4) and re-suspended to obtain a 2×10^8 cells/ suspension. This was incubated with equal volumes of increasing concentrations of the respective peptides up to 200 µM at 310K in shaking condition for 1 hr. and 4 hr., respectively. Samples were again centrifuged at 8000 × g for 10 min at 277 K and the absorbance of supernatant was measured at 414 nm to quantify RBC lysis and heme release. Heme released by 2% per volume Triton X 100 was taken as 100% and data from other samples were normalized against it. All experiments were performed in triplicates.

2.2.7. Cell Viability Assay:

The effects of the peptides on the cell viability were studied by MTT assay. HEK-293 cells were seeded into 96 well plate at the density of 10^4 cells/well. After overnight incubation, cells were treated with different concentrations (0 µM to 100 µM) of the P4 and P5 for 24 hr. MTT (0.3 mg/) reagent in DMEM was then incubated for 3 h and the formed formazan crystals were solubilized by adding 200 µL DMSO. Cell viability was calculated by measuring absorbance at 570 nm using a Tecan plate reader.

2.2.8. Liposome Preparation and Calcein Leakage Assay:

Approximately 1 mg each of DOPE and DOPG were weighed and dissolved in chloroform ($CHCl_3$) to obtain stock solutions which were further mixed to obtain the model liposomes investigated; 3:1 molar ratio of anionic DOPE/DOPG, reported to be used extensively as a

model system for negatively charged bacterial membrane in the literature. This was followed by drying of model liposomes in a nitrogen stream and overnight lyophilization to form a lipid film. The film was re-suspended in 10 mM Tris pH 7.4, containing 70 mM calcein, by vigorously vortexing for 30 min, followed by five freeze-thaw cycles in liquid nitrogen to obtain calcein entrapped vesicles. To obtain unilamellar vesicles, the suspension was passed through a mini extruder (Avanti Polar Lipids, Alabaster, AL) using stacked 100-nm pore-size polycarbonate membrane filters. Samples were subjected to 21 passes through filter. To avoid contamination of the sample by vesicles that have not passed through the first filter, an odd number of passages was performed. Untrapped calcein was eliminated, by loading on to a gel filtration-based hydrated Centrisep-Spin Column and centrifuging at 3000 rpm for 2 min to obtain a light orange iridescent suspension. The size of the LUVs were confirmed by dynamic light scattering experiments (Figure 2.7b, inset).

Calcein release from 20 μM dye-entrapped liposomes in six-hundred microliters of extra vesicular buffer (10 mM Tris, 100 mM NaCl, pH 7.4) was determined by monitoring the emitted fluorescence at 520 nm from liposome dispersion using Hitachi F-700 FL spectrometer, with a slit width of 2.5 nm. After stabilization of calcein fluorescence, peptide in different increasing concentrations was added to individual experiments and fluorescence enhancement was measured after 5 min of each addition. An absolute leakage scale was obtained by disrupting the liposomes at the end of each experiment through addition of 0.1% per volume Triton X-100. Measurements were performed in triplicate at 298 K.

An independent control, containing only 0.1% per volume Triton X-100 added to calcein loaded LUVs, was performed to ascertain the maximum disruption possible. Similar results were obtained in both the cases.

Percent leakage was calculated using the equation:

% leakage = $[(F-F_o)/(F_T-F_o)] \times 100$ %

Where, F, F_O and F_T are fluorescence intensity after addition of peptide, basal fluorescence intensity, and maximum fluorescence intensity obtained after addition of 0.1% per volume Triton X-100 respectively.

The time kinetics of calcein release upon peptide application was monitored by treating 20 μM liposomes in six-hundred microliters of extra vesicular buffer (10 mM Tris, 100 mM NaCl, pH 7.4) with 50 μM of the respective peptides, P4 and P5. A control experiment containing LUV alone was also maintained and monitored for 2 hr. Measurements were performed at 298K by monitoring the emitted fluorescence at 520 nm from liposome dispersion using Hitachi F-700 FL spectrometer, with a slit width of 2.5 nm.

2.2.9. Dynamic Light Scattering (DLS):

DLS experiment was performed using Malvern ZetasizerNano S (Malvern Instruments, UK) provided with a 4-mW He-Ne laser (λ= 633 nm) and a back scattering angle of 173°. 20 μM LUVs were dissolved in 10 mM Tris buffer, 100mM NaCl (pH 7.4), filtered using Millipore 0.45-μm polycarbonate membrane filters, degassed prior to use and measured at 298 K in low volume disposable sizing cuvettes. For data analysis, the viscosity and refractive index of 10 mM Tris buffer, 100mM NaCl buffer (pH 7.4) were taken to be 0.89 and 1.33, respectively.

2.2.10. CD Spectroscopy:

The CD spectra were recorded on a Jasco J-815 spectropolarimeter (Tokyo, Japan) calibrated with (±)–10-camphorsulfonic acid for optical rotation. The spectra were measured from $\lambda_{250\ nm}$ to $\lambda_{190\ nm}$, using a 1-mm path length suprasil quartz cuvette at a scan rate of 100 nm/min, interval of 0.5 nm, time constant of 1 s, and taking an accumulation of three scans at 298 K. For CD studies, P4 and P5 were dissolved in deionized water and 30 mM SDS or DPC to

give a final concentration of 25 µM peptide. The acquired CD signal spectra were then converted to the mean residue ellipticity using the following equation:

$$\theta_M = (1000.\ \theta_{obs})/(c.l.n)$$

where θ_M is the mean residue ellipticity [deg·cm^2 ·dmol^{-1}], θ_{obs} is the observed ellipticity corrected for the water and 30 mM SDS at a given wavelength [mdeg], *c* is the peptide concentration [mM], *l* is the path length [mm], and *n* is the number of amino acids.

2.2.11. NMR Spectroscopy:

All NMR experiments were carried out at 310 K using Bruker Avance III 500 MHz NMR spectrometer, equipped with 5 mm SMART probe. NMR samples were prepared in 10% deuterated water (pH 4.5) and DSS (2, 2-Dimethyl-2-silapentane-5- sulfonate sodium salt) was used as an internal chemical shift standard. Next, 1D proton NMR spectra of two active peptides, P4 and P5 with a concentration of 0.5 mM each were recorded in the presence of 200 mM per-deuterated SDS micelle (d_{25}-SDS). Subsequently, two-dimensional ^{1}H-^{1}H total correlation spectroscopy (2D TOCSY), and two-dimensional ^{1}H-^{1}H Nuclear Over Hauser Spectroscopy (2D NOESY) were recorded for the two peptides with a mixing time of 80 ms and 150 ms, respectively. The spectral width was 12 ppm in both dimensions. Water suppression was done using excitation-sculpting scheme and the States-TPPI was used for quadrature detection in the t1 dimension.[61] The total number of scans was fixed to 28 and 80 for TOCSY and NOESY, respectively per t1 increment with 16 dummy scans.

For Paramagnetic Relaxation Enhancement (PRE) NMR, a series of two-dimensional ^{1}H-^{1}H total correlation spectroscopy (2D TOCSY) were recorded upon titration with increasing concentration of Manganese Chloride ($MnCl_2$), a paramagnetic quencher. The number of scans was fixed to 32 per t1 increment with 16 dummy scans. NMR data processing, and analysis, were performed using Topspin (Bruker) and SPARKY[62] software, respectively. The Hα/NH

cross peak intensities of P4/ P5 in SDS micelle were calculated before and after addition of respective amount of $MnCl_2$ and remaining amplitudes were calculated using the following equation:

Remaining amplitude = $I_{H\alpha/NH(MnCl2)} / I_{H\alpha/NH(no\ MnCl2)}$

Where, $I_{H\alpha/NH(MnCl2)}$ and $I_{H\alpha/NH(no\ MnCl2)}$ indicates the Hα/NH peaks intensities of respective amino acid residues in the presence and absence of $MnCl_2$, respectively.

2.2.12. Live-cell NMR spectroscopy:

To gain further insights into the atomic level killing of bacterial and fungal cells upon treatment with the respective peptides, live cell NMR experiments were conducted to monitor broadening of ^1H-^1H proton resonances of peptide upon interaction with microbial cells and time-dependent release of metabolites from injured and dead cells.

Overnight grown cultures of respective pathogens were used to obtain the mid log phase cultures of *E. coli* DH5α, and *C. grubii*. The cell suspensions were centrifuged at 6000 rpm for 5 min. Cell pellets were washed thrice with 10 mM phosphate buffer of pH 7.4 alone and re-suspended in the same buffer to obtain a cell suspension containing 10^6 CFU/.

In brief, One-dimensional proton NMR spectra of 1mM solution of the respective peptide, P4 or P5 in 90% of 10 mM phosphate buffer (pH 6.5) and 10% D_2O was recorded on a Bruker Avance III 500 MHz NMR spectrometer (equipped with smart probe). The temperature for each experiment was adjusted as per the standard growing temperature of *E. coli* (310 K) and *C. grubii* (298 K). This was followed by addition of the peptide solution to 10^6 CFU/ of log phase microbial cells and subsequent recording of a series of 1D proton NMR spectra. It is worth mentioning that the experimental conditions used had no effect on the innate growth of

either of the two microbial cells. The same was repeated for both free bacterial and fungal cells as well as cells treated with the control peptide P1.

2.2.13. Scanning Electron Microscopy (SEM):

E. coli DH5α cells were cultured to mid-log phase and were harvested by centrifugation at 6,000 rpm for 5 min, washed thrice and re-suspended in phosphate buffer, pH 7.4 to a final number of 10^6 cells/ml. The cell suspensions were incubated with P4 and P5 at 1×, 2×, and 5× MIC value for 4 hr. at 310 K. Untreated cells, and P1 treated cells were set as control.

After incubation, 10 µl of bacterial suspension was spotted on a clean poly L-lysine coated glass slide and fixed with 2.5% (v/v) glutaraldehyde in phosphate buffer, overnight at 277K. Thereafter, the slides were washed twice with phosphate buffer, and dehydrated by treatment with a graded series of ethanol (30%, 50%, 70%, 90%, and 100%), each for 15 min. The samples were next air dried, followed by gold coating and observed under a SEM at 4000× magnification.

2.2.14. Tryptophan Fluorescence Measurements:

Intrinsic fluorescence of tryptophan (W3) of P4 and P5 in water and SDS were recorded by using a Horiba Jobin YVON Fluoromax-4 spectrofluorometer. The emission spectra was recorded from 295 to 500 nm after excitation at 295 nm. The studies were carried out at a peptide concentration of 50 µM and SDS concentration 30 mM at 25^0C.

2.2.15. MD Simulations:

2.2.15.1. Modelling of SDS and DPC Micelles in Water Box:

SDS and DPC micelles were modelled using CHARM-GUI Membrane Builder[467,483-485] for GROMACS[486-489] inputs.[490]

Total 60 SDS/DPC molecules were used for modelling the micelles. 60 Na^+ ions were added for neutralizing the simulation box. DPC micelles were neutral as each monomer was neutral in nature. The simulations were done by overlaying an equilibrated water box. Molecular Dynamics simulation was done to equilibrate the SDS/DPC micelles at 300K for 20 ns. The equilibrated SDS/DPC micelles were used for peptide binding studies. Total 169626/99015 atoms were considered for MD simulations of SDS/DPC micelle in water.

2.2.15.2. Modelling of Peptides:

Atomic coordinates of three seven residues peptides with sequence LKWLKKL, LRWLRRL & LHWLHHL were designed using Discovery Studio visualiser. The N- and C- termini were capped with $-NH_3^+$ and $-CONH_2$ respectively. Peptides were initially modelled as a linear chain with dihedral angle phi 150º (±5º) and psi -150º (±5º). The side chain of lysine was positively charged in our models. We performed MD, with a linear chain of peptide solvated with a water box as input. The total number of atoms considered for MD was 169747.

2.2.15.3. Setup for Peptide-SDS/DPC System:

Linear peptides were placed ~10Å away from the surface of equilibrated SDS micelles (Figure 2.1.) and the same geometry was used as an initial input for running molecular dynamics simulations. Along with 7-residue peptide and 60 SDS molecules, Model I/II/III/IV consisted of 55648/55639/55643/56532 water molecules, 60 Na^+ ions and 4/4/1/3 Cl^- ions. Our simulation model consisted of a total of 169680, 169659, 169647 and 169679 atoms for model I, II, III and IV respectively. Three structures from the MD simulations corresponding to SDS micelle bound peptide P4, P5 and P6 are deposited as .pdb files in the supporting information. Same setup has been used to study binding of P4 with DPC micelles. The P4-DPC system consist of total 98617 atoms out of which 32820 water molecules, 4 Cl^- ions were present.

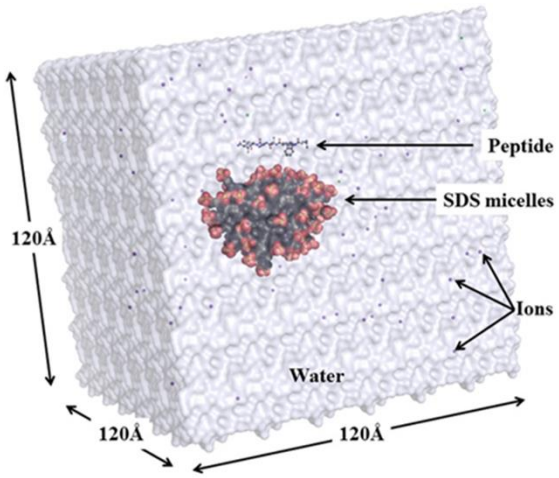

Figure 2.1. Molecular dynamics setup

2.2.15.4. Simulation Specifications:

Simulations were performed in the cubic water box of dimension 120Å X 120Å X 120Å centered at a SDS micelle. DPC micelle was solvated with 100Å X 100Å X 100Å cubic water box. TIP3P[73] (transferable intermolecular potential 3P) water model was used for modelling water molecules. The overall charge of the simulation box was neutralized by monovalent Na^+ and Cl^- counter ions. Each simulation model was minimized (step size = 0.01 nm, steps ~50000) by steepest descent algorithm. Maximum forces for the minimization convergence was set to 1000.0 kJ mol^{-1} nm^{-1}. After minimization, MD was performed with GROMACS V5.14 using the CHARMM36[74] force field. Simulations were done considering NPT (number of particle, volume, temperature) ensemble using Leap-frog algorithm. Bond lengths were restrained using LINCS[491] algorithms. Temperature and pressure of the system were maintained at 300K and 1 bar pressure respectively. Long range electrostatic interactions were treated using Particle Mesh Ewald[492] algorithm. Temperature was controlled using modified Berendsen thermostat[493] (coupling with a time constant of 0.1ps at 300 K) and maintained using Nose-Hoover[494,495] method implemented in GROMACS. Constant pressure simulation was maintained using Parrinello-Rahman[496,497] algorithms. We used 2fs MD time step and van der Waals cutoff at 12

Å distance. Initial velocities were generated using Maxwell distribution at 300 K. 50 ns simulation was performed for each complex. Structures were collected for analysis at an interval of every 10 ps. Output data was analyzed using GROMACS utilities.

2.3. Results and Discussions

The peptides, P1-P6 (Table 2.1, Figure 2.2) were synthesized, purified and characterized using analytical HPLC (Appendix, Figure A5) ESI-MS (Appendix, Figure A18-A23) and ^{1}H NMR (Appendix, Figure A40-A45).

2.3.1. Antimicrobial Potency of the Designed Peptides:

The five designed peptides, P2-P6 along with the control peptide P1 were initially screened for their antimicrobial potency against Gram-negative bacterial and human fungal pathogens by broth dilution assay as mentioned above. Microbes (5×10^4 cells) of each species were incubated with 2-fold increasing dilution of the respective peptides and incubated for 4 h. Bacteriolytic activity and hence $MIC_{90\%}$ was measured by taking the absorbance at 630 nm. Among the six peptides, only P4 and P5 showed good antibacterial/antifungal activity against all the organisms tested (Table 2.2, Figure 2.3).

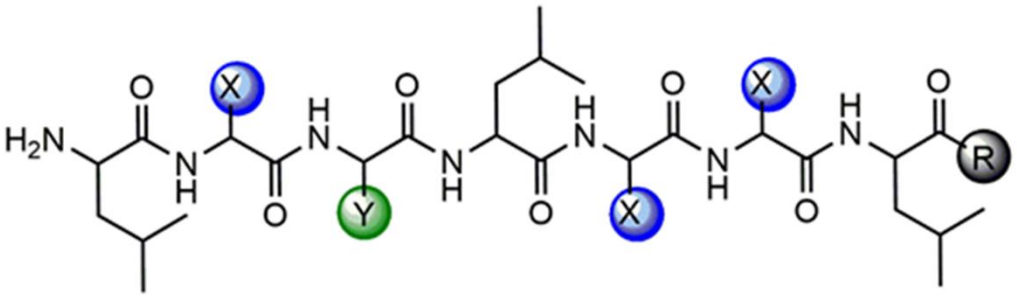

P1, P2, P3: X = K, R, H resp. ; Y = L; R = OH

P4, P5, P6: X = K, R, H resp. ; Y = W; R = NH_2

Figure 2.2. Schematic diagram of the peptides (**P1-P6**) studied in the present report.

Table 2.1. Peptide Sequences with Code

Sl. No.	Peptide Code	Peptide Sequence
1	P1(Reference)	H-LKLLKKL-OH
2	P2	H-LRLLRRL-OH
3	P3	H-LHLLHHL-OH
4	P4	H-LKWLKKL-NH_2
5	P5	H-LRWLRRL-NH_2
6	P6	H-LHWLHHL-NH_2

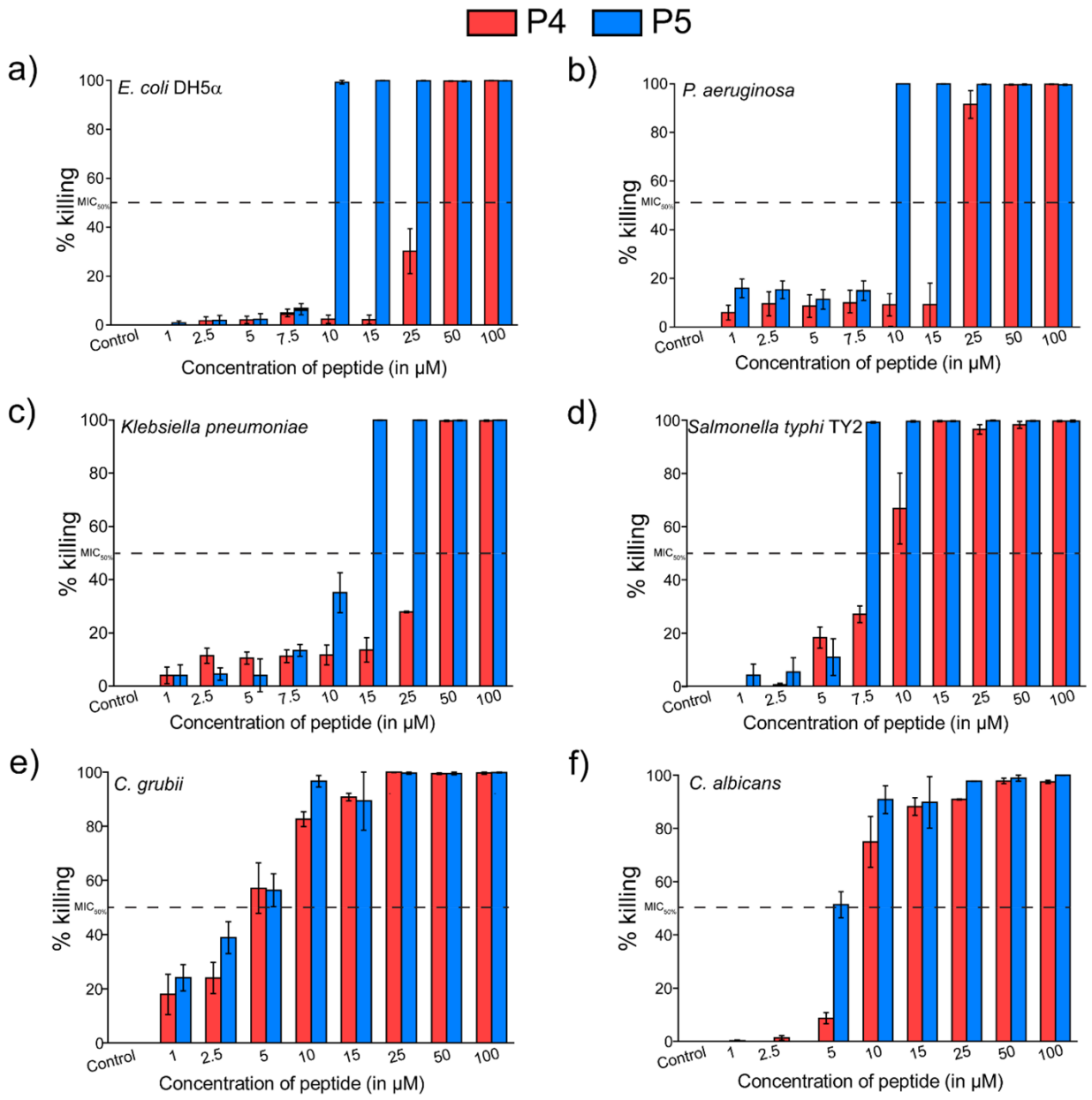

Figure 2.3. $MIC_{90\%}$ of the peptides P4 and P5. Microbroth dilution assay was done with increasing concentration of the respective peptides against various bacterial and fungal strains. After allowing for overnight recovery, the percentage of killing was calculated and represented in the form of $MIC_{90\%}$ value. Both P4 and P5 showed potent antimicrobial activity at low concentrations. All experiments were performed in triplicates and the $MIC_{50\%}$ values have been marked by broken black line.

Table 2.2. $MIC_{90\%}$ and $MIC_{50\%}$ for P1-P6 against several bacterial and fungal strains in the absence and presence of salts.

	In Absence of Salts $MIC_{90\%}$ in μM				**In Presence of 150 mM NaCl $MIC_{50\%}$ in μM**			
	P1/P2/P3	**P4**	**P5**	**P6**	**P1/P2/P3**	**P4**	**P5**	**P6**
E. coli DH5α	≥500	50	10	≥100	-	≥100	≥100	-
P. aeruginosa	≥500	50	10	≥100	-	≥100	≥100	-
K. pneumoniae	≥500	50	15	≥100	-	-	-	-
S. typhi TY2	≥500	15	7.5	≥100	-	-	-	-
S. aureus	≥500	50	50	≥100	-	-	-	-
C. albicans	≥500	50	50	≥100	-	50	25	-
C. grubii	≥500	25	15	≥100	-	50	25	-

An important observation here was that both peptides exhibited quite convincing activity against *P. aeruginosa*, a nosocomial bacterial pathogen. This organism expresses extracellular alginate capsules on its outer membrane, which is a potent antigen involved in *Pseudomonas* pathogenesis. The presence of an alginate capsule is known to inhibit the entry of antimicrobial agents, thus rendering them inactive.[498] It is worth mentioning that alginate production is also associated with formation of surface-attached biofilms which exhibit high resistance to most of the existing drugs and antibiotics. *P. aeruginosa* along with *K. pneumoniae* and *S. aureus*, forms a part of the ESKAPE group of pathogens listed by the Infectious Disease Society of America as highly biocidal resistant strains forming a new era in microbial pathogenesis and

resistance. Additionally, we have also tested our peptides against *S. typhi*, known to cause typhoid fever, a highly prevalent disease in Asia. Our designed peptides exhibited moderate to good activity against all these strains as shown in Table 2.2 and Figure 2.4 P4 and P5 also retained their antifungal activity in presence of physiological concentration of salt (150 mM NaCl) exhibiting 50% killing at 50 µM and 25 µM for P4 and P5, respectively against both fungal species tested. An important point of consideration here is that peptide P5 was more potent than P4 for all the microorganisms tested and under both conditions (Figure 2.4, Table 2.2). This is most probably owing to the guanidine group present in the side chain of Arg in comparison to the primary amine group present in the side chain of Lys.

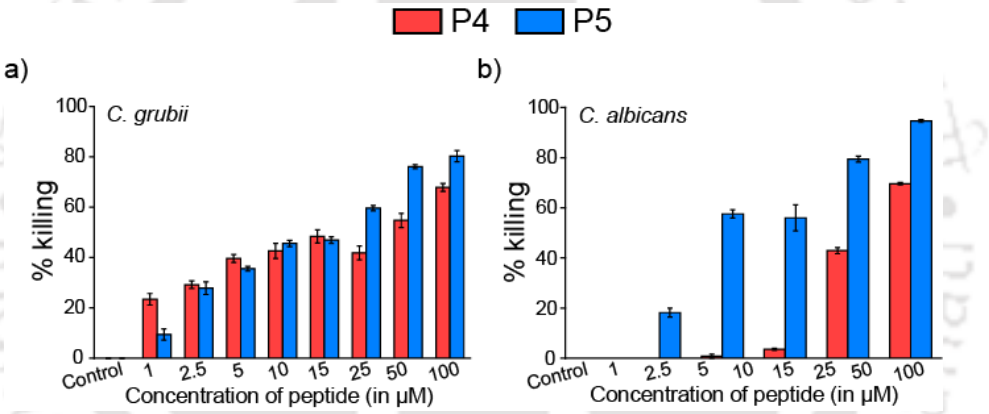

Figure 2.4. $MIC_{50\%}$ of the peptides, P4 and P5 in presence of salt. Microbroth dilution assay was done with increasing concentration of the respective peptides, in the presence of 150 mM of NaCl, the physiological salt concentration. After allowing for overnight recovery, percentage of killing was calculated and represented in the form of $MIC_{50\%}$ value. All experiments were performed in triplicates.

2.3.2. Cytotoxicity and Hemolytic Activity of Designed AMPs:

Over the last couple of decades, AMPs have become quite widespread due to their unique characteristics, including high potency and membranolytic mechanism of killing.[499,500] However, their usage is still very limited due to reports of cytotoxicity and hemolytic activity.

In order to be applied as therapeutic agents, the peptides should be non-cytotoxic and non-hemolytic. Therefore, we tested the hemolytic potential of our two active peptides, P4 and P5, against human RBCs by analyzing heme release. As seen in Figure 2.5, both the peptides were non-hemolytic even after 4 h of treatment with concentration as high as 200 µM of the respective peptides. Cell viability of P4 and P5, on the other hand was tested on normal human embryonic kidney epithelium (HEK 293) cells.

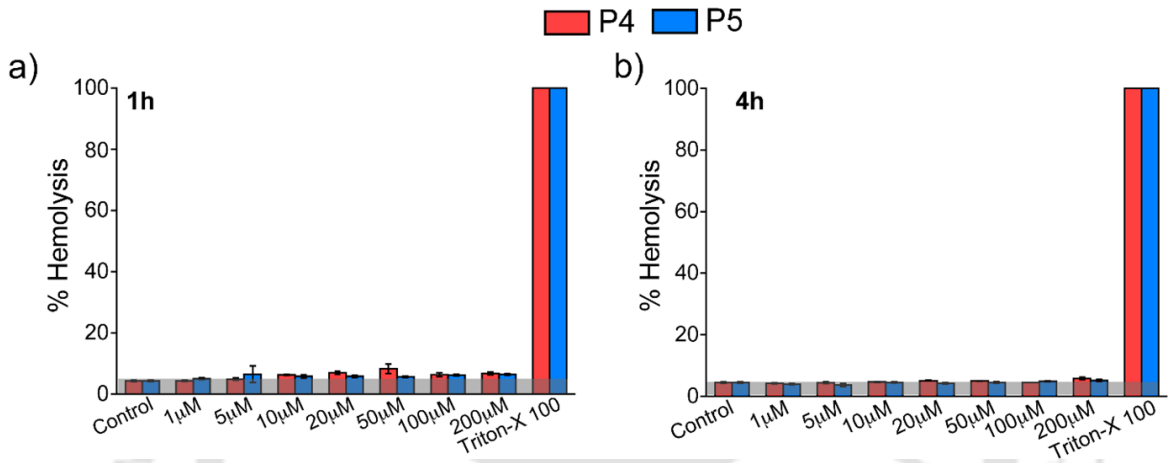

Figure 2.5. Hemolytic assay of P4 and P5. Heme release was quantified by measuring the absorbance at 410 nm after treatment with increasing concentration of P4 and P5 for 1 and 4 hr. Maximum heme release was < 10% in case of both P4 and P5, clearly indicating that they were non-hemolytic. All experiments were performed in triplicates and 2% per volume of Triton X-100 was used to normalize all data.

As shown in Figure 2.6, treatment of the cells with P4 and P5 did not result in significant cytotoxicity even after 24 hr. At higher concentrations (≥100 µM), cell viability was reduced by less than 10%.

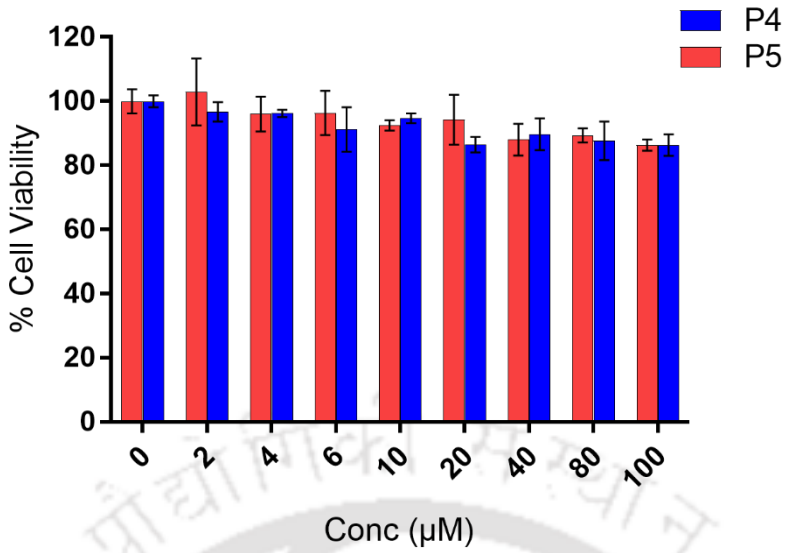

Figure 2.6. MTT Assay of peptides P4 and P5 on HEK-293 cells. Viability was quantified by measuring the absorption at 570 nm. All experiments were performed in triplets.

2.3.3. Membranolytic Activity of Designed Peptides: Calcein Dye Leakage Assay

Majority of cationic AMPs are known to be membranolytic in action, *i.e.* they kill the target cell through membrane perturbation and pore formation leading to cell death due to lysis and loss of osmolarity.[498] Initial interactions with the cell membrane is a prerequisite for peptide-mediated lysis to occur. In order to probe the membrane binding and perturbing activity of our peptides, calcein-entrapped large unilamellar vesicles (LUVs) composed of 3:1 DOPE/DOPG, were prepared to mimic negatively charged bacterial membrane and their interaction with the active peptides P4 and P5 was studied. Both the peptides, showed a concentration-dependent permeabilization of the LUVs, with around 27% and 45% disruption at concentrations of 30 μM for P4 and P5, respectively (Figure 2.7a). This data confirmed that P4 and P5 interacted with the membrane and possessed a membranolytic mode of action. Further, time kinetics profile of the LUVs treated with 50 μM of the respective peptides clearly indicated that P5 was comparatively more vigorous in binding and disrupting the bacterial membrane mimic, as also

depicted by its lower $MIC_{90\%}$ values (Figure 2.7b). In contrast, in the absence of peptides, we did not find leakage of calcein from the 3:1 DOPE/DOPG LUV till 10hr. of measuring time. In addition, dynamic light scattering (DLS) experiments confirmed that the hydrodynamic radius of fresh 3:1 DOPE/DOPG LUV was almost identical even after 24hr., suggesting that the LUV was stable in nature (Figure 2.7b, inset).

2.3.4. Membranolytic Activity of Designed Peptides: FESEM

Furthermore, to study the bacteriolytic activity of P4 and P5, we probed their action using scanning electron microscopy (SEM). *E. coli* cells (10^6 cells/) were incubated with 1×, 2×, and 5× $MIC_{90\%}$ of the respective peptides to study and interpret the extent of peptide-mediated cell perturbation and hence lysis. It is noteworthy to mention that the *E. coli* bacterial cell is rod shaped with a smooth outer membrane. However, in the presence of different concentrations of peptide P4 or P5, we observed cell wall shrinkage and the leakage of intracellular materials due to cell lysis. At low concentration, distorted cell morphology in the form of dents and membrane blebbing was clearly visible (Figure 2.7 c iii-iv), while non-uniform cell debris with leaked intracellular material, indicating complete cell lysis, was visible at higher concentration of peptides (Figure 2.7 c iii-iv). Strikingly, control sets comprising of peptide untreated cells showed intact morphology (Figure 2.7 c i) while negligible morphological change was observed in the presence of inactive peptide, P1 at 100 μM concentration (Figure 2.7 c ii).

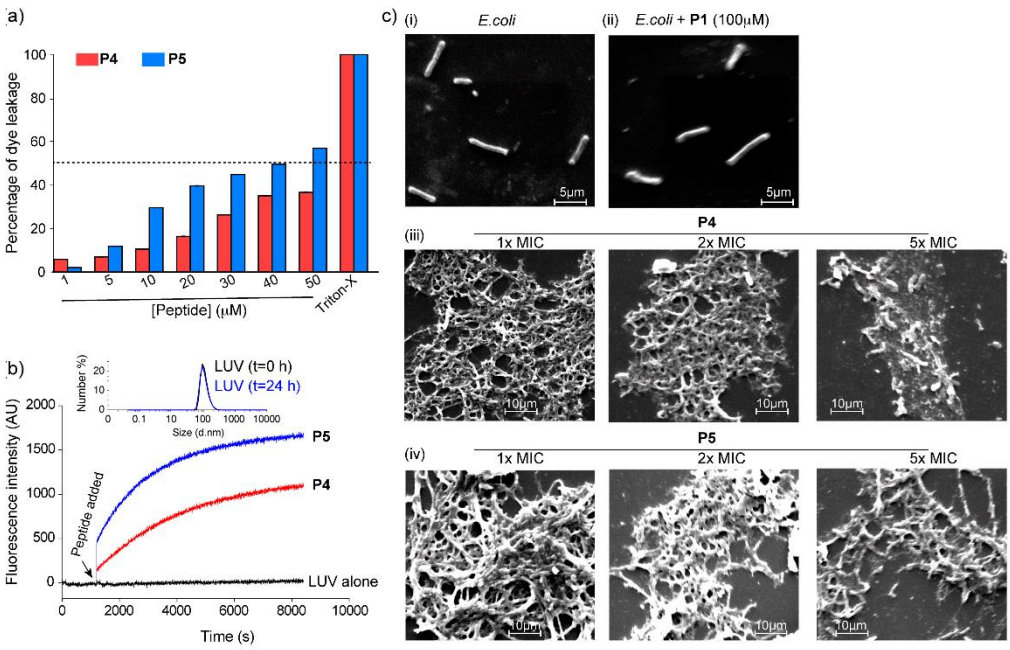

Figure 2.7. Membranolytic peptides, P4 and P5: (a) Calcein dye leakage assay was done with increasing concentration of P4 and P5 in 10 mM phosphate buffer, 100 mM NaCl, pH 7.4. Percentage of calcein leakage was calculated with respect to 0.1% per volume Triton-X (used as control). Maximum leakage was 37% and 57% for P4 and P5, respectively. All experiments were performed in triplicates. (b) The time kinetics of peptide-induced calcein dye leakage was monitored over a period of 7200 s after treatment with 50 μM of the respective peptides. Peptide P5 showed more extensive effects on the LUVs, compared to P4. Untreated LUVs did not show any change in hydrodynamic radius (inset) or any leakage even up till 24hr. indicating that they were stable in nature. (c) SEM images depicted the interaction of the respective peptides with *E. coli* cells. (i-ii) Untreated and P1-treated control cells did not show any significant morphological changes. (iii-iv) Cells treated with varying concentrations of P4 and P5 showed cell disruption and loss of cellular morphology with leakage of intracellular contents. The samples were observed at 4000× magnification.

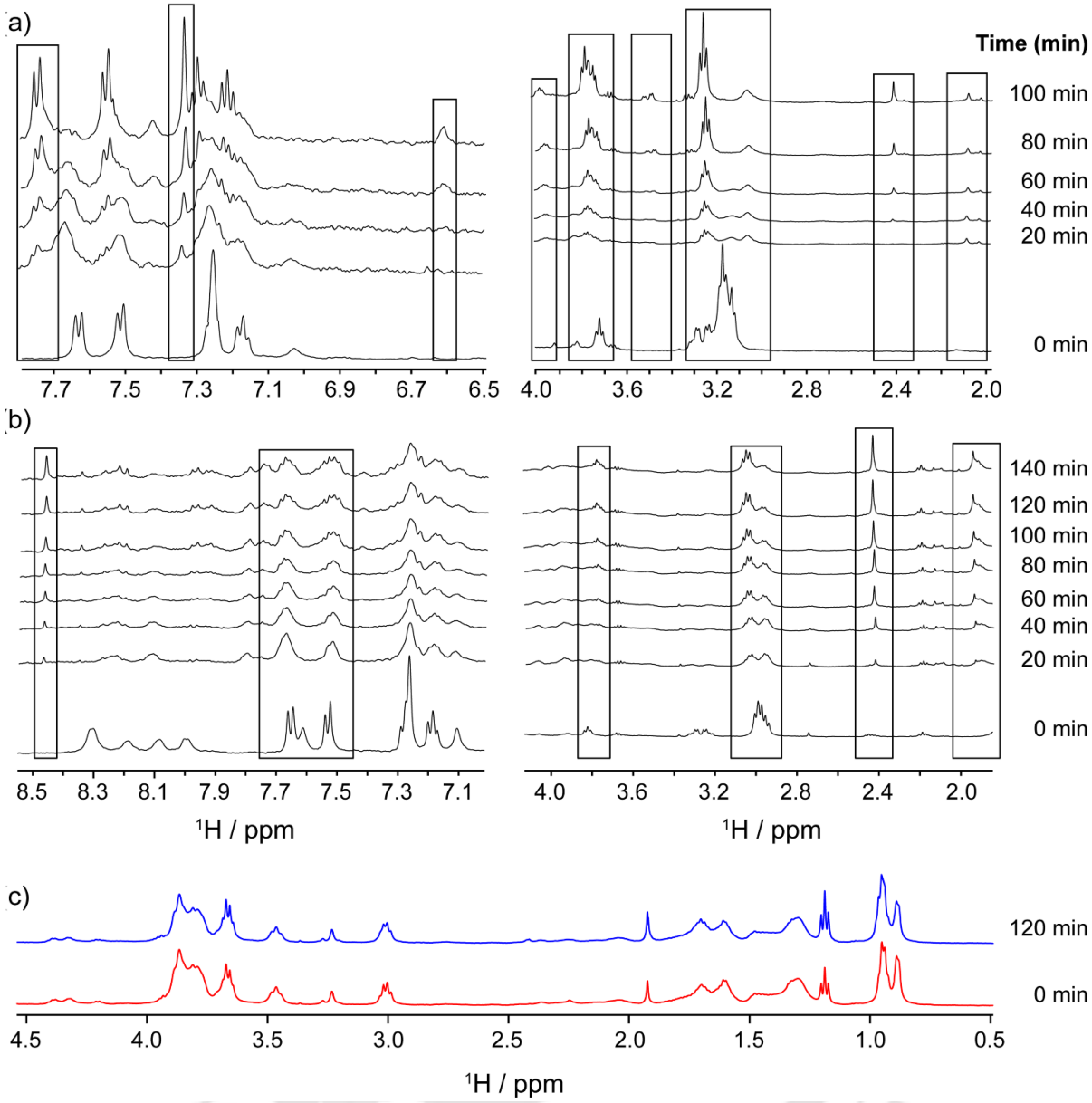

Figure 2.8. Live cell NMR spectroscopy with P4 and P5: (a-b) 1D ^{1}H NMR spectra of either P4 or P5 in the presence of live *C. grubii* cells showed the line broadening effect of the peptides due to enhanced T_2 relaxation and concomitant appearance of newer peaks corroborating with the release of cellular metabolites. (c) On the contrary, P1 treated cells did not show any membrane lysis even after 2hr. Most importantly, the intensities of both P4 and P5 returned to their original unbound conformation, indicating significant cell killing and hence peptide dissociation from the cells. All the experiments were performed with Bruker Avance III 500 MHz NMR spectrometer at 298 K.

2.3.5. Membranolytic Activity of Designed Peptides: Live cell NMR

To provide auxiliary support to the dye leakage data, as well as to probe peptide-cell interaction at an atomistic level, we conducted live cell NMR experiments with bacterial and fungal cells, monitoring (i) line broadening effect of peptide depicting the peptide-cell interaction; and (ii) appearance of new peaks, analogous to the release of metabolites from wounded/dead cells. Addition of peptide solution to the microbial cells led to immediate line broadening of the ^{1}H signal due to enhanced T_2 relaxation of both the peptides. Additionally, chemical shift perturbation and reduction in resonance intensity in the amide, aromatic as well as methyl and other aliphatic regions of the NMR spectra were observed, giving clear indications for the interaction of the peptides (P4 and P5) with the microbial cells (Figure 2.8 a-b). Moreover, generation of new metabolite peaks distinctly supported the membranolytic mechanism of peptide action, causing cell death due to lysis. Interestingly, after several hrs. of co-incubation, the peptide resonance intensities substantially increased for both P4 and P5, as well as the line shape returned back to their respective initial phases, remarkably similar to those of the peptide alone, indicating substantial cell death and ensuing peptide dissociation from the cell (Figure 2.8 a-b).

In contrast, under similar conditions, P1 treated (Figure 2.8 c) and untreated cells (Figure 2.9) failed to show any such changes or release of metabolites, suggesting that the cells remain stable throughout the experiment.

Taken together, all the above data, obtained from live cell NMR and morphological changes using SEM, confirmed that the mechanism of action for the cell lysis by P4 and P5 is membranolytic.

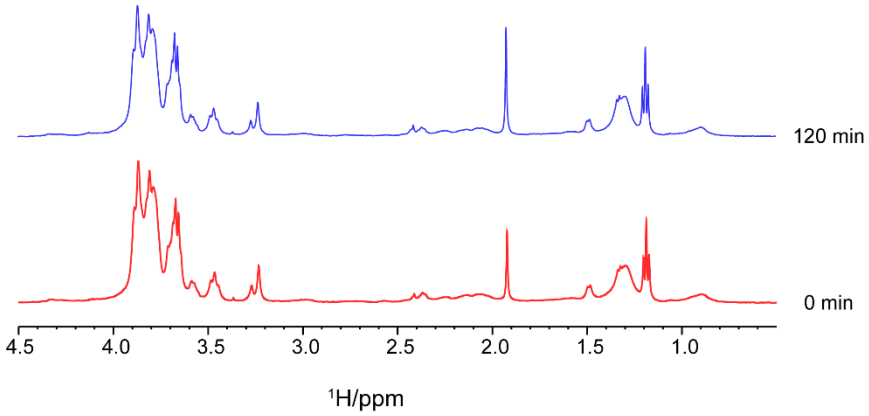

Figure 2.9. Live cell NMR of untreated cells. 1D ^{1}H NMR spectra of live untreated *C. grubii* cells neither exhibited the line broadening effect of the peptides nor showed appearance of newer peaks resulting from cell lysis and cellular leakage.

2.3.6. Secondary Structure of Designed AMPs through CD Spectroscopy:

Since the inner membrane of the bacteria is negatively charged in nature, a series of low- and high-resolution biophysical experiments were performed with negatively charged model membrane mimic (SDS) to understand the interaction between P4/P5 and the negatively charged bacterial membrane. To get preliminary idea regarding the secondary structure adopted by P4 and P5 in different membrane mimetic environments and a hint of interaction between the two, we performed circular dichroism experiment (Figure 2.10 a-b). The peptides P4 and P5 were seen to adopt random coil conformation in water. In the presence of 30 mM SDS, an anionic surfactant mimicking the negatively charged microbial membrane, the CD spectra of P4 and P5 changed slightly, with the appearance of a positive band at around 193 nm, red shift of the negative band at 196 nm to about 204 nm and the appearance of a negative shoulder at 218 nm. However, this CD feature could not be conclusively classified as any kind of well-defined secondary structure. A deviation in the secondary structure of the peptides P4 and P5 in the presence of SDS indicated some interaction between the two. It could be concluded that even though in the presence of SDS, there was a deviation from the typical random coil like

structure, peptides P4 and P5 did not adopt any well-defined secondary structure upon binding to the micelle.

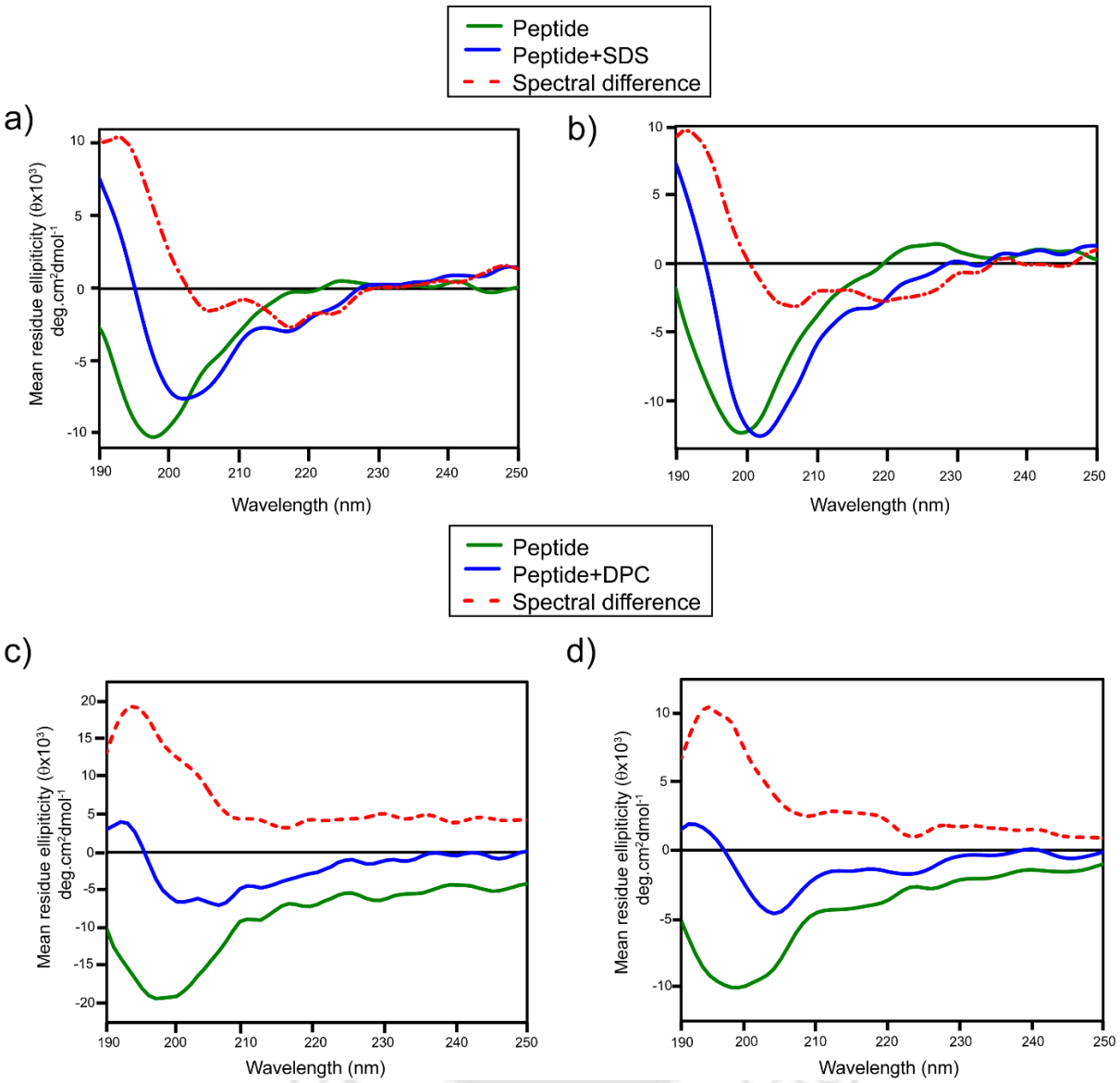

Figures 2.10. Structure of P4 and P5 studied using CD spectroscopy. CD spectroscopy in water (green) and SDS/DPC (blue) of a)/c) P4 and b)/d) P5. Difference spectrum is shown in red dotted line.

In order to further validate our finding, the CD spectra of P4 and P5 was also recorded in presence of 30 mM DPC micelle, a zwitterionic lipid micelle mimicking the zwitterion mammalian membrane. As seen in the figures 2.10 c-d, no significant change was seen in the structure of P4 and P5 in presence of DPC micelle, suggesting that there was probably no binding between the two.

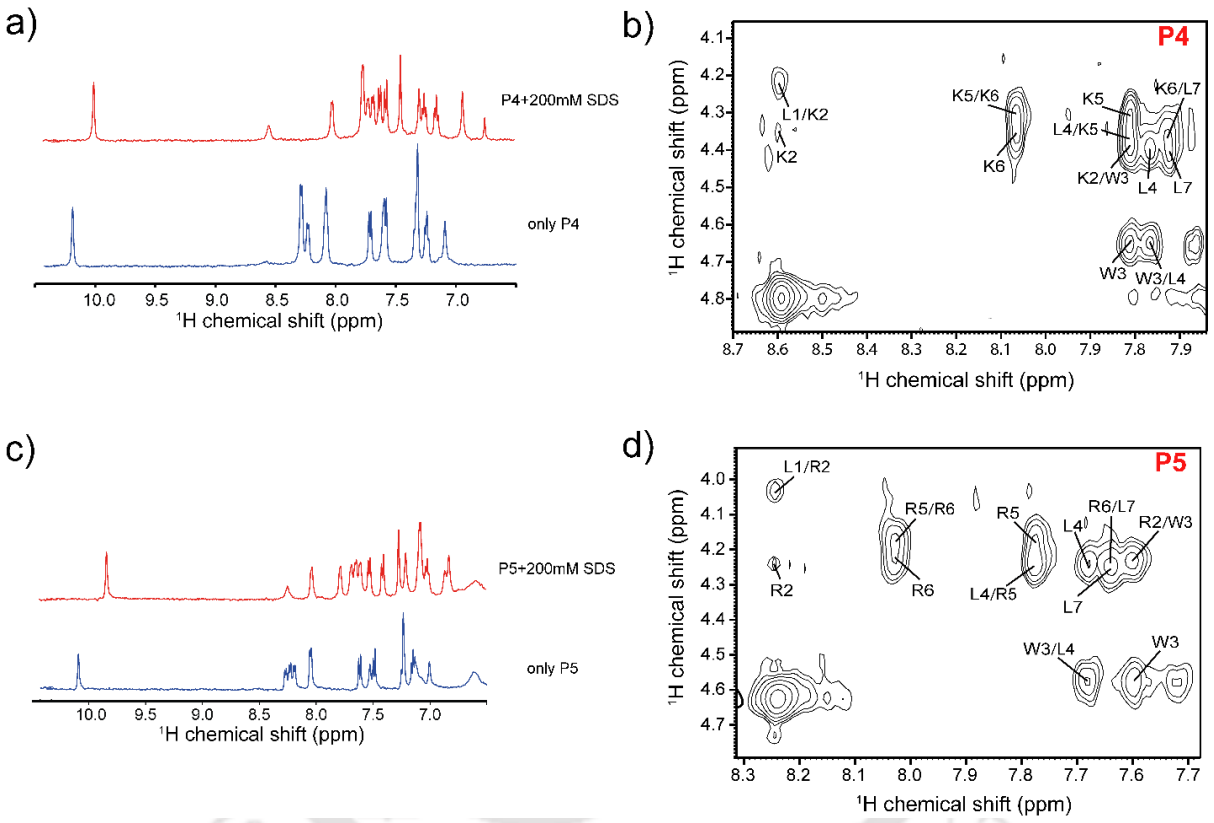

Figure 2.11. High resolution NMR spectroscopy of the peptides, P4 and P5: a), c) 1D ^{1}H NMR spectrum of P4 and P5 showed significant resonance broadening and chemical shift perturbation as well as newer peaks at all region of the spectrum, in presence of SDS micelles. The indole ring proton (NεH) of W5 underwent an upfield shift, indicating membrane acyl chain interaction. b), d) The 2D ^{1}H-^{1}H NOESY spectra, also showed the presence of all sequential and backbone peaks, however medium (i, i+2/i+3) and long (i, ≥i+5) range peaks were missing indicating that the peptide assumed a random coil orientation in SDS. The NMR

experiments were carried out using Bruker Avance III 500 MHz NMR spectrometer at 310 K. Peptides stock solution was prepared in water, pH 4.5.

2.3.7. Secondary Structure of Designed AMPs through NMR Spectroscopy:

Further, structure-function correlation for the activity of peptides P4 and P5 was obtained by recording one-dimensional ^{1}H NMR spectrum in the presence of perdeuterated SDS (d_{25}-SDS) micelles (Figure 2.11 a, c). SDS micellar system is a well-accepted membrane mimetic environment, and has been reported to be useful for studying interaction and structure of small membrane perturbing peptides, as it forms smaller micelles having faster tumbling and T_2 relaxation[501] at high temperature. One-dimensional ^{1}H NMR spectrum of both peptides in the presence of 200 mM SDS micelles showed significantly dispersed proton resonances, which were well resolved, signifying the binding of the peptide to negatively charged membrane. The indole ring proton (NεH) of W3, resonating at approximately 10.17 ppm showed an upfield shift, which might indicate the interaction of W3 with the acyl chain of the SDS micelle (Figure 2.11a, c). Such association could corroborate the bacteriolytic activity of these peptides. This prompted us to further probe the SDS micelle bound functionally active conformations of the two peptides using two-dimensional NMR spectroscopy.

In aqueous solution, the peptides, P4 and P5 lacked any medium or long range NOEs, indicating a random coil conformation. However, the NOESY spectra of both peptides in SDS micelle exhibited the presence of sequential αN (i, i+1) as well as NH/NH (i, i+1) NOEs for all the residues (Figure 2. 11 b, d). The absence of medium (i, i+2/i+3), side chain/ side chain or side chain/NH and long range (i, ≥i+5) NOEs for the residues confirmed that P4 and P5 adopted a random coil conformation in SDS micelle. Due to absence of signature NOEs, it was difficult to determine the exact secondary structure assumed by the two peptides in micelle

environment. Taken together, the peptides P4 and P5 did not adopt any classical secondary structure in association with SDS micelles.[502]

2.3.8. Residue Specific Peptide: Membrane Mimic Interaction by PRE NMR:

To probe the residue-specific membrane bound orientation of the peptides in SDS and DPC micelle, PRE NMR was performed.[503] For this, manganese chloride ($MnCl_2$), containing five unpaired electrons, was used as the paramagnetic probe. T_2 relaxation rate of solvent-exposed residues were selectively quenched while those which were solvent shielded residues interacting with the hydrophobic core of the micelles and thus in close proximity to the membrane mimic, were not quenched. The PRE spectra for both P4 and P5 did not show significant broadening of the Hx/NH protons (where x=α, β, γ, or δ protons, respectively) (Figure 2.12 a-b) in the presence of 0.1 mM $MnCl_2$, indicating a stabilised interaction of the peptides with SDS micelle. However, in case of P4, with increasing concentration up to 0.5 mM of $MnCl_2$ significant quenching for specific residues was observed (Figure 2.12 a). This clearly gave an indication for a sequential or step-wise insertion of the peptide into the SDS micelles. As shown in Figure 2.12a, the N-terminal region of P4 comprised of residues K2 and W3 were comparatively less quenched for Hα/NH peaks in comparison to other residues. In addition, the aromatic or CβHs/NH peaks of W3 did not quench even in the presence of 0.5 mM $MnCl_2$, indicating their direct interaction with the acyl chain of the SDS micelle. In contrast, the aliphatic side chains (especially CγHs/NH and CδHs/NH) of the cationic residues, K2, K5 and K6 showed prominent quenching (Figure 2.12 a), suggesting the side chain atoms of Lysine residues were exposed to solvent for either strong electrostatic or hydrogen bond interaction between positively charged $–NH_3^+$ and negatively charged SDS head group.

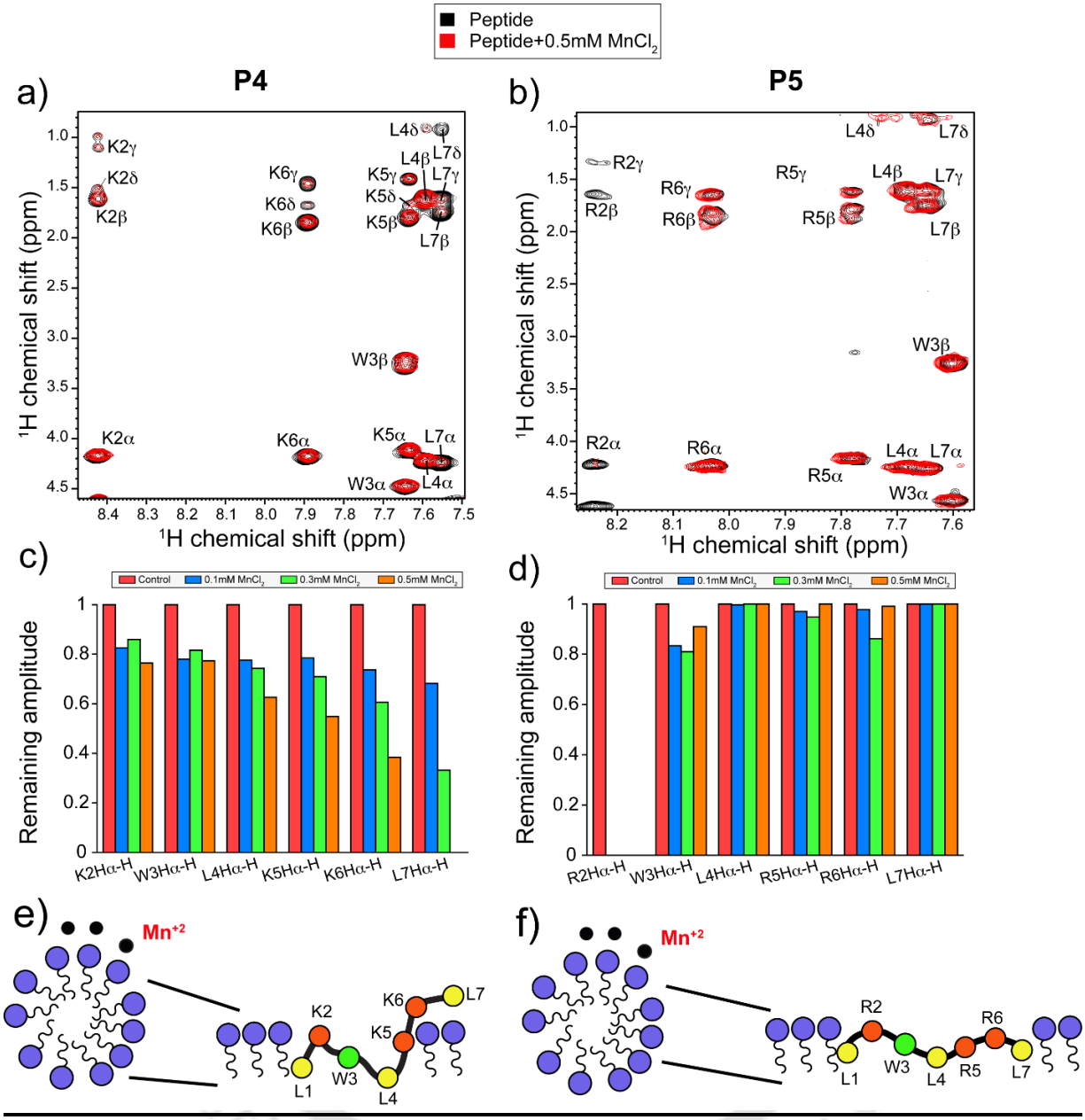

Figure 2.12. Solvent accessibility of the peptides, P4 and P5: a), b) Two-dimensional ^{1}H-^{1}H TOCSY NMR spectra of P4 (left panel) and P5 (right panel) in perpetuated SDS micelle, in the absence (black contour) and presence of $MnCl_2$ (red contour). c), d) Plot showing the relative change of intensities of Hα/NH cross peaks of P4/P5 bound to SDS in the presence of $MnCl_2$. e), f) Schematic representation of the orientation of the two peptides in SDS membrane. All data were recorded in Bruker Avance III 500 MHz NMR spectrometer and at 310 K.

In case of peptide P5, no significant Hα/NH quenching were observed for majority of residues except R2, even in presence of 0.5 mM of $MnCl_2$. However, the CβHs/NH and CγHs/NH of R5 and R6 did show some quenching in the presence of $MnCl_2$. This observation clearly justified the fact that the net positive charge due to guanidium group of Arg residues provided preferential interaction property with the negatively charged membrane *via* formation of stronger electrostatic and hydrogen bond interactions when compared to the $-NH_3^+$ group of Lys.[504] Such interactions played a primary role in promoting the anchoring of the peptide moiety to the microbial membrane by facilitating hydrophobic contact between the hydrophobic/aromatic residues and the acyl side chains of the micelles. This further helped in justifying the higher reported antimicrobial and dye-leakage activity of P5 when compared to P4.

In contrast, the PRE spectra of P4 and P5 in presence of DPC micelle was quenched almost completely, illustrating very weak to no interaction between the peptides and the zwitterionic model membrane (Figure 2.13). In other words, the data indicated that both the peptides P4 and P5 were mostly solvent exposed. However, transient electrostatic interactions cannot be ruled out. As the AMPs were unable to bind with the mammalian model membrane mimic, it could be concluded that the AMPs were non-cytotoxic, which supported our earlier conclusions from the cell viability studies.

2.3.9. Structure Determination and Peptide: Membrane Interaction Studies through MD Simulations:

To probe this interaction further, we performed MD simulations with three different N-terminal protonated peptides P4, P5, P6 in presence and absence of SDS micelles.

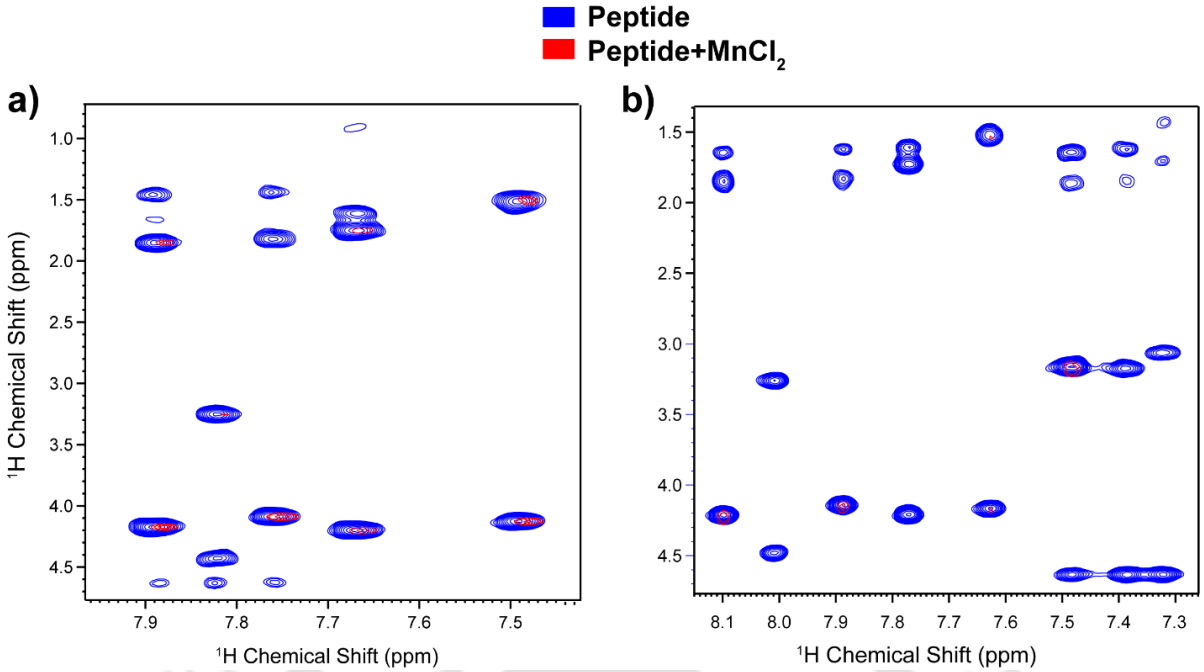

Figure 2.13. Solvent accessibility of the peptides, P4 and P5 in DPC micelle: Two-dimensional ^{1}H-^{1}H TOCSY NMR spectra of (a) P4 and (b) P5 in perpetuated DPC micelle (black contour) and in the presence of $MnCl_2$ (red contour). The experiment was recorded using a Bruker Avance III 500 MHz NMR spectrometer and at 310 K. Most of the cross-peaks (including Trp) broadened in the presence of 0.1 mM $MnCl_2$ solution. The data conformed that the peptides were mostly solvent exposed in DPC micelle.

Free peptides in aqueous environment showed various random coil conformations (Figure 2.14a), which validated the observation from NMR and CD. In order to understand the binding event, we carried out MD simulations with an initial configuration where peptides were placed 10 Å away from SDS micelle (Figure 2.1). The MD trajectory analysis suggested that peptides started interacting with micelles within ~ 1 ns and a stable bound conformation (Figure 2.14 b) was attained within ~ 15 ns, which remained stable throughout the molecular dynamics trajectory (total ~ 50 ns). SDS bound peptides sampled limited conformational space or attained a specific conformation with respect to the flexible random coil SDS free state (Figure 2.15).

Though the conformation of micelle bound peptide was distinct and stable, it could not be categorized as any classical secondary structure.

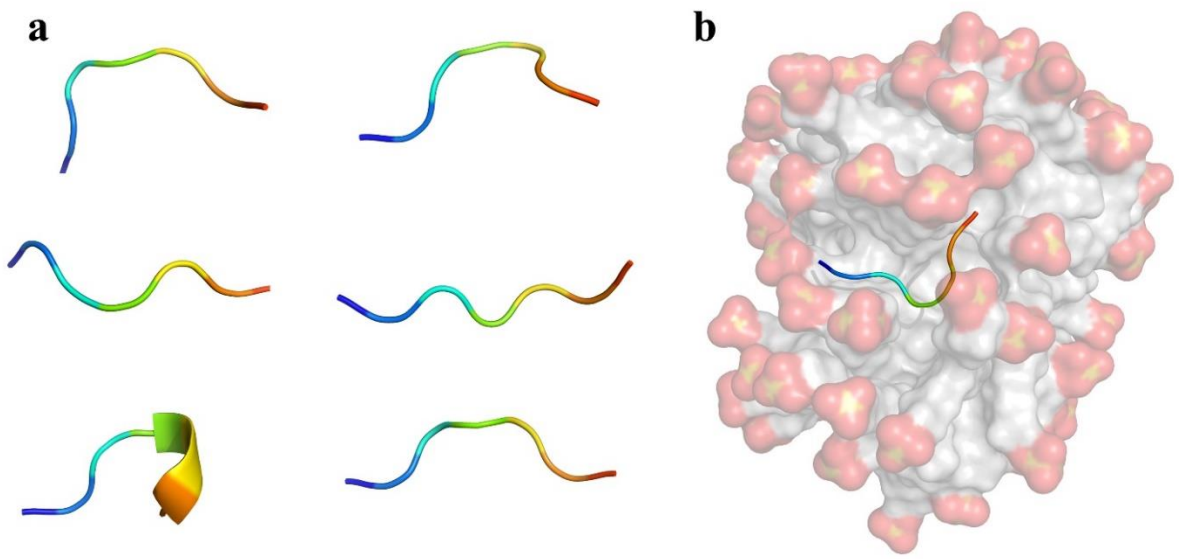

Figure 2.14. Structure from molecular dynamics trajectory. (a) Few representative random coil structures of peptide P4 in water, (b) SDS Micelle bound P4 peptide conformation after 50 ns of molecular dynamics run. N-terminal has been colored blue and C-terminal red in the peptide (cartoon); SDS micelle (surface and lines) has sulfates in red and aliphatic side chain in grey. Hydrogens are not shown for clarity.

The binding of the peptide to the SDS micelle followed a sequential order (Figure 2.16). At first, the positively charged peptide landed on the surface of negatively charged SDS micelles through electrostatic interaction. Subsequently, the SDS bound peptide was further stabilized by hydrophobic interaction between neutral side chains of the peptide and aliphatic chain of micelle, leading to a local deformation on micelle surface.

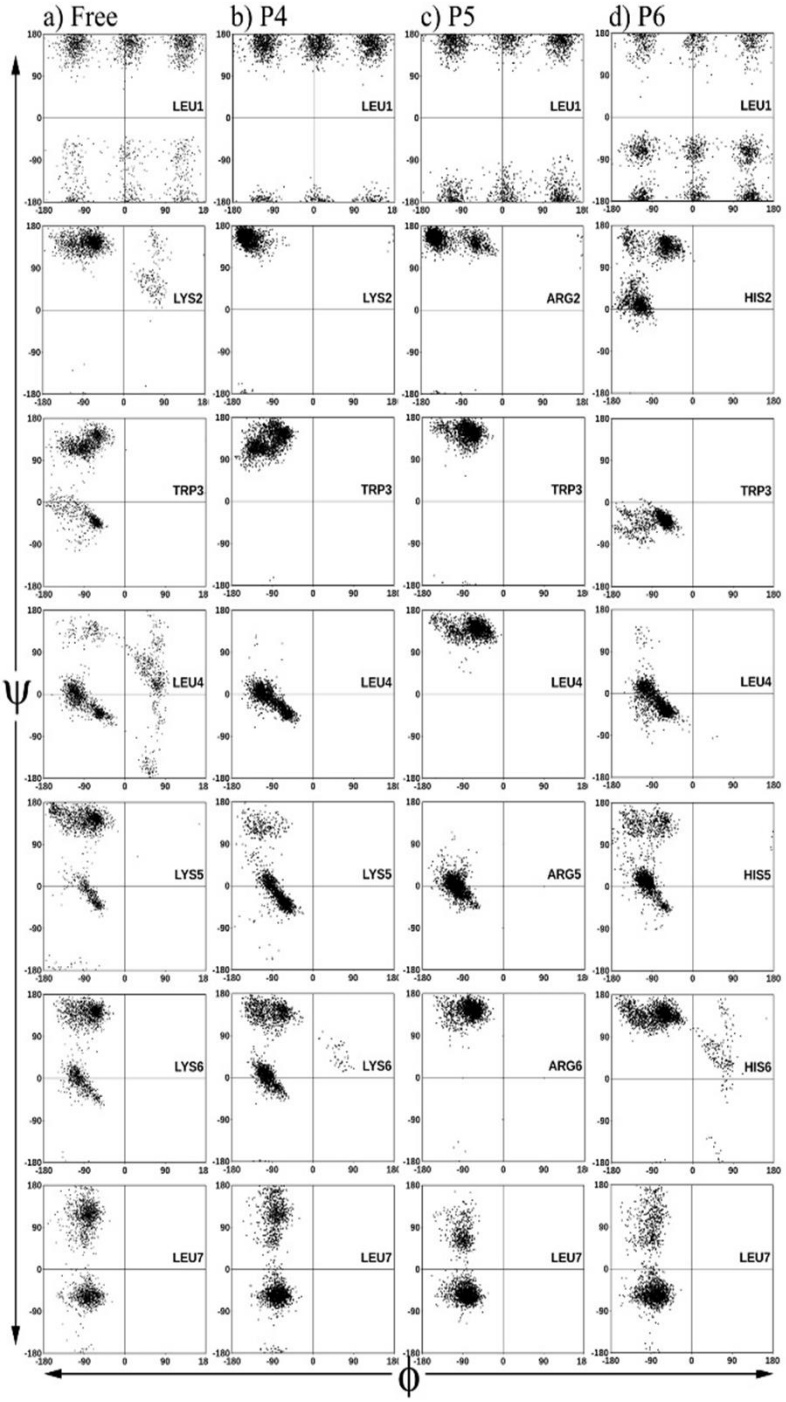

Figure 2.15. Residue specific Ramachandran Map for a) Free P4, SDS micelle bound b) P4, c) P5 and d) P6, indicating the flexible conformation of P4 in Free State vs the fixed random coil conformations of P4, P5 and P6 upon binding to SDS during the MD trajectory.

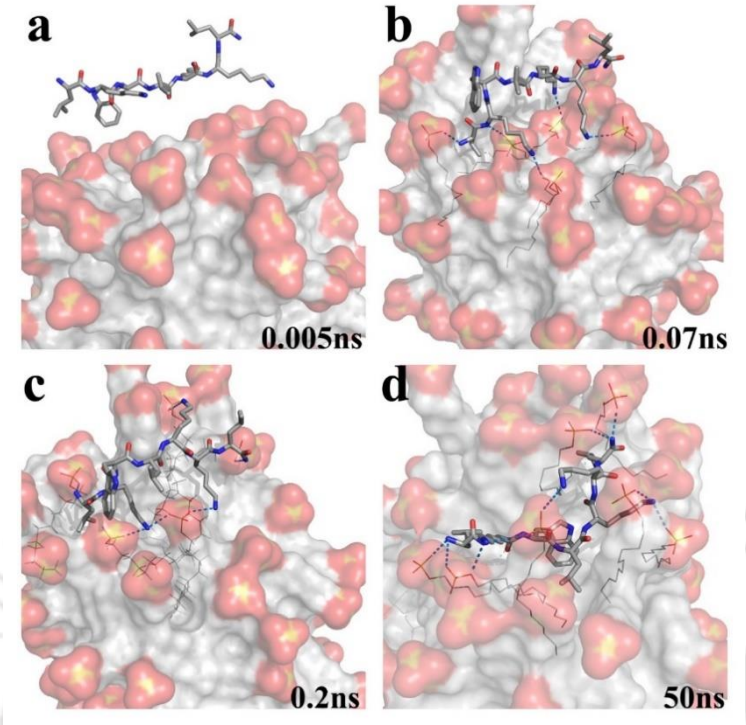

Figure 2.16. MD Snapshots of peptide (sticks, NH_3^+-LKWLKKL-$CONH_2$: Model I) binding to SDS micelle (surface and lines). a) Peptide approaching to micelle at 5 ps, b) anchoring interaction between peptide and micelle is established at 0.07 ns, c) hydrophobic interaction along with the electrostatic anchoring could be seen at 0.2 ns, d) representative snapshot at 50 ns describing stable conformation of peptide bound to the micelle.

Peptide backbone satisfied its hydrogen bond requirement by interacting with waters and/or sulfates of SDS micelle. Micelle-peptide interaction has been shown in Figure 2.17 a-c for P4, P5 and P6 respectively.

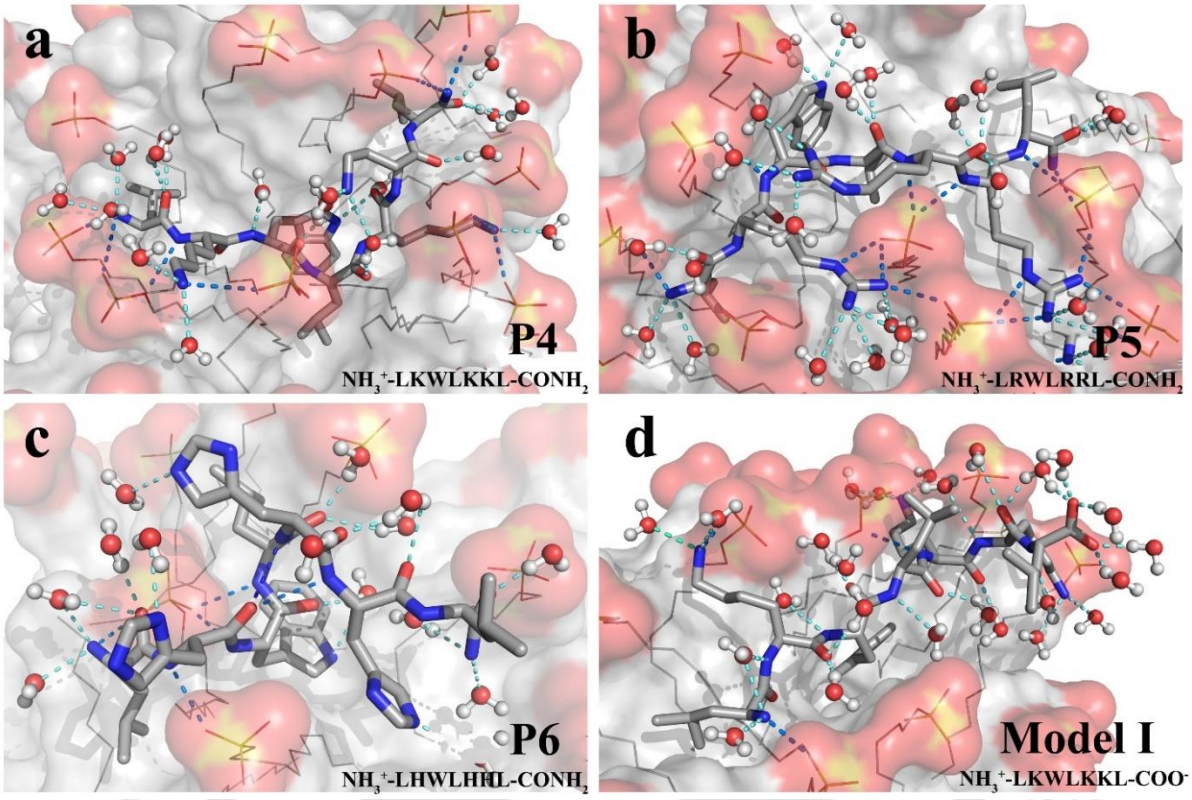

Figure 2.17. MD snapshot describing the electrostatic, hydrophobic and hydrogen bonding interactions between peptide and micelle. Water as ball and stick, micelle as surface and lines, peptide as stick. Only water hydrogens are shown. Oxygen is red, Nitrogen is blue and carbon is gray. a) P4 bound micelle, b) P5 bound micelle, c) P6 bound micelle and d) peptide with deprotonated carboxy terminal $–COO^-$ (derived from P4) bound to micelle.

Similarly, side chain residues of L1, W3 and L4 in P5 were buried inside the micelle, whereas L7 was present at the membrane water interphase (Figure 2.17b). R2, R5, R6 side chains of P5 formed anchoring interaction by direct and water mediated interactions with sulfates of micelle (Figure 2.17b). In case of peptide P6, only L1 and W3 primarily formed hydrophobic interactions with aliphatic side chains of the micelles (Figure 2.17c). The hydrogen bond requirement of peptide backbone was satisfied by interaction with water molecules and/or sulfate of micelles. Interaction area between the peptides and SDS micelles were ~ 753 (±92)

$Å^2$, 778 (±108) $Å^2$ and 519 (±66) $Å^2$ for P4, P5 and P6, respectively. Lack of positively charged side chains (Neutral His has pka ~ 6.0) in P6 was responsible for lowest interaction area.

In order to understand the role of the C-terminal end of the peptides, in their interaction with SDS micelle, we performed simulations with a peptide containing $-COO^-$ terminus (Model I, Figure 2.17d). Model I was similar to P4, differing only at the C-terminal end with a carboxyl group instead of the amide ($-CONH_2$) group. The C-terminal end of Model I lost its interaction with micelles due to electrostatic reasons. The calculated area of interaction for Model I was ~ 670 (±88) $Å^2$. This proved that electrostatic interaction between peptide and the micelle was crucial for initial binding. The removal of positive charge (as in P6) or deprotonation of the carboxyl group at the C-terminal end (as in Model I) led to poor association, which was reflected in the poor anti-microbial activity of P6 and P1-3, respectively (Table 2.2).

To prove our point further, we performed MD simulation with P4 in the presence of DPC micelle, a neutral lipid mimicking the zwitterionic mammalian membrane. It is interesting to note that P4 could not bind with dodecylphosphocholine micelles (DPC) even after 50 ns of dynamics due to electrostatic reasons. This clearly proved that electrostatic interaction was the primary and crucial interaction between the peptide and the membrane-mimic (SDS/DPC). Trp residue W3 in both P4 and P5 was seen to be buried in the hydrophobic core of the SDS micelles from MD simulations and PRE NMR experiments. Significant blue shift in the fluorescence emission of the two peptides (Figure 2.18) in presence of SDS (about 9 nm in case of P4 and 11 nm in the case of P5) supported our claim for the burial of the Trp residue within the hydrophobic core of the SDS micelle. This might be the second additional drive for the interaction of P4 and P5 with the membrane and hence their activity.

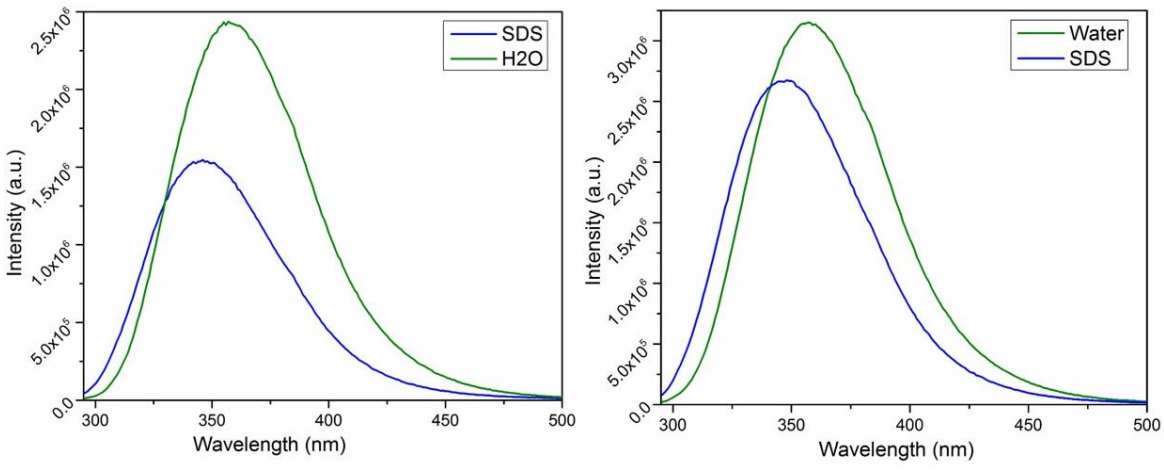

Figure 2.18. Trp emission spectra for a) P4 and b) P5 in water (green line) and in the presence of 30 mM SDS (blue line).

2.4. Conclusion

In this chapter, we have developed two small economically viable cationic peptides P4 and P5 with broad-spectrum antimicrobial activity against various members of ESKAPE group of pathogens and fungal strains like *C. albicans* and *C grubii*. P4 and P5 retained their anti-fungal activity in the presence of physiological salt conditions. They were anti-hemolytic and non-cytotoxic to human cells making them potential therapeutic agents. Between the two AMPs, P5 was found to be more active than P4 against all the strains tested, in the presence and absence of salt. We established that our active peptides P4 and P5 employed a primary membranolytic mode of action by conducting spectroscopic and microscopic experiments with membrane mimics as well live microbial cell. Selective binding of these cationic AMPs with the negatively charged microbial membrane mimic, SDS micelles in comparison to the zwitterionic DPC micelles indicated, that electrostatic interactions were of primary importance in the AMP: membrane mimic binding. Free carboxy terminus and His containing AMPs had

reduced charge and hence lesser surface area of interaction with the SDS micelles as seen from the MD simulations. The peptide membrane interaction was established to be sequential in nature. The initial binding was guided by the electrostatics in between the cationic AMPs and the negatively charged microbial membrane. This was followed by the hydrophobic interactions in between neutral side chains of AMPs and the acyl chains of the SDS. The Trp residue was found to be solvent shielded and hence was assumed to play an important role in the peptide binding. Free peptides were flexible in water and adopted random coil conformation. In the presence of SDS micellar system, the available conformational space reduced for these peptides and a specific conformation bound to the membrane mimic. However, this bound conformation could not be classified as any well-defined secondary structure. This indicated that secondary structure was not essential for the activity of the AMPs. Such fundamental understanding of the mechanism of action and the peptide membrane interactions will definitely stimulate the design of better antimicrobial agents in the future.

Chapter 3

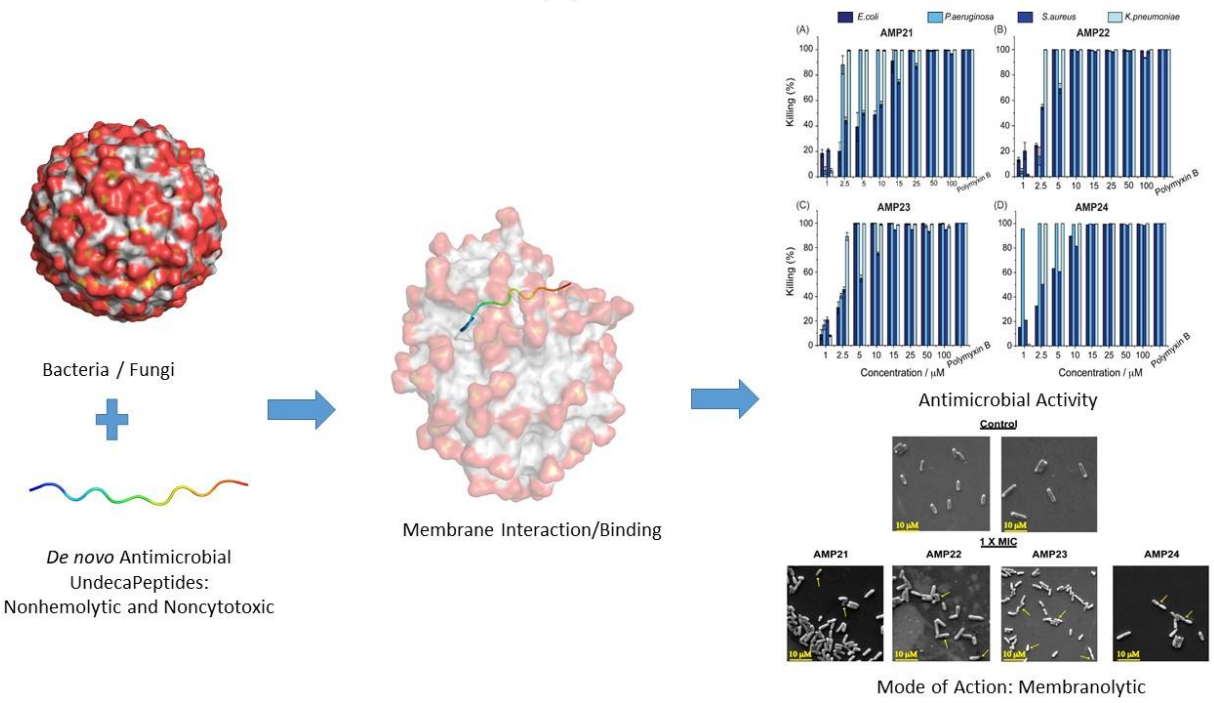

Rationally Designed AMPs: Insight into the Mechanism of Eleven Residue Peptides against Microbial Infections

3.1. **Introduction:**

In the last chapter, we developed heptapeptide AMPs with moderate activity against broad-spectrum of microbes. In this present study, we intended to improve on the activity of the designed AMPs by incorporating an active tetra peptide sequence from the natural AMP human lactoferrin into P4 (AMP21), developed in the earlier study. Later AMP21 was further modified to generate AMP22-24 by (Table 3.2) using an educated guess based on the existing literature. AMP21-24 possessed much higher activity in comparison to P5. AMP21-24 possessed broad-spectrum antimicrobial properties against *E. coli* DH5α as well as various pathogens from the ESKAPE group like *S. aureus, K. pneumoniae, P. aeruginosa* and also fungal strains like *C. albicans* and *C. neoformans var. grubii*. We have used various spectroscopic, biophysical and molecular dynamics simulation techniques to delineate the structure, membrane interactions and the mode of action of these AMPs.

3.2. Experimental Section:

Peptide synthesis and purification of the AMPs21-24 was done using standard SPPS and reverse phase semi preparative HPLC using ACN-H_2O gradients as discussed previously (Section 2.2.2.). The purity of the peptides was checked using Analytical HPLC (Appendix, Figure A6, A7) and they were characterized thoroughly using ESI-MS (Appendix, Figure A24-A31) and ^{1}H NMR (Appendix, Figure A46-A49).

3.2.1. Micro broth Dilution Assay:

Antimicrobial activity of the AMP21-24 was studied in the absence and presence of 150 mM sodium chloride (NaCl) using standard micro dilution broth assay[60] as described earlier (Section 2.2.5.).

3.2.2. Cell Viability and Hemolysis Assay:

MTT assay was performed as described earlier for AMP21-24 to determine their cytotoxicity towards the mammalian cell line L132 (Section 2.2.7.). Activity of AMP21-24 against human RBCs was determined both quantitatively using hemolytic assay as described earlier (Section 2.2.6.).

3.2.3. AMPs-Membrane Mimetic Interaction: Tryptophan Fluorescence Measurements:

Intrinsic fluorescence of tryptophan (W5 and W7) of AMP22 in 10 mM phosphate buffer and D8PG and DPC were recorded by using Hitachi F-7000 FL spectrophotometer (Tokyo, Japan). The intrinsic Trp-fluorescence emission spectra of 10 µM peptide upon titration with increasing concentration of D8PG and DPC ranging from (10 µM to 100 µM) from 6 mM stock was measured at an emission spectral range of 300-400 nm using an excitation wavelength of 295 nm, and excitation and emission slit of 2.5 nm. All the fluorescence experiments were performed at 25°C in a quartz cuvette of path length 0.1 cm.

Solvent accessibility of AMP22 in the vicinity of D8PG was determined by fluorescence quenching experiments. A static quencher, acrylamide (stock solution of 10 M) was added to the peptide-D8PG complex as well as free peptide solution upto 0.25 M. The resultant fluorescence intensity of the peptide was analyzed by fitting to Stern-Volmer equation.

$F_0/F = 1 + K_{SV}[Q]$

Where, F_0 denotes initial fluorescence intensity in absence of the quencher. F stands for the fluorescence intensity at each quencher concentration [Q] denoted in terms of molarity. K_{SV} represents the Stern –Volmer Quenching Constant expressed in M^{-1} calculated from the above equation, both in free and bound state of AMP22.

3.2.4. Isothermal Titration Calorimetry (ITC):

The binding interaction of AMP22 and AMP24 with D8PG was assessed using TA-affinity ITC (TA Instruments, New Castle, USA). Peptide and D8PG stocks were prepared in 10 mM

phosphate buffer (pH 7.4). The buffer, peptide stocks as well as D8PG stock were degassed. A 182 µl sample cell containing 0.5 mM peptide concentration was titrated with D8PG from a stock solution of 25 mM at 310 K and stirring speed of 75 rpm. A total of 20 injections, at an interval of 180 s with 2 µl of D8PG aliquots per injection were performed. Nano Analyze 3.7.5 software was used to plot the raw data. Each plot was fitted using a nonlinear equation, and an independent binding site model was utilized to analyze number of binding sites (n) and the thermodynamic parameters, which include dissociation constant (K_d), change in enthalpy (ΔH), free energy of binding (ΔG) and entropy (ΔS).

$\Delta G = -RT \ln K_a$ and $\Delta G = \Delta H - T\Delta S$.

3.2.5. Calcein Leakage Assay:

The calcein dye leakage assay was performed to investigate whether the AMP22 and 24 were membranolytic in their mechanism of action. Calcein loaded LUV's that mimicked the bacterial cell membranes (3:1 POPE/POPG, 25 mg/ stock solution for each) and fungal cell membranes (5:4:3 POPC/POPE/Ergesterol, 25 mg/ stock solution for each) were prepared and calcein leakage of from them in the presence of AMP22 and AMP24 was performed as described in a process detailed earlier in Section 2.2.8.

Time kinetics of calcein release upon treatment with test peptides were also carried out maintaining similar conditions. Calcein release from free unilamellar vesicle was performed for 60 min and the change in fluorescence intensity was monitored to check the stability of the formed vesicles. Test peptides were then titrated at selected concentrations and change in emitted fluorescence intensity was observed for 60 min at 519 nm.

3.2.6. Live Cell NMR Spectroscopy:

For further detailed study of the atomic level killing of *P. aeruginosa* upon treatment with AMP22 and AMP24, live cell NMR experiments were carried out as discussed earlier[505] to

monitor the broadening of ^{1}H proton resonances of peptide on interaction with *P. aeruginosa* cells and subsequently time-dependent release of metabolites from the injured cells.

Overnight grown cultures of *P. aeruginosa* were used to obtain mid-logarithmic culture. The culture was centrifuged at 5500 rpm for 5 minutes and the pellet was washed thrice in phosphate buffer (pH 6.5) followed by resuspension in the same buffer to obtain a cell suspension containing 10^{8} CFU/.

1 mM peptide stock solution of AMP22 and AMP24 was prepared in 90% phosphate buffer (pH 6.5) and 10% D_2O and one-dimensional proton NMR spectra of the peptide along and in presence of live cell was recorded on a Bruker Avance III 500 MHz NMR spectrometer. The temperature for each experiment was adjusted as per the growing condition of *P. aeruginosa* (310 K). A series of 1D ^{1}H proton NMR spectra was recorded of the peptides in presence of live cells.

3.2.7. Assay of Membrane Permeabilization:

Overnight grown cultures of *P. aeruginosa* cells and *C. albicans* were used to obtain mid-logarithmic phase**.** The cells were washed in sodium phosphate buffer (pH 7.4) and resuspended in the same to obtain a concentration of 10^{6} CFU/ and 10^{5} CFU/ for *P. aeruginosa* and *C. albicans* respectively. 10 µM Propidium Iodide (PI) dye was added to 1 of the cell suspension and incubated at room temperature for 30 min under shaking conditions. The fluorescence of the dye was measured at 298 K for 40 min at an excitation wavelength of 535 nm (slit width: 10 nm) and emission wavelength of 617 nm (slit width: 10 nm) using Hitachi F-7000 FL spectrophotometer. The fluorescence intensity of the free cell suspension was monitored for any fluctuations in the intensity to test the stability of the cells. After a stable intensity was obtained addition of our designed peptides to the bacterial and fungal suspension was followed. An increase in dye fluorescence was indicative of permeabilization of the inner

membrane. Hence, this indicated the active interaction of our peptides with the cell membrane of the microorganisms, which further allow the permeabilization of PI into the cells and bind with the DNA, resulting the increase in the fluorescence intensity.

3.2.8. Assay of Depolarization of Cytoplasmic Membrane:

Overnight grown cultures of *P. aeruginosa* cells and *C. albicans* were used to obtain mid-logarithmic phase. *P. aeruginosa* culture was centrifuged at 5500 rpm, washed thrice with 5 mM HEPES buffer (pH 7.4) and resuspended in the same to obtain a cell suspension of 10^6 CFU/. Measurements were recorded in a cuvette containing 600 µl bacterial suspension and 1 µM 3,3'-Dipropylthiadicarbocyanine Iodide ($DiSC_3$) dye using Hitachi F-7000 FL spectrophotometer. In case of *C. albicans,* the overnight culture was centrifuged at 5500 rpm for 5 min and the pellet was washed with 5 mM HEPES buffer thrice. The washed pellet was re-suspended in the same buffer and a cell suspension of 10^5 CFU/ was obtained. 1 µM $DiSC_3$ was added to the cell suspension and incubated at 37º C for 90 min. The fluorescence of the dye was measured at 298 K for 40 min at an excitation wavelength of 622 nm (slit width: 10 nm) and emission wavelength of 670 nm (slit width: 5 nm). After reaching the maximum uptake of the dye by the bacteria and the fungus, which is the resultant of membrane potential, an indication of minimum in dye fluorescence was observed.[466] This was followed by addition of our designed peptides to the bacterial and fungal suspension. An increase in dye fluorescence was indicative of decrease in membrane potential.

3.2.9. Field Emission Scanning Electron Microscopy (FESEM):

Effect of AMP21-24 (at their respective 1X and 2X MIC) on the *P. aeruginosa* cells was visualized through FESEM in a process described earlier (Section 2.2.13).

3.2.10. Confocal Laser Scanning Microscopy (CLSM):

C.albicans cells were grown overnight to obtain mid-log phase. The culture was then centrifuged at 5500 rpm for 5 min followed by washing the pellet thrice in phosphate buffer (pH 7.4). Resuspension was done in the same buffer to obtain a cell suspension of 10^6 CFU/. The cell suspension was treated with carboxyfluorescein tagged peptide at a concentration of 10µM and incubated for 10 min at 28ºC. Clean glass slides were taken and 3 µl of sample was dropped on the slide and covered with coverslip. Untreated cell was taken as control. Fluorescent and differential interference contrast images were captured with a 488 nm band-pass filter for excitation of carboxyfluorescein using a No. TCS SP8 confocal microscope (Leica, Wetzlar, Germany) at a magnification of 63 ×(oil immersion) having a numerical aperture of 1.4. Acquisition Suite X software (Leica) was used for capturing images.

3.2.11. Molecular Dynamics (MD) Setup for Micelle (SDS, DPC), Bilayer (Coli*, Albi*) in Water:

CHARM-GUI membrane builder was used to model micelles (SDS, DPC), bilayers (mimicking *E. coli* and *C. albicans* lipid profile) and prepare the GROMACS input files.[470,486,506,507] 100 SDS and DPC molecules were considered for initial structural model of micelle. DPC micelle was neutral due to the zwitterionic nature of monomer (dodecylphosphocholine) units (Figure 3.13). SDS being negatively charged, 100 Na^+ counter ions were added for charge neutrality.

In order to mimic *E. coli* and *C. albicans* membranes, we considered only the major phospholipid compositions[421,508] of few important lipids and built models of bilayer for studying the peptide bilayer interactions. *Escherichia coli* membrane mimic bilayer (Coli*) was prepared by considering dielaidoylphosphatidylethanolamine (DEPE) and dioleoylphosphatidylglycerol (DOPG) in a ratio of 8:1.5.[507] Each layer of Coli* was composed of 160 DEPE and 30 DOPG molecules (Figure 3.13). *C. albicans* membrane mimic bilayer

(Albi*) was prepared by considering four key lipid molecules (Figure 3.13), phosphatidylcholine (PC), phosphatidylethanolamine (PE), phosphatidylinositol (PI), and ergosterol in a ratio of 5:4:1:2.[421] Each layer of Albi* was composed of 100 POPC, 80 POPE, 20 POPI and 40 ergosterol molecules (Figure 3.13). Na^+ counter ions were added to maintain charge neutrality for our simulation models.

Keeping micelle/bilayer at the center, a water box of dimension 12×12×12 nm^3 was overlaid and subjected to energy minimization. The energy minimized geometry was considered for MD simulations using GROMACS software.[486,506] Micelles and bilayers were equilibrated for 12 ns at 300 K. Equilibrated structures of micelles/bilayer were then used for peptide-lipid interaction studies. MD simulations considered total of 169952, 170353, 100954 and 121780 atoms for SDS, DPC, Coli* and Albi* in water, respectively.

3.2.12. Modeling of AMPs in Water:

Linear chain of 11 residue peptides (AMP21, AMP22, AMP23 and AMP24) were modelled using PyMOL software.[509] N- and C-terminal of peptides were modelled as $-NH_3^+$ and $-CONH_2$, respectively. MD study considered standard protonation states corresponding to neutral pH=7 for the ionizable side chains. Water box (dimension 8x8x8 nm^3) centered at the liner peptide chain was overlaid. In the next step, energy minimization followed by MD simulations were performed. Total ~50850 atoms were considered for simulations of free peptides in water.

3.2.13. MD Setup for AMP–Micelle/Bilayer Simulation:

Micelles/bilayer structures were taken from equilibrated water solvated MD simulations. Linear peptides were initially placed ~10-15 Å away from the surface of the equilibrated micelles/bilayer, re-solvated with water box (dimension 12x12x12 nm^3) centered at the micelles/bilayer and subjected to energy minimization and subsequent MD simulations (Figure 3.1). More than 100000 atoms were considered for simulating AMP-SDS, AMP-DPC, AMP-Coli* and AMP-Albi* systems (Table 3.1). Energy minimization (step size of 0.01 nm and ~50000 steps, steepest descent algorithm followed by MD simulation) was performed using CHARMM36 force field.[510,511] Temperature and pressure of the simulation system were kept fixed at 300 K and 1 bar, respectively. Electrostatic interactions were computed using the particle-mesh Ewald algorithm.[512] Temperature and pressure were controlled by Berendsen thermostat[496] and Parrinello-Rahman[497,513] algorithms, respectively. MD simulations were performed with 2 fs time step and van der Waals cutoff of 12 Å. A total of 50 ns of simulation was performed for each model system. Water was modeled using TIP3P water model.[514] Output data were analyzed using GROMACS utilities. Cutoff heavy atom distance (Donor-Acceptor =0.35 nm) and angle (Hydrogen-Donor-Acceptor = 30^0) was considered for hydrogen bond calculations. The area of interaction between peptide and micelle/bilayer was defined as = (SASA of peptide + SASA of micelle or bilayer –SASA of complex)/2, where SASA = solvent accessible surface area. Total number of hydrogen bonds, interaction area and RMSF (root mean square of fluctuation) were calculated for each snapshot (every 1 ps interval) of the last 20 ns trajectory from 50 ns MD. The MD averaged results (hydrogen bonds, interaction area, peptide RMSF) are reported in this manuscript.

Table 3.1: Total number of atoms considered as in our MD simulations of peptides in free and micelle/bilayer bound water simulations

Box Dimension (nm^3)	**FREE** 8×8×8	**SDS** 12×12×12	**DPC** 12×12×12	**Coli*** 12×12×12	**Albi*** 12×12×12
AMP21	50850	169731	170137	103384	122092
AMP22	50863	169724	170125	100726	124587
AMP23	50836	169727	170108	103901	121762
AMP24	50837	169716	170115	103869	121574

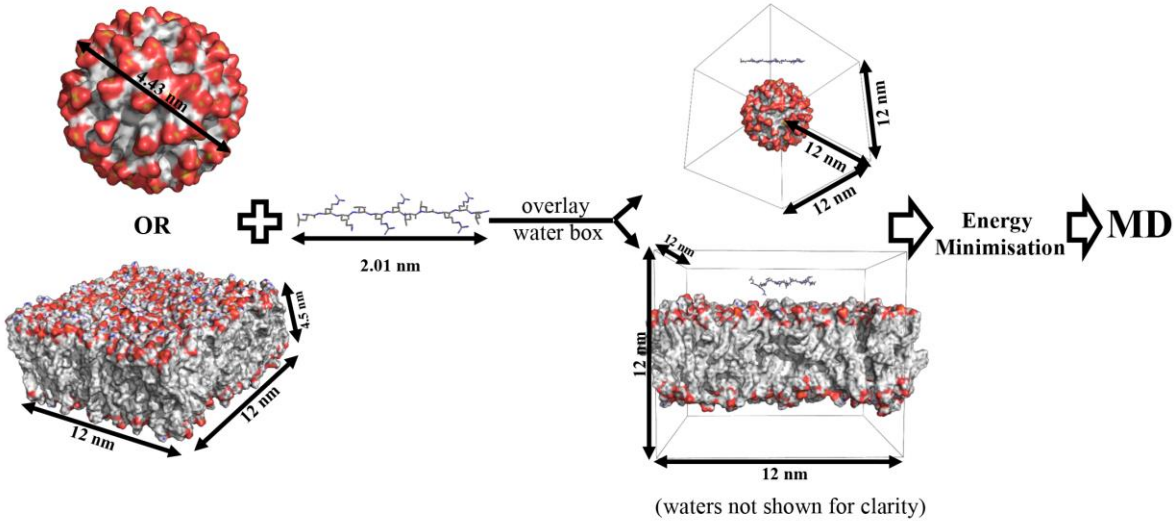

Figure 3.1. Scheme of our MD setup.

3.3. Results and Discussions:

3.3.1. Peptide Design:

Lactoferrin is an avidly iron-binding glycoprotein of the transferrin family with a N-terminus that possesses high antimicrobial activity against a broad range of Gram-positive bacteria, Gram-negative bacteria and fungi.[515] Proteolytic digestion of human lactoferrin in *in vitro* yields a peptide fragment[516] , which has enhanced antimicrobial activity due to presence of two cationic peptide fragments namely RRRR and RKVR. In this study, we incorporated RKVR fragment in an LR peptide (H-LRLLRRL-NH_2), which was shown to have potent antimicrobial properties in chapter 2 (AMP21). The peptides have been made rich in Arg residues, based on literature review of the guanidium group in the side chain of Arg being more potent in inducing antimicrobial properties than the primary amine present in the Lys. In AMP22, a basic Arg (R5) and a hydrophobic Leu (L7) residue of AMP21 have been replaced by Trp residue. AMP23 has been designed by substituting the Val (V4) residue of RKVR fragment with a Phe residue. AMP24 is derived from AMP21 by substituting all the hydrophobic and hydrophilic amino acid residues to Leu and Arg, respectively (Table 3.2).

Table 3.2: Peptide sequences with code.

Peptide Codes	Sequences
AMP 21	H-LRKVRRLLRRL-NH_2
AMP 22	H-LRKVWRWLRRL-NH_2
AMP 23	H-LRKFRRLLRRL-NH_2
AMP 24	H-LRRLRRLLRRL-NH_2

3.3.2. Antimicrobial Property of AMP 21-24:

The peptides AMP21-24 showed high potency against both Gram–negative bacteria like *E. coli*, *P. aeruginosa* and *K. pneumoniae* as well as Gram–positive bacteria like *S. aureus.* (Table 3.3). ESKAPE pathogens have been reported to be majorly involved in various nosocomial infections and are also responsible in escaping the biocidal action of various existing antimicrobial agents.[517] *P. aeruginosa* mainly owes its antigenic property to its alginate capsule which forms an extra-cellular matrix that not only hinders the entry of the various antimicrobial agent but also assists in the formation of biofilm adding to the resistive property of the pathogen. All the four designed peptides AMP21-24 exhibited very good activity against *P. aeruginosa.* Additionally, all the designed AMPs had very good activity against *K. pneumoniae* (Figure 3.2). These peptides also displayed excellent potency against fungal pathogens such as *C. albicans* and *C. grubii* (Table 3.3, Figure 3.3), which are also actively involved in various human infections such as Candidiasis and fungal meningitis respectively. AMP23 and AMP24 specifically seemed to be highly active against the fungal strains tested. Thus, in summary, the designed AMPs showed very high as well as broad-spectrum activity against all the tested strains.

3.3.3. Salt Tolerant Property of the Designed Peptides:

All the tested peptides, AMP21-24 also displayed considerable antibacterial activity against *P. aeruginosa* as well as antifungal activity against *C. albicans* in the presence of physiological concentration of salt (150 mM NaCl) (Table 3.3).

Table 3.3: MIC values of AMP21-24 in µM concentrations against bacterial and fungal pathogens in presence and absence of physiological concentration of salts (150 mM NaCl).

	In Absence of Salts $MIC_{90\%}$ in µM				**In Presence of Salts $MIC_{50\%}$ in µM**			
	AMP21	AMP22	AMP23	AMP24	AMP21	AMP22	AMP23	AMP24
E. coli DH5α	**25**	**5**	**5**	**15**	**-**	**-**	**-**	**-**
S.aureus	**50**	**10**	**15**	**10**	**-**	**-**	**-**	**-**
K. pneumoniae	**3**	**3**	**5**	**10**	**-**	**-**	**-**	**-**
P. aeruginosa	**5**	**5**	**5**	**2.5**	**15**	**10**	**10**	**10**
C. albicans	**1**	**2.5**	**1**	**1**	**15**	**15**	**15**	**10**
C. grubii	**2.5**	**2.5**	**1**	**1**	**-**	**-**	**-**	**-**

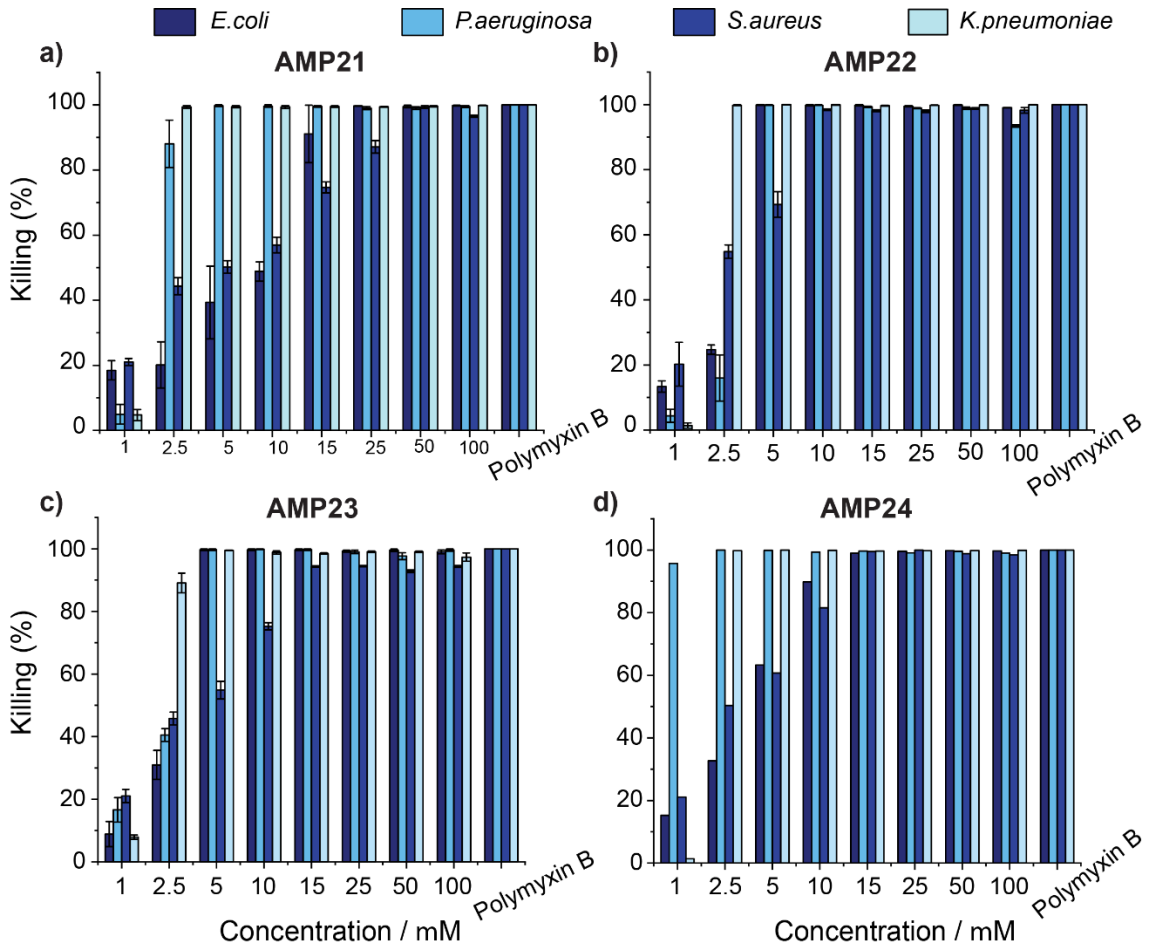

Figure 3.2. $MIC_{90\%}$ of AMP21-24 against Bacterial Cells: Micro broth dilution assay was done with increasing concentration of the respective peptides. After allowing for overnight recovery, the percentage of killing was calculated and represented in the form of $MIC_{90\%}$ value. All experiments were performed in triplicates.

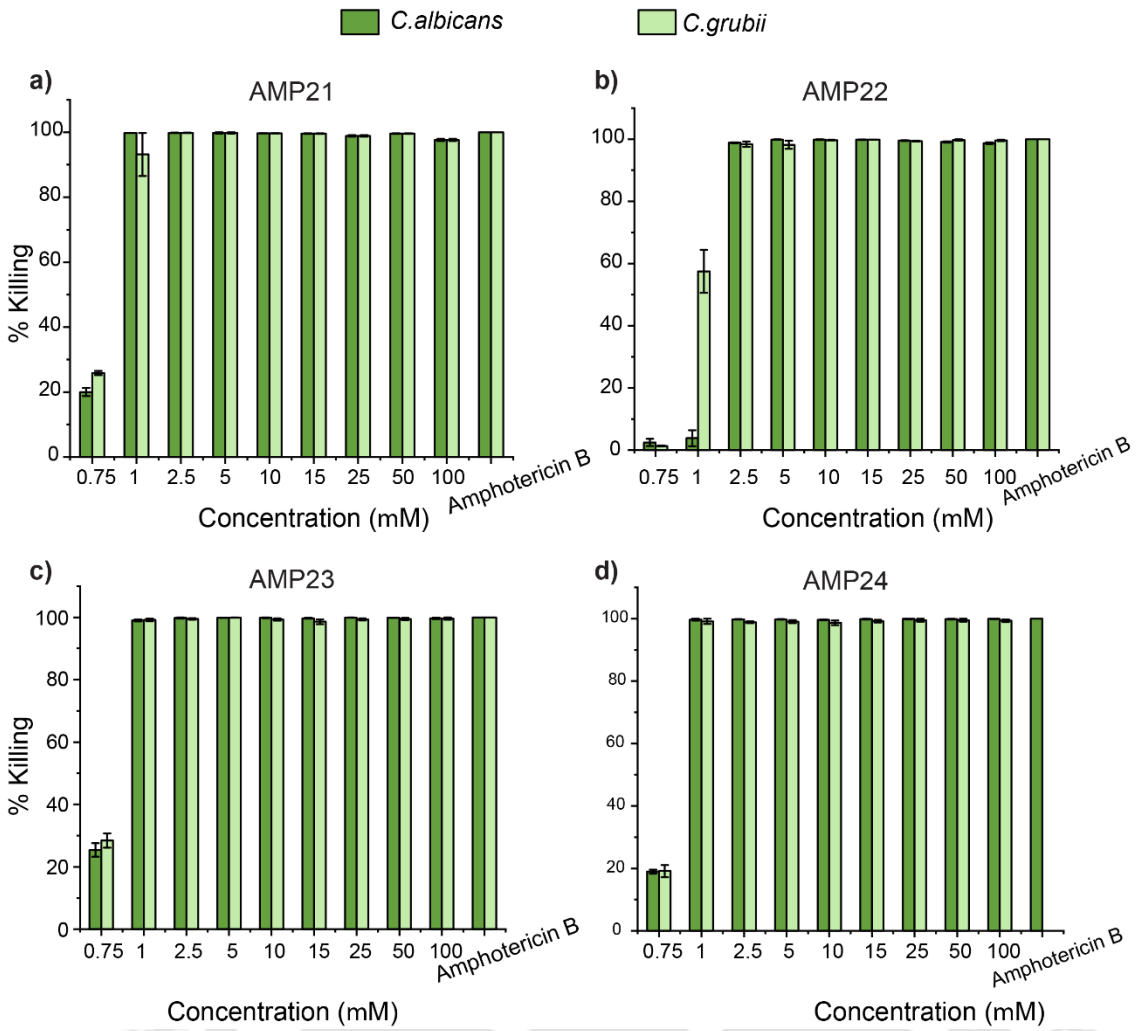

Figure 3.3. $MIC_{90\%}$ of the peptides against Fungal Cells. Micro broth dilution assay was done with increasing concentration of the respective peptides. After allowing for overnight recovery, the percentage of killing was calculated and represented in the form of $MIC_{90\%}$ value. All experiments were performed in triplicates.

3.3.4. Cytotoxicity of Designed AMPs:

One of the major bottlenecks in being able to use the naturally occurring AMPs as therapeutic molecules is related to their cytotoxicity and hemolytic property. Thus we looked into the cell viability and the non-hemolytic ability of our designed peptides AMP21-24. Figure 3.4 shows the effect of the peptides AMP21-24 on the cell viability of Hela and L132 cells. Till 30 µM concentration, none of the peptides showed any cytotoxicity for 24 hrs. At higher concentration

(≥ 40 µM), AMP22 specifically showed diminished cell viability. Other AMPs showed diminished cell viability at higher concentrations. However, all the AMPs have good cell viability at their biologically active concentrations.

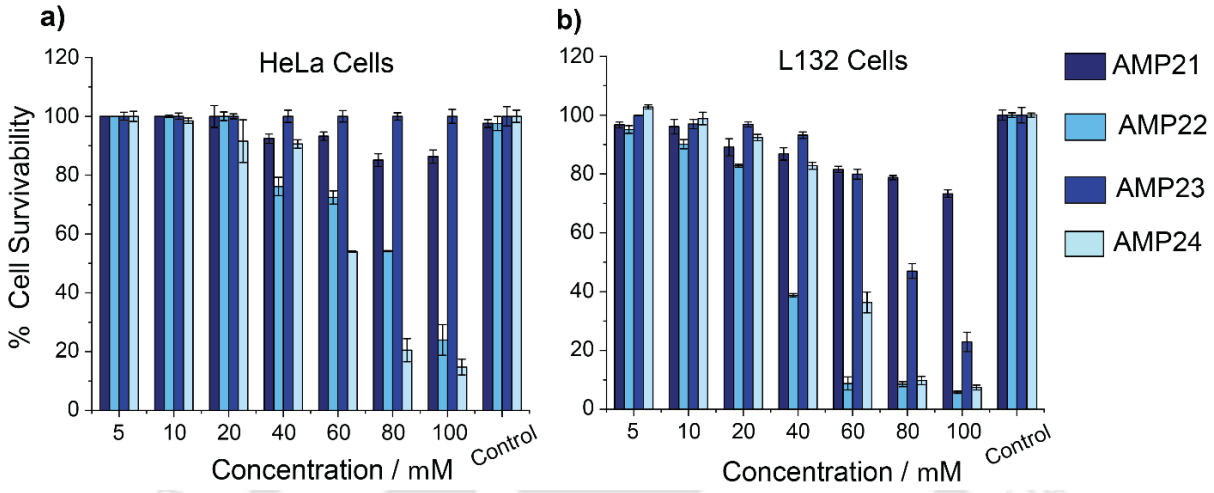

Figure. 3.4. Cytotoxicity of AMP21-24: MTT Assay of peptides AMP21-24 on (a) Hela cells and (b) L132 cells. Viability was quantified by measuring the absorption at 570 nm. All experiments were performed in triplets.

3.3.5. Non-Hemolytic Potential of the Peptides:

The hemolytic potential of our peptides was tested by evaluating the release of heme after disruption of human RBCs in presence of AMP21-24 (Figure 3.5). Till 4 hrs, none of the tested peptides showed significant hemolysis upto 100 µM concentration, which was considerably higher than their biologically active concentrations.

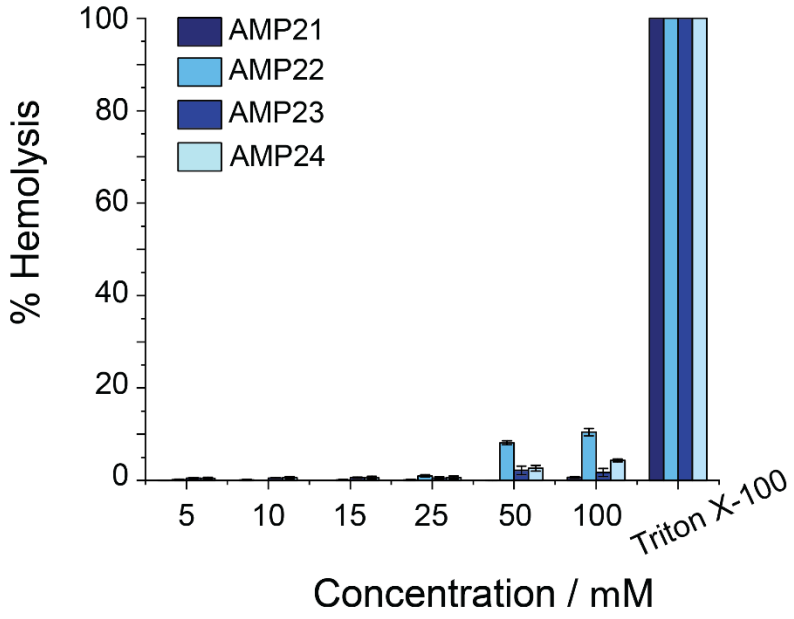

Figure 3.5. Non-hemolytic activity of AMP21-24: Heme release was quantified for hemolytic assay by measuring the absorbance at 410 nm after treating cells with increasing concentration of AMP21-24 for 4 hr. Maximum heme release was < 10% in case of all the peptides, clearly indicating that they were non-hemolytic. All experiments were performed in triplicates and 2% per volume of Triton X-100 was used to normalize all data.

3.3.6. Interaction of AMPs with the Microbial Membranes: As mentioned earlier, AMPs exhibit multimode mechanisms for effective killing and inhibition of growth of microbes. In majority of the cases, it is, however, observed that the primary mode basically involves interaction with the microbial membrane.[436,518] Hence, to probe the activity of our designed peptides and to study the interaction of the AMPs with the membrane, several low-resolution as well as high-resolution spectroscopic techniques were employed.

3.3.7. Fluorescence Spectroscopy:

Intrinsic tryptophan fluorescence was monitored for understanding the interaction between peptides and bacterial/mammalian membrane mimics. AMP22 consisted of two Trp residues (W5 and W7) in its sequence. Changes in the intrinsic tryptophan fluorescence usually occured due to change in the microenvironment around the Trp residue, upon interaction of the peptide with bacterial membrane/ membrane mimics like D8PG. Free peptide displayed an emission maxima at ~350 nm in aqueous solution hinting towards high solvent accessibility of Trp. Upon titrating the peptide with increasing micromolar concentrations of D8PG, a hypsochromic shift was observed in the emission maxima (λ_{max}) of Trp. A shift of upto 11 nm was observed when the ratio of peptide and D8PG was 1:8 and above as shown in Figure 3.6a. This change in λ_{max} could be attributed to the changes in the surrounding environment of Trp in presence of D8PG. Presence of D8PG micelles led to the probable incorporation of Trp residue into the hydrophobic core of the micelle, preventing solvent exposure. However, upon titrating with increasing concentrations of DPC, an accepted mammalian membrane mimic, there was no significant change in the emission maxima (λ_{max}) of Trp (Figure 3.6a). This data suggested that there was no or very little interaction of AMP22 with the mammalian membrane mimic and validated the non-cytotoxicity observed earlier for our designed AMPs.

Fluorescence quenching experiments of AMP22 alone and mixtures of AMP22 and D8PG or DPC (1:10 molar ratio), were performed in the presence of a static quencher acrylamide, for better understanding of solvent exposure. The extent of quenching in fluorescence of the free peptide as well as the peptide-membrane mimic mixtures was expressed in terms of Stern-Volmer Constant (K_{SV}) (Figure 3.6b). It was observed that the K_{SV} value for the AMP22 alone and in the presence of DPC were significantly higher than in the presence of D8PG, suggesting a decrease in solvent exposure of Trp in the presence of D8PG. As mentioned above, this might be due to localization of the Tryptophan residues within the D8PG micelle core that hindered the exposure of the Trp residues to the quencher.

3.3.8. Determination of the Thermodynamic Parameters of the Binding Interaction of the Peptides and D8PG:

Isothermal titration calorimetry (ITC) experiments were performed to determine the thermodynamical parameters guiding the binding interaction of AMP22 (Figure 3.6c) and AMP24 (Figure 3.6d) with D8PG. Gibb's Free Energy was calculated as shown in Table 3.4 and its negative value for both the peptides showed that the interaction was spontaneous and thermodynamically driven. A greater negative value of ΔG for AMP24 compared to that of AMP22 indicated that the interaction of the former with the microbial membrane was more thermodynamically favorable. Further, the dissociation constant (K_D) value was also determined. The lower K_D value of AMP24 as compared to that of AMP22, indicated that AMP24 had higher affinity towards D8PG. This might be a direct consequence of the positive charge content of the AMPs. Peptide 22 had the lowest positive charge (6) at physiological pH among all the AMPs studied here. This was a hint that the interaction between the peptides and the microbial membranes was electrostatically driven.

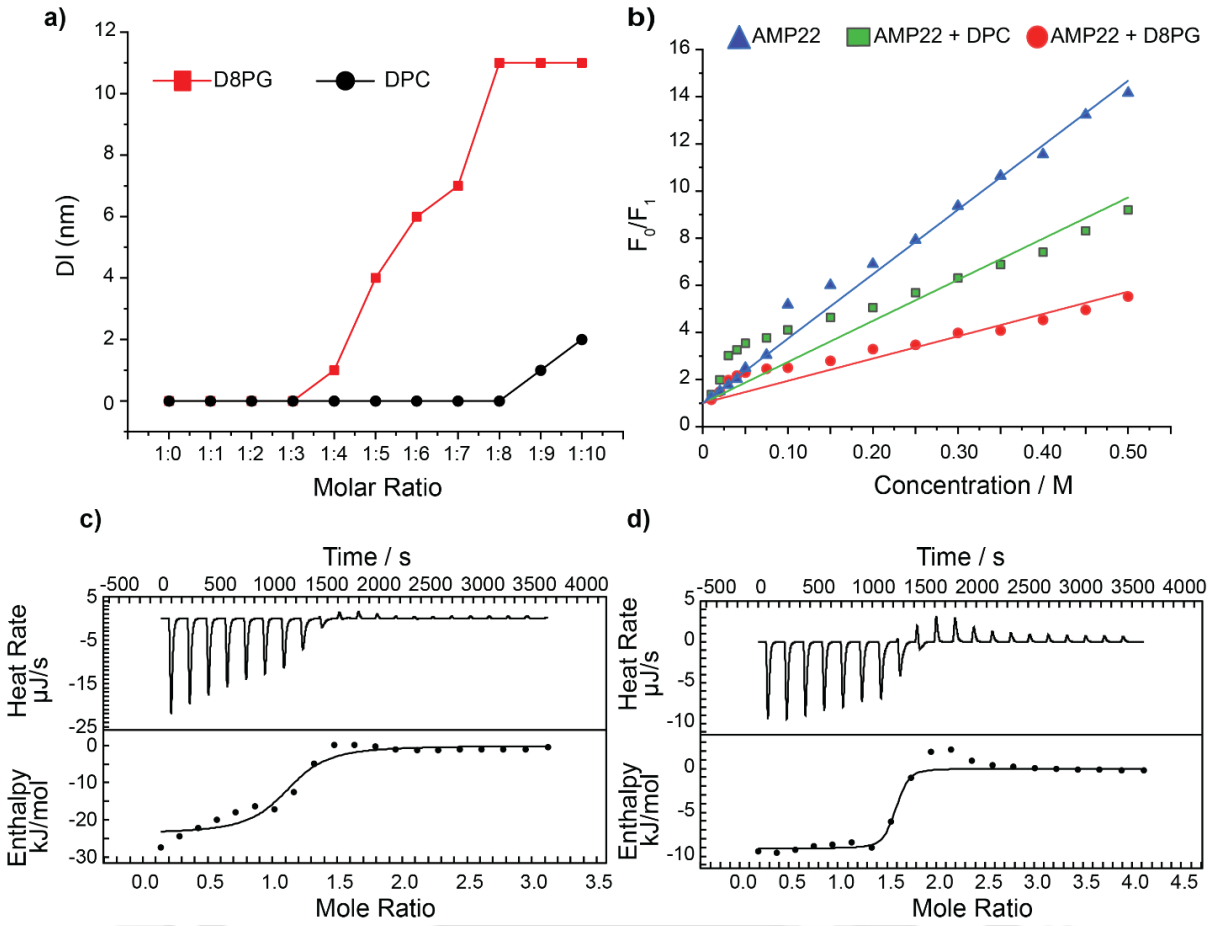

Figure 3.6. Interaction of AMPs with the membrane. (a) Change in the fluorescence emission maxima (λ_{max}) of Trp of AMP22 in presence of varying ratios of peptide: lipids (DPC and D8PG). No change in the emission maxima (λ_{max}) of Trp occured in presence of increasing concentration of DPC (black), a mammalian membrane mimic, indicating no interaction in between the two. Hypsochromic shift in the emission maxima of Trp occured in presence of increasing concentration of D8PG (red), a bacterial mimic, suggesting an interaction in between peptide and the D8PG micelles. (b) Plot representing the F_0/F_1 values against concentration of AMP22 alone and in presence of DPC and D8PG. (c, d) Isothermal titration calorimetry of AMP22 and AMP24 in presence of D8PG, a bacterial membrane mimic. Upper panels depict exothermic heat of reaction vs. time (seconds) upon interaction of D8PG micelle with AMP22-24. Lower panels depict enthalpy change per mole of D8PG injection vs. molar ratio (D8PG:AMP22 and 24).

Table 3.4: Thermodynamic parameters of the binding interaction of AMP22 and AMP24 with D8PG at 310 K. n is the stoichiometry of binding.

Peptide	n	K_D (μM)	ΔH (kJ mol^{-1})	ΔS (kJ. mol^{-1} K^{-1}) x 10^3	ΔG (kJ mol^{-1})
AMP22	1.07	21.56	-23.72 ± 2.152	12.84	-27.7
AMP24	1.5	1.46	-9.12 ± 0.211	82.33	-34.65

3.3.9. Mode of Action:

Majority of the AMPs possess membranolytic mode of action, wherein they cause membrane deformation, permeabalization, depolarization, lysis, leading to leakage of the intracellular contents. They also act via impairment of membrane transport and loss of osmolarity[515] , indicating that the designed AMPs have strong interactions with the microbial membrane.

3.3.9.1. Permeabilization of Model Membrane Mimic LUVs by Designed AMPs:

Model bacterial membrane as well as fungal membrane mimics were prepared to study their interaction with AMP22 and AMP24. Increase in fluorescence intensity denoted the calcein release, hence membrane perturbation.[144] Concentration dependent permeabilization of large unilamellar vesicles (LUVs) was shown by AMP22 as well as AMP24 against both bacterial and fungal model membranes. AMP22 caused a calcein release of about 47% and 82% from bacterial and fungal model membranes, respectively (Figure 3.7 a, b) AMP24, on the other hand caused a release of about 36% from both bacterial and fungal model membranes. AMP22, thus showed a higher membrane perturbation potency than AMP24 against both bacterial and fungal membrane model, but the disruption property was significantly high in case of fungal model membrane. The very high antifungal activity of AMP24 as seen from the MIC values,

might suggest a secondary mode of action in addition to membrane perturbation for this antimicrobial peptide.

Time-dependent calcein release in presence of AMP22 and AMP24 was studied (Figure 3.7 c, d). Time dependence of LUV permeabilization was observed only at lower peptide concentrations for both AMP22 and AMP24. Free LUVs, on the other hand, did not show significant calcein release even after 24 hr.

3.3.10. Designed AMPs Cause Efflux of Metabolites from Microbial Cells:

To determine the atomistic level effect of the peptides on *P. aeruginosa* and *C. albicans* cells, live cell NMR spectroscopy was performed (Figure 3.8). Two major changes in the NMR spectra were observed, (i) immediate line broadening effect of the peptides, (ii) emergence of new peaks symbolizing release of intracellular metabolites following membrane lysis and/or disruption. Line broadening of the ^{1}H signal was mainly attributed to the increased T_2 relaxation of both the peptides upon interaction with the live cells. Changes in the resonance intensity in the amide, aromatic, methyl as well as other aliphatic regions of the NMR spectra clearly indicated peptide-cell interaction. The new peaks that appeared increased in intensity over the time as seen in the ^{1}H NMR spectra upon incubation of the peptide with the live cells. Emergence of these new peaks corresponded to efflux of metabolites from the *P. aeruginosa* and *C. albicans* cells. In case of AMP22, upon co-incubation of peptide and *P. aeruginosa* cells (Figure 3.8a i), emergence of newer peaks was observed as well as line broadening was visible. After 2 hrs of co-incubation, substantial increase in the peptide resonance and return of the line shape began to occur.

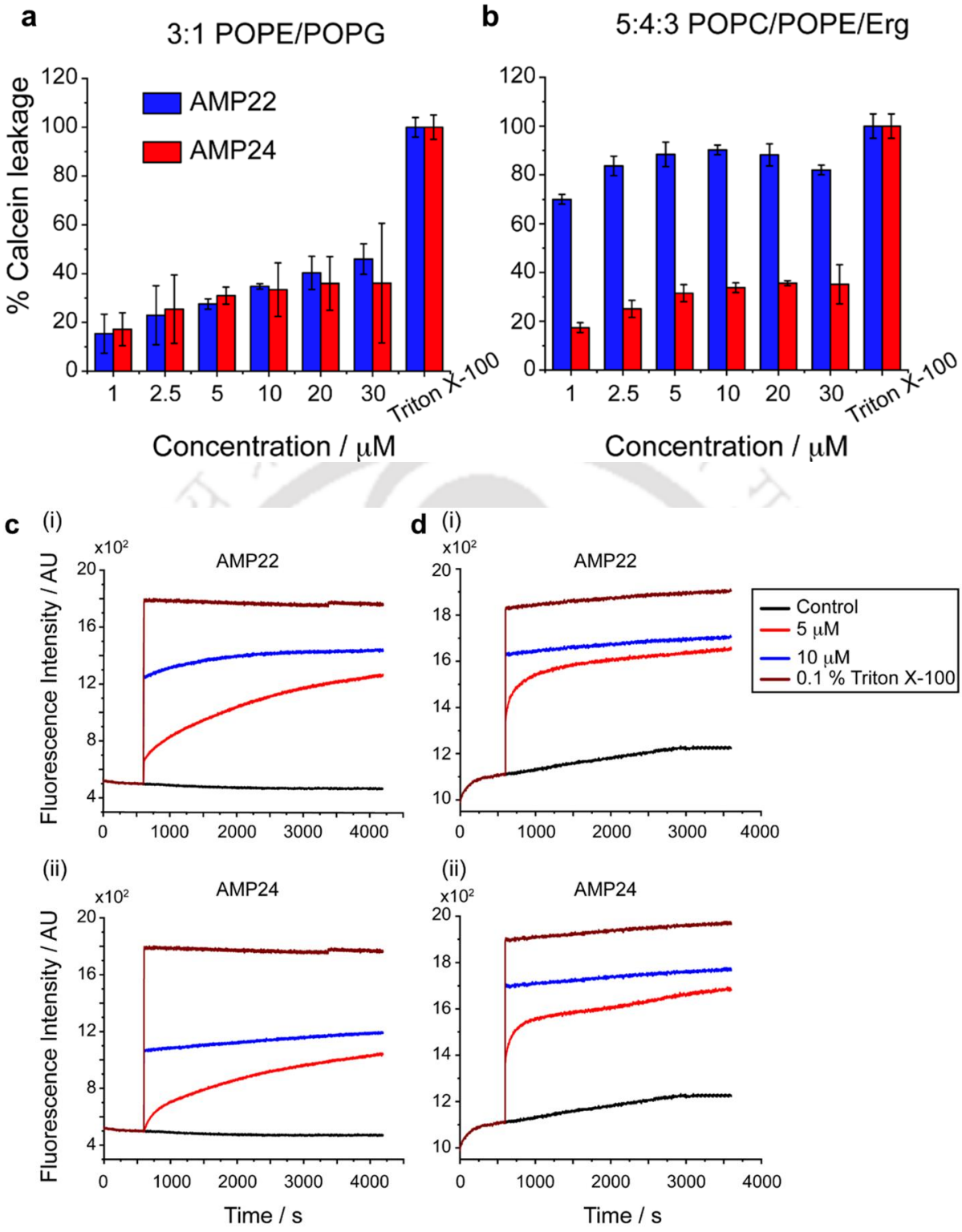

Figure 3.7. Calcein-leakage assay for AMP22 and AMP24. Calcein release in the presence of varying concentrations of AMPs upon interaction with (a) bacterial model membrane and (b) fungal model membrane. Time- dependent release of calcein from dye- encapsulated vesicles mimicking (c) bacterial model membrane and (d) fungal model membrane upon interaction

with AMP22(i) and AMP24 (ii) for a period of 4200 seconds. Triton X-100 was used as a control.

On incubation upto 6 hr., peptide resonance increased significantly and line shape also returned close to its initial phase. This was attributed to the dissociation of the peptide from the cells after membrane disruption. However, in case of AMP24, appearance of new peaks was observed but line shape did not return to its initial position, suggesting there could be slow conformational exchange in the NMR time scale (Figure 3.8 a ii).

In case of *C. albicans*, the emergence of new peaks was rapid and significant line broadening was observed within a short span (5 minutes) of co-incubation with both AMP22 and AMP24 (Figure 3.8 b i, ii). Even in this case the peptide lines returned to original shape after long incubation times for the AMP22 but not for AMP24 hinting at the weaker membrane binding capability of the former with respect to the later. This result was in lines with the change in free energy (ΔG) upon membrane binding, obtained from the ITC experiment suggesting that electrostatics played a major role in interaction of the peptides with the membrane.

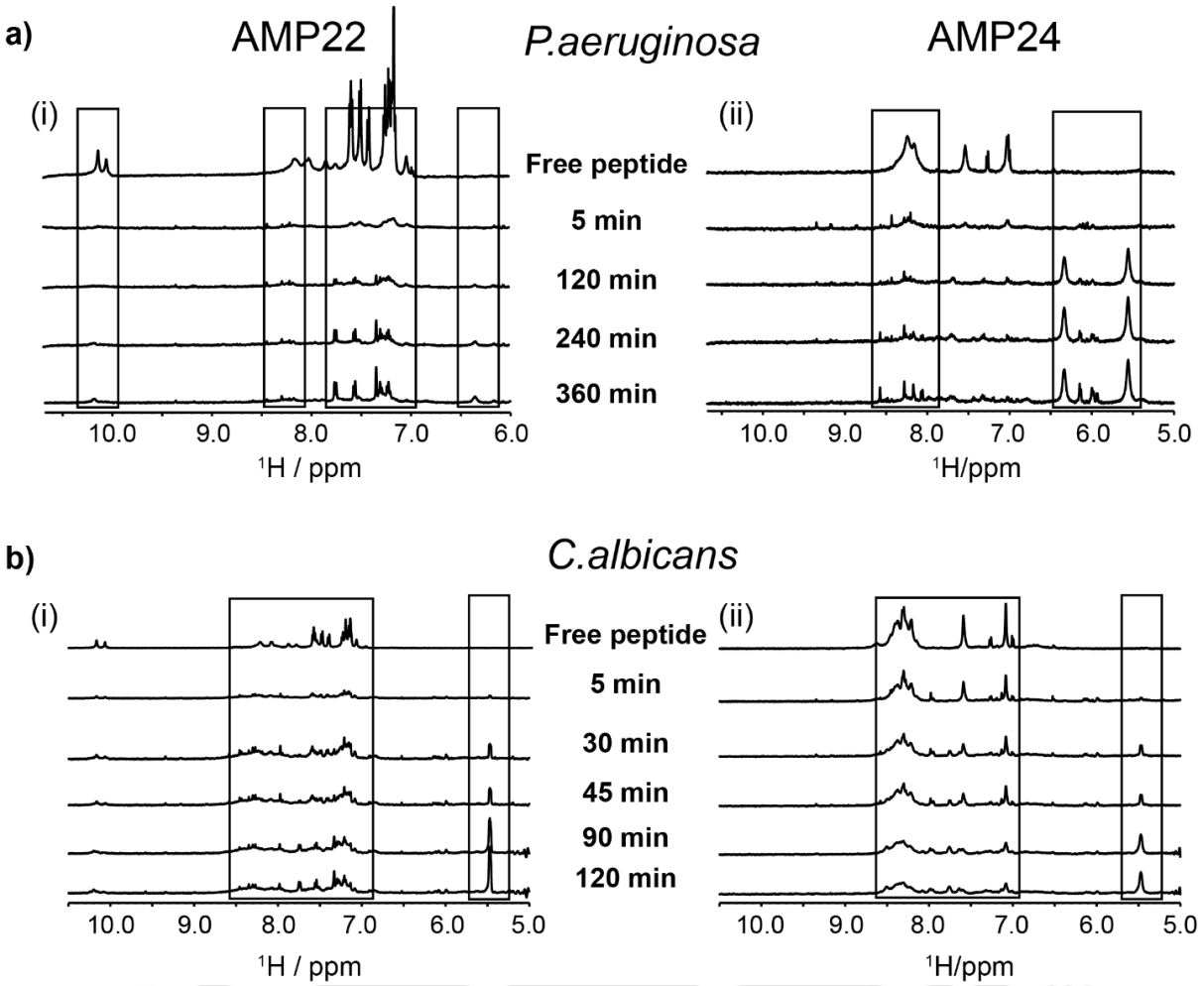

Figure 3.8. Live Cell NMR spectroscopy of AMP22 and AMP24 in presence of *P. aeruginosa* and *C. albicans* cells. Partial stacked plots of one-dimensional NMR spectra at different times of incubation of AMP22 (i) and AMP24 (ii) with (a) *P. aeruginosa* and (b) *C. albicans*.

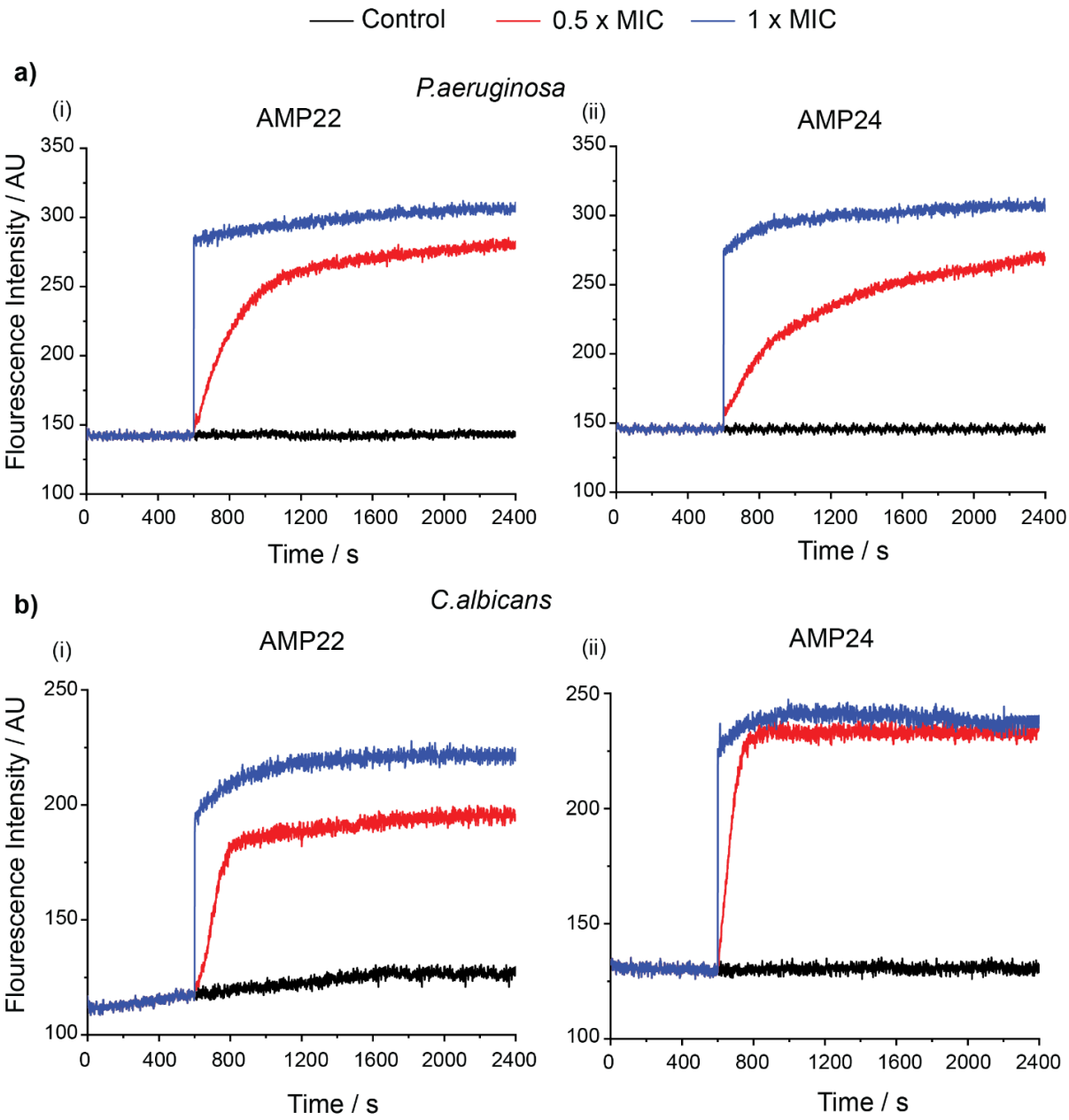

Figure 3.9. (a), (b) Propidium Iodide staining assay for AMP22 and AMP24. PI fluorescence was observed for AMP22 (i) and AMP24 (ii) at 0.5x and 1x % with *P. aeruginosa* and *C. albicans* respectively for 2400 s.

3.3.11. Membrane Permeabilization by designed AMPs:

Interaction of AMP22 and AMP24 with the live cell membrane of *P. aeruginosa* and *C. albicans* was studied using Propidium Iodide (PI) dye (Figure 3.9 a, b). PI cannot penetrate intact cell membrane. However, membrane perturbation or disruption of the cell membrane,

allows the dye to penetrate the cell and bind with the nucleic acid. Half- MIC and MIC values of the peptides were titrated to detect the change in the fluorescence intensity of the dye, indicative of the permeabilization of the dye, hence, membrane disruption in the presence of the peptides. AMP22 and AMP24 showed similar activity both in case of *P. aeruginosa* as well as *C. albicans* cells. Highest fluorescence intensity was observed in case of MIC concentration, after which there was no significant change in fluorescence.

3.3.12. Cytoplasmic Membrane Depolarization Caused by Designed Peptides:

Membrane depolarization capability of AMP22 and AMP24 was studied using $DiSC_3$ dye to determine the change in membrane potential of *P. aeruginosa* and *C. albicans* (Figure 3.10 a, b)[144]. Both the peptides were titrated at concentrations of 5 µM and 10 µM against *P. aeruginosa* and *C. albicans*. Increase in the fluorescence intensity of the dye indicated a decrease in the membrane potential of cells. Significant changes were observed in the membrane potential of both *P. aeruginosa* and *C. albicans* in the presence of the peptides. AMP24 showed slightly higher membrane polarizing activity than AMP22 in case of *P. aeruginosa* cells (Figure 3.10a). In case of *C. albicans*, however AMP22 displayed higher activity (Figure 3.10b). Only *P. aeruginosa* and *C. albicans* cells were also incubated in the presence of $DiSC_3$ to observe the dye uptake by the cells. 0.1% Triton X-100 served as a control responsible for absolute decrease in membrane potential and subsequent increase in fluorescence intensity of the dye.

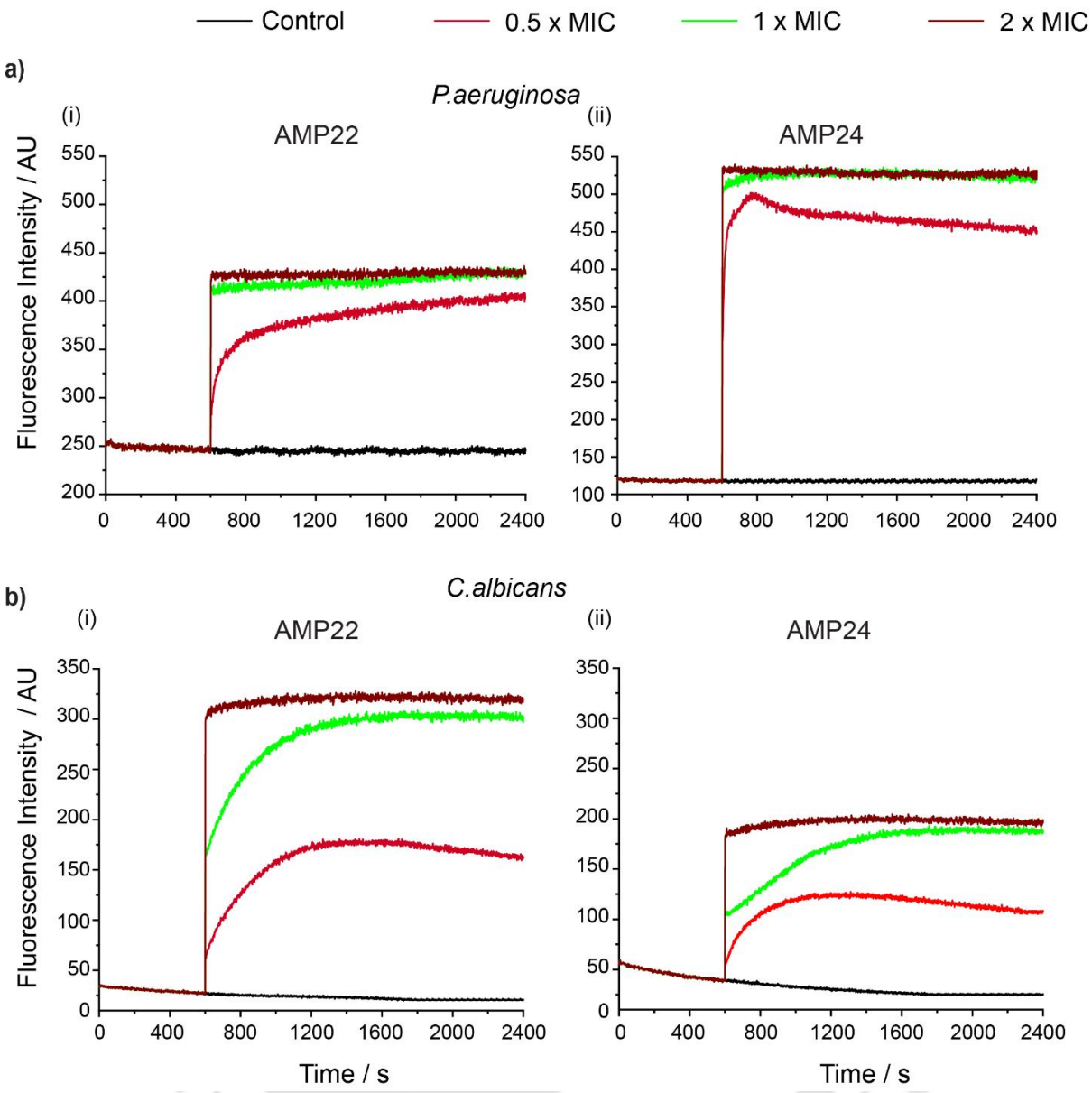

Figure 3.10. (a), (b) Cytoplasmic Depolarization assay caused by AMP22 and AMP24 in case of *P. aeruginosa* and *C. albicans*. Decrease in membrane potential of *P. aeruginosa* and *C. albicans* cells was monitored by increase in dye fluorescence over a period of 2400 seconds in presence of i) AMP22 and ii) AMP24. 0.1% Triton X-100 served as control.

3.3.13. Membrane Deformation Caused by Designed AMPs:

To investigate the mechanism of action of the peptides further, FESEM studies were performed. *P. aeruginosa* cells (10^6 cells/) were incubated with 1×, and 2× % of AMP21-24 to study and interpret the extent of peptide-mediated cell perturbation and hence lysis (Figure

3.11 a). *P. aeruginosa* bacterial cell is rod shaped with a smooth outer membrane. Control experiments comprising of peptide untreated cells showed intact morphology. However, in the presence of different concentrations of AMP21, AMP22, AMP23 and AMP24, deformations in the outer membrane including blebbing, disruption followed by leakage of intracellular materials due to cell lysis was observed. At low concentration, distorted cell morphology in the form of dents and membrane blebbing was clearly visible, while non-uniform cell debris with leaked intracellular material, indicating complete cell lysis, was visible at higher concentration of peptides. Establishment of membrane deformation as well as disruption was observed at 1× % concentration, post 30 min treatment. In case of 2× % concentration, complete lysis of the cells as well as leaked intracellular components were observed. Interestingly, in treated samples, notable change in cell size was also observed in some cases.

3.3.14. Intracellular Permeability of AMPs:

To determine the ability of translocation of the AMPs across the cell membrane and intracellular localization of the peptides, confocal microscopy technique was employed. 10 µM carboxyfluorescein tagged peptides were used to treat *C. albicans* and confocal imaging was performed. It was interesting to observe that there was green fluorescence throughout the cell, indicative of cellular uptake and an unspecific localization of the peptides (Figure 3.11b). Membrane blebbing as well as disruption of the cell was observed in some cases. This also hinted towards the possibility of secondary mode of action of these peptides against *C. albicans* cells.

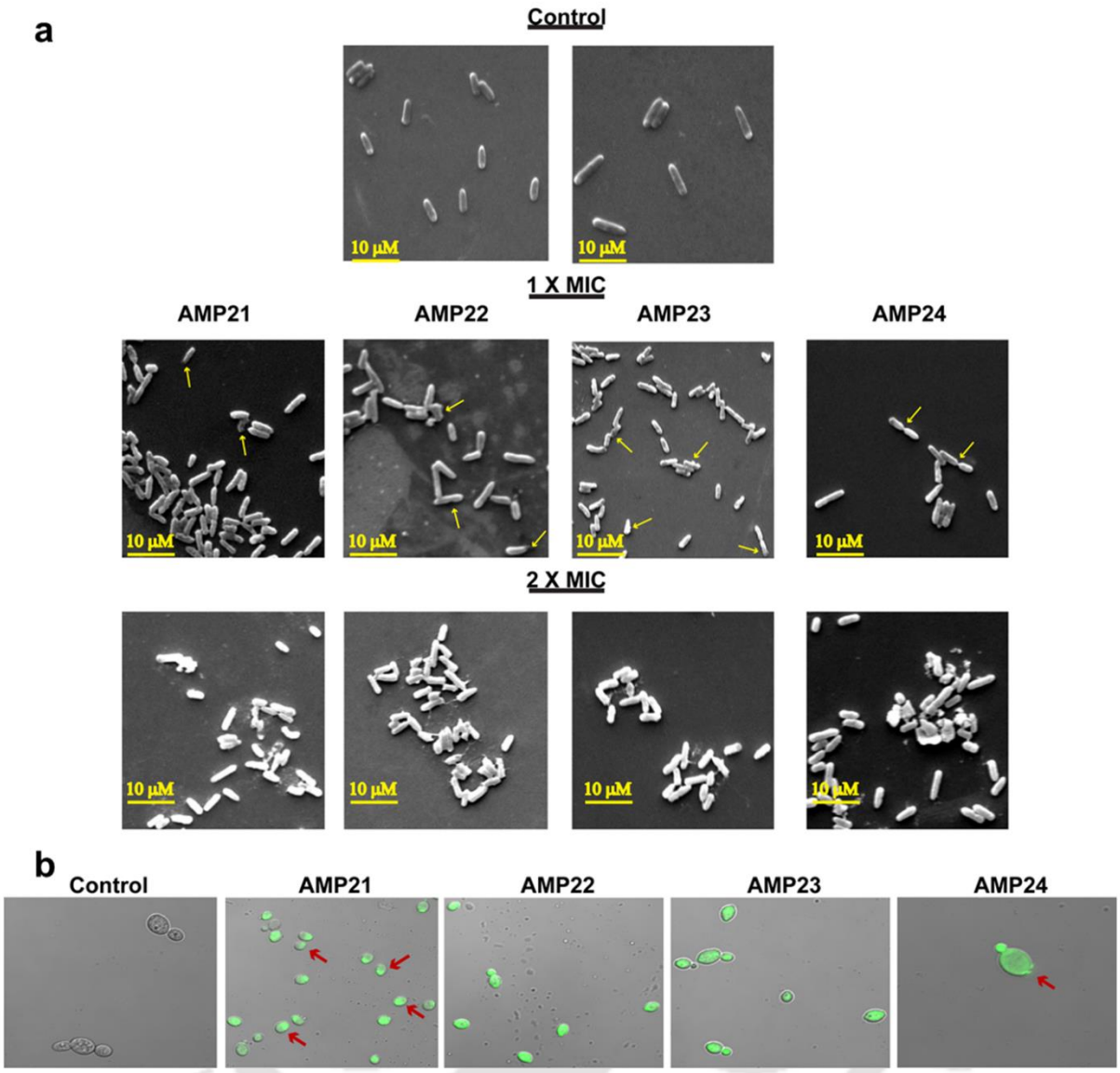

Fig. 3.11. (a) FESEM of AMP21-24 with *P. aeruginosa* cells. Untreated and Triton X-treated cells were used as positive and negative control respectively. While the former did not show any significant morphological changes, the later showed complete disruption of the bacterial cells. Cells treated with 1x and 2x % concentrations of AMP21-24 showed considerable morphological changes. The designed peptides showed significant membranolytic activity. (b) CLSM of AMP21-24 treated *C. albicans* cells showing cellular uptake and unspecific cytosolic localization of the peptides.

In brief, summing up the results from dye leakage, live cell NMR and FESEM experiments, the AMPs seemed to function primarily via acting on the membrane surfaces of both bacteria

and fungus hampering the membrane architecture, leading to efflux of cellular constituents, and further death. Significant membrane lysis occurred for the designed AMPs at high concentration. At lower concentration, considerable change in the membrane morphology was noted in case of *P. aeruginosa* cells. Membrane permeabilization assay as well as cytoplasmic depolarization assay indicated strong peptide- membrane interaction. An alternative mode of action for the AMPs might not be ruled out based on the confocal microscopy observation of the cellular internalization of the peptides.

3.3.15. Structure of the AMPs:

AMPs adopt diverse secondary structures from being amphipathic helical, to amphipathic β sheets, to cyclic, to being irregularly structured.

We wanted to probe the secondary structure of our designed peptides AMP21-24 in the free state and in presence of bacterial –membrane mimic using CD and MD simulations. This would help us understand the structure-function relationship, if any for the designed AMPs.

3.3.16. CD Spectroscopy:

For looking at the structure of the peptides in solution in free state and in the presence of microbial membrane environments, CD was performed in the presence of water, TFE (helix promoting solvent), SDS micelles, D8PG micelles (microbial membrane mimic), and DPC micelles (zwitterionic mammalian membrane mimic). Figure 3.12 shows the CD spectra of the four peptides that were recorded in the various environments.

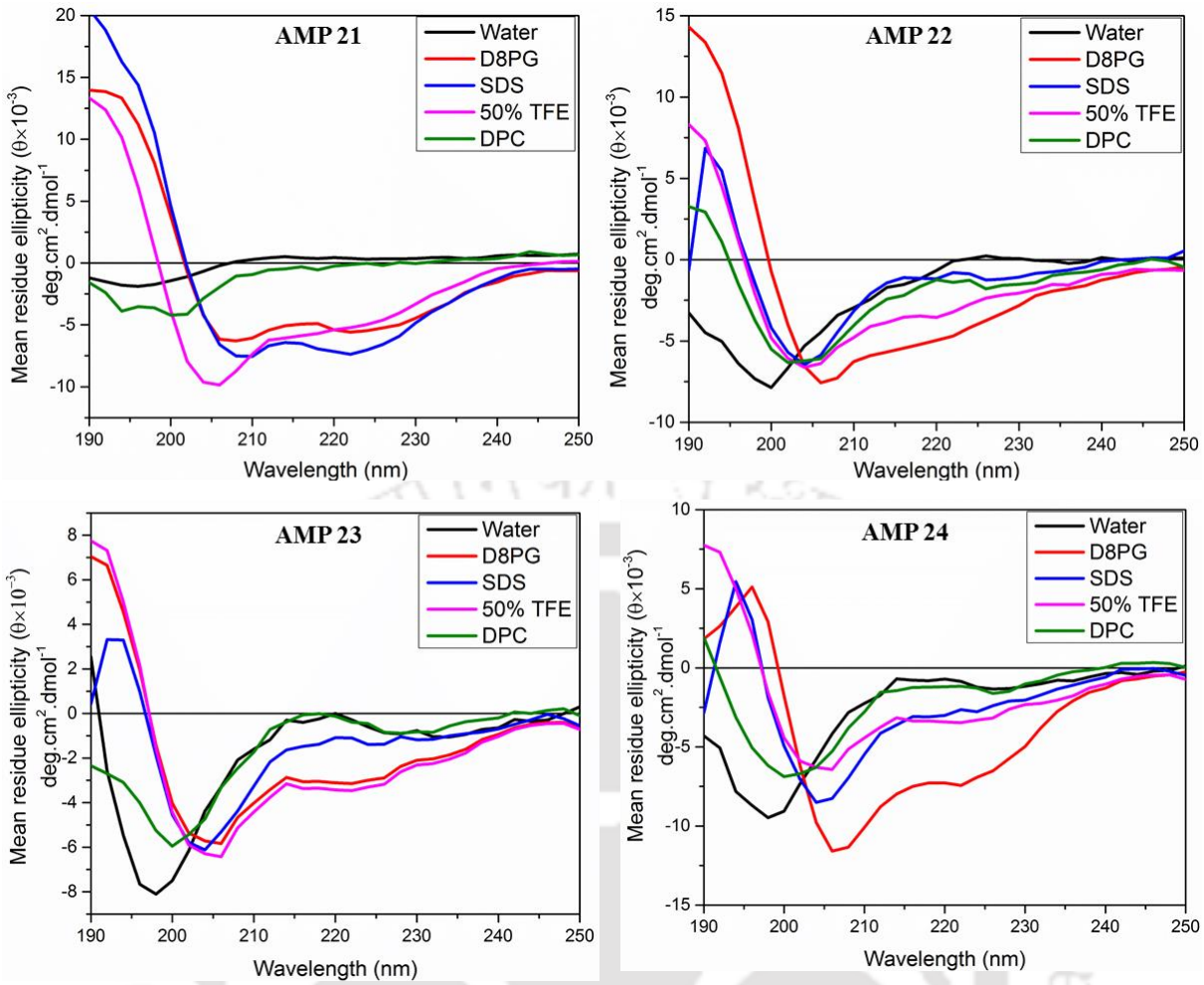

Figure 3.12. CD spectroscopy of AMP21-24 in the presence of water, SDS, 50%TFE and DPC. All the peptides adopted random coil conformation in water and DPC membrane mimetic environment. In the presence of 50% TFE, D8PG and SDS, the conformation of the peptide changed to helical-like.

In water, the free peptides adopted random coil like structures with a negative cotton effect at around 200 nm. In the presence of the helix promoting solvent TFE, there was a stark shift in the CD peaks. All the peptides tended to adopt a helix-like conformation with positive peaks at ~196 nm and negative peaks at ~ 205 and 222 nm. In the presence of D8PG (all AMP's) and SDS (for AMP21) micellar environments, the CD spectra deviated from the random coil like signature observed in the aqueous environment to an α-helical like secondary structure. However, in the presence of DPC micellar environment, all the peptides predominantly

exhibited random coil like secondary structure just like in aqueous solution. However, from MD simulations, the peptides were seen to be mostly unstructured even in the presence of bacterial membrane mimics. Thus the α-helix like conformation hinted from CD, in the presence of bacterial membrane mimics like D8PG and SDS, might just be a transient dynamic conformation.

3.3.17. NMR Spectroscopy:

We have performed the 2D NMR experiments for the AMPs in water as well as in lipid systems (D8PG as well as SDS) that were worked with throughout the study (Figure 3.13). Since the designed peptides had repetitive amino acid sequences, we observed severe signal overlaps both in TOCSY and NOESY spectra, making the assignment as well as three-dimensional structure determination of the peptides in the water as well as in lipid difficult.

3.3.18. Molecular Insights from MD Simulations:

Understanding peptide-membrane interactions in terms of its structure and dynamics is challenging. Bio membranes are inhomogeneous and are composed of various types of proteins and lipids. Hence, peptide binding is a complex process involving large and small biomolecules in their different conformations, protonation states and in presence of different ions.

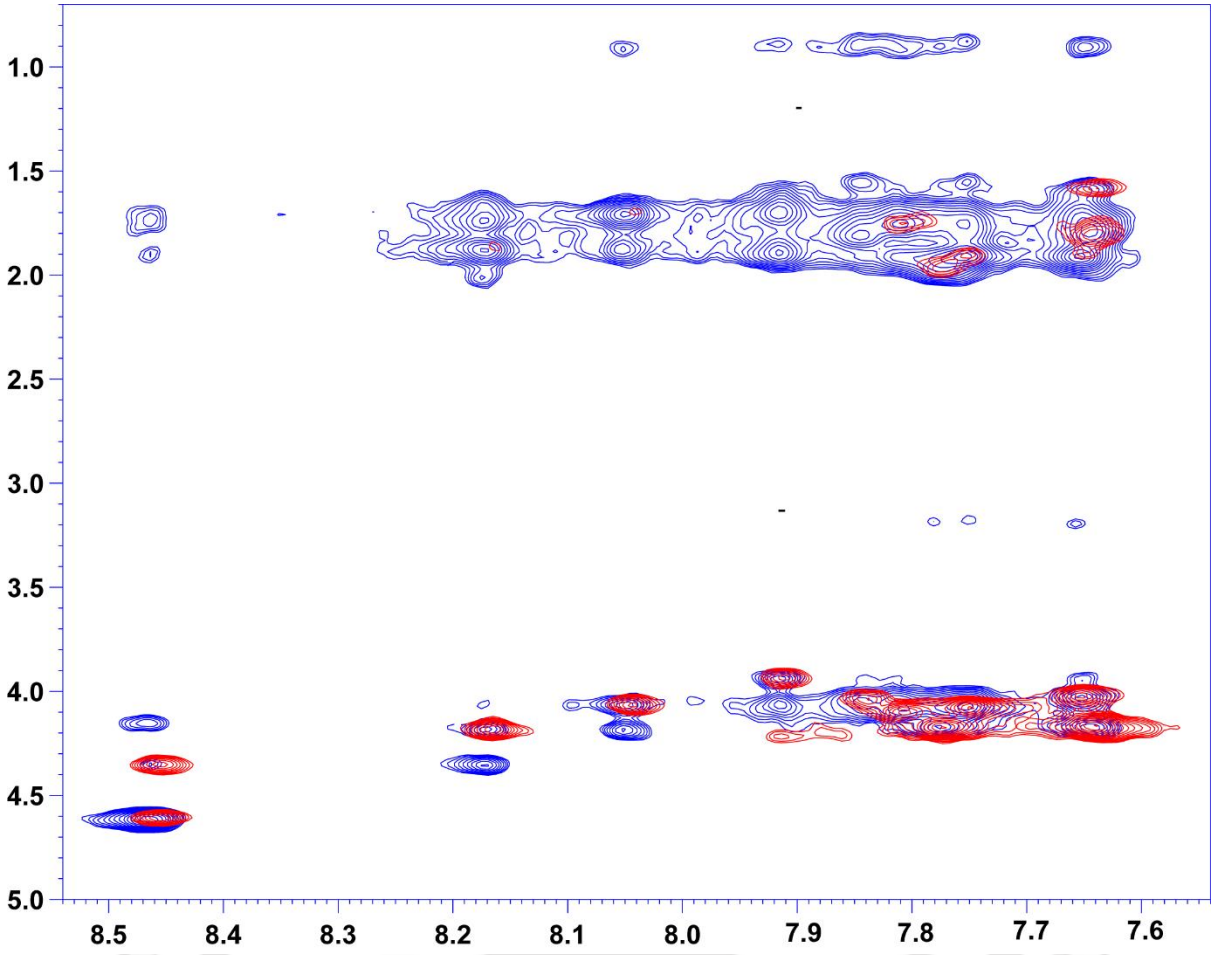

Figure 3.13. 2D NMR spectra of AMP24 in presence of 200 mM SDS. The blue peaks are obtained performing 2D NOESY whereas the red peaks are obtained performing 2D TOCSY NMR experiments.

Modelling true membrane is very complicated and we are no way close to understanding the mechanism of peptide-membrane interaction in its atomic terms. MD simulations can partially fill up the gap by modelling membrane in a very simplistic way, e.g., by mimicking the composition of few lipids of real membrane (Figure 3.13).

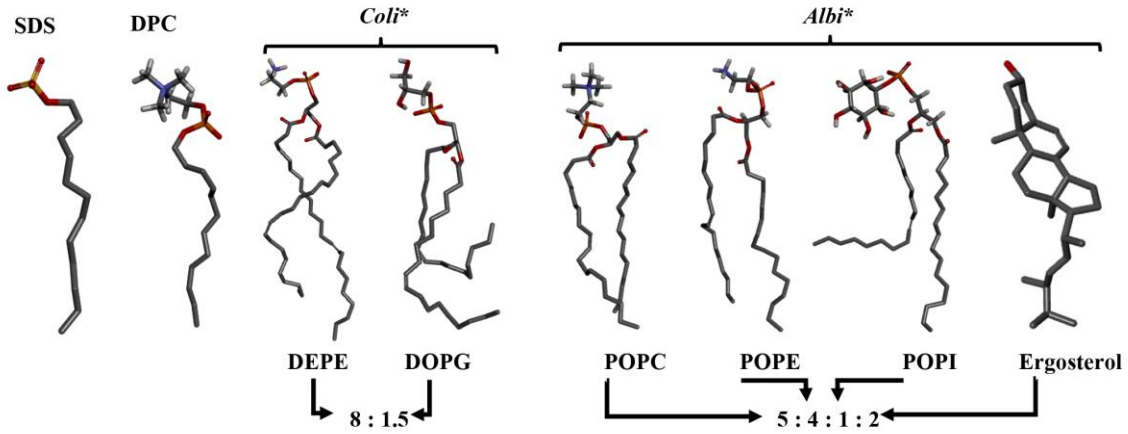

Figure 3.13. Molecules used for modelling micelle (SDS, DPC)/bilayer (Coli*, Albi*). SDS (negatively charged); DPC (zwitterionic); Coli* bilayer is composed of dielaidoylphosphatidylethanolamine (DEPE, zwitterionic) and dioleoylphosphatidylglycerol (DOPG, negatively changed); Albi* bilayer is composed of phosphatidylcholine (PC, zwitterionic), phosphatidylethanolamine (PE, zwitterionic), phosphatidylinositol (PI, negatively charged), and ergosterol (neutral). The ratio considered for modelling is mentioned in the experimental section. Aliphatic chain (Gray), oxygen (red), nitrogen (blue).

In order to gain insight into the atomic interactions between the AMPs and membrane lipids, we performed MD simulations with the four peptides (AMP21, AMP22, AMP23 and AMP24) in the presence and absence of SDS (sodium dodecyl sulfate micelle), DPC (dodecylphosphocholine micelle), Coli* (bilayer mimic of *E. coli* membrane based on major phospholipid composition) and Albi* (bilayer mimic of *C. albicans* membrane based on major phospholipid composition). Radius of SDS micelle was 2.22 nm and the bilayer dimension was 12x12x4.5 nm^3 respectively (Figure 14a, b). MD trajectories clearly showed unstructured random coil conformations of the

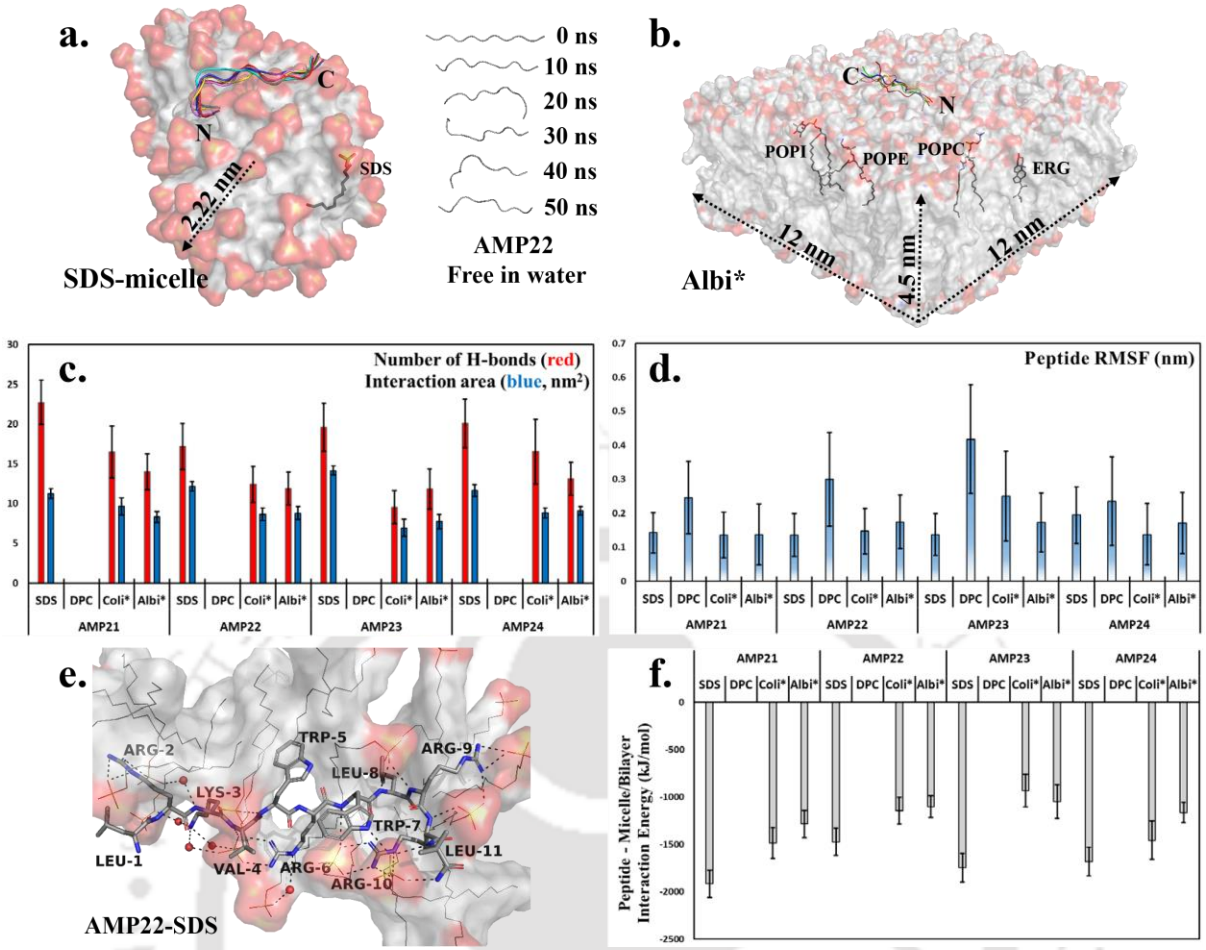

Figure 3.14. Conformations of peptide (AMP22) in (a) SDS micelle bound and unbound form and (b) Albi* bilayer bound form in water. (c) Trajectory averaged number of hydrogen bonds and interaction area between peptide and micelle/bilayer. (d) Trajectory averaged root mean square fluctuation (RMSF) of the peptides. (e) Interaction between SDS and AMP22 after 50 ns of MD; SDS on surface are shown with lines while peptides are shown in sticks. Interaction between peptide main-chain C=O and bulk water is not shown for clarity. (f) Trajectory averaged peptide-micelle/bilayer non-bonded interaction energies. SDS micelle/Albi* (surface); SDS molecule shown as lines with sulfate (red) and aliphatic side chains (grey); Albi* bilayer is composed of phosphatidylcholine (PC), phosphatidylethanolamine (PE), phosphatidylinositol (PI), and ergosterol (ERG) shown as lines. Hydrogens are not shown for clarity. Dimension of the micelle/bilayer is shown with broken arrow. MD averages were done from last 40 ns of total 50 ns molecular dynamics simulations.

free peptides in water (Figure 3.14a), corroborating CD experiments. MD trajectories starting with the geometries where peptides were placed 10-15 Å away from the micelle/bilayer (Figure 3.1) showed direct interaction between peptides and the lipids within ~0.75-2 ns of MD simulations (Figure 3.14 a, b), except for DPC micelle. The resulting lipid-peptide complex (Figure 3.14 a, b) was stable throughout the MD trajectory (upto 50 ns). MD simulations in presence of micelle/bilayer revealed the following robust features:

(a) Number of hydrogen bonds between peptides and SDS micelle were maximum, supported by largest peptide-micelle interaction area (Figure 8C). SDS micelle being negatively charged on the outer surface showed strongest interaction with the positively charged peptides (Figure 3.14c), evident from maximum number of hydrogen bonds and largest interaction area. Both Coli* and Albi* formed an almost equal number of H-bonds with peptides. No favorable interactions between peptide and zwitterionic DPC micelle was observed till 50 ns of dynamics. This corroborated the non-cytotoxicity and the non-hemolytic nature of the peptides. The favorable electrostatic attraction between –ve charge on DPC micelle and positively charged peptides was offset completely due to the presence of +ve charge on the DPC lipids, resulting in no net interaction (upto 50 ns of MD simulations) between the two. Electrostatic interactions seemed to play the key role for peptide binding.

(b) Conformational flexibility of the peptides could be indicated by the RMSF fluctuations. Small RMSF corresponded to less flexibility. MD averaged RMSF of free peptides in water showed large values of 0.31±0.16 nm, 0.32±0.15 nm, 0.42±0.17 nm and 0.32±0.16 nm for AMP21, AMP22, AMP23 and AMP24 respectively. MD simulation of peptides in presence of micelle/bilayer demonstrated that peptides exhibited a reduction in RMSF or conformational flexibility in response to binding to the surface of SDS/Coli*/Albi* (Figure

3.14d). As expected, the RMSF of peptides in presence of DPC micelle were largest and were almost identical to that of free peptides in water (Figure 3.14d).

(c) Comparison of Ramachandran plot (Figure 3.15) of peptide residues (bound and unbound peptide in water) from MD simulations suggested that micelle/bilayer binding certainly reduced the possible conformational space for the peptide. N-Cα (ϕ) and Cα-C (ψ) torsion angles of peptide residues (Ramachandran Plot) were computed from MD trajectories of free and micelle/bilayer bound peptide-simulations (Figure 3.15). Distribution of (ϕ, ψ) torsion angles was linked to available conformational space

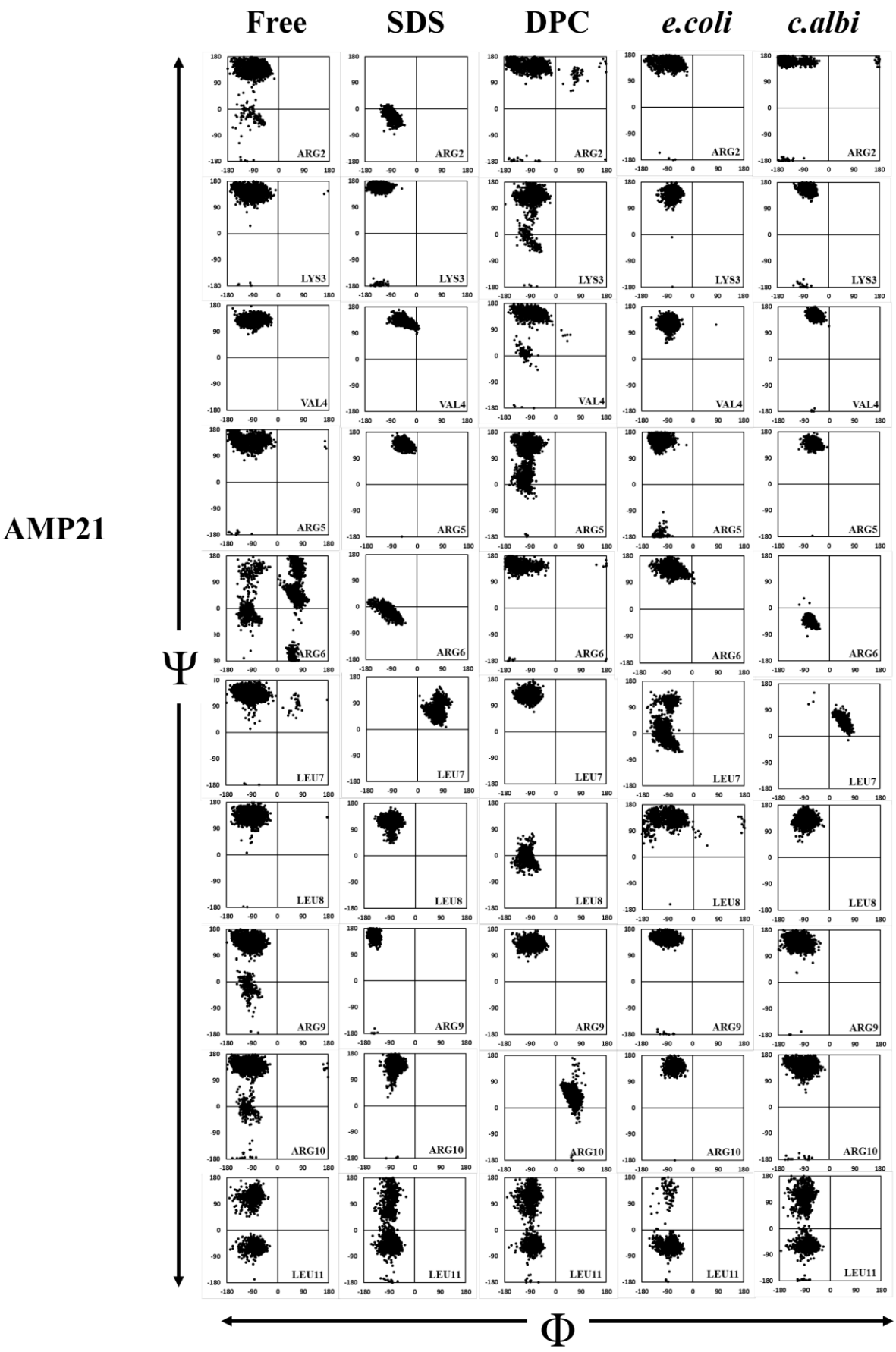
Free
SDS
DPC
e.coli
c.albi
AMP21
Ψ
Φ
ARG2
LYS3
VAL4
ARG5
ARG6
LEU7
LEU8
ARG9
ARG10
LEU11

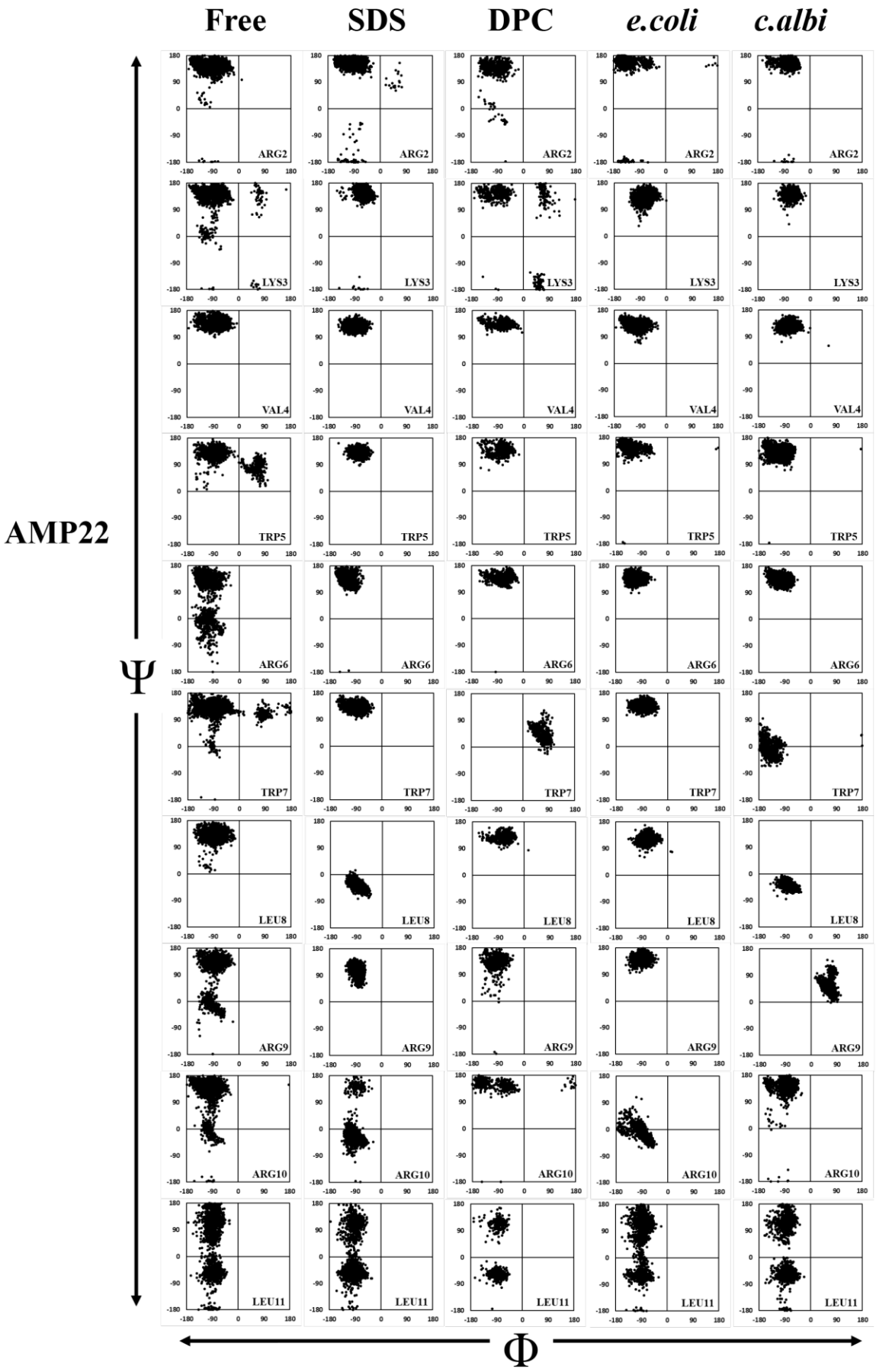
Free
SDS
DPC
e.coli
c.albi
AMP22
Ψ
Φ
ARG2
LYS3
VAL4
TRP5
ARG6
TRP7
LEU8
ARG9
ARG10
LEU11

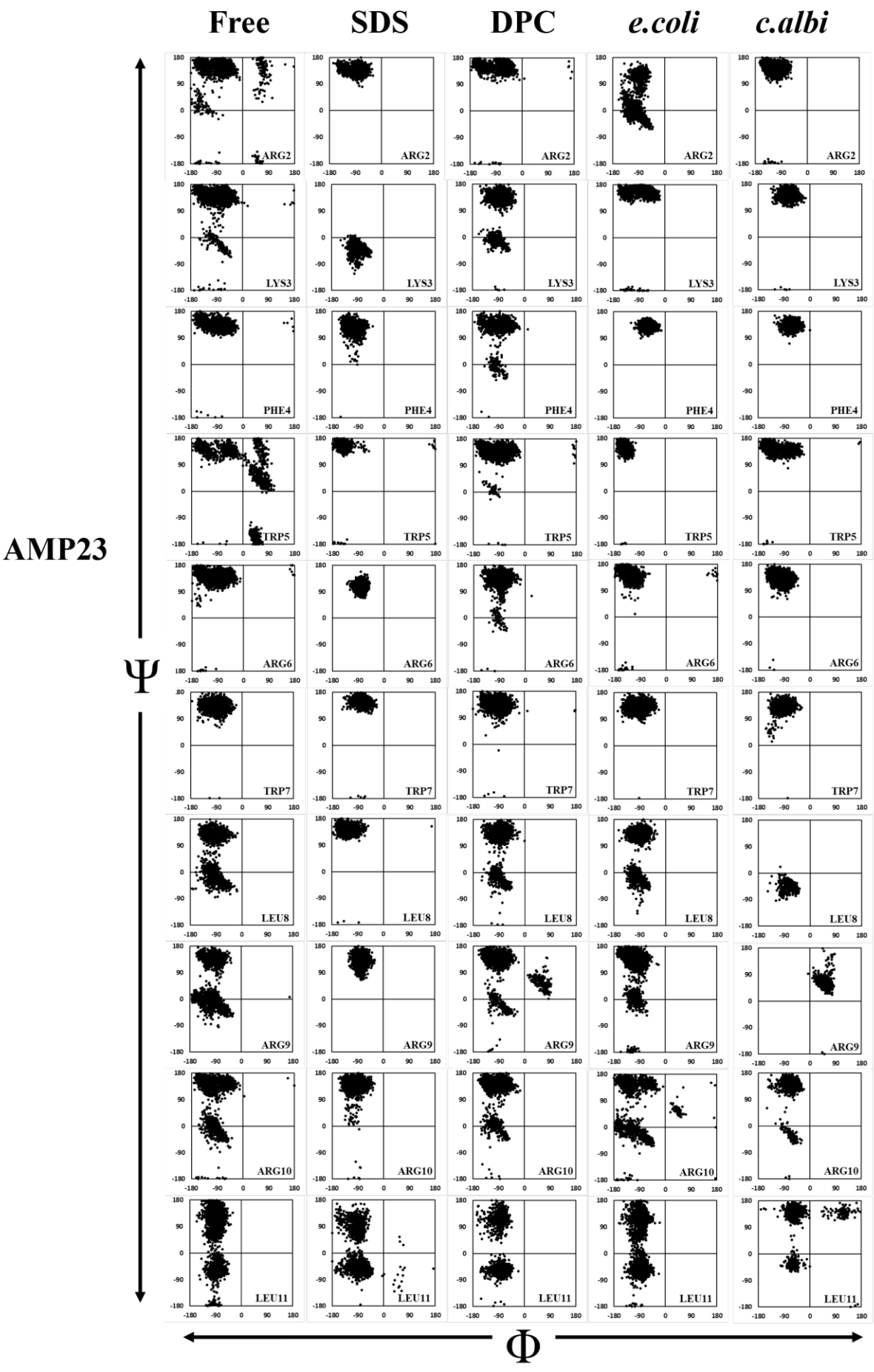
Free
SDS
DPC
e.coli
c.albi
AMP23
Ψ
Φ
ARG2
LYS3
PHE4
TRP5
ARG6
TRP7
LEU8
ARG9
ARG10
LEU11

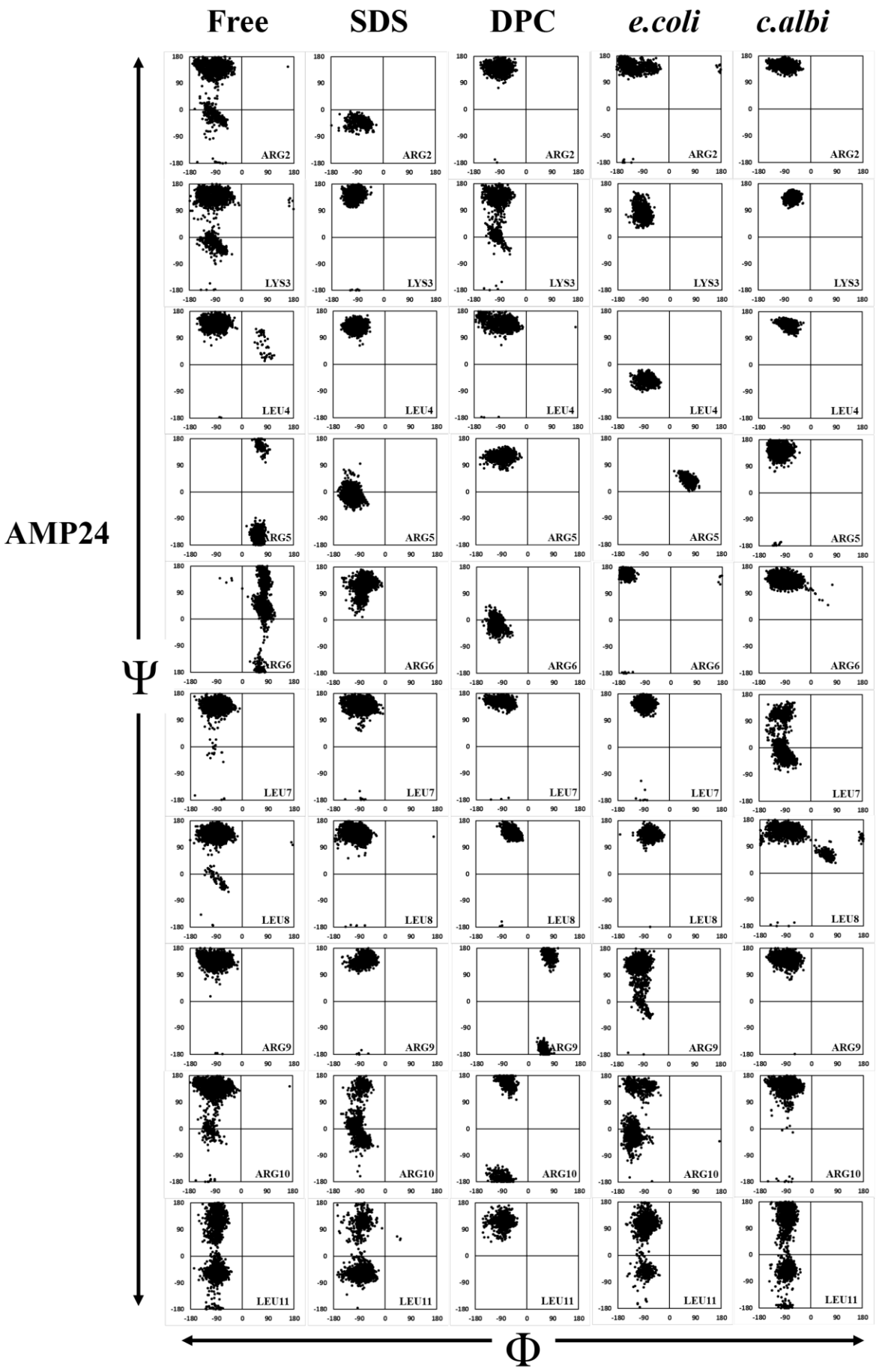
Free
SDS
DPC
e.coli
c.albi
AMP24
ARG2
LYS3
LEU4
ARG5
ARG6
LEU7
LEU8
ARG9
ARG10
LEU11
Ψ
Φ

Figure 3.15: Comparison of Ramachandran plot of each residue of AMP21-24 from MD simulations. There was a reduction in the available conformational space of the residues of all the peptides in the presence of SDS, Ecoli*and Albi* in comparison to the peptides in water alone. This reduction in flexibility of the backbone indirectly suggested binding of the peptides to the microbial membrane mimics. There was less/no significant reduction in the conformational space available to the peptide in the presence of DPC micelles indirectly suggesting little or no interaction with DPC.

for the peptide residue. Reduction of peptide conformational space in response to SDS/Ecoli*/Albi*-binding was evident for the non-terminal residues of the peptides (Figure 3.15)

(d) The conformation of micelle/bilayer-bound peptides could not be classified as any canonical secondary structural structures of proteins. The micelle/bilayer bound peptide was a random coil dynamically less flexible, relative to its unbound form.

(e) Peptide backbone –NH's formed favourable electrostatic interactions (direct or water mediated) with the negatively charged phosphates of the membrane/micelle (Figure 3.14 e), whereas the backbone C=O groups fulfilled their hydrogen bonding requirement by interaction with the bulk water (not shown in Figure 3.14e). The positively charged side-chains of peptide residues formed salt-bridges with the micelle/bilayer phosphates and interacted with bulk waters ensuring hydration. Hydrophobic side-chains were either embedded into the lipid part of the membrane or exposed to the bulk. Overall interaction network between other peptides (AMP21, 23 and 24) and micelle were more or less similar (Figure 3.16).

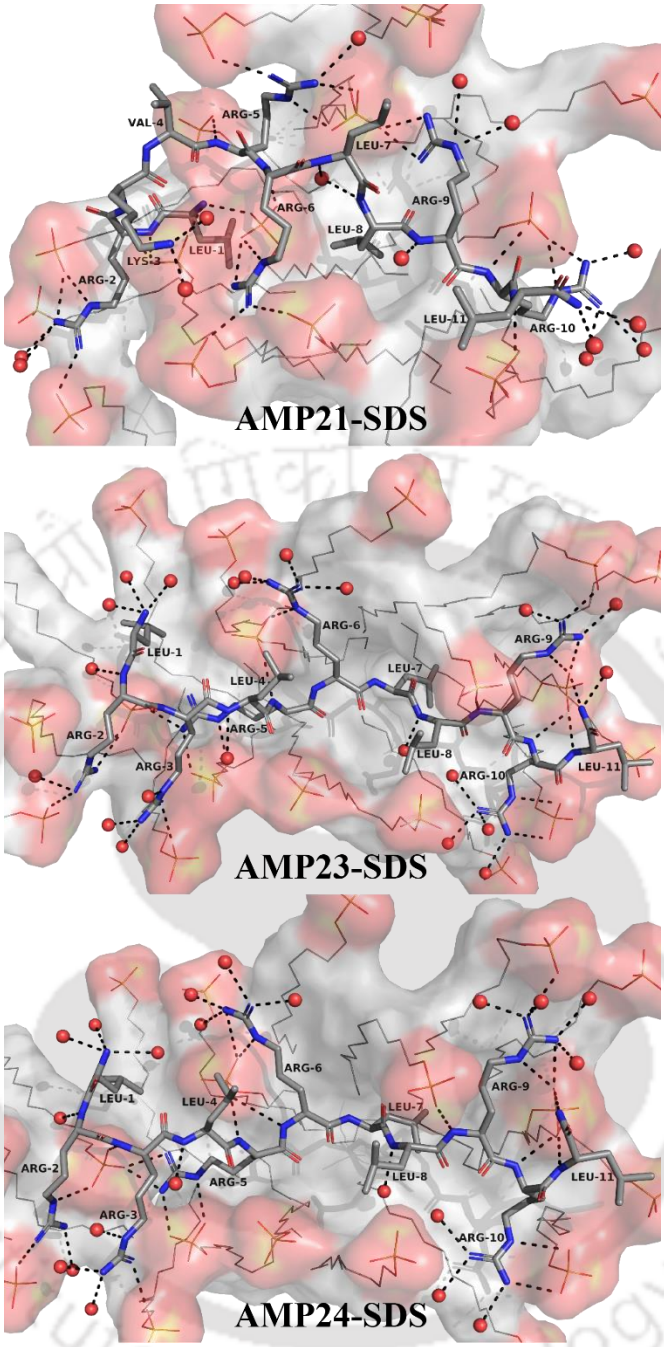

Figure 3.16. Zoomed in view of the interactions between peptides and SDS micelle. Electrostatic contact between peptide amines (backbone and sidechain) and negatively charged phosphates of SDS (direct or water mediated) and bulk water are shown in black broken lines. Hydrophobic side-chains were either embedded into the lipid part of SDS or exposed to bulk water. Peptide backbone C=O interaction with bulk water is not shown for clarity.

(f) Non-bonded interaction energies i.e., coulomb (electrostatic) and Lennard Jones (van der Waals) terms turned out to be favourable for Peptide-micelle/bilayer binding (Table 3.5) except for the DPC micelle (Figure 3.14 f). However, the magnitude of coulomb interaction was larger than the Lennard Jones term (Table 3.5) throughout the MD trajectory (Figure 3.17). Thus, we might conclude that electrostatic interaction was the key factor for peptide-micelle/bilayer binding for AMP 21-24.

Table 3.5. Peptide-micelle/bilayer non-bonded interaction energies (Coulomb, Lennard-Jones) averaged over last 40 ns of MD trajectories. Energies are expressed in kJ/mol and standard deviations are given after ±.

		AMP21	**AMP22**	**AMP23**	**AMP24**
SDS	Coulomb	-1581.56 ±148.41	-1098.24 ±144.43	-1306.26 ±150.12	-1338.11 ±146.64
	Lennard Jones	-337.52 ±35.18	-374.785 ±34.75	-440.69 ±35.82	-345.69 ±37.45
	TOTAL	**-1919.08 ±143.83**	**-1473.02 ±145.81**	**-1746.94 ±150.61**	**-1683.8 ±150.26**
Coli*	Coulomb	-1274.28 ±151.22	-949.77 ±142.49	-786.33 ±156.36	-1252.1 ±203.24
	Lennard Jones	-211.45 ±38.79	-195.31 ±32.96	-144.74 ±39.72	-205.79 ±32.23
	TOTAL	**-1485.72 ±161.53**	**-1145.07 ±142.05**	**-931.07 ±173.7**	**-1457.89 ±201.36**
Albi*	Coulomb	-1111.53 ±145.25	-898.04 ±109.58	-889.62 ±165.42	-952.06 ±112.52
	Lennard Jones	-174.09 ±31.98	-205.36 ±40.42	-161.65 ±31.03	-212.54 ±30.86
	TOTAL	**-1285.61 ±144.83**	**-1103.4 ±116.2**	**-1051.27 ±178.28**	**-1164.6 ±106.37**

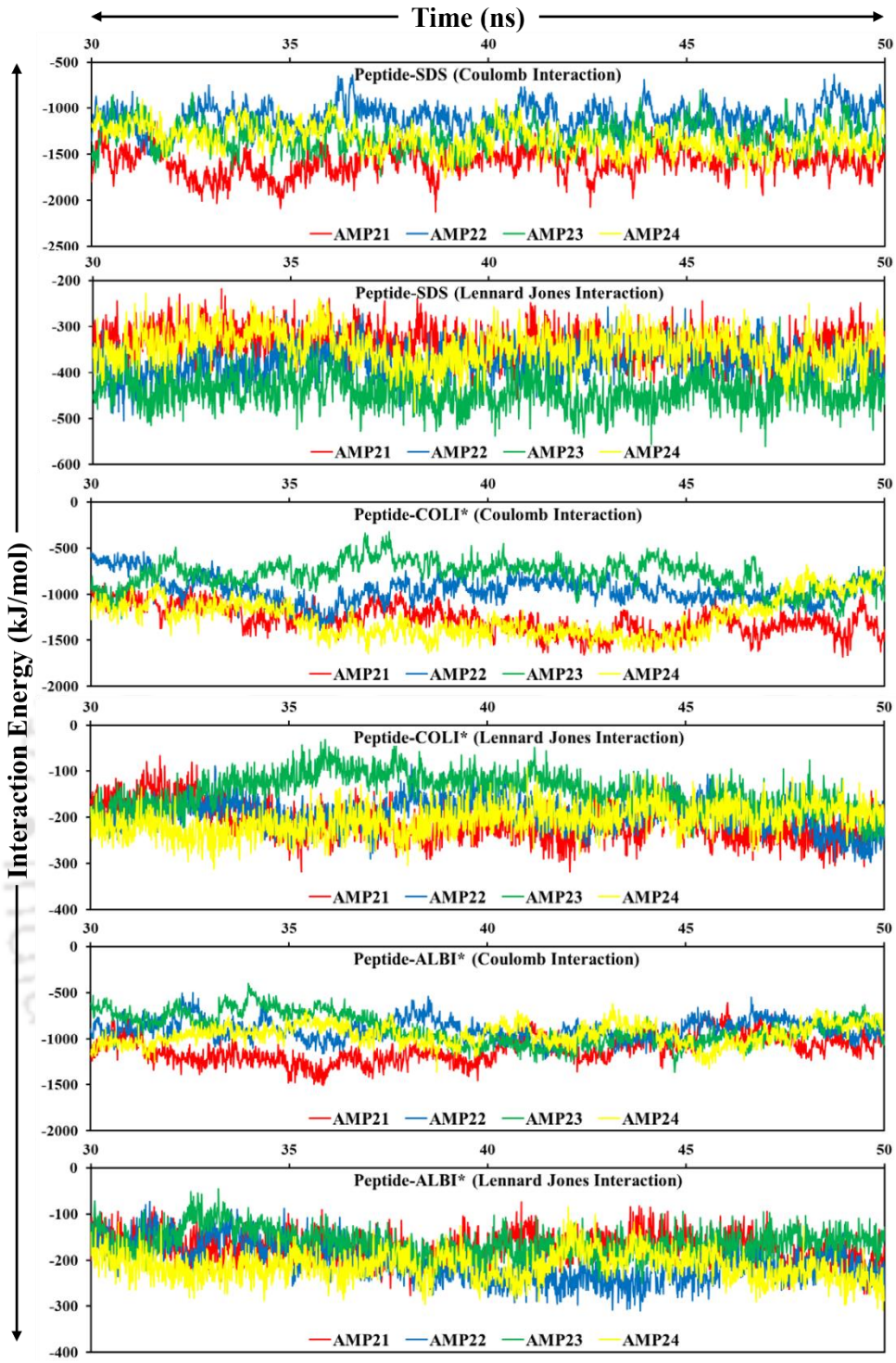
Time (ns)
Interaction Energy (kJ/mol)
Peptide-SDS (Coulomb Interaction)
Peptide-SDS (Lennard Jones Interaction)
Peptide-COLI* (Coulomb Interaction)
Peptide-COLI* (Lennard Jones Interaction)
Peptide-ALBI* (Coulomb Interaction)
Peptide-ALBI* (Lennard Jones Interaction)
AMP21
AMP22
AMP23
AMP24

Figure 3.17: Non-bonded interaction energetics (Coulomb and Lennard-Jones in kJ/mol) as a function of time (ns), between peptide and micelle/mimicked-bilayer from last 20 ns of 50 ns trajectory.

(g) Upon comparison of the no. of hydrogen bonds formed in between AMP22/AMP24 with the lipid membrane mimics, the former clearly scored lower in comparison to the later owing to its lesser positive charge. This was supported by several experimental evidences where AMP22 having lesser positive charge than AMP24 had a weaker interaction with the membrane. This also supported the fact that electrostatics played a major role in peptide membrane interactions.

3.4. Conclusions

We designed four salt tolerant highly efficient small AMPs 21-24 with diminished expenses and time. AMP21-24 were non-hemolytic and non-cytotoxic in nature and hence they could be used as promising candidates for therapeutic use. As AMP21-24 were unstructured, their activity was independent of secondary structure. The primary mode of action of the AMPs was through interaction with the membranes, causing membrane permeabilization, depolarization, deformation and lysis leading to efflux of intracellular materials and eventual cell death. The interaction of the AMPs with the membrane was governed primarily by electrostatics. A secondary mode of action of these AMPs on intracellular targets was suggestive from the unspecific cytosolic localization of the peptides as seen from the confocal laser microscopy. The fundamental understanding about the design and mechanism of action of AMPs developed in this study would not only enrich the existing literature but also trigger the design of better antimicrobials in the future.

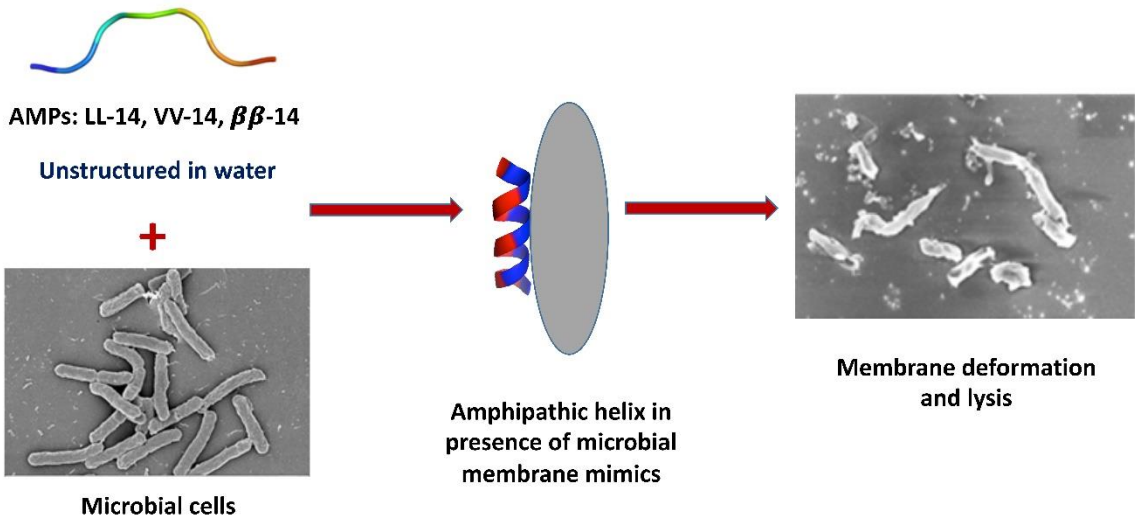

Hydrophobic side chain length, Antimicrobial Activity, Cytotoxicity:

LL-14 > VV-14 > ββ-14

Chapter 4

Effect of Secondary Structure and Side Chain Length of Hydrophobic Amino Acid Residues on the Antimicrobial Activity and Toxicity of 14-Residue-Long de novo AMPs

4.1. Introduction

Cationic amphipathic α-helical peptides are the most promising, well-characterized and abundant AMPs in nature. Leu and Lys residues which have strong helix promoting abilities are often used to design prototype α-helices, called LK peptides with strong antimicrobial activities. Length of the LK peptides plays a crucial role in their antimicrobial activity and the cytotoxicity. Increasing the length promotes enhanced activity, however, compromising the cytotoxicity of these peptides. In chapter 2, we have developed an unstructured LK heptapeptide P4, with broad-spectrum antimicrobial activity. In the present study, we attempted to improve upon its activity by lengthening the sequence. The peptide LL-14 (Table 4.1) was derived by the doubling the sequence of AMP P4 twice. We speculated that doubling the length of P4 would promote helical structure to the peptide, which in turn might improve its antimicrobial efficacy without compromising the cytotoxicity. The primary sequence of LL-14 was designed to have facial amphipathicity upon attainment of helical structure. Val is known for its propensity to occur in β-sheets and discouraging the helical secondary structure. In the peptide VV-14, we replaced all the Leu residues from LL-14 to Val, to study the effect of secondary structure and altering the side chain length of the hydrophobic residues on the activity and cytotoxicity of LL-14. To improve on the protease susceptibility of our designed AMPs, we designed ββ-14 where unnatural amino acid residue β-Ala replaced most of the hydrophobic Leu residues in LL-14. While higher homologues of α amino acid residues increase the backbone flexibility of the peptides in general, there are several reports of these amino acid residues being accommodated into the well-defined secondary structures as well. It would be interesting to study the structural implications of the use of β-Ala as the hydrophobic residue in the AMP sequence ββ-14, and its consequence on the activity. It is important to mention that this amino acid residue does not

Table 4.1. Peptide Sequences with Code.

Peptide Code	Peptide Sequences
LL-14	H-LKWLKKLLKWLKKL-NH_2
VV-14	H-VKWVKKVVKWVKKV-NH_2
ββ-14	H-LKWβ_{ala}KKβ_{ala}LKWβ_{ala}KKβ_{ala}-NH_2

contain any side chains like Leu and Val residues used in the earlier designs. In short, our design intended to study the effect of (a) peptide length, (b) length of side chains and (c) secondary structures on the antimicrobial activity and toxicity of the AMPs. In a study by Hicks and coworkers, the side chain length of the basic amino acid residues was systematically varied by the use of amino acids Lys, Orn, Dab, Dpr and Arg to study its effect on the antimicrobial property of the peptides.[519] We have studied the mechanism of action of the potent AMPs in details by using various biophysical, spectroscopic and electron microscopic techniques in this chapter.

4.2. Experimental Section

Peptide synthesis, purification, characterization (Appendix, Figure A8-A10, A32, A50-52), MIC studies, hemolytic assay, cytotoxicity assay done according to the protocol discussed in Chapter 2.

4.2.1. Hemolytic and Bactericidal Activity Assay of VV-14 in Presence of both RBCs and Bacteria:

This experimental method is the little modified version of previously reported protocol.[520] Over-night grown culture of *S. typhi* TY2 cells were centrifuged at 6000 rpm for 5 min and fresh human blood cell suspension was centrifuged at 8000 rpm for 10 min at 277 K. The pellets were washed three times with 10mM PBS (pH 7.4) and suspended in the same buffer to

obtain 10^5 CFU/ suspension in case of bacteria and 5×10^9 cells/ in case of RBCs. 50 µL bacterial cell suspension and 5 µL blood cell suspension together were incubated with different concentrations of peptide VV-14 (ranging from 1-50 µM) prepared from 1mM stock, made the reaction volume to 100 µL and incubated at 310 K with shaking for 4 h. After incubation, 5 µL was taken from reaction volume, diluted in the same buffer and spread onto the NB agar plates for CFU counting after overnight incubation at 310K. The remaining volume was centrifuged and the absorbance of supernatant was measured at 414 nm using a sterile 96 well plate. For comparison, experiments were performed also with *S. typhi* TY2 cells and RBCs only, under the same conditions. All experiments were performed in triplicate.

4.2.2. Time Course of Bactericidal Activity Assay of VV-14:

Overnight grown culture of *S. typhi* TY2 was centrifuged at 6000 rpm for 5 min and the pellet was washed three times with 10 mM phosphate buffer (pH 7.4) and resuspended to obtained 10^5 CFU/ suspension. 50 µL of bacterial cell suspension was incubated with minimum inhibitory concentration of peptide VV-14 and incubated at 310 K for different time intervals (5-120 min). After each incubation time, 5 µl aliquot was taken from each reaction volume, diluted in the same buffer and spread onto the NB agar plates for CFU counting after overnight incubation at 310 K. All experiments were performed in triplicate.

4.2.3. Membrane Permeabilization Assay of VV-14:

To determine the outer membrane permeabalization ability of VV-14, NPN uptake assay was performed. Overnight grown culture of *S. typhi* TY2 cells was washed and resuspended in 10 mM sodium phosphate buffer (pH 7.4) to a final cell concentration of 10^6 CFU/ml. The peptide was added with increasing concentrations to a cuvette containing 1 of cells and 10 µM NPN. The fluorescence of the dye was monitored for 10 min at room temperature and after peptide addition, increased fluorescence was monitored for 10 min using Hitachi F-7000 FL

spectrometer at excitation wavelength of 350 nm (slit width: 5 nm) and emission wavelength of 410 nm (slit width: 5 nm) to determine the NPN uptake.

Next, inner membrane permeabilization ability of VV-14 in *S. typhi* TY2 was examined by performing PI uptake assay as described earlier in Chapter 3, section 3.2.7.

4.2.4. Calcein Leakage Assay:

Two kinds of calcein encapsulated LUVs, mimicking anionic bacterial cell membranes and zwitterionic cell membranes were used to study calcein leakage in the presence of AMPs. Anionic bacterial membrane and eukaryotic cell membrane mimicking model LUVs were made with the composition of 1-palmitoyl-2-oleoyl-sn-glycero-3-phosphoetanolamine (POPE), 1-palmitoyl-2-oleoyl-sn-glycero-3-phosphoglycerol (POPG) at 3:1 ratio and 1-palmitoyl-2-oleoyl-sn-glycero-3-phosphocholine (POPC), cholesterol lipid at 6:4 ratio respectively, with a final concentration of 2 mg/. The rest of the experiment was performed as described earlier in Chapter 2 Section 2.2.8.

4.2.5. Fluorescence Spectroscopic Studies:

The intrinsic tryptophan fluorescence property of VV-14 peptide was used to analyse interaction and conformational transition of VV-14 with bacterial and eukaryotic cell membrane mimics. Intrinsic tryptophan of VV-14 was exited at 295 nm and emission spectra was recorded from 300-400 nm in presence of 10 mM phosphate buffer (pH 7.4), SDS and DPC using Hitachi F-7000 FL spectrometer at 25°C temperature. The experiments were performed at 5 µM peptide concentration and added SDS and DPC, in increasing concentrations ranging from 5-40 µM.

4.2.6. Fluorescence Anisotropy:

The binding affinity of VV-14 to SDS was determined by steady-state fluorescence anisotropy on the basis of intrinsic tryptophan fluorescence property of VV-14 peptide. The experiments were carried out using Hitachi F-7000 FL spectrometer equipped with a polariser. Initially fluorescence measurement was performed at 5 µM peptide concentration in 10 mM phosphate buffer (pH 7.4) and then SDS was added with increasing concentrations ranging from 5-40 µM. The fluorescence anisotropy values were calculated from the equation (2)

$$\text{Anisotropy } (r) = (I_{VV}-G\times I_{VH})/(I_{VV}+2\times G\times I_{VH}) \qquad (2)$$

Where, I_{VV} and I_{VH} are the emission intensity with fixed excitation polariser at vertical orientation, when the orientation of emission polariser varied vertically and horizontally. G is the sensitivity parameter for the spectrometer (Hitachi F-7000 FL spectrometer), which is represented as $G = I_{HV}/I_{HH}$. To determine the equilibrium dissociation constant (K_D) of peptide and SDS micelle, the anisotropy values were plotted against SDS concentration (µM) and fitted using the Hill equation.

4.2.7. Flied Emission Scanning Electron Microscopy (FESEM):

The effect of VV-14 on the *S. typhi* TY2 cells was visualized by performing FESEM as described earlier in Chapter 2, Section 2.2.13.

4.2.8. Field Emission Transmission Electron Microscopy (FETEM):

Overnight grown culture of *S. typhi* TY2 cells were collected by centrifugation at 6000 rpm for 5 min, washed three times and resuspended in 10 mM sodium phosphate buffer at pH 7.4 to final number of 10^5 cells/. The cell suspensions were incubated with VV-14 at MIC for 1 hrs. at 310 K and untreated cells were set as the control. After incubation, 2 µL aliquot was placed on a copper grid, stained with 1% uranyl acetate and air dried.

4.2.9. CD experiment:

CD spectroscopy of all the designed AMPs were recorded in water, TFE, and different membrane mimetic environments (SDS (30 mM) and DPC (2.5 mM)) as described in Chapter 2 section 2.2.10.

4.2.10. NMR Experiments:

All NMR spectra were recorded at 37°C using either a Bruker Avance III 500 MHz spectrometer equipped with a 5 mm SMART probe or a 700 MHz spectrometer equipped with a RT probe. For SDS bound structure calculation of VV-14, 1mM peptide dissolved in 10 mM sodium phosphate buffer (pH -4.5) was used for two-dimensional (2D) $^1H-^1H$ total correlation spectroscopy (2D TOCSY) and 2D $^1H-^1H$ nuclear Overhauser effect spectroscopy (2D NOESY) with mixing times of 80 and 150 ms, respectively. The experiments were performed in absence and presence of 200 mM deuterated SDS (SDS-D_{25}, Cambridge Isotope Laboratories, USA) to compare free and bound structures. 10% D_2O was added into the tube for locking purposes and 3-(trimethylsilyl)propanoic acid (TSP) was used as an internal standard (0.0 ppm).[521] The recycle delay was set to 1.5 sec and the experiments were performed with 2K (t2) x 456 (t1) increments with excitation sculpting for water suppression. States TPPI was used for quadrature detection in t1 dimension. Number of scans were 20 and 40 for TOCSY and NOESY, respectively.

Live cell NMR experiment was recorded on a Bruker Avance III 500 MHz spectrometer as described in chapter 3. Briefly, S. typhi TY2 cells were grown in Nutrient Broth containing 50 µg/ streptomycin and maintained at 310 K with shaking conditions to reach logarithmic phase (OD_{600}=0.4 – 0.6). Then the cells were washed three times by using 10mM phosphate buffer (pH-6.5) and re-suspended in the same buffer to a final concentration of approximately 1×10^8 cells/. The suspension was then divided into two aliquots of the same volume and centrifuged for 5 min at 7000 rpm to remove the supernatant and obtain two pellets containing approximately the same number of living cells. The first pellet was re-suspended in 10 mM sodium phosphate buffer (pH 6.5) and subjected to NMR analysis in presence of 1 mM VV-14 peptide, while the second was re-suspended in the same buffer and subjected to time kinetics using agar plate method. The duration of each experiment was set around 5 min keeping the recycle delay at 1 s.

All NMR data processing and analysis were carried out using the Topspin v3.1 (Bruker Biospin, Switzerland) and SPARKY (Goddard, T. D., and Kneller, D. G. University of California, San Francisco) programs, respectively.

4.2.11. Calculation of NMR Derived Structures:

For calculation of the SDS-bound three dimensional structure of the VV-14 peptide, the volume integrals of their respective NOE cross-peaks were qualitatively differentiated into strong, medium and weak, depending on their intensities in the NOESY spectra. This information was further transformed to inter-proton upper bound distances of 3.0, 4.0 and 5.0 Å for strong, medium and weak NOEs respectively, while the lower bound distance was fixed to 2.0 Å. The dihedral angle restraint for phi (φ) angles were obtained from PREDITOR web server with the

help of H^{α} and $^{13}C^{\alpha}H$ chemical shifts and the predicted torsional angles were further relaxed with ± 20° as upper and lower limits for further structure calculation while the values for psi (ψ) angles were kept flexible (120 º to -120°) for all non-glycine residues to limit the conformational space. CYANA program v2.1 was used for all structure calculations with iterative refinement of the structure based on distance violation. Hydrogen bonding constraints were excluded from structure calculation. The NMR-derived ensemble structures were analysed using PyMol™ (2.0.4, student version), chimera (1.13.1)[522] and their stereochemistry was checked using Procheck.[523]

4.3. Results and Discussions

4.3.1. Antimicrobial Activity:

All the three peptides were active against bacterial strains such as *E. coli DH5α, P. aeruginosa* (ATCC 27853), *S. typhi (gifts from J. Parkhill Sanger Institute, Hinxton, United Kingdom), K. pneumoniae, S. aureus* as well as human opportunist fungal strains such as *C. albicans* SC5314 and *C. neoformans* var. *grubii* H99. *P. aeruginosa*, *K. pneumoniae* and *S. aureus* belongs to the ESKAPE group of pathogens, which are potential multi drug resistant strains, challenging clinical practices.[524] *S. typhi*, a causative agent of typhoid fever, is very widespread in the world, mainly in developing regions.[525] Among three peptides, ββ-14 showed least activity, having none against *S. aureus* and *S. typhi TY2*. Higher antimicrobial activity was shown in case of LL-14 and VV-14 (Table 4.2, Figure 4.1). Peptide LL-14, derived directly from doubling of the sequence of P4 (from Chapter 2) had a better activity than P4. This suggested that, increasing the length of the peptide generally led to better activity.

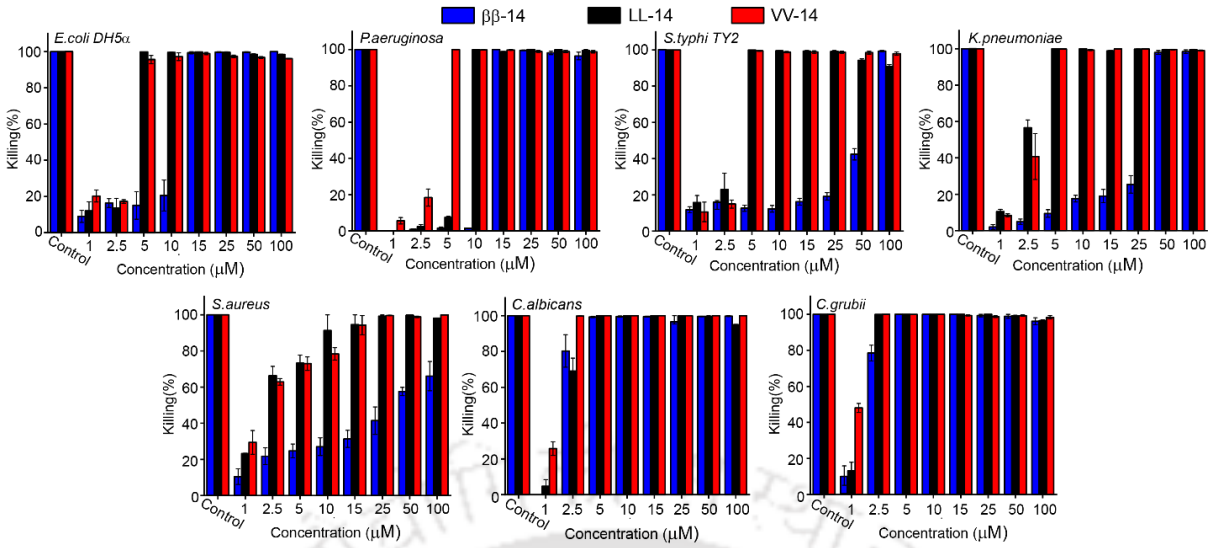

Figure 4.1. The bar plots represent $MIC_{99\%}$ of LL-14, VV-14 and ββ-14 in absence of 10 mM phosphate buffer. The micro broth dilution assay was performed in increasing concentration of respective peptides and killing percentage was calculated, after overnight incubation. LL-14 (black) and VV-14 (red) peptides showed higher potentiality than ββ-14(blue).

Biological systems generally contain high concentration of salt that hamper antimicrobial activity of many AMPs.[526] To check the physiological salt tolerance ability of our designed AMPs, the micro broth dilution assay was performed in presence of 10 mM phosphate buffer saline (pH 7.4). At this concentration, ββ-14 completely lost its activity and VV-14 reduced its activity against all the other strains except *S. typhi* TY2 (Table 4.2, Figure 4.2). Interestingly, LL-14 showed unaltered activity against *E. coli DH5α, K. pneumoniae, S. typhi, C. albicans* and slightly reduced activity against *P. aeruginosa*, *S. aureus* and *C. neoformans* var. *grubii.* Additionally, LL-14 also showed unaltered activity against *S. typhi TY2*. From these experiments it was confirmed that among the three peptides, LL-14 was the most active AMP with the best salt tolerance property (Table 4.2). As the activity of LL-14 was the best, followed

by VV-14 and ββ-14, it may be assumed that, the activity diminishes gradually with the reducing size of the side chain of hydrophobic amino acid residues in the sequence.

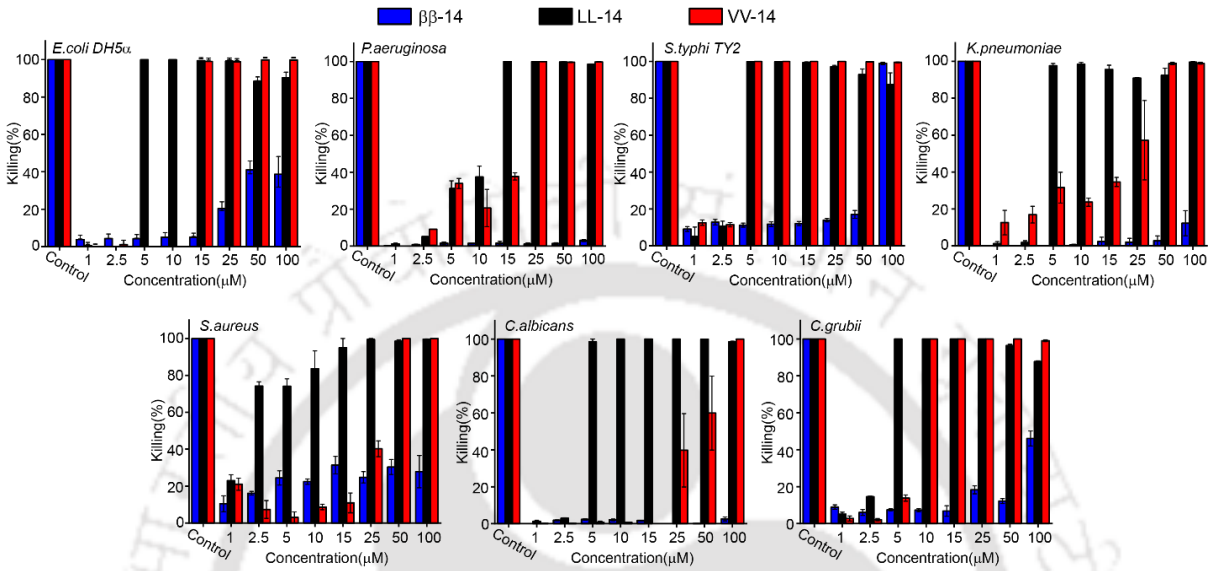

Figure 4.2. The bar plots represent $MIC_{99\%}$ of LL-14, VV-14 and ββ-14 in presence of 10mM phosphate buffer saline. The micro broth dilution assay was performed in increasing concentration of respective peptides to calculate the killing percentage. ββ-14 (blue) completely loose its activity, VV-14 (red) reduced its antimicrobial activity against all microorganisms except *S. typhi TY2* but, in case of LL-14 (black) antimicrobial activity was not that much altered.

Table 4.2: MIC of LL-14, VV-14 and ββ-14 in presence and absence of salts.

	In Absence of Salts MIC$_{99\%}$ in µM			**In Presence of 150 mM NaCl MIC$_{99\%}$ in µM**		
	LL-14	**VV-14**	**ββ-14**	**LL-14**	**VV-14**	**ββ-14**
E. coli DH5α	5	5	15	**5**	**15**	>100
P. aeruginosa	10	5	15	**15**	**25**	>100
K. pneumoniae	5	5	50	**5**	50	>100
S. typhi TY2	5	5	100	**5**	**5**	100
S. aureus	10	15	>100	NA	NA	NA
C. albicans	5	2.5	5	**5**	50	>100
C. grubii	2.5	2.5	5	**5**	**10**	>100

4.3.2. Hemolytic Activity:

Non-Hemolytic potency of a peptide is a major governing factor in its practical applicability as an antimicrobial therapeutic and hence the hemolytic activity of the designed peptides, LL-14, VV-14, ββ-14 was tested against human red blood cells. As seen in Figure 4.3, VV-14 and ββ-14 showed very negligible percentage of hemolysis, making them non-hemolytic, while LL-14 showed about 90% hemolysis at 5 µM concentration. This may be a consequence of the large size of the Leu side chains, in comparison to Val or β-Ala. Due to this, in spite of its higher activity, biological application of LL-14 was not considered for further experiments.

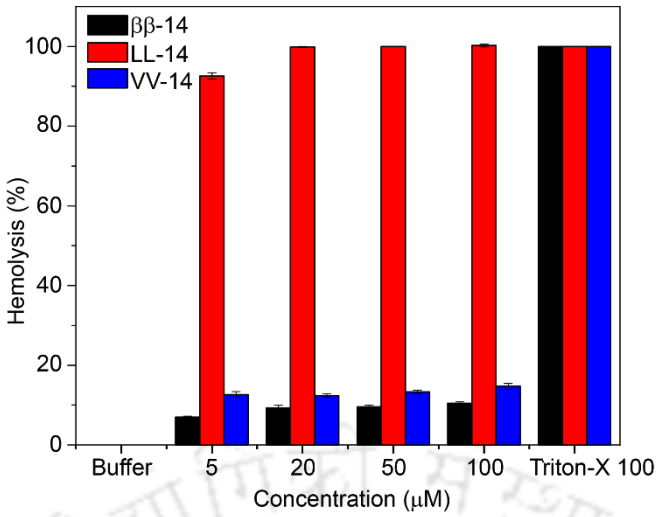

Figure 4.3. Hemolytic activity of LL-14, VV-14 and ββ-14. The haemolytic activity was determined by treating RBCs with increasing concentration of peptides and after 4 hr. of incubation, amount of hemoglobin release was quantified by measuring absorbance at 414 nm. LL-14 (red) showed high haemolytic activity but ββ-14 (black) and VV-14 (blue) showed negligible haemolysis. All experiments were performed in triplicate.

4.2.3. Cytotoxicity of the AMPs:

Cell viability of normal human embryonic kidney (HEK 293) and human embryonic lungs (L132) cell lines in the presence of all the designed AMPs was studied. As shown in Figure 4.4, upon treatment of the cells with the peptides for 24 hr., only peptide LL-14 showed significant toxicity even at low concentration. In contrast, cell viability was reduced only by 10% for VV-14 and ββ-14 even at higher concentrations (≥100 μM). This is a quite spectacular observation. As the peptides only differ in their hydrophobic amino acid residues, which have varying length of side chains, this difference in their cytotoxicity can be related to it. Leu with the longest side chain interacts with mammalian membranes generating cytotoxicity, while Val and β-Ala with smaller side chains do not interact, causing non-cytotoxicity.

Collectively, after the initial screening, among the three designed peptides, VV-14 was the best candidate from both the potency and cytotoxicity perspective and was considered for further studies. As the activity of VV-14 was unaltered against *S. typhi TY2* in the presence of salt, all the future experiments on VV-14 was performed on this microbe.

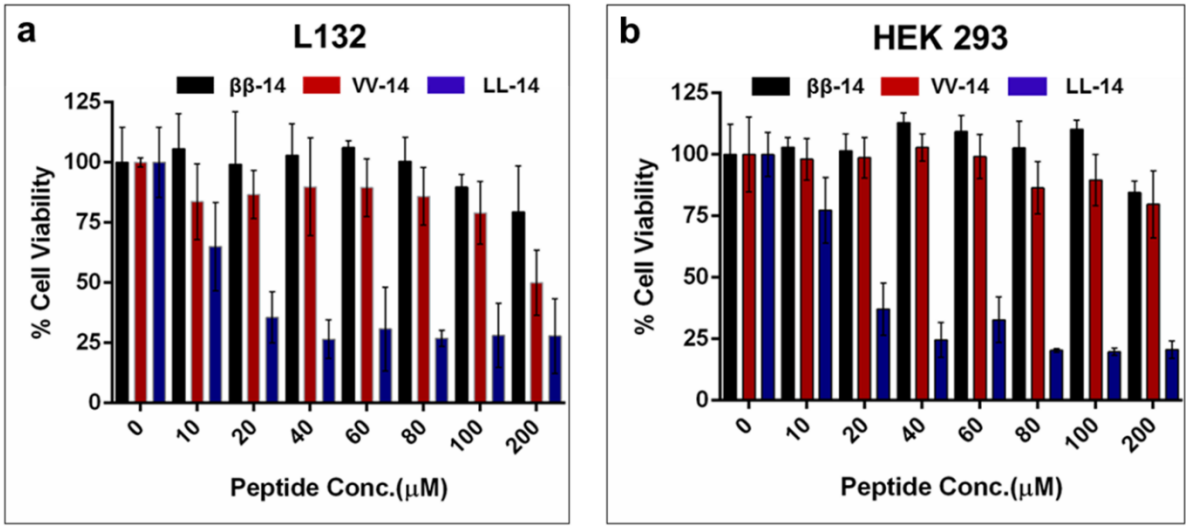

Figure 4.4. MTT Assay of peptides LL-14 (Blue), VV-14 (Red), ββ-14 (Black) on HEK 293 and L132 cells. Viability was quantified by measuring the absorption at 570 nm. All experiments were performed in triplicate.

4.3.4. Time Course of Bactericidal Activity for VV-14 on *S. typhi TY2*:

To determine the time needed for expressing bactericidal activity of VV-14 peptide, the time kinetics assay was performed. The cells were treated with VV-14 at its $MIC_{99\%}$ value and at different time points, treated cells were spread onto the NB agar plate for CFU counting. After overnight incubation, percentage of viable cells was calculated. From this we concluded that (a) 60 minutes of incubation was sufficient for lysing 90% of the cells and (b) at 70 minutes, almost complete killing the cells occurred when compared with control experiment (Figure 4.5).

4.3.5. Bactericidal and Non-Hemolytic Activity in the presence of both Bacteria and RBCs:

It was known that the activity of some AMPs is higher in the *in vitro* microbiological studies; however, when the bacteria are exposed to excess human cells, the activity of the peptides gets suppressed due to complex mechanisms of host cell.[520]

In order to bridge this gap between *in vitro* and *in vivo* conditions, we set up an experimental condition to identify the antimicrobial activity in the presence of human RBCs. Here, we have used 5×10^4 *S. typhi* TY2 cells/ and 1×10^7 RBCs/, ie. a large amount of host cells in comparison to bacterial cells which represents a simple model to predict about selectivity of the peptide.[51] To our surprise, the antimicrobial as well as hemolytic activity of VV-14 was not altered drastically, suggesting that presence of excess RBC's as in the *in vivo* conditions, did not affect the potency of the peptide (Figure 4.6, 4.7). Taken together, our findings confirm on strong selectivity VV-14 peptide against *S. typhi* TY2 even in presence of eukaryotic host cells.

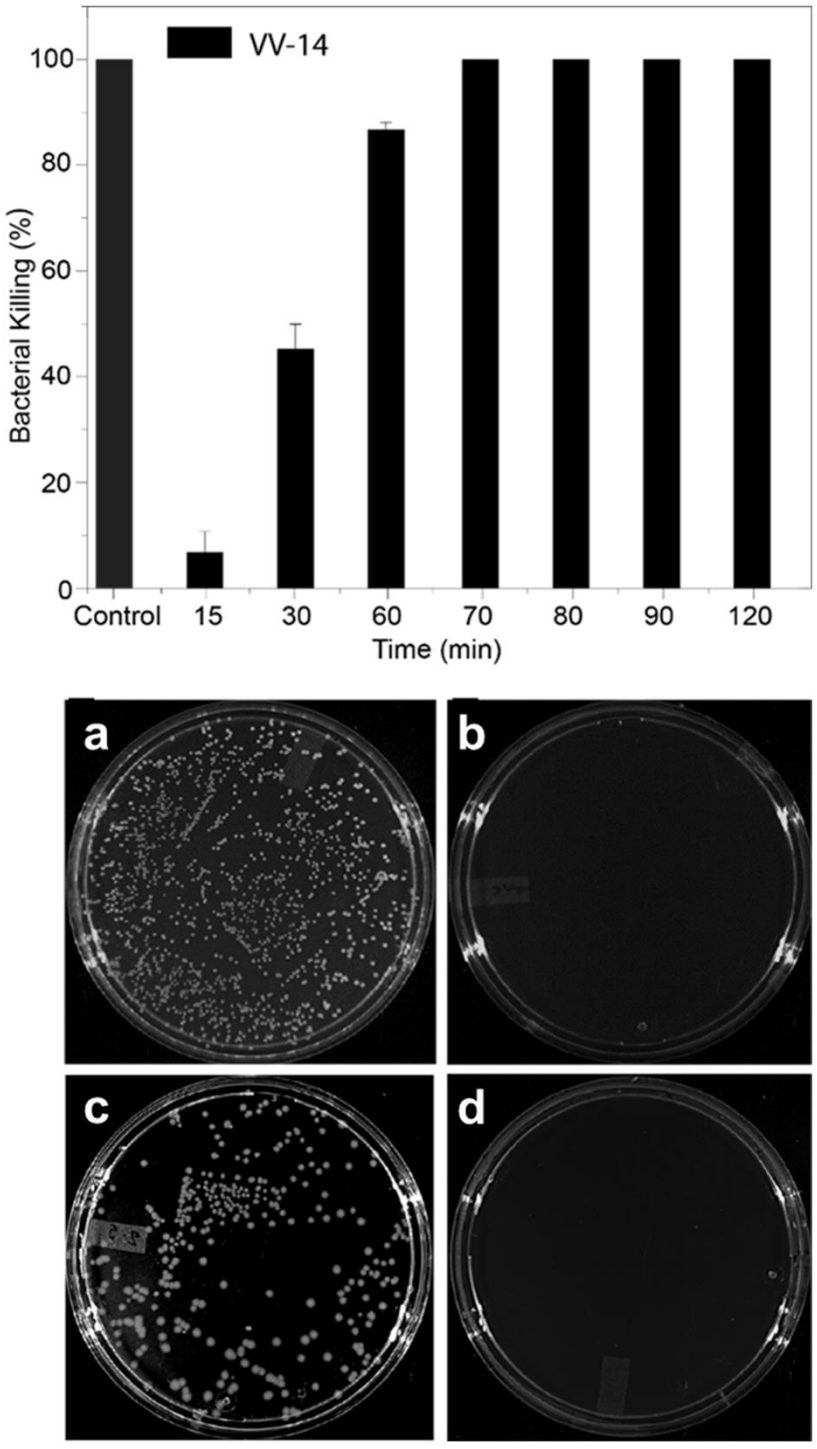

Figure 4.5. Time course study of bactericidal activity of VV-14 peptide at MIC against *S. typhi* TY2 cells. *S. typhi* TY2 cells were treated with VV-14 at MIC for different time intervals and cells were spread on NA plate for CFU count after overnight incubation. Bacterial killing percentage was calculated from CFU count of the plate in comparison to the control plate. At 70 min time point, completely clear plate was observed, indicating 100% killing of bacterial

cells. (a) Negative control plate (i.e. no AMP), (b) Positive control plate (i.e. 10 µM Polymyxin B treated cells), (c) 60 min time point plate, (d) 70 min time point plate. All experiments were performed in triplicate.

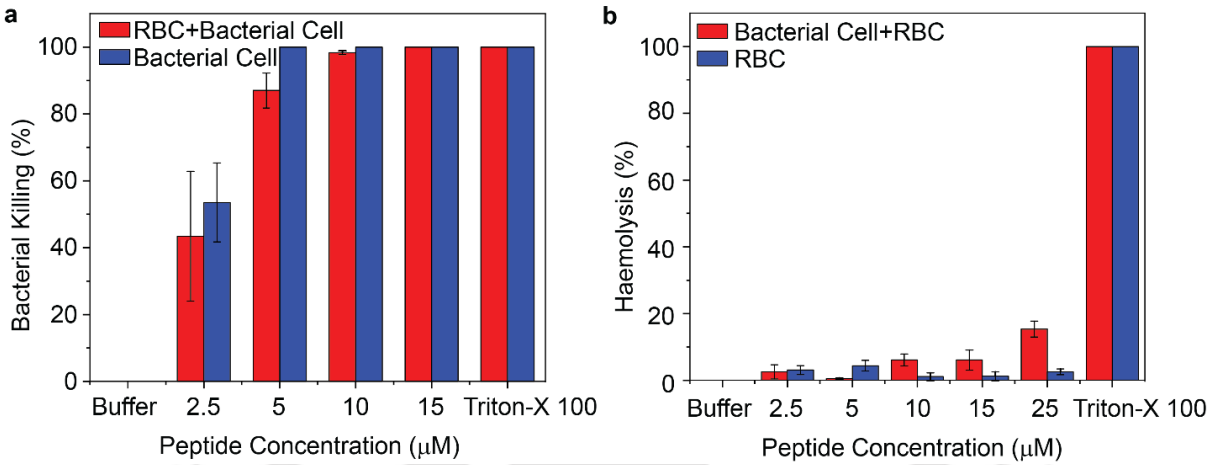

Figure 4.6. (a) Bactericidal and (b) hemolytic activity of VV-14 in presence of both bacterial cells and RBCs. To check membrane binding selectivity and sequestration effect by host cells on antimicrobial activity of VV-14, bactericidal and hemolytic assays were performed in presence of both *S. typhi TY2* cells and RBCs. Bacterial cells and RBCs together were treated with increasing concentration of VV-14. After 4 hr. of incubation, hemolysis was checked by measuring absorbance at 414 nm and bactericidal activity was checked by spreading the cells on NA plate for CFU count after overnight incubation. A negligible amount of antimicrobial activity alteration and hemolysis was observed. All experiments were performed in triplicate. please

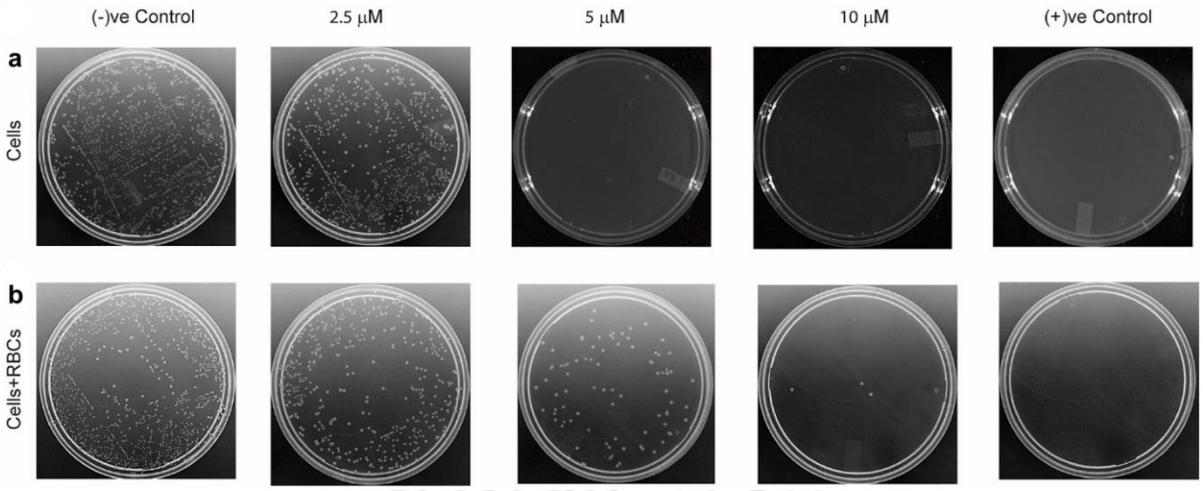

Figure 4.7. The images depicting the CFU/ on nutrient agar plates at various peptide concentration. The bactericidal assay was performed in the presence of both *S. typhi* TY2 cells and human RBCs to check altered antimicrobial activity of VV-14. (a) The images of the plates represents control experiment, where only *S. typhi* TY2 cells were treated with VV-14 in increasing concentration. $MBC_{90\%}$ was observed at 5 μM concentration of VV-14. (b) In presence of RBCs, *S. typhi* TY2 cells were treated with VV-14 in increasing concentration. Negligible alteration of $MBC_{90\%}$ was observed compared to the control experiment.

4.3.6. Killing Kinetics of VV-14 using Live Cell NMR:

To understand the atomistic detail of this interaction between VV-14 and microbial cells, real time NMR experiment using live bacterial cells was performed. Immediate line width broadening for all the residues of the peptide VV-14 was observed due to T_2 relaxation, in the presence of bacterial cells, suggesting interaction in between them. Additionally, release of metabolites from the lysed, dead or wounded cells were also observed as early as 20 minutes after incubating the cells with the peptide (Figure 4.8). Kinetics experiments using agar plate method (Figure 4.8, Right panel) further confirmed the time required to kill 99% of the bacterial cells in presence of the peptide. The increment of the metabolite peaks (5.4-9.40 ppm) from

the VV-14 peptide treated cells over the time, also confirmed that the peptide had a persistent activity on the negatively charged bacterial membranes (Figure 4.8, inset). Under similar conditions, untreated control cells did not show any metabolite release.

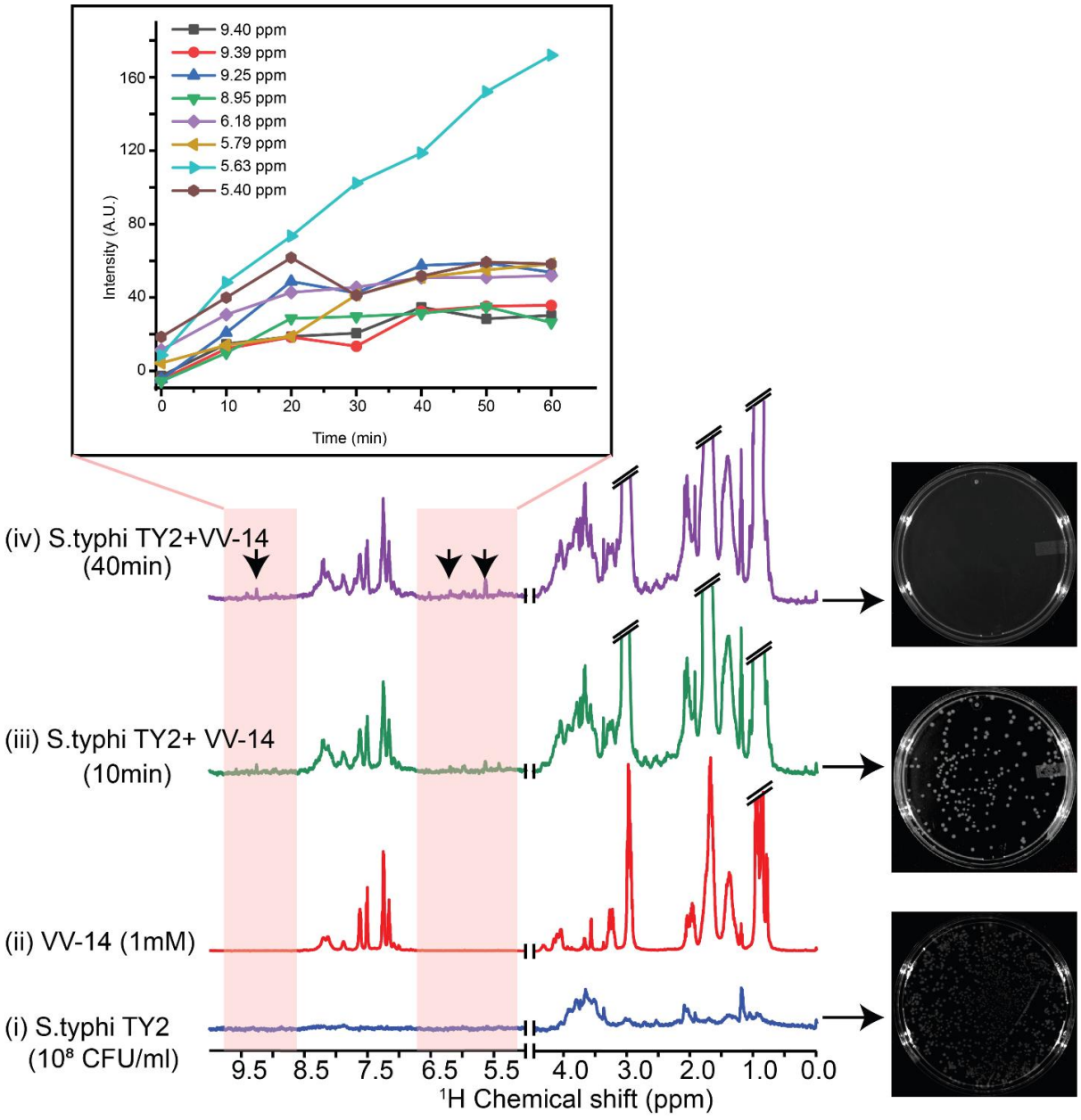

Figure 4.8. Killing kinetics of *S. typhi* TY2 by using live cell NMR and correlating with agar plate method. 1D ^{1}H spectra of (i) *S. typhi TY2* (10^{8} CFU/ml), (ii) 1mM VV-14 peptide in

10mM phosphate buffer (pH-6.5) and (iii-iv) VV-14 in presence of S. typhi TY2 cells at 10 and 40 minutes respectively. Agar plate corresponding to the untreated and treated cells has been shown accordingly. Inset: Intensity of the newly generated peaks from the metabolites as a result of peptide action on the cells plotted against time shows a gradual increase in the peak intensities.

4.3.7. Membrane Permeabilization Assay:

Generally**,** most of the AMPs are known to target the cells though membrane perturbation and pore formation. To probe the membrane binding and perturbing activity of VV-14, we performed a series of biophysical experiments. The outer membrane permeabilization of *S. typhi* TY2 was determined using NPN dye uptake assay. N-phenyl-1- naphthyl – amine (NPN), a hydrophobic fluorophore, is generally excluded by the outer membrane due to permeability barrier. Disruption of the outer membrane by membranolytic agent, allows NPN to interact with membrane lipids, which enhances its fluorescence emission.[527] In this study increase in NPN fluorescence was observed when it was incubated with peptide treated cells. Around 90% of NPN uptake was showed upon addition of 5 µM VV-14 (i.e. its 1×MIC), whereas around 70% NPN uptake was observed at 2.5 µM concentration (i.e. its 0.5×MIC) (Figure 4.9 a). Untreated cells did not show any increase in NPN fluorescence intensity, and cells treated with 10 µM Polymyxin-B used as positive control showed 100% uptake. Next, Propidium Iodide (PI) uptake assay was performed to access the inner membrane permeability of VV-14 through *S. typhi* TY2 cells. PI is a fluorophore that binds to DNA by intercalating in between two bases. As it is permeable through the membrane, it can be successfully used to study the membrane integrity of the cells.[528]

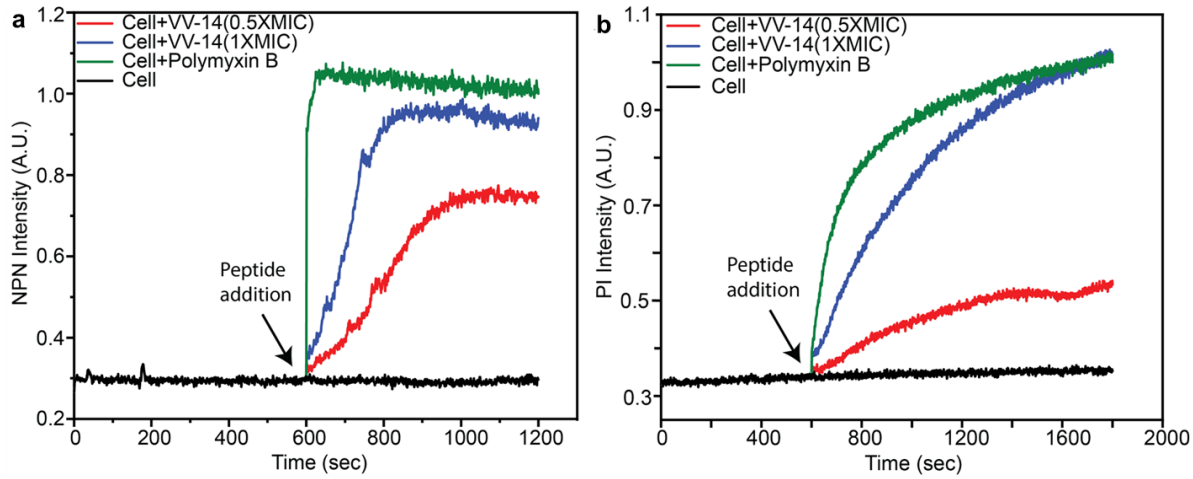

Figure 4.9. Membrane permeabilization effect of VV-14. (a) Time kinetics of NPN and (b) PI uptake was monitored after addition of peptide at 0.5x MIC (red) and 1x MIC (blue) respectively, to *S. typhi TY2* cells, indicating outer membrane and inner membrane permeability of VV-14 respectively. Maximum NPN uptake was observed upon treating the cells with 10 µM Polymixin B (green), which was used as positive control.

We observed almost 100% and around 40% PI uptake upon addition of 5 µM (i.e. its 1×MIC) and 2.5 µM (i.e. its 0.5×MIC) of VV-14 to the cells respectively. In contrast, untreated cells did not show any significant PI fluorescence. 10 µM Polymyxin-B served as positive control (Figure 4.9b).

4.3.8. Membrane Specificity of VV-14 Using Calcein Dye Leakage Assay:

In order to understand the membrane specificity of the peptide, calcein dye leakage assay was performed using two different model membrane systems. The calcein dye was entrapped in two different liposome systems composed of 3:1 POPE/POPG, and 6:4 POPC/Cholesterol, mimicking negatively charged bacterial membrane and mammalian membranes, respectively.[529] These compositions facilitate stable, unilamellar vesicles. The stability of

liposomes was checked by performing time kinetics of calcein dye leakage (Figure 4.10) for one hr. wherein no leakage was observed. The fluorescence intensity of calcein is very low when it is entrapped in large unilamellar vesicals (LUV). Upon addition of the peptide VV-14, fluorescence intensity increased to 50% at 5µM concentration after which there was saturation at 70% (Figure 4.11), suggesting the disruption of membrane by the peptide. In case of LUVs composed of 6:4 POPC/Cholesterol, which mimiced mammalian cell membrane, only 10% leakage was observed at 10 µM peptide concentration. Hence, VV-14 showed distinctive selectivity towards bacterial cell membrane mimics but not eukaryotic cell membrane mimics.

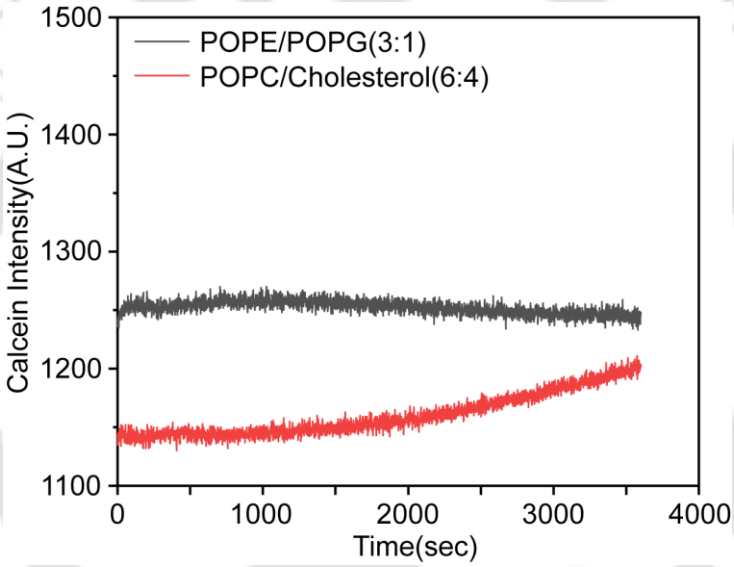

Figure 4.10. Time dependent calcein dye leakage assay of the model membranes. The release of calcein dye was monitored for one hr. to ensure the stability of model membranes composed of POPE/POPG at 3:1 ratio (black) and POPC/Cholesterol at 6:4 ratio (red) respectively. No significant calcein was observed, indicating stability of model membranes.

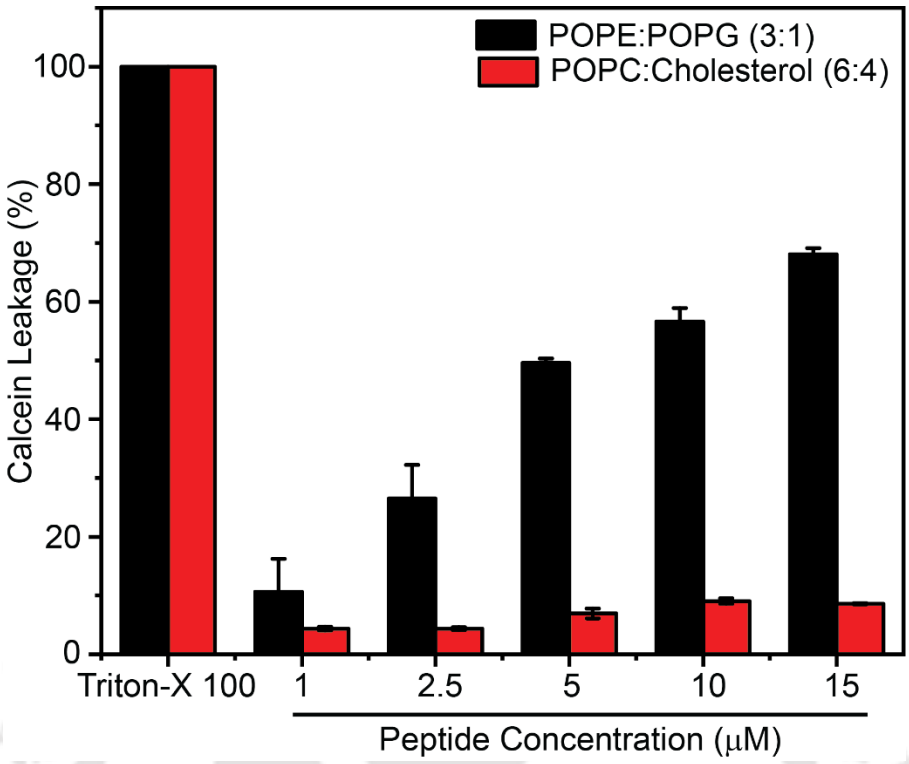

Figure 4.11. Bar plot representing calcein dye leakage percentage upon addition of increasing concentrations of VV-14 to dye entrapped microbial (3:1 ratio POPE/POPG (black)) and mammalian membrane (6:4 ratio POPC/Cholesterol (red)) mimics respectively. Triton X-100 (0.1%) was used as positive control. All the experiments were done in triplicates.

4.3.9. AMP-Model Membrane Interaction:

Peptide interaction with cell membrane is a prerequisite for the membranolytic mode of action. Intrinsic fluorescence properties of the aromatic Trp residues present in VV-14 was used to explore the interaction of peptide with bacterial and eukaryotic cell membrane mimics. Upon addition of increasing concentration of negatively charged SDS micelle, a bacterial membrane mimic, substantial blue shift of 16 nm in the emission maxima was observed (Figure 4.12a), implying the insertion of the Trp residues into the hydrophobic environment of the SDS acyl chains. On the contrary, titration with eukaryotic membrane mimic DPC micelles did not cause

any considerable blue shift of the emission maxima (Figure 4.12 b). This suggested lack of any interaction in between the peptide and the eukaryotic membrane mimic DPC.

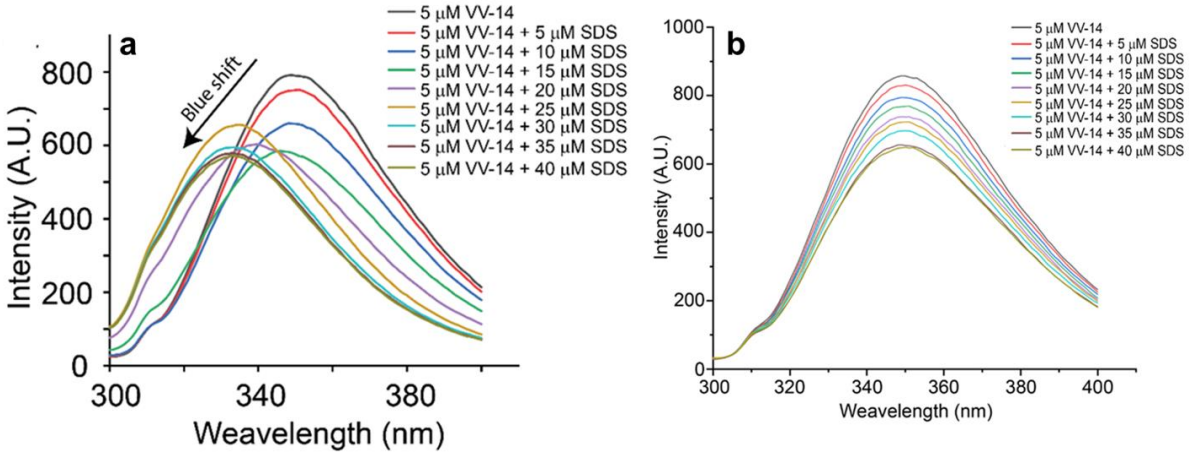

Figure 4.12. Interaction and binding property of VV-14 towards SDS micelles was studied by intrinsic Trp fluorescence emission spectra. (a) Blue shift of intrinsic Trp fluorescence emission spectra was observed upon addition of SDS micelles with increasing concentration up to 40 μM, indicating strong interactions between VV-14 and SDS micelles. (b) Increasing fluorescence anisotropy of VV-14 with increasing concentration of SDS micelles, demonstrated the restricted dynamicity of VV-14 in presence of SDS micelles. After fitting the anisotropy values using Hill equation, the equilibrium dissociation constant (K_D) was calculated.

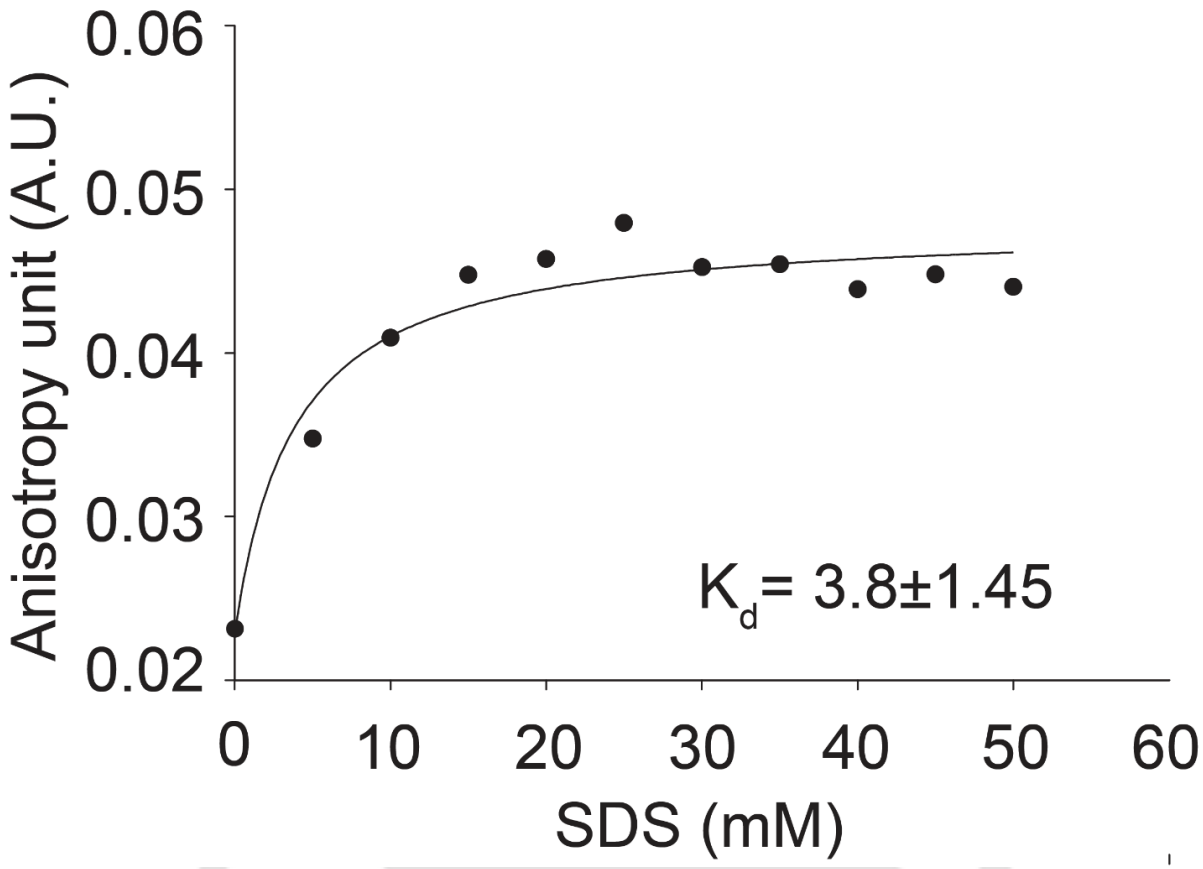

Figure 4.13. Blue shift assay of VV-14 in presence of DPC micelles. The spectral shift of intrinsic Trp fluorescence of VV-14 was not observed, after the addition of DPC micelles in increasing concentration, indicating no significant interaction between VV-14 and DPC micelles.

Next, the binding affinity of VV-14 to bacterial cell membrane mimic was studied using fluorescence anisotropy experiment (Figure 4.13). In case of free peptides, anisotropy values were significantly low, due to the rapid tumbling motion in the solvent.[530] Interestingly, the addition of SDS micelles with increasing concentration showed increment of anisotropy value, indicating slower tumbling motion of peptide due to the strong association between negatively charged SDS micelles and peptide. To calculate equilibrium dissociation constant (K_D), the

anisotropy values were plotted against the SDS concentration and the data was fitted using Hill equation (Figure 4.13).[530]

4.3.10. Delineation of the Structure of the AMPs using CD and NMR:

To get a primary idea about the secondary structure of the peptides, CD experiment was performed in water (peptide in free state) as well as in different membrane mimetic environments like 50% TFE (helix promoting solvent), 30 mM SDS (negatively charged microbial membrane mimic) and DPC (zwitterionic mammalian membrane mimic) (Figure 4.14). All the peptides were seen to adopt random coil like conformation in water in the free state, with a negative cotton effect between 195 nm to 200 nm. In 50% TFE, both LL-14 and VV-14 adopted helix conformation while ββ-14 failed.

Inability of the formation of any helical conformation by ββ-14 even in the presence of helix promoting solvent suggests, the backbone flexibility introduced by the use of β-Ala. In presence of 30 mM SDS, peptides LL-14 and VV-14 adopted α-helical conformation with negative cotton effects around 208 nm and 222 nm and a positive cotton effect around 192 nm. The helical conformations of LL-14 and VV-14 were induced by the interaction of the peptides with the microbial membrane mimics. VV-14, despite of having a number of β-sheet promoter Val residues, adopted helical conformation upon membrane interaction. ββ-14 still remained as a random coil in SDS which explained its inability of interaction with the microbial membrane mimic and its relatively lesser potency. Thus antimicrobial activity of these designed peptides was directly related to their helix forming ability. In the presence of DPC micelles, LL-14 adopted an α-helix like conformation but VV-14 and ββ-14 adopted random coil like conformation, with a negative band at 195 nm as in water. This suggested that LL-14 interacted with the mammalian membrane mimic, while VV-14 or ββ-14 did not, in turn

explaining the cytotoxicity of LL-14 towards the mammalian cells in contrast to VV-14 and ββ-14.

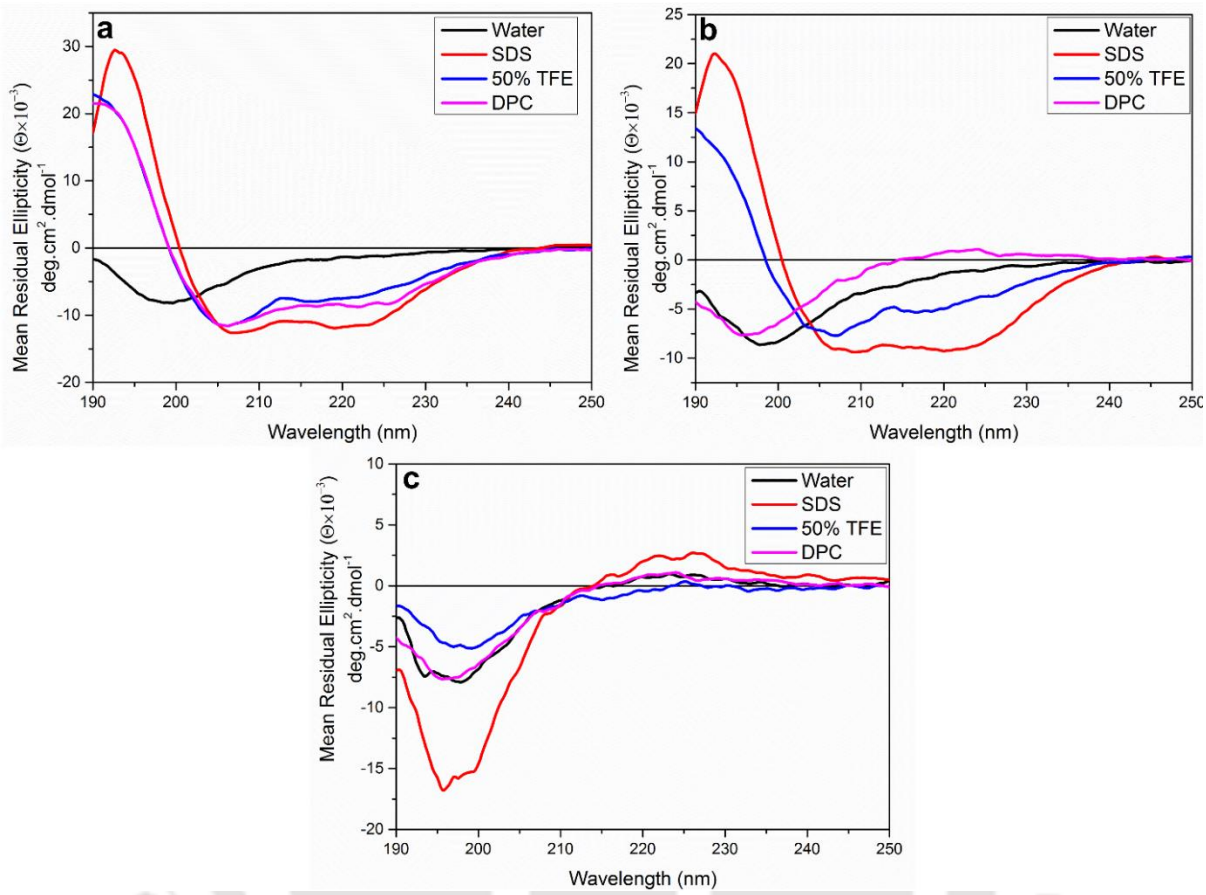

Figure 4.14. Structure determination of AMPs using CD spectroscopy. CD spectra of (a) LL-14, (b) VV-14 and (c) ββ-14 recorded in water (black), 50% TFE (blue), SDS (red) and DPC (magenta).

In summary, findings from the CD spectroscopy established a structure activity relation (SAR) in the designed AMPs. Attainment of helical structure upon interaction with the microbial membrane mimic, explained the high potency of LL-14 and VV-14 in comparison to ββ-14. Secondly, cytotoxicity of LL-14, among all the three AMPs, could be understood from

attainment of helical structure of this peptide alone in the presence of mammalian membrane mimic.

Two-dimensional homonuclear (^{1}H-^{1}H) TOCSY and NOESY experiments are highly useful tools for the unambiguous assignment of chemical shifts of protons that are connected either via covalent bonds or through space. This provides significant information about the secondary structures of the peptides at an atomistic level. In order to get an insight of the bound conformation of VV-14 peptide in SDS micelle, a sequence specific complete assignment of the TOCSY and NOESY spectrum of the peptide was done.[531] The primary amino acid sequence of 14-residue VV-14 peptide contained as many as six Val, six Lys and two Trp residues. Most of the resonances from these amino acids were unambiguously assigned. The NOESY spectrum of the free-state peptide (in water) contained only intra-residue and sequential NOEs between the backbone protons and the side-chain protons. The absence of any significant long range NOEs clearly depicted that VV-14 did not adopt any unique conformation(s) in the free solution, which is in agreement with the CD data. Addition of 200 mM SDS into 1 mM peptide solution showed significant broadening of the overall proton resonances of the peptide in one dimensional ^{1}H spectra due to interaction of the peptide with the micelles in the NMR time scale. The NOESY spectra also showed sufficient number of sequential and medium range NOE (i to i+2/3/4) cross peaks suggesting the existence of a folded conformation in the negatively charged environment (Figure 4.15). Sequential and medium range connectivities could be observed in between dαN (i, i+1), dβN (i, i+1), dNN (i, i+1) and dαN (i, i+2/3/4), respectively as shown in the Figure 4.16.

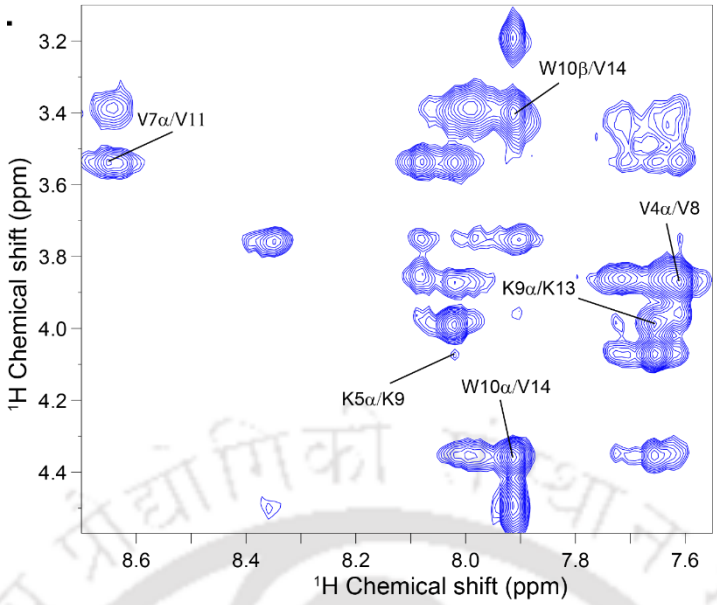

Figure 4.15. Section of two dimensional ^{1}H-^{1}H NOESY spectra of VV-14 showing medium range (i – i+4) NOEs that took important role in the peptide structure as well as in function.

4.3.11. Three-Dimensional Structure of VV-14 in SDS Micelle:

The NOESY derived distance constraints were further used to elucidate the three dimensional solution NMR structure using CYANA programme. In order to calculate the structure in SDS micelles, total 98 distance constraints including 26 medium range constraints (i, i+2/3/4) were used (Table 4.3). After carefully analysing the structure from several calculations, finally 20 lower energy structures were obtained from the CYANA where the average root mean square deviation value of the backbone and heavy atoms were 0.43± 0.10 Å and 1.17 ± 0.14 Å respectively (Table 4.3). Figure 4.16 (a) shows the superimposition of all the 20 lowest energy structures of the VV-14 peptide bound to SDS micelle. The C-terminal end was a little more flexible than the N-terminal end (Figure 4.16 d) while the hydrophobic and aromatic residues like Val and Trp adopted very rigid conformation.

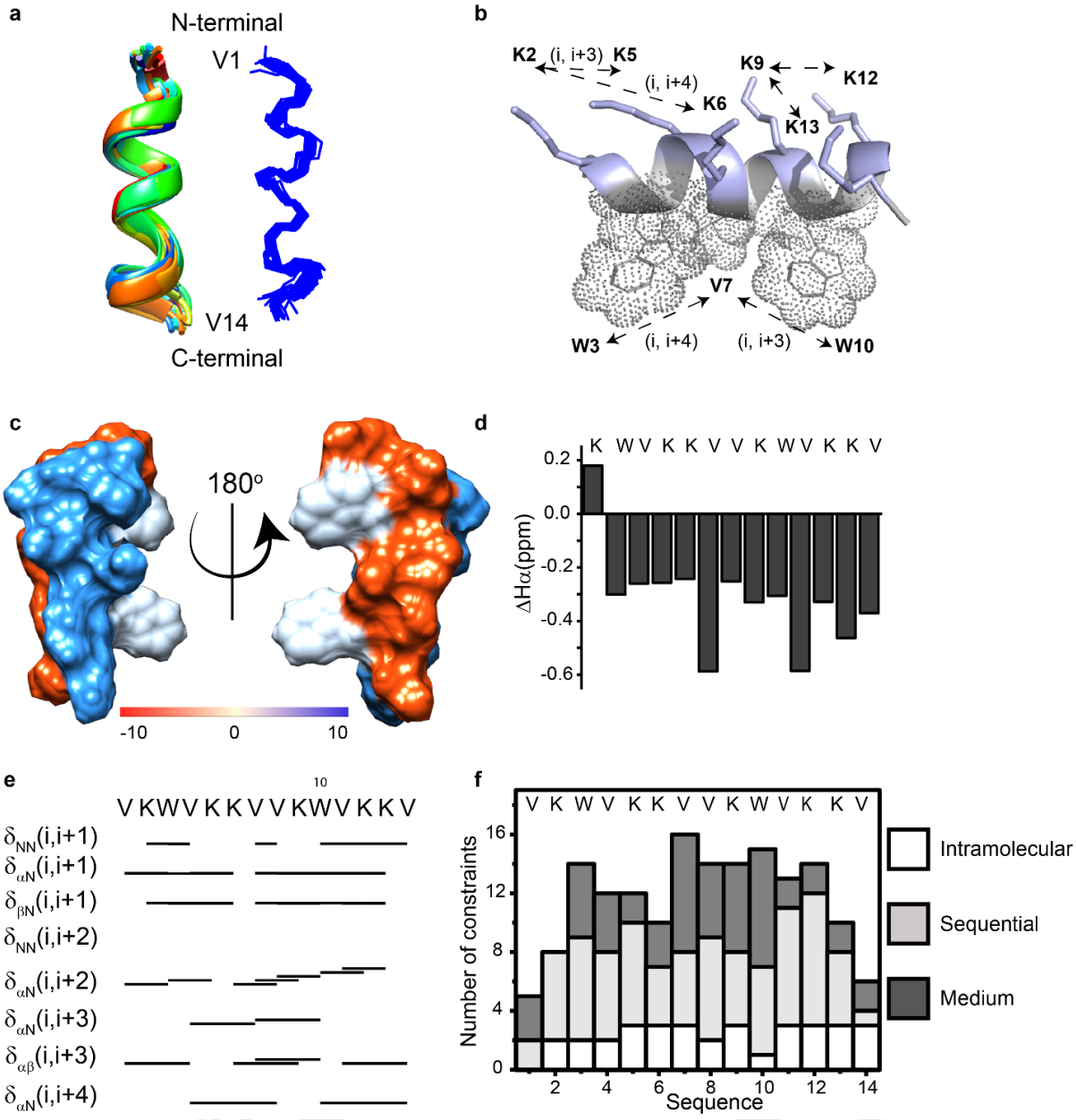

Figure 4.16. Three-dimensional structure of VV-14 in SDS micelles. (a) Superposition of backbone of the twenty lowest energy structures of VV-14 bound to SDS as obtained from CYANA. (b) Representative cartoon structure of SDS-bound VV-14, showing side-chain orientation of polar (Lys), non-polar (Val) and aromatic (Trp) side chains where the respective residues have an i, i+3 and i, i+4 connectivity. This figure was produced using PyMol. (c) Electrostatic surface potential of VV-14 structure in SDS micelles. The figure was colored

according to the local values of the electrostatic potential. The color palette ranges from −10 kcal/(mole) (red) to +10 kcal/(mole) (blue). (d) Chemical shift index of $C^{\alpha}H$ for VV-14, from random coil to SDS micelle bound conformation showing majorly negative deviations. (e) Bar diagram summarizing the sequential and medium range NOE's observed for SDS micelle-bound VV-14 obtained from two-dimensional ^{1}H-^{1}H NOESY spectrum. The thickness of the bar corresponds to the relative intensities of NOE cross-peak. Sequence of the VV-14 peptide is shown above. (F) Histogram plot showing the number and type (intra, sequential, and medium) of NOEs of VV-14 peptide as a function of the residue number in complex with the SDS micelle.

In contrast, the positively charged Lys residues had highly dynamic side chains (Figure 4.16 d). Moreover, the overall structure of VV-14 peptide bound with SDS micelle showed a clear separation between polar and non-polar or aromatic residues, essentially providing an amphipathic structure to the peptide (Figure 4.16 b).

This seemed to be a consequence of the design of primary sequence of the peptide, wherein charged or hydrophobic residues were placed at either i+3 or i+4 positions relative to each other, so that in case the peptide adopted helical structure it would naturally gain amphipathicity with distinct charged and hydrophobic faces.[532] The chemical shift deviation of $C^{\alpha}H$ resonances of VV-14 from the random coil values also supported a well-defined secondary conformation of the peptide in SDS micelles (Figure 9.16 d).[533] The amphipathic structure was further stabilised by the hydrophobic interactions between the aromatic residues W3 and W10 with V7 which again maintained the i+4 and i+3 relationships, respectively.

Table 4.3. Summary of Statistical Analysis of the 20 Lowest-Energy Structures of Peptide VV-14 in SDS Micelles.

Distance restraints	
Intra residue (i – j = 0)	33
Sequential (|i – j| = 1)	39
Medium range (2 ≤ |i – j| ≤ 4)	26
Long range (|i – j| ≥ 5)	0
Total	98
Angular restraints	
Φ (PREDITOR predicted angular values +/- 20)	12
Ψ (Full freedom for rotation within allowed region, -120 to +120)	12
Distance restraints from violation (≥0.4 Å)	0
Deviation from mean structure (Å)	
Average backbone to mean structure	0.43 ± 0.10
Average heavy atom to mean structure	1.17 ± 0.14
Ramachandran plot*	
% residues in the most favored regions	100%
% residues in the additional allowed region	0%
% residues in the generously allowed region	0%
% residues in the disallowed region	0%

The delineation of three dimensional helical structure of VV-14 helped us to understand the structure function relationship (SAR) of the designed AMPs. We hypothesised that the positively charged AMPs initially anchored on the negatively charged microbial membrane due to favourable electrostatic interactions. They then folded into helical secondary structures

because of the favourable interactions of the side chains of hydrophobic residues with the nonpolar acyl chains of the lipid molecules by insertion of the former in between the later. This in turn destabilised the integrity of the membrane and caused microbial cell death. It was favourable hydrophobic interaction that drove VV-14 to adopt helical conformation in the membrane mimetic environment even though Val is known to have a high propensity for occurring in β sheets. As in ββ-14, there are no side chains in the hydrophobic amino acid residues, no favourable hydrophobic interaction existed and thus the backbone flexibility prevented the peptide from formation of helical structure. Thus, the membrane damage caused by ββ-14 decreased which explains its lower microbial activity. As all the peptides carried same positive charge, the electrostatic component of interaction in between the designed AMPs and the microbial membranes remained the same. However, it is the hydrophobic interaction in between the side chains of the hydrophobic amino acid residues and the lipids in the membrane that varied among the three designed AMPs. The hydrophobic interaction required insertion of the hydrophobic side chains into the lipid bilayers. Thus longer the chain, better their lodging in between the lipids, better the interaction and better the activity. This explained the diminishing activity from LL-14 to ββ-14. LL-14 with the longest side chain containing Leucine residues could also interact with the zwitterionic mammalian membranes and adopt helical conformations, as seen from CD, in spite of the diminished favourable electrostatic interaction. This explained the cytotoxicity of LL-14 in comparison to the VV-14 and LL-14.

4.3.12. Membrane Deformation Caused by Designed AMPs:

In order to investigate the role of the VV-14 on the membrane integrity and visualize the effect on their morphology, electron microscopic studies were performed. S. typhi cells were treated with VV-14 at its 1x, 2x and 3x MIC values to study the effect of peptide mediated membrane perturbation and lysis. Control experiment in the absence of VV-14 showed the intact rod like

cellular morphology of the bacteria with a smooth outer membrane (Figure 4.17a). Upon addition of various concentration of VV-14, a clear deformation of the outer membrane was noticed. At 1x MIC of the peptide, there was presence of cell debris and intracellular material, resulting from the lysis of the bacterial cells (Figure 4.17b). There were few some unaltered cells, however their membrane morphology was severely deformed. In the presence of higher concentration (2x and 3x MIC) of VV-14, the percentage of lysed cells increased visibly indicating greater damage to the cells (Figure 4.17c and d). At 1x and 2x MIC concentration of the peptide, the unlysed cells showed altered cell shape and size. Exactly similar results were seen upon treating VV-14 with *E. Coli* cells (Figure 4.18) further confirming its membranolytic activity.

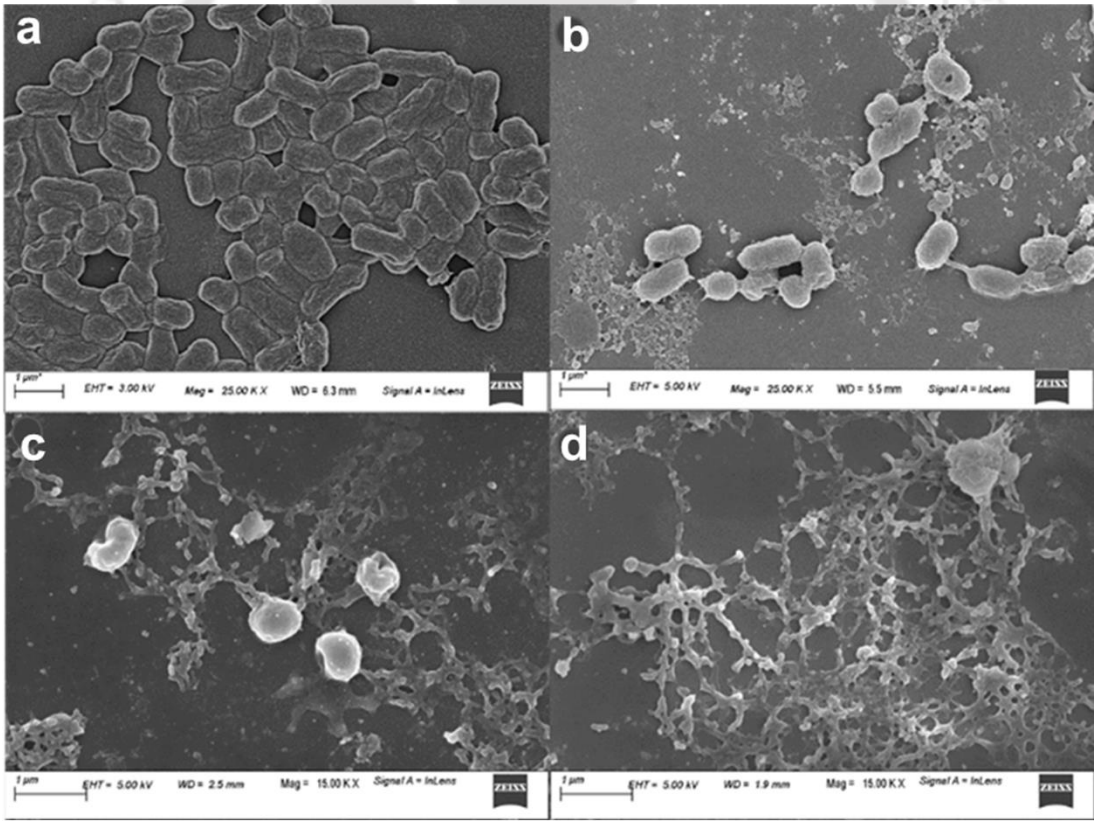

Figure 4.17: Field emission scanning electron microscopy (FESEM) image for *S. typhi* (a) Control (b) 1x MIC (c) 2x MIC (d) 3x MIC.

To further visualize the membrane perturbation and deformation, Field emission scanning electron microscopy, FETEM was performed on the *S. typhi* cells (10^5 cells/) treated with VV-14 at its 1x $MIC_{99\%}$ value. Membrane deformation and distortion in the shape and size of the microbial cell was clearly visible at 1x MIC concentration of VV-14 in Figure 4.19 b. The smoothness of the control microbial cell membrane was clearly lost upon treatment of the peptide, showing the effect of the peptide on the membrane. Additionally, in the presence of the peptide, there was presence of some cellular debri and intracellular metabolites in the background suggesting a lysis of the cell membrane.

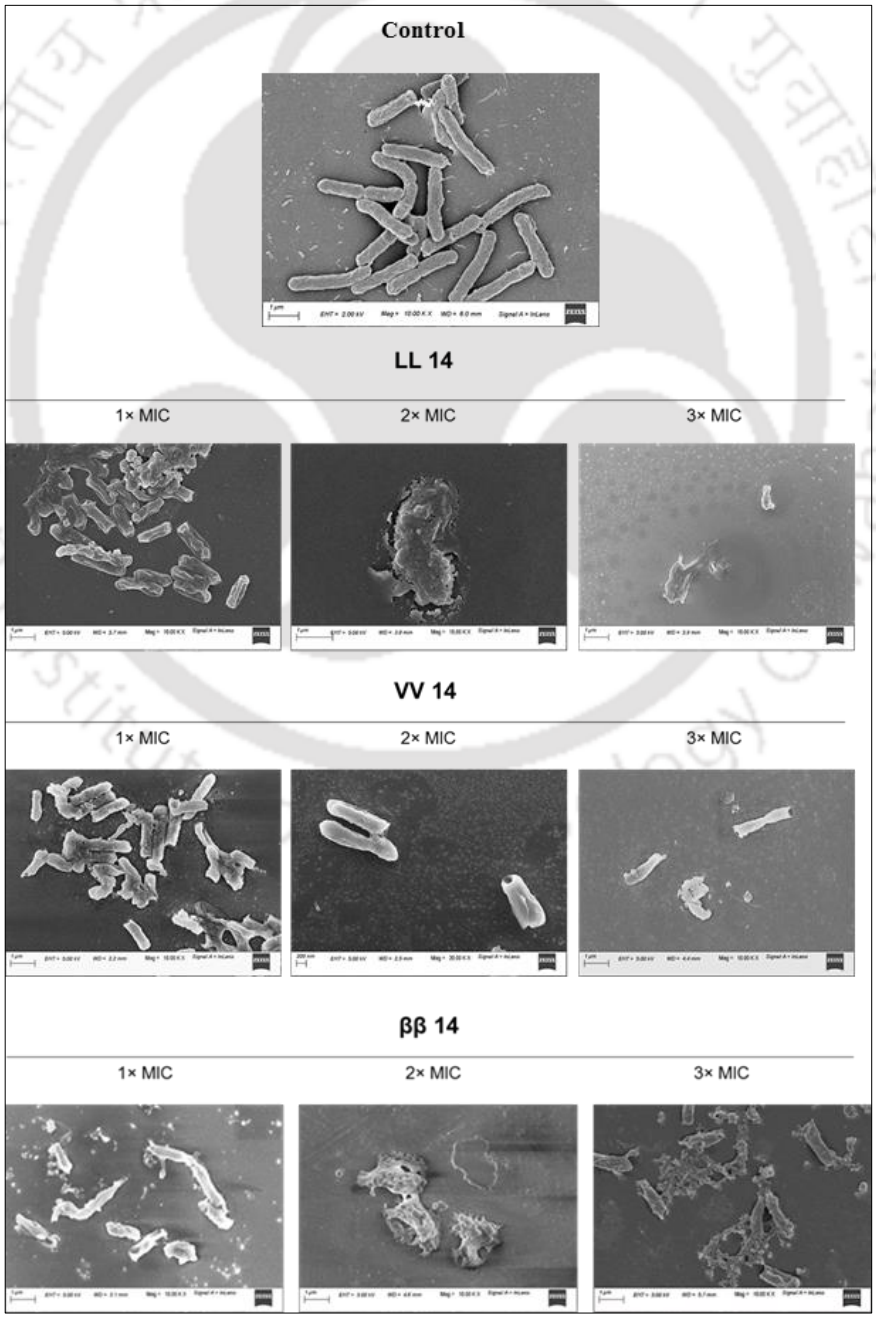

Figure 4.18. FESEM image for untreated *E. coli* cells and treated with LL-14, VV-14, ββ-14 at different concentration.

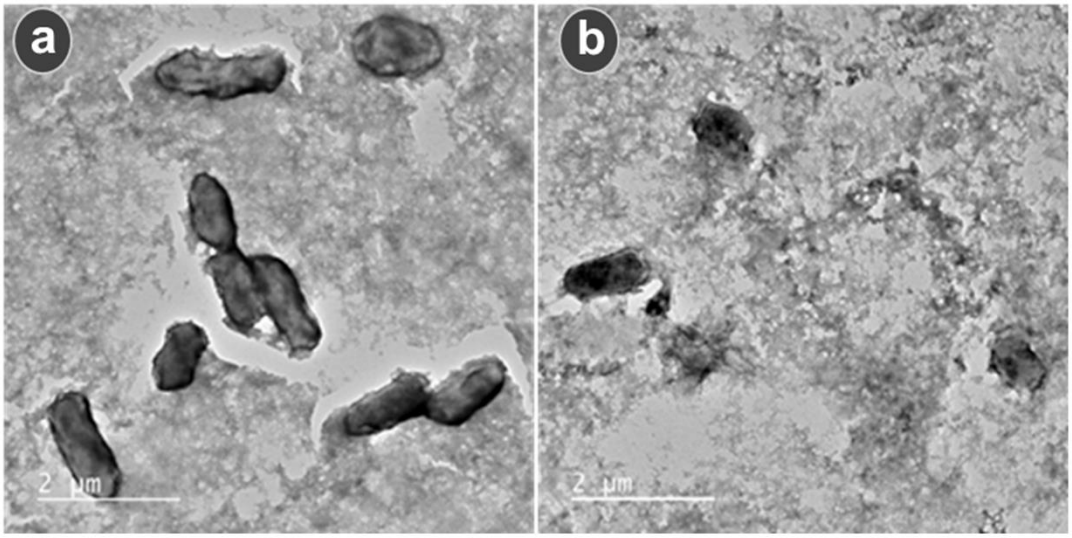

Figure 4.19. Field emission transmission electron microscopy (FETEM) image for *S. typhi.* (a) Control and (B) 1× MIC.

4.4. Conclusion

We have designed three similarly charged cationic AMPs (LL-14, VV-14 and ββ-14) with hydrophobic residues of varying length. The AMPs have broad-spectrum antimicrobial activity and are effective against three pathogens from ESKAPE group and two fungal strains. We have demonstrated that too long and too short side chains resulted in cytotoxicity and diminished activity respectively. Optimum length of side chain of Valine residue gave rise to the non-cytotoxic and highly potent AMP VV-14, which was salt tolerant and specifically effective against *S. typhi*. The AMPs acted via membrane permeabilization, deformation and lysis. The activity of the AMPs was related to their ability to form amphipathic helical conformation in presence of microbial membrane mimics. Interaction of the side chains with the membrane

lipids played the determining role in potency and cytotoxicity of designed AMPs. Thus in summary, an optimum hydrophobic interaction remains the key factor in developing highly potent non-cytotoxic AMPs.

Chapter 5

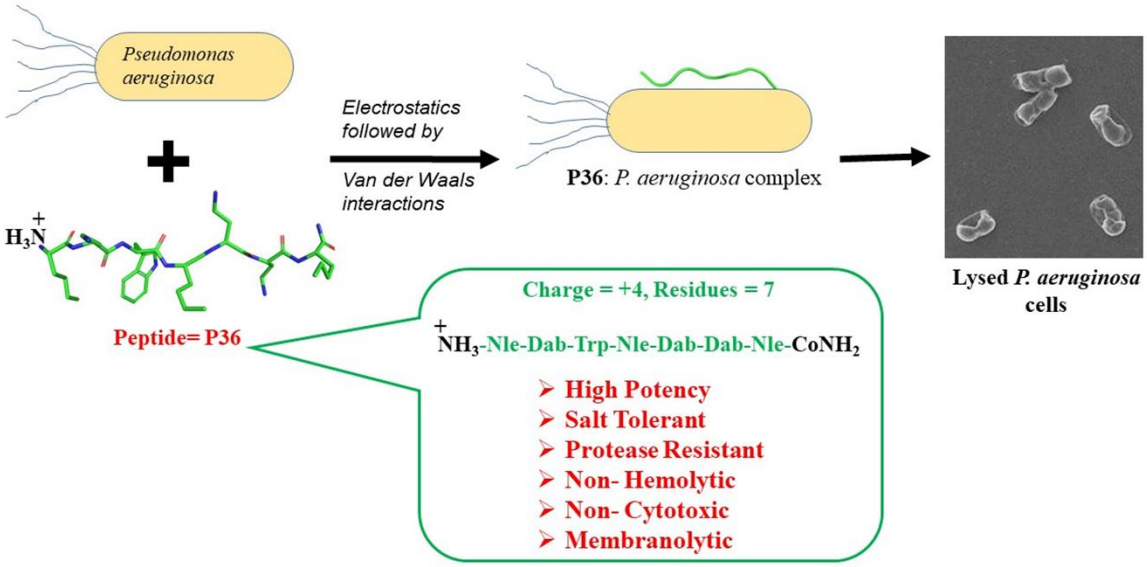

Delineating the Mechanism of Action of a Protease Resistant and Salt Tolerant Synthetic Antimicrobial Peptide against P. aeruginosa

5.1. Introduction

One of the most important disadvantages of the AMPs lies in their short systemic half-life owing to the protease degradation. Cationic AMPs. AMP have large quantities of Lysine (Lys) and Arginine (Arg), making them highly susceptible to serine proteases like Trypsin, which specifically hydrolyzes the peptide bond at the C-terminal end of the Lys and Arg. In an effort to overcome the protease degradability of the AMPs different strategies have been adopted like a) insertion of non-standard ω amino acids[401,534-537] and side chain modified α-amino acids[538,539] in the AMP sequence, b) peptide terminal modifications,[537] c) insertion of amino acids of opposite chirality[540-542] d) cyclization of the AMP sequences,[543-546] e) insertion of peptidomimetic blocks in key positions of the sequence,[127,539,547-549] f) pegylation,[421,550,551] g) lipidation[358,516,552] and h) construction of hybrids.[553] Of all the strategies employed, modification of the side chain length of the positively charged amino acid residues such as Lys and Arg, is the most common one. Many non-standard amino acids are used as analogs of Lys like Ornithine (Orn), Dab (di-amino butyric acid), Dap (di-amino propionic acid), and Arg like homoarginine, 2-amino-(3-guanidino) propanoic acid.[505,540,554-558] In general, the short side chain analogs for Lys and the long side chain analogs for Arg, improved the activity of the AMPs.

The Gram-negative bacterial infections are more difficult to treat than the Gram-positive bacterial infections.[559,560,] This is owing to the lipopolysaccharide (LPS) layer which forms the outer leaflet of the asymmetrical lipid bilayer in the Gram-negative bacteria.[561-563] The AMP encounters the LPS layer before it can assess the inner plasma membrane.[564-566] The LPS layer interacts with the antibiotics and the AMPs rendering them inactive. The resistance of the Gram -negative bacteria against the AMPs is partially attributed to LPS layer though there are other known mechanisms of the development of resistance against them like chemical modification

of the lipid membranes, sequestration, proteolytic degradation, release of glycosaminoglycans (GAGs), polysaccharides and polyanionic scavenging species.[567,568]

In the second chapter, we had developed a cationic heptapeptide, P4 (H-LKWLKKL-NH_2), with broad-spectrum activity against ESKAPE pathogens and fungal strains and non-cytotoxicity towards the mammalian cells.[334,569] Due to the all α-amino acid backbone and high content of Lys, P4 was be anticipated to be susceptible to protease degradation in vivo. In the present study, we wanted to impart protease resistance to P4 by replacing the α-amino acids by their non-standard analogous amino acids. The designed analogs of P4 (P31-P37), had identical charge but differed in their hydrophobic-hydrophilic balance. As the hydrophobic-hydrophilic balance plays a crucial role in determining the bioactivities of the AMPs, we investigated the antimicrobial potency, salt tolerance of the antimicrobial potency and cytotoxicity of the designed peptides P31-P37. Mechanism of action of the lead AMP was studied in details using various biophysical, spectroscopic and microscopic techniques while computational studies were performed to understand the interaction of the peptides with the microbial membrane mimics in atomistic details.

5.2. Experimental Section

Peptide synthesis and purification of the peptides P31-37 were done using standard SPPS and reverse phase semi preparative HPLC using ACN-H_2O gradients as discussed previously. The purity of the peptides was checked using Analytical HPLC (Appendix, Figure A11-A17) and they were characterized thoroughly using ESI-MS (Appendix, Figure A33-A39) and ^{1}H NMR (Appendix, Figure A53-A59).

5.2.1. Micro Broth Dilution Assay:

Antimicrobial activity of the P31-37 was studied in the absence and presence of different salts ((a) 150 mM sodium chloride (NaCl), (b) 1.25 mM magnesium chloride ($MgCl_2$) and 1mM

calcium chloride ($CaCl_2$)) using standard micro dilution broth assay as described earlier.[569] In addition, in order to investigate the antimicrobial activity of P36 in the presence of enzymes, microbroth dilution assay was performed with P36 incubated with enzyme cocktail (trypsin, chymotrypsin and Proteinase K) for 4 hr.

5.2.2. Cell Viability Assay:

Cell viability assay was performed as described earlier for all the peptides P31-37 to determine the cytotoxicity of the AMPs towards the mammalian cell line L132 (Section 2.2.7).

5.2.3. Hemolytic Assay:

Activity of AMPs against human RBCs was determined both quantitatively and qualitatively using hemolytic assay as described earlier (Section 2.2.6)

5.2.4. Time Course of Bactericidal Activity:

Time required to manifest the bactericidal activity was studied by performing time course bactericidal assay as described in section 4.2.2. of chapter 4.

5.2.5. Proteolytic Stability Assay:

a) HPLC Experiment:

10 mM P4 and P36 were treated with a 1:1:1 mixture of enzymes trypsin, chymotrypsin and protease K (0.3 mg/) at 37 ˚C for 0 to 6 hrs. After incubation, 50 µL of reaction solution was taken and mixed with 50 µL of acetonitrile with 1% TFA at 4°C and kept for 15 min to inactivate the enzymes. The mixture was then diluted with HPLC grade water and 20 µL was injected onto the C18 reverse-phase column for HPLC analysis. Samples were eluted by a linear gradient of 10%–100% CH_3CN/H_2O in 0.1% TFA at a flow rate of 1mL /min for 25 min. The UV absorbance of the eluted peptides was detected at 214 nm and 280 nm with a UV monitor.

b) Mass Spectrometry:

In order to determine the chemical integrity of the most active peptides P4 and **P36** upon protease degradation, a mass spectrometric analysis of the peptide-enzyme reaction mixture, post incubation and the subsequent deactivation of the enzymes, was carried out on an Agilent-Q-TOF 6500 instrument equipped with Mass Hunter workstation software in the electrospray ionization positive mode.

c) In order to see if P36 retained its activity upon incubation with the proteases, MIC of the enzyme incubated P36 against *P. aeruginosa* was delineated (Figure 5.11). P36 was shown to retain most of its activity even after protease treatment proving the protease resistance of the peptides.

5.2.6. Calcein Leakage Assay:

The calcein dye leakage assay was performed with LUV's that mimicked the microbial cell membranes in a process detailed earlier in section 2.2.8 to establish the membranolytic nature of P32 and P36.

5.2.7. Assay of Outer and Inner Membrane Permeabilization:

Outer and inner membrane permeabilization capability of P32 and P36 were studied using the NPN assay and PI assay as described earlier in the sections 4.2.3 and 3.2.7.

5.2.8. Fluorescence Experiments:

a. Blue Shift Experiment:

ii) In Presence of Membrane Mimetics:

Membrane association of P32/P36 was performed in the presence of membrane mimics (SDS/DPC) using the intrinsic fluorescence signal of the Trp residue present in the AMP, as described in the section 2.2.14.

i) In Presence of Live Cells:

In a similar experiment as above, intrinsic tryptophan fluorescence was utilized to analyze the interaction between the peptide and live *P. aeruginosa* cells. *P. aeruginosa* cells were collected, washed, and re-suspended in 10 mM phosphate buffer (pH 7.4). Cells (5 µL) were added (stock: 10^8 CFU/mL) in subsequent steps to the P32 and P36 solutions. Trp fluorescence emission was monitored (for an excitation wavelength of 280 nm, excitation and emission slit width of 2.5 nm) only for P32 and P36 and in the presence of live *P. aeruginosa* cells.

5.2.9. Solvent Accessibility:

Solvent accessibility of the AMPs P32/36 in the presence of different membrane mimics was studied in the presence of static quencher acrylamide, by calculating the Stern Volmer constant as described in the Section 3.2.3.

5.2.10. ITC Experiments:

Isothermal Calorimetry was performed to calculate the thermodynamic parameters involved in the AMP: membrane mimic interactions as described in the Section 3.2.4

5.2.11. Circular Dichroism Spectroscopy:

Solution structure of the peptides was studied using Circular Dichroism (CD) spectroscopy in water and in various membrane mimic environments as described earlier in Section 4.2.9.

5.2.12. Live Cells CD Spectroscopy:

Overnight grown *P. aeruginosa* cells were collected, washed, and re-suspended in 10 mM phosphate buffer (pH 7.4) to a final cell count of 5 ×10^5 cells /. Cells (50 µL) were added (stock: 10^8 CFU/) to P36 solution (25 µM, 250 µL), and CD spectra were recorded after different incubation times (till 2.5 hr.) using a 1 cm quartz cell, 260−190 nm measurement range, 100

nm/min scanning speed, 2 nm bandwidth, 4s response time, and 1.0 nm data pitch up to 2.5 hr. of incubation at 37°C. Similarly, the CD spectrum for *P. aeruginosa* cells only was measured under identical conditions. The peptide concentration was 25 μM in 10 mM phosphate buffer (pH 7.4).[570]

5.2.13. Live Cells Zeta Potential:

Zeta potential was measured with the help of a Zetasizer Nano ZS 90 instrument (Malvern, UK), containing Helium–Neon laser (633 nm) as a source of light, with the detection at 90 degree scattering angle at room temperature (28° C). Overnight grown *P. aeruginosa* cells were washed three times by DI water and re-suspended in the same to obtain a cell suspension of 5 $\times 10^5$ cells /mL. To minimize the effect of buffer on zeta potential value, cells were suspended in DI water instead of buffer. P36 (1mM stock solution, 5μL) was added to 1 of *P. aeruginosa* cells ($5x10^5$) at different time intervals and its zeta potential value was checked after each addition.[571]

5.2.14. NMR Experiments:

a. NMR in Presence of Microbial Membrane Mimics (SDS and LPS):

AMP: membrane mimic interaction was studied using ^{1}H NMR in 90% of 10 mM phosphate buffer (pH 6.5) and 10% D_2O alone, in the presence of SDS (200 mM) and LPS (3 μM, outer layer of the bacterial cell membrane) and as described earlier in section 2.2.11.

b. Live- Cell NMR Experiments: *P. aeruginosa* cultures were grown overnight and used to perform the experiment. The cell suspensions were centrifuged at 6000 rpm for 5 min. Cell pellets were washed three times with 10 mM phosphate buffer at pH 6.5 and later re-suspended in the same buffer to obtain a cell suspension containing 10^6 CFU/. One-dimensional proton NMR spectra of 1 mM solution of P36 in a mixture of 90% of 10 mM phosphate buffer (pH 6.5) and 10% D_2O was recorded on a Bruker Avance III 600 MHz NMR spectrometer. In

another experiment, 500 μg of solid peptide P36 was added to a 500 μL solution of the cells (10^6 CFU/), and the mixture was thoroughly vortexed to achieve a final peptide concentration of 1mM. A series of 1D ^{1}H NMR spectra were recorded at different time points after addition of P36 to the *P. aeruginosa* cells. The temperature for experiment was adjusted as per the standard growing temperature of *P. aeruginosa* at 310 K.

5.2.15. Field Emission Scanning Electron Microscopy (FESEM):

The effect of the P36 on the *P. aeruginosa* cells was visualized by performing FESEM experiment as described earlier in Section 2.2.13.

5.2.16. MD Simulations:

a. Modelling of Peptides (P32, P36) in Water:

The most active peptides P32 and P36 (in the presence or absence of micelle) were considered for molecular dynamics simulations. The initial linear model of P32 and P36 were generated using PyMOL version 2.4.1 software.[572] N- and C-termini of these peptides were modelled as $-NH_3^+$ and $-CONH_2$ respectively. A water box of dimensions 60×60×60 Å^3 was overlaid keeping the linear peptide model at the center. The overall charge (+4) of the peptide was neutralized by adding four chloride ions. A total of ~21075 atoms were considered for MD simulations of peptides in water. Topology descriptions of the non-standard amino acids (Dab and Nle) were retrieved from Swiss Side Chain database.[573]

b. Modelling of Membrane-Mimetic Systems (SDS/ DPC Micelles):

CHARMM-GUI Micelle Builder[574,575] was used to build SDS/DPC micelles. SDS micelle was modelled by including a total of 60 molecules of SDS. The experimental value of the aggregation number was reported to be close to 60. Simulations with 60 SDS molecule is a popular choice for computational analysis.[576-581] The micelle was placed at the center and solvated by overlaying a water-box of dimension 100 x 100 x 100 Å^3. 60 Na^+ counter-ions

were added for neutralizing the simulation box. A total of ~98230 atoms were considered for MD simulations of SDS in water. DPC micelle was modelled in the same way as SDS. DPC is a neutral zwitterionic molecule, thus no counter-ion was added. The final snapshot produced from the molecular dynamics was considered for studying peptide-micelle interactions.

c. Simulation Setup for Studying Peptide-Micelle Interaction:

First, the center of mass of the model linear peptide (P32 or P36) was initially placed ~55 Å away from the center of mass of the micelle (SDS or DPC) (Figure 5.1a). The water padding was extended in the peptide direction and the solvated water box of dimension 100×100×140 $Å^3$ was subjected to MD simulation (Figure 5.1b). More than 145530 atoms were considered for MD simulations. To check convergence and ensure efficient sampling, we performed various independent MD replicas differing in the initial setup (Setup A, Setup B, and Setup C: orientations of the peptide relative to micelle) (Figure 5.1a) as well as in their initial velocities (Table 5.1).

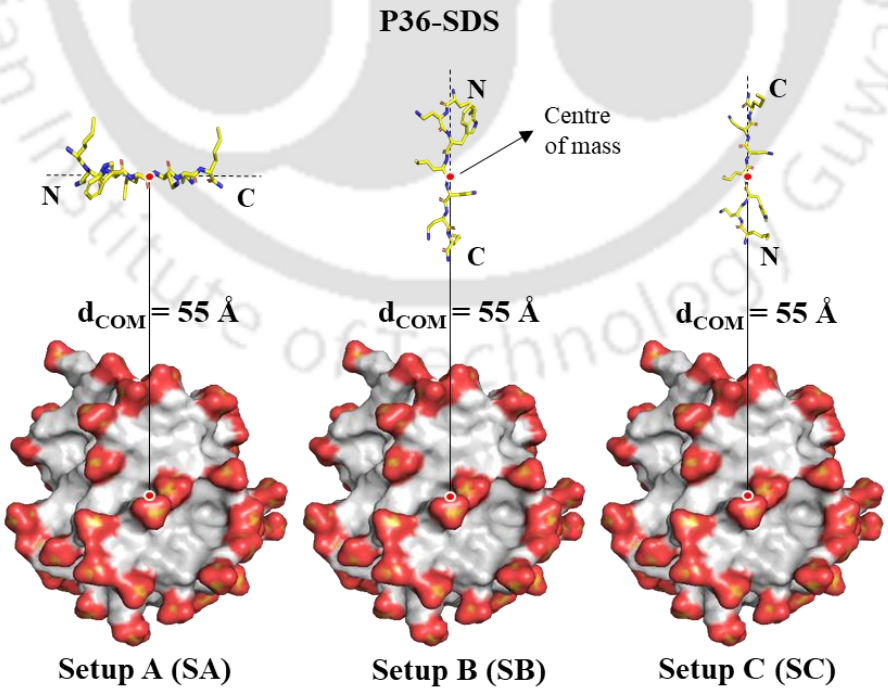

a) Peptide-Micelle initial models (MD Simulation set-up)

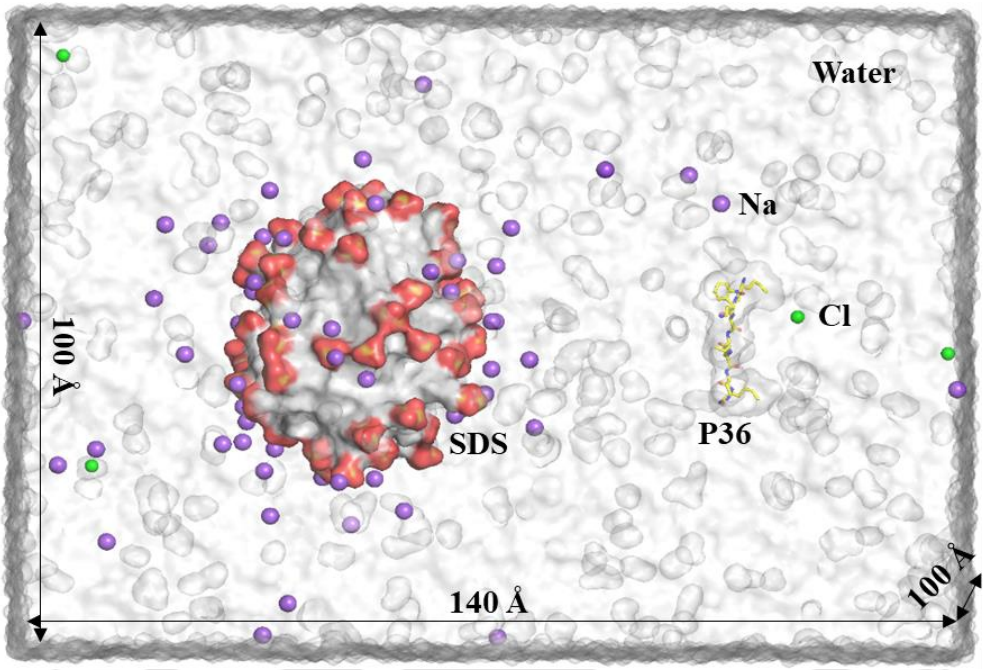

b) Peptide-Micelle MD Simulation Box (Including water and ions)

Figure 5.1. (a) Initial MD setup models (SA, SB, SC): varying relative orientation of P36/P32 and SDS micelle. N- and C-termini are highlighted. (b) Typical MD simulation system (P36 in presence of SDS micelle), solvated with a water box of dimension 100×100×140 $Å^3$, SDS micelle (red- white surface), P36 (sticks), Na^+ ions (violet sphere), Cl^- (green sphere) and water (white transparent surface).

Table 5.1. Peptide (P32/P36) in the presence and absence of micelle (SDS/DPC) is considered for MD simulations. The number of independent replicas (varying the initial velocities), box size, composition and post-equilibrated MD run-length. A total of 810 ns of production MD was performed.

S. No	System (Simulation Setup A/B/C)	No of replicas (replica label)	Box Size ($Å^3$)	No of Molecules	Simulation Time (ns)
1	Free SDS	1 (R1)	100×100×100	SDS – 60 SOL – 31861 Na – 60	5
2	Free DPC	1 (R1)	100×100×100	DPC – 60 SOL –31684	5

3	Free P32	1 (R1)	60×60×60	Peptide – 1 SOL – 6979 Cl – 4	50
4	P32-SDS (SA)	2 (R1, R2)	100×100×140	Peptide – 1 SDS – 60 SOL – 47606 Cl – 4 Na – 60	50,50
5	P32-SDS (SB)	2 (R1, R2)			50,50
6	P32-SDS (SC)	2 (R1, R2)			50,50
7	P32-DPC (SA)	1 (R1)	100×100×140	Peptide – 1 DPC – 60 SOL – 47364 Cl – 4	50
8	Free P36	1 (R1)	60×60×60	Peptide – 1 SOL – 6978 Cl – 4	50
9	P36-SDS (SA)	2 (R1, R2)	100×100×140	Peptide – 1 SDS – 60 SOL – 47597 Cl – 4 Na – 60	50,50
10	P36-SDS (SB)	2 (R1, R2)			50,50
11	P36-SDS (SC)	2 (R1, R2)			50,50
12	P36-DPC (SA)	1 (R1)	100×100×140	Peptide – 1 DPC – 60 SOL – 47355 Cl – 4	50

Table 5.2. Parameters used in MD simulations.

Molecular Dynamics Parameters (NPT ensemble)	
Integrator, time step	Leap-frog algorithm, 2 fs

Hydrogen Bonds Constraint Algorithm	LINCS [SI1]
Long range electrostatics, short range electrostatic cut-off	Particle Mesh Ewald (PME) [SI2], 12 Å
Short range van der Waals cut-off	12 Å
Boundary Conditions	Periodic Boundary condition
Temperature control, coupling constant	Velocity rescaling algorithm [SI3], 0.1 ps
Pressure control, coupling constant	Parrinello-Rahman algorithm [SI4], 2.0 ps
Temperature	310 K
Pressure	1 bar

d. Simulation Parameters:

All the simulations in this study were performed in GROMACS version 2019 package,[582] with CHARMM36 (version March 2019)[583] as force field parameters. TIP3P[584] water model was used to model waters. Energy minimization was performed using the steepest descent algorithm (step size=0.1 Å, 50000 steps). After energy minimization, 200 ps of equilibration was performed (restraining only the micelle and peptide) considering NVT ensemble (first 100 ps) followed by NPT ensemble. After equilibration, the production run for 50 ns was performed and the last 30ns was considered for analysis. The simulation parameters adopted for this work are given in Table 5.2. Co-ordinates were saved at every 10 ps from the MD trajectories for analysis.

e. MD Trajectory Analysis:

Secondary structural content of the peptides was obtained by processing the MD trajectories using *gmx dssp* tool.[575] Structural deformation of micelles in response to peptide binding was

characterized by estimating trajectory averaged radius of gyration (R_G) and micelle eccentricity using *gmx gyrate* tool.[582] SASA (solvent accessible surface area) values are the geometric estimation of the exposure of molecule surface to the bulk solvent. SASA values were computed by *gmx sasa* [526] using a probe radius of 1.4 Å. *gmx distance*[73] tool was used to plot the distance between the center of mass of micelle and peptide as a function of simulation time. Peptide-micelle distance and SASA of peptide were obtained from the MD trajectories and plotted using OriginPro and images were generated using PyMOL visualization software.[572]

5.3. Results and Discussion

5.3.1. Rational Design of the AMPs:

Peptides P31-P37 were designed based on P4, from chapter 2 as a template (Figure 5.2, Table 5.3). In an attempt to improve the activity and protease resistance of P4, Lys and Leu in the sequence were systematically mutated by side chain modified analogs of Lys (Orn, Dab, Dap) and Leu (Nle). Mutations were systematically incorporated to change the polar (P31-P33) and hydrophobic (P34) amino acid residues, one type at a time or both simultaneously (P35-P37). The side chain length and the hydrophobicity of Lys and its analogs diminish in the order of Lys, Orn, Dab and Dap. Though the side chain carbon atoms are the same for Nle and Leu, the former is longer being unbranched in comparison to the later, which is branched. Thus, though all the P4 analogs (P31-37) studied here had identical charge to P4, their overall hydrophobicities were different due to incorporation of various non-standard amino acid analogs of Lys and Leu.

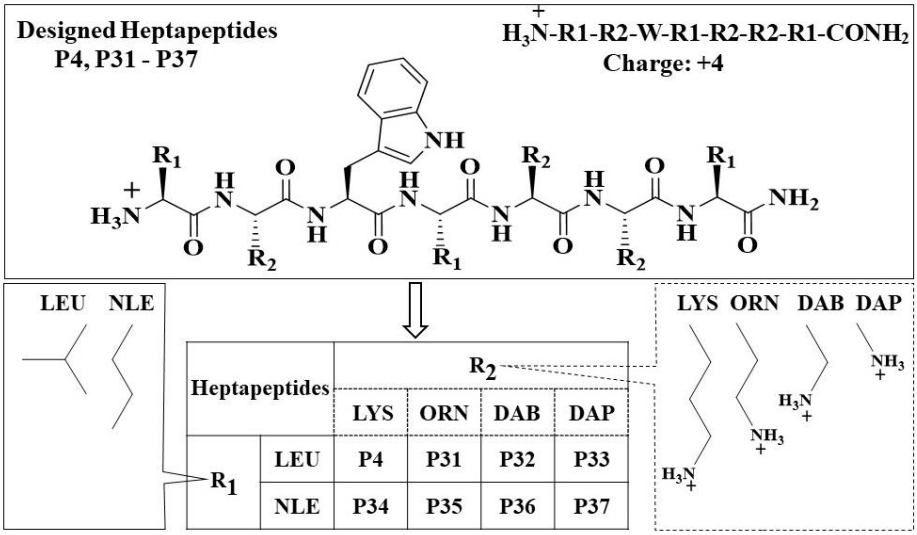

Figure 5.2. Schematic representation of the heptapeptide (P31-P37) designed from the all α amino acid containing template peptide P4. In peptides P31-33, polar amino acid Lys of P4 was replaced by unnatural analogs like Orn, Dab and Dap, in P34, all the non-polar hydrophobic Leu residues in P4 were replaced by Nle and in P35-37, both the Lys and Leu residues were simultaneously replaced by the unnatural analogs. The side chains of the unnatural amino acid residues are illustrated in the figure 5.2.

Table 5.3. Sequence of the Peptides P31-37

Sl. NO	Peptide name	Peptide sequence
1	P4	H-LKWLKKL-NH_2
2	P31	H-LOrnWLOrnOrnL-NH_2
3	P32	H-LDabWLDabDabL-NH_2
4	P33	H-LDapWLDapDapL-NH_2
5	P34	H-NleKWNleKKNle-NH_2
6	P35	H-NleOrnWNleOrnOrnNle-NH_2
7	P36	H-NleDabWNleDabDabNle-NH_2
8	P37	H-NleDapWNleKKNle-NH_2

5.3.2. Peptide Synthesis and Characterization:

All the designed peptides were synthesized using solid phase synthesis protocol as described in the experimental section. The purified peptides were characterized using analytical HPLC (Appendix, Figure A11-A17), ESI-MS (Appendix, Figure A33-A39) and ^{1}H NMR (Appendix, Figure A53-A59) spectra.

5.3.3. Antimicrobial Activity of the Designed AMPs:

Antimicrobial activities of P31-37 were tested against both Gram-negative (*P. aeruginosa* and *K. pneumoniae*) and Gram-positive (*S. aureus*) ESKAPE pathogens. The activity of all the peptides were compared with P4 (Table 5.4, Figure 5.3). Activity of the peptides were dependent both on the individual sequences as well as on the bacterial strain. Activity against *P. aeruginosa* improved upon substitution of Lys with shorter side chains containing amino acids like Orn and Dab in P31 and P32/ P36 respectively. Upon further shortening the side length of Lys by substituting it with Dap, the activity of P33 diminished against *P. aeruginosa*. However, upon introducing the second type of substitution of Leu with Nle in P37, in addition to substitution of Lys with Dap, the activity against *P. aeruginosa* was partially recovered. In case of P35 and P36 though, substitution of Leu with Nle did not improve the activity of P31 and P32 respectively. None of the analogs of P4 showed enhanced activity compared to P4 against *K. pneumoniae*. However, among the various analogs those containing Dab (P32/P36) mutated in the place of Lys, showed best activity. In the case of Gram-positive bacteria *S. aureus*, P32 containing Dab residues had improved activity in comparison to P4. The activity of P32 further improved upon additional mutation of the Leu residues to Nle in P36. Activities of P31 containing Lys to Orn substitution was somewhat comparable to that of P4, while the activity was lost upon introducing the double mutation involving both Lys and Leu residues in P35. Peptides P33 and P37 containing Dap mutations were completely inactive against *S. aureus.* AMP 34, with Leu to Nle mutations, had somewhat diminished activity against *P.*

aeruginosa and completely lost activity against *K. pneumoniae* and *S. aureus* in comparison to P4. This differential behavior of the designed AMPs against a specific microbes suggested that the hydrophobic-hydrophilic balance of the AMPs and the length of the side chains of the constituent amino acid residues were very important for their activities. Among the similarly charged cationic AMPs, this might be the factor that modulates activity. Secondly, the differential potency of a particular AMP towards the various microbial strains suggested that the activity depended on the membrane diversity of these strains.

Table 5.4. $MIC_{99\%}$ of P31-P37 against ESKAPE pathogens *P. aeruginosa*, *K. pneumoniae* and *S. aureus*. All the $MIC_{99\%}$ are reported in μM. ND = Not detectable, ND* = Not Done

Microbes / Peptides	$MIC_{99\%}$ (μM)					
	Gram-negative bacteria				*Gram-positive bacteria*	
	P. aeruginosa		*K. pneumoniae*		*S. aureus*	
	Absence of salts	Presence of Salts	Absence of salts	Presence of Salts	Absence of salts	Presence of Salts
P4 (Control)	30	ND*	50	ND*	80	ND*
P31	20	ND*	200	ND*	60	ND*
P32	20	100	60	ND*	40	ND*
P33	200	ND*	>200	ND*	200	ND*
P34	60	ND	200	ND	200	ND
P35	60	ND	200	ND	200	ND
P36	20	50	80	ND	20	ND
P37	60	ND	>200	ND	200	ND

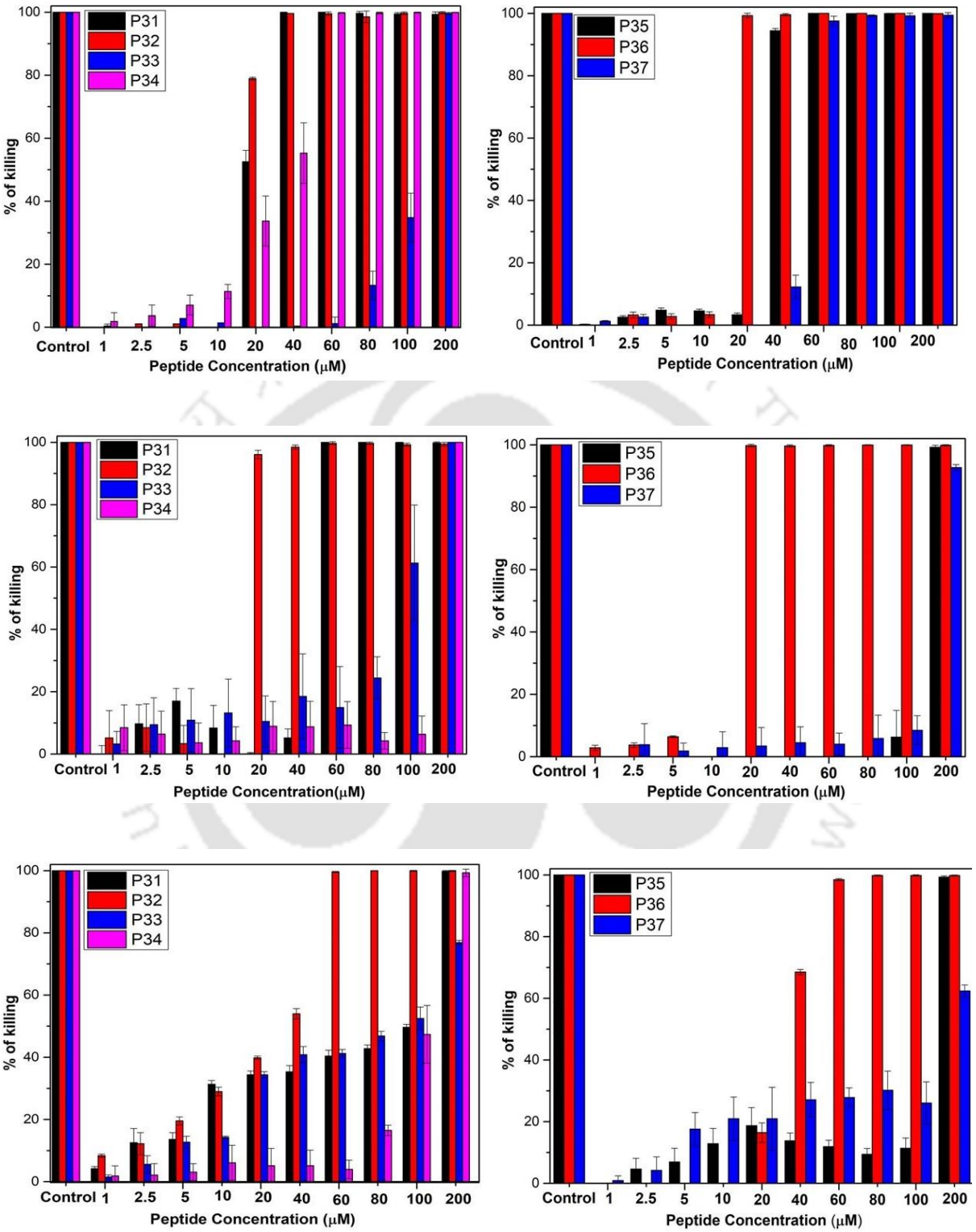

Figure 5.3. The bar plots represent $MIC_{99\%}$ of P31 to P37 in presence of 10 mM phosphate buffer. The micro broth dilution assay was performed in increasing concentration of respective

peptides and killing percentage was calculated, after overnight incubation. (Upper Panel: against *P. aeruginosa*; middle: against *S. aureus*; lower: against *K. pneumoniae*). Control experiment was done in presence of 100 μM polymixin B and other readings were normalized against it.

As most of the AMPs lose their activity in the presence of physiological concentration of salt, we investigated the salt tolerance of the antimicrobial activity of P31-P37 in the presence of physiological concentrations of NaCl (150 mM), the most abundant salt in the serum. The loss of activity in the presence of salts is generally attributed to the electrostatic reasons that decrease the affinity of the cationic AMPs towards the negatively charged microbial membranes. The presence of salt delays the kinetics of the interaction in between the peptide and the membrane surface though, post the initial interactions, final peptide: membrane mimetic complex is independent to the presence of salts. Of all the peptides designed, P36 exhibited moderate NaCl tolerant activity respectively against *P. aeruginosa* (Figure 5.4a). P32 and P36 lost their activity completely towards the other strains in the presence of salts. All the other analogs completely lost their activity in the presence of NaCl against all the microbial

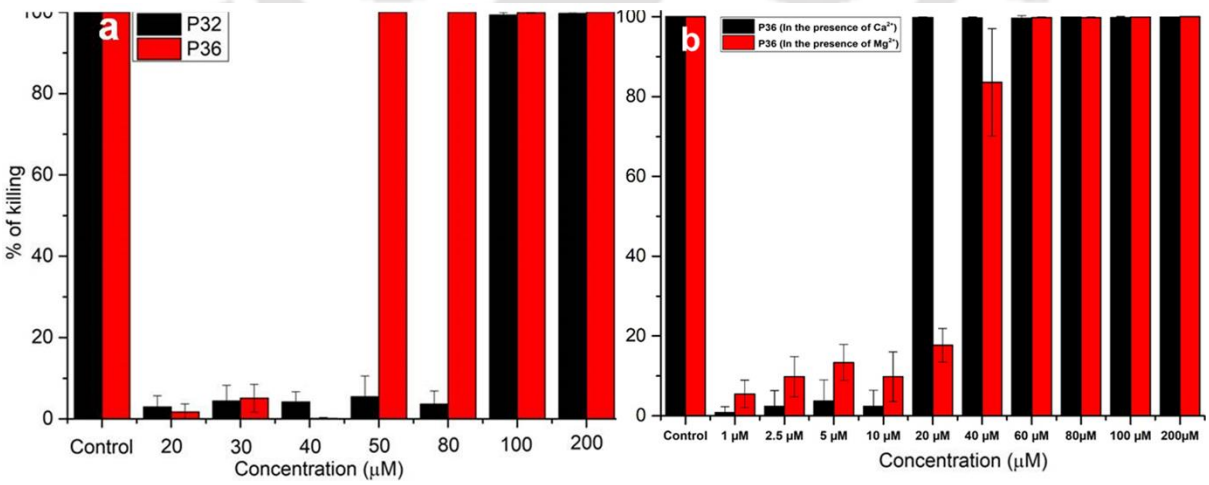

Figure 5.4. (a) Salt tolerant activity of P32 (black) and P36 (red) against *P. aeruginosa*. MIC99% was calculated from the micro broth dilution assay performed in the presence of 150

mM NaCl. The control experiment was performed in the presence of 10 μM Polymixin B and other readings were normalized against it. (b) MIC of P36 against *P. aeruginosa* in the presence of Ca^{2+} and Mg^{2+} ions.

strains tested (Table 5.4). It is mention worthy that the template peptide P4 also had a salt sensitive activity towards the microbes. Salt tolerance of the most active peptide P36 against *P. aeruginosa* was further performed in the presence of some physiologically lesser abundant salts like $MgCl_2$ and $CaCl_2$ (Figure 5.4b). Activity of P36 against *P. aeruginosa* was completely retained in the presence of $CaCl_2$ (20 μM) while it was partially compromised in the presence of $MgCl_2$ ($MIC_{99\%}$ ~ 60 μM). However, even being compromised in the presence of $MgCl_2$, P36 retains a moderate antimicrobial activity.

In summary, from the above discussion, it might be concluded that the activities of the different analogs were dependent on the specific microbial species. This was not surprising, as the membranes of different microbial species were quite unique and most of the cationic AMPs manifested their action through membrane interactions. The designed analogs were most potent against *P. aeruginosa*. Decrease in the length of the side chain of the charged amino acid residue led to the increase in the activity of the analogs as seen in the Orn and Dab substituted peptides.

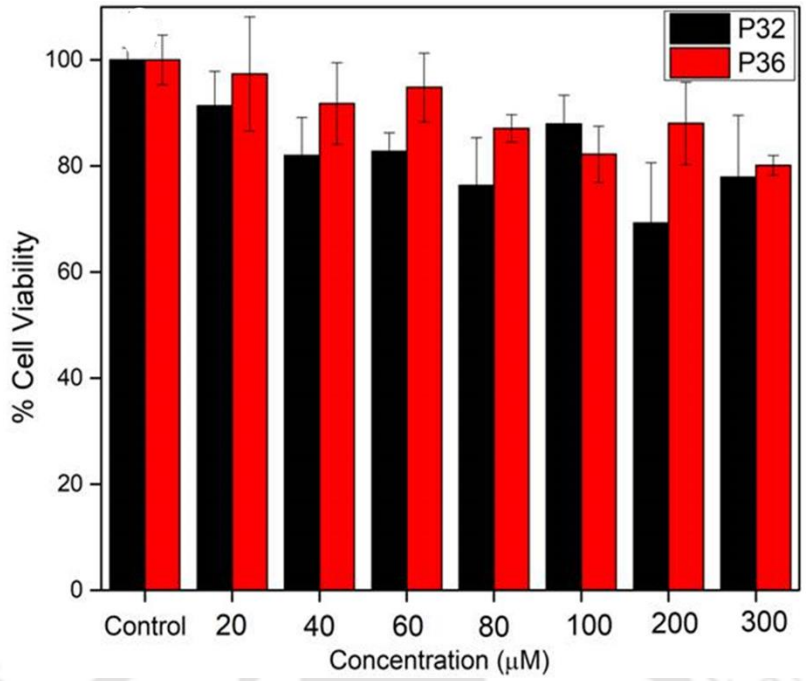

Figure 5.5. MTT assay of the peptides P32 (red) and P36 (black) on L132 cell lines. Cell viability was measured by monitoring the absorbance at 570 nm upon addition of increasing concentrations of peptide to the cells. All the experiments were performed in triplicates.

However, upon decreasing the side chain length too much as in Dap substituted peptides, there was a loss in activity which could be recovered partially by the second type of substitution of Leu to Nle. Though Leu and Nle have same hydrophobicities, the length of the side chains in Nle being longer compared to Leu, improved the activity. In the cases of peptides P31 or P32 where the charged side chain was longer, there was effective interaction with the microbial membrane already leading to high activity. Thus, in those cases a second type of mutation of Leu to Nle did not improve the activity further. Additionally, in P34, where the hydrophobic-hydrophilic balance was identical to P4 but the length of the hydrophobic chain was varied, the peptide either had diminished or lost activity against the different microbes. This indicated that in addition to the optimum hydrophobic hydrophilic ratio, the antimicrobial activity depended

on the length of the side chains in being able to make the best interaction with the microbial cell membrane.

P32 and P36 were found to be the most active peptides against all the strains tested, with best activity against *P. aeruginosa*. Additionally, P36 showed salt tolerant activity against *P. aeruginosa*. *P. aeruginosa* is a multi-drug resistant opportunist pathogen that causes diseases in plants, animals and humans. The organism causes serious infection during existing diseases or conditions like cystic fibrosis or traumatic burns. It is generally problematic to treat infections caused by this organism owing to its intrinsically advanced antibiotic resistance. Though not extremely virulent, this pathogen is capable of extensive colonization and formation of enduring biofilms. Thus in the later part of the study, we have only focused on the bioactivities, biophysical attributes and the mode of action in details against *P. aeruginosa* for the two most active peptides i.e. P32 and P36.

5.3.4. Cytotoxicity of the AMPs:

Being non-cytotoxic to the mammalian cells is one of the basic criteria for being an effective antimicrobial therapeutic. Effect of P32 and P36 on the viability of the human embryonic lungs (L132) cell lines was determined using MTT assay. Upon treatment of the cells for 4 hrs. with 100 μM (concentration greater than $MIC_{99\%}$) of P32 and P36, they exhibited a cell viability of ~ 90% (Figure 5.5), suggesting a very low cytotoxicity at the biologically relevant concentration.

5.3.5. Hemolytic Activity:

Being non- hemolytic is yet another basic criterion for any peptide to be used as a therapeutic molecule and hence the hemolytic activities of P32 and P36 against human RBCs were studied. Figure 5.6 represents the digital image of the hemolytic assay performed against human RBCs at different concentrations of P32 and P36 (25, 50, 100, 200 μM). Incubation of the RBCs with

buffer and Triton-X 100 were treated as negative and positive control respectively. Till 4 hrs. both P32 and P36 were found to be very weakly hemolytic (% hemolysis < 10%) till a concentration of 100 µM, which was much greater than their biologically active concentrations.

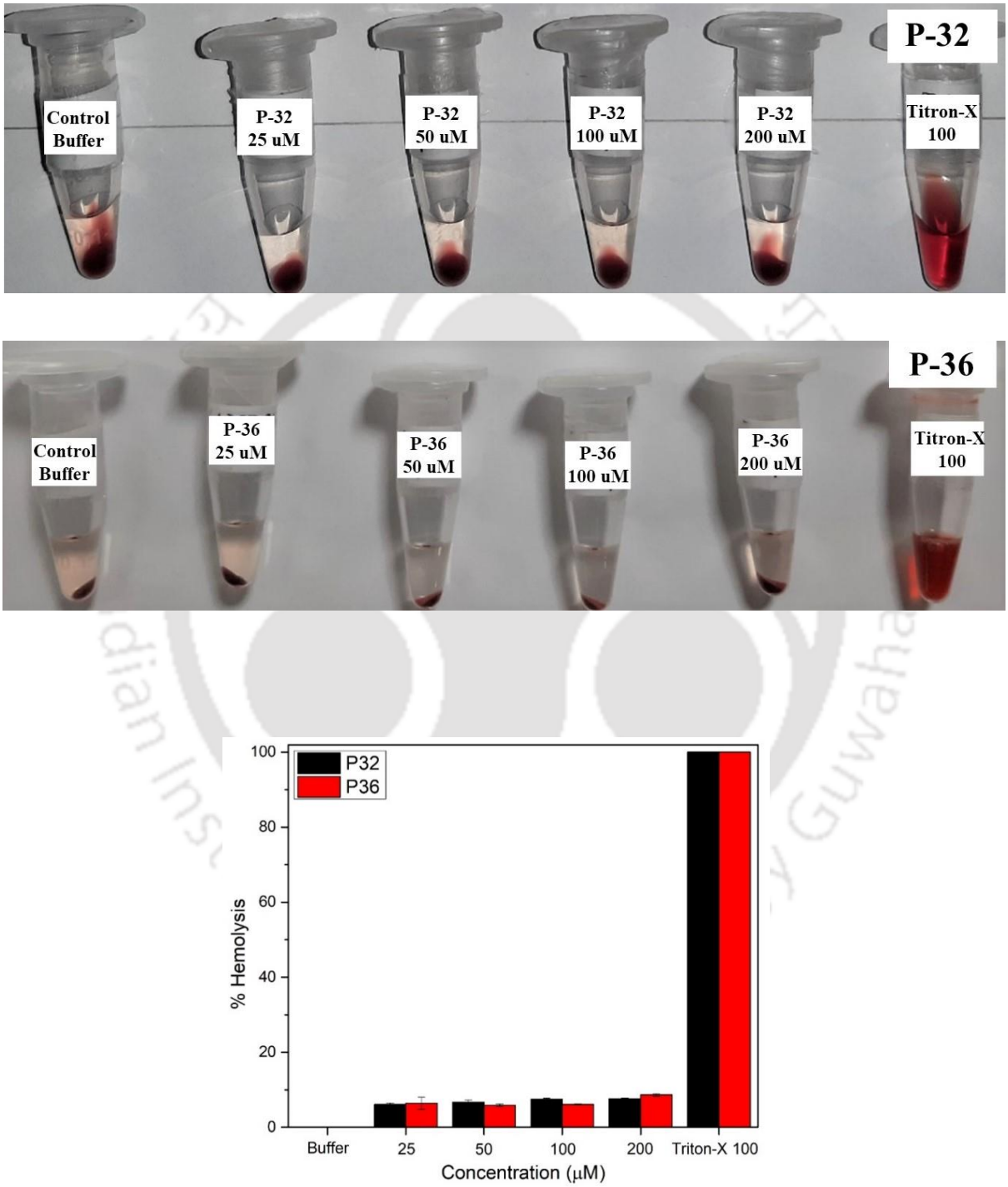

Figure 5.6. Above: Digital image represent hemolytic assay for P32 and P36 against human RBC at different peptide concentration (25, 50, 100, 200 µM). Bottom: Bar diagram showing

the % hemolysis for P32 (black) and P36 (red) against different concentrations of the peptides. Buffer and Triton-X 100 treated as negative and positive control.

5.3.6. Time Course for Bactericidal Activity of P36 on *P. aeruginosa*:

To determine the time needed by P32 and P36 to express their bactericidal activity against *P. aeruginosa* at its $MIC_{99\%}$, a time course experiment was performed (Figure 5.7, 5.8). Cells were incubated with P32 and P36 at their respective $MIC_{99\%}$ for different time span and then spread onto NB agar plates for CFU counting. After overnight incubation of the agar plate, number of viable cells were calculated. It was observed that almost complete killing of *P. aeruginosa* cells was observed within 45 min for P36 (Figure 5.7) and within 60 min for P32 (Figure 5.8).

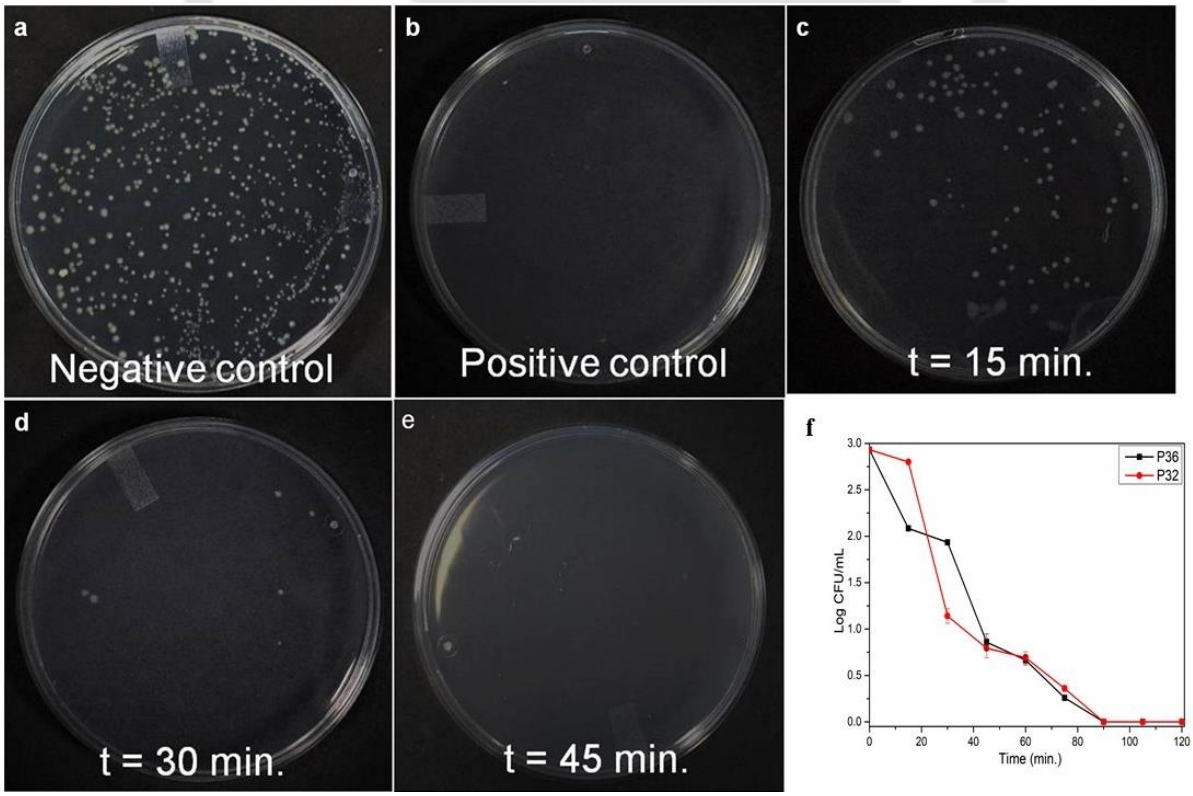

Figure 5.7. Time kinetics of the bactericidal activity of P36 at its $MIC_{99\%}$ against *P. aeruginosa* cells. *P. aeruginosa* cells were treated with P36 at MIC for different time intervals and cells were spread on NA plate for CFU count after overnight incubation at 37 °C. Bacterial killing percentage was calculated from CFU count of the plate in comparison to the control plate. At 45 min time point, a completely clear plate was observed, suggesting a 100% killing of the microbial cells. (a) Negative control plate (no P36 added), (b) Positive control plate (10 µM Polymyxin B treated cells) and (c), (d), (e) are plates at time points 15 min, 30 min and 45 min respectively. (f) The time kill kinetics of P32 and P36 against *P. aeruginosa* shown in log scale.

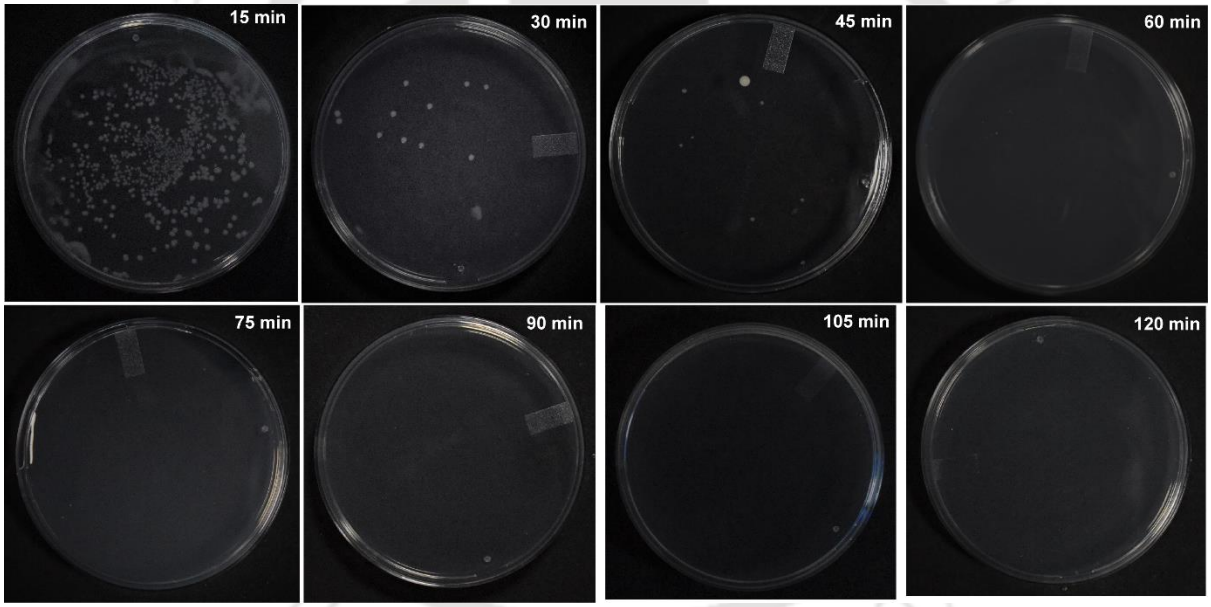

Figure 5.8. The bactericidal assay against P. *aeruginosa* in presence of P32. The images depict the CFU/ on nutrient agar plates at different time point.

5.3.7. Protease Resistance of P36:

The main bottle neck in the application of the AMPs as therapeutic agents arises from their short serum half-life owing to their protease degradability. To test if our lead peptide P36 was

immune to protease resistance, we checked its chemical integrity upon incubation with a mixture of various proteases like trypsin, chymotrypsin and proteinase K in comparison to the template AMP P4, using analytical HPLC (Figure 5.9) and ESI-MS (Figure 5.10 a-f). Peptide P36 maintained its retention time when injected into the analytical HPLC, even after incubation with the mixture of proteases till 6 hrs. , suggesting its robustness to the protease degradation (Figure 5.9 a-f). This was corroborated from the ESI-MS analysis of the reaction mixture post incubation with the enzyme cocktail, which contained only intact P36 (differently ionized, Figure 5.10 a-c) peaks. In contrast, incubation of P4 with proteases resulted in the appearance of several new peaks at different retention times in the HPLC chromatogram (Figure 5.9 d-f).

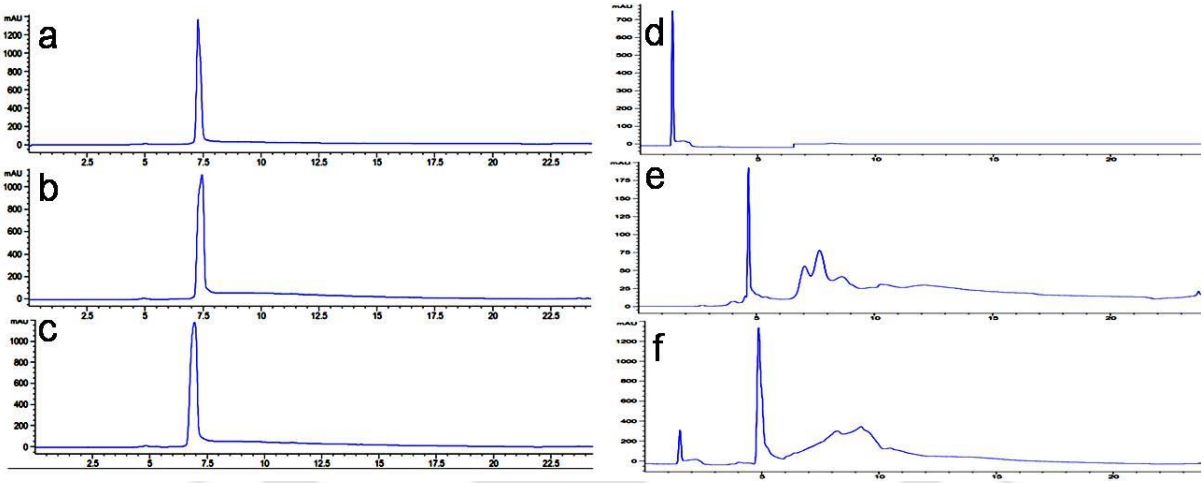

Figure 5.9. Protease resistance of P36 and P4. Analytical HPLC traces of the P36 (Left panel) and P4 (Right panel), after incubation with an enzyme cocktail (trypsin, chymotrypsin and proteinase K) for different time intervals. Chromatogram of P36 and P4: (a, d) in the absence of enzymes, (b, e) after 1hr. in the presence of enzyme cocktail and (c, f) after 12 hr. in presence of enzyme cocktail.

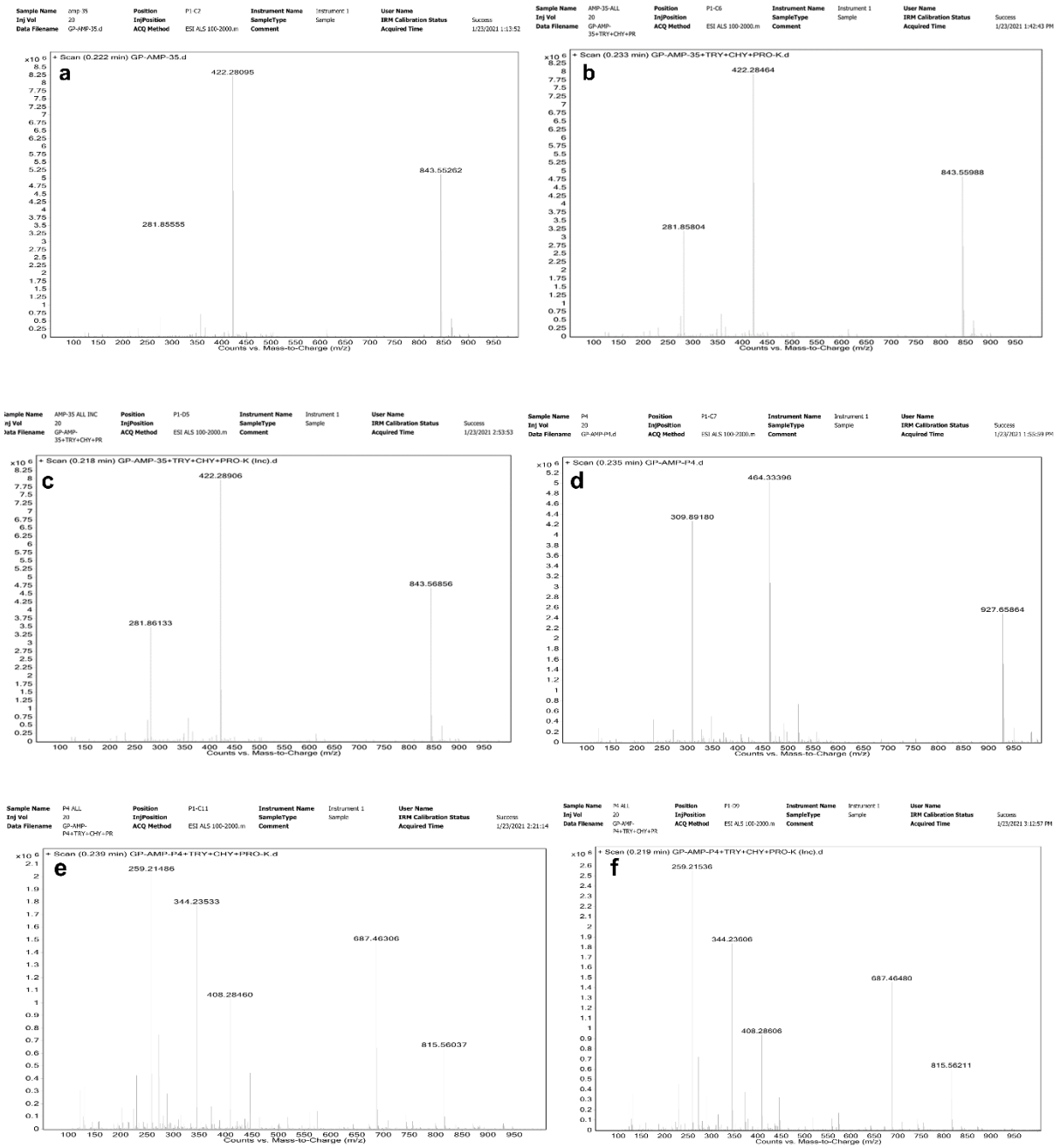

Figure 5.10. (a) Control ESI MS of P36 for enzymatic action study. Calc. $(M+H)^+$ for $C_{41}H_{70}N_{12}O_7$= 843.5524 Da; Obs. $(M+H)^+$ = 843.5526 Da, $(M+2H)^{2+}$ = 422.2809 Da, $(M+3H)^{3+}$ = 281.8555 Da. (b) ESI MS of P36 in presence of enzyme mixture (30 min. approximately). Calc. $(M+H)^+$ for $C_{41}H_{70}N_{12}O_7$= 843.5524 Da; Obs. $(M+H)^+$ = 843.5598 Da, $(M+2H)^{2+}$ = 422.2846 Da, $(M+3H)^{3+}$ = 281.8580 Da. (c) ESI MS of P36 in presence of enzyme mixture (6 hr. approximately). Calc. $(M+H)^+$ for $C_{41}H_{70}N_{12}O_7$= 843.5524 Da; Obs. $(M+H)^+$ = 843.5604 Da, $(M+2H)^{2+}$ = 422.2845 Da, $(M+3H)^{3+}$ = 281.8595 Da. (d) Control ESI MS of P4 for enzymatic action study. Calc. $(M+H)^+$ for $C_{47}H_{82}N_{12}O_7$= 927.6502 Da; Obs. $(M+H)^+$ = 927.6586 Da, $(M+2H)^{2+}$ = 464.3339 Da, $(M+3H)^{3+}$ = 309.8918 Da. (e) ESI MS of P4 in

presence of enzyme mixture (30 min. approximately). Calc. $(M+H)^+$ for C47H82N12O7= 927.6502 Da. (f) ESI MS of P4 in presence of enzyme mixture (6 hr. approximately). Calc. $(M+H)^+$ for $C_{47}H_{82}N_{12}O_7$= 927.6502 Da.

Fragment analysis for **5.9 (e)**

815.5603 corresponds to $(M+H)^+$ of the fragment LKWLKK

408.2846 corresponds to $(M+2H)^{2+}$ of the fragment LKWLKK

687. 46306 corresponds to $(M+H)^+$ of the fragment LKWLK

344.2353 corresponds to $(M+2H)^{2+}$ of the fragment LKWLK

258.2148 corresponds to $(M+H)^+$ of the fragment LK

Others small peaks seen corresponds to several other fragments of the peptide **P4**: LKWLKKL-NH_2

Fragment analysis for **5.9 (f)**

815.5603 corresponds to $(M+H^+)$ of the fragment LKWLKK

408.2846 corresponds to $(M+2H)^{2+}$ of the fragment LKWLKK

687. 46306 corresponds to $(M+H)^+$ of the fragment LKWLK

344.2353 corresponds to $(M+2H)^{2+}$ of the fragment LKWLK

258.2148 corresponds to $(M+H)^+$ of the fragment LK

Others small peaks seen corresponds to several other fragments of the peptide **P4**: LKWLKKL-NH_2

The protease treated P4 reaction mixture was analyzed using ESI-MS, which led to the identification of various degraded species (Figure 5.10 d-f). The above results conclusively proved the resistance of P36 towards enzymatic degradation in comparison to earlier reported all α amino acid containing P4. Further, to investigate if the activity of P36 was retained upon

protease treatment, $MIC_{99\%}$ of protease treated P36 was studied against *P. aeruginosa*. Figure 5.11 shows that the activity of P36 remained unaltered even upon incubating it with proteases for 6 hr. confirming that P36 was indeed protease resistant.

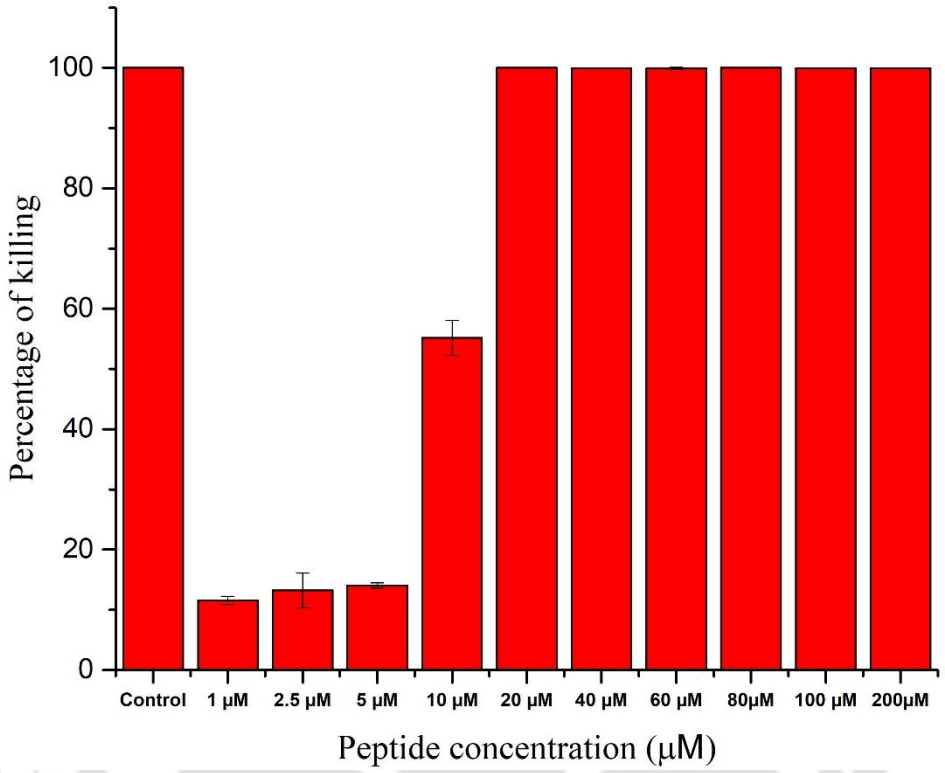

Figure 5.11. MIC of P36 against *P. aeruginosa*, post 6 hr. incubation of P36 with the enzyme cocktail (Mixture of Chymotrypsin, Proteinase-K and Trypsin in the ratio 1:1:1). Experiment was performed in triplicates.

5.3.8. Mechanism of Action of P36:

In order to study the mechanism of action of P32 and P36 against *P. aeruginosa* and membrane mimic systems, we performed a series of biophysical experiments as reported below.

5.3.9. Calcein Dye Leakage Assay

In a pursuit to understand the effect of AMPs on the microbial membrane integrity, leakage of calcein dye from POPE/POPG (3:1) LUVs was studied. The composition of the lipids that

constitute the LUVs, mimic the microbial membrane environment and thus these LUVs act as microbial cell mimics. DLS studies confirmed the structural stability of the LUVs up to 24 hrs. (Figure 5.12 a, inset). Stability of calcein laden LUVs was also checked by performing a time kinetics of the calcein leakage over one hr., wherein no detectable calcein fluorescence was observed (Figure 5.12 a). The fluorescence of calcein is not observed when trapped inside the LUVs while it enhances greatly upon leakage from them. Thus the enhancement of calcein fluorescence intensity is directly related to the dye leakage from the LUVs and thus membrane disruption. Upon treating the LUVs with 0.5X, 1X and 2X MIC of P32, about 18%, 41% and 81% enhancement of calcein fluorescence intensity was observed while 0.5X, 1X and 2X MIC of P36 led to 53%, 76% and 85 % enhancement of fluorescence signal (Figure 5.12 b). This study clearly indicated a membrane disruptive mode of action for both P32 and P36, with a greater efficiency in the later.

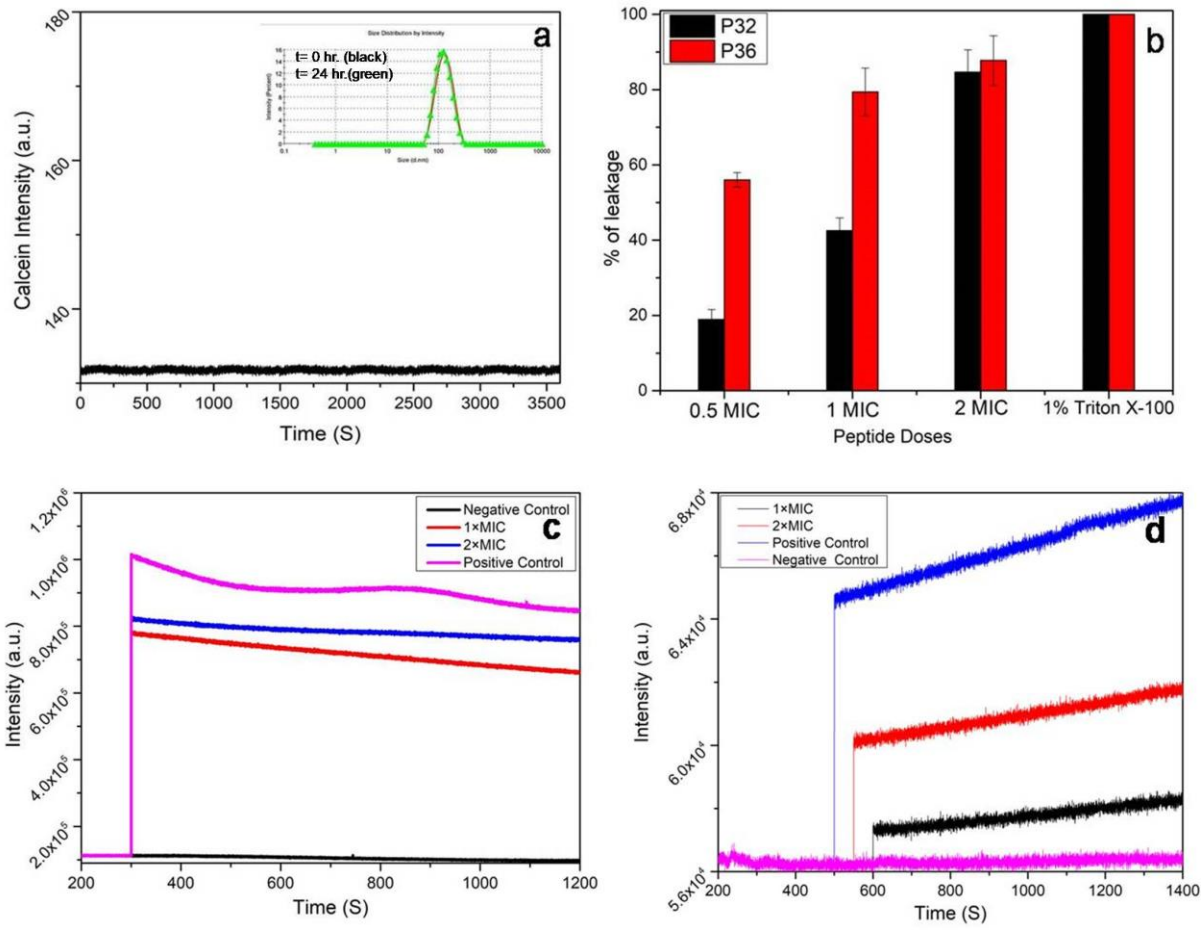

Figure 5.12. Membrane permeabilization effect of P32 and P36. (a) Structural stability of calcein entrapped LUVs (3:1 ratio POPE/POPG) in the absence of peptides (Inset) monitored over a time period of 3600 s. Unchanged hydrodynamic radius of the LUVs after 24 hrs. (green line) as seen from DLS. Absence of calcein leakage in the untreated LUV's. (b) Calcein dye leakage assay. Bar diagram representing calcein leakage from dye entrapped LUV's (3:1 ratio of POPE: POPG), a microbial membrane mimic system, upon addition of increasing concentrations of P32 and P36. Triton X 100 (0.1%) was used as the positive control. Time kinetics of (c) NPN and (d) PI uptake after addition of 1X and 2X MIC P36 to *P. aeruginosa* cells, which indicate the outer and inner membrane permeability respectively. All the experiments were performed in triplets.

5.3.10. NPN Uptake Assay (Outer Membrane Permeability):

Outer membrane permeabilization of *P. aeruginosa* was studied by NPN dye uptake assay. NPN, a hydrophobic dye is usually excluded by the outer membrane due to permeability barrier from interacting with the membrane lipids. However, disruption of the outer membrane upon treatment with AMPs or other membranolytic agents, enables the binding of NPN to the membrane lipids generating an enhanced fluorescence signal. In the present study, an enhancement of 75% and 80% in the fluorescence intensity of NPN was observed upon incubating *P. aeruginosa* cells with 1X and 2X MIC of P36 respectively (Figure 5.12 c). Similarly, an enhancement of 20% and 80% in the fluorescence intensity of NPN was observed upon incubation of *P. aeruginosa* cells with 1X and 2X MIC of P32 respectively (Figure 5.13). In the negative control experiment, the untreated cells did not show any increase the fluorescence of NPN while in the positive control experiment, Triton X 100 led to 100% enhancement of the fluorescence signal. It can thus be concluded that P36 causes considerable disruption of the outer membrane of *P. aeruginosa* and much more efficiently than P32.

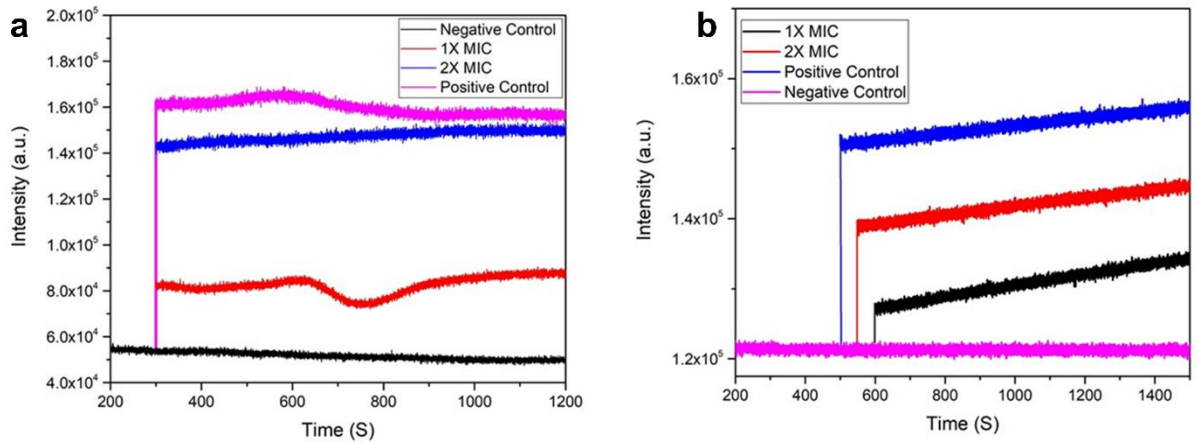

Figure 5.13. Time kinetics of (a) NPN and (b) PI uptake after addition of 1X and 2X MIC P32 to *P. aeruginosa* cells, which indicate the outer and inner membrane permeability respectively. All the experiments were performed in triplets.

5.3.11. PI Uptake Assay (Inner Membrane Permeability):

The inner membrane permeability of P36 for the *P. aeruginosa* cells was studied using Propidium Iodide Assay. Propidium iodide (PI) is a fluorophore that generates high fluorescence signal upon intercalating with the bases of DNA. As PI is impermeable through healthy membrane, and only permeates through compromised membrane, this assay is used to study the inner membrane permeability of the AMPs. Figure 5.12 d shows a 20% and 40% increment in intensity of PI upon incubating *P. aeruginosa* cells with P36 for 0.5 hrs. at its 1X and 2X MIC respectively. Figure 5.13 shows ~ 15% and 60% increase in the intensity of PI upon using 1X and 2X MIC of P32. In contrast, in the negative control, untreated cells did not show any enhancement in the PI fluorescence. This proved that both P32 and P36 caused inner membrane permeability of the *P. aeruginosa* cells, with the latter being marginally more efficient at the MIC concentrations

5.3.12. Peptide-Membrane Mimetic/Live Cell Interactions by Fluorescence Spectroscopy:

From the above biophysical studies, P36 has been shown to be highly membrane active. Membrane association is a prerequisite for the membrane activity needed to manifest the antimicrobial activity of AMPs. For understanding the selectivity in the membrane association of P32 and P36, their interactions with the microbial and mammalian membrane mimics and live cells were studied by using intrinsic fluorescence of the aromatic amino acid residue Trp. SDS and DPC micellar systems, containing negative and zwitterionic charges on the surface respectively, were considered to be microbial and mammalian membrane mimetic systems respectively.

Upon addition of increasing amounts of SDS micelles to the solutions of P32 and P36, the fluorescence emission of Trp underwent a blue shift of around 22 nm (Figure 5.14a). This indicated insertion of Trp into the hydrophobic environment of the SDS acyl chains, in turn suggesting an interaction in between the peptides and the SDS micelles. Upon similar addition of increasing amounts of DPC micelles to the peptides, no blue shift in the fluorescence emission of Trp was observed suggesting no interaction in between them (Figure 5.14a). Fluorescence quenching experiments of P36 alone and in membrane mimetic environments like SDS and DPC were performed in the presence of a static quencher like bisacrylamide for understanding the solvent exposure (Figure 5.14b). The extent of quenching of Trp fluorescence the free peptide and that in presence of the membrane mimetic environment were expressed in terms of Stern Volmer constant (K_{sv}). It was observed that the K_{sv} value for the peptide alone

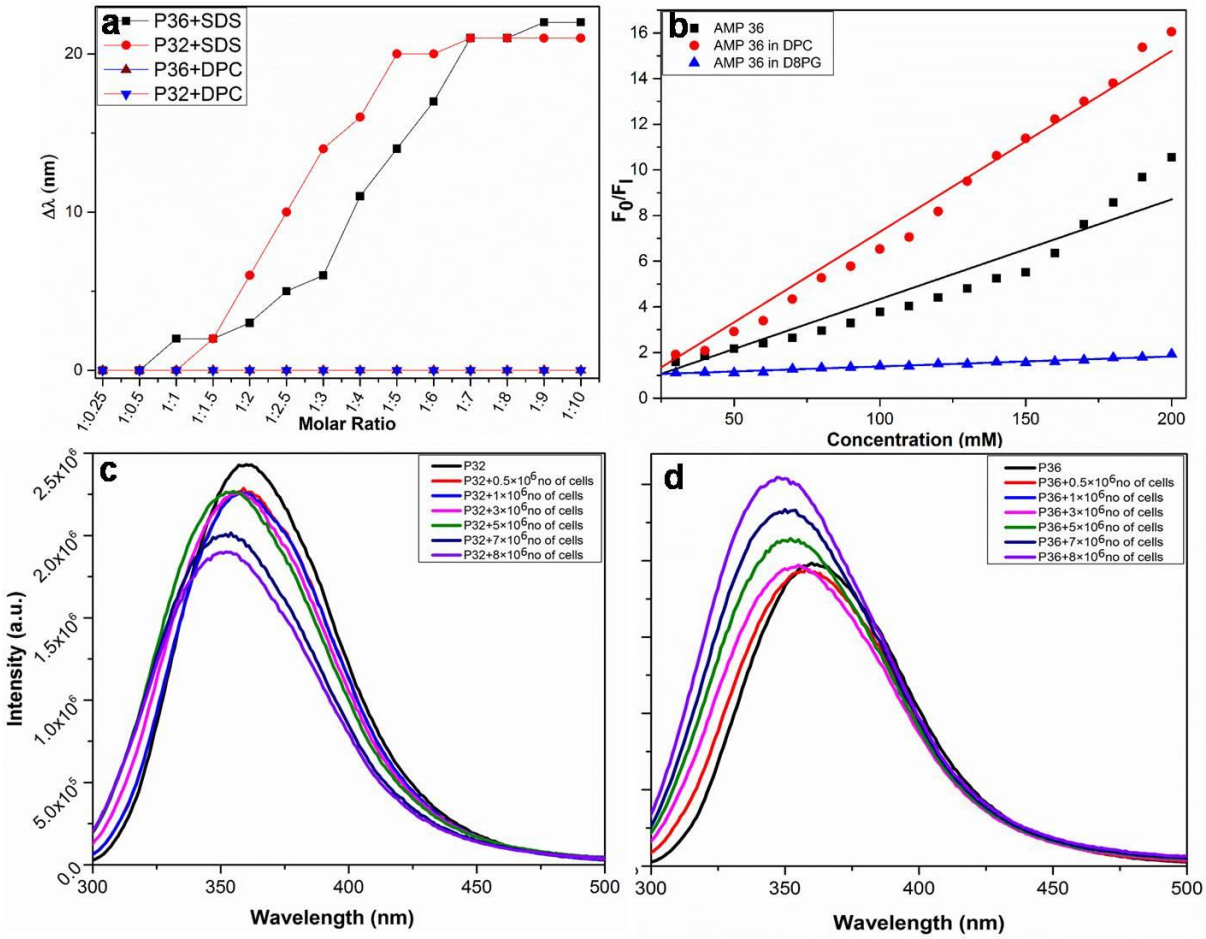

Figure 5.14. Interaction of P32 and P36 with membrane mimics/ live membranes. (a) Change in fluorescence emission maxima (Δλ) of Trp residues of P32 and P36 in the presence of varying ratios of peptide: lipids (SDS and DPC). A blue shift in the emission maxima occurs for both P32 and P36 with increasing concentrations of SDS, a bacterial membrane mimic suggesting an interaction in between the two, while there is no change in the fluorescence maxima upon addition of DPC, indicating no interaction in between them. (b) Plot of F0/F1 against concentration of peptide alone and in the presence of membrane mimics like D8PG and DPC. Change in the fluorescence emission maxima of the tryptophan fluorescence of (c) P32 and (d) P36 respectively in the presence of increasing concentration of live *P. aeruginosa* cells.

and the peptide in DPC was higher than that seen in SDS. This indicated that the peptide was much more solvent exposed in DPC, the mammalian membrane mimetic environment than in SDS, the microbial membrane mimetic environment. Or in other words, P36 selectively interacted with the microbial membrane mimetic environment over the mammalian membrane mimetic environment leading to the lesser exposure of Trp in the former.

Next, in order to understand the interaction of P32 and P36 with the live *P. aeruginosa* cell membranes, increasing amounts of cells were added to the peptides while monitoring the Trp fluorescence (Figure 5.14c and 5.14d). Upon increasing the concentration of the cells, an increasing blue shift in the emission maxima was observed for both P32 and P36, which might be attributed to the embedding of the Trp in the hydrophobic environment of the microbial membranes. This observation conclusively established the interaction in between P32 and P36 with *P. aeruginosa* cell membranes.

5.3.13. Determination of the Thermodynamic Factors in the Binding of P32/P36 with Lipopolysaccharide (LPS):

P32 and P36 exhibited best activity towards *P. aeruginosa*, a gram-negative bacteria. The outermost leaflet of the asymmetrical bilayer of the outer membrane of the gram-negative bacteria is composed of Lipopolysaccharide (LPS). Hence, any antimicrobial agent that acts on the Gram-negative bacteria first encounters LPS layer. We wanted to look at the thermodynamic parameters associated with the interaction in between the P32/P36 and LPS through ITC (Figure 5.15). The isotherm obtained for both P32 and P36, indicated a negative enthalpy change or an exothermic reaction with LPS (Figure 5.15 a, b). Gibb's free energies of the interactions were calculated (Table 5.7). The negative values of ΔG indicated that the binding of the peptides to LPS were thermodynamically favorable. P36 had a more negative value for the ΔG for binding than P32. The association constants of binding of P32 and P36 to

LPS were determined. P36 clearly had a higher affinity towards LPS than P32. From the ITC studies, P36 seemed to have a better membrane affinity than P32.

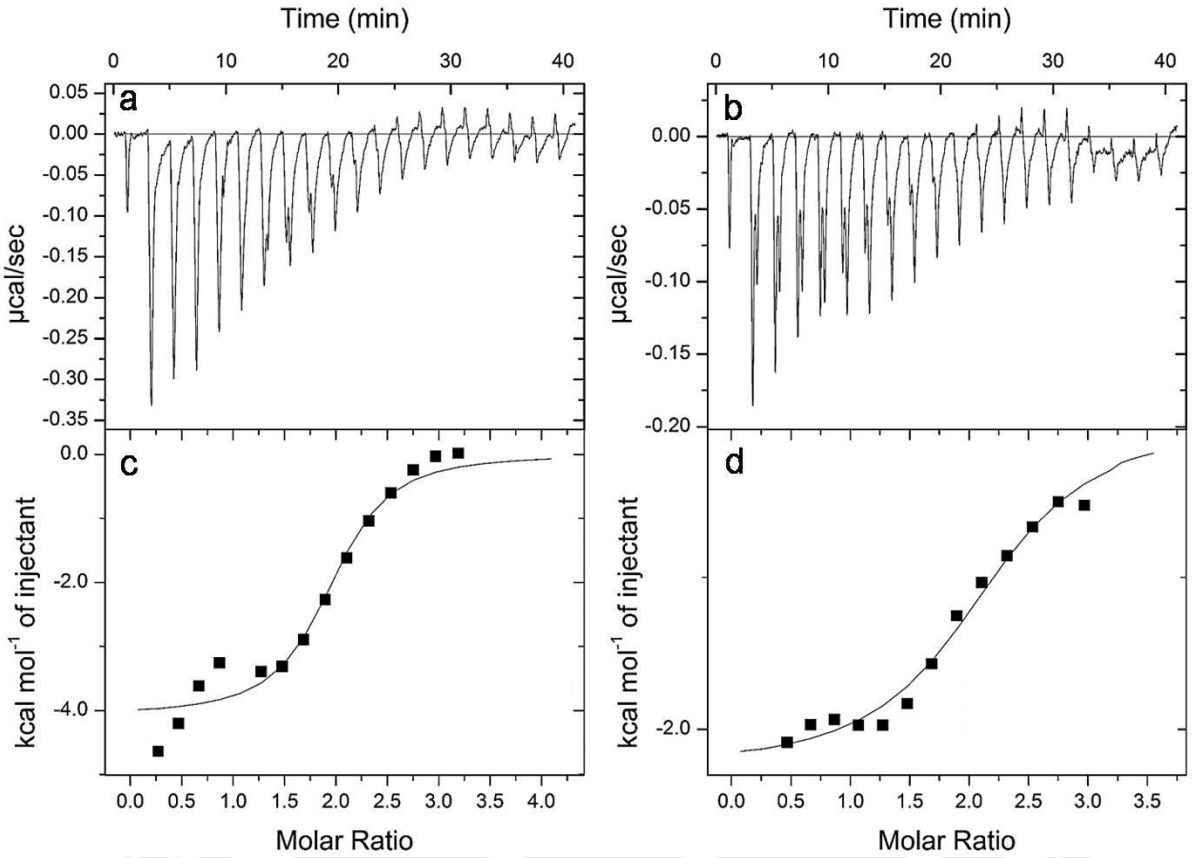

Figure 5.15: Isothermal Titration calorimetry (ITC) for P32 and P36 in the presence of LPS (50 µM), a component of the outer leaflet of the bacterial membrane. Exothermic heat of reaction with LPS micelles vs time of interaction for (a) P32 and (b) P36. Enthalpy change per mole of peptide (c) P32 and (d) P36 injection with the Peptide: LPS molar ratio.

5.3.14. Peptide-Live Cell Interaction Studied through Microbial Surface Zeta Potential:

Interaction of P36 with the live *P. aeruginosa* cells was studied by monitoring the surface zeta potential of the cells. Microbial cells are negatively charged and hence have a negative surface zeta potential. Upon binding of the cationic peptides to the negatively charged microbial membranes, the surface zeta potential of the cell surface becomes less negative.

Table 5.7. Thermodynamic parameters in the interaction of P32 and P36 with SDS calculated from ITC experiments performed at 298K.

Thermodynamic parameters	Peptides	
	P32	**P36**
$K_A(M^{-1})$	1.83×10^5	4.72×10^5
$\Delta G(kcal.mol^{-1}) = RTlnK_A$	-7.18	-7.74
N	2.13	1.90
$\Delta H(kcal.mol^{-1})$	-2.26	-4.08
$\Delta S(kcal.mol^{-1}K^{-1})$	16.6	12.4
$T\Delta S(kcal.mol^{-1})$	415	310
K_D (M)	$5.46 \text{ X } 10^{-6}$	$2.12 \text{ X } 10^{-6}$

Thus a decreasing negative zeta potential is an indication of the peptide-membrane interaction. Upon addition of P36 to the live cells, the surface zeta potential of the *P. aeruginosa* cells became less negative, and plateaued out beyond 1X MIC to about 0 mV (Figure 5.16 a). This observation conclusively proved binding of P36 to the *P. aeruginosa* cell membrane.

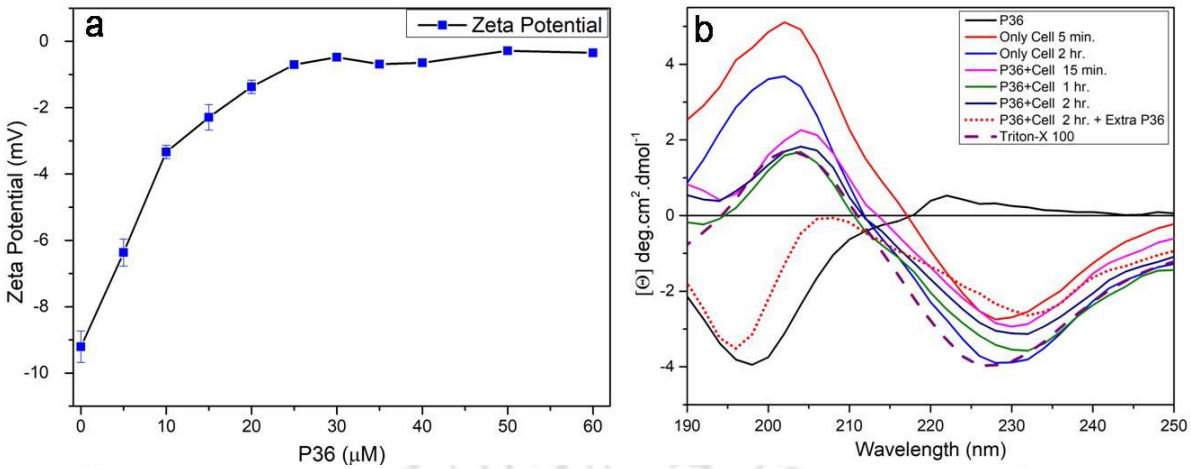

Figure 5.16. (a) Surface zeta potential of live *P. aeruginosa* cells upon addition of increasing concentration of P36. (b) CD spectra of P36 alone in phosphate buffer and in the presence of live *P. aeruginosa* cells at different incubation times.

5.3.15. Structure of AMP upon AMP-Membrane Mimic/Live Cell Interactions using CD:

Secondary structure of the peptides often plays an important role in the peptide membrane interactions and hence the activity of the peptides. We wanted to study the structure of the two most active peptides P32 and P36 in free state and in the presence of membrane mimetic systems. Figure 5.17 shows the change in molar ellipticity of P32 and P36 in water, 50% TFE (a helix promoting solvent), SDS micelles and DPC micelles. Both the peptides adopted a random coil conformation in water and also in the presence of the different membrane mimetic environments. This suggested that the peptides bound to the membranes mimics as random coils.

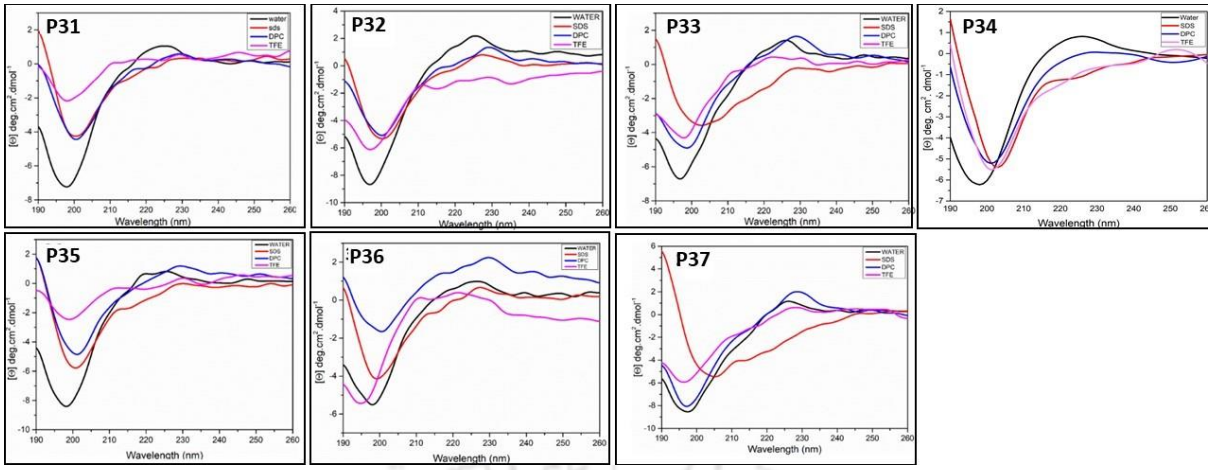

Figure 5.17. CD spectral study of P31 to P37 in presence of different membrane mimetic environments: SDS mimics the bacterial membrane and DPC mimics the mammalian membrane. 50% TFE promotes the α-helical propensity.

We further wanted to study the P36-*P. aeruginosa* interactions through Circular Dichroism spectroscopy. CD was performed on P36 alone in phosphate buffer and on P36-*P. aeruginosa* cell mixture at different time points (Figure 5.16b). Later, fresh P36 was added to the peptide-live cell mixtures and CD was studied. P36 formed a random coil conformation with a negative peak at 200 nm. The live *P. aeruginosa* cells in phosphate buffer at pH 7.4 showed a positive peak at 200 nm and a negative peak at around 228 nm. Upon addition of 1x MIC of P36 to the cells, the positive and the negative CD peaks red-shifted to around 205 nm and 232 nm respectively. The positive peak intensity was significantly diminished upon addition of P36. This was due to the cancellation of positive peak from the *P. aeruginosa* cells by the negative peak of P36. The negative peak of the cells remained almost similar in intensity in the P36: *P. aeruginosa* complex due to absence of any peaks from P36 in this region. The slight red shift in the peak positions of the final P36- *P. aeruginosa* system was owing to the interactions in between them. The spectra of the P36- *P. aeruginosa* mixture remained almost unchanged from 15 min to 2.5 hrs., indicating completion of interaction within the first 15 minutes. Upon

addition of fresh P36 after 2.5 hrs. , a negative peak re-appeared at 195 nm, suggesting random coil conformation of the freshly added P36 in addition to the negative cotton effect peak at ~ 230 nm from the P36-*P. aeruginosa* complex. The positive peak of the P36: *P. aeruginosa* cell complex was not observed as it was cancelled by the negative peak of the free peptide. The peptide added in the second slot was excess in comparison to the cells, which were already completely complexed with the peptide added in the first slot. Hence, the peak due to the free P36 reappeared in this case. Thus we concluded that the peptide existed as random coil in the free state as well as in the live *P. aeruginosa* cell bound systems. Adoption of random coil conformation in the presence of membrane mimics and live cells may be attributed to the very small size of the AMPs.

5.3.16. P36-Membrane Mimic Interaction through NMR:

Next, we wanted to study the interaction of P36 with (a) SDS, the microbial membrane mimic, (b) LPS, constituent of the Gram-negative microbial membrane and (c) DPC, the mammalian membrane mimic using NMR. Figure 5.18 shows the stacked plots of the aromatic region of the ^{1}H NMR spectra of P36 (1mM) in 10% D_2O (containing 10 mM phosphate buffer pH 6.5) and in the presence of membrane mimetic environments like SDS, LPS and DPC. The sharp NMR signals of P36 became broad in the presence of SDS and LPS, while it remained unaffected in the presence of DPC. Broadening of the NMR signals was a clear indication of the interaction in between P36 and SDS and LPS. Unchanged line widths of P36 in the presence of DPC micellar system suggested the absence of interaction in between them. These observations conclusively explained the high antimicrobial potency of P36 against the *P. aeruginosa* in contrast to its non-cytotoxicity towards mammalian cells.

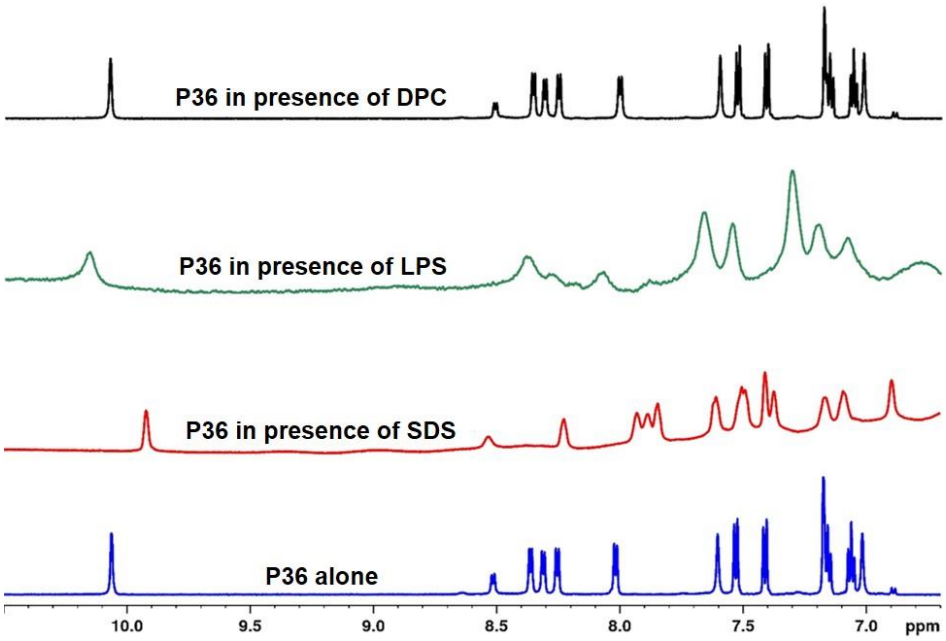

Figure 5.18. Stacked plots of the NH region of the ^{1}H NMR spectra of P36 (1mM) alone and in the presence of SDS, LPS and DPC. Broadening of the line widths and the change in the chemical shifts of the peptide signals in the presence of SDS and LPS indicates interaction in between them. Unchanged line widths and the chemical shifts of the peptide in the presence of DPC suggests absence of interaction between them.

5.3.17. Live Cell NMR:

To understand the details of the mechanism of action of P36 on *P. aeruginosa* cells, we performed a real time NMR experiment with cells added to the peptide (Figure 5.19). Line width broadening of all the signals of the peptide was observed upon incubation with the cells, due to the increase in the t2 relaxation time, suggesting an interaction in between P36 and the live cells. Additionally, new peaks attributed to the leaked metabolites from the lysed, wounded and dead cells were observed as early as 30 minutes. The time kill kinetics of bactericidal activity of P36 against *P. aeruginosa* cells, which had earlier shown considerable

killing within 30 minutes of incubation corroborated with the NMR observation. The appearance of the metabolite peaks, supported the previous biophysical studies and indicated the membranolytic mode of action for P36.

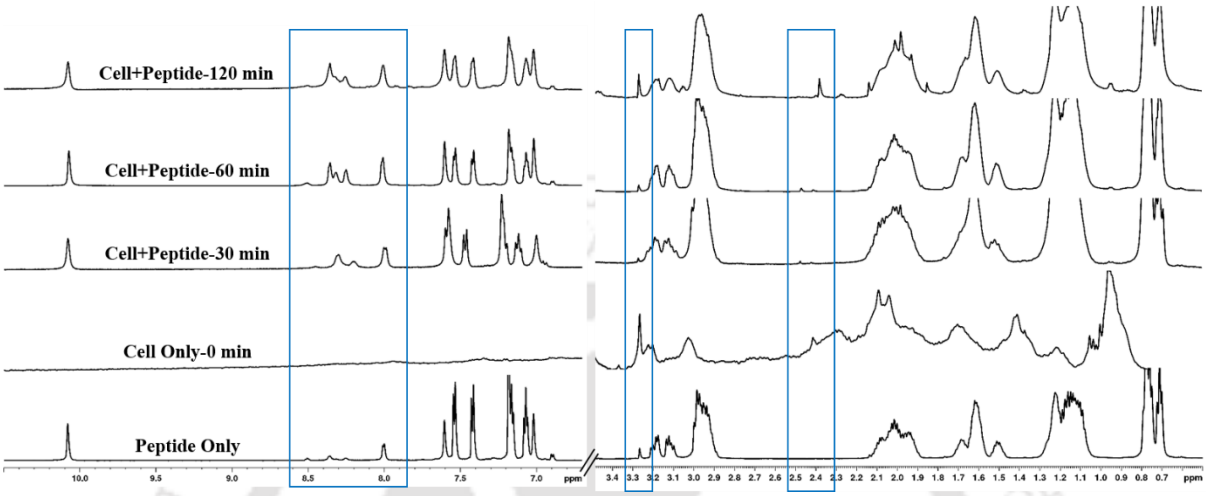

Figure 5.19. Live cell NMR spectroscopy of P36 in the presence of *P. aeruginosa* cells. Partial stacked plots of 1D ^{1}H NMR spectra at different times of incubation of P36 with *P. aeruginosa*. The blue boxes highlight the newly appeared spectral lines over the time interval.

5.3.18. Microscopic Visualization of the Membranolytic Mechanism of Action of P36:

In order to visualize the effect of P36 on the membrane integrity and the morphology of *P. aeruginosa* cells, FESEM was performed. *P. aeruginosa* cells were incubated with the P36 at their 1X and 2X MIC concentrations to study the peptide mediated deformation and cell lysis. Cells not treated with P36 retained their healthy morphology with a smooth outer membrane while the cells treated with Triton X for 4 hrs., showed complete disruption of the cellular morphology and presence of cell debri (Figure 5.20 a and b). Upon addition of 1X and 2X MIC concentration of P36 to the *P. aeruginosa* cells, cellular morphology was severely deformed accompanied by the disruption of the cell membrane (Figure 5.20 c and d).

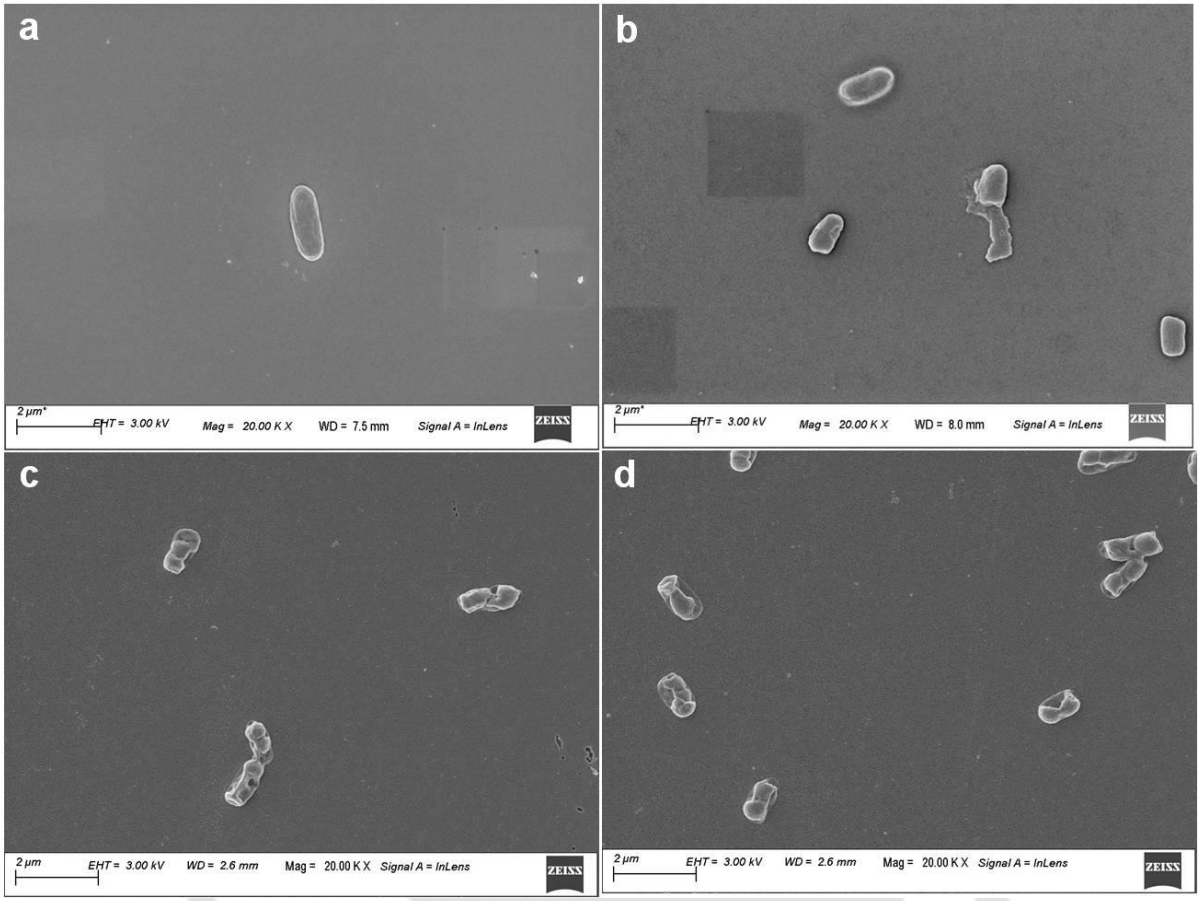

Figure 5.20. Field emission scanning electron microscopic (FESEM) images of the *P. aeruginosa* cells in the absence and presence of P36. (a) Negative control and (b) positive control in presence of 10 µM Polymixin B. Considerable deformation in cellular morphology was observed upon incubation of cells with (c) 1X MIC and (d) 2X MIC of P36.

5.3.19. Atomistic Visualization of P36 Structure and Membrane Interaction: Insight from MD Simulations:

MD simulations of the free peptides (P36, P32) showed that the peptides remained as a random coil along the MD trajectory (Table 5.8), in lines with the CD experiment. SDS micelle is a popular mimic of the bacterial membrane[70-72] and was adopted for simulation studies in this work.

Table 5.8. Structural Parameters. Data averaged from the last 30 ns of the 50 ns MD trajectory, except * & # systems. (* & # are calculated from the last 1 ns and 5 ns respectively).

S. No	Simulation Systems	Eccentricity	Micelle Radius (Å)	Peptide Secondary Structures		
		AVG±SD	AVG±SD	Coil (%)	Bend (%)	Turn (%)
1	Free SDS*	0.176±0.07	21.64±0.32			
2	Free DPC*	0.105±0.04	22.66±0.18			
3	Free P32-R1			94	5	1
4	P32-SDS-SA-R1	0.151±0.06	21.66±0.28	91	9	-
5	P32-SDS-SA-R2	0.150±0.05	21.67±0.26	92	8	-
6	P32-SDS-SB-R1	0.170±0.06	21.66±0.29	97	3	-
7	P32-SDS-SB-R2	0.153±0.06	21.55±0.29	100	-	-
8	P32-SDS-SC-R1	0.136±0.05	21.55±0.26	81	19	-
9	P32-SDS-SC-R2	0.165±0.06	21.72±0.32	83	16	1
10	P32-DPC-SA-R1	0.104±0.04	22.92±0.20	100	-	-
11	Free P36-R1			93	7	-
12	P36-SDS-SA-R1	0.169±0.06	22.20±0.86	97	2	1
13	P36-SDS-SA-R2	0.157±0.06	21.71±0.31	98	2	-
14	P36-SDS-SB-R1	0.148±0.06	21.50±0.28	86	13	1
15	P36-SDS-SB-R2	0.154±0.06	21.48±0.35	73	23	4
16	P36-SDS-SC-R1	0.143±0.06	21.45±0.34	85	8	7
17	P36-SDS-SC-R2	0.156±0.06	21.69±0.30	94	6	-
18	P36-DPC-SA-R1#	0.105±0.04	22.79±0.22	73	27	-

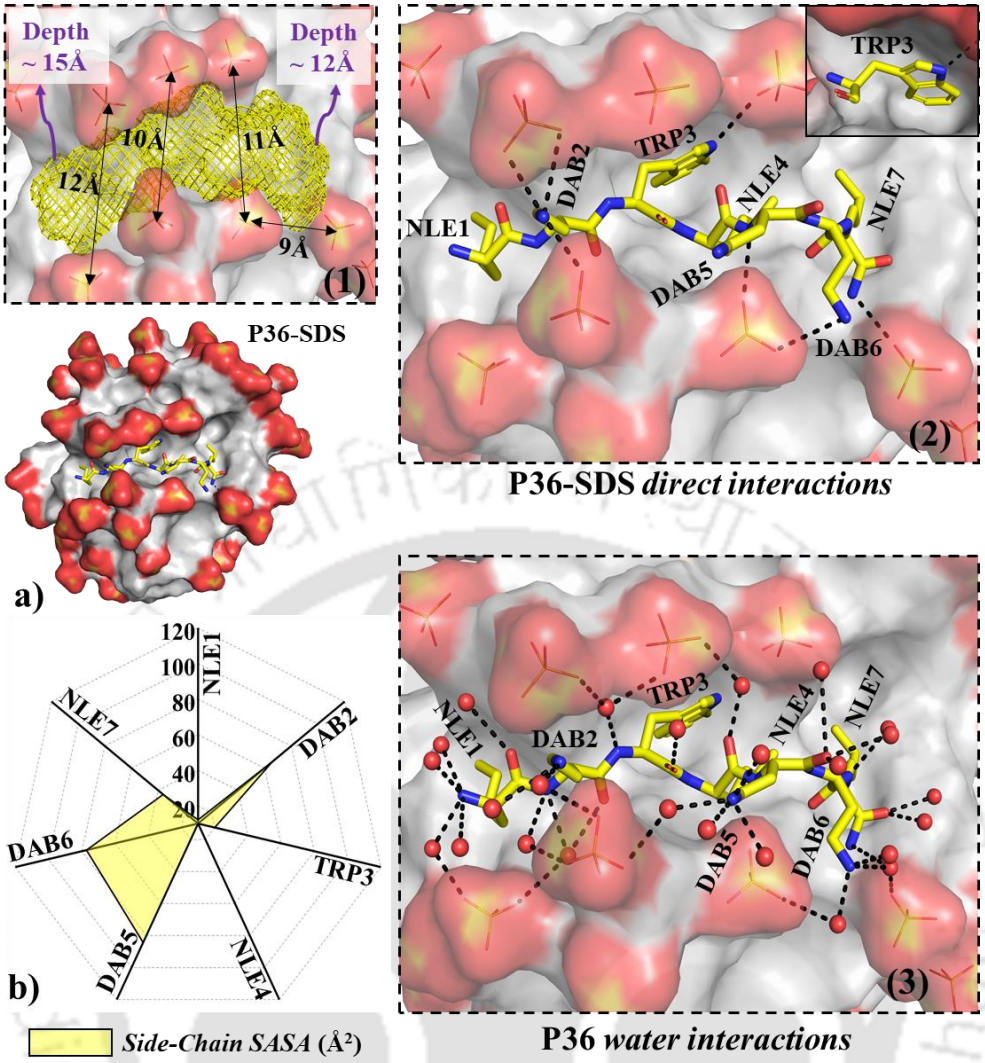

Figure 5.21. (a) Representative snapshot of P36: micelle (SDS) complex (without ions and water) after 50 ns of MD. Peptide P36 is shown as yellow sticks (Nitrogen: blue, Oxygen: red) and SDS micelle is shown as surface representation. Zoomed-in view of the peptide: micelle binding pockets are shown in the black-broken boxes: (1) SDS micelle pocket hosting the peptide is shown as yellow mesh (dimension: width ~ 10-12 Å, depth ~12-15 Å). (2) Direct peptide: micelle interaction. Trp3 side-chain is found to be buried in a dry (no waters found within 3.4Å of Trp side-chain) hydrophobic core of the micelle that satisfied hydrogen bonding requirement of the indole –NH, forming direct interaction with sulphate of SDS (shown explicitly in the solid box).

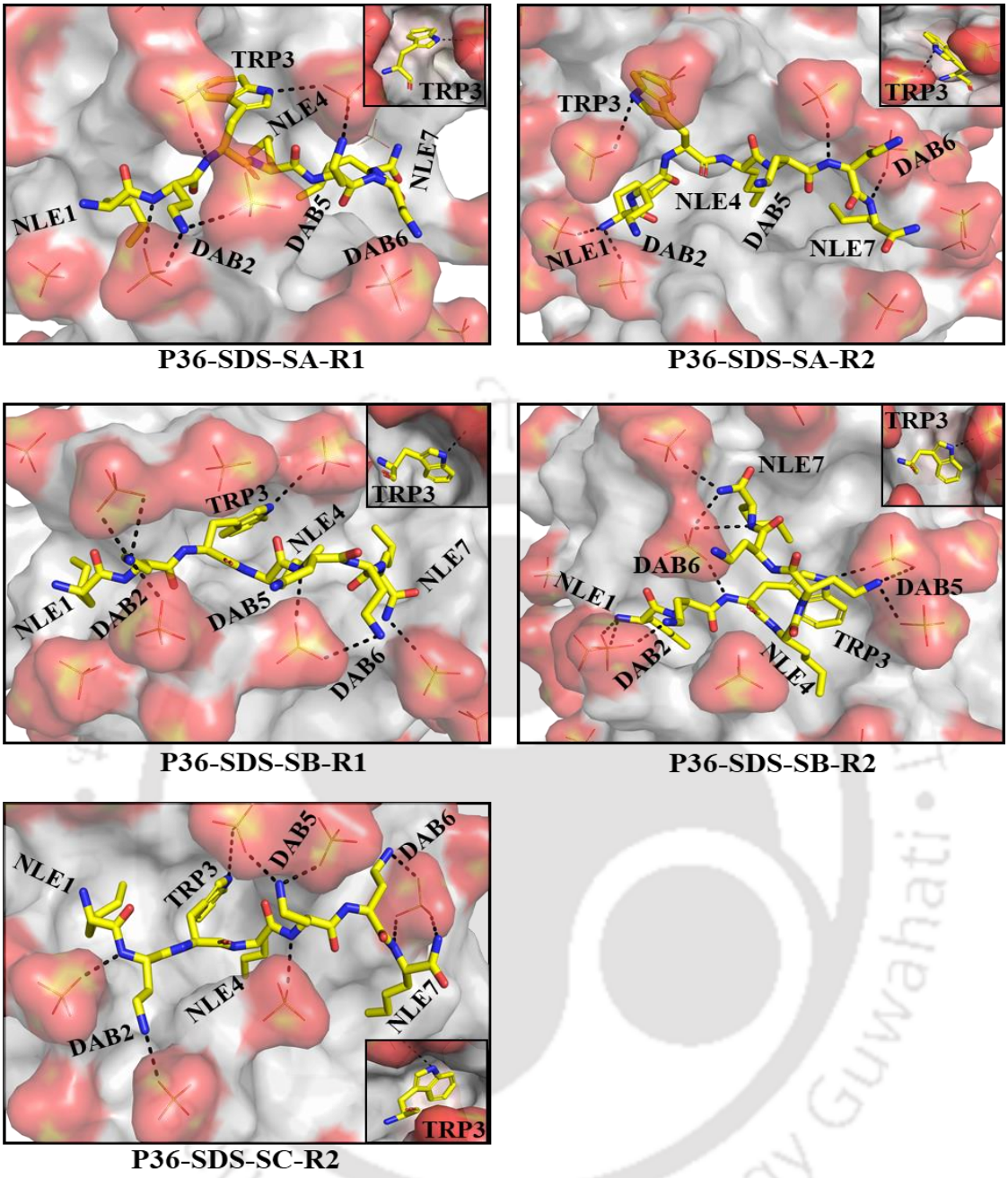

Figure 5.22. P36-SDS direct interactions are portrayed from the final structure of the P36: SDS micelle MD simulation after 50 ns. Positively charged tips of the peptide (N-terminal, side-chains of Dab2, Dab5 and Dab6) interact directly with sulphates of SDS. P36 is represented in yellow coloured sticks (Nitrogen: blue, Oxygen: red). SDS is shown in surface representation and sulphates of SDS interacting with P36 are shown in sticks form (Sulphur: yellow, Oxygen: red). The local environment of Trp3 is shown explicitly in a solid box. (SA, SB, SC) represent

distinctly different simulation setups, (R1, R2) indicate two independent replicas for each simulation setup. Hydrogens are not shown for clarity. Broken black lines represent the interactions (heavy atom distances ≤ 3.4 Å).

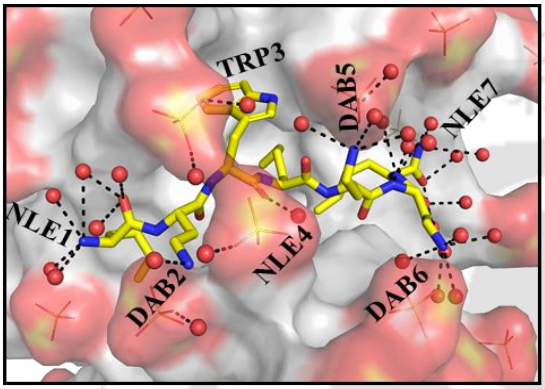

P36-SDS-SA-R1

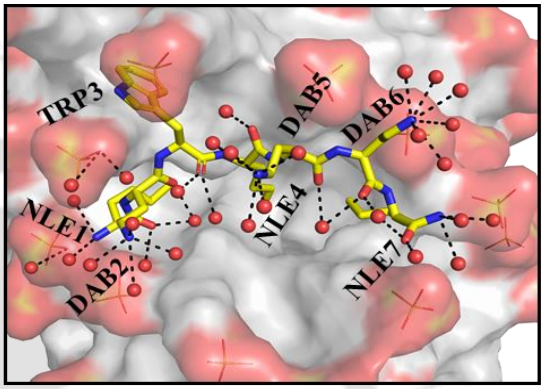

P36-SDS-SA-R2

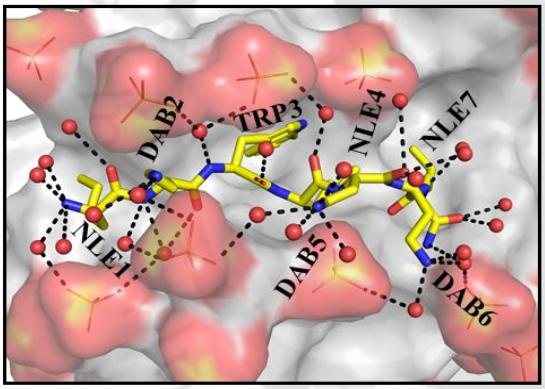

P36-SDS-SB-R1

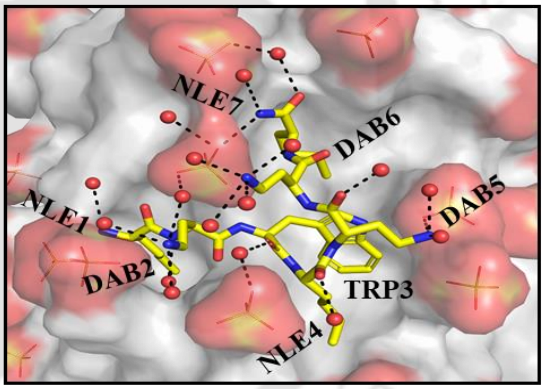

P36-SDS-SB-R2

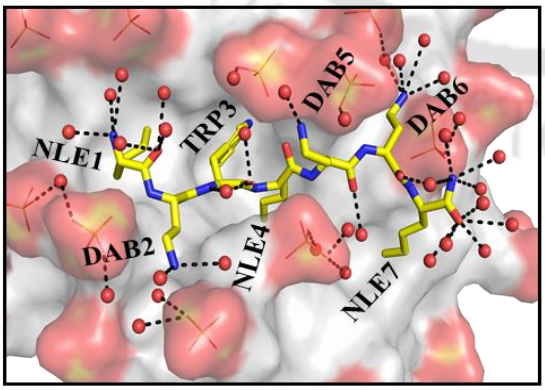

P36-SDS-SC-R2

Figure 5.23. P36 water interactions are observed from the final MD structure of the P36: SDS complex after 50 ns. Waters interact with the positively charged tips of the peptide (N-terminal, side-chain of Dab2, Dab5 and Dab6). Water mediated interactions between peptide positive charges and the negatively charged sulphates of SDS are frequently observed. Nle1 and Nle4 had less solvent exposure than Nle7. P36 is represented in yellow coloured sticks (Nitrogen: blue, Oxygen: red) and oxygens of water are shown in red spheres. SDS is shown in surface representation and sulphates of SDS interacting with water are shown in sticks form (Sulphur: yellow, Oxygen: red). Hydrogens are not shown for clarity. Broken black lines represent the interactions (distances ≤ 3.4 Å).

No secondary structure of the peptide was attained in response to SDS micelle binding (Table 5.8). Micelle structure (eccentricity, micellar radius) was independent of peptide binding (Table 5.8). Noticeable structural features observed from the MD structure of the P36-SDS complex were: (1) The peptide lied over the surface of the micelle with noticeable local deformation (~ 11Å width and ~13Å deep peptide binding pocket, Figure 5.21a) of the micelle surface. (2) Trp3 and Nle4 side-chains were found to be on the same side relative to peptide-backbone. (3) Trp3 was found to be buried in the dry hydrophobic core of the SDS micelle, in lines with the experimentally observed shift in the emission maxima of the tryptophan fluorescence (Figure 5.14a and c). No water was found within 3.4 Å of the Trp3 side chain. The hydrogen bonding requirement of the polar "-NH" of the indole ring of Trp3 was found to be satisfied by establishing direct interaction with the oxygen of the terminal sulphate of SDS (Figure 5.21 a). (4) Hydrophobic side chains of Nle1 and Nle4 were found to be more buried relative to Nle7 in the hydrophobic core of SDS micelle (Figure 5.21 a, b). (4) High solvent exposure was observed for the positively charged side-chains of Dab2, Dab5 and Dab6 (Figure 5.21 b). The interaction network of the positively charged terminals of Dab2, Dab5, and Dab6,

were of three kinds: (I) direct interaction with the negatively charged sulphate oxygens of SDS (Figure 5.22), (II) water-mediated interaction with SDS and (III) interaction with the bulk water. (5) The peptide backbone satisfied its hydrogen bonding requirement by forming H-bonds with water molecules or sulphates of the SDS micelle or both (Figure 5.21a, Figure 5.23). The above structural observations were robust features of our MD simulations (confirmed from 6 independent MD runs differing in the initial structural model and initial velocities, see methods section). A similar observation was confirmed from **P32** simulations in presence of SDS micelles (Figure 5.24, 5.25).

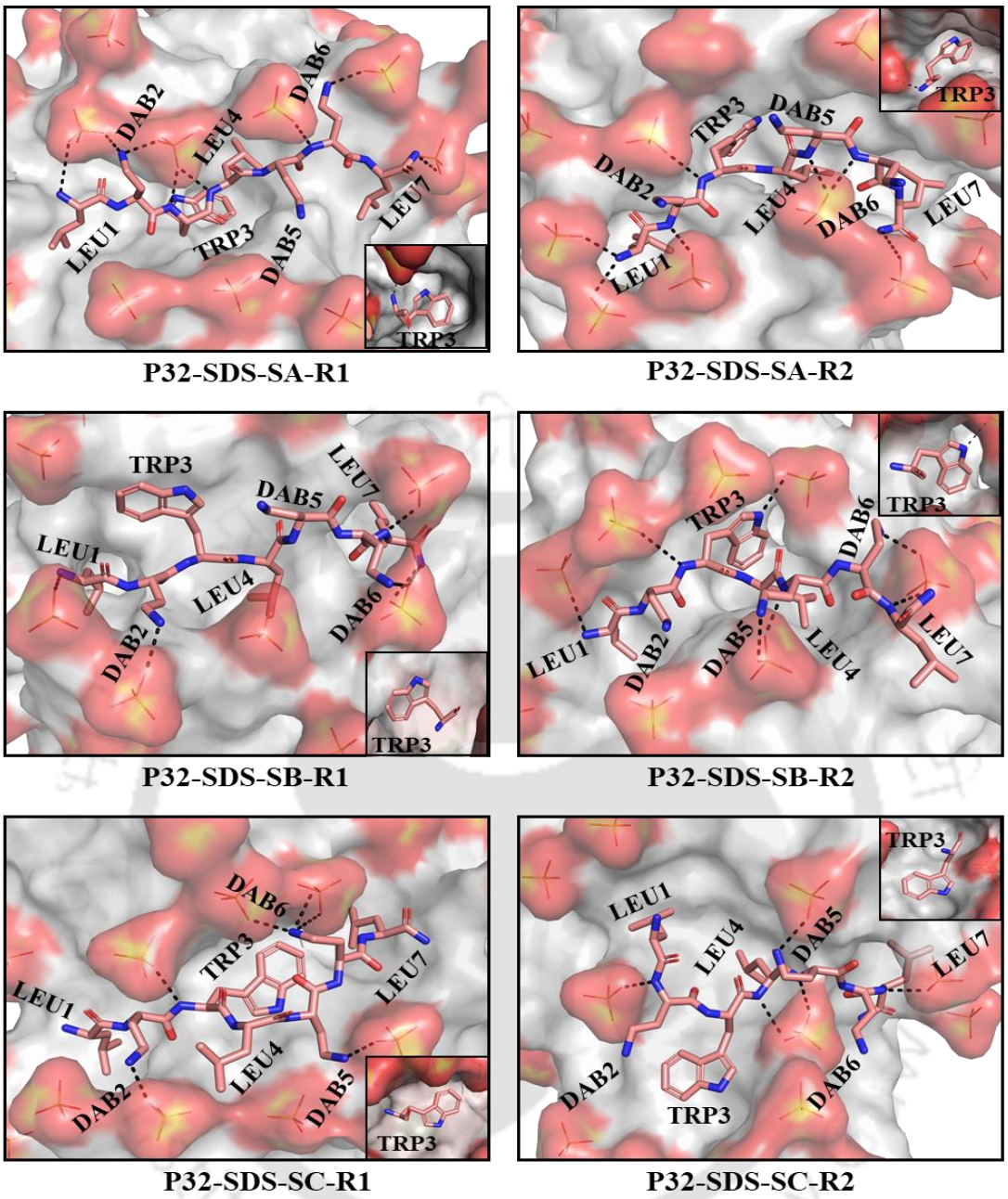

Figure 5.24. P32-SDS direct interactions are portrayed from the final structure of the P32: SDS micelle MD simulation after 50 ns. Positively charged tips of the peptide (N-terminal, side-chains of Dab2, Dab5 and Dab6) interact directly with sulphates of SDS. P32 is represented in salmon coloured sticks (Nitrogen: blue, Oxygen: red). SDS is shown in surface representation and sulphates of SDS interacting with P32 are shown in sticks form (Sulphur: yellow, Oxygen: red). The local environment of Trp3 is shown explicitly in a solid box. (SA, SB, SC) represent distinctly different simulation setups, (R1, R2) indicate two independent replicas for each

simulation setup. Hydrogens are not shown for clarity. Broken black lines represent the interactions (heavy atom distances ≤ 3.4 Å).

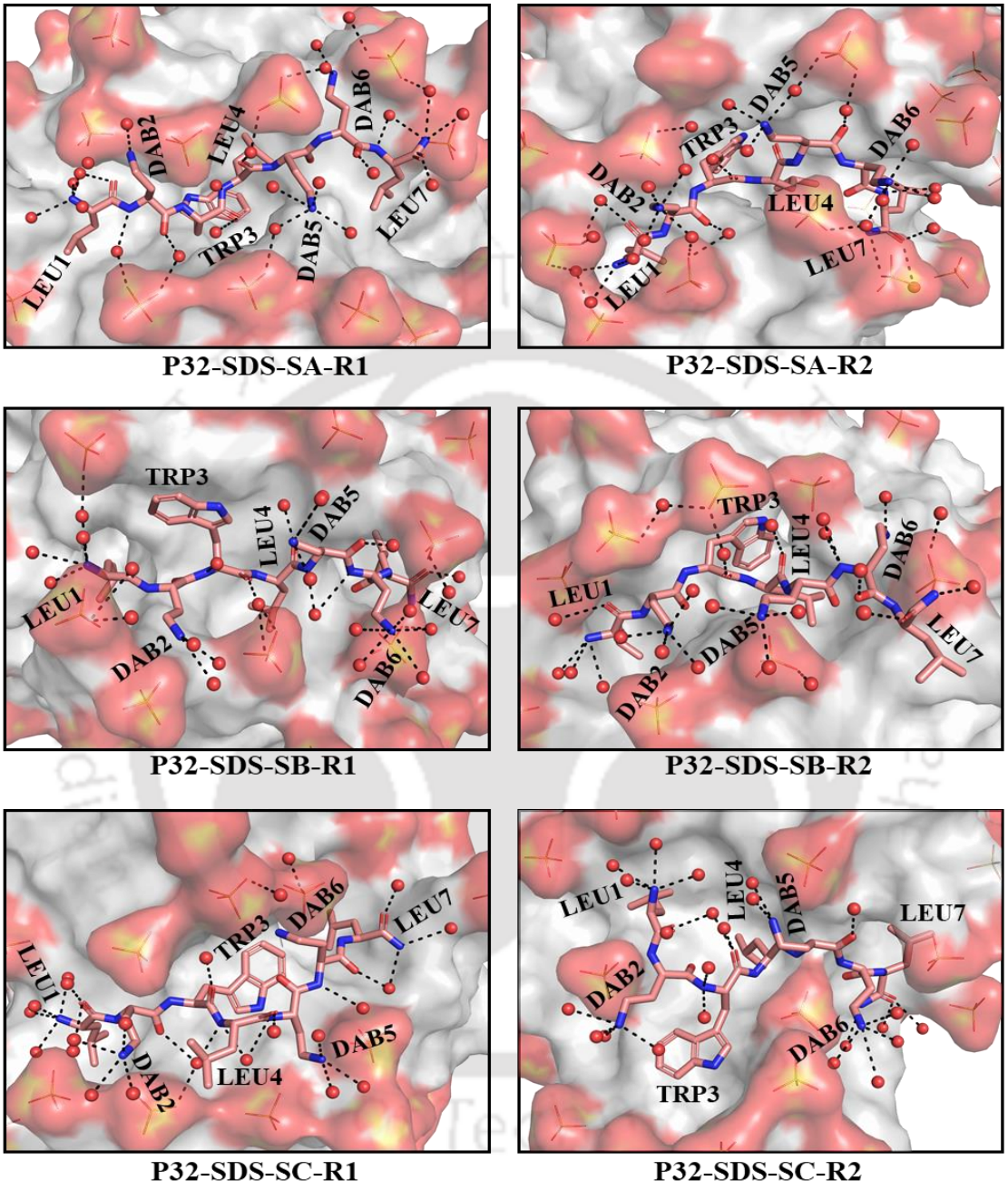

Figure 5.25. P32 water interactions observed from the final MD structure of the P32: SDS complex after 50 ns. Waters interact with the positively charged tips of the peptide (N-terminal, side-chain of Dab2, Dab5 and Dab6). Water mediated interactions between peptide positive charges and the negatively charged sulphates of SDS are frequently observed. Leu1 and Leu4

have less solvent exposure than Leu7. P32 is represented in salmon coloured sticks (Nitrogen: blue, Oxygen: red) and oxygens of water are shown in red spheres. SDS is shown in surface representation and sulphates of SDS interacting with water are shown in sticks form (Sulphur: yellow, Oxygen: red). Hydrogens are not shown for clarity. Broken black lines represent the interactions (heavy atom distances ≤ 3.4 Å).

P32 and P36 binding to the SDS micelles was found to be significantly faster relative to zwitterionic DPC micelles, due to obvious electrostatic reasons (Figure 5.26). P36 was able to bind DPC micelle surface after 38 ns of dynamics, much slower relative to the initial SDS binding event which took place within 1-3 ns (Figure 5.28). The results indicated that electrostatic interactions were crucial for initial peptide: micelle binding kinetics. Although the kinetics of the initial peptide binding event depended on the nature of the micelles (SDS or DPC), the interaction network between the peptide and micelle in the final equilibrated peptide: micelle complex was more or less similar between peptide: SDS and peptide: DPC micelles (Figure 5.22-5.24).

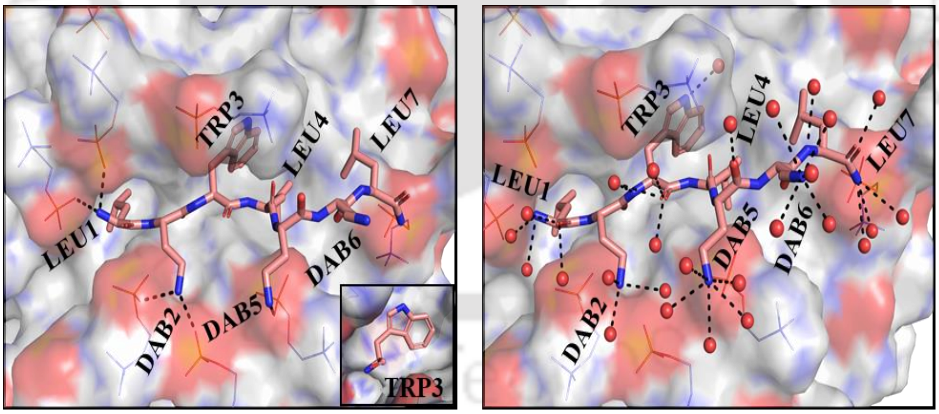

a) P32-DPC-SA-R1

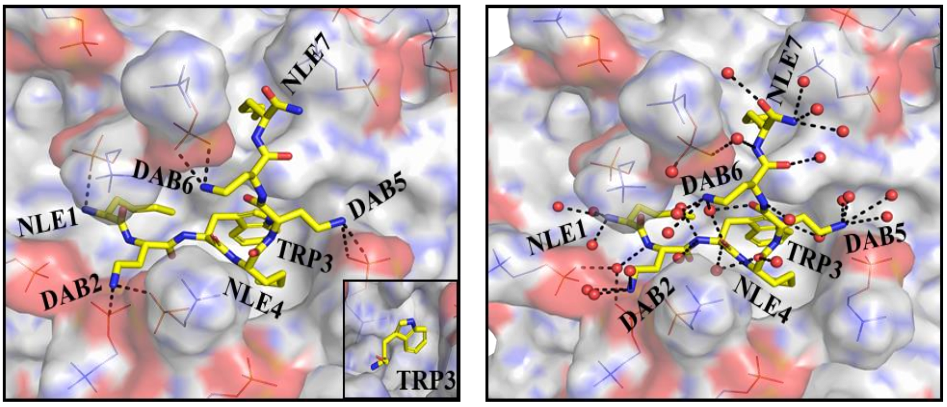

b) P36-DPC-SA-R1

Figure 5.26. P32(P36): DPC direct and water mediated interactions. Representative MD snapshot (after 50ns trajectory). Positively charged tips of the peptide (N-terminal, side-chains of Dab2, Dab5 and Dab6) interact directly with phosphates of DPC and waters. Water mediated interactions between peptide positive charges and the negatively charged phosphates of DPC are frequently observed. The local environment of Trp3 is shown explicitly in a solid box. (SA) represent distinct simulation setup and (R1) indicate independent run for the simulation setup. (a) Left image: P32-DPC direct interaction. Right Image: P32-DPC water interactions. Leu1 and Leu4 have less solvent exposure than Leu7. P32 is represented in salmon colored sticks (Nitrogen: blue, Oxygen: red). (b) Left image: P36-DPC direct interaction.

Right Image: P36-DPC water interactions. Nle1 and Nle7 have less solvent exposure than Nle4. P36 is represented in yellow colored sticks (Nitrogen: blue, Oxygen: red). DPC is shown in surface representation and phosphates of DPC interacting with P32 (P36) are shown in sticks form (Carbon: blue, Phosphorus: orange, Oxygen: red) and oxygens of water are shown in red spheres. Hydrogens are not shown for clarity. Broken black lines represent the interactions (heavy atom distances $\leq$ 3.4 Å).

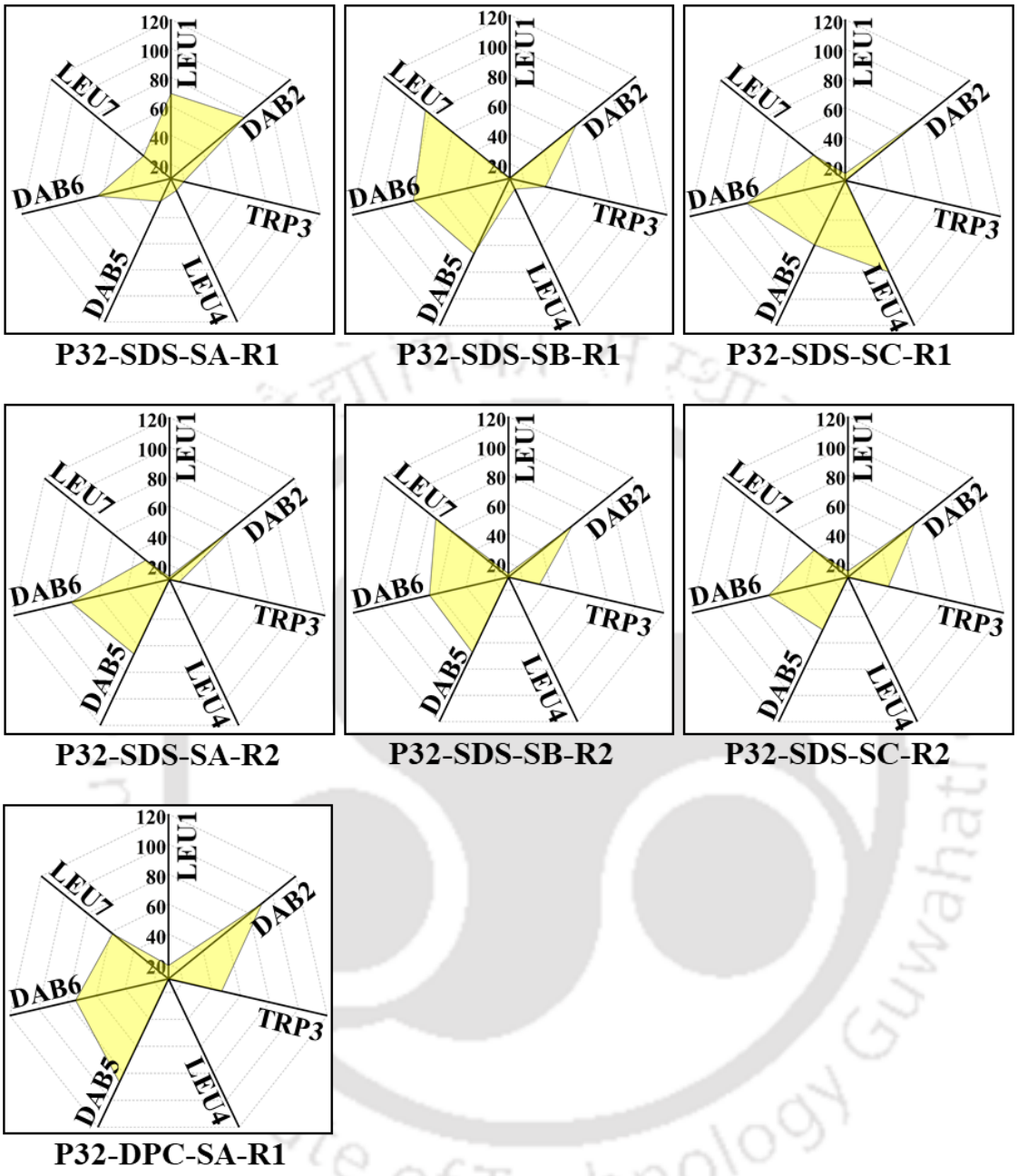

Figure 5.27 Trajectory averaged (last 30 ns) residue-wise solvent exposure (SASA in $Å^2$) of P32 sidechain are shown in the yellow net-plot with contours of constant solvent exposure (increases as one goes away from the center).

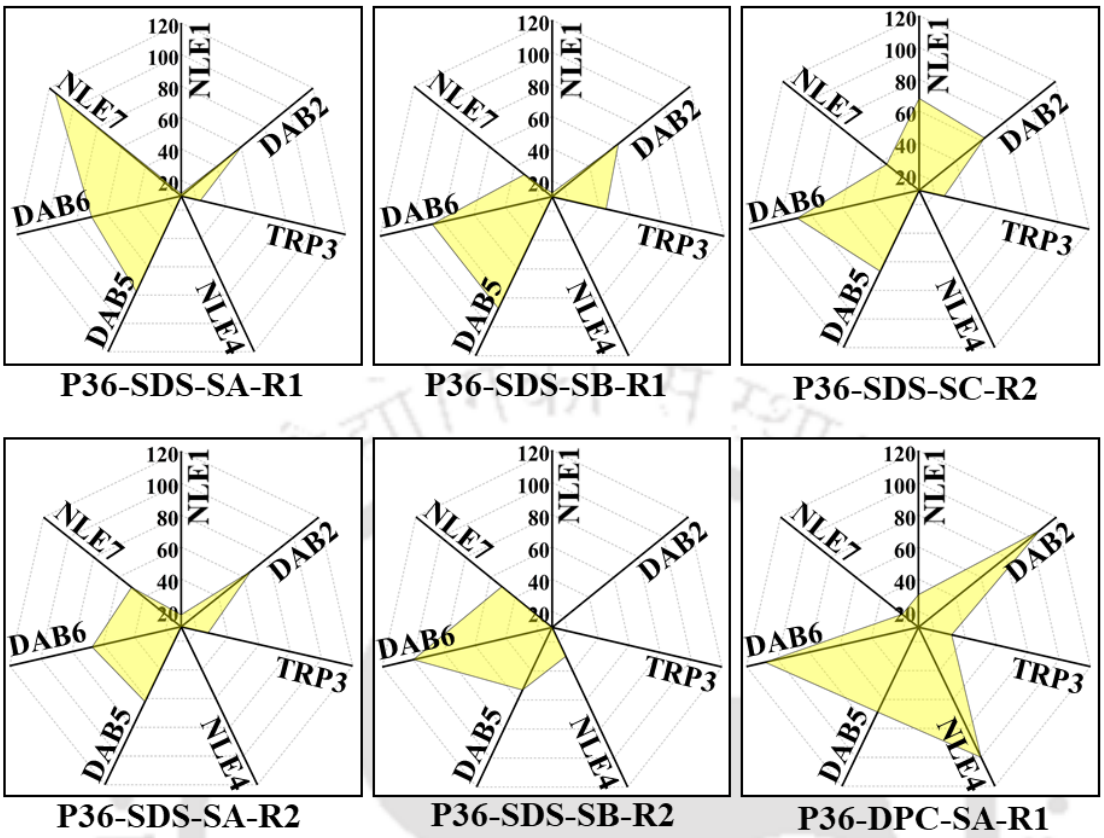

Figure 5.28. Trajectory averaged (last 30 ns*) residue-wise solvent exposure (SASA in $Å^2$) of P36 sidechain are shown in the yellow net-plot with contours of constant solvent exposure (increases as one goes away from the center). [*except P36-DPC-SA-R1 (last 5ns)]

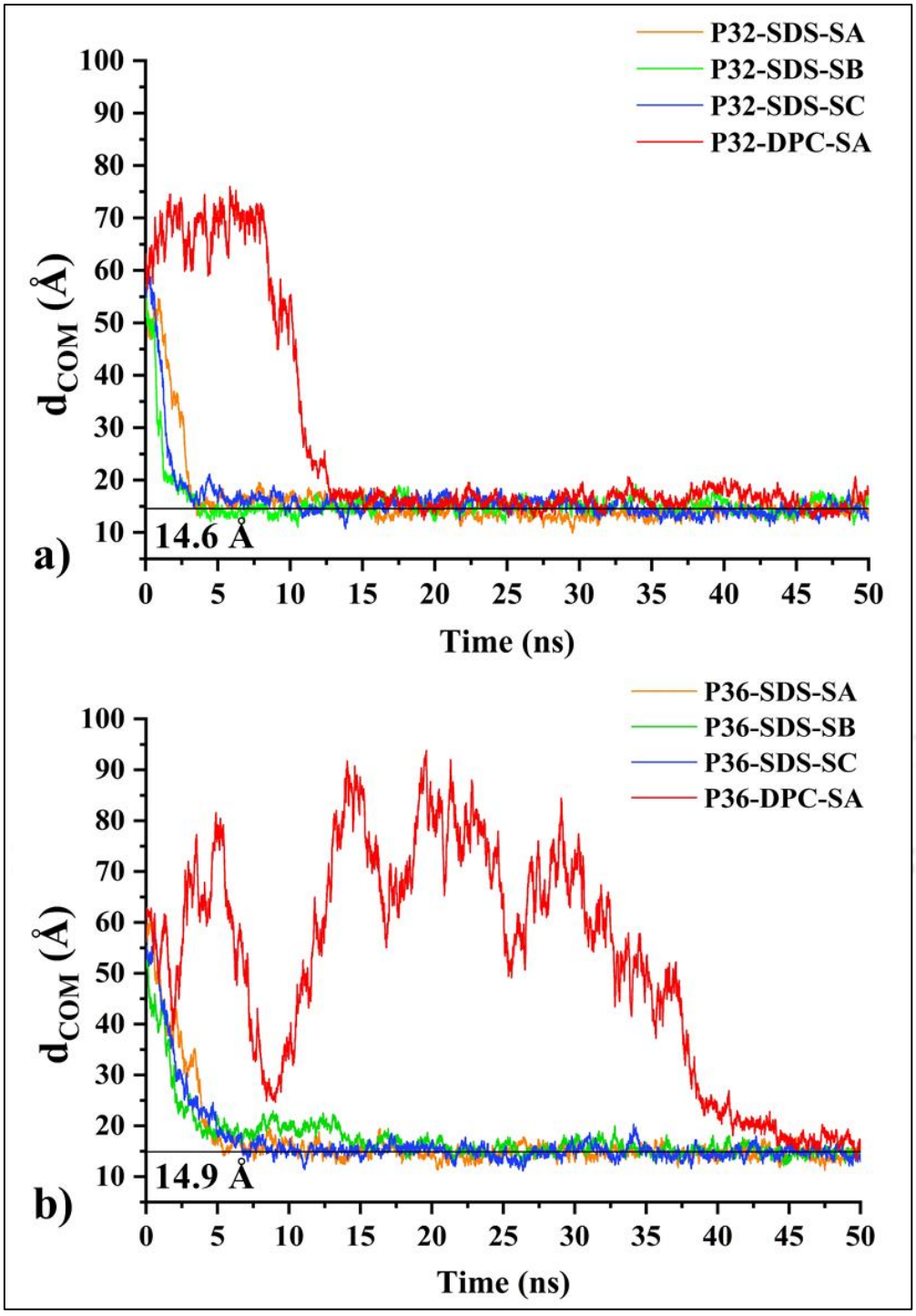

Figure 5.29. Peptide- Micelle distance as a function of time. d_{COM} is the distance between the center of mass of peptide and the center of mass of micelle (SDS/DPC). For the peptide- SDS simulations (Setup: SA, SB, and SC of Figure 5.1. a), temporally averaged d_{COM} (averaging over 2 independent MD runs, see Table 5.1) is plotted. (a) P32-micelle (SDS/DPC) d_{COM} plot. (b) P36-micelle (SDS/DPC) d_{COM} plot. The black horizontal line is the averaged d_{COM} obtained

from the last 30 ns of the 50ns trajectory that corresponds to stable peptide: SDS complex. 14.6Å (14.9Å) for stable P32 (P36): SDS micelle.

5.4. Conclusions

We have successfully designed a lead protease resistant AMP P36, with high salt tolerant potency against gram-negative bacteria *P. aeruginosa*. P36 manifested non-cytotoxic and non-hemolytic behavior against mammalian cell lines. We established the membranolytic mode of action of P36 using several biophysical, spectroscopic and microscopic tools. The study illustrated that the antimicrobial activity of AMPs was dependent on the hydrophobic-hydrophilic balance and the length of the side chains of amino acid residues, disruption of which led to the loss in activity or increase in the cytotoxicity. In this work, we have overcome several significant shortcomings of the AMPs, viz. the salt induced inactivation of the bioactivity protease degradability and cytotoxicity, which limit their therapeutic potential and applicability. Antimicrobials like P36 hold immense potential of being commercialized as antimicrobial agents of the future.

Chapter 6

Conclusions and Future prospects

AMPs are a group of molecules, which have the potential of acting as an alternative to the conventional class of antibiotics, in combating microbial infections. In fact, AMPs are better therapeutic candidates than antibiotics, owing to the slow development of resistance against them in microbes. However, AMPs have shown limited commercial success due to some of the inherent shortcomings like moderate activity, salt sensitivity of antimicrobial potency, short systemic half-life and toxicity. Scientists all over the world are working on development of synthetic AMPs which can circumvent the shortcomings of the natural AMPs. Additionally, good therapeutic molecules should also be economically viable for commercial success.

In this thesis we have developed various types short cationic AMPs, which economize the cost and time of production. The AMPs were de novo designed and targeted to achieve high potency accompanied by reduced cytotoxicity. Another noteworthy feature of the AMPs studied in this thesis is that they are highly active against gram-negative bacteria like *P. aeruginosa, S. Typhi* and *K. Pseudomonas*, which are more difficult to kill in general. In addition, all the AMPs developed here are membranolytic in nature and hence development of resistance against them probably would not be easy. Membranes being an integral part of the microbial systems and a complex assembly of lipids and proteins, it cannot be easily mutated. Thus, in general it is difficult for the microbes to develop resistance against membrane active AMPs. Throughout the thesis, we have developed new AMPs on one hand and thoroughly investigated their mechanism of action and molecular interactions involved in their activity on the other. We have used several experimental techniques and MD simulations to completely understand the structure function relationship.

In chapter 2, we developed cationic heptapeptide AMPs P4 and P5 with moderate broad-spectrum activity against ESKAPE group of pathogens. These AMPs were non-hemolytic and non-cytotoxic with membranolytic mode of action. These AMPs were unstructured in free and membrane bound state, establishing that their activity was independent of secondary structure. We established that the peptide membrane interaction was sequential in nature and was primarily driven by electrostatics. We established that the optimal charge on the AMPs was crucial for their activity.

In chapter 3, we modified P5 by insertion of RKVR fragment to improve the activity. AMP21 thus obtained was further modified by mutation of specific amino acid residues to obtain a series of peptides AMP22-24. All the peptides showed very good antimicrobial properties against a broad-spectrum of ESKAPE pathogens, with AMP22 and AMP24 being the most active. The developed AMPs were non-cytotoxic, non-hemolytic and moderately salt tolerant in their activity against P. *aeruginosa* and *C. albicans.* We established that these AMPS were primarily membranolytic in their mechanism of action, though there might be secondary intracellular mechanisms as well. The activity of these peptide was independent of their secondary structure as they adopted no specific structure even upon binding to the membranes. In chapter 4, P4 sequence was doubled to generate 14 residues long peptide LL-14. Role of side chain of the hydrophobic amino acid residues on the activity of the AMPs was studied by mutating the Leu residues to Val and β Ala residues thus generating VV-14 and ββ-14 respectively. We established that the long side chain of Leu lead to indiscriminate binding of microbial and mammalian membranes, rendering LL-14 both highly active and salt tolerant. Shorter side chains of Val on the other hand led to selective binding of the microbial membranes in comparison to the mammalian membranes generating good antimicrobial activity accompanied by non-cytotoxicity. We also established that adoption of helical conformation upon binding to the membrane mimics was crucial for gaining activity.

Membrane binding led to the attainment of helical conformation. As β-Ala in ββ14 did not have any side chain, it could not bind to the membrane and hence did not show any antimicrobial activity. Thus for similarly charged peptides, length of hydrophobic side chains plays a crucial role in the determining their activity and toxicity.

In the fifth chapter, we have developed P36 a salt tolerant, protease resistant AMP against *P. aeruginosa.* In order to develop protease resistance, Lys and Leu residues were systematically mutated by their nonstandard analogs Orn/ Dab/Dap and Nle respectively. Among all the peptides generated, P36 containing Nle and Dab showed best activity against several microbial strains studied. However, among different strains, P36 showed best activity towards *P. aeruginosa*. The peptide was unstructured and membranolytic in its mode of action. We established that a fine hydrophobic- hydrophilic balance is essential in developing a good AMP.

We believe that the understanding developed from our studies presented in this thesis about the design principles, structure-function relations and interactions driving the activity of the AMPs will help in development of better AMPS in the future.

In the future we want to develop better therapeutically component AMPs with high potency, salt tolerance of antimicrobial activity, protease resistance and non-cytotoxicity. Other than existing in the planktonic form, microbes often exist in a more dangerous colonial form called the biofilm. Microbial cells exist as an assembly on a surface and is covered by an extracellular polymeric matrix. This matrix protects the microbial cells by rendering the antimicrobials ineffective by several mechanisms. Biofilms cause serious dangers in biomedical procedures like surgery, organ transplants, catheters etc. Thus, eradication of biofilms is hugely challenging and much more complicated than treating planktonic forms of the microbes. In the future, we intend to develop AMPs that can prevent the growth of AMPs on surfaces and/or

eradicate the preformed biofilms. We want to test our developed AMPs in the in vivo animal infection models and wound healing models. In addition, we look forward to developing AMPs with multiple modes of action, which might increase its overall activity. Finally, we want to study combinatorial therapy of our AMPs with existing conventional antibiotics against multi drug resistant superbugs in the future. Our long term goals would be to develop AMPs that can be translated to industry and eventually to the market.

References

(1) Penesyan, A.; Gillings, M.; Paulsen, I. T. Antibiotic discovery: combatting bacterial resistance in cells and in biofilm communities. *Molecules* **2015**, *20*, 5286-5298.

(2) Xu, Z.-Q.; Flavin, M. T.; Flavin, J. Combating multidrug-resistant Gram-negative bacterial infections. *Expert Opin. Invest. Drugs* **2014**, *23*, 163-182.

(3) Fair, R. J.; Tor, Y. Antibiotics and bacterial resistance in the 21st century. *Perspect. Med. Chem.* **2014**, *6*, 1-40.

(4) Izadpanah, M.; Khalili, H. Antibiotic regimens for treatment of infections due to multidrug-resistant Gram-negative pathogens: An evidence-based literature review. *J. Res. Pharm. Pract.* **2015**, *4*, 105-114.

(5) Long, S. W.; Linson, S. E.; Ojeda Saavedra, M.; Cantu, C.; Davis, J. J.; Brettin, T.; Olsen, R. J. Whole-genome sequencing of human clinical Klebsiella pneumoniae isolates reveals misidentification and misunderstandings of Klebsiella pneumoniae, Klebsiella variicola, and Klebsiella quasipneumoniae. *Msphere* **2017**, *2*, 1-15.

(6) Antibiotic resistance threats in the United States, 2013. Centers for Disease Control and Prevention, **2013**, *114*, 1-114.

(7) Ebenhan, T.; Gheysens, O.; Kruger, H. G.; Zeevaart, J. R.; Sathekge, M. M. Antimicrobial peptides: their role as infection-selective tracers for molecular imaging. *BioMed Res. Int.* **2014**, *2014*, 1-16.

(8) Bechinger, B.; Gorr, S.-U. Antimicrobial peptides: mechanisms of action and resistance. *J. Dent. Res.* **2017**, *96*, 254-260.

(9) O'Neill, J. Tackling drug-resistant infections globally: final report and recommendations. **2016**.

(10) Westblade, L. F.; Simon, M. S.; Satlin, M. J. Bacterial coinfections in coronavirus disease 2019. *Trends Microbiol.* **2021**, *29*, 930-941.

(11) Alpert, P. T. Superbugs: antibiotic resistance is becoming a major public health concern. *Home Health Care Manag. Pract.* **2017**, *29*, 130-133.

(12) Silver, L. L. Challenges of antibacterial discovery. *Clin. Microbiol. Rev.* **2011**, *24*, 71-109.

(13) Kase, H.; Iwahashi, K.; Matsuda, Y. J. Antibiot.(Tokyo). **1986**, *32*, 1059-1065.

(14) Steckbeck, J. D.; Deslouches, B.; Montelaro, R. C. Antimicrobial peptides: new drugs for bad bugs? *Expert Opin. Biol. Ther.* **2014**, *14*, 11-14.

(15) de Kraker, M. E.; Stewardson, A. J.; Harbarth, S. Will 10 million people die a year due to antimicrobial resistance by 2050? *PLoS Med.* **2016**, *13*, 1-6.

(16) Tossi, A.; Sandri, L.; Giangaspero, A. Amphipathic, α-Helical Antimicrobial Peptides. *Biopolymers* **2000**, *55*, 4-30.

(17) Cardoso, P.; Glossop, H.; Meikle, T. G.; Aburto-Medina, A.; Conn, C. E.; Sarojini, V.; Valery, C. Molecular engineering of antimicrobial peptides: Microbial targets, peptide motifs and translation opportunities. *Biophys Rev* . **2021**, *13*, 35-69.

(18) Davies, J.; Davies, D. Origins and evolution of antibiotic resistance. *Microbiol. Mol. Biol. Rev.* **2010**, *74*, 417-433.

(19) Wright, G. D. Q&A: Antibiotic resistance: where does it come from and what can we do about it? *BMC Biol.* **2010**, *8*, 1-6.

(20) Aslam, B.; Wang, W.; Arshad, M. I.; Khurshid, M.; Muzammil, S.; Rasool, M. H.; Nisar, M. A.; Alvi, R. F.; Aslam, M. A.; Qamar, M. U. Antibiotic resistance: a rundown of a global crisis. *Infect. Drug Resist.* **2018**, *11*, 1645-1658.

(21) Gibson, E. G. A., R. E.; Kerns, R. J.; Osheroff, N. ; : *Bacterial Type II Topoisomerases and Target-Mediated Drug Resistance. In Antimicrobial Resistance in the*

21st Century. Emerging Infectious Diseases of the 21st Century. Fong, I., Shlaes, D., Drlica, K., Eds. ; Springer: Cham, 2018.

(22) Malmir, S.; Bahreinian, M.; Zahiri Yeganeh, S.; Mirnejad, R.; Moosazadeh Moghaddam, M.; Saberi, F. Molecular mechanisms of resistance to conventional antibiotics in bacteria. *Int. J. Med. Rev.* **2018**, *5*, 118-129.

(23) Duval, R. E.; Grare, M.; Demoré, B. Fight against antimicrobial resistance: we always need new antibacterials but for right bacteria. *Molecules* **2019**, *24*, 3152-3161.

(24) Farrell, L.; Lo, R.; Wanford, J.; Jenkins, A.; Maxwell, A.; Piddock, L. Revitalizing the drug pipeline: AntibioticDB, an open access database to aid antibacterial research and development. *J. Antimicrob. Chemother.* **2018**, *73*, 2284-2297.

(25) Magana, M.; Pushpanathan, M.; Santos, A. L.; Leanse, L.; Fernandez, M.; Ioannidis, A.; Giulianotti, M. A.; Apidianakis, Y.; Bradfute, S.; Ferguson, A. L. The value of antimicrobial peptides in the age of resistance. *Lancet Infect. Dis.* **2020**, *20*, 216-230.

(26) Osei Sekyere, J. Genomic insights into nitrofurantoin resistance mechanisms and epidemiology in clinical Enterobacteriaceae. *Future Sci. OA* **2018**, *4*, 1-14.

(27) Dharmadana, D.; Reynolds, N. P.; Conn, C. E.; Valéry, C. Molecular interactions of amyloid nanofibrils with biological aggregation modifiers: implications for cytotoxicity mechanisms and biomaterial design. *Interface Focus* **2017**, *7*, 1-14.

(28) Schwarz, S.; Shen, J.; Kadlec, K.; Wang, Y.; Michael, G. B.; Feßler, A. T.; Vester, B. Lincosamides, streptogramins, phenicols, and pleuromutilins: mode of action and mechanisms of resistance. *Cold Spring Harbor Perspect. Med.* **2016**, *6*, 1-30.

(29) Li, Y.; Xiang, Q.; Zhang, Q.; Huang, Y.; Su, Z. Overview on the recent study of antimicrobial peptides: origins, functions, relative mechanisms and application. *Peptides* **2012**, *37*, 207-215.

(30) Otvos Jr, L. Antibacterial peptides and proteins with multiple cellular targets. *J. Pept. Sci.* **2005**, *11*, 697-706.

(31) Vanzolini, T.; Bruschi, M.; Rinaldi, A. C.; Magnani, M.; Fraternale, A. Multitalented Synthetic Antimicrobial Peptides and Their Antibacterial, Antifungal and Antiviral Mechanisms. *Int. J. Mol. Sci.* **2022**, *23*, 545-565.

(32) Jenssen, H.; Hamill, P.; Hancock, R. E. Peptide antimicrobial agents. *Clin. Microbiol. Rev.* **2006**, *19*, 491-511.

(33) Boman, H. Antibacterial peptides: basic facts and emerging concepts. *J. Intern. Med.* **2003**, *254*, 197-215.

(34) de Souza Nascimento, A. M.; de Oliveira Segundo, V. H.; Felipe Camelo Aguiar, A. J.; Piuvezam, G.; Souza Passos, T.; Florentino da Silva Chaves Damasceno, K. S. F. d. S.; de Araújo Morais, A. H. Antibacterial action mechanisms and mode of trypsin inhibitors: a systematic review. *J. Enzyme Inhib. Med. Chem.* **2022**, *37*, 749-759.

(35) Nayab, S.; Aslam, M. A.; Sajid, S.; Zafar, N.; Razaq, M.; Kanwar, R. A Review of Antimicrobial Peptides: Its Function, Mode of Action and Therapeutic Potential. *Int. J. Pept. Res. Ther.* **2022**, *28*, 1-15.

(36) Du, Z.; Fan, B.; Dai, Q.; Wang, L.; Guo, J.; Ye, Z.; Cui, N.; Chen, J.; Tan, K.; Li, R. Supramolecular peptide nanostructures: Self-assembly and biomedical applications. *Giant* **2022**, *9*, 1-36.

(37) Fernández de Ullivarri, M.; Arbulu, S.; Garcia-Gutierrez, E.; Cotter, P. D. Antifungal peptides as therapeutic agents. *Front. Cell Dev. Biol.* **2020**, *10*, 105-127.

(38) Heydari, H.; Golmohammadi, R.; Mirnejad, R.; Tebyanian, H.; Fasihi-Ramandi, M.; Moghaddam, M. M. Antiviral peptides against Coronaviridae family: A review. *Peptides* **2021**, *139*, 1-11.

(39) Vilas Boas, L. C. P.; Campos, M. L.; Berlanda, R. L. A.; de Carvalho Neves, N.; Franco, O. L. Antiviral peptides as promising therapeutic drugs. *Cell. Mol. Life Sci.* **2019**, *76*, 3525-3542.

(40) Agarwal, G.; Gabrani, R. Antiviral peptides: identification and validation. *Int. J. Pept. Res. Ther.* **2021**, *27*, 149-168.

(41) Skalickova, S.; Heger, Z.; Krejcova, L.; Pekarik, V.; Bastl, K.; Janda, J.; Kostolansky, F.; Vareckova, E.; Zitka, O.; Adam, V. Perspective of use of antiviral peptides against influenza virus. *Viruses* **2015**, *7*, 5428-5442.

(42) Skwarecki, A. S.; Nowak, M. G.; Milewska, M. J. Amino Acid and Peptide-Based Antiviral Agents. *ChemMedChem* **2021**, *16*, 3106-3135.

(43) Pan, Y.; Lee, A.; Wan, J.; Coventry, M.; Michalski, W.; Shiell, B.; Roginski, H. Antiviral properties of milk proteins and peptides. *Int. Dairy J.* **2006**, *16*, 1252-1261.

(44) Kuroki, A.; Tay, J.; Lee, G. H.; Yang, Y. Y. Broad-Spectrum Antiviral Peptides and Polymers. *Adv. Healthcare Mater.* **2021**, *10*, 2101113.

(45) Pärn, K.; Eriste, E.; Langel, Ü. The antimicrobial and antiviral applications of cell-penetrating peptides. *Cell-Penetrating Pept.* **2015**, *1324*, 223-245.

(46) Hsieh, I.-N.; Hartshorn, K. L. The role of antimicrobial peptides in influenza virus infection and their potential as antiviral and immunomodulatory therapy. *Pharmaceuticals* **2016**, *9*, 53-68.

(47) De Lucca, A. J.; Walsh, T. J. Antifungal peptides: novel therapeutic compounds against emerging pathogens. *Antimicrob. Agents Chemother.* **1999**, *43*, 1-11.

(48) Rautenbach, M.; Troskie, A. M.; Vosloo, J. A. Antifungal peptides: to be or not to be membrane active. *Biochimie* **2016**, *130*, 132-145.

(49) Akkam, Y. A Review of Antifungal Peptides: Basis to New Era of Antifungal Drugs. *Jordan J. Pharm. Sci.* **2016**, *9*, 1-25.

(50) Ciociola, T.; Giovati, L.; Conti, S.; Magliani, W.; Santinoli, C.; Polonelli, L. Natural and synthetic peptides with antifungal activity. *Future Med. Chem.* **2016**, *8*, 1413-1433.

(51) Struyfs, C.; Cammue, B.; Thevissen, K. Membrane-interacting antifungal peptides. *Front. Cell Dev. Biol.* **2021**, *9*, 706-723.

(52) Mehra, T.; Köberle, M.; Braunsdorf, C.; Mailänder-Sanchez, D.; Borelli, C.; Schaller, M. Alternative approaches to antifungal therapies. *Exp. Dermatol.* **2012**, *21*, 778-782.

(53) De Lucca, A. J. Antifungal peptides: potential candidates for the treatment of fungal infections. *Expert Opin. Invest. Drugs* **2000**, *9*, 273-299.

(54) Sharma, D.; Bisht, G. S. Recent updates on antifungal peptides. *Mini-Rev. Med. Chem.* **2020**, *20*, 260-268.

(55) Kavanagh, K.; Dowd, S. Histatins: antimicrobial peptides with therapeutic potential. *J. Pharm. Pharmacol.* **2004**, *56*, 285-289.

(56) Yan, J.; Yuan, S.-s.; Jiang, L.-l.; Ye, X.-j.; Ng, T. B.; Wu, Z.-j. Plant antifungal proteins and their applications in agriculture. *Appl. Microbiol. Biotechnol.* **2015**, *99*, 4961-4981.

(57) Zasloff, M. Antimicrobial peptides of multicellular organisms. *Nature* **2002**, *415*, 389-395.

(58) Zasloff, M. Antimicrobial peptides of multicellular organisms: my perspective. *Antimicrob. Pept.* **2019**, *1117*, 3-6.

(59) Bulet, P.; Stöcklin, R.; Menin, L. Anti-microbial peptides: from invertebrates to vertebrates. *Immunol.* **2004**, *198*, 169-184.

(60) Pag, U.; Sahl, H.-G.: Lanthionine-containing bacterial peptides. In *Peptide Antibiotics: Discovery, Mode of Actions, and Applications*; Dekker, M New York, 2002; pp 47-80.

(61) Dutton, C.; Haxwell, M.; McArthur, H.; Wax, R. G.: *Peptide Antibiotics: Discovery Modes Of Action And Applications*; CRC Press, 2001.

(62) García-Olmedo, F.; Molina, A.; Alamillo, J. M.; Rodríguez-Palenzuéla, P. Plant defense peptides. *Pept. Sci.* **1998**, *47*, 479-491.

(63) Demori, I.; El Rashed, Z.; Corradino, V.; Catalano, A.; Rovegno, L.; Queirolo, L.; Salvidio, S.; Biggi, E.; Zanotti-Russo, M.; Canesi, L. Peptides for skin protection and healing in amphibians. *Molecules* **2019**, *24*, 347-362.

(64) Xiao, Y.; Liu, C.; Lai, R. Antimicrobial peptides from amphibians. *Biomol. Concepts* **2011**, *2*, 27-38.

(65) Ghasemian, A.; Nojoomi, F.; Najafi-olya, Z.; Rajabi-Vardanjani, H. Antimicrobial Features of Cerastoderma and Didacna Double Basins Peptides. *Int. J. Enteric. Pathog.* **2018**, *6*, 75-78.

(66) Chaithanya, E. Molecular and Functional Characterization of Antimicrobial Peptides in Marine Fishes. Doctoral dissertation,. Cochin University of Science and Technology, 2016.

(67) Hancock, R. E. Peptide antibiotics. *Lancet* **1997**, *349*, 418-422.

(68) Wang, G.; Li, X.; Wang, Z. APD3: the antimicrobial peptide database as a tool for research and education. *Nucleic Acids Res.* **2016**, *44*, 1087-1093.

(69) Henzler Wildman, K. A.; Lee, D.-K.; Ramamoorthy, A. Mechanism of lipid bilayer disruption by the human antimicrobial peptide, LL-37. *Biochemistry* **2003**, *42*, 6545-6558.

(70) Yamaguchi, S.; Huster, D.; Waring, A.; Lehrer, R. I.; Kearney, W.; Tack, B. F.; Hong, M. Orientation and dynamics of an antimicrobial peptide in the lipid bilayer by solid-state NMR spectroscopy. *Biophys. J.* **2001**, *81*, 2203-2214.

(71) Shi, J.; Ross, C. R.; Chengappa, M.; Sylte, M. J.; McVey, D. S.; Blecha, F. Antibacterial activity of a synthetic peptide (PR-26) derived from PR-39, a proline-arginine-rich neutrophil antimicrobial peptide. *Antimicrob. Agents Chemother.* **1996**, *40*, 115-121.

(72) Subbalakshmi, C.; Sitaram, N. Mechanism of antimicrobial action of indolicidin. *FEMS Microbiol. Lett.* **1998**, *160*, 91-96.

(73) Salomon, R.; Farías, R. N. Microcin 25, a novel antimicrobial peptide produced by Escherichia coli. *J. Bacteriol. Res.* **1992**, *174*, 7428-7435.

(74) Bowdish, D. M.; Davidson, D. J.; Hancock, R. A re-evaluation of the role of host defence peptides in mammalian immunity. *Curr. Protein Pept. Sci.* **2005**, *6*, 35-51.

(75) Finlay, B. B.; Hancock, R. E. Can innate immunity be enhanced to treat microbial infections? *Nat. Rev. Microbiol.* **2004**, *2*, 497-504.

(76) Artamonov, A. Y.; Shanin, S.; Orlov, D.; Shamova, O.; Kolodkin, N.; Rybakina, E. Immunomodulatory activity of antimicrobial peptide indolicidin and its structural analogues. *Med. Immunol.* **2014**, *11*, 101-104.

(77) Thaker, H. D.; Som, A.; Ayaz, F.; Lui, D.; Pan, W.; Scott, R. W.; Anguita, J.; Tew, G. N. Synthetic mimics of antimicrobial peptides with immunomodulatory responses. *J. Am. Chem. Soc.* **2012**, *134*, 11088-11091.

(78) Lima, S. M. F.; Freire, M. S.; Gomes, A. L. O.; Cantuária, A. P. C.; Dutra, F. R. P.; Magalhães, B. S.; Sousa, M. G. C.; Migliolo, L.; Almeida, J. A.; Franco, O. L. Antimicrobial and immunomodulatory activity of host defense peptides, clavanins and LL-37, in vitro: An endodontic perspective. *Peptides* **2017**, *95*, 16-24.

(79) Popov, C. S.; Magalhães, B. S.; Goodfellow, B. J.; Bocca, A. L.; Pereira, D. M.; Andrade, P. B.; Valentão, P.; Pereira, P. J. B.; Rodrigues, J. E.; Júnior, P. H. d. H. V. Host-defense peptides AC12, DK16 and RC11 with immunomodulatory activity isolated from Hypsiboas raniceps skin secretion. *Peptides* **2019**, *113*, 11-21.

(80) Drayton, M.; Deisinger, J. P.; Ludwig, K. C.; Raheem, N.; Müller, A.; Schneider, T.; Straus, S. K. Host Defense Peptides: Dual Antimicrobial and Immunomodulatory Action. *Int. J. Mol. Sci.* **2021**, *22*, 11172-11188.

(81) Chessa, C.; Bodet, C.; Jousselin, C.; Wehbe, M.; Lévêque, N.; Garcia, M. Antiviral and immunomodulatory properties of antimicrobial peptides produced by human keratinocytes. *Front. Microbiol.* **2020**, *11*, 1155-1170.

(82) Bahar, A. A.; Ren, D. Antimicrobial peptides. *Pharmaceuticals* **2013**, *6*, 1543-1575.

(83) Zhu, Y.; Hao, W.; Wang, X.; Ouyang, J.; Deng, X.; Yu, H.; Wang, Y. Antimicrobial peptides, conventional antibiotics, and their synergistic utility for the treatment of drug-resistant infections. *Med. Res. Rev.* **2022**, *https://doi.org/10.1002/med.21879*.

(84) Silva, A. R. P.; Guimarães, M.; Rabelo, J.; Belen, L.; Perecin, C.; Farias, J.; Santos, J. H. P. M.; Rangel-Yagui, C. O. Recent advances in the design of antimicrobial peptide conjugates. *J. Mater. Chem. B* **2022**, *10*, 3587-3600.

(85) Erdem Büyükkiraz, M.; Kesmen, Z. Antimicrobial peptides (AMPs): A promising class of antimicrobial compounds. *J. Appl. Microbiol.* **2022**, *132*, 1573-1596.

(86) Tarín-Pelló, A.; Suay-García, B.; Pérez-Gracia, M.-T. Antibiotic resistant bacteria: current situation and treatment options to accelerate the development of a new antimicrobial arsenal. *Expert Rev. Anti-Infect. Ther.* **2022**, https://doi.org/10.1080/14787210.14782022.12078308.

(87) Saeed, S. I.; Mergani, A.; Aklilu, E.; Kamaruzzman, N. F. Antimicrobial Peptides: Bringing Solution to the Rising Threats of Antimicrobial Resistance in Livestock. *Front. Vet. Sci.* **2022**, 319-328.

(88) Cheng, J. T. J.; Hale, J. D.; Elliott, M.; Hancock, R. E. W.; Straus, S. K. The importance of bacterial membrane composition in the structure and function of aurein 2.2 and selected variants. *Biochim. Biophys. Acta, Biomembr.*. **2011**, *1808*, 622-633.

(89) Jin L, B. X., Luan N, Yao H, Zhang Z, Liu W, Chen Y, Yan X, Rong M, Lai R, Lu Q. A Designed Tryptophan- and Lysine/Arginine-Rich Antimicrobial Peptide with Therapeutic Potential for Clinical Antibiotic-Resistant Candida albicans Vaginitis. *J. Med. Chem.* **2016**, *59*, 1791-17999.

(90) Wang, G.; Li, X.; Wang, Z. APD2: the updated antimicrobial peptide database and its application in peptide design. *Nucleic Acids Res.* **2009**, *37*, 933-937.

(91) Wang, Z.; Wang, G. APD: the antimicrobial peptide database. *Nucleic Acids Res.* **2004**, *32*, 590-592.

(92) Waghu, F. H.; Idicula-Thomas, S. Collection of antimicrobial peptides database and its derivatives: Applications and beyond. *Protein Sci.* **2020**, *29*, 36-42.

(93) Kang, X.; Dong, F.; Shi, C.; Liu, S.; Sun, J.; Chen, J.; Li, H.; Xu, H.; Lao, X.; Zheng, H. DRAMP 2.0, an updated data repository of antimicrobial peptides. *Sci. Data* **2019**, *6*, 1-10.

(94) Koo, H. B.; Seo, J. Antimicrobial peptides under clinical investigation. *Pept. Sci.* **2019**, *111*, 1-15.

(95) Jaumaux, F.; P Gómez de Cadiñanos, L.; Gabant, P. In the Age of Synthetic Biology, Will Antimicrobial Peptides be the Next Generation of Antibiotics? *Antibiotics* **2020**, *9*, 484-497.

(96) Divyashree, M.; Mani, M. K.; Reddy, D.; Kumavath, R.; Ghosh, P.; Azevedo, V.; Barh, D. Clinical applications of antimicrobial peptides (AMPs): where do we stand now? *Protein Pept. Lett.* **2020**, *27*, 120-134.

(97) Sarkar, T.; Chetia, M.; Chatterjee, S. Antimicrobial peptides and proteins: from nature's reservoir to the laboratory and beyond. *Front. Chem.* **2021**, *9*, 432-472.

(98) Stevens, K. A.; Sheldon, B. W.; Klapes, N. A.; Klaenhammer, T. R. Effect of treatment conditions on nisin inactivation of gram-negative bacteria. *J. Food Prot.* **1992**, *55*, 763-766.

(99) Prenner, E. J.; Lewis, R. N.; McElhaney, R. N. The interaction of the antimicrobial peptide gramicidin S with lipid bilayer model and biological membranes. *Biochim. Biophys. Acta, Biomembr.* **1999**, *1462*, 201-221.

(100) Poirel, L.; Jayol, A.; Nordmann, P. Polymyxins: antibacterial activity, susceptibility testing, and resistance mechanisms encoded by plasmids or chromosomes. *Clin. Microbiol. Rev.* **2017**, *30*, 557-596.

(101) Steenbergen, J. N.; Alder, J.; Thorne, G. M.; Tally, F. P. Daptomycin: a lipopeptide antibiotic for the treatment of serious Gram-positive infections. *J. Antimicrob. Chemother.* **2005**, *55*, 283-288.

(102) Ling, L. L.; Schneider, T.; Peoples, A. J.; Spoering, A. L.; Engels, I.; Conlon, B. P.; Mueller, A.; Schäberle, T. F.; Hughes, D. E.; Epstein, S. A new antibiotic kills pathogens without detectable resistance. *Nature* **2015**, *517*, 455-459.

(103) Fennell, J. F. S., William H Cole, Leonard J. Antibacterial action of melittin, a polypeptide from bee venom. *Exp. Biol. Med.* **1968**, *127*, 707-710.

(104) Zasloff, M. Magainins, a class of antimicrobial peptides from Xenopus skin: isolation, characterization of two active forms, and partial cDNA sequence of a precursor. *Proc. Natl. Acad. Sci.* **1987**, *84*, 5449-5453.

(105) Kościuczuk, E. M.; Lisowski, P.; Jarczak, J.; Strzałkowska, N.; Jóźwik, A.; Horbańczuk, J.; Krzyżewski, J.; Zwierzchowski, L.; Bagnicka, E. Cathelicidins: family of antimicrobial peptides. A review. *Mol. Biol. Rep.* **2012**, *39*, 10957-10970.

(106) Park, C. B.; Kim, H. S.; Kim, S. C. Mechanism of action of the antimicrobial peptide buforin II: buforin II kills microorganisms by penetrating the cell membrane and inhibiting cellular functions. *Biochem. Biophys. Res. Commun.* **1998**, *244*, 253-257.

(107) da Costa, A.; Pereira, A. M.; Sampaio, P.; Rodríguez-Cabello, J. C.; Gomes, A. C.; Casal, M.; Machado, R. Protein-based films functionalized with a truncated antimicrobial peptide sequence display broad antimicrobial activity. *ACS Biomater. Sci. Eng.* **2021**, *7*, 451-461.

(108) Lee, D. G.; Hahm, K.-S.; Shin, S. Y. Structure and fungicidal activity of a synthetic antimicrobial peptide, P18, and its truncated peptides. *Biotechnol. Lett.* **2004**, *26*, 337-341.

(109) Lin, M.-C.; Hui, C.-F.; Chen, J.-Y.; Wu, J.-L. Truncated antimicrobial peptides from marine organisms retain anticancer activity and antibacterial activity against multidrug-resistant Staphylococcus aureus. *Peptides* **2013**, *44*, 139-148.

(110) Zhu, W. L.; Lan, H.; Park, Y.; Yang, S.-T.; Kim, J. I.; Park, I.-S.; You, H. J.; Lee, J. S.; Park, Y. S.; Kim, Y. Effects of Pro→ peptoid residue substitution on cell selectivity and mechanism of antibacterial action of tritrpticin-amide antimicrobial peptide. *Biochemistry* **2006**, *45*, 13007-13017.

(111) Deslouches, B.; Phadke, S. M.; Lazarevic, V.; Cascio, M.; Islam, K.; Montelaro, R. C.; Mietzner, T. A. De novo generation of cationic antimicrobial peptides: influence of length and tryptophan substitution on antimicrobial activity. *Antimicrob. Agents Chemother.* **2005**, *49*, 316-322.

(112) Zelezetsky, I.; Pag, U.; Sahl, H.-G.; Tossi, A. Tuning the biological properties of amphipathic α-helical antimicrobial peptides: rational use of minimal amino acid substitutions. *Peptides* **2005**, *26*, 2368-2376.

(113) Rodríguez, A.; Villegas, E.; Satake, H.; Possani, L.; Corzo, G. Amino acid substitutions in an α-helical antimicrobial arachnid peptide affect its chemical properties and biological activity towards pathogenic bacteria but improves its therapeutic index. *Amino acids* **2011**, *40*, 61-68.

(114) Gunasekera, S.; Muhammad, T.; Strömstedt, A. A.; Rosengren, K. J.; Göransson, U. Backbone cyclization and dimerization of LL-37-derived peptides enhance antimicrobial activity and proteolytic stability. *Front. Microbiol.* **2020**, *11*, 168-183.

(115) Dathe, M.; Nikolenko, H.; Klose, J.; Bienert, M. Cyclization increases the antimicrobial activity and selectivity of arginine-and tryptophan-containing hexapeptides. *Biochemistry* **2004**, *43*, 9140-9150.

(116) Wessolowski, A.; Bienert, M.; Dathe, M. Antimicrobial activity of arginine-and tryptophan-rich hexapeptides: the effects of aromatic clusters, d-amino acid substitution and cyclization. *J. Pept. Sci.* **2004**, *64*, 159-169.

(117) Chan, L. Y.; Zhang, V. M.; Huang, Y. h.; Waters, N. C.; Bansal, P. S.; Craik, D. J.; Daly, N. L. Cyclization of the antimicrobial peptide gomesin with native chemical ligation: influences on stability and bioactivity. *ChemBioChem* **2013**, *14*, 617-624.

(118) Reuther, J. F.; Goodrich, A. C.; Escamilla, P. R.; Lu, T. A.; Del Rio, V.; Davies, B. W.; Anslyn, E. V. A versatile approach to noncanonical, dynamic covalent single-and multi-loop peptide macrocycles for enhancing antimicrobial activity. *J. Am. Chem. Soc.* **2018**, *140*, 3768-3774.

(119) Lu, J.; Xu, H.; Xia, J.; Ma, J.; Xu, J.; Li, Y.; Feng, J. D-and unnatural amino acid substituted antimicrobial peptides with improved proteolytic resistance and their proteolytic degradation characteristics. *Front. Microbiol.* **2020**, *11*, 2869-2886.

(120) Oliva, R.; Chino, M.; Pane, K.; Pistorio, V.; De Santis, A.; Pizzo, E.; D'Errico, G.; Pavone, V.; Lombardi, A.; Del Vecchio, P. Exploring the role of unnatural amino acids in antimicrobial peptides. *Sci. Rep.* **2018**, *8*, 1-16.

(121) Hicks, R. P.; Abercrombie, J.; Wong, R.; Leung, K. Antimicrobial peptides containing unnatural amino acid exhibit potent bactericidal activity against ESKAPE pathogens. *Bioorg. Med. Chem.* **2013**, *21*, 205-214.

(122) Oh, J. E.; Lee, K. H. Synthesis of novel unnatural amino acid as a building block and its incorporation into an antimicrobial peptide. *Bioorg. Med. Chem.* **1999**, *7*, 2985-2990.

(123) Kapil, S.; Sharma, V. d-Amino acids in antimicrobial peptides: A potential approach to treat and combat antimicrobial resistance. *Can. J. Microbiol.* **2021**, *67*, 119-137.

(124) Jia, F.; Wang, J.; Peng, J.; Zhao, P.; Kong, Z.; Wang, K.; Yan, W.; Wang, R. D-amino acid substitution enhances the stability of antimicrobial peptide polybia-CP. *Acta Biochimica et Biophysica Sinica* **2017**, *49*, 916-925.

(125) Albada, H. B.; Prochnow, P.; Bobersky, S.; Langklotz, S.; Bandow, J. E.; Metzler-Nolte, N. Short antibacterial peptides with significantly reduced hemolytic activity can be identified by a systematic L-to-D exchange scan of their amino acid residues. *ACS Combinatorial Science* **2013**, *15*, 585-592.

(126) Jahnsen, R. D.; Frimodt-Møller, N.; Franzyk, H. Antimicrobial activity of peptidomimetics against multidrug-resistant Escherichia coli: a comparative study of different backbones. *J. Med. Chem.* **2012**, *55*, 7253-7261.

(127) Padhee, S.; Hu, Y.; Niu, Y.; Bai, G.; Wu, H.; Costanza, F.; West, L.; Harrington, L.; Shaw, L. N.; Cao, C. Non-hemolytic α-AApeptides as antimicrobial peptidomimetics. *Chem. Commun.* **2011**, *47*, 9729-9731.

(128) Méndez-Samperio, P. Peptidomimetics as a new generation of antimicrobial agents: current progress. *Infect. Drug Resist.* **2014**, *7*, 229-237.

(129) Molchanova, N.; Wang, H.; Hansen, P. R.; Høiby, N.; Nielsen, H. M.; Franzyk, H. Antimicrobial activity of α-peptide/β-peptoid lysine-based peptidomimetics against colistin-resistant pseudomonas aeruginosa isolated from cystic fibrosis patients. *Front. Microbiol.* **2019**, *10*, 275-284.

(130) Frederiksen, N.; Hansen, P. R.; Björkling, F.; Franzyk, H. Peptide/peptoid hybrid oligomers: The Influence of hydrophobicity and relative side-chain length on antibacterial activity and cell Selectivity. *Molecules* **2019**, *24*, 4429-4447.

(131) Molchanova, N.; Hansen, P. R.; Damborg, P.; Franzyk, H. Fluorinated antimicrobial lysine-based peptidomimetics with activity against methicillin-resistant Staphylococcus pseudintermedius. *J. Pept. Sci.* **2018**, *24*, 1-8.

(132) Srinivas, N.; Moehle, K.; Abou-Hadeed, K.; Obrecht, D.; Robinson, J. A. Biaryl amino acid templates in place of D-Pro-L-Pro in cyclic ß-hairpin cationic antimicrobial peptidomimetics. *Org. Biomol. Chem.* **2007**, *5*, 3100-3105.

(133) Goodman, M.; Shao, H. Peptidomimetic building blocks for drug discovery: an overview. *Pure Appl. Chem.* **1996**, *68*, 1303-1308.

(134) Teng, P.; Wu, H.; Cai, J. Peptidomimetics as Antimicrobial Agents. *Novel Antimicrob. Agents Strategies* **2015**, 91-108.

(135) Goodman, M.; Zapf, C.; Rew, Y. New reagents, reactions, and peptidomimetics for drug design. *Pept. Sci.* **2001**, *60*, 229-245.

(136) Haney, E. F.; Mansour, S. C.; Hancock, R. E. Antimicrobial peptides: an introduction. *Antimicrob. Pept.* **2017**, *1548*, 3-22.

(137) Saravanan, R.; Li, X.; Lim, K.; Mohanram, H.; Peng, L.; Mishra, B.; Basu, A.; Lee, J. M.; Bhattacharjya, S.; Leong, S. S. J. Design of short membrane selective antimicrobial peptides containing tryptophan and arginine residues for improved activity, salt-resistance, and biocompatibility. *Biotechnol. Bioeng.* **2014**, *111*, 37-49.

(138) Findlay, B.; Zhanel, G. G.; Schweizer, F. Cationic amphiphiles, a new generation of antimicrobials inspired by the natural antimicrobial peptide scaffold. *Antimicrob. Agents Chemother.* **2010**, *54*, 4049-4058.

(139) Gopal, R.; Seo, C. H.; Song, P. I.; Park, Y. Effect of repetitive lysine–tryptophan motifs on the bactericidal activity of antimicrobial peptides. *Amino acids* **2013**, *44*, 645-660.

(140) Vogel, H. J.; Schibli, D. J.; Jing, W.; Lohmeier-Vogel, E. M.; Epand, R. F.; Epand, R. M. Towards a structure-function analysis of bovine lactoferricin and related tryptophan-and arginine-containing peptides. *Biochem. Cell Biol.* **2002**, *80*, 49-63.

(141) Wiradharma, N.; Khoe, U.; Hauser, C. A.; Seow, S. V.; Zhang, S.; Yang, Y.-Y. Synthetic cationic amphiphilic α-helical peptides as antimicrobial agents. *Biomaterials* **2011**, *32*, 2204-2212.

(142) Stone, T. A.; Cole, G. B.; Ravamehr-Lake, D.; Nguyen, H. Q.; Khan, F.; Sharpe, S.; Deber, C. M. Positive charge patterning and hydrophobicity of membrane-active antimicrobial peptides as determinants of activity, toxicity, and pharmacokinetic stability. *J. Med. Chem.* **2019**, *62*, 6276-6286.

(143) Wang, J.; Dou, X.; Song, J.; Lyu, Y.; Zhu, X.; Xu, L.; Li, W.; Shan, A. Antimicrobial peptides: Promising alternatives in the post feeding antibiotic era. *Med. Res. Rev.* **2019**, *39*, 831-859.

(144) Giangaspero, A.; Sandri, L.; Tossi, A. Amphipathic α helical antimicrobial peptides. A systematic study of the effects of structural and physical properties on biological activity. *Eur. J. Biochem.* **2001**, *268*, 5589-5600.

(145) Jiang, Z.; Mant, C. T.; Vasil, M.; Hodges, R. S. Role of positively charged residues on the polar and non-polar faces of amphipathic α-helical antimicrobial peptides on specificity and selectivity for Gram-negative pathogens. *Chem. Biol. Drug Des.* **2018**, *91*, 75-92.

(146) Hollmann, A.; Martínez, M.; Noguera, M. E.; Augusto, M. T.; Disalvo, A.; Santos, N. C.; Semorile, L.; Maffía, P. C. Role of amphipathicity and hydrophobicity in the balance between hemolysis and peptide–membrane interactions of three related antimicrobial peptides. *Colloids Surf., B* **2016**, *141*, 528-536.

(147) Wood, S. J.; Park, Y. A.; Kanneganti, N. P.; Mukkisa, H. R.; Crisman, L. L.; Davis, S. E.; Vandenbosch, J. L.; Scaglione, J. B.; Heyl, D. L. Modified cysteine-deleted tachyplesin (CDT) analogs as linear antimicrobial peptides: influence of chain length, positive charge, and hydrophobicity on antimicrobial and hemolytic activity. *Int. J. Pept. Res. Ther.* **2014**, *20*, 519-530.

(148) Yin, L. M.; Edwards, M. A.; Li, J.; Yip, C. M.; Deber, C. M. Roles of hydrophobicity and charge distribution of cationic antimicrobial peptides in peptide-membrane interactions. *J. Biol. Chem.* **2012**, *287*, 7738-7745.

(149) Hong, S. Y.; Park, T. G.; Lee, K.-H. The effect of charge increase on the specificity and activity of a short antimicrobial peptide. *Peptides* **2001**, *22*, 1669-1674.

(150) Soares, J. W.; Mello, C. M. Antimicrobial peptides: a review of how peptide structure impacts antimicrobial activity. *Monitoring Food Safety, Agriculture, and Plant Health* **2004**, *5271*, 20-27.

(151) Konz, D.; Marahiel, M. A. How do peptide synthetases generate structural diversity? *Chem. Biol.* **1999**, *6*, 39-48.

(152) Mootz, H. D.; Marahiel, M. A. The tyrocidine biosynthesis operon of Bacillus brevis: complete nucleotide sequence and biochemical characterization of functional internal adenylation domains. *J. Bacteriol. Res.* **1997**, *179*, 6843-6850.

(153) Nissen-Meyer, J.; Nes, I. F. Ribosomally synthesized antimicrobial peptides: their function, structure, biogenesis, and mechanism of action. *Arch. Microbiol.* **1997**, *167*, 67-77.

(154) Wijaya, R.; Neumann, G. M.; Condron, R.; Hughes, A. B.; Polya, G. M. Defense proteins from seed of Cassia fistula include a lipid transfer protein homologue and a protease inhibitory plant defensin. *Plant Sci. J.* **2000**, *159*, 243-255.

(155) Segura, A.; Moreno, M.; Molina, A.; García-Olmedo, F. Novel defensin subfamily from spinach (Spinacia oleracea). *FEBS Lett.* **1998**, *435*, 159-162.

(156) Van Parijs, J.; Broekaert, W. F.; Goldstein, I. J.; Peumans, W. J. Hevein: an antifungal protein from rubber-tree (Hevea brasiliensis) latex. *Planta* **1991**, *183*, 258-264.

(157) Ganz, T. Defensins in the urinary tract and other tissues. *J. Infect. Dis.* **2001**, *183*, 41-42.

(158) Goldman, M. J.; Anderson, G. M.; Stolzenberg, E. D.; Kari, U. P.; Zasloff, M.; Wilson, J. M. Human β-defensin-1 is a salt-sensitive antibiotic in lung that is inactivated in cystic fibrosis. *Cell* **1997**, *88*, 553-560.

(159) Bals, R.; Wang, X.; Wu, Z.; Freeman, T.; Bafna, V.; Zasloff, M.; Wilson, J. M. Human beta-defensin 2 is a salt-sensitive peptide antibiotic expressed in human lung. *J. Clin. Invest.* **1998**, *102*, 874-880.

(160) Harder, J. r.; Bartels, J.; Christophers, E.; Schröder, J.-M. Isolation and Characterization of Human μ-Defensin-3, a Novel Human Inducible Peptide Antibiotic. *J. Biol. Chem.* **2001**, *276*, 5707-5713.

(161) Hoffmann, J. A.; Hetru, C. Insect defensins: inducible antibacterial peptides. *Immunol. Today* **1992**, *13*, 411-415.

(162) Gomes, P. d. S.; Fernandes, M. H. Defensins in the oral cavity: distribution and biological role. *J. Oral Pathol. Med.* **2010**, *39*, 1-9.

(163) Zou, G.; de Leeuw, E.; Li, C.; Pazgier, M.; Li, C.; Zeng, P.; Lu, W.-Y.; Lubkowski, J.; Lu, W. Toward understanding the cationicity of defensins: Arg and Lys versus their noncoded analogs. *J. Biol. Chem.* **2007**, *282*, 19653-19665.

(164) Zimmermann, G. R.; Legault, P.; Selsted, M. E.; Pardi, A. Solution structure of bovine neutrophil. beta.-defensin-12: the peptide fold of the. beta.-defensins is identical to that of the classical defensins. *Biochemistry* **1995**, *34*, 13663-13671.

(165) Cornet, B.; Bonmatin, J.-M.; Hetru, C.; Hoffmann, J. A.; Ptak, M.; Vovelle, F. Refined three-dimensional solution structure of insect defensin A. *Structure* **1995**, *3*, 435-448.

(166) Hoover, D. M.; Chertov, O.; Lubkowski, J. The structure of human β-defensin-1: new insights into structural properties of β-defensins. *J. Biol. Chem.* **2001**, *276*, 39021-39026.

(167) Fant, F.; Vranken, W.; Broekaert, W.; Borremans, F. Determination of the three-dimensional solution structure of Raphanus sativus antifungal protein 1 by 1H NMR. *J. Mol. Biol.* **1998**, *279*, 257-270.

(168) Conibear, A. C.; Rosengren, K. J.; Harvey, P. J.; Craik, D. J. Structural characterization of the cyclic cystine ladder motif of θ-defensins. *Biochemistry* **2012**, *51*, 9718-9726.

(169) Shi, J.; Ganz, T. The role of protegrins and other elastase-activated polypeptides in the bactericidal properties of porcine inflammatory fluids. *Infect. Immun.* **1998**, *66*, 3611-3617.

(170) Zhang, G.; Wu, H.; Shi, J.; Ganz, T.; Ross, C. R.; Blecha, F. Molecular cloning and tissue expression of porcine β-defensin-1. *FEBS Lett.* **1998**, *424*, 37-40.

(171) Oppenheim, F. X., T McMillian, FM Levitz, SM Diamond, RD Offner, GD Troxler, RF. Histatins, a novel family of histidine-rich proteins in human parotid secretion. Isolation, characterization, primary structure, and fungistatic effects on Candida albicans. *J. Biol. Chem.* **1988**, *263*, 7472-7477.

(172) Cole, A. M.; Kim, Y.-H.; Tahk, S.; Hong, T.; Weis, P.; Waring, A. J.; Ganz, T. Calcitermin, a novel antimicrobial peptide isolated from human airway secretions. *FEBS Lett.* **2001**, *504*, 5-10.

(173) Wang, Y.; Wang, M.; Shan, A.; Feng, X. Avian host defense cathelicidins: Structure, expression, biological functions, and potential therapeutic applications. *Poult. Sci.* **2020**, *99*, 6434-6445.

(174) Braff, M. H.; Zaiou, M.; Fierer, J.; Nizet, V.; Gallo, R. L. Keratinocyte production of cathelicidin provides direct activity against bacterial skin pathogens. *Infect. Immun.* **2005**, *73*, 6771-6781.

(175) Yang, D.; Chertov, O.; Oppenheim, J. J. Participation of mammalian defensins and cathelicidins in anti-microbial immunity: receptors and activities of human defensins and cathelicidin (LL-37). *J. Leukocyte Biol.* **2001**, *69*, 691-697.

(176) Weber, G.; Borregaard, N.; Nilsson, M. M. F.; Sandstedt, B.; Sørensen, O. The Human Cationic Antimicrobial Protein. *Infect. Immun.* **1999**, *67*, 2561-2566.

(177) Frohm, M.; Agerberth, B.; Ahangari, G.; Ståhle-Bäckdahl, M.; Lidén, S.; Wigzell, H.; Gudmundsson, G. H. The expression of the gene coding for the antibacterial peptide LL-37 is induced in human keratinocytes during inflammatory disorders. *J. Biol. Chem.* **1997**, *272*, 15258-15263.

(178) Bals, R.; Wang, X.; Zasloff, M.; Wilson, J. M. The peptide antibiotic LL-37/hCAP-18 is expressed in epithelia of the human lung where it has broad antimicrobial activity at the airway surface. *Proc. Natl. Acad. Sci.* **1998**, *95*, 9541-9546.

(179) Yang, D.; Chen, Q.; Schmidt, A. P.; Anderson, G. M.; Wang, J. M.; Wooters, J.; Oppenheim, J. J.; Chertov, O. LL-37, the neutrophil granule–and epithelial cell–derived cathelicidin, utilizes formyl peptide receptor–like 1 (FPRL1) as a receptor to chemoattract

human peripheral blood neutrophils, monocytes, and T cells. *J. Exp. Med.* **2000**, *192*, 1069-1074.

(180) Agerberth, B.; Charo, J.; Werr, J.; Olsson, B.; Idali, F.; Lindbom, L.; Kiessling, R.; Jörnvall, H.; Wigzell, H.; Gudmundsson, G. H. The human antimicrobial and chemotactic peptides LL-37 and α-defensins are expressed by specific lymphocyte and monocyte populations. *Am. J. Hematol.* **2000**, *96*, 3086-3093.

(181) Zanetti, M.; Gennaro, R.; Romeo, D. Cathelicidins: a novel protein family with a common proregion and a variable C-terminal antimicrobial domain. *FEBS Lett.* **1995**, *374*, 1-5.

(182) Van Dijk, A.; Molhoek, E.; Bikker, F.; Yu, P.-L.; Veldhuizen, E.; Haagsman, H. Avian cathelicidins: paradigms for the development of anti-infectives. *Vet. Microbiol.* **2011**, *153*, 27-36.

(183) Zanetti, M. Cathelicidins, multifunctional peptides of the innate immunity. *J. Leukocyte Biol.* **2004**, *75*, 39-48.

(184) Cuperus, T.; Coorens, M.; van Dijk, A.; Haagsman, H. P. Avian host defense peptides. *Dev. Comp. Immunol.* **2013**, *41*, 352-369.

(185) Zhang, G.; Sunkara, L. T. Avian antimicrobial host defense peptides: from biology to therapeutic applications. *Pharmaceuticals* **2014**, *7*, 220-247.

(186) Young-Speirs, M.; Drouin, D.; Cavalcante, P. A.; Barkema, H. W.; Cobo, E. R. Host defense cathelicidins in cattle: types, production, bioactive functions and potential therapeutic and diagnostic applications. *Int. J. Antimicrob. Agents* **2018**, *51*, 813-821.

(187) Lamiable, A.; Thévenet, P.; Rey, J.; Vavrusa, M.; Derreumaux, P.; Tufféry, P. PEP-FOLD3: faster de novo structure prediction for linear peptides in solution and in complex. *Nucleic Acids Res.* **2016**, *44*, 449-454.

(188) Hwang, P. M.; Vogel, H. J. Structure-function relationships of antimicrobial peptides. *Biochem. Cell Biol.* **1998**, *76*, 235-246.

(189) Van Den Hooven, H. W.; Doeland, C. C.; Van De Kamp, M.; Konings, R. N.; Hilbers, C. W.; Van De Ven, F. J. Three-dimensional structure of the lantibiotic nisin in the presence of membrane-mimetic micelles of dodecylphosphocholine and of sodium dodecylsulphate. *Eur. J. Biochem.* **1996**, *235*, 382-393.

(190) Franklin, J. C.; Ellena, J. F.; Jayasinghe, S.; Kelsh, L. P.; Cafiso, D. S. Structure of micelle-associated alamethicin from 1H NMR. Evidence for conformational heterogeneity in a voltage-gated peptide. *Biochemistry* **1994**, *33*, 4036-4045.

(191) Koehbach, J.; Craik, D. J. The vast structural diversity of antimicrobial peptides. *Trends Pharmacol. Sci.* **2019**, *40*, 517-528.

(192) Jamasbi, E.; Lucky, S. S.; Li, W.; Hossain, M. A.; Gopalakrishnakone, P.; Separovic, F. Effect of dimerized melittin on gastric cancer cells and antibacterial activity. *Amino Acids* **2018**, *50*, 1101-1110.

(193) Chen, J.; Guan, S.-M.; Sun, W.; Fu, H. Melittin, the major pain-producing substance of bee venom. *Neurosci. Bull.* **2016**, *32*, 265-272.

(194) Asthana, N.; Yadav, S. P.; Ghosh, J. K. Dissection of antibacterial and toxic activity of melittin: a leucine zipper motif plays a crucial role in determining its hemolytic activity but not antibacterial activity. *J. Biol. Chem.* **2004**, *279*, 55042-55050.

(195) Lee, G.; Bae, H. Anti-inflammatory applications of melittin, a major component of bee venom: Detailed mechanism of action and adverse effects. *Molecules* **2016**, *21*, 616-626.

(196) Shi, W.; Li, C.; Li, M.; Zong, X.; Han, D.; Chen, Y. Antimicrobial peptide melittin against Xanthomonas oryzae pv. oryzae, the bacterial leaf blight pathogen in rice. *Appl. Microbiol. Biotechnol.* **2016**, *100*, 5059-5067.

(197) Jamasbi, E.; Mularski, A.; Separovic, F. Model membrane and cell studies of antimicrobial activity of melittin analogues. *Curr. Top. Med. Chem.* **2016**, *16*, 40-45.

(198) Lee, J.; Lee, D. G. Melittin triggers apoptosis in Candida albicans through the reactive oxygen species-mediated mitochondria/caspase-dependent pathway. *FEMS Microbiol. Lett.* **2014**, *355*, 36-42.

(199) Akbari, R.; Hakemi-Vala, M.; Pashaie, F.; Bevalian, P.; Hashemi, A.; Pooshang Bagheri, K. Highly synergistic effects of melittin with conventional antibiotics against multidrug-resistant isolates of acinetobacter baumannii and pseudomonas aeruginosa. *Microb. Drug Resist.* **2019**, *25*, 193-202.

(200) Choi, J. H.; Jang, A. Y.; Lin, S.; Lim, S.; Kim, D.; Park, K.; Han, S. M.; Yeo, J. H.; Seo, H. S. Melittin, a honeybee venom-derived antimicrobial peptide, may target methicillin-resistant Staphylococcus aureus. *Mol. Med. Rep.* **2015**, *12*, 6483-6490.

(201) Simmaco, M.; Mignogna, G.; Barra, D.; Bossa, F. Antimicrobial peptides from skin secretions of Rana esculenta. Molecular cloning of cDNAs encoding esculentin and brevinins and isolation of new active peptides. *J. Biol. Chem.* **1994**, *269*, 11956-11961.

(202) Ponti, D.; Mignogna, G.; Mangoni, M. L.; De Biase, D.; Simmaco, M.; Barra, D. Expression and activity of cyclic and linear analogues of esculentin-1, an anti-microbial peptide from amphibian skin. *Eur. J. Biochem.* **1999**, *263*, 921-927.

(203) Mangoni, M. L.; Papo, N.; Saugar, J. M.; Barra, D.; Shai, Y.; Simmaco, M.; Rivas, L. Effect of natural L-to D-amino acid conversion on the organization, membrane binding, and biological function of the antimicrobial peptides bombinins H. *Biochemistry* **2006**, *45*, 4266-4276.

(204) Vasu, S.; McGahon, M. K.; Moffett, R. C.; Curtis, T. M.; Conlon, J. M.; Abdel-Wahab, Y.; Flatt, P. R. Esculentin-2CHa (1-30) and its analogues: Stability and mechanisms of insulinotropic action. *J. Endocrinol.* **2017**, *232*, 423-435.

(205) Othon, C. M.; Kwon, O.-H.; Lin, M. M.; Zewail, A. H. Solvation in protein (un) folding of melittin tetramer–monomer transition. *Proc. Natl. Acad. Sci.* **2009**, *106*, 12593-12598.

(206) Gesell, J.; Zasloff, M.; Opella, S. J. Two-dimensional 1H NMR experiments show that the 23-residue magainin antibiotic peptide is an α-helix in dodecylphosphocholine micelles, sodium dodecylsulfate micelles, and trifluoroethanol/water solution. *J. Biomol. NMR* **1997**, *9*, 127-135.

(207) Wang, G. Structures of human host defense cathelicidin LL-37 and its smallest antimicrobial peptide KR-12 in lipid micelles. *J. Biol. Chem.* **2008**, *283*, 32637-32643.

(208) Saravanan, R.; Joshi, M.; Mohanram, H.; Bhunia, A.; Mangoni, M. L.; Bhattacharjya, S. NMR structure of temporin-1 ta in lipopolysaccharide micelles: mechanistic insight into inactivation by outer membrane. *PLoS One* **2013**, *8*, 1-9.

(209) Manzo, G.; Ferguson, P. M.; Gustilo, V. B.; Hind, C. K.; Clifford, M.; Bui, T. T.; Drake, A. F.; Atkinson, R. A.; Sutton, J. M.; Batoni, G. Minor sequence modifications in temporin B cause drastic changes in antibacterial potency and selectivity by fundamentally altering membrane activity. *Sci. Rep.* **2019**, *9*, 1-16.

(210) Baek, M. H.; Kamiya, M.; Kushibiki, T.; Nakazumi, T.; Tomisawa, S.; Abe, C.; Kumaki, Y.; Kikukawa, T.; Demura, M.; Kawano, K. Lipopolysaccharide-bound structure of the antimicrobial peptide cecropin P1 determined by nuclear magnetic resonance spectroscopy. *J. Pept. Sci.* **2016**, *22*, 214-221.

(211) Steiner, H. H., D Engström, Å Bennich, H Boman, HG. Sequence and specificity of two antibacterial proteins involved in insect immunity. *Nature* **1981**, *292*, 246-248.

(212) Hultmark, D. E., Åke B., Hans K., Rashmi B., Hans G. Insect immunity: isolation and structure of cecropin D and four minor antibacterial components from Cecropia pupae. *Eur. J. Biochem.* **1982**, *127*, 207-217.

(213) Andreu, D. M., RB Steiner, H Boman, HG. Solid-phase synthesis of cecropin A and related peptides. *Proc. Natl. Acad. Sci.* **1983**, *80*, 6475-6479.

(214) Bechinger, B.; Lohner, K. Detergent-like actions of linear amphipathic cationic antimicrobial peptides. *Biochim. Biophys. Acta, Biomembr.* **2006**, *1758*, 1529-1539.

(215) Ouyang, L.; Xu, X.; Freed, S.; Gao, Y.; Yu, J.; Wang, S.; Ju, W.; Zhang, Y.; Jin, F. Cecropins from Plutella xylostella and Their Interaction with Metarhizium anisopliae. *PLoS One* **2015**, *10*, 1-16.

(216) Mangoni, M. Temporins, anti-infective peptides with expanding properties. *Cell. Mol. Life Sci.* **2006**, *63*, 1060-1069.

(217) Giacometti, A.; Cirioni, O.; Kamysz, W.; D'amato, G.; Silvestri, C.; Del Prete, M. S.; Licci, A.; Łukasiak, J.; Scalise, G. In vitro activity and killing effect of temporin A on nosocomial isolates of Enterococcus faecalis and interactions with clinically used antibiotics. *J. Antimicrob. Chemother.* **2005**, *55*, 272-274.

(218) Mangoni, M. L.; Saugar, J. M.; Dellisanti, M.; Barra, D.; Simmaco, M.; Rivas, L. Temporins, small antimicrobial peptides with leishmanicidal activity. *J. Biol. Chem.* **2005**, *280*, 984-990.

(219) Park, C. B.; Kim, M. S.; Kim, S. C. A novel antimicrobial peptide frombufo bufo gargarizans. *Biochem. Biophys. Res. Commun.* **1996**, *218*, 408-413.

(220) Yi, G.-S.; Park, C. B.; Kim, S. C.; Cheong, C. Solution structure of an antimicrobial peptide buforin II. *FEBS Lett.* **1996**, *398*, 87-90.

(221) Oishi, O.; Yamashita, S.; Nishimoto, E.; Lee, S.; Sugihara, G.; Ohno, M. Conformations and orientations of aromatic amino acid residues of tachyplesin I in phospholipid membranes. *Biochemistry* **1997**, *36*, 4352-4359.

(222) Kawano, K.; Yoneya, T.; Miyata, T.; Yoshikawa, K.; Tokunaga, F.; Terada, Y.; Iwanaga, S. Antimicrobial peptide, tachyplesin I, isolated from hemocytes of the horseshoe crab (Tachypleus tridentatus). NMR determination of the beta-sheet structure. *J. Biol. Chem.* **1990**, *265*, 15365-15367.

(223) Kokryakov, V. N. H., Sylvia SL Panyutich, Elena A Shevchenko, Andrei A Aleshina, Galina M Shamova, Olga V; Korneva, H. A. L., Robert I. Protegrins: leukocyte antimicrobial peptides that combine features of corticostatic defensins and tachyplesins. *FEBS Lett.* **1993**, *327*, 231-236.

(224) Fahrner, R. L.; Dieckmann, T.; Harwig, S. S.; Lehrer, R. I.; Eisenberg, D.; Feigon, J. Solution structure of protegrin-1, a broad-spectrum antimicrobial peptide from porcine leukocytes. *Chem. Biol.* **1996**, *3*, 543-550.

(225) Hwang, P. M.; Zhou, N.; Shan, X.; Arrowsmith, C. H.; Vogel, H. J. Three-dimensional solution structure of lactoferricin B, an antimicrobial peptide derived from bovine lactoferrin. *Biochemistry* **1998**, *37*, 4288-4298.

(226) Jordan, J. B.; Poppe, L.; Haniu, M.; Arvedson, T.; Syed, R.; Li, V.; Kohno, H.; Kim, H.; Schnier, P. D.; Harvey, T. S. Hepcidin revisited, disulfide connectivity, dynamics, and structure. *J. Biol. Chem.* **2009**, *284*, 24155-24167.

(227) McManus, A. M.; Dawson, N. F.; Wade, J. D.; Carrington, L. E.; Winzor, D. J.; Craik, D. J. Three-dimensional structure of RK-1: a novel α-defensin peptide. *Biochemistry* **2000**, *39*, 15757-15764.

(228) Hur, G. H.; Vickery, C. R.; Burkart, M. D. Explorations of catalytic domains in non-ribosomal peptide synthetase enzymology. *Nat. Prod. Rep.* **2012**, *29*, 1074-1098.

(229) Mizuhara, N.; Kuroda, M.; Ogita, A.; Tanaka, T.; Usuki, Y.; Fujita, K.-i. Antifungal thiopeptide cyclothiazomycin B1 exhibits growth inhibition accompanying morphological changes via binding to fungal cell wall chitin. *Bioorg. Med. Chem.* **2011**, *19*, 5300-5310.

(230) Vijayakumar, E.; Roy, K.; Chatterjee, S.; Deshmukh, S.; Ganguli, B.; Fehlhaber, H.-W.; Kogler, H. Arthrichitin. A new cell wall active metabolite from Arthrinium phaeospermum. *J. Org. Chem.* **1996**, *61*, 6591-6593.

(231) Smits, G. J.; Kapteyn, J. C.; van d. E., H.; Klis, F. M. Cell wall dynamics in yeast. *Curr. Opin. Microbiol.* **1999**, *2*, 348-352.

(232) Thimon, L.; Peyoux, F.; Maget-Dana, R.; Michel, G. Surface-active properties of antifungal lipopeptides produced byBacillus subtilis. *J. Am. Oil Chem. Soc.* **1992**, *69*, 92-93.

(233) Lee, D. W.; Kim, B. S. Antimicrobial cyclic peptides for plant disease control. *J. Plant Pathol.* **2015**, *31*, 1-11.

(234) Mishra, A. K.; Choi, J.; Moon, E.; Baek, K.-H. Tryptophan-rich and proline-rich antimicrobial peptides. *Molecules* **2018**, *23*, 815-838.

(235) Zanjani, N. T.; Miranda-Saksena, M.; Cunningham, A. L.; Dehghani, F. Antimicrobial peptides of marine crustaceans: The potential and challenges of developing therapeutic agents. *Curr. Med. Chem.* **2018**, *25*, 2245-2259.

(236) Tam, J. P.; Wang, S.; Wong, K. H.; Tan, W. L. Antimicrobial peptides from plants. *Pharmaceuticals* **2015**, *8*, 711-757.

(237) Wang, G. Human antimicrobial peptides and proteins. *Pharmaceuticals* **2014**, *7*, 545-594.

(238) Dutta, P.; Das, S. Mammalian antimicrobial peptides: promising therapeutic targets against infection and chronic inflammation. *Curr. Top. Med. Chem.*. **2016**, *16*, 99-129.

(239) Hassan, M.; Kjos, M.; Nes, I.; Diep, D.; Lotfipour, F. Natural antimicrobial peptides from bacteria: characteristics and potential applications to fight against antibiotic resistance. *J. Appl. Microbiol.* **2012**, *113*, 723-736.

(240) Matejuk, A.; Leng, Q.; Begum, M.; Woodle, M.; Scaria, P.; Chou, S.; Mixson, A. Peptide-based antifungal therapies against emerging infections. *Drugs Future* **2010**, *35*, 197-232.

(241) Masso-Silva, J. A.; Diamond, G. Antimicrobial peptides from fish. *Pharmaceuticals* **2014**, *7*, 265-310.

(242) Li, C.; Blencke, H.-M.; Haug, T.; Stensvåg, K. Antimicrobial peptides in echinoderm host defense. *Dev. Comp. Immunol.* **2015**, *49*, 190-197.

(243) Hancock, R. E.; Rozek, A. Role of membranes in the activities of antimicrobial cationic peptides. *FEMS Microbiol. Lett.* **2002**, *206*, 143-149.

(244) Powers, J.-P. S.; Hancock, R. E. The relationship between peptide structure and antibacterial activity. *Peptides* **2003**, *24*, 1681-1691.

(245) Brown, K. L.; Hancock, R. E. Cationic host defense (antimicrobial) peptides. *Curr. Opin. Immunol.* **2006**, *18*, 24-30.

(246) Fernández-Vidal, M.; Jayasinghe, S.; Ladokhin, A. S.; White, S. H. Folding amphipathic helices into membranes: amphiphilicity trumps hydrophobicity. *J. Mol. Biol.* **2007**, *370*, 459-470.

(247) Mangoni, M. L.; Marcellini HG, L.; Simmaco, M. Biological characterization and modes of action of temporins and bombinins H, multiple forms of short and mildly cationic anti-microbial peptides from amphibian skin. *J. Pept. Sci.* **2007**, *13*, 603-613.

(248) Mookherjee, N.; Anderson, M. A.; Haagsman, H. P.; Davidson, D. J. Antimicrobial host defence peptides: functions and clinical potential. *Nat. Rev. Drug Discovery* **2020**, *19*, 311-332.

(249) Hussain, S.; Güzel, Y.; Pezzei, C.; Rainer, M.; Huck, C. W.; Bonn, G. K. Solid-phase extraction of plant thionins employing aluminum silicate based extraction columns. *J. Sep. Sci.* **2014**, *37*, 2200-2207.

(250) Park, C. H.; Valore, E. V.; Waring, A. J.; Ganz, T. Hepcidin, a urinary antimicrobial peptide synthesized in the liver. *J. Biol. Chem.* **2001**, *276*, 7806-7810.

(251) Krause, A.; Neitz, S.; Mägert, H.-J.; Schulz, A.; Forssmann, W.-G.; Schulz-Knappe, P.; Adermann, K. LEAP-1, a novel highly disulfide-bonded human peptide, exhibits antimicrobial activity. *FEBS Lett.* **2000**, *480*, 147-150.

(252) Krause, A.; Sillard, R.; Kleemeier, B.; Klüver, E.; Maronde, E.; Conejo-García, J. R.; Forssmann, W. G.; Schulz-Knappe, P.; Nehls, M. C.; Wattler, F. Isolation and biochemical characterization of LEAP-2, a novel blood peptide expressed in the liver. *Protein Sci.* **2003**, *12*, 143-152.

(253) Epand, R. M.; Vogel, H. J. Diversity of antimicrobial peptides and their mechanisms of action. *Biochim. Biophys. Acta, Biomembr.* **1999**, *1462*, 11-28.

(254) Sansom, M. S. The biophysics of peptide models of ion channels. *Prog. Biophys. Mol. Biol.* **1991**, *55*, 139-235.

(255) Ketchem, R.; Hu, W.; Cross, T. High-resolution conformation of gramicidin A in a lipid bilayer by solid-state NMR. *Science* **1993**, *261*, 1457-1460.

(256) Caverly, J. M.; Radi, Z. A.; Andreasen, C. B.; Dixon, R. A.; Brogden, K. A.; Ackermann, M. R. Comparison of bronchoalveolar lavage fluid obtained from Mannheimia haemolytica-inoculated calves with and without prior treatment with the selectin inhibitor TBC1269. *Am. J. Vet. Res.* **2001**, *62*, 665-672.

(257) Brogden, K. A.; De Lucca, A. J.; Bland, J.; Elliott, S. Isolation of an ovine pulmonary surfactant-associated anionic peptide bactericidal for Pasteurella haemolytica. *Proc. Natl. Acad. Sci.* **1996**, *93*, 412-416.

(258) Harris, F.; Dennison, S. R.; Phoenix, D. A. Anionic antimicrobial peptides from eukaryotic organisms. *Curr. Protein Pept. Sci.* **2009**, *10*, 585-606.

(259) Brogden, K. A.; Ackermann, M.; Huttner, K. M. Small, anionic, and charge-neutralizing propeptide fragments of zymogens are antimicrobial. *Antimicrob. Agents Chemother.* **1997**, *41*, 1615-1617.

(260) Lai, R.; Liu, H.; Lee, W. H.; Zhang, Y. An anionic antimicrobial peptide from toad Bombina maxima. *Biochem. Biophys. Res. Commun.* **2002**, *295*, 796-799.

(261) Steffen, H.; Rieg, S.; Wiedemann, I.; Kalbacher, H.; Deeg, M.; Sahl, H.-G.; Peschel, A.; Gotz, F.; Garbe, C.; Schittek, B. Naturally processed dermcidin-derived peptides do not permeabilize bacterial membranes and kill microorganisms irrespective of their charge. *Antimicrob. Agents Chemother.* **2006**, *50*, 2608-2620.

(262) Lee, I. H.; Cho, Y.; Lehrer, R. I. Effects of pH and salinity on the antimicrobial properties of clavanins. *Infect. Immun.* **1997**, *65*, 2898-2903.

(263) Tam, J. P.; Lu, Y.-A.; Yang, J.-L. Design of salt-insensitive glycine-rich antimicrobial peptides with cyclic tricystine structures. *Biochemistry* **2000**, *39*, 7159-7169.

(264) Rothstein, D. M.; Spacciapoli, P.; Tran, L. T.; Xu, T.; Roberts, F. D.; Dalla Serra, M.; Buxton, D. K.; Oppenheim, F. G.; Friden, P. Anticandida activity is retained in P-113, a 12-amino-acid fragment of histatin 5. *Antimicrob. Agents Chemother.* **2001**, *45*, 1367-1373.

(265) Hiemstra, P. Antimicrobial peptides in the real world: implications for cystic fibrosis. *Eur. Respir. J.* **2007**, *29*, 617-618.

(266) Kandasamy, S. K.; Larson, R. G. Effect of salt on the interactions of antimicrobial peptides with zwitterionic lipid bilayers. *Biochim. Biophys. Acta, Biomembr.* **2006**, *1758*, 1274-1284.

(267) Ghosh, S.; Pandit, G.; Debnath, S.; Chatterjee, S.; Satpati, P. Effect of monovalent salt concentration and peptide secondary structure in peptide-micelle binding. *RSC Adv.* **2021**, *11*, 36836-36849.

(268) Rydlo, T.; Rotem, S.; Mor, A. Antibacterial properties of dermaseptin S4 derivatives under extreme incubation conditions. *Antimicrob. Agents Chemother.* **2006**, *50*, 490-497.

(269) Friedrich, C.; Scott, M. G.; Karunaratne, N.; Yan, H.; Hancock, R. E. Salt-resistant α-helical cationic antimicrobial peptides. *Antimicrob. Agents Chemother.* **1999**, *43*, 1542-1548.

(270) Mohanram, H.; Bhattacharjya, S. Salt-resistant short antimicrobial peptides. *Pept. Sci.* **2016**, *106*, 345-356.

(271) Olli, S.; Rangaraj, N.; Nagaraj, R. Effect of selectively introducing arginine and D-amino acids on the antimicrobial activity and salt sensitivity in analogs of human beta-defensins. *PLoS One* **2013**, *8*, 1-10.

(272) Yu, H. Y.; Tu, C. H.; Yip, B. S.; Chen, H. L.; Cheng, H. T.; Huang, K. C.; Lo, H. J.; Cheng, J. W. Easy strategy to increase salt resistance of antimicrobial peptides. *Antimicrob. Agents Chemother.* **2011**, *55*, 4918-4921.

(273) Chu, H.-L.; Yu, H.-Y.; Yip, B.-S.; Chih, Y.-H.; Liang, C.-W.; Cheng, H.-T.; Cheng, J.-W. Boosting salt resistance of short antimicrobial peptides. *Antimicrob. Agents Chemother.* **2013**, *57*, 4050-4052.

(274) Wang, C.-W.; Yip, B.-S.; Cheng, H.-T.; Wang, A.-H.; Chen, H.-L.; Cheng, J.-W.; Lo, H.-J. Increased potency of a novel D-β-naphthylalanine-substituted antimicrobial peptide against fluconazole-resistant fungal pathogens. *FEMS Yeast Res.* **2009**, *9*, 967-970.

(275) Harwig, S. S.; Waring, A.; Yang, H. J.; Cho, Y.; Tan, L.; Lehrer, R. I. Intramolecular disulfide bonds enhance the antimicrobial and lytic activities of protegrins at physiological sodium chloride concentrations. *Eur. J. Biochem.* **1996**, *240*, 352-357.

(276) Nan, Y.-H.; Bang, J.-K.; Shin, S.-Y. Effects of Lys-linked Dimerization of an α-Helical Leu/Lys-rich Model Antimicrobial Peptide on Salt Resistance and LPS-neutralizing Activity. *Bull. Korean Chem. Soc.* **2011**, *32*, 4055-4058.

(277) Nan, Y.-H.; Shin, S.-Y. Effect of disulphide bond position on salt resistance and LPS-neutralizing activity of α-helical homo-dimeric model antimicrobial peptides. *BMB Rep.* **2011**, *44*, 747-752.

(278) Park, I. Y.; Cho, J. H.; Kim, K. S.; Kim, Y.-B.; Kim, M. S.; Kim, S. C. Helix stability confers salt resistance upon helical antimicrobial peptides. *J. Biol. Chem.* **2004**, *279*, 13896-13901.

(279) Malik, E.; Dennison, S. R.; Harris, F.; Phoenix, D. A. pH dependent antimicrobial peptides and proteins, their mechanisms of action and potential as therapeutic agents. *Pharmaceuticals* **2016**, *9*, 67-102.

(280) Nekoofar, M. H.; Namazikhah, M.; Sheykhrezae, M.; Mohammadi, M.; Kazemi, A.; Aseeley, Z.; Dummer, P. M. H. pH of pus collected from periapical abscesses. *Int. Endod. J.* **2009**, *42*, 534-538.

(281) Grinstein, S.; Swallow, C. J.; Rotstein, O. D. Regulation of cytoplasmic pH in phagocytic cell function and dysfunction. *Clin. Biochem.* **1991**, *24*, 241-247.

(282) Schneider, L. A.; Korber, A.; Grabbe, S.; Dissemond, J. Influence of pH on wound-healing: a new perspective for wound-therapy? *Arch. Dermatol. Res.* **2007**, *298*, 413-420.

(283) Liu, Y.; Kalén, A.; Risto, O.; Wahlström, O. Fibroblast proliferation due to exposure to a platelet concentrate in vitro is pH dependent. *Wound Repair Regen* **2002**, *10*, 336-340.

(284) Walkenhorst, W. F. Using adjuvants and environmental factors to modulate the activity of antimicrobial peptides. *Biochim. Biophys. Acta, Biomembr.*. **2016**, *1858*, 926-935.

(285) Kacprzyk, L.; Rydengård, V.; Mörgelin, M.; Davoudi, M.; Pasupuleti, M.; Malmsten, M.; Schmidtchen, A. Antimicrobial activity of histidine-rich peptides is dependent on acidic conditions. *Biochim. Biophys. Acta, Biomembr.* **2007**, *1768*, 2667-2680.

(286) Yount, N. Y.; Kupferwasser, D.; Spisni, A.; Dutz, S. M.; Ramjan, Z. H.; Sharma, S.; Waring, A. J.; Yeaman, M. R. Selective reciprocity in antimicrobial activity versus cytotoxicity of hBD-2 and crotamine. *Proc. Natl. Acad. Sci.* **2009**, *106*, 14972-14977.

(287) Dashper, S. G.; O'Brien-Simpson, N. M.; Cross, K. J.; Paolini, R. A.; Hoffmann, B.; Catmull, D. V.; Malkoski, M.; Reynolds, E. C. Divalent metal cations increase the activity of the antimicrobial peptide kappacin. *Antimicrob. Agents Chemother.* **2005**, *49*, 2322-2328.

(288) Paulmann, M.; Arnold, T.; Linke, D.; Özdirekcan, S.; Kopp, A.; Gutsmann, T.; Kalbacher, H.; Wanke, I.; Schuenemann, V. J.; Habeck, M. Structure-activity analysis of the dermcidin-derived peptide DCD-1L, an anionic antimicrobial peptide present in human sweat. *J. Biol. Chem.* **2012**, *287*, 8434-8443.

(289) Walkenhorst, W. F.; Klein, J. W.; Vo, P.; Wiey, W. C. pH dependence of microbe sterilization by cationic antimicrobial peptides. *Antimicrob. Agents Chemother.* **2013**, *57*, 3312-3320.

(290) Abou Alaiwa, M. H.; Reznikov, L. R.; Gansemer, N. D.; Sheets, K. A.; Horswill, A. R.; Stoltz, D. A.; Zabner, J.; Welsh, M. J. pH modulates the activity and synergism of the airway surface liquid antimicrobials β-defensin-3 and LL-37. *Proc. Natl. Acad. Sci.* **2014**, *111*, 18703-18708.

(291) Wang, G.; Hanke, M. L.; Mishra, B.; Lushnikova, T.; Heim, C. E.; Chittezham Thomas, V.; Bayles, K. W.; Kielian, T. Transformation of human cathelicidin LL-37 into selective, stable, and potent antimicrobial compounds. *ACS Chem. Biol.* **2014**, *9*, 1997-2002.

(292) Zai, Y.; Ying, Y.; Ye, Z.; Zhou, M.; Ma, C.; Shi, Z.; Chen, X.; Xi, X.; Chen, T.; Wang, L. Broad-spectrum antimicrobial activity and improved stability of a D-Amino acid enantiomer of DMPC-10A, the designed derivative of dermaseptin truncates. *Antibiotics* **2020**, *9*, 627-646.

(293) Li, X.; Li, Y.; Han, H.; Miller, D. W.; Wang, G. Solution structures of human LL-37 fragments and NMR-based identification of a minimal membrane-targeting antimicrobial and anticancer region. *J. Am. Chem. Soc.* **2006**, *128*, 5776-5785.

(294) Meng, H.; Kumar, K. Antimicrobial activity and protease stability of peptides containing fluorinated amino acids. *J. Am. Chem. Soc.* **2007**, *129*, 15615-15622.

(295) Molhoek, E. M.; Van Dijk, A.; Veldhuizen, E. J.; Haagsman, H. P.; Bikker, F. J. Improved proteolytic stability of chicken cathelicidin-2 derived peptides by D-amino acid substitutions and cyclization. *Peptides* **2011**, *32*, 875-880.

(296) Shagaghi, N.; Clayton, A. H.; Aguilar, M.-I.; Lee, T.-H.; Palombo, E. A.; Bhave, M. Effects of rationally designed physico-chemical variants of the peptide PuroA on biocidal activity towards bacterial and mammalian cells. *Int. J. Mol. Sci.* **2020**, *21*, 8624-8647.

(297) Avrahami, D.; Shai, Y. Conjugation of a magainin analogue with lipophilic acids controls hydrophobicity, solution assembly, and cell selectivity. *Biochemistry* **2002**, *41*, 2254-2263.

(298) Chionis, K.; Krikorian, D.; Koukkou, A. I.; Sakarellos-Daitsiotis, M.; Panou-Pomonis, E. Synthesis and biological activity of lipophilic analogs of the cationic antimicrobial active peptide anoplin. *J. Pept. Sci.* **2016**, *22*, 731-736.

(299) Lau, Y. H.; De Andrade, P.; Wu, Y.; Spring, D. R. Peptide stapling techniques based on different macrocyclisation chemistries. *Chem. Soc. Rev.* **2015**, *44*, 91-102.

(300) Lai, Z.; Yuan, X.; Chen, H.; Zhu, Y.; Dong, N.; Shan, A. Strategies employed in the design of antimicrobial peptides with enhanced proteolytic stability. *Biotechnol. Adv.* **2022**, *59*, 107962-107982.

(301) Chou, P. Y. F., Gerald D. Empirical predictions of protein conformation. *Annu. Rev. Biochem.* **1978**, *47*, 251-276.

(302) Blondelle, S. E.; Houghten, R. A. Hemolytic and antimicrobial activities of the twenty-four individual omission analogs of melittin. *Biochemistry* **1991**, *30*, 4671-4678.

(303) Blondelle, S. E.; Houghten, R. A. Probing the relationships between the structure and hemolytic activity of melittin with a complete set of leucine substitution analogs. *Pept. Res.* **1991**, *4*, 12-18.

(304) Chen, H.-C. B., Judith H Morell, John L Huang, CM. Synthetic magainin analogues with improved antimicrobial activity. *FEBS Lett.* **1988**, *236*, 462-466.

(305) Dathe, M.; Wieprecht, T. Structural features of helical antimicrobial peptides: their potential to modulate activity on model membranes and biological cells. *Biochim. Biophys. Acta, Biomembr.* **1999**, *1462*, 71-87.

(306) Moore, A. J.; Beazley, W. D.; Bibby, M. C.; Devine, D. A. Antimicrobial activity of cecropins. *J. Antimicrob. Chemother.* **1996**, *37*, 1077-1089.

(307) Thennarasu, S.; Nagaraj, R. Specific antimicrobial and hemolytic activities of 18-residue peptides derived from the amino terminal region of the toxin pardaxin. *Protein Eng., Des. Sel.* **1996**, *9*, 1219-1224.

(308) Andreu, D. M., RB Steiner, Haakan Boman, Hans G. N-terminal analogs of cecropin A: synthesis, antibacterial activity, and conformational properties. *Biochemistry* **1985**, *24*, 1683-1688.

(309) Gazit, E.; Boman, A.; Boman, H. G.; Shai, Y. Interaction of the mammalian antibacterial peptide cecropin P1 with phospholipid vesicles. *Biochemistry* **1995**, *34*, 11479-11488.

(310) Pouny, Y.; Rapaport, D.; Mor, A.; Nicolas, P.; Shai, Y. Interaction of antimicrobial dermaseptin and its fluorescently labeled analogs with phospholipid membranes. *Biochemistry* **1992**, *31*, 12416-12423.

(311) Oren, Z.; Lerman, J. C.; Gudmundsson, G. H.; Agerberth, B.; Shai, Y. Structure and organization of the human antimicrobial peptide LL-37 in phospholipid membranes: relevance to the molecular basis for its non-cell-selective activity. *Biochem. Cell Biol.* **1999**, *341*, 501-513.

(312) Krause, E.; Beyermann, M.; Fabian, H.; Dathe, M.; Rothemund, S.; Bienert, M. Conformation of a water-soluble β-sheet model peptide. A circular dichroism and Fourier-transform infrared spectroscopie study of double D-amino acid replacements. *Int. J. Pept. Res. Ther.* **1996**, *48*, 559-568.

(313) Conlon, J. M.; Mechkarska, M. Host-defense peptides with therapeutic potential from skin secretions of frogs from the family pipidae. *Pharmaceuticals* **2014**, *7*, 58-77.

(314) Dathe, M.; Nikolenko, H.; Meyer, J.; Beyermann, M.; Bienert, M. Optimization of the antimicrobial activity of magainin peptides by modification of charge. *FEBS Lett.* **2001**, *501*, 146-150.

(315) Schibli, D. J.; Hunter, H. N.; Aseyev, V.; Starner, T. D.; Wiencek, J. M.; McCray, P. B.; Tack, B. F.; Vogel, H. J. The solution structures of the human β-defensins lead to a better understanding of the potent bactericidal activity of HBD3 against Staphylococcus aureus. *J. Biol. Chem.* **2002**, *277*, 8279-8289.

(316) Dathe, M.; Wieprecht, T.; Nikolenko, H.; Handel, L.; Maloy, W. L.; MacDonald, D. L.; Beyermann, M.; Bienert, M. Hydrophobicity, hydrophobic moment and

angle subtended by charged residues modulate antibacterial and haemolytic activity of amphipathic helical peptides. *FEBS Lett.* **1997**, *403*, 208-212.

(317) Bessalle, R.; Haas, H.; Goria, A.; Shalit, I.; Fridkin, M. Augmentation of the antibacterial activity of magainin by positive-charge chain extension. *Antimicrob. Agents Chemother.* **1992**, *36*, 313-317.

(318) Matsuzaki, K.; Nakamura, A.; Murase, O.; Sugishita, K.-i.; Fujii, N.; Miyajima, K. Modulation of magainin 2− lipid bilayer interactions by peptide charge. *Biochemistry* **1997**, *36*, 2104-2111.

(319) Matsuzaki, K.; Sugishita, K.-i.; Harada, M.; Fujii, N.; Miyajima, K. Interactions of an antimicrobial peptide, magainin 2, with outer and inner membranes of Gram-negative bacteria. *Biochim. Biophys. Acta, Biomembr.* **1997**, *1327*, 119-130.

(320) Blondelle, S. E.; Houghten, R. A. Design of model amphipathic peptides having potent antimicrobial activities. *Biochemistry* **1992**, *31*, 12688-12694.

(321) Kiyota, T.; Lee, S.; Sugihara, G. Design and Synthesis of Amphiphilic α-Helical Model Peptides with Systematically Varied Hydrophobic− Hydrophilic Balance and Their Interaction with Lipid-and Bio-Membranes. *Biochemistry* **1996**, *35*, 13196-13204.

(322) Ganz, T. Defensins: antimicrobial peptides of innate immunity. *Nat. Rev. Immunol.* **2003**, *3*, 710-720.

(323) Lehrer, R. I. Primate defensins. *Nat. Rev. Microbiol.* **2004**, *2*, 727-738.

(324) Selsted, M. E.; Ouellette, A. J. Mammalian defensins in the antimicrobial immune response. *Nat. Immunol.* **2005**, *6*, 551-557.

(325) Unger, T.; Oren, Z.; Shai, Y. The effect of cyclization of magainin 2 and melittin analogues on structure, function, and model membrane interactions: implication to their mode of action. *Biochemistry* **2001**, *40*, 6388-6397.

(326) Wieprecht, T.; Dathe, M.; Krause, E.; Beyermann, M.; Maloy, W. L.; MacDonald, D. L.; Bienert, M. Modulation of membrane activity of amphipathic, antibacterial peptides by slight modifications of the hydrophobic moment. *FEBS Lett.* **1997**, *417*, 135-140.

(327) Dathe, M.; Macdonald, D.; Maloy, W.; Beyermann, M.; Krause, E.; Bienert, M.: The influence of structural motifs of amphipathic peptides on the permeabilization of lipid bilayers and the antibacterial and hemolytic activity. In *Peptide Science—Present and Future*; Springer, 1999; pp 684-686.

(328) Tossi, A.; Sandri, L.; Giangaspero, A. Amphipathic, α-helical antimicrobial peptides. *Pept. Sci.* **2000**, *55*, 4-30.

(329) Yeaman, M. R.; Yount, N. Y. Mechanisms of antimicrobial peptide action and resistance. *Pharmacol. Rev.* **2003**, *55*, 27-55.

(330) Eisenberg, D. Three-dimensional structure of membrane and surface proteins. *Annu. Rev. Biochem.* **1984**, *53*, 595-623.

(331) Brasseur, R. Differentiation of lipid-associating helices by use of three-dimensional molecular hydrophobicity potential calculations. *J. Biol. Chem.* **1991**, *266*, 16120-16127.

(332) Matsuzaki, K.; Sugishita, K.; Fujii, N.; Miyajima, K. Molecular basis for membrane selectivity of an antimicrobial peptide, magainin 2. *Biochemistry* **1995**, *34*, 3423-3429.

(333) Dathe, M.; Schümann, M.; Wieprecht, T.; Winkler, A.; Beyermann, M.; Krause, E.; Matsuzaki, K.; Murase, O.; Bienert, M. Peptide helicity and membrane surface charge modulate the balance of electrostatic and hydrophobic interactions with lipid bilayers and biological membranes. *Biochemistry* **1996**, *35*, 12612-12622.

(334) Chen, Y.; Guarnieri, M. T.; Vasil, A. I.; Vasil, M. L.; Mant, C. T.; Hodges, R. S. Role of peptide hydrophobicity in the mechanism of action of α-helical antimicrobial peptides. *Antimicrob. Agents Chemother.* **2007**, *51*, 1398-1406.

(335) Bessalle, R.; Gorea, A.; Shalit, I.; Metzger, J. W.; Dass, C.; Desiderio, D. M.; Fridkin, M. Structure-function studies of amphiphilic antibacterial peptides. *J. Med. Chem.* **1993**, *36*, 1203-1209.

(336) Ohmori, N.; Niidome, T.; Hatakeyama, T.; Mihara, H.; Aoyagi, H. Interaction of α-helical peptides with phospholipid membrane: effects of chain length and hydrophobicity of peptides. *J. Pept. Sci.* **1998**, *51*, 103-109.

(337) Chan, D. I.; Prenner, E. J.; Vogel, H. J. Tryptophan-and arginine-rich antimicrobial peptides: structures and mechanisms of action. *Biochim. Biophys. Acta, Biomembr.* **2006**, *1758*, 1184-1202.

(338) Yau, W.-M.; Wiey, W. C.; Gawrisch, K.; White, S. H. The preference of tryptophan for membrane interfaces. *Biochemistry* **1998**, *37*, 14713-14718.

(339) Dougherty, D. A. Cation-π interactions in chemistry and biology: a new view of benzene, Phe, Tyr, and Trp. *Science* **1996**, *271*, 163-168.

(340) Mojsoska B, Z. R., Jenssen H. Structure-Activity Relationship Study of Novel Peptoids That Mimic the Structure of Antimicrobial Peptides. *Antimicrob. Agents Chemother.* **2015**, *59*, 4112-4120.

(341) Brogden, N. K.; Brogden, K. A. Will new generations of modified antimicrobial peptides improve their potential as pharmaceuticals? *Int. J. Antimicrob. Agents* **2011**, *38*, 217-225.

(342) Tam, J. P.; Lu, Y.-A.; Yang, J.-L. Correlations of cationic charges with salt sensitivity and microbial specificity of cystine-stabilized β-strand antimicrobial peptides. *J. Biol. Chem.* **2002**, *277*, 50450-50456.

(343) Hua, J. e. a. Activity of antimicrobial peptide mimetics in the oral cavity: I. Activity against biofilms of Candida albicans. *Mol. Oral Microbiol.* **2010**, *25*, 418-425.

(344) Mojsoska, B.; Zuckermann, R. N.; Jenssen, H. Structure-activity relationship study of novel peptoids that mimic the structure of antimicrobial peptides. *Antimicrob. Agents Chemother.* **2015**, *59*, 4112-4120.

(345) Radzishevsky, I. S.; Rotem, S.; Bourdetsky, D.; Navon-Venezia, S.; Carmeli, Y.; Mor, A. Improved antimicrobial peptides based on acyl-lysine oligomers. *Nat. Biotechnol.* **2007**, *25*, 657-659.

(346) Piers, K. L. B., Melissa H Hancock, Robert EW. Recombinant DNA procedures for producing small antimicrobial cationic peptides in bacteria. *Gene* **1993**, *134*, 7-13.

(347) Piers, K. L.; Brown, M. H.; Hancock, R. Improvement of outer membrane-permeabilizing and lipopolysaccharide-binding activities of an antimicrobial cationic peptide by C-terminal modification. *Antimicrob. Agents Chemother.* **1994**, *38*, 2311-2316.

(348) Wade, D.; Andreu, D.; Mitchell, S.; Silveira, A.; Boman, A.; Boman, H.; Merrifield, R. B. Antibacterial peptides designed as analogs or hybrids of cecropins and melittin. *Int. J. Pept. Protein Res.* **1992**, *40*, 429-436.

(349) Steiner, H., David Merrifield, Ri B. Binding and action of cecropin and cecropin analogues: antibacterial peptides from insects. *Biochim. Biophys. Acta, Biomembr.* **1988**, *939*, 260-266.

(350) Qiu, X.-Q.; Wang, H.; Lu, X.-F.; Zhang, J.; Li, S.-F.; Cheng, G.; Wan, L.; Yang, L.; Zuo, J.-Y.; Zhou, Y.-Q. An engineered multidomain bactericidal peptide as a model for targeted antibiotics against specific bacteria. *Nat. Biotechnol.* **2003**, *21*, 1480-1485.

(351) Qiu, X.-Q.; Zhang, J.; Wang, H.; Wu, G. Y. A novel engineered peptide, a narrow-spectrum antibiotic, is effective against vancomycin-resistant Enterococcus faecalis. *Antimicrob. Agents Chemother.* **2005**, *49*, 1184-1189.

(352) Eckert, R.; He, J.; Yarbrough, D. K.; Qi, F.; Anderson, M. H.; Shi, W. Targeted killing of Streptococcus mutans by a pheromone-guided "smart" antimicrobial peptide. *Antimicrob. Agents Chemother.* **2006**, *50*, 3651-3657.

(353) He, J.; Anderson, M. H.; Shi, W.; Eckert, R. Design and activity of a 'dual-targeted'antimicrobial peptide. *Int. J. Antimicrob. Agents* **2009**, *33*, 532-537.

(354) Rozgonyi, F.; Szabo, D.; Kocsis, B.; Ostorhazi, E.; Abbadessa, G.; Cassone, M.; Wade, J.; Otvos Jr, L. The antibacterial effect of a proline-rich antibacterial peptide A3-APO. *Curr. Med. Chem.* **2009**, *16*, 3996-4002.

(355) Szabo, D.; Ostorhazi, E.; Binas, A.; Rozgonyi, F.; Kocsis, B.; Cassone, M.; Wade, J. D.; Nolte, O.; Otvos Jr, L. The designer proline-rich antibacterial peptide A3-APO is effective against systemic Escherichia coli infections in different mouse models. *Int. J. Antimicrob. Agents* **2010**, *35*, 357-361.

(356) Fox, M. A.; Thwaite, J. E.; Ulaeto, D. O.; Atkins, T. P.; Atkins, H. S. Design and characterization of novel hybrid antimicrobial peptides based on cecropin A, LL-37 and magainin II. *Peptides* **2012**, *33*, 197-205.

(357) Morris, C. J.; Beck, K.; Fox, M. A.; Ulaeto, D.; Clark, G. C.; Gumbleton, M. Pegylation of antimicrobial peptides maintains the active peptide conformation, model membrane interactions, and antimicrobial activity while improving lung tissue biocompatibility following airway delivery. *Antimicrob. Agents Chemother.* **2012**, *56*, 3298-3308.

(358) Tan, T.; Wu, D.; Li, W.; Zheng, X.; Li, W.; Shan, A. High specific selectivity and membrane-active mechanism of synthetic cationic hybrid antimicrobial peptides based on the peptide FV7. *Int. J. Mol. Sci.* **2017**, *18*, 339-356.

(359) Klubthawee, N.; Adisakwattana, P.; Hanpithakpong, W.; Somsri, S.; Aunpad, R. A novel, rationally designed, hybrid antimicrobial peptide, inspired by cathelicidin and

aurein, exhibits membrane-active mechanisms against Pseudomonas aeruginosa. *Sci. Rep.* **2020**, *10*, 1-17.

(360) Shang, L.; Li, J.; Song, C.; Nina, Z.; Li, Q.; Chou, S.; Wang, Z.; Shan, A. Hybrid Antimicrobial Peptide Targeting Staphylococcus aureus and Displaying Anti-infective Activity in a Murine Model. *Front. Microbiol.* **2020**, *11*, 1767-1780.

(361) Kim, H.; Jang, J. H.; Kim, S. C.; Cho, J. H. Development of a novel hybrid antimicrobial peptide for targeted killing of Pseudomonas aeruginosa. *Eur. J. Med. Chem.* **2020**, *185*, 111814-111824.

(362) Eckert, R.; He, J.; Yarbrough, D. K.; Qi, F.; Anderson, M. H.; Shi, W. Targeted killing of Streptococcus mutans by a pheromone-guided "smart" antimicrobial peptide. *Antimicrobial agents and chemotherapy* **2006**, *50*, 3651-3657.

(363) Schroeder, B. O.; Wu, Z.; Nuding, S.; Groscurth, S.; Marcinowski, M.; Beisner, J.; Buchner, J.; Schaller, M.; Stange, E. F.; Wehkamp, J. Reduction of disulphide bonds unmasks potent antimicrobial activity of human β-defensin 1. *Nature* **2011**, *469*, 419-423.

(364) Larrick, J. W. H., Michimasa Shimomoura, Yuko Yoshida, Masao Zheng, Hui Zhong, Jian Wright, Susan C. Antimicrobial activity of rabbit CAP18-derived peptides. *Antimicrob. Agents Chemother.* **1993**, *37*, 2534-2539.

(365) Larrick, J. W.; Hirata, M.; Zhong, J.; Wright, S. C. Anti-microbial activity of human CAP18 peptides. *Immunotechnology* **1995**, *1*, 65-72.

(366) Travis, S. M.; Anderson, N. N.; Forsyth, W. R.; Espiritu, C.; Conway, B. D.; Greenberg, E.; McCray Jr, P. B.; Lehrer, R. I.; Welsh, M. J.; Tack, B. F. Bactericidal activity of mammalian cathelicidin-derived peptides. *Infect. Immun.* **2000**, *68*, 2748-2755.

(367) Valdezate, S.; Vindel, A.; Loza, E.; Baquero, F.; Cantón, R. Antimicrobial susceptibilities of unique Stenotrophomonas maltophilia clinical strains. *Antimicrob. Agents Chemother.* **2001**, *45*, 1581-1584.

(368) Brogden, K. A.; Kalfa, V.; Ackermann, M. R.; Palmquist, D.; McCray Jr, P. B.; Tack, B. The ovine cathelicidin SMAP29 kills ovine respiratory pathogens in vitro and in an ovine model of pulmonary infection. *Antimicrob. Agents Chemother.* **2001**, *45*, 331-334.

(369) Suzuki, M. M.; Matsumoto, M.; Yamamoto, A.; Ochiai, M.; Horiuchi, Y.; Niwa, M.; Omi, H.; Kobayashi, T.; Takagi, T. Molecular design of LPS-binding peptides. *J. Microbiol. Methods* **2010**, *83*, 153-155.

(370) Yu, Q.; Lehrer, R. I.; Tam, J. P. Engineered salt-insensitive α-defensins with end-to-end circularized structures. *J. Biol. Chem.* **2000**, *275*, 3943-3949.

(371) Levengood, M. R.; van der Donk, W. A. Use of lantibiotic synthetases for the preparation of bioactive constrained peptides. *Bioorg. Med. Chem. Lett.* **2008**, *18*, 3025-3028.

(372) De Veer, S. J.; Kan, M.-W.; Craik, D. J. Cyclotides: from structure to function. *Chem. Rev.* **2019**, *119*, 12375-12421.

(373) Peschen, D.; Li, H.-P.; Fischer, R.; Kreuzaler, F.; Liao, Y.-C. Fusion proteins comprising a Fusarium-specific antibody linked to antifungal peptides protect plants against a fungal pathogen. *Nat. Biotechnol.* **2004**, *22*, 732-738.

(374) Chu-Kung, A. F.; Nguyen, R.; Bozzelli, K. N.; Tirrell, M. Chain length dependence of antimicrobial peptide–fatty acid conjugate activity. *J. Colloid Interface Sci.* **2010**, *345*, 160-167.

(375) Ding, B.; Taotofa, U.; Orsak, T.; Chadwell, M.; Savage, P. B. Synthesis and characterization of peptide− cationic steroid antibiotic conjugates. *Org. Lett.* **2004**, *6*, 3433-3436.

(376) Leupold, E.; Nikolenko, H.; Dathe, M. Apolipoprotein E peptide-modified colloidal carriers: the design determines the mechanism of uptake in vascular endothelial cells. *Biochim. Biophys. Acta, Biomembr.* **2009**, *1788*, 442-449.

(377) Chou PY, Fasman, GD. Conformational parameters for amino acids in helical, β-sheet, and random coil regions calculated from protein. *Biochemistry* **1974**, *13*, 211-222.

(378) Blondelle SE, H. R. Design of model amphipathic peptides having potent antimicrobial activities. *Biochemistry* **1992**, *31*, 12688-12694.

(379) Beven L, C. S., Dufourcq J, Wieslander Å, Wr´ oblewski H. T. The´ antibiotic activity of cationic linear amphipathic peptides: lessons from the action of leucine/lysine copolymers on bacteria of the class Mollicutes. . *Eur. J. Biochem.* **2003**, *270*, 2207-2217.

(380) Haynie SL, C. G., Doele BA. Antimicrobial Activities of Amphiphilic Peptides Covalently Bonded to a Water-Insoluble Resin. *Antimicrob. Agents Chemother.* **1995**, *39*, 301–307.

(381) Won HS, S. M., Jung SJ, Lee SJ, Kang SJ, Son WS, Kim HJ, Park TK, Park SJ, Lee BJ. Structural determinants for the membrane interaction of novel bioactive undecapeptides derived from gaegurin 5. *J. Med. Chem.* **2006**, *49*, 4886–4895.

(382) Oh D, S. S., Lee S, Kang JH, Kim SD, Ryu PD, Hahm KS, Kim Y. . Role of the hinge region and the tryptophan residue in the synthetic antimicrobial peptides, cecropin A(1–8)-Magainin 2(1–12) and its analogues, on their antibiotic activities and structures. *Biochemistry* **2000**, *39*, 11855–11964.

(383) Ridder ANJA, M. S., Stam JG, Kuhn A, de Kruijff B, Killian JA. Analysis of the role of interfacial tryptophan residues in controlling the topology of membrane proteins. *Biochemistry* **2000**, *39*, 6521-6528.

(384) Hu W, L. K., Cross TA.. Tryptophans in membrane proteins: indole ring orientations and functional implications in the gramicidin channel. *Biochemistry* **1993**, *32*, 7035-7047.

(385) Chou PY, F. G. Conformational parameters for amino acids in helical, β-sheet, and random coil regions calculated from proteins. *Biochemistry* **1974**, *13*, 211-222.

(386) Park K, O. D., Shin SY, Hahm KS, Kim Y. Structural studies of porcine myeloid antibacterial peptide PMAP-23 and its analogues in DPC micelles by NMR spectroscopy. *Biochem. Biophys. Res. Commun.* **2002**, *290*, 204-212.

(387) Won, H. S.; Park, S. H.; Kim, H. E.; Hyun, B.; Kim, M.; Lee, B. J.; Lee, B. J. Effects of a tryptophanyl substitution on the structure and antimicrobial activity of C-terminally truncated gaegurin 4. *Eur. Biochem. J.* **2002**, *269*, 4367-4374.

(388) Epand RM, V. H. Diversity of antimicrobial peptides and their mechanisms of action. . *Biochim. Biophys. Acta* **1999**, *1462*, 11-28.

(389) N., S. Antimicrobial peptides with unusual amino acid compositions and unusual structures. *Curr. Med. Chem.* **2006**, *13*, 679–696

(390) Won HS, J. S., Kim HE, Seo MD, Lee BJ. Systematic peptide engineering and structural characterization to search for the shortest antimicrobial peptide analogue of gaegurin 5. *J. Biol. Chem.* **2004**, *279*, 14784-14791.

(391) Won HS, K. S., Lee BJ. Action mechanism and structural requirements of the antimicrobial peptides, gaegurins. *Biochim. Biophys. Acta* **2008**, *1788*, 1620-1629.

(392) H.J. Vogel, D. J. S., W. Jing, E.M. Lohmeier-Vogel, R.F. Epand, R.M. Towards a structure–function analysis of bovine lactoferricin and related tryptophan- and arginine-containing peptides. *Biochem. Cell Biol.* **2002**, *80*, 49-63.

(393) M.B. Strøm, B. E. H., Ø. Rekdal, M.L. Skar, W. Stensen, J.S. Svendsen, I. Important structural features of 15-residue lactoferricin derivatives and methods for improvement of antimicrobial activity,. *Biochem. Cell Biol.* **2002**, *80*, 65-74.

(394) Denning, D. W. Echinocandins and pneumocandins--a new antifungal class with a novel mode of action. *J. Antimicrob. Chemother.* **1997**, *40*, 611-614.

(395) L. Ofek, S. C., R. Rahmani, K. Kabha, D. Tamarkin, Y. Herzig, E. Rubinstein, Antibacterial synergism of polymyxin B nonapeptide andhydrophobic antibiotics in

experimental Gram-negative infections in mice, . *Antimicrob. Agents Chemother.* **1994**, *38*, 374-377.

(396) W. E . Alborn , N. E. A., D. A. Preston ,. Daptomycin disrupts membrane potential in growing Staphylococcus aureus. *Antimicrob. Agents Chemother.* **1991**, *35*, 2282-2287.

(397) C. Auvin-Guette, S. R., Y. Prigent, B. Bodo,. Trichogin A IV, an 11-residue lipopeptaibol from Trichoderma longibrachiatum. *J. Am. Chem. Soc.* **1992**, *114*, 2170-2174.

(398) C. Toniolo, M. C., F. Formaggio, C. Peggion, R.F. Epand, R.M. Lipopeptaibols, a novel family of membrane active, antimicrobial peptides,. *Cell. Mol. Life Sci.* **2001**, *58*, 1179-1188.

(399) C.L. Bender, F. A.-C., D.C. Gross, P 63. seudomonas syringae phytotoxins: mode of action, regulation, and biosynthesis by peptide and polyketide synthetases, . *Microbiol. Mol. Biol. Rev.* **1999**, *63*, 266-292.

(400) M.D. Resh, B. Fatty acylation of proteins: new insights into membrane targeting of myristoylated and palmitoylated proteins,. *Biophys. Acta* **1999**, *1451*, 1-16.

(401) D.W. Denning, r. Echinocandins and pneumocandins—a new antifungal class with a novel mode of action,. *J. Antimicrob. Chemother.* **1997**, *40*, 611-614.

(402) H. Wakabayashi, H. M., K. Hashimoto, S. Teraguchi, M. Takase, H. Hayasawa,y,. N-acylated and d enantiomer derivatives of a nonamer core peptide of lactoferricin B showing improved antimicrobial activit. *Antimicrob. Agents Chemother.* **1999**, *43*, 1267-1269.

(403) N.A. Lockwood, J. R. H., M.V. Tirrell, K.H. Mayo,. Acylation of SC4 dodecapeptide increases bactericidal potency against Grampositive bacteria, including drug-resistant strains,. *Biochem. J.* **2004**, *378*, 93-103.

(404) D. Avrahami, Y. S. Bestowing antifungal and antibacterial activities by lipophilic acid conjugation to d,l-amino acid-containing antimicrobial peptides: a plausible mode of action,. *Biochemistry* **2003**, *42*, 14946-14956.

(405) A.F. Chu-Kung, K. N. B., N.A. Lockwood, J.R. Haseman, K.H. Mayo, M.V. Tirrell,. Promotion of peptide antimicrobial activity by fatty acid conjugation. *Bioconjug. Chem* **2004**, *15*, 530-535.

(406) P. Mak, J. P., A. Dubin, M.S. Reed, S.E. Bowers, M.T. Fallon, W.M. Shafer,. The increased bactericidal activity of a fatty acidmodified synthetic antimicrobial peptide of human cathepsin G correlates with its enhanced capacity to interact with model membranes,. *Int. J. Antimicrob. Agents* **2003**, *21*, 13-19.

(407) A. Majerle, J. K., P. Jerala,. Enhancement of antibacterial and lipopolysaccharide binding activities of a human lactoferrin peptide fragment by the addition of acyl chain. *J. Antimicrob. Chemother.* **2003**, *51*, 1159-1165.

(408) A. Rustici, M. V., R. Faggioni, M. Sironi, P. Ghezzi, S. Quataert, B. Green, M. Porro,. Molecular mapping and detoxification of the lipid A binding site by synthetic peptides,. *Science* **1993**, *259*, 361-365.

(409) A.K. Duwe, C. A. R., G.B. Horsman, S.I. Vas,. In vitro cytotoxicity and antibiotic activity of polymyxin B nonapeptide,. *Antimicrob. Agents Chemother.* **1986**, *30*, 340-341.

(410) Thennarasu S, L. D., Tan A, Kari UP, Ramamoorthy A. Antimicrobial activity and membrane selective interactions of a synthetic lipopeptide MSI-843. *Biochim. Biophys. Acta* **2005**, *1711*, 49-58.

(411) Arik Makovitzki, D. A., and Yechiel Shai. Ultrashort antibacterial and antifungal lipopeptides. *Proc. Natl. Acad. Sci.* **2006**, *103*, 15997-16002.

(412) Azmi, F. E., A. G.; Khalil, Z. G.; Hussein, W. M.; Kavanagh, A.; Huang, J. X.; Quezada, M.; Blaskovich, M. A. T.; Capon, R. J.; Cooper, M. A.; Skwarczynski, M.; Toth, I. Self-assembling lipopeptides with a potent activity against Gram-positive bacteria, including multidrug resistant strains. *Nanomedicine* **2015**, *10*, 3559-3371.

(413) Yuxin Fang, W. Z., Yue Wang, Tianrong Xun, Dongguo Lin, Wenjun Liu, Jingyu Wang, Lin Lv, Shuwen Liu , Jian He. Tuning the antimicrobial phar macophore t o enable discovery of short lipopeptides with multipl e modes of action. *Eur. J. Med. Chem.* **2014**, *83*, 36-44.

(414) Sikorska E, D. M., Greber K, Iłowska E, Pogorzelska A, Kamysz W. Self-assembly and interactions of short antimicrobial cationiclipopeptides with membrane lipids: ITC, FTIR and molecular dynamics studies. *Biochim. Biophys. Acta* **2014**, *1838*, 2625-2634.

(415) Ghosh C, M. G., Akkapeddi P, Yarlagadda V, Hoque J, Uppu DS, Konai MM, Haldar J. Small Molecular Antibacterial Peptoid Mimics: The Simpler the Better! *J. Med. Chem.* **2014**, *57*, 1428 −1436.

(416) Konai, M. M.; Haldar, J., Lysine-Based Small Molecules That Disrupt Biofi lms and Kill bothActively Growing Planktonic and Nondividing Stationary Phase Bacteria. *ACS Infect. Dis.* **2015,** *1*, 469-478.

(417) Sandeep Lohan, S. S. C., Gopal S. Bisht. Systematic Study of Non-Natural Short Cationic Lipopeptides as Novel Broad-Spectrum Antimicrobial Agents. *Chem. Biol. Drug Des.* **2013**, *82*, 557-566.

(418) Thennarasu, S.; Lee, D.-K.; Tan, A.; Kari, U. P.; Ramamoorthy, A. Antimicrobial activity and membrane selective interactions of a synthetic lipopeptide MSI-843. *Biochim. Biophys. Acta, Biomembr.* **2005**, *1711*, 49-58.

(419) Laverty, G.; McLaughlin, M.; Shaw, C.; Gorman, S. P.; Gilmore, B. F. Antimicrobial activity of short, synthetic cationic lipopeptides. *Chem. Biol. Drug Des.* **2010**, *75*, 563-569.

(420) Fang, Y.; Zhong, W.; Wang, Y.; Xun, T.; Lin, D.; Liu, W.; Wang, J.; Lv, L.; Liu, S.; He, J. Tuning the antimicrobial pharmacophore to enable discovery of short lipopeptides with multiple modes of action. *Eur. J. Med. Chem.* **2014**, *83*, 36-44.

(421) Makovitzki, A.; Avrahami, D.; Shai, Y. Ultrashort antibacterial and antifungal lipopeptides. *Proc. Natl. Acad. Sci.* **2006**, *103*, 15997-16002.

(422) Grgurina, I.; Bensaci, M.; Pocsfalvi, G.; Mannina, L.; Cruciani, O.; Fiore, A.; Fogliano, V.; Sorensen, K. N.; Takemoto, J. Y. Novel cyclic lipodepsipeptide from Pseudomonas syringae pv. lachrymans strain 508 and syringopeptin antimicrobial activities. *Antimicrob. Agents Chemother.* **2005**, *49*, 5037-5045.

(423) Lavermicocca, P.; Iacobellis, N. S.; Simmaco, M.; Graniti, A. Biological properties and spectrum of activity ofPseudomonas syringaepv. syringaetoxins. *Physiol. Mol. Plant Pathol.* **1997**, *50*, 129-140.

(424) Burr, D. B.; Milgrom, C.; Fyhrie, D.; Forwood, M.; Nyska, M.; Finestone, A.; Hoshaw, S.; Saiag, E.; Simkin, A. In vivo measurement of human tibial strains during vigorous activity. *Bone* **1996**, *18*, 405-410.

(425) Bassarello, C.; Lazzaroni, S.; Bifulco, G.; Lo Cantore, P.; Iacobellis, N. S.; Riccio, R.; Gomez-Paloma, L.; Evidente, A. Tolaasins A− E, Five new lipodepsipeptides produced by Pseudomonas tolaasii. *J. Nat. Prod.* **2004**, *67*, 811-816.

(426) Pedras, M. H.; de Lemos, M. J. Computation of Turbulent Flow in Porous Media Using a Low-Reynolds K-ε Modeland AN Infinite Array of Transversally Displaced Elliptic Rods. *NUMER HEAT TR A-APPL* **2003**, *43*, 585-602.

(427) Ledger, E. V.; Sabnis, A.; Edwards, A. M. Polymyxin and lipopeptide antibiotics: membrane-targeting drugs of last resort. *Microbiology* **2022**, *168*, 1-20.

(428) Zhang, Y.-M.; Rock, C. O. Membrane lipid homeostasis in bacteria. *Nat. Rev. Microbiol.* **2008**, *6*, 222-233.

(429) Matsuzaki, K. Control of cell selectivity of antimicrobial peptides. *Biochim. Biophys. Acta, Biomembr.* **2009**, *1788*, 1687-1692.

(430) Tang, Y.-W.; Sails, A.: *Molecular medical microbiology*; Academic press, 2014.

(431) Gan, B. H.; Gaynord, J.; Rowe, S. M.; Deingruber, T.; Spring, D. R. The multifaceted nature of antimicrobial peptides: Current synthetic chemistry approaches and future directions. *Chem. Soc. Rev.* **2021**, *50*, 7820-7880.

(432) Wiedemann, I.; Breukink, E.; van Kraaij, C.; Kuipers, O. P.; Bierbaum, G.; de Kruijff, B.; Sahl, H.-G. Specific binding of nisin to the peptidoglycan precursor lipid II combines pore formation and inhibition of cell wall biosynthesis for potent antibiotic activity. *J. Biol. Chem.* **2001**, *276*, 1772-1779.

(433) Pokhrel, R.; Bhattarai, N.; Baral, P.; Gerstman, B. S.; Park, J. H.; Handfield, M.; Chapagain, P. P. Molecular mechanisms of pore formation and membrane disruption by the antimicrobial lantibiotic peptide Mutacin 1140. *Phys. Chem. Chem. Phys.* **2019**, *21*, 12530-12539.

(434) Kreutzberger, M. A. P., Antje A., Paulo F. Daptomycin–phosphatidylglycerol domains in lipid membranes. *Langmuir* **2017**, *33*, 13669-13679.

(435) Brogden, K. Antimicrobial Peptides: Pore Formers or Metabolic Inhibitors in Bacteria? *Nat. Rev. Microbiol.* **2005**, *3*, 238-250.

(436) Wiey, W. C. Describing the mechanism of antimicrobial peptide action with the interfacial activity model. *ACS Chem. Biol.* **2010**, *5*, 905-917.

(437) Lee, T.-H.; N Hall, K.; Aguilar, M.-I. Antimicrobial peptide structure and mechanism of action: a focus on the role of membrane structure. *Curr. Top. Med. Chem.* **2016**, *16*, 25-39.

(438) Teixeira, V.; Feio, M. J.; Bastos, M. Role of lipids in the interaction of antimicrobial peptides with membranes. *Prog. Lipid Res.* **2012**, *51*, 149-177.

(439) Brogden, K. A. Antimicrobial peptides: pore formers or metabolic inhibitors in bacteria? *Nat. Rev. Microbiol.* **2005**, *3*, 238-250.

(440) Miteva, M.; Andersson, M.; Karshikoff, A.; Otting, G. Molecular electroporation: a unifying concept for the description of membrane pore formation by antibacterial peptides, exemplified with NK-lysin. *FEBS Lett.* **1999**, *462*, 155-158.

(441) Ehrenstein, G. L., Harold. Electrically gated ionic channels in lipid bilayers. *Q. Rev. Biophys.* **1977**, *10*, 1-34.

(442) Breukink, E.; de Kruijff, B. The lantibiotic nisin, a special case or not? *Biochim. Biophys. Acta, Biomembr.* **1999**, *1462*, 223-234.

(443) Béven, L.; Helluin, O.; Molle, G.; Duclohier, H.; Wróblewski, H. Correlation between anti-bacterial activity and pore sizes of two classes of voltage-dependent channel-forming peptides. *Biochim. Biophys. Acta, Biomembr.* **1999**, *1421*, 53-63.

(444) Shai, Y.; Oren, Z. From "carpet" mechanism to de-novo designed diastereomeric cell-selective antimicrobial peptides. *Peptides* **2001**, *22*, 1629-1641.

(445) Sitaram, N.; Nagaraj, R. Interaction of antimicrobial peptides with biological and model membranes: structural and charge requirements for activity. *Biochim. Biophys. Acta, Biomembr.*. **1999**, *1462*, 29-54.

(446) Rozek, A.; Friedrich, C. L.; Hancock, R. E. Structure of the bovine antimicrobial peptide indolicidin bound to dodecylphosphocholine and sodium dodecyl sulfate micelles. *Biochemistry* **2000**, *39*, 15765-15774.

(447) Matsuzaki, K. Why and how are peptide–lipid interactions utilized for self-defense? Magainins and tachyplesins as archetypes. *Biochim. Biophys. Acta, Biomembr.* **1999**, *1462*, 1-10.

(448) Hara, T.; Kodama, H.; Kondo, M.; Wakamatsu, K.; Takeda, A.; Tachi, T.; Matsuzaki, K. Effects of peptide dimerization on pore formation: Antiparallel disulfide-dimerized magainin 2 analogue. *Biopolymers: Original Research on Biomolecules* **2001**, *58*, 437-446.

(449) Yang, L.; Weiss, T. M.; Lehrer, R. I.; Huang, H. W. Crystallization of antimicrobial pores in membranes: magainin and protegrin. *Biophys. J.* **2000**, *79*, 2002-2009.

(450) Uematsu, N.; Matsuzaki, K. Polar angle as a determinant of amphipathic α-helix-lipid interactions: a model peptide study. *Biophys. J.* **2000**, *79*, 2075-2083.

(451) Yonezawa, A.; Kuwahara, J.; Fujii, N.; Sugiura, Y. Binding of tachyplesin I to DNA revealed by footprinting analysis: significant contribution of secondary structure to DNA binding and implication for biological action. *Biochemistry* **1992**, *31*, 2998-3004.

(452) Patrzykat, A.; Friedrich, C. L.; Zhang, L.; Mendoza, V.; Hancock, R. E. Sublethal concentrations of pleurocidin-derived antimicrobial peptides inhibit macromolecular synthesis in Escherichia coli. *Antimicrob. Agents Chemother.* **2002**, *46*, 605-614.

(453) Piers, K. L.; Brown, M. H.; Hancock, R. Improvement of outer membrane-permeabilizing and lipopolysaccharide-binding activities of an antimicrobial cationic peptide by C-terminal modification. *Antimicrob. Agents Chemother.* **1994**, *38*, 2311-2316.

(454) Andreu, D.; Rivas, L. Animal antimicrobial peptides: an overview. *Pept. Sci.* **1998**, *47*, 415-433.

(455) Otvos, L.; O, I.; Rogers, M. E.; Consolvo, P. J.; Condie, B. A.; Lovas, S.; Bulet, P.; Blaszczyk-Thurin, M. Interaction between heat shock proteins and antimicrobial peptides. *Biochemistry* **2000**, *39*, 14150-14159.

(456) Gray, D. A.; Wenzel, M. Multitarget approaches against multiresistant superbugs. *ACS Infect. Dis.* **2020**, *6*, 1346-1365.

(457) Hancock, R. E.; Sahl, H.-G. Antimicrobial and host-defense peptides as new anti-infective therapeutic strategies. *Nat. Biotechnol.* **2006**, *24*, 1551-1557.

(458) Blazyk, J.; Wiegand, R.; Klein, J.; Hammer, J.; Epand, R. M.; Epand, R. F.; Maloy, W. L.; Kari, U. P. A novel linear amphipathic β-sheet cationic antimicrobial peptide with enhanced selectivity for bacterial lipids. *J. Biol. Chem.* **2001**, *276*, 27899-27906.

(459) Pandit, G.; Chowdhury, N.; Abdul Mohid, S.; Bidkar, A. P.; Bhunia, A.; Chatterjee, S. Effect of Secondary Structure and Side Chain Length of Hydrophobic Amino Acid Residues on the Antimicrobial Activity and Toxicity of 14-Residue-Long de novo AMPs. *ChemMedChem* **2021**, *16*, 355-367.

(460) Cheng, J. T.; Hale, J. D.; Elliott, M.; Hancock, R. E.; Straus, S. K. The importance of bacterial membrane composition in the structure and function of aurein 2.2 and selected variants. *Biochim. Biophys. Acta, Biomembr.* **2011**, *1808*, 622-633.

(461) Lee, D.-K.; Bhunia, A.; Kotler, S. A.; Ramamoorthy, A. Detergent-type membrane fragmentation by MSI-78, MSI-367, MSI-594, and MSI-843 antimicrobial peptides and inhibition by cholesterol: a solid-state nuclear magnetic resonance study. *Biochemistry* **2015**, *54*, 1897-1907.

(462) Fernandez, D. I.; Sani, M.-A.; Gehman, J. D.; Hahm, K.-S.; Separovic, F. Interactions of a synthetic Leu–Lys-rich antimicrobial peptide with phospholipid bilayers. *Eur. Biophys. J.* **2011**, *40*, 471-480.

(463) Lee, D.-K.; Brender, J. R.; Sciacca, M. F.; Krishnamoorthy, J.; Yu, C.; Ramamoorthy, A. Lipid composition-dependent membrane fragmentation and pore-forming mechanisms of membrane disruption by pexiganan (MSI-78). *Biochemistry* **2013**, *52*, 3254-3263.

(464) Bhattacharyya, D.; Kim, M.; Mroue, K. H.; Park, M.; Tiwari, A.; Saleem, M.; Lee, D.; Bhunia, A. Role of non-electrostatic forces in antimicrobial potency of a dengue-virus derived fusion peptide VG16KRKP: Mechanistic insight into the interfacial peptide-lipid interactions. *Biochim. Biophys. Acta, Biomembr.* **2019**, *1861*, 798-809.

(465) Alexander, N.; Woetzel, N.; Meiler, J. In *Tilte*2011; IEEE.

(466) Yarlagadda, V.; Akkapeddi, P.; Manjunath, G. B.; Haldar, J. Membrane active vancomycin analogues: a strategy to combat bacterial resistance. *J. Med. Chem.* **2014**, *57*, 4558-4568.

(467) Jo, S.; Kim, T.; Im, W. Automated builder and database of protein/membrane complexes for molecular dynamics simulations. *PLoS One* **2007**, *2*, 1-9.

(468) Wu, E. L.; Cheng, X.; Jo, S.; Rui, H.; Song, K. C.; Dávila-Contreras, E. M.; Qi, Y.; Lee, J.; Monje-Galvan, V.; Venable, R. M. CHARMM-GUI membrane builder toward realistic biological membrane simulations. *J. Comput. Chem.* **2014**, *35*, 1997-2004.

(469) Lindahl, E.; Hess, B.; Van Der Spoel, D. GROMACS 3.0: a package for molecular simulation and trajectory analysis. *Molecular modeling annual* **2001**, *7*, 306-317.

(470) Van Der Spoel, D.; Lindahl, E.; Hess, B.; Groenhof, G.; Mark, A. E.; Berendsen, H. J. GROMACS: fast, flexible, and free. *J. Comput. Chem.* **2005**, *26*, 1701-1718.

(471) Datta, A.; Yadav, V.; Ghosh, A.; Choi, J.; Bhattacharyya, D.; Kar, R. K.; Ilyas, H.; Dutta, A.; An, E.; Mukhopadhyay, J.; Lee, D.; Sanyal, K.; Ramamoorthy, A.; Bhunia, A. Mode of Action of a Designed Antimicrobial Peptide: High Potency against Cryptococcus neoformans. *Biophys. J.* **2016**, *111*, 1724-1737.

(472) Monroc, S.; Badosa, E.; Feliu, L.; Planas, M.; Montesinos, E.; Bardají, E. De Novo Designed Cyclic Cationic Peptides as Inhibitors of Plant Pathogenic Bacteria. *Peptides* **2006**, *27*, 2567-2574.

(473) Haynie, S. L.; Crum, G. A.; Doele, B. A. Antimicrobial Activities of Amphiphilic Peptides Covalently Bonded to a Water-Insoluble Resin. *Antimicrob. Agents Chemother.* **1995**, *39*, 301-307.

(474) Sitaram, N. Antimicrobial Peptides with Unusual Amino Acid Compositions and Unusual Structures. *Curr. Med. Chem.* **2006**, *13*, 679-696.

(475) Won, H. S.; Park, S. H.; Kim, H. E.; Hyun, B.; Kim, M.; Lee, B. J.; Lee, B. J. Effects of a Tryptophanyl Substitution on the Structure and Antimicrobial Activity of C-Terminally Truncated Gaegurin 4. *Eur. J. Biochem.* **2002**, *269*, 4367-4374.

(476) Lee, S. H.; Kim, S. J.; Lee, Y. S.; Song, M. D.; Kim, I. H.; Won, H. S. De Novo Generation of Short Antimicrobial Peptides with Simple Amino Acid Composition. *Regul. Pept.* **2011**, *166*, 36-41.

(477) Kang, S. J.; Won, H. S.; Choi, W. S.; Lee, B. J. De Novo Generation of Antimicrobial LK Peptides with a Single Tryptophan at the Critical Amphipathic Interface. *J. Pept. Sci.* **2009**, *15*, 583-589.

(478) Kim, S. J.; Kim, J. S.; Lee, Y. S.; Sim, D. W.; Lee, S. H.; Bahk, Y. Y.; Lee, K. H.; Kim, E. H.; Park, S. J.; Lee, B. J.; Won, H. S. Structural Characterization of de Novo Designed L5K5W Model Peptide Isomers with Potent Antimicrobial and Varied Hemolytic Activities. *Molecules* **2013**, *18*, 859-476.

(479) Zaiou, M. Multifunctional Antimicrobial Peptides: Therapeutic Targets in Several Human Diseases. *J. Mol. Med.* **2007**, *85*, 317-329.

(480) Giuliani, A.; Pirri, G.; Nicoletto, S. F. Antimicrobial Peptides: An Overview of a Promising Class of Therapeutics. *Cent. Eur. J. Biol.* **2007**, *2*, 1-33.

(481) Oyston, P. C. F.; Fox, M. A.; Richards, S. J.; Clark, G. C. Novel Peptides Therapeutics for Treatment of Infections. *J. Med. Microbiol.* **2009**, *58*, 977-987.

(482) Blazyk, J.; Wiegand, R.; Klein, J.; Hammer, J.; Epand, R. M.; Epand, R. F.; Maloy, W. L.; Kari, U. P. A Novel Linear Amphipathic Beta-Sheet Cationic Antimicrobial Peptide with Enhanced Selectivity for Bacterial Lipids. *J. Biol. Chem.* **2001**, *276*, 27899-27906.

(483) Jo, S.; Kim, T.; Iyer, V.; Im, W. CHARMM-GUI: A Web-Based Graphical User Interface for CHARMM. *J. Comput. Chem.* **2008**, *29*, 1859-1865.

(484) Jo, S.; Lim, J. B.; Klauda, J.; Im, W. CHARMM-GUI Membrane Builder for Mixed Bilayers and its Application to Yeast Membranes. *Biophys. J.* **2009**, *97*, 50-58.

(485) Wu, E.; Cheng, X.; Jo, S.; Rui, H.; Song, K.; Dávila-Contreras, E.; Qi, Y.; Lee, J.; Monje-Galvan, V.; Venable, R.; Klauda, J.; Im, W. CHARMM-GUI Membrane Builder Toward Realistic Biological Membrane Simulations. *J. Comput. Chem.* **2014**, *35*, 1997-2004.

(486) Lindahl, E.; Hess, B.; Van Der Spoel, D. GROMACS 3.0: a package for molecular simulation and trajectory analysis. *J. Mol. Model.* **2001**, *7*, 306-317.

(487) Abraham, M. J.; Murtola, T.; Schulz, R.; Páll, S.; Smith, J. C.; Hess, B.; Lindahl, E. GROMACS: High Performance Molecular Simulations Through Multi-Level Parallelism from Laptops to Supercomputers. *SoftwareX*. **2015**, *1*, 19-25.

(488) Berendsen, H. J. C.; van der Spoel, D.; van Drunen, R. GROMACS: A Message-Passing Parallel Molecular Dynamics Implementation. *Comput. Phys. Commun.* **1995**, *91*, 43-56.

(489) van der Spoel, D.; Lindahl, E.; Hess, B.; Groenhof, G.; Mark, A. E.; Berendsen, H. J. C. GROMACS: Fast, Flexible, and Free. *J. Comput. Chem.* **2005**, *26*, 1701-1718.

(490) Lee, J.; Cheng, X.; Swails, J. M.; Yeom, M. S.; Eastman, P. K.; Lemkul, J. A.; Wei, S.; Buckner, J.; Jeong, J. C.; Qi, Y.; Jo, S.; Pande, V. S.; Case, D. A.; Brooks, C. L.; MacKerell, A. D.; Klauda, J. B.; Im, W. CHARMM-GUI Input Generator for NAMD, GROMACS, AMBER, OpenMM, and CHARMM/OpenMM Simulations Using the CHARMM36 Additive Force Field. *J. Chem. Theory Comput.* **2016**, *12*, 405-413.

(491) Hess, B.; Bekker, H.; Berendsen, H. J. C.; Fraaije, J. G. E. M. A Linear Constraint Solver for Molecular Simulations. *J. Comput. Chem.* **1997**, *18*, 1463-1472.

(492) Darden, T.; York, D.; Pedersen, L. Particle Mesh Ewald: An N·log(N) Method for Ewald Sums in Large Systems. *J. Chem. Phys.* **1993**, *98*, 10089-10092.

(493) Berendsen, H. J. C. P., J. P. M. van Gunsteren, W. F. DiNola, A. Haak, J. R. Molecular Dynamics with Coupling to an External Bath. *J. Chem. Phys.* **1984**, *81*, 3684-3691.

(494) Nosé, S. A. Unified Formulation of the Constant Temperature Molecular Dynamics Methods. *J. Chem. Phys.* **1984**, *81*, 511-519.

(495) Hoover, W. G. Canonical Dynamics: Equilibrium Phase-space Distributions. *Phys. Rev. A: At., Mol., Opt. Phys.* **1985**, *31*, 1695-1698.

(496) Parrinello, M. R., A. Strain fluctuations and elastic constants. *J. Chem. Phys.* **1982**, *76*, 2662-2666.

(497) Parrinello, M. R., Aneesur. Polymorphic transitions in single crystals: A new molecular dynamics method. *J. Appl. Phys.* **1981**, *52*, 7182-7190.

(498) Ghosh, A.; Bhattacharyya, D.; Bhunia, A. Structural Insights of a Self-assembling 9-residue Peptide from the C-Terminal Tail of the SARS Corona Virus E-Protein in DPC and SDS Micelles: A Combined High- and Low-Resolution Spectroscopic Study. *Biochim. Biophys. Acta* **2017**, *17*, 335-346.

(499) Kosikowska, P.; Lesner, A. Antimicrobial Peptides (AMPs) as Drug Candidates: A Patent Review (2003–2015). *Expert Opin. Ther. Pat.* **2016**, *26*, 689-702.

(500) Gordon, Y. J.; Romanowski, E. G.; McDermott, A. M. A Review of Antimicrobial Peptides and Their Therapeutic Potential as Anti-Infective Drugs. *Curr. Eye Res.* **2005**, *30*, 505-515.

(501) Damberg, P.; Jarvet, J.; Graslund, A. MIcellar Systems as Solvents in Peptide and Protein Structure Determination. *Methods Enzymol.* **2001**, *339*, 271-285.

(502) Bai, Y.; Chung, J.; Dyson, H. J.; Wright, P. E. Structural and Dynamic Characterization of an Unfolded State of Poplar Apo-Plastocyanin formed under Nondenaturing Conditions. *Protein Sci.* **2001**, *10*, 1056-1066.

(503) Tseng, T. S.; Wang, S. H.; Chang, T. W.; Wei, H. M.; Wang, Y. J.; Tsai, K. C.; Liao, Y. D.; Chen, C. Sarkosyl-Induced Helical Structure of an Antimicrobial Peptide GW-Q6 Plays an Essential Role in the Binding of Surface Receptor OprI in Pseudomonas aeruginosa. *PLoS One* **2016**, *11*, 1-21.

(504) Nguyen, L. T.; de Boer, L.; Zaat, S. A.; Vogel, H. J. Investigating the Cationic Side Chains of the Antimicrobial Peptide Tritrpticin: Hydrogen Bonding Properties Govern its Membrane-Disruptive Activities. *Biochim. Biophys. Acta, Biomembr.* **2011**, *1808*, 2297-2303.

(505) Pandit, G.; Ilyas, H.; Ghosh, S.; Bidkar, A. P.; Mohid, S. A.; Bhunia, A.; Satpati, P.; Chatterjee, S., Insights into the mechanism of antimicrobial activity of seven-residue peptides. *J. Med. Chem.* **2018,** *61*, 7614-7629.

(506) Berendsen, H. J.; van der Spoel, D.; van Drunen, R. GROMACS: A message-passing parallel molecular dynamics implementation. *Comput. Phys. Commun.* **1995**, *91*, 43-56.

(507) Lee, J.; Cheng, X.; Swails, J. M.; Yeom, M. S.; Eastman, P. K.; Lemkul, J. A.; Wei, S.; Buckner, J.; Jeong, J. C.; Qi, Y. CHARMM-GUI input generator for NAMD, GROMACS, AMBER, OpenMM, and CHARMM/OpenMM simulations using the CHARMM36 additive force field. *J. Chem. Theory Comput.* **2016**, *12*, 405-413.

(508) Epand, R. F.; Savage, P. B.; Epand, R. M. Bacterial lipid composition and the antimicrobial efficacy of cationic steroid compounds (Ceragenins). *Biochim. Biophys. Acta, Biomembr.* **2007**, *1768*, 2500-2509.

(509) Arfken, G. The method of steepest descents. *Math. Models Methods Appl. Sci.* **1985**, *3*, 428-436.

(510) Klauda, J. B.; Monje, V.; Kim, T.; Im, W. Improving the CHARMM force field for polyunsaturated fatty acid chains. *J. phys. Chem. B* **2012**, *116*, 9424-9431.

(511) Darden, T.; York, D.; Pedersen, L. Particle mesh Ewald: An N· log (N) method for Ewald sums in large systems. *J. Chem. Phys.* **1993**, *98*, 10089-10092.

(512) Berendsen, H. J. P., JPM van Van Gunsteren, Wilfred F DiNola, ARHJ Haak, Jan R. Molecular dynamics with coupling to an external bath. *J. Chem. Phys.* **1984**, *81*, 3684-3690.

(513) Jorgensen, W. L. C., Jayaraman Madura, Jeffry D Impey, Roger W Klein, Michael L. Comparison of simple potential functions for simulating liquid water. *J. Chem. Phys.* **1983**, *79*, 926-935.

(514) Tomita, M.; Takase, M.; Wakabayashi, H.; Bellamy, W.: Antimicrobial peptides of lactoferrin. In *Lactoferrin*; Springer, 1994; pp 209-218.

(515) Nibbering, P.; Ravensbergen, E.; Welling, M.; Van Berkel, L.; Van Berkel, P.; Pauwels, E.; Nuijens, J. Human lactoferrin and peptides derived from its N terminus are highly effective against infections with antibiotic-resistant bacteria. *Infect. Immun.* **2001**, *69*, 1469-1476.

(516) Pendleton, J. N.; Gorman, S. P.; Gilmore, B. F. Clinical relevance of the ESKAPE pathogens. *Expert Rev. Anti-Infect. Ther.* **2013**, *11*, 297-308.

(517) Ghosh, A.; Bhattacharyya, D.; Bhunia, A. Structural insights of a self-assembling 9-residue peptide from the C-terminal tail of the SARS corona virus E-protein in DPC and SDS micelles: A combined high and low resolution spectroscopic study. *Biochim. Biophys. Acta, Biomembr.* **2018**, *1860*, 335-346.

(518) Wang, G.; Keifer, P. A.; Peterkofsky, A. Solution structure of the N-terminal amphitropic domain of Escherichia coli glucose-specific enzyme IIA in membrane-mimetic micelles. *Protein Sci.* **2003**, *12*, 1087-1096.

(519) Russell, A. L.; Williams, B. C.; Spuches, A.; Klapper, D.; Srouji, A. H.; Hicks, R. P. The effect of the length and flexibility of the side chain of basic amino acids on the binding of antimicrobial peptides to zwitterionic and anionic membrane model systems. *Bioorg. Med. Chem.* **2012**, *20*, 1723-1739.

(520) Savini, F.; Luca, V.; Bocedi, A.; Massoud, R.; Park, Y.; Mangoni, M. L.; Stella, L. Cell-density dependence of host-defense peptide activity and selectivity in the presence of host cells. *ACS Chem. Biol.* **2017**, *12*, 52-56.

(521) Pohl, L. E., M. Sodium 3-trimethylsilyltetradeuteriopropionate, a new water-soluble standard for 1H-NMR. *Angew. Chem. Int. Ed.* **1969**, *8*, 381-381.

(522) Pettersen, E. F.; Goddard, T. D.; Huang, C. C.; Couch, G. S.; Greenblatt, D. M.; Meng, E. C.; Ferrin, T. E. UCSF Chimera—a visualization system for exploratory research and analysis. *J. Comput. Chem.* **2004**, *25*, 1605-1612.

(523) Laskowski, R. A.; Rullmann, J. A. C.; MacArthur, M. W.; Kaptein, R.; Thornton, J. M. AQUA and PROCHECK-NMR: programs for checking the quality of protein structures solved by NMR. *J. Biomol. NMR* **1996**, *8*, 477-486.

(524) Sun, J.; Zhang, H.; Liu, Y.-H.; Feng, Y. Towards understanding MCR-like colistin resistance. *Trends Microbiol.* **2018**, *26*, 794-808.

(525) Bhutta, Z. A. Current concepts in the diagnosis and treatment of typhoid fever. *BMJ* **2006**, *333*, 78-82.

(526) Aoki, W.; Ueda, M., Characterization of antimicrobial peptides toward the development of novel antibiotics. *Pharmaceuticals* **2013,** *6*, 1055-1081.

(527) Datta, A.; Ghosh, A.; Airoldi, C.; Sperandeo, P.; Mroue, K. H.; Jiménez-Barbero, J.; Kundu, P.; Ramamoorthy, A.; Bhunia, A. Antimicrobial peptides: insights into membrane permeabilization, lipopolysaccharide fragmentation and application in plant disease control. *Sci. Rep.* **2015**, *5*, 1-15.

(528) Romoli, O.; Mukherjee, S.; Mohid, S. A.; Dutta, A.; Montali, A.; Franzolin, E.; Brady, D.; Zito, F.; Bergantino, E.; Rampazzo, C.; Tettamanti, G.; Bhunia, A.; Sandrelli, F. Enhanced Silkworm Cecropin B Antimicrobial Activity against. *ACS Infect. Dis.* **2019**, *5*, 1200-1213.

(529) Varnava, K. G.; Mohid, S. A.; Calligari, P.; Stella, L.; Reynison, J.; Bhunia, A.; Sarojini, V. Design, Synthesis, Antibacterial Potential, and Structural Characterization of N-Acylated Derivatives of the Human Autophagy 16 Polypeptide. *Bioconjugate Chem.* **2019**, *30*, 1998-2010.

(530) Bera, S.; Ghosh, A.; Sharma, S.; Debnath, T.; Giri, B.; Bhunia, A. Probing the role of Proline in the antimicrobial activity and lipopolysaccharide binding of indolicidin. *J. Colloid Interface Sci.* **2015**, *452*, 148-159.

(531) Wüthrich, K. NMR with proteins and nucleic acids. *Europhys. News* **1986**, *17*, 11-13.

(532) Richardson, J. S. The anatomy and taxonomy of protein structure. *Adv. Protein Chem.* **1981**, *34*, 167-339.

(533) Wishart, D. S.; Sykes, B. D.; Richards, F. M. Relationship between nuclear magnetic resonance chemical shift and protein secondary structure. *J. Mol. Biol.* **1991**, *222*, 311-333.

(534) Ghosh, C.; Haldar, J. Membrane-active small molecules: designs inspired by antimicrobial peptides. *ChemMedChem* **2015**, *10*, 1606-1624.

(535) Molchanova, N.; Hansen, P. R.; Franzyk, H. Advances in development of antimicrobial peptidomimetics as potential drugs. *Molecules* **2017**, *22*, 1430-1490.

(536) Raguse, T. L.; Porter, E. A.; Weisblum, B.; Gellman, S. H. Structure− activity studies of 14-helical antimicrobial β-peptides: probing the relationship between conformational stability and antimicrobial potency. *J. Am. Chem. Soc.* **2002**, *124*, 12774-12785.

(537) Drayton, M.; Kizhakkedathu, J. N.; Straus, S. K. Towards robust delivery of antimicrobial peptides to combat bacterial resistance. *Molecules* **2020**, *25*, 3048-3072.

(538) Gentilucci, L.; De Marco, R.; Cerisoli, L., Chemical modifications designed to improve peptide stability: incorporation of non-natural amino acids, pseudo-peptide bonds, and cyclization. *Curr. Pharm. Des.* **2010,** *16*, 3185-3203.

(539) Ting, D. S. J.; Beuerman, R. W.; Dua, H. S.; Lakshminarayanan, R.; Mohammed, I. Strategies in translating the therapeutic potentials of host defense peptides. *Front. Immunol.* **2020**, *11*, 983-999.

(540) Berthold, N.; Czihal, P.; Fritsche, S.; Sauer, U.; Schiffer, G.; Knappe, D.; Alber, G.; Hoffmann, R., Novel apidaecin 1b analogs with superior serum stabilities for treatment of infections by gram-negative pathogens. *Antimicrob. Agents Chemother.* **2013,** *57*, 402-409.

(541) Nguyen, L. T.; Chau, J. K.; Perry, N. A.; De Boer, L.; Zaat, S. A.; Vogel, H. J. Serum stabilities of short tryptophan-and arginine-rich antimicrobial peptide analogs. *PLoS One* **2010**, *5*, 1-8.

(542) Liang, X.; Liu, K.; Zhao, P.; Zhou, J.; Zhang, F.; He, Y.; Zhang, H.; Fareed, M. S.; Lu, Y.; Xu, Y. The effects of incorporation of the counterparts and mimics of l-lysine on the antimicrobial activity, hemolytic activity, cytotoxicity and tryptic stability of antimicrobial peptide polybia-MPII. *Amino acids* **2021**, *54*, 123-135.

(543) Gunasekaran, P.; Kim, E. Y.; Lee, J.; Ryu, E. K.; Shin, S. Y.; Bang, J. K. Synthesis of Fmoc-Triazine Amino Acids and Its Application in the Synthesis of Short Antibacterial Peptidomimetics. *Int. J. Mol. Sci.* **2020**, *21*, 3602-3623.

(544) Dathe, M.; Nikolenko, H.; Klose, J.; Bienert, M., Cyclization increases the antimicrobial activity and selectivity of arginine-and tryptophan-containing hexapeptides. *Biochemistry* **2004,** *43*, 9140-9150.

(545) Oh, D.; Sun, J.; Nasrolahi Shirazi, A.; LaPlante, K. L.; Rowley, D. C.; Parang, K., Antibacterial activities of amphiphilic cyclic cell-penetrating peptides against multidrug-resistant pathogens. *Mol. Pharmaceutics* **2014,** *11*, 3528-3536.

(546) Lohner, K.; Sevcsik, E.; Pabst, G., Chapter five liposome-based biomembrane mimetic systems: Implications for lipid–peptide interactions. *Adv. Planar Lipid Bilayers Liposomes* **2008,** *6*, 103-137.

(547) Lee, J.; Kang, D.; Choi, J.; Huang, W.; Wadman, M.; Barron, A. E.; Seo, J., Effect of side chain hydrophobicity and cationic charge on antimicrobial activity and cytotoxicity of helical peptoids. *Bioorg. Med. Chem. Lett.* **2018,** *28*, 170-173.

(548) Imura, Y.; Nishida, M.; Ogawa, Y.; Takakura, Y.; Matsuzaki, K. Action mechanism of tachyplesin I and effects of PEGylation. *Biochim. Biophys. Acta, Biomembr.* **2007**, *1768*, 1160-1169.

(549) Chongsiriwatana, N. P.; Patch, J. A.; Czyzewski, A. M.; Dohm, M. T.; Ivankin, A.; Gidalevitz, D.; Zuckermann, R. N.; Barron, A. E. Peptoids that mimic the structure, function, and mechanism of helical antimicrobial peptides. *Proc. Natl. Acad. Sci.* **2008**, *105*, 2794-2799.

(550) Singh, S.; Papareddy, P.; Morgelin, M.; Schmidtchen, A.; Malmsten, M. J. B. Effects of PEGylation on membrane and lipopolysaccharide interactions of host defense peptides. **2014**, *15*, 1337-1345.

(551) Albada, H. B.; Prochnow, P.; Bobersky, S.; Langklotz, S.; Schriek, P.; Bandow, J. E.; Metzler-Nolte, N. J. A. m. c. l. Tuning the activity of a short Arg-Trp antimicrobial peptide by lipidation of a C-or N-terminal lysine side-chain. **2012**, *3*, 980-984.

(552) Bagheri, M.; Hancock, R. E.: High-performance liquid chromatography and mass spectrometry-based design of proteolytically stable antimicrobial peptides. In *Antimicrob. Pept.*; Springer, 2017; pp 61-71.

(553) Bagheri, M.; Arasteh, S.; Haney, E. F.; Hancock, R. E., Tryptic stability of synthetic bactenecin derivatives is determined by the side chain length of cationic residues and the peptide conformation. *J. Med. Chem.* **2016,** *59*, 3079-3086.

(554) Chen, C.; Hu, J.; Zeng, P.; Chen, Y.; Xu, H.; Lu, J. R., High cell selectivity and low-level antibacterial resistance of designed amphiphilic peptide G (IIKK) 3I-NH2. *ACS Appl. Mater. Interfaces* **2014,** *6*, 16529-16536.

(555) Nguyen, L. T.; de Boer, L.; Zaat, S. A.; Vogel, H. J., Investigating the Cationic Side Chains of the Antimicrobial Peptide Tritrpticin: Hydrogen Bonding Properties Govern its Membrane-Disruptive Activities. *Biochim. Biophys. Acta, Biomembr.* **2011,** *1808*, 2297-2303.

(556) Russell, A. L.; Williams, B. C.; Spuches, A.; Klapper, D.; Srouji, A. H.; Hicks, R. P., The effect of the length and flexibility of the side chain of basic amino acids on the binding of antimicrobial peptides to zwitterionic and anionic membrane model systems. *Bioorg. Med. Chem.* **2012,** *20*, 1723-1739.

(557) Pandit, G.; Chowdhury, N.; Abdul Mohid, S.; Bidkar, A. P.; Bhunia, A.; Chatterjee, S. J. C. Effect of Secondary Structure and Side Chain Length of Hydrophobic Amino Acid Residues on the Antimicrobial Activity and Toxicity of 14-Residue-Long de novo AMPs. **2021**, *16*, 355-367.

(558) Arias, M.; Piga, K. B.; Hyndman, M. E.; Vogel, H. J. Improving the activity of Trp-rich antimicrobial peptides by Arg/Lys substitutions and changing the length of cationic residues. *Biomolecules* **2018**, *8*, 19-36.

(559) Delcour, A. H., Outer membrane permeability and antibiotic resistance. *Biochim. Biophys. Acta, Proteins Proteomics* **2009,** *1794*, 808-816.

(560) Blair, J.; Webber, M. A.; Baylay, A. J.; Ogbolu, D. O.; Piddock, L. J., Molecular mechanisms of antibiotic resistance. *Nat. Rev. Microbiol.* **2015,** *13*, 42-51

(561) Nikaido, H., Molecular basis of bacterial outer membrane permeability revisited. *Microbiol. Mol. Biol. Rev.* **2003,** *67*, 593-656.

(562) Miller, S. I. Antibiotic resistance and regulation of the gram-negative bacterial outer membrane barrier by host innate immune molecules. *mBio* **2016**, *7*, 1-3.

(563) Silhavy, T. J.; Kahne, D.; Walker, S. The bacterial cell envelope. *Cold Spring Harbor Perspect. Biol.* **2010**, *2*, 1-17.

(564) Snyder, D. S.; McIntosh, T. J. J. B. The lipopolysaccharide barrier: correlation of antibiotic susceptibility with antibiotic permeability and fluorescent probe binding kinetics. **2000**, *39*, 11777-11787.

(565) Rosenfeld, Y.; Barra, D.; Simmaco, M.; Shai, Y.; Mangoni, M. L., A synergism between temporins toward Gram-negative bacteria overcomes resistance imposed by the lipopolysaccharide protective layer. *J. Biol. Chem.* **2006,** *281*, 28565-28574.

(566) LaRock, C. N.; Nizet, V. Cationic antimicrobial peptide resistance mechanisms of streptococcal pathogens. *Biochim. Biophys. Acta, Biomembr.* **2015**, *1848*, 3047-3054.

(567) Maria-Neto, S.; de Almeida, K. C.; Macedo, M. L. R.; Franco, O. L., Understanding bacterial resistance to antimicrobial peptides: From the surface to deep inside. *Biochim. Biophys. Acta, Biomembr.* **2015,** *1848*, 3078-3088.

(568) Matamouros, S.; Miller, S., S. Typhimurium strategies to resist killing by cationic antimicrobial peptides. *Biochim. Biophys. Acta, Biomembr.* **2015,** *1848*, 3021-3025.

(569) Pandit, G.; Biswas, K.; Ghosh, S.; Debnath, S.; Bidkar, A. P.; Satpati, P.; Bhunia, A.; Chatterjee, S. Rationally designed antimicrobial peptides: Insight into the mechanism of eleven residue peptides against microbial infections. *Biochim. Biophys. Acta, Biomembr.*. **2020**, *1862*, 1-16.

(570) Halder, S.; Yadav, K. K.; Sarkar, R.; Mukherjee, S.; Saha, P.; Haldar, S.; Karmakar, S.; Sen, T. J. S. Alteration of Zeta potential and membrane permeability in bacteria: a study with cationic agents. **2015**, *4*, 1-14.

(571) Gfeller, D.; Michielin, O.; Zoete, V. SwissSidechain: a molecular and structural database of non-natural sidechains. *Nucleic Acids Res.* **2012**, *41*, 327-332.

(572) Cheng, X.; Jo, S.; Lee, H. S.; Klauda, J. B.; Im, W. CHARMM-GUI micelle builder for pure/mixed micelle and protein/micelle complex systems. *J. Chem. Inf. Model.* **2013**, *53*, 2171-2180.

(573) Mackerell Jr, A. D., Molecular dynamics simulation analysis of a sodium dodecyl sulfate micelle in aqueous solution: decreased fluidity of the micelle hydrocarbon interior. *J. Phys. Chem.* **1995,** *99*, 1846-1855.

(574) Rakitin, A. R.; Pack, G. R. Molecular dynamics simulations of ionic interactions with dodecyl sulfate micelles. *J. phys. Chem. B* **2004**, *108*, 2712-2716.

(575) Bondi, A. v. vander Waals volumes and radii. *J. Phys. Chem.* **1964**, *68*, 441-451.

(576) Brötz, H.; Bierbaum, G.; Leopold, K.; Reynolds, P. E.; Sahl, H.-G. The lantibiotic mersacidin inhibits peptidoglycan synthesis by targeting lipid II. *Antimicrob. Agents Chemother.* **1998**, *42*, 154-160.

(577) Wang, Q.; Hong, G.; Johnson, G. R.; Pachter, R.; Cheung, M. S., Biophysical properties of membrane-active peptides based on micelle modeling: a case study of cell-penetrating and antimicrobial peptides. *J. phys. Chem. B* **2010,** *114*, 13726-13735.

(578) Lebecque, S. C., Jean-Marc Nasir, Mehmet Nail Deleu, Magali Lins, Laurence, Molecular dynamics study of micelles properties according to their size. *J. Mol. Graphics Modell.* **2017,** *72*, 6-15.

(579) Oliveira Bortot, L.; Bashardanesh, Z.; Van der Spoel, D. Making soup: preparing and validating models of the bacterial cytoplasm for molecular simulation. *J. Chem. Inf. Model.* **2019,** *60*, 322-331.

(580) Best, R. B.; Zhu, X.; Shim, J.; Lopes, P. E.; Mittal, J.; Feig, M.; MacKerell Jr, A. D. Optimization of the additive CHARMM all-atom protein force field targeting improved sampling of the backbone ϕ, ψ and side-chain χ1 and χ2 dihedral angles. *J. Chem. Theory Comput.* **2012,** *8*, 3257-3273.

(581) Lebecque, S. C., Jean-Marc Nasir, Mehmet Nail Deleu, Magali Lins, Laurence. Molecular dynamics study of micelles properties according to their size. *J. Mol. Graphics Modell.* **2017**, *72*, 6-15.

(582) Durell, S. R.; Brooks, B. R.; Ben-Naim, A. Solvent-induced forces between two hydrophilic groups. *J. Phys. Chem.* **1994**, *98*, 2198-2202.

(583) Frishman, D.; Argos, P. Function,; Bioinformatics. Knowledge-based protein secondary structure assignment. *Proteins: Struct., Funct., Genet.* **1995**, *23*, 566-579.

(584) Eisenhaber, F. L., Philip Argos, Patrick Sander, Chris Scharf, Michael. The double cubic lattice method: efficient approaches to numerical integration of surface area and volume and to dot surface contouring of molecular assemblies. *J. Comput. Chem.* **1995**, *16*, 273-284.

APPENDIX

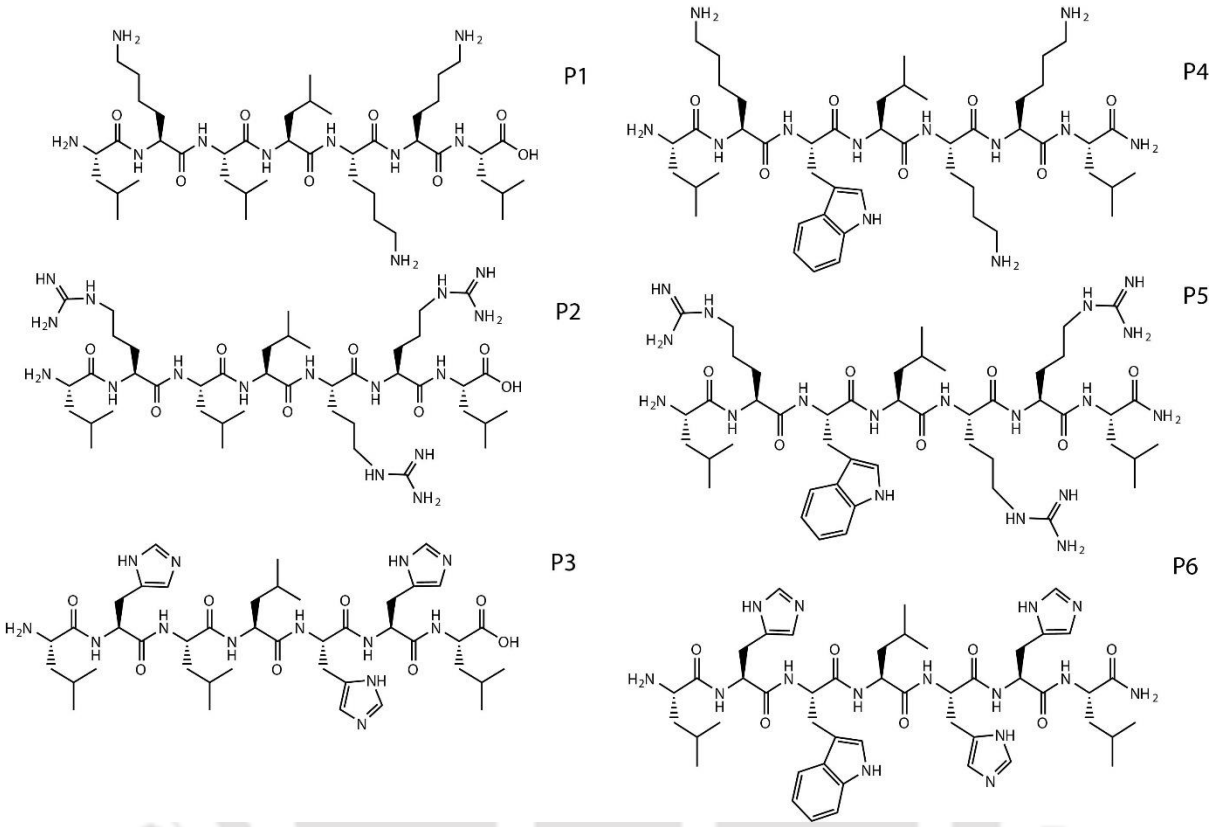

Figure A1: Chemical Structure of Peptide P1 to P6

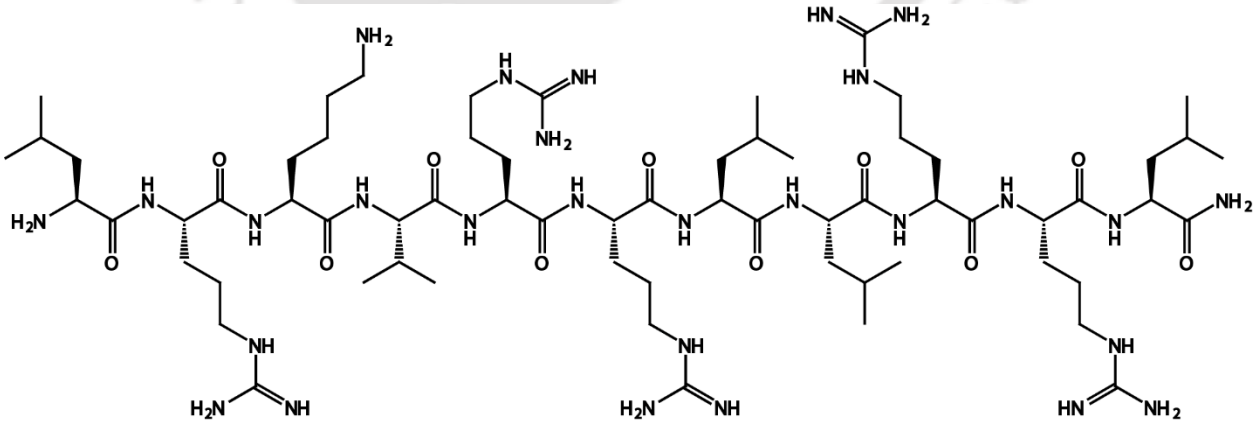

AMP 21

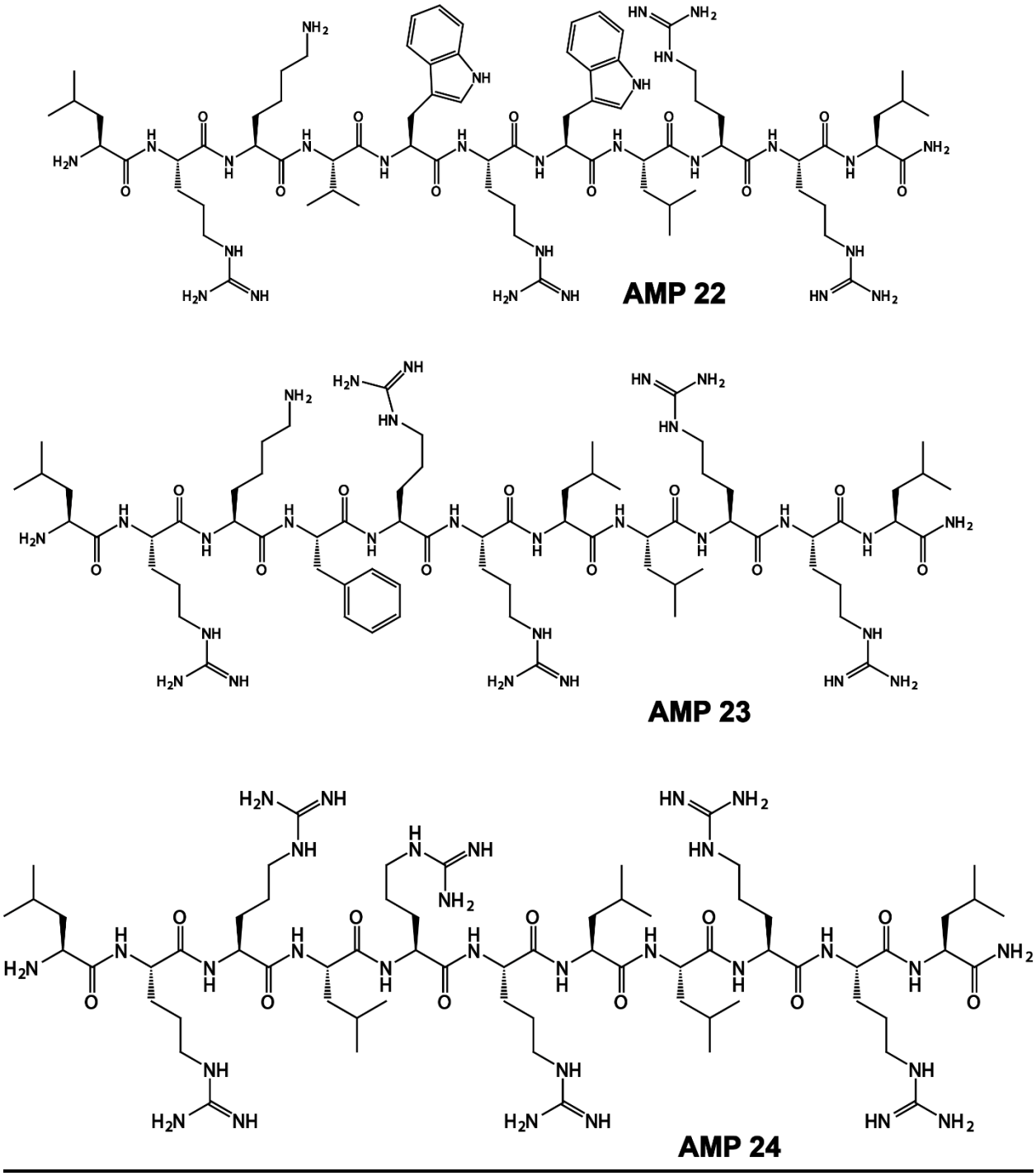

Figure A2: Chemical Structure of Peptide AMP21 to AMP24

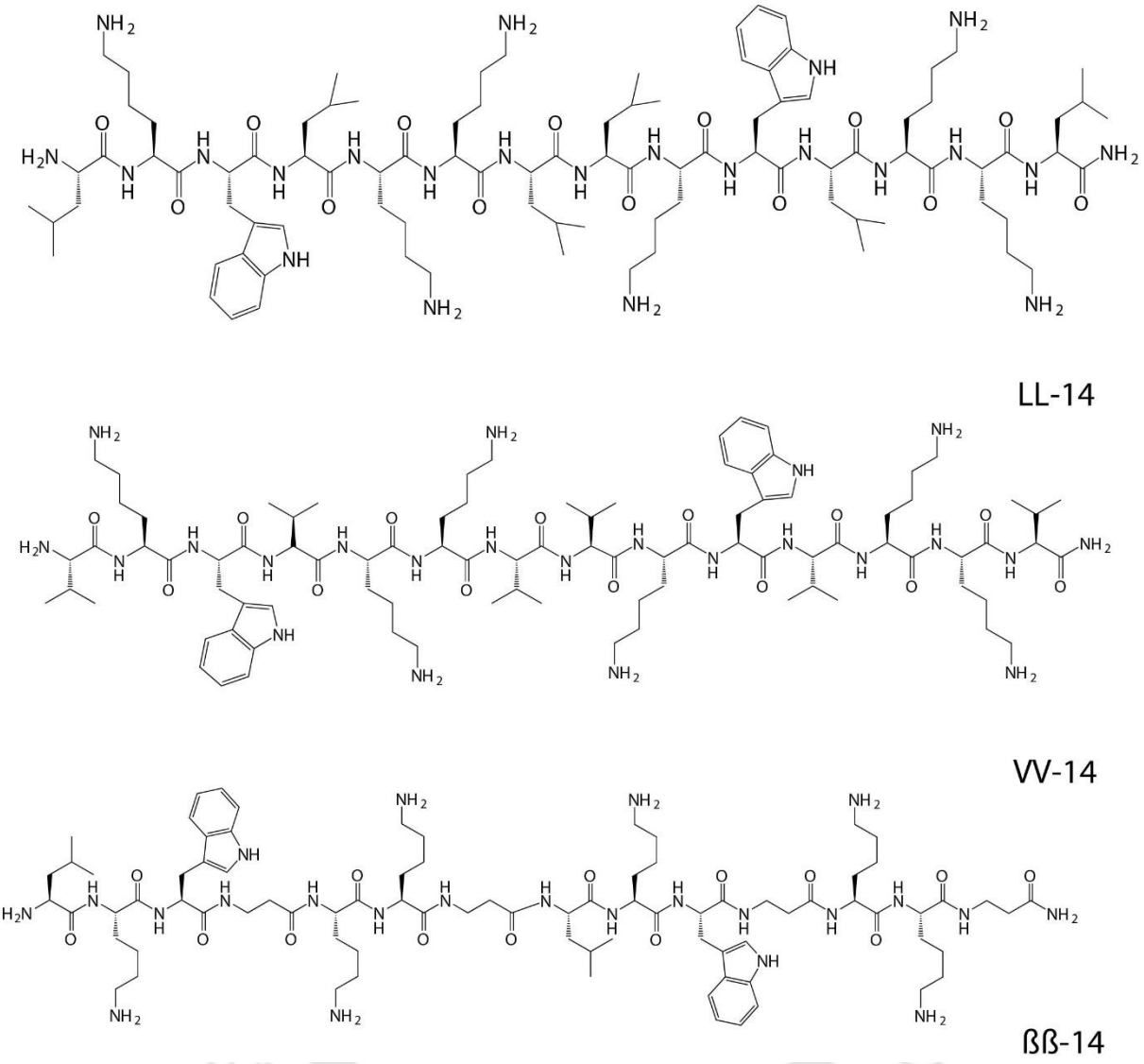

Figure A3: Chemical Structure of Peptide LL-14, VV-14 & ββ-14

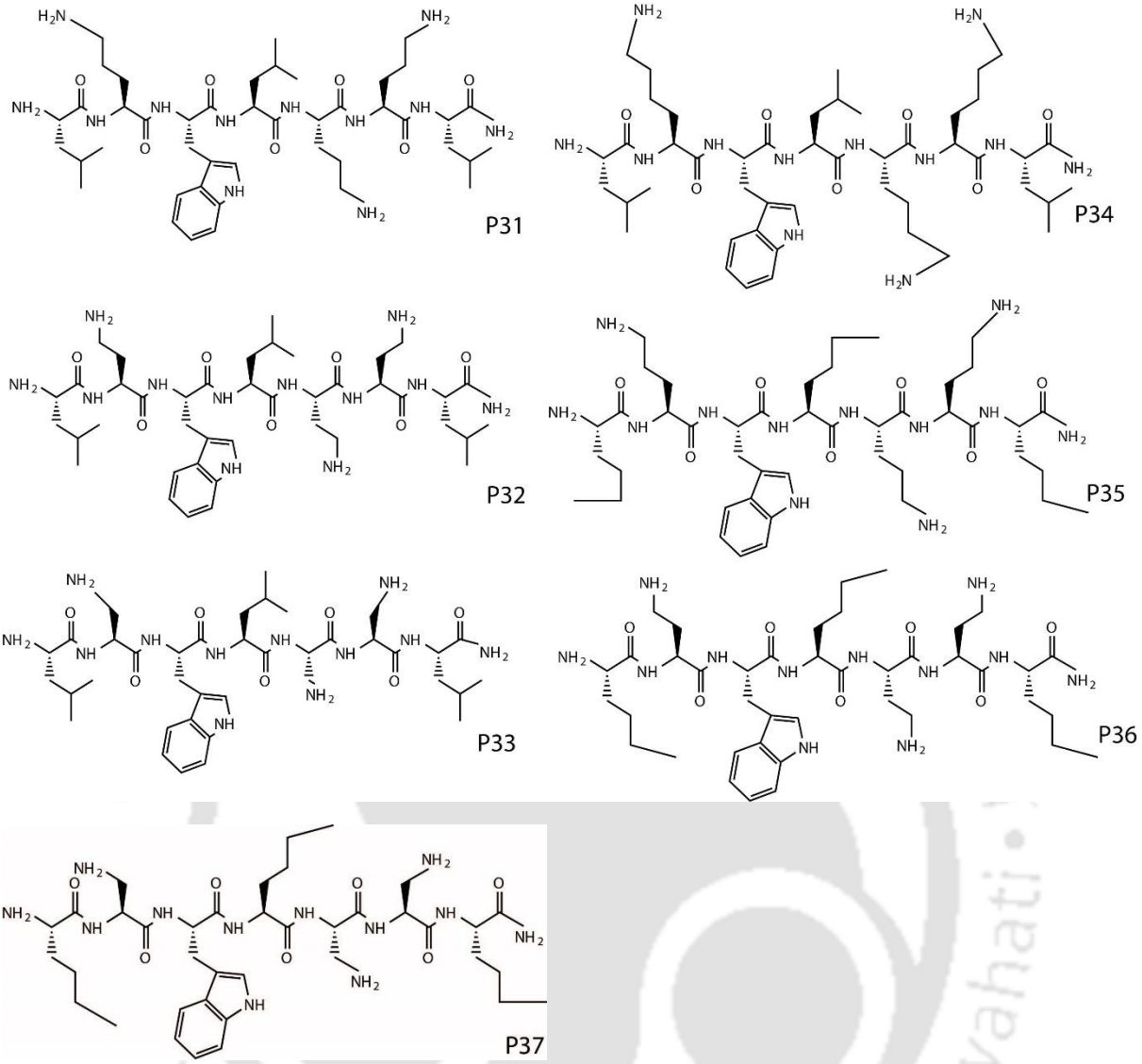

Figure A4: Chemical Structure of Peptide P31 to P37

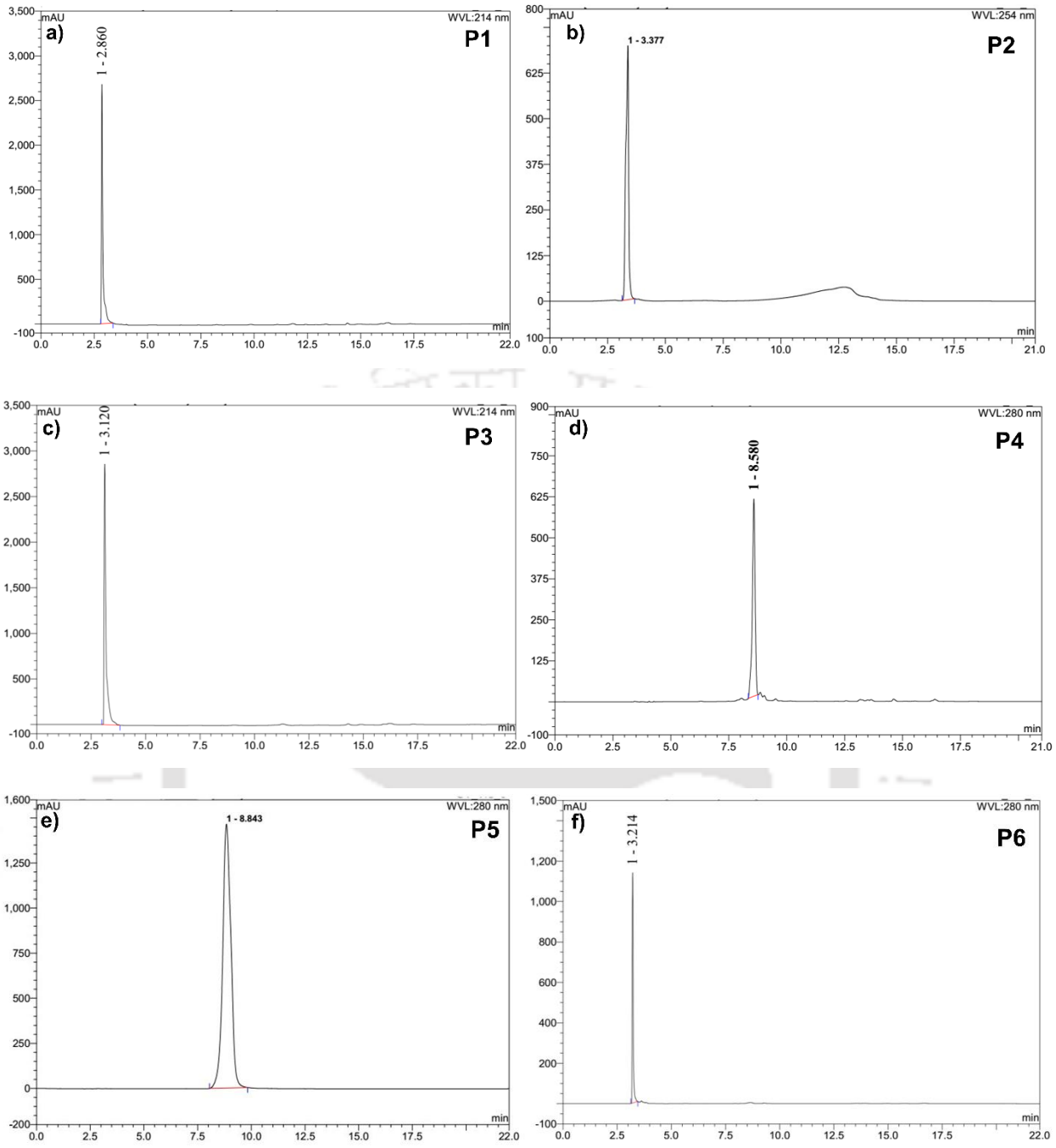

Figure A5: Analytical HPLC Traces for peptide (a-f) P1-P6.

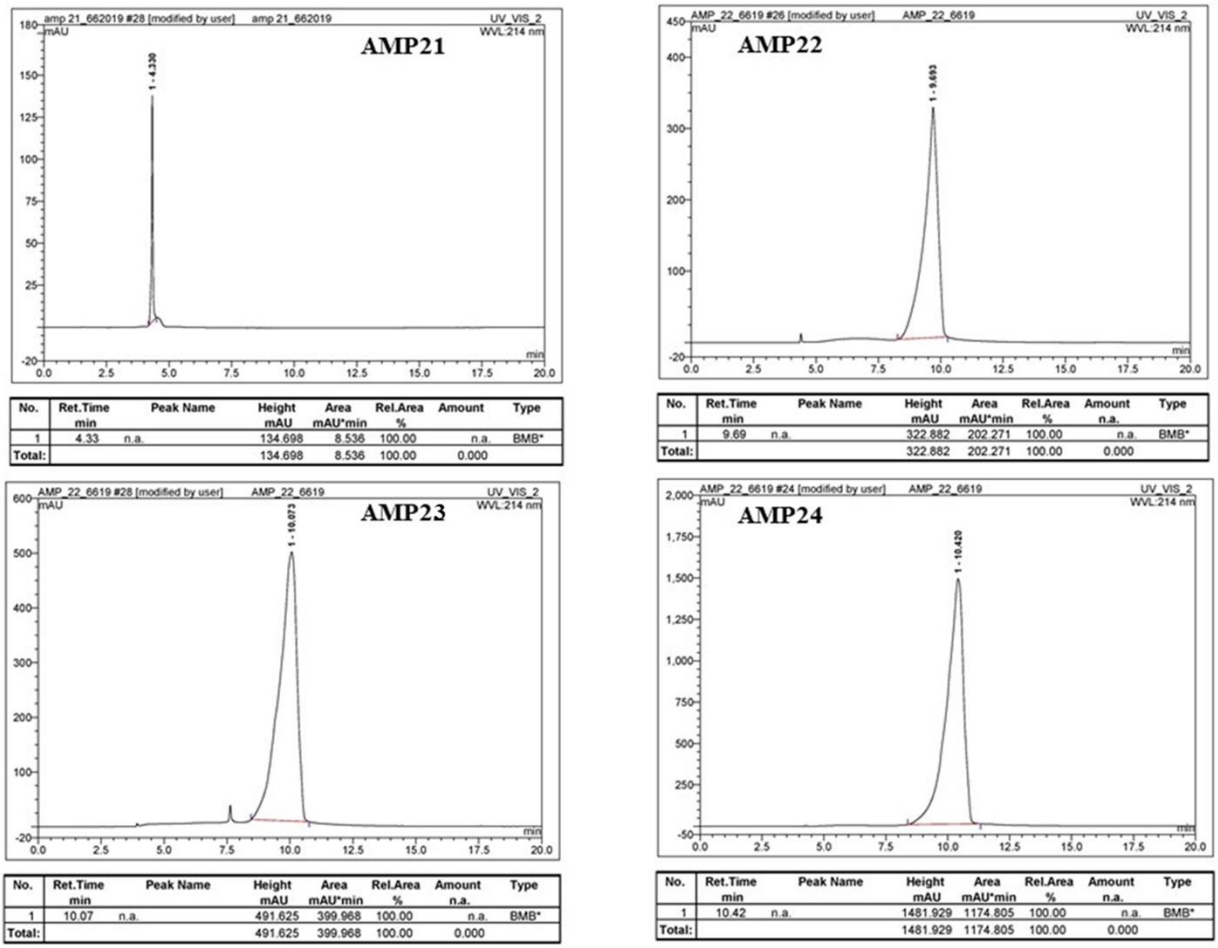

No.	Ret.Time min	Peak Name	Height mAU	Area mAU*min	Rel.Area %	Amount n.a.	Type
1	4.33	n.a.	134.698	8.536	100.00	n.a.	BMB*
Total:			134.698	8.536	100.00	0.000	

No.	Ret.Time min	Peak Name	Height mAU	Area mAU*min	Rel.Area %	Amount n.a.	Type
1	9.69	n.a.	322.882	202.271	100.00	n.a.	BMB*
Total:			322.882	202.271	100.00	0.000	

No.	Ret.Time min	Peak Name	Height mAU	Area mAU*min	Rel.Area %	Amount n.a.	Type
1	10.07	n.a.	491.625	399.968	100.00	n.a.	BMB*
Total:			491.625	399.968	100.00	0.000	

No.	Ret.Time min	Peak Name	Height mAU	Area mAU*min	Rel.Area %	Amount n.a.	Type
1	10.42	n.a.	1481.929	1174.805	100.00	n.a.	BMB*
Total:			1481.929	1174.805	100.00	0.000	

Figure A6: Analytical HPLC traces for peptide AMP21, AMP22, AMP23, AMP24.

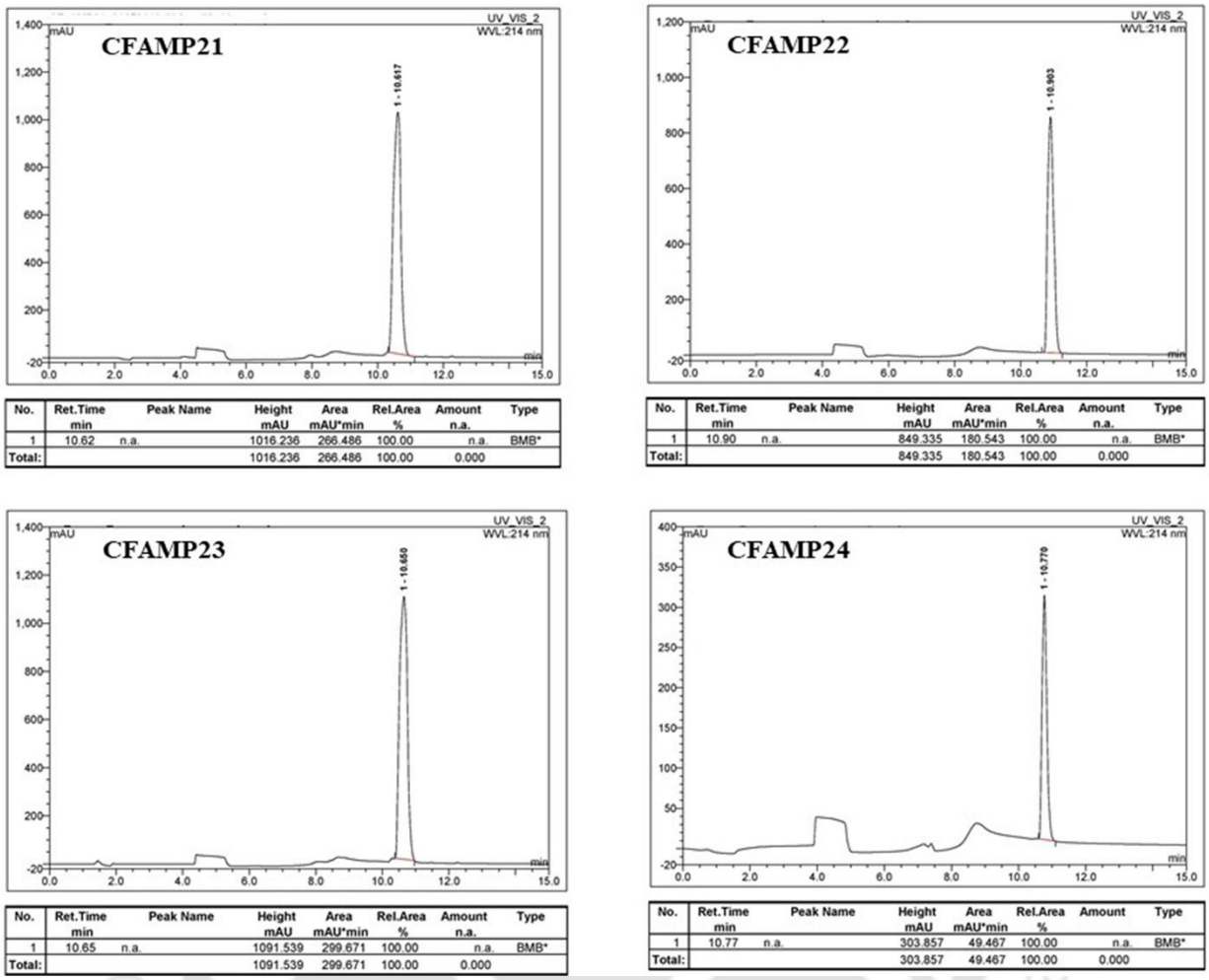

No.	Ret.Time min	Peak Name	Height mAU	Area mAU*min	Rel.Area %	Amount n.a.	Type
1	10.62	n.a.	1016.236	266.486	100.00	n.a.	BMB*
Total:			1016.236	266.486	100.00	0.000	

No.	Ret.Time min	Peak Name	Height mAU	Area mAU*min	Rel.Area %	Amount n.a.	Type
1	10.90	n.a.	849.335	180.543	100.00	n.a.	BMB*
Total:			849.335	180.543	100.00	0.000	

No.	Ret.Time min	Peak Name	Height mAU	Area mAU*min	Rel.Area %	Amount n.a.	Type
1	10.65	n.a.	1091.539	299.671	100.00	n.a.	BMB*
Total:			1091.539	299.671	100.00	0.000	

No.	Ret.Time min	Peak Name	Height mAU	Area mAU*min	Rel.Area %	Amount n.a.	Type
1	10.77	n.a.	303.857	49.467	100.00	n.a.	BMB*
Total:			303.857	49.467	100.00	0.000	

Figure A7: Analytical HPLC traces for peptide CF-AMP21, CF-AMP22, CF-AMP23, CF-AMP24.

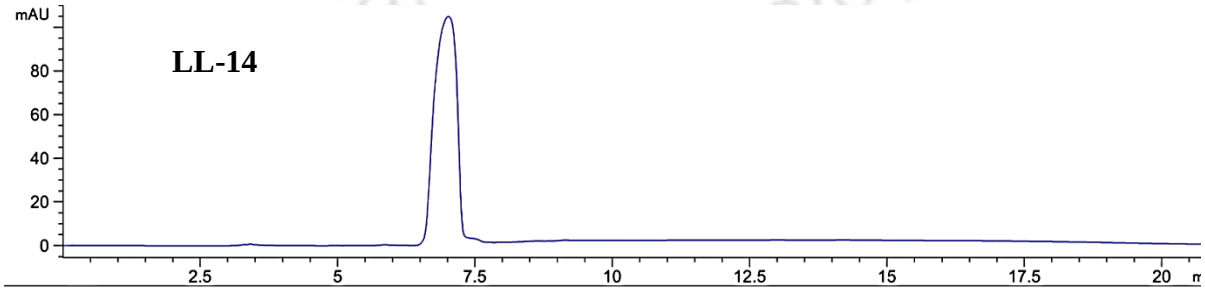

Figure A8: Analytical HPLC trace for peptide LL-14

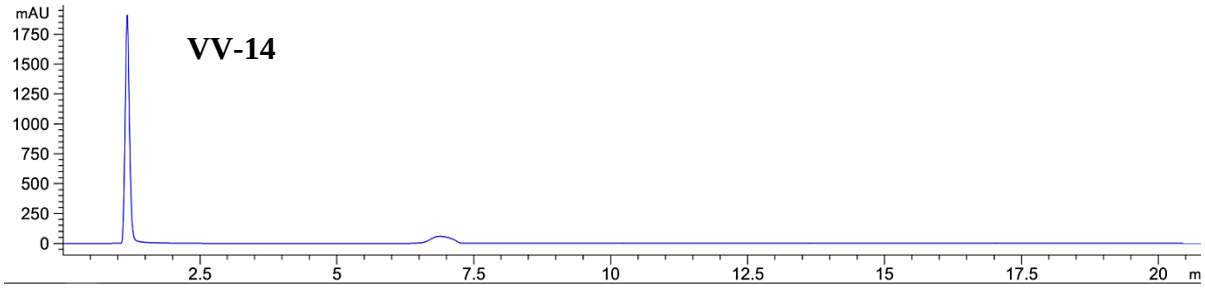

Figure A9: Analytical HPLC trace for peptide VV-14

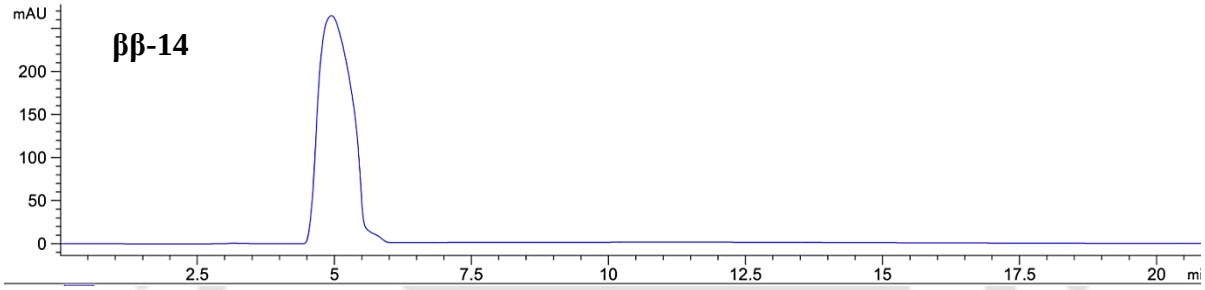

Figure A10: Analytical HPLC trace for peptide ββ-14

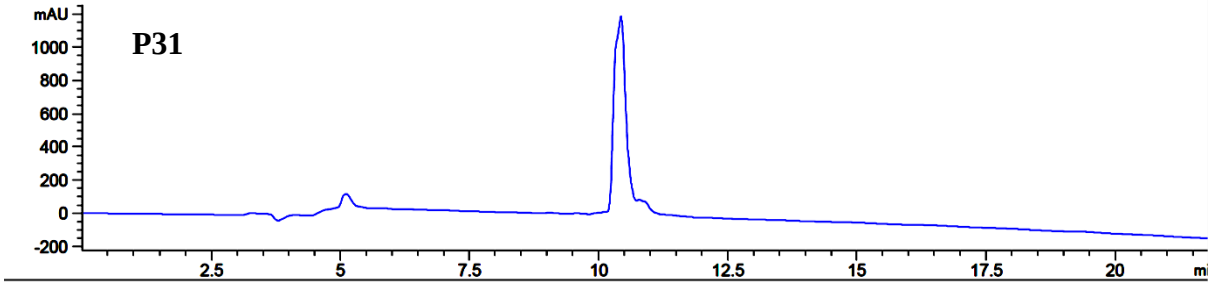

Figure A11: Analytical HPLC trace for peptide **P31**.

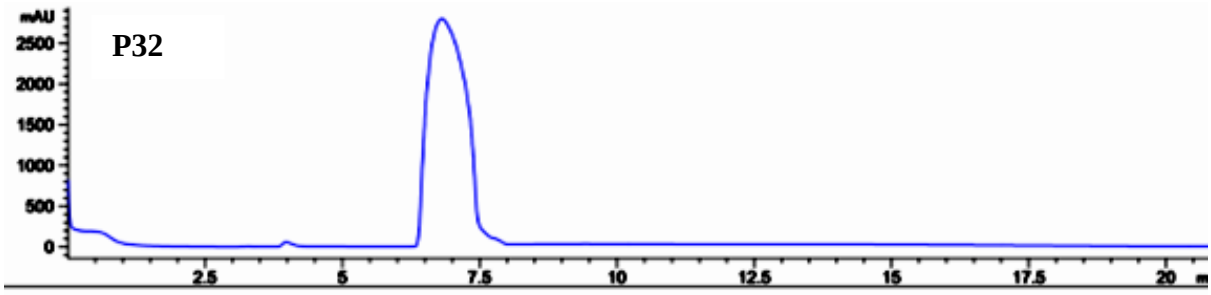

Figure A12: Analytical HPLC trace for peptide **P32**.

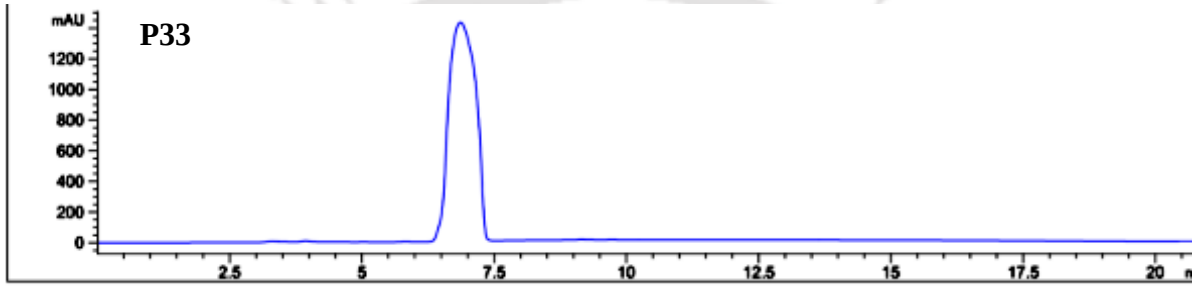

Figure A13: Analytical HPLC trace for peptide **P33**.

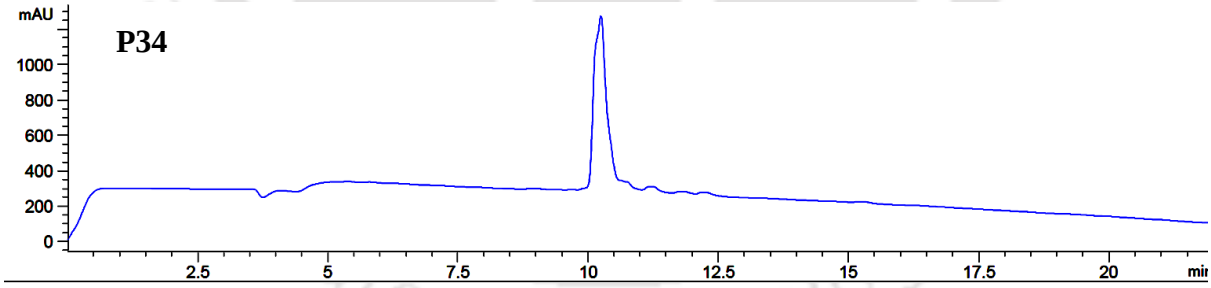

Figure A14: Analytical HPLC trace for peptide **P34**.

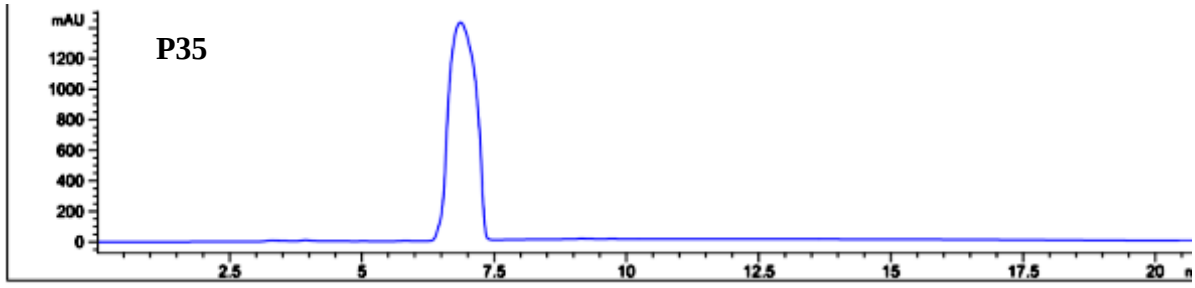

Figure A15: Analytical HPLC trace for peptide **P35**.

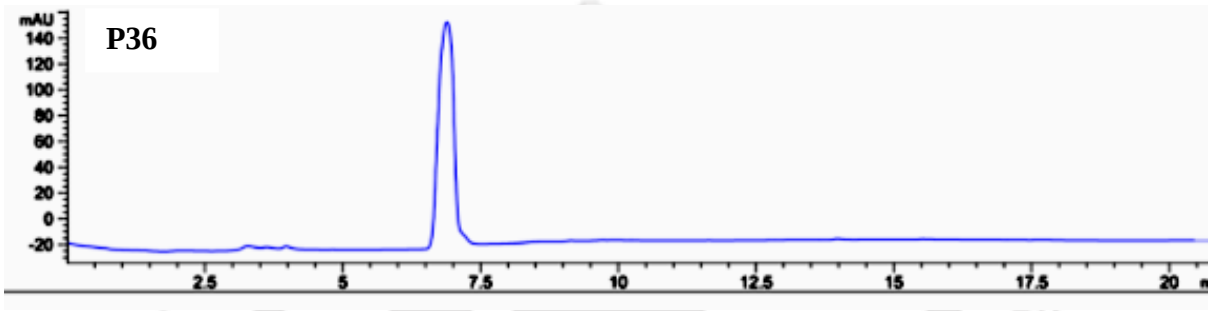

Figure A16: Analytical HPLC trace for peptide **P36**.

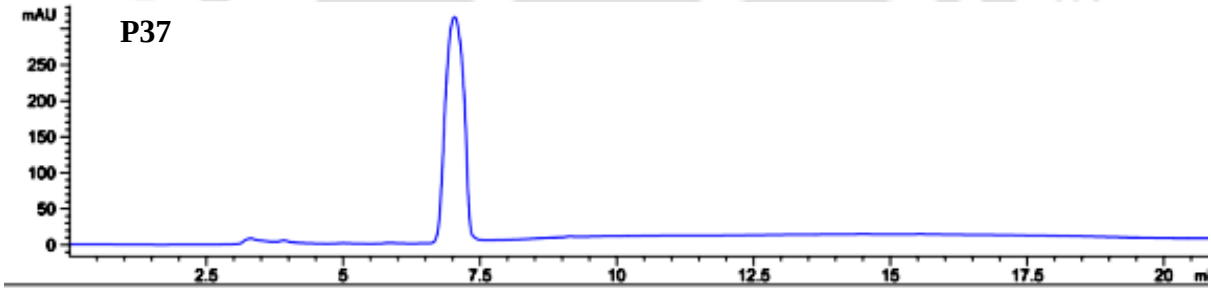

Figure A17: Analytical HPLC trace for peptide **P37**.

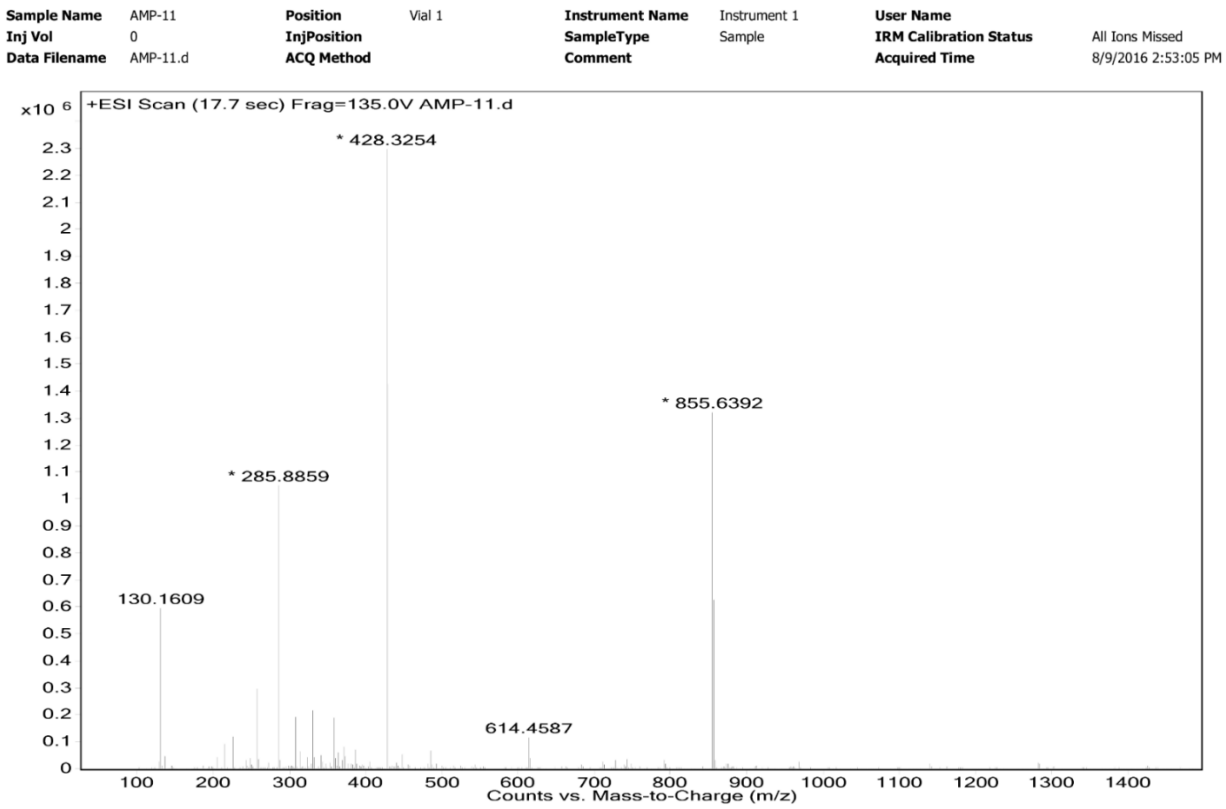

Figure A18: ESI-MS of P1. Calc. $(M+H)^+$ for $C_{42}H_{82}N_{10}O_8$= 855.639 Da; Obs. $(M+H)^+$ = 855.6392Da, $(M+2H)^+$=428.3254Da, $(M+3H)^+$ = 285.8859 Da.

Sample Name	Unavailable	**Position**	Unavailable	**Instrument Name**	Unavailable	**User Name**	Unavailable
Inj Vol	Unavailable	**InjPosition**	Unavailable	**SampleType**	Unavailable	**IRM Calibration Status**	Success
Data Filename	GP-R.d	**ACQ Method**		**Comment**	Sample information is unavailable	**Acquired Time**	Unavailable

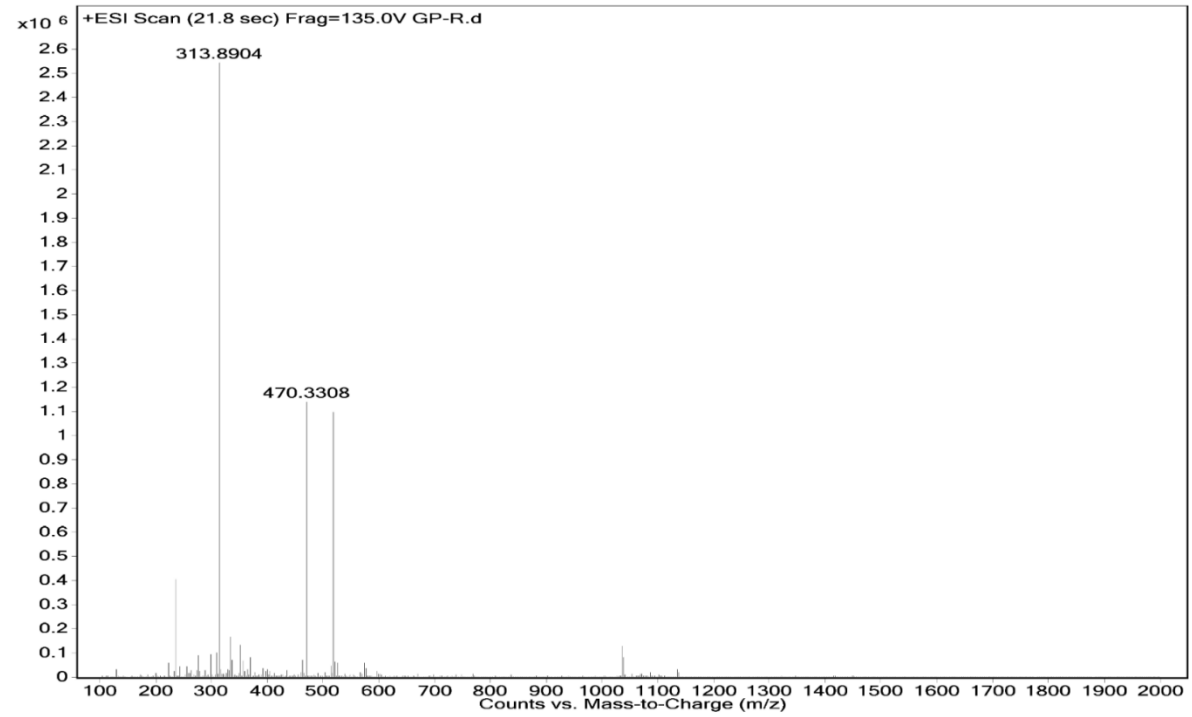

Figure A19: ESI-MS of P2. Calc. $(M+H)^+$ for $C_{42}H_{82}N_{16}O_8$= 939.6574 Da; Obs. $(M+2H)^+$ = 470.3308 Da, $(M+3H)^+$ = 313.8904 Da.

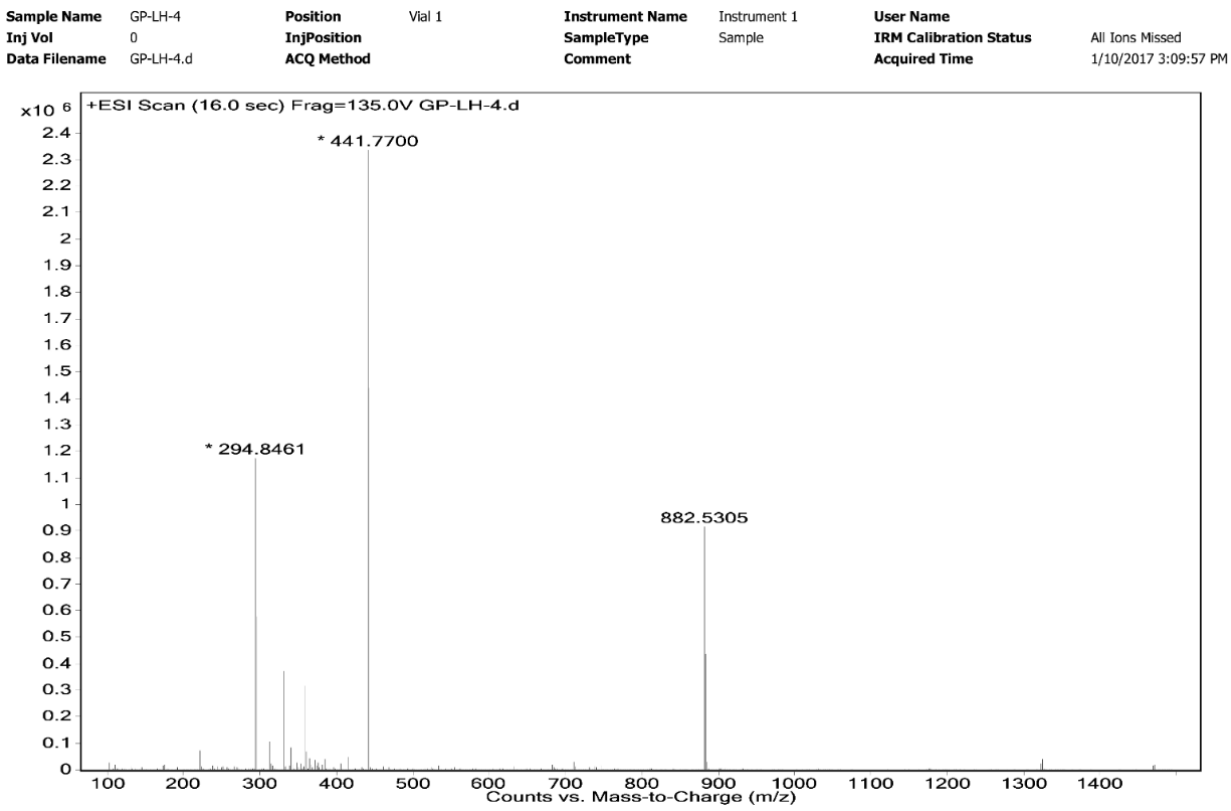

Figure A20: ESI-MS of P3. Calc. $(M+H)^+$ for $C_{42}H_{67}N_{13}O_8$= 882.5308 Da; Obs. $(M+H)^+$ = 882.5305 Da, $(M+2H)^+$ = 441.77 Da, $(M+3H)^+$ = 294.8461 Da.

Sample Name	GP-LKWL	**Position**	Vial 1	**Instrument Name**	Instrument 1	**User Name**	
Inj Vol	0	**InjPosition**		**SampleType**	Sample	**IRM Calibration Status**	Success
Data Filename	GP-LKWL.d	**ACQ Method**		**Comment**		**Acquired Time**	10/10/2017 5:08:09 PM

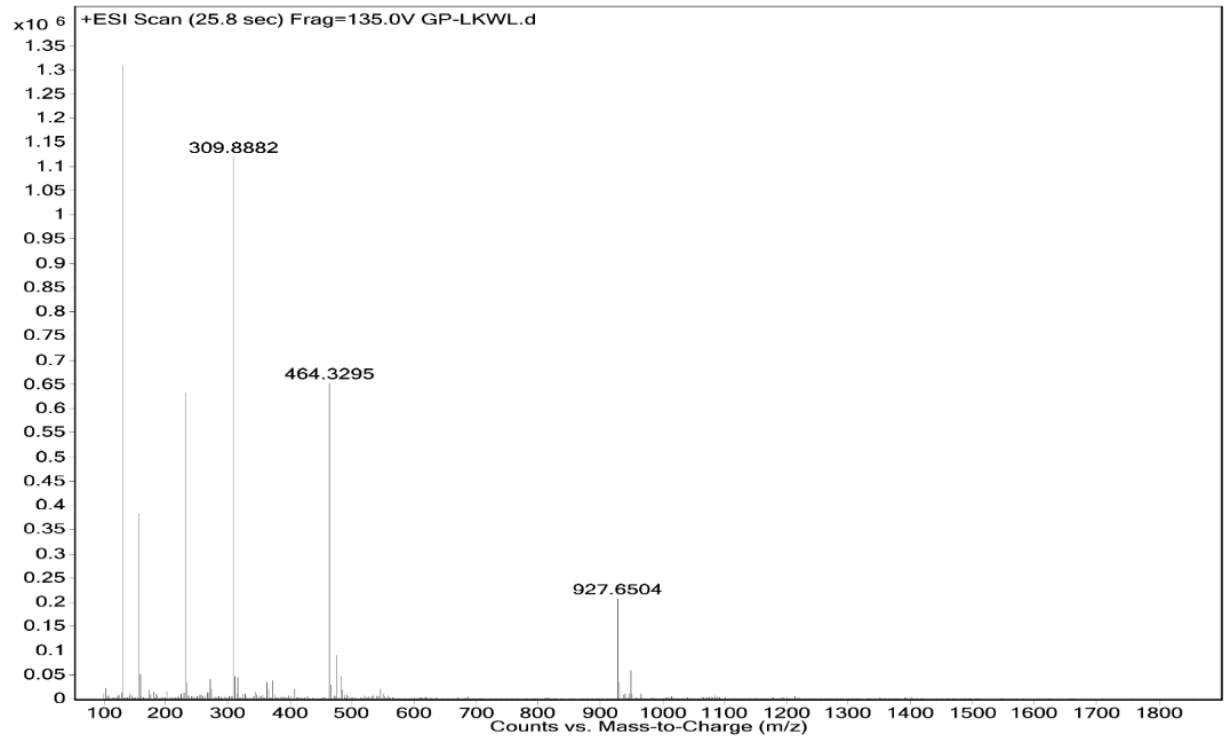

Figure A21: ESI-MS of P4. Calc. $(M+H)^+$ for $C_{47}H_{82}N_{12}O_7$= 927.6502 Da; Obs. $(M+H)^+$ = 927.6504 Da, $(M+2H)^+$ = 464.3295 Da, $(M+3H)^+$ = 309.8882 Da.

Sample Name	GP-LRW	**Position**	Vial 1	**Instrument Name**	Instrument 1	**User Name**	
Inj Vol	0	**InjPosition**		**SampleType**	Sample	**IRM Calibration Status**	All Ions Missed
Data Filename	GP-LRW.d	**ACQ Method**		**Comment**		**Acquired Time**	1/19/2017 12:36:58 PM

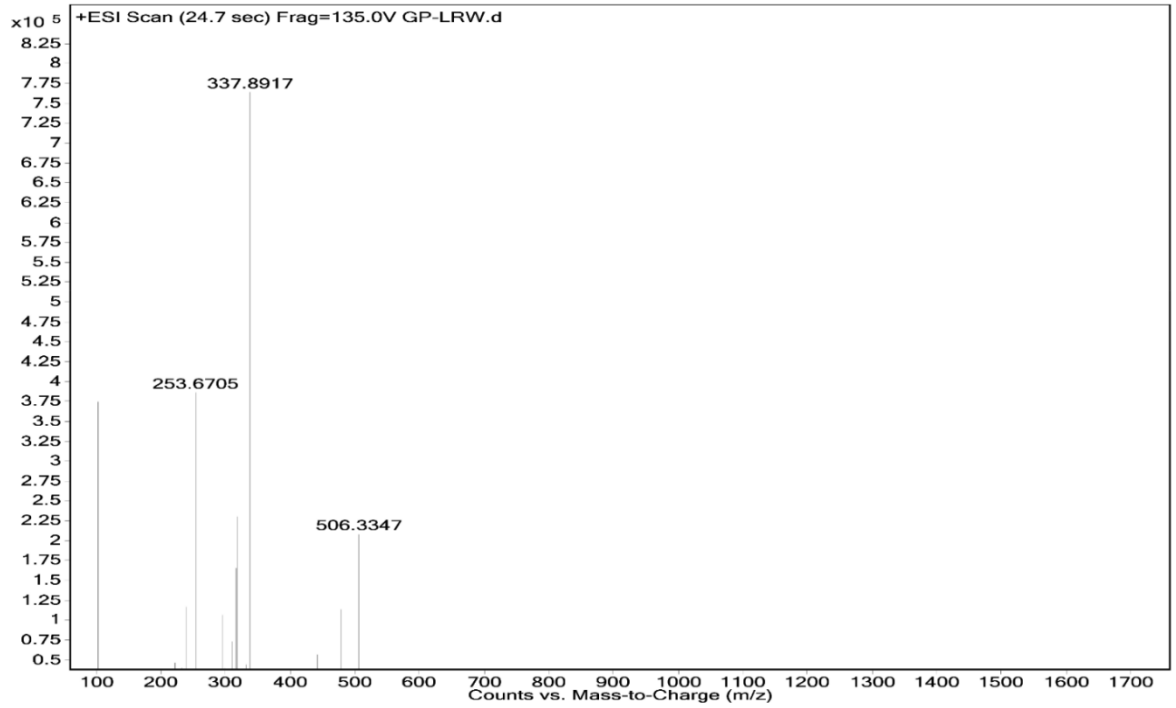

Figure A22: ESI-MS of P5. Calc. $(M+H)^+$ for $C_{47}H_{82}N_{18}O_7$ = 1011.6687 Da; Obs. $(M+2H)^+$ = 506.3347 Da, $(M+3H)^+$ = 337.8917 Da, $(M+4H)^+$ = 253.6705 Da.. $(M+H)^+$ = 882.5305 Da, $(M+2H)^+$ = 441.77 Da, $(M+3H)^+$ = 294.8461 Da.

Sample Name	GP-LHW-11	**Position**	Vial 1	**Instrument Name**	Instrument 1	**User Name**	
Inj Vol	0	**InjPosition**		**SampleType**	Sample	**IRM Calibration Status**	All Ions Missed
Data Filename	GP-LHW-11.d	**ACQ Method**		**Comment**		**Acquired Time**	1/19/2017 12:31:40 PM

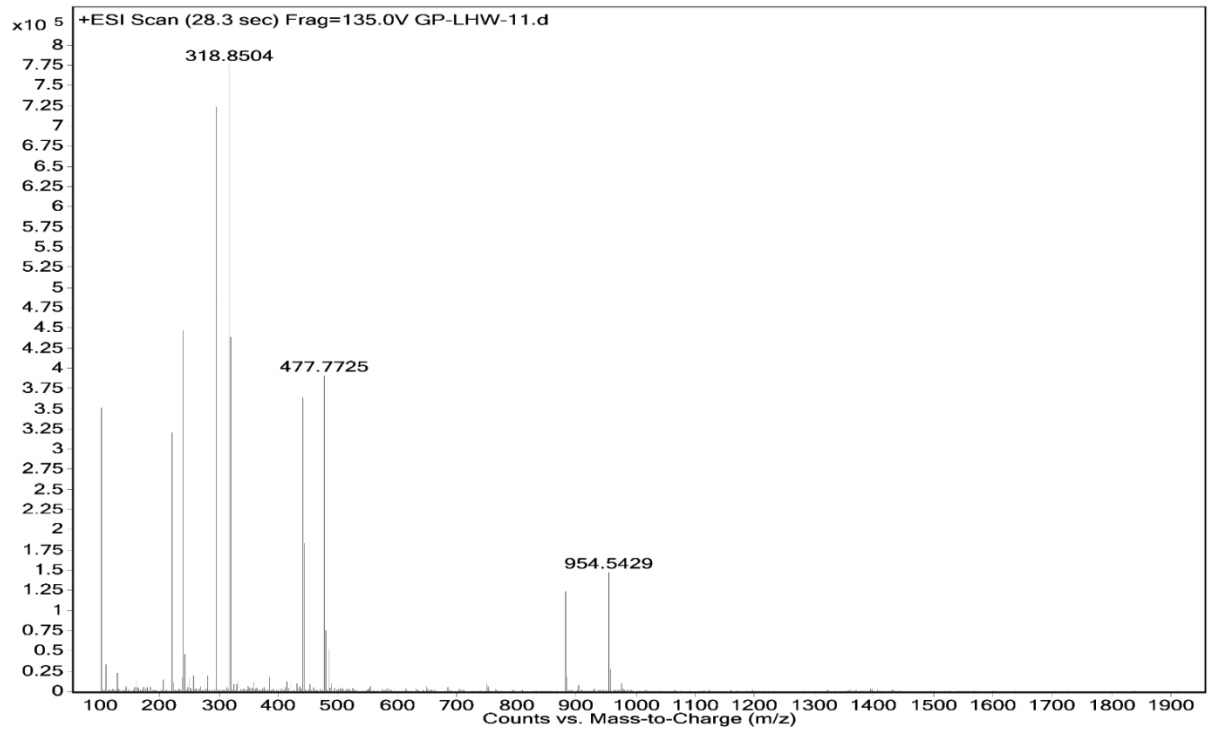

Figure A23: ESI-MS of P6. Calc. $(M+H)^+$ for $C_{47}H_{67}N_{15}O_7$ = 954.5421 Da; Obs. $(M+H)^+$ = 954.5429 Da, $(M+2H)^+$ = 477.7725 Da, $(M+3H)^+$ = 318.8504 Da.. $(M+H)^+$ = 882.5305 Da, $(M+2H)^+$ = 441.77 Da, $(M+3H)^+$ = 294.8461 Da.

Sample Name	SAMPLE 2	**Position**	P1-B1	**Instrument Name**	Instrument 1	**User Name**	
Inj Vol	20	**InjPosition**		**SampleType**	Sample	**IRM Calibration Status**	Success
Data Filename	GP-21.d	**ACQ Method**	ESI ALS 100-3000.m	**Comment**		**Acquired Time**	6/6/2019 5:55:07 PM

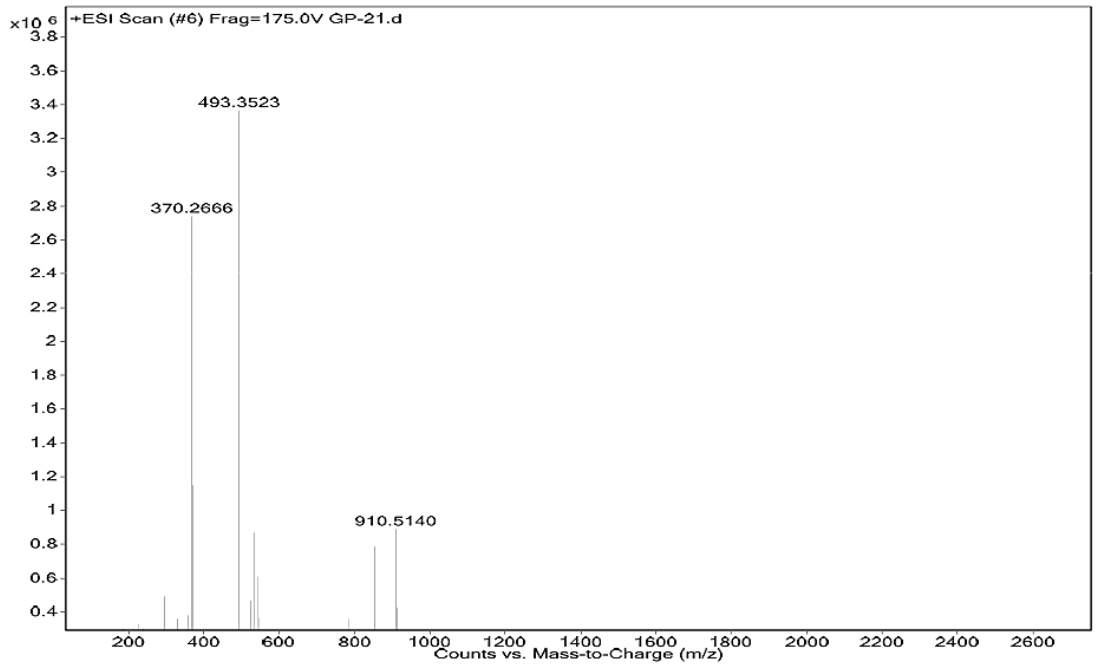

Figure A24: ESI-MS of AMP21. Calc. $(M+H)^+$ for $C_{65}H_{128}N_{28}O_{11}$= 1477.0317 Da; Obs. $(M+3H)^+$ = 493.3523 Da, $(M+4H)^+$ = 370.2666 Da, $(M+5H)^+$ = 296.4063 Da

Sample Name	SAMPLE 2	**Position**	P1-B2	**Instrument Name**	Instrument 1	**User Name**	
Inj Vol	20	**InjPosition**		**SampleType**	Sample	**IRM Calibration Status**	Success
Data Filename	GP-22.d	**ACQ Method**	ESI ALS 100-3000.m	**Comment**		**Acquired Time**	6/6/2019 5:56:58 PM

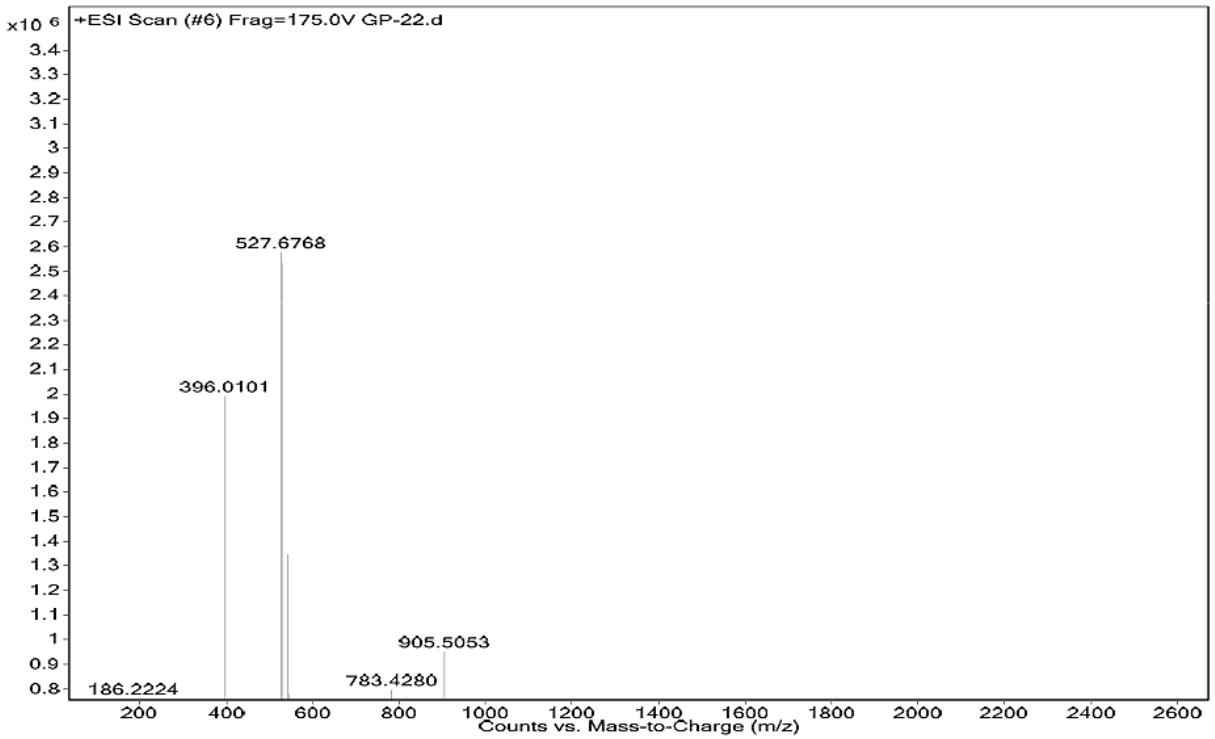

Figure A25: ESI-MS of AMP22. Calc. $(M+H)^+$ for $C_{75}H_{125}N_{27}O_{11}$= 1580.0052 Da; Obs. $(M+3H)^+$ = 527.6768 Da, $(M+4H)^+$ = 396.0101 Da, $(M+2H+TFA)^+$ = 905.5053 Da.

Sample Name	SAMPLE 2	**Position**	P1-B3	**Instrument Name**	Instrument 1	**User Name**	
Inj Vol	20	**InjPosition**		**SampleType**	Sample	**IRM Calibration Status**	Success
Data Filename	GP-23.d	**ACQ Method**	ESI ALS 100-3000.m	**Comment**		**Acquired Time**	6/6/2019 5:58:44 PM

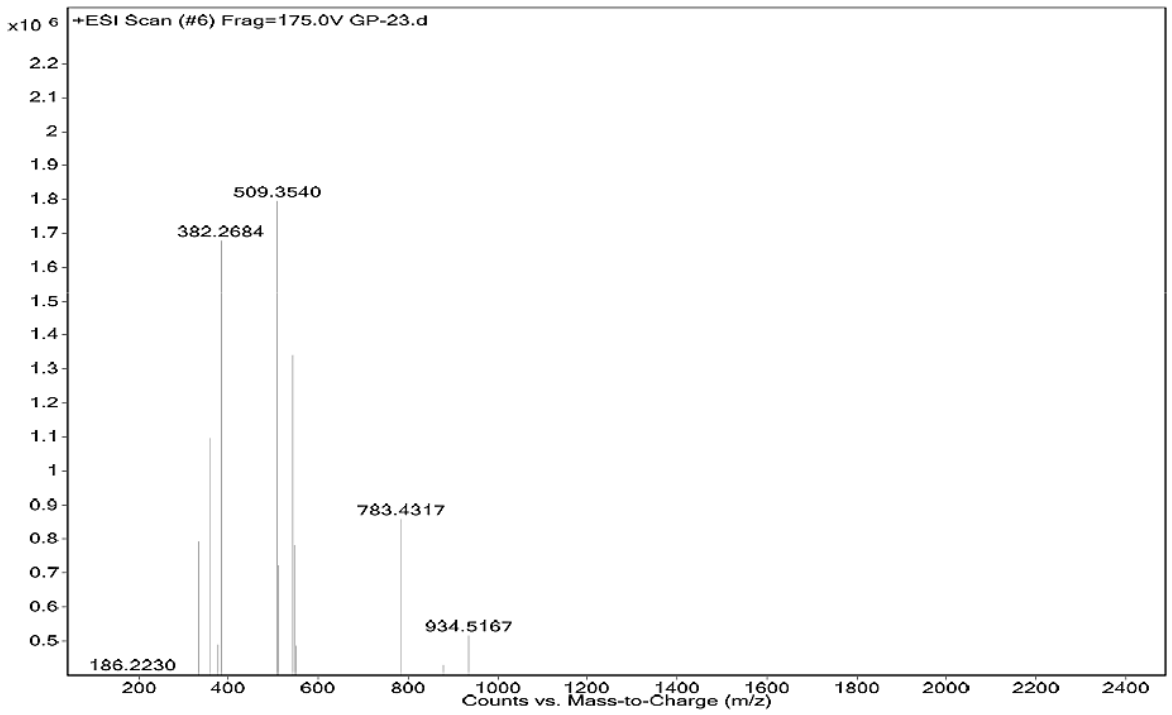

Figure A26: ESI-MS of AMP23. Calc. $(M+H)^+$ for $C_{69}H_{128}N_{28}O_{11}$= 1525.0317 Da; Obs. $(M+3H)^+$ = 509.3540 Da, $(M+4H)^+$ = 382.2684 Da.

Sample Name	SAMPLE 2	**Position**	P1-B4	**Instrument Name**	Instrument 1	**User Name**	
Inj Vol	20	**InjPosition**		**SampleType**	Sample	**IRM Calibration Status**	Success
Data Filename	GP-24-r001.d	**ACQ Method**	ESI ALS 100-3000.m	**Comment**		**Acquired Time**	6/6/2019 6:00:32 PM

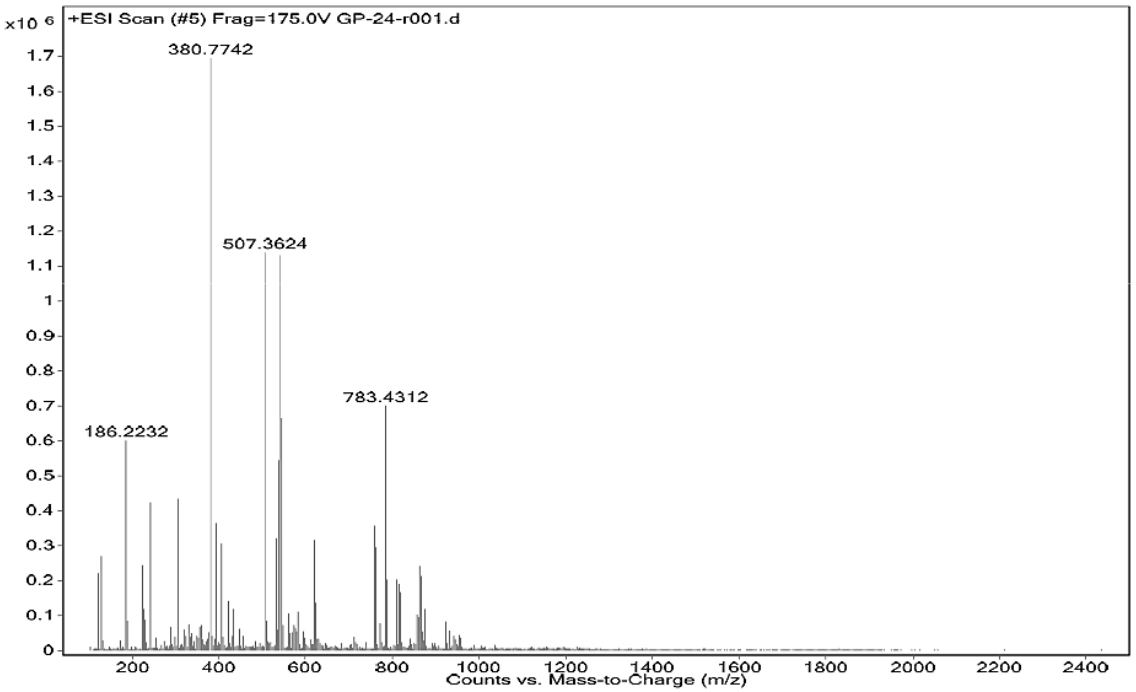

Figure A27: ESI-MS of AMP24. Calc. $(M+H)^+$ for $C_{66}H_{130}N_{30}O_{16}$= 1519.0535 Da; Obs. $(M+3H)^+$ = 507.3624 Da, $(M+4H)^+$ =380.7742 Da, $(M+5H)^+$ = 304.9891 Da, $(M+2H+Na)^+$ = 783.4312 Da.

Sample Name	SAMPLE	**Position**	P2-D7	**Instrument Name**	Instrument 1	**User Name**	
Inj Vol	20	**InjPosition**		**SampleType**	Sample	**IRM Calibration Status**	Success
Data Filename	CF-21-I1-6.7-7.2.d	**ACQ Method**	ESI ALS 100-3000.m	**Comment**		**Acquired Time**	6/13/2019 5:43:53 PM

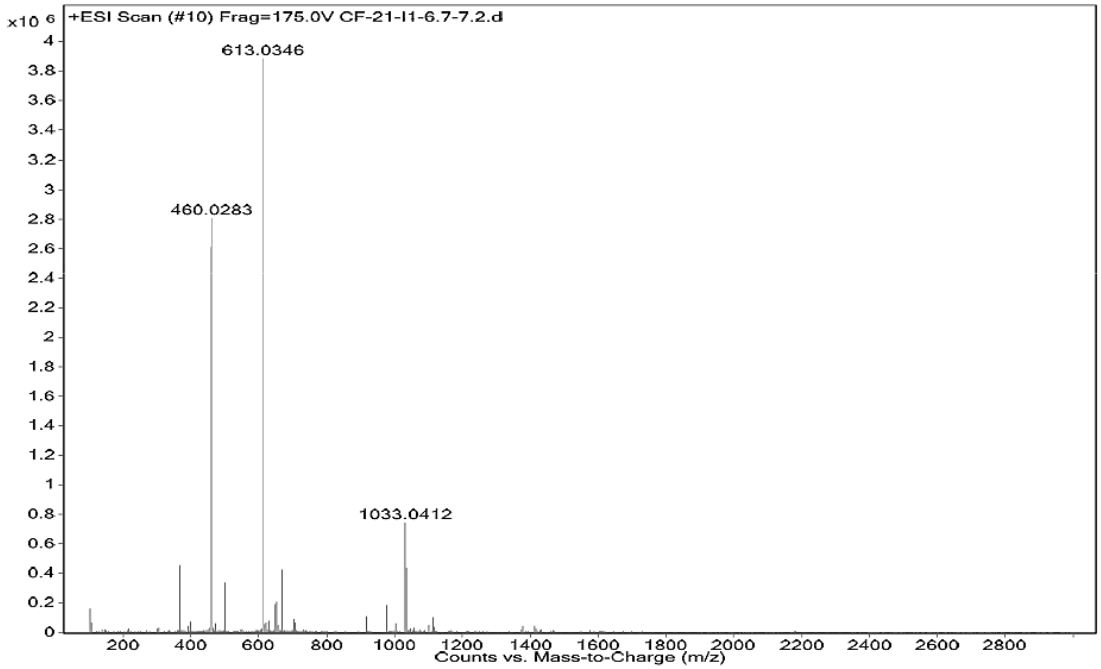

Figure A28: ESI-MS of CF-AMP21. Calc. $(M+H)^+$ for $C_{86}H_{138}N_{28}O_{17}$= 1835.0795 Da; Obs. $(M+3H)^+$ = 613.0346 Da, $(M+4H)^+$ = 460.0283 Da, $(M+2H+TFA)^+$ = 1033.0412 Da.

Sample Name	SAMPLE	**Position**	P2-D9	**Instrument Name**	Instrument 1	**User Name**	
Inj Vol	20	**InjPosition**		**SampleType**	Sample	**IRM Calibration Status**	Success
Data Filename	CF-22-I1-8.1-8.5.d	**ACQ Method**	ESI ALS 100-3000.m	**Comment**		**Acquired Time**	6/13/2019 5:49:02 PM

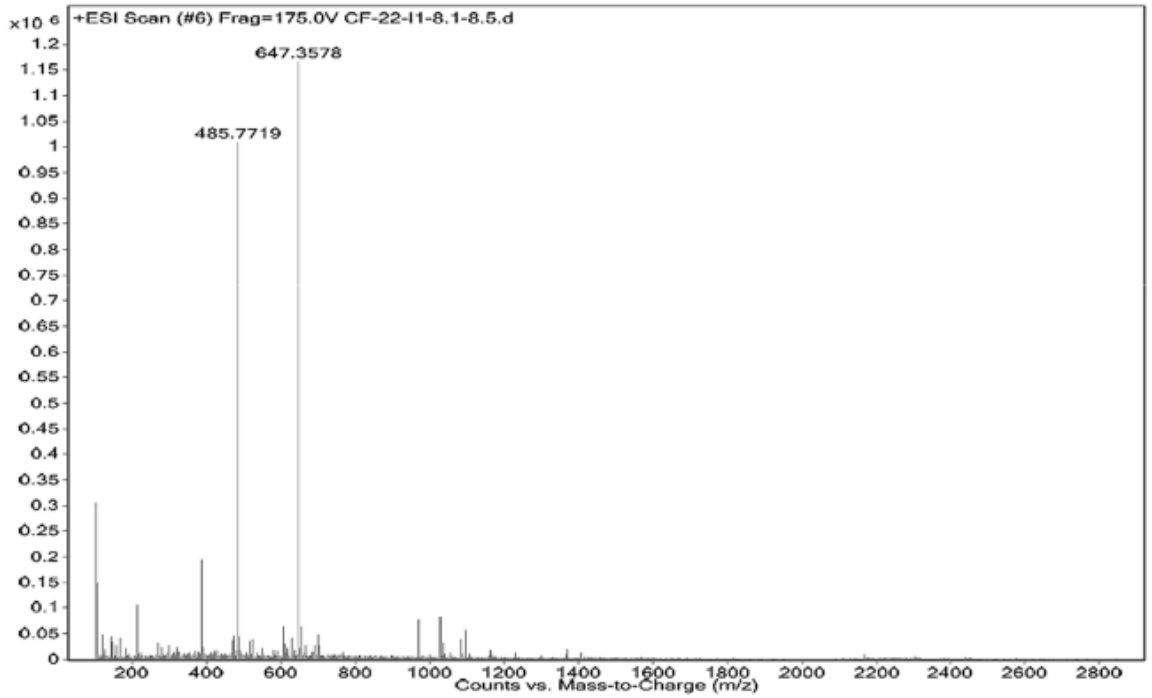

Figure A29: ESI-MS of CF-AMP22. Calc. $(M+H)^+$ for $C_{96}H_{135}N_{27}O_{17}$= 1939.0563 Da; Obs. $(M+3H)^+$ = 647.3578 Da, $(M+4H)^+$ = 485.7719 Da.

Sample Name	SAMPLE	**Position**	P2-D4	**Instrument Name**	Instrument 1	**User Name**	
Inj Vol	20	**InjPosition**		**SampleType**	Sample	**IRM Calibration Status**	Success
Data Filename	CF-23-I1-4-r001.d	**ACQ Method**	ESI ALS 100-3000.m	**Comment**		**Acquired Time**	6/13/2019 5:38:51 PM

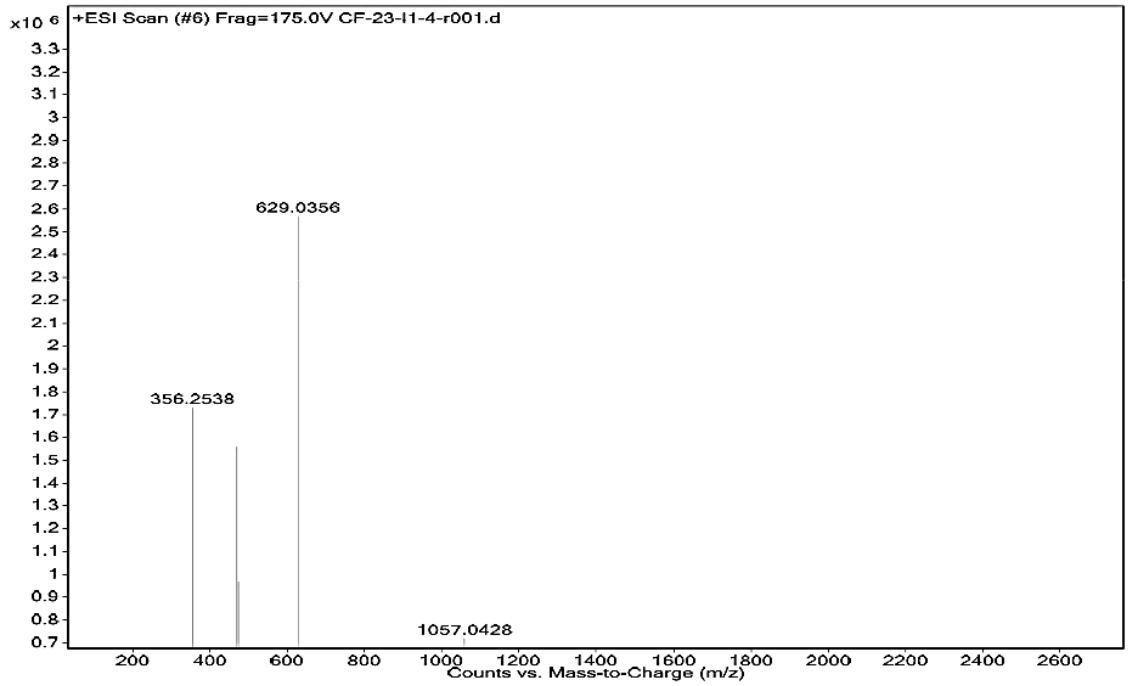

Figure A30: ESI-MS of CF-AMP23. Calc. $(M+H)^+$ for $C_{90}H_{138}N_{28}O_{17}$= 1883.0795 Da; Obs. $(M+3H)^+$ = 629.0356 Da, $(M+4H)^+$ = 472.0301 Da, $(M+2H+TFA)^+$ = 1057.0428 Da

Sample Name	CF-24-I3-3.7-4.1	**Position**	P1-B9	**Instrument Name**	Instrument 1	**User Name**	
Inj Vol	20	**InjPosition**		**SampleType**	Sample	**IRM Calibration Status**	Success
Data Filename	CF-24-I3-3.7-4.1.d	**ACQ Method**	ESI ALS 100-3000.m	**Comment**		**Acquired Time**	6/13/2019 11:15:43 AM

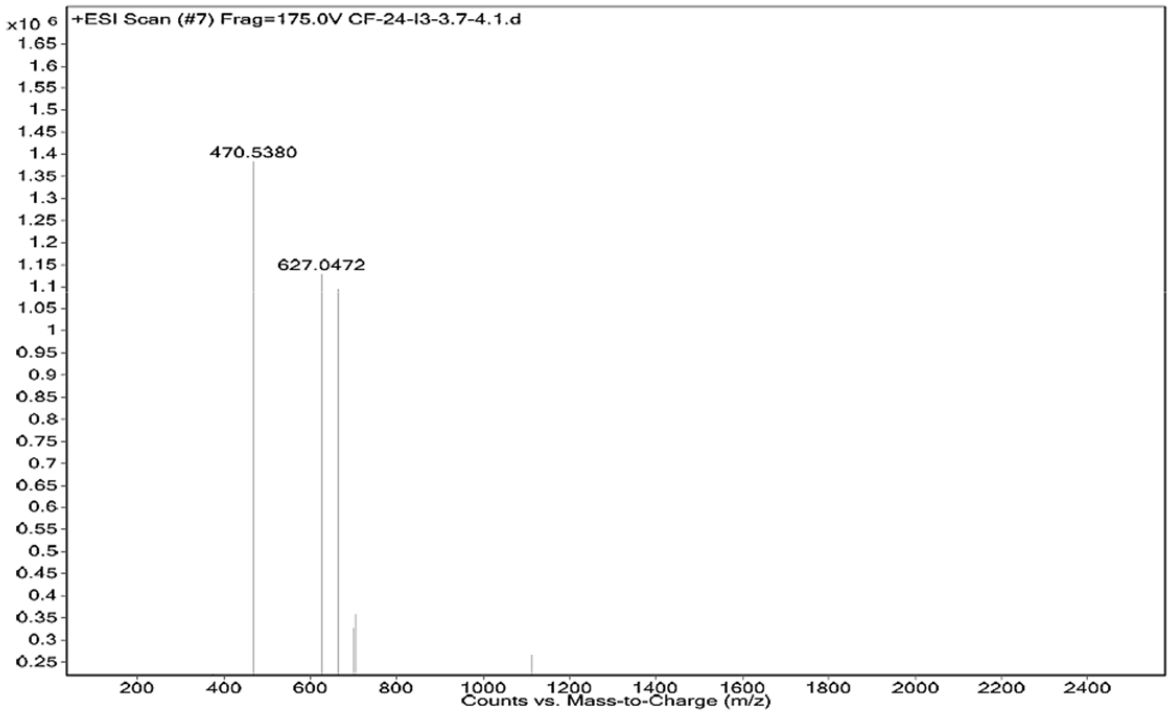

Figure A31: ESI-MS of CF-AMP24. Calc. $(M+H)^+$ for $C_{87}H_{140}N_{30}O_{17}$= 1877.1013 Da; Obs. $(M+3H)^+$ = 627.0472 Da, $(M+4H)^+$ = 470.5380 Da.

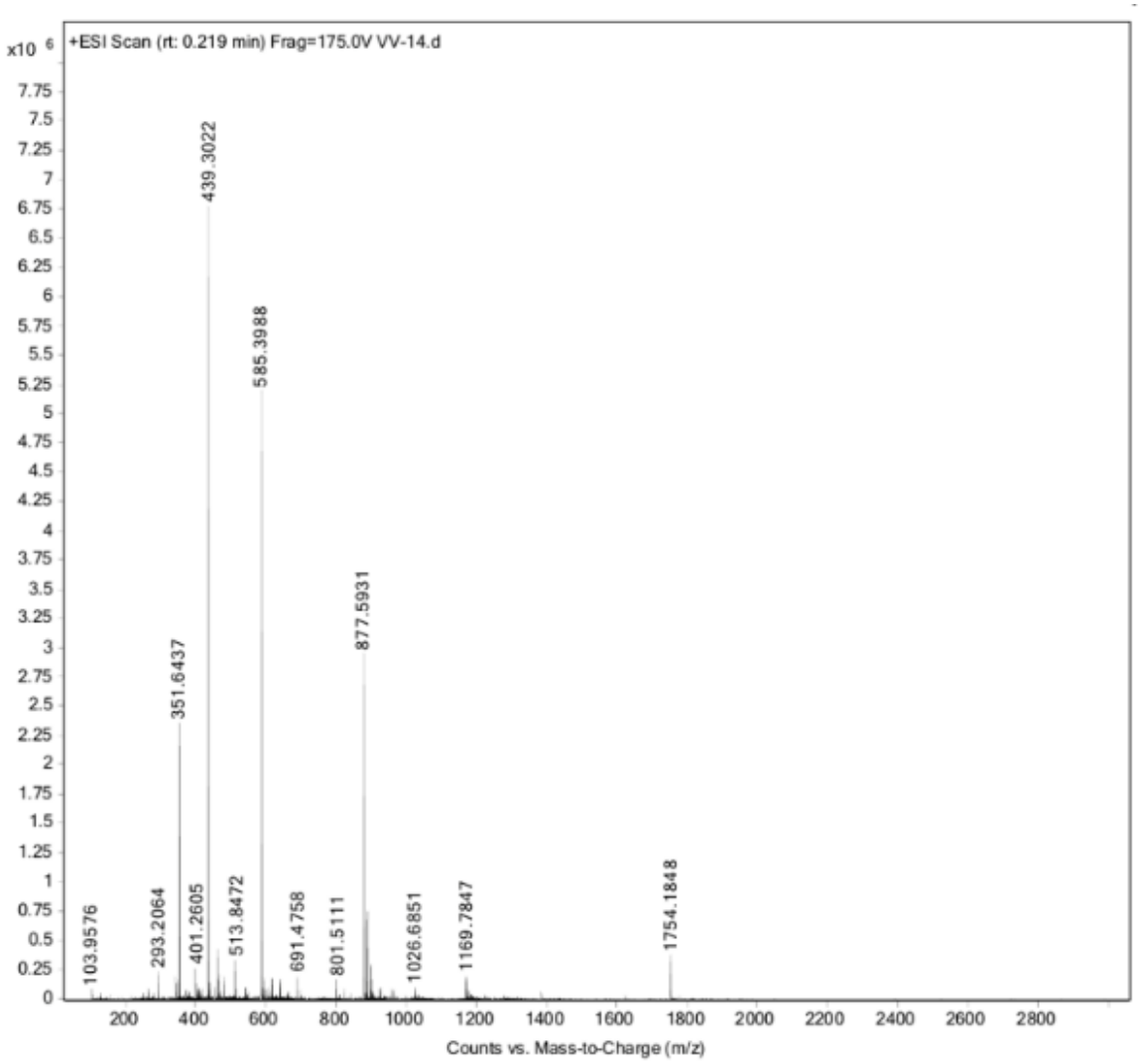

Figure A32: ESI-MS of VV-14. $(M+H)^+$ =1754.184 Da, $(M+2H)^+$ = 877.593 Da, $(M+3H)^+$ = 585.398 Da, $(M+4H)^+$ = 439.302 Da, $(M+5H)^+$ = 351.643 Da, $(M+6H)^+$ = 293.206 Da.

Sample Name	GP-31-1	**Position**	P2-F1	**Instrument Name**	Instrument 1	**User Name**	
Inj Vol	20	**InjPosition**		**SampleType**	Sample	**IRM Calibration Status**	Success
Data Filename	GP-31-1.d	**ACQ Method**	ESI ALS 100-2000.m	**Comment**		**Acquired Time**	5/14/2019 5:15:37 PM

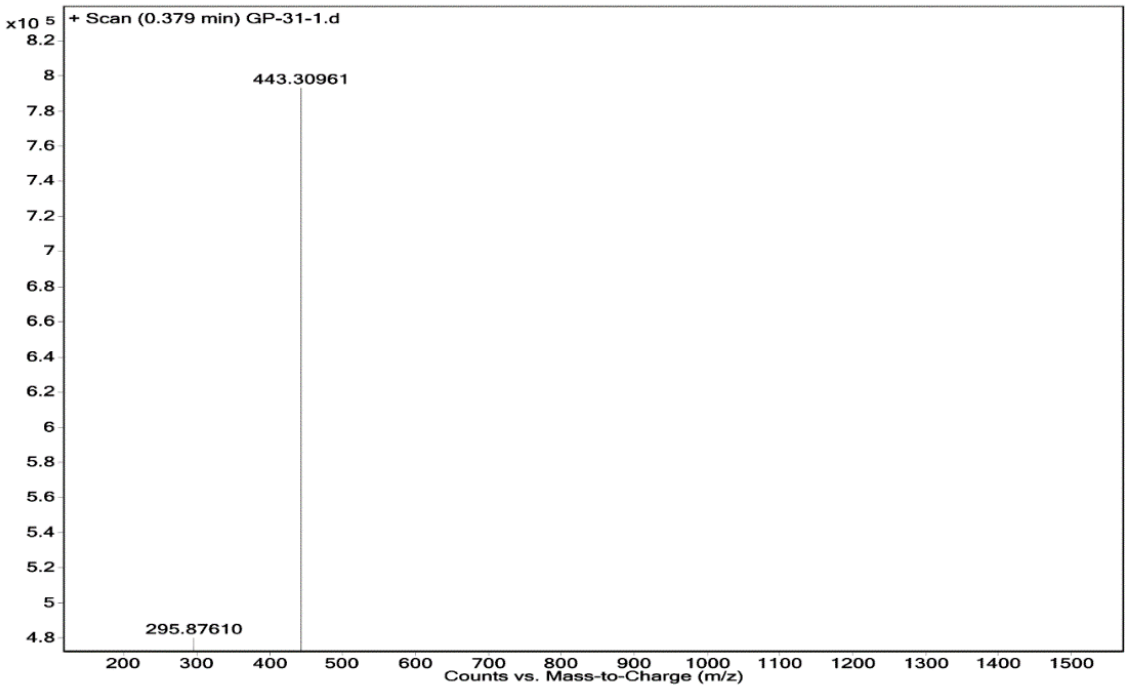

Figure A33: ESI-MS of P31. Calc. $(M+H)^+$ for $C_{44}H_{76}N_{12}O_7$= 885.5993 Da; Obs. $(M+2H)^+$= 443.3096 Da, $(M+3H)^+$= 295.8761 Da.

Sample Name	SAMPLE 42	**Position**	P2-E3	**Instrument Name**	Instrument 1	**User Name**	
Inj Vol	20	**InjPosition**		**SampleType**	Sample	**IRM Calibration Status**	Success
Data Filename	GP-32.d	**ACQ Method**	ESI ALS 100-3000.m	**Comment**		**Acquired Time**	5/13/2019 6:26:48 PM

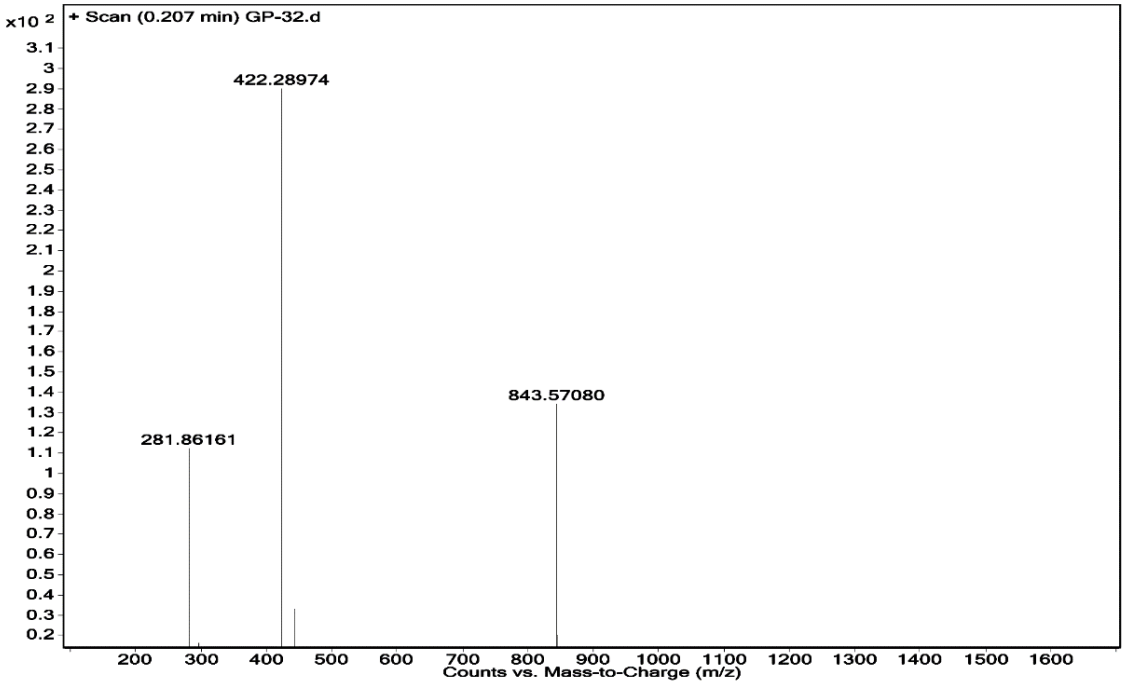

Figure A34: ESI-MS of P32. Calc. $(M+H)^+$ for $C_{41}H_{70}N_{12}O_7$= 843.5524 Da; Obs. $(M+H)^+$=843.5708 Da, $(M+2H)^+$= 422.2897 Da, $(M+3H)^+$= 281.8616 Da.

Sample Name	SAMPLE 43	**Position**	P2-E4	**Instrument Name**	Instrument 1	**User Name**	
Inj Vol	20	**InjPosition**		**SampleType**	Sample	**IRM Calibration Status**	Success
Data Filename	GP-33.d	**ACQ Method**	ESI ALS 100-3000.m	**Comment**		**Acquired Time**	5/13/2019 6:28:39 PM

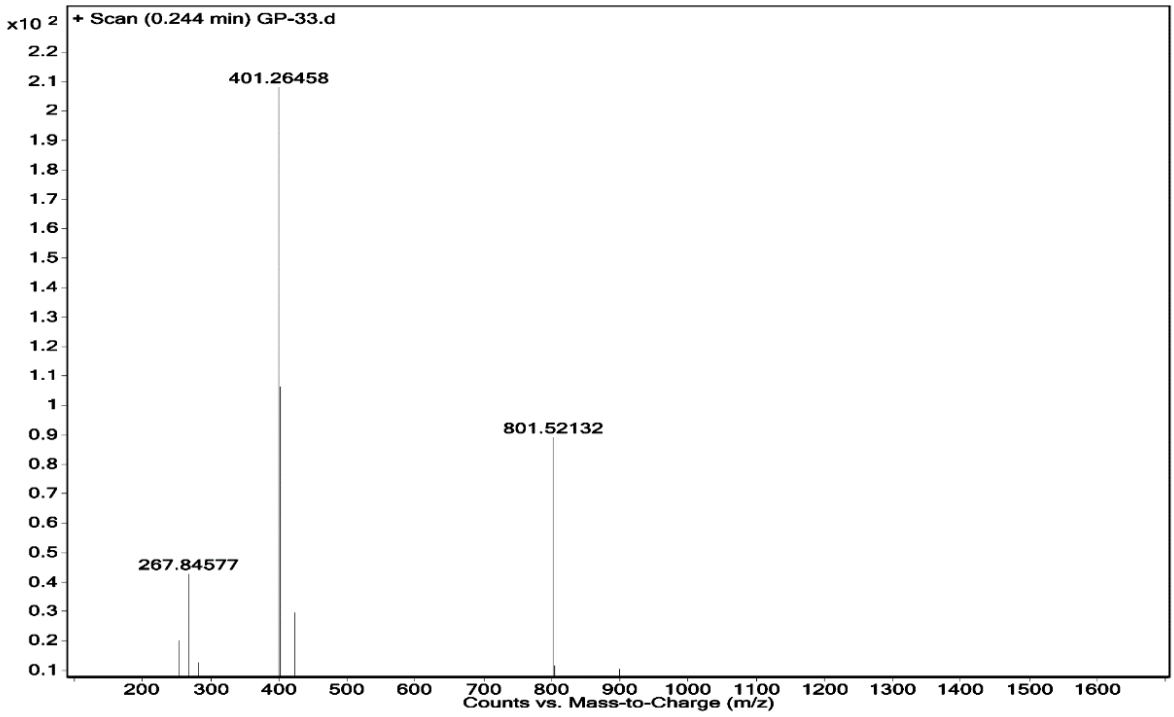

Figure A35: ESI-MS of P33. Calc. $(M+H)^+$for $C_{38}H_{64}N_{12}O_7$= 801.5054 Da; Obs. $(M+H)^+$=801.5213 Da, $(M+2H)^+$= 401.2645 Da, $(M+3H)^+$= 267.8457 Da.

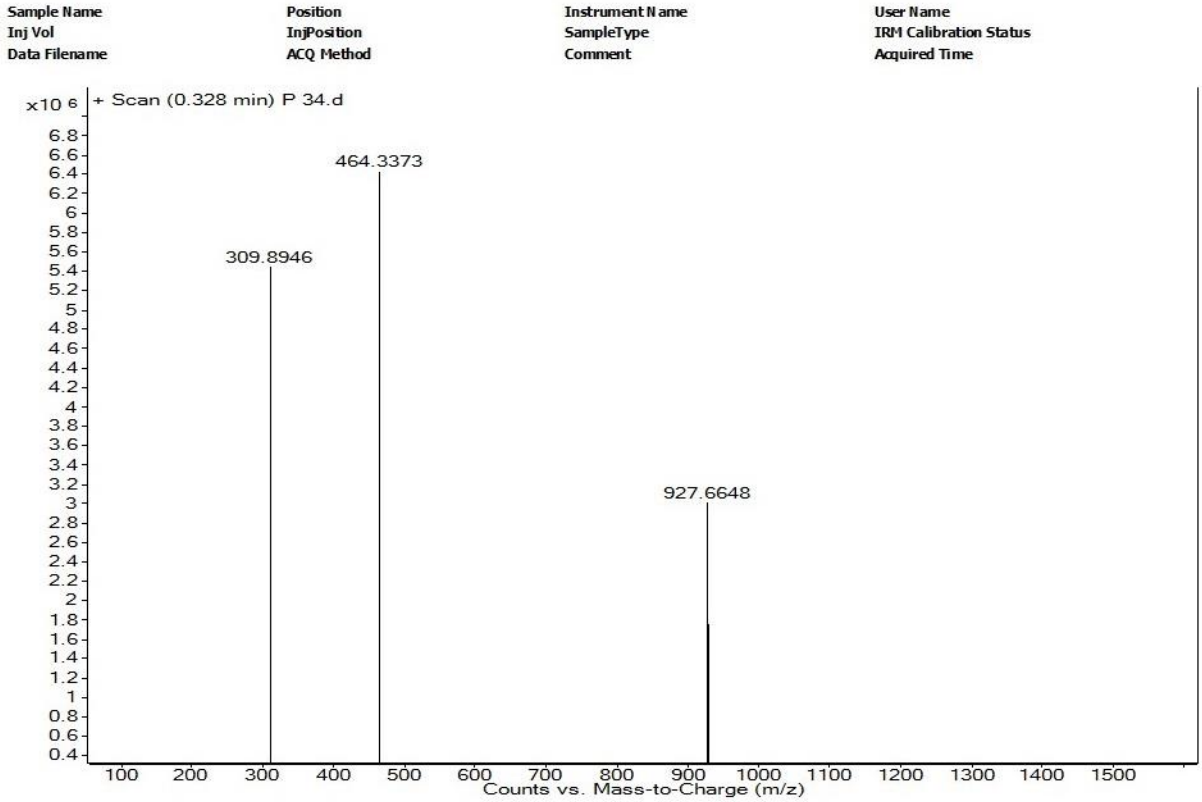

Figure A36: MS of P34. Calc. $(M+H)^+$ for $C_{47}H_{82}N_{12}O_7$= 927.6502 Da; Obs. $(M+H)^+$=927.6648 Da, $(M+2H)^+$= 464.3373 Da, $(M+3H)^+$= 309.8946 Da.

Sample Name	SAMPLE 44	**Position**	P2-E5	**Instrument Name**	Instrument 1	**User Name**	
Inj Vol	20	**InjPosition**		**SampleType**	Sample	**IRM Calibration Status**	Success
Data Filename	GP-34.d	**ACQ Method**	ESI ALS 100-3000.m	**Comment**		**Acquired Time**	5/13/2019 6:30:29 PM

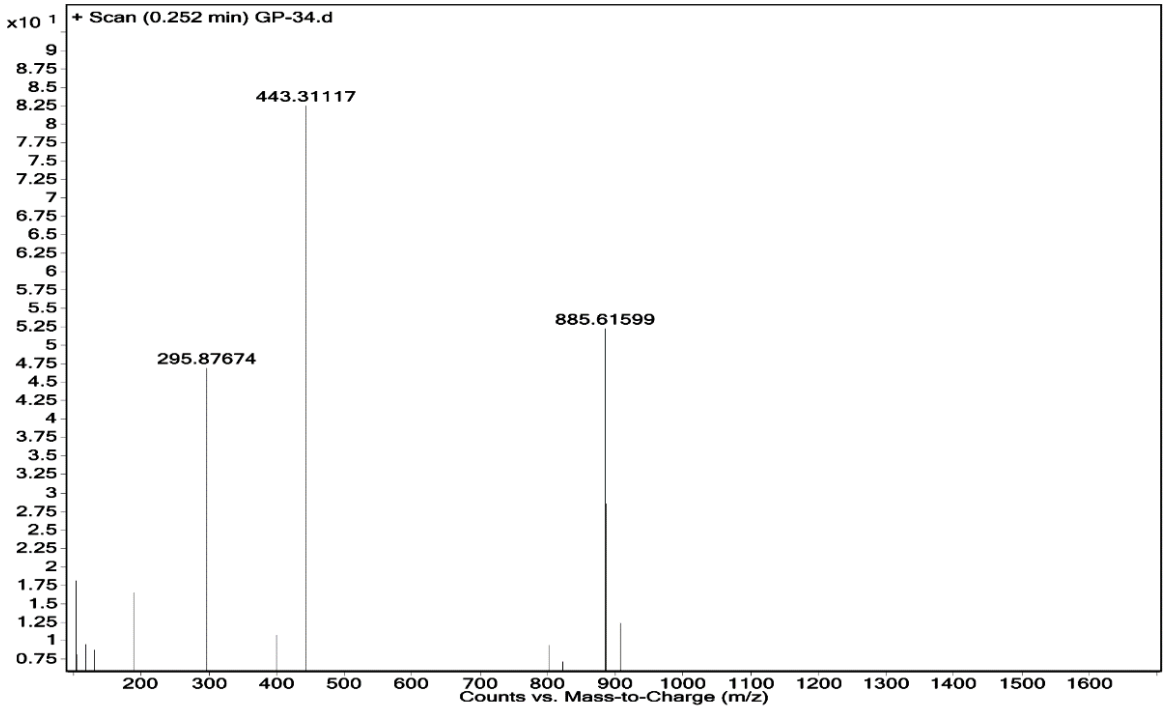

Figure A37: ESI-MS of P35. Calc. $(M+H)^+$for $C_{44}H_{76}N_{12}O_7$= 885.5993 Da; Obs. $(M+H)^+$=885.6159 Da, $(M+2H)^+$= 443.3112 Da, $(M+3H)^+$= 295.8767 Da

Sample Name	GP-35-1	**Position**	P2-F5	**Instrument Name**	Instrument 1	**User Name**	
Inj Vol	20	**InjPosition**		**SampleType**	Sample	**IRM Calibration Status**	Success
Data Filename	GP-35-1.d	**ACQ Method**	ESI ALS 100-2000.m	**Comment**		**Acquired Time**	5/14/2019 5:23:03 PM

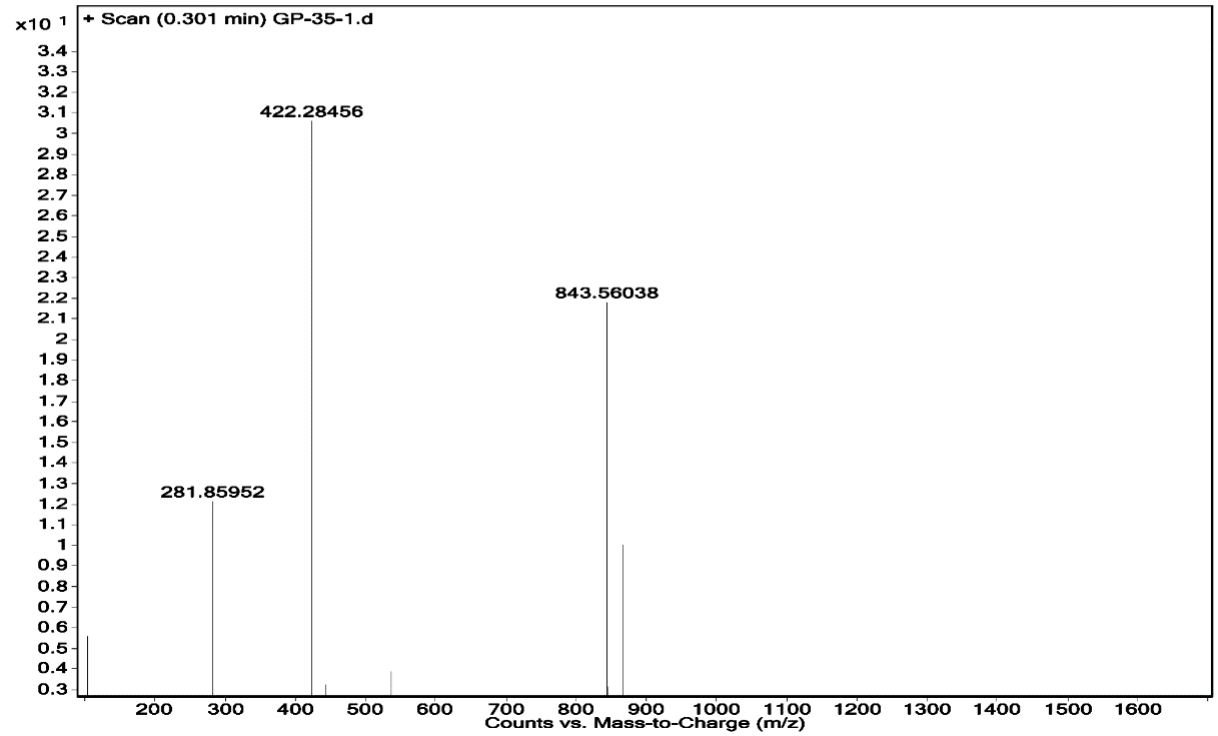

Figure A38: ESI-MS of P36. Calc. $(M+H)^+$for $C_{41}H_{70}N_{12}O_7$= 843.5524 Da; Obs. $(M+H)^+$=843.5604 Da, $(M+2H)^+$= 422.2845 Da, $(M+3H)^+$= 281.8595 Da.

Sample Name	GP-36-1	**Position**	P2-F6	**Instrument Name**	Instrument 1	**User Name**	
Inj Vol	20	**InjPosition**		**SampleType**	Sample	**IRM Calibration Status**	Success
Data Filename	GP-36-1.d	**ACQ Method**	ESI ALS 100-2000.m	**Comment**		**Acquired Time**	5/14/2019 5:24:52 PM

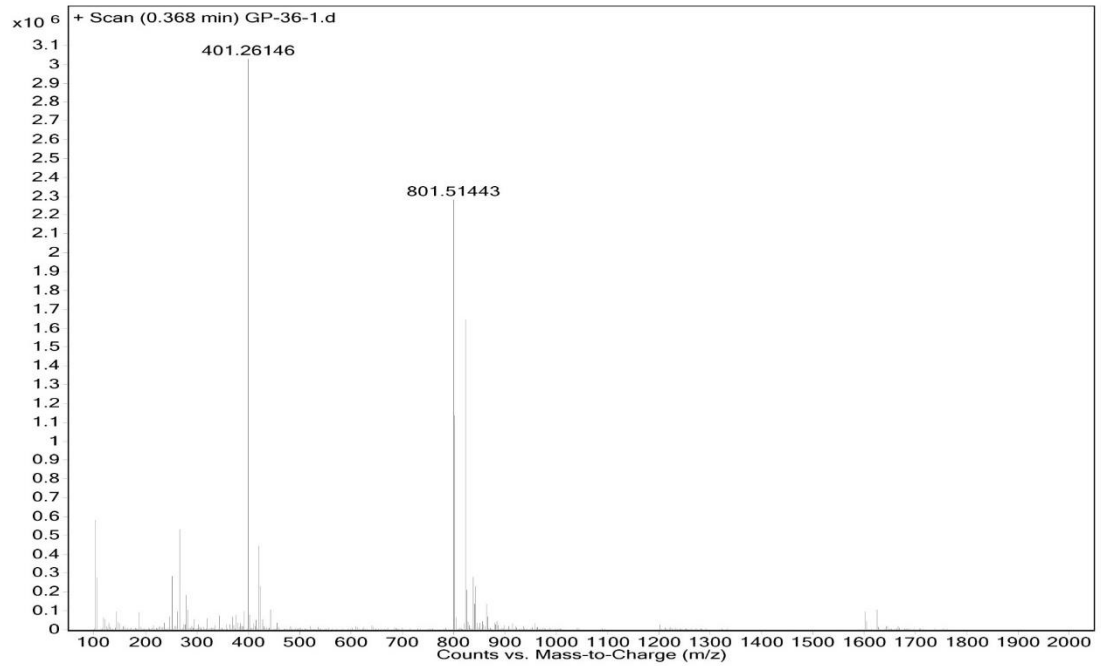

Figure A39: ESI-MS of P37. Calc. $(M+H)^+$ for $C_{38}H_{64}N_{12}O_7$= 801.5054 Da; Obs. $(M+H)^+$ = 801.5143 Da, $(M+2H)^+$ = 401.2614 Da

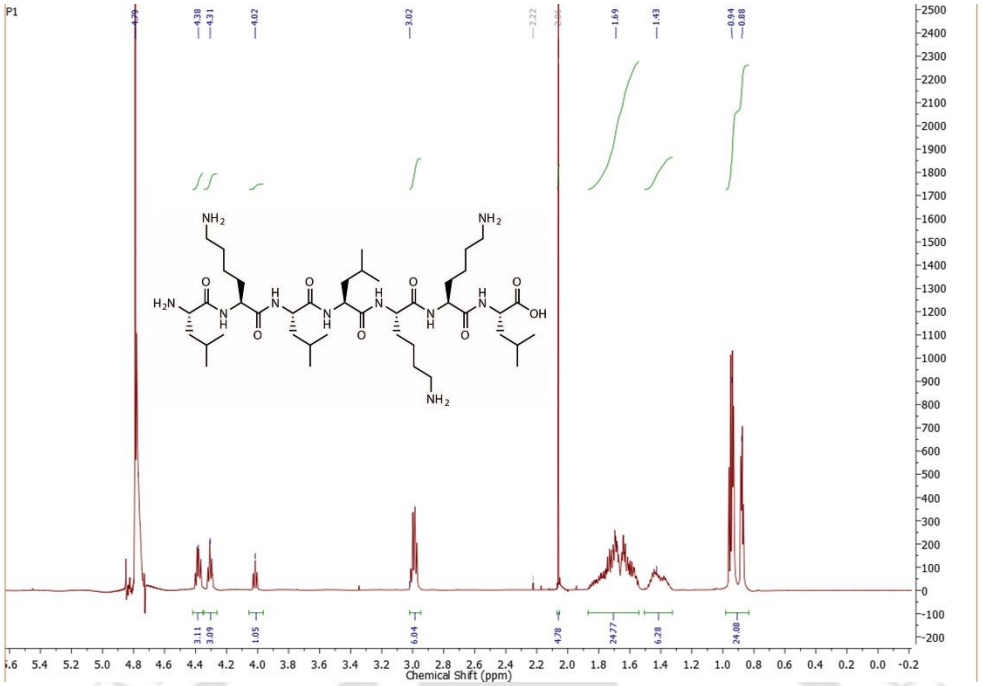

Figure A40: qHNMR of **P1** at a concentration of 15.97 mM in D_2O at room temperature. Acetonitrile was added as an internal calibrant.^{1}H NMR (600 MHz, D_2O) δ 0.88-0.94 (m, 24H, Leu), 1.35-1.88 (m, 27H, Leu and Lys), 2.22 (acetone, solvent residue), 2.96-3.04 (6H, m, Lys), 4.02, 4.31, 4.38 (7 αH).

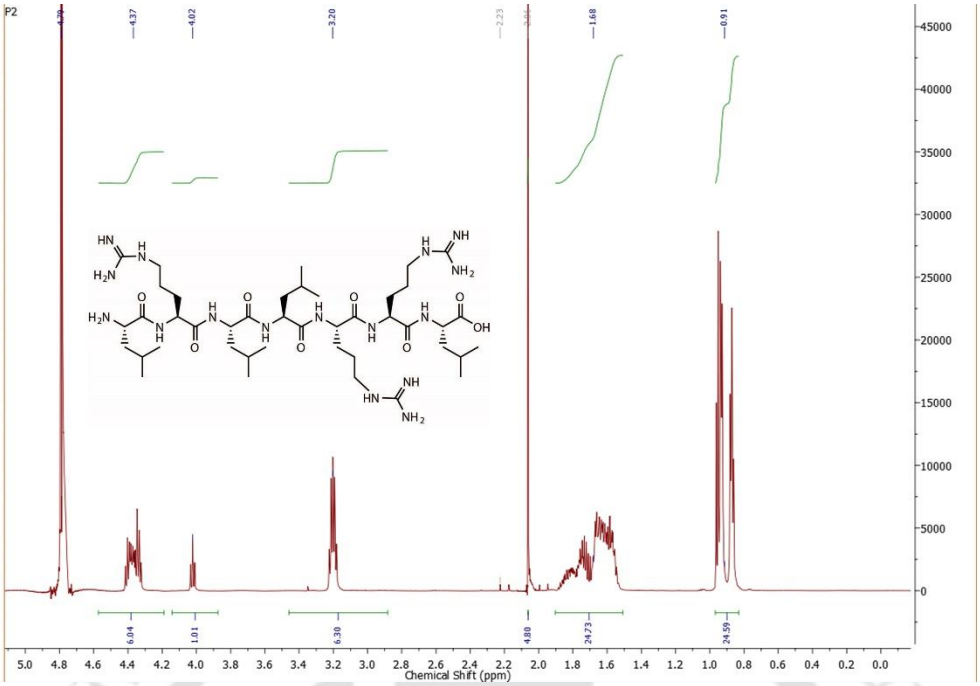

Figure A41: qHNMR of **P2** at a concentration of 15.97 mM in D_2O at room temperature. Acetonitrile was added as an internal calibrant.^{1}H NMR (600 MHz, D_2O) δ 0.83-0.97 (m, 24H, Leu), 1.57-1.9 (m, 21H, Leu and Arg), 3.15-3.26 (6H, Arg), 4.02, 4.37 (7 αH).

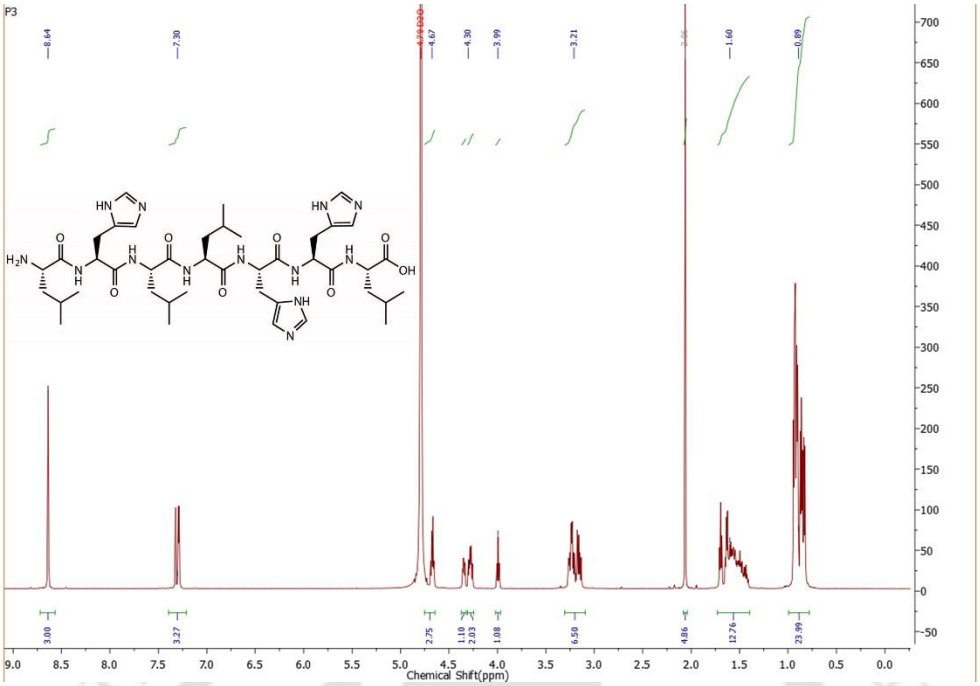

Figure A42: qHNMR of **P3** at a concentration of 15.97 mM in D_2O at room temperature. Acetonitrile was added as an internal calibrant.^{1}H NMR (600 MHz, D_2O) δ 0.75-0.96 (m, 24H, Leu), 1.37-1.72 (12H, Leu), 3.11-3.32 (6H, His), 3.99, 4.3, 4.67 (7 αH), 7.3 (3H, His), 8.64(3H, His).

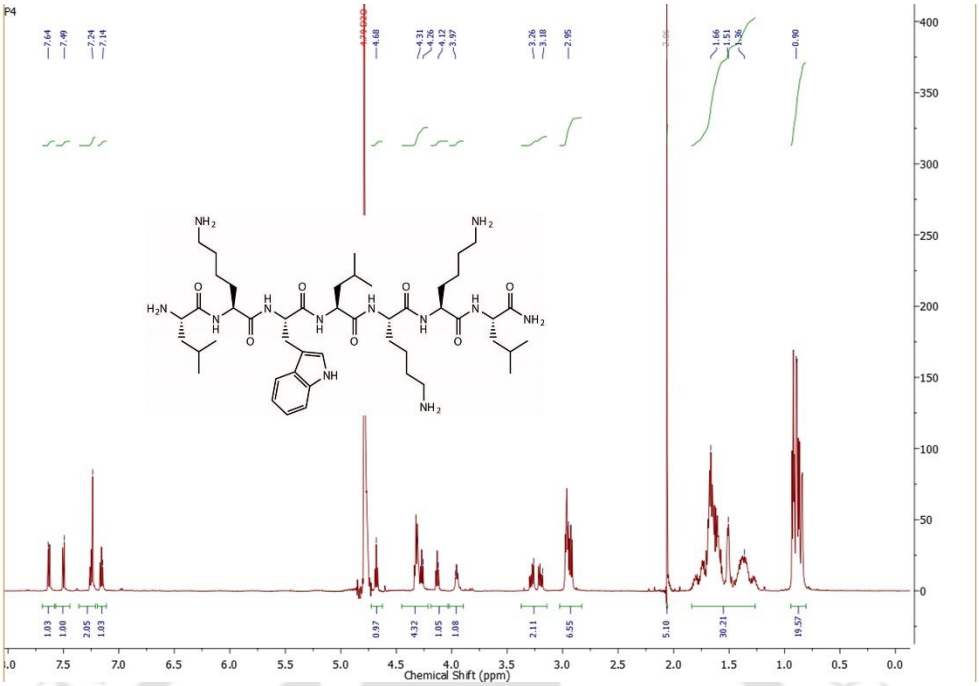

Figure A43: qHNMR of **P4** at a concentration of 15.97 mM in D_2O at room temperature. Acetonitrile was added as an internal calibrant.^{1}H NMR (600 MHz, D_2O) δ 0.8-0.96 (18H, Leu), 1.19-1.87 (27H, Leu and Lys), 2.9-3.3 (8H, m, Lys and Trp), 3.97, 4.12, 4.26, 4.31, 4.68 (7 αH), 7.14, 7.24, 7.49, 7.64 (5H, Trp).

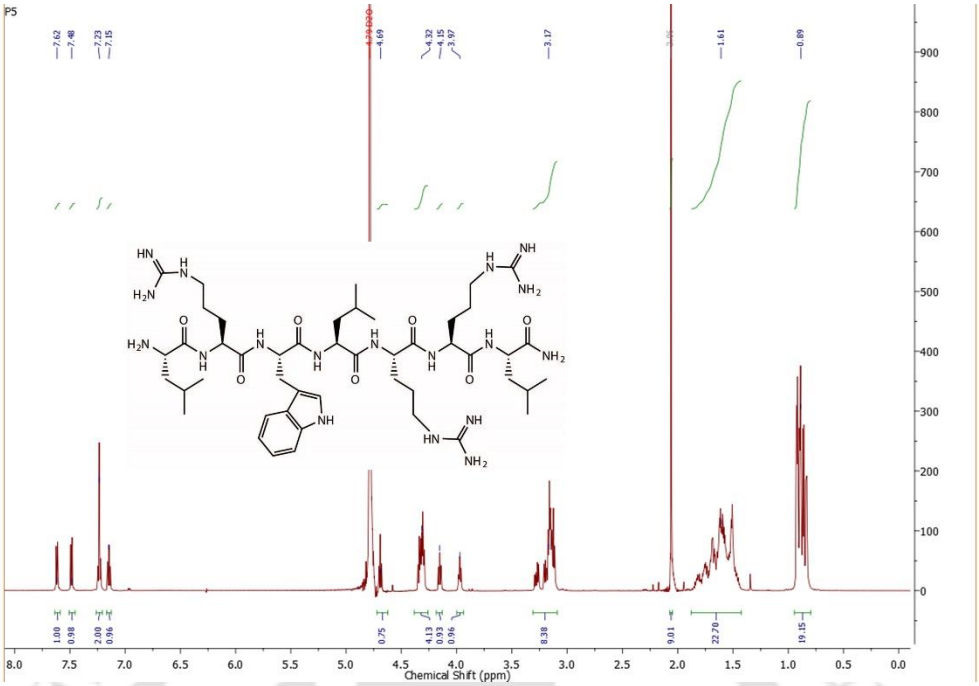

Figure A44: qHNMR of **P5** at a concentration of 15.97 mM in D_2O at room temperature. Acetonitrile was added as an internal calibrant.^{1}H NMR (600 MHz, D_2O) δ 0.8-0.98 (18H, Leu), 1.4-1.8 (21H, Leu and Arg), 3.09-3.33 (8 H, Arg,Trp), 3.97, 4.15, 4.32, 4.69 (7 αH, 1 merged with D_2O signal), 7.15, 7.23, 7.48, 7.62 (5H, Trp).

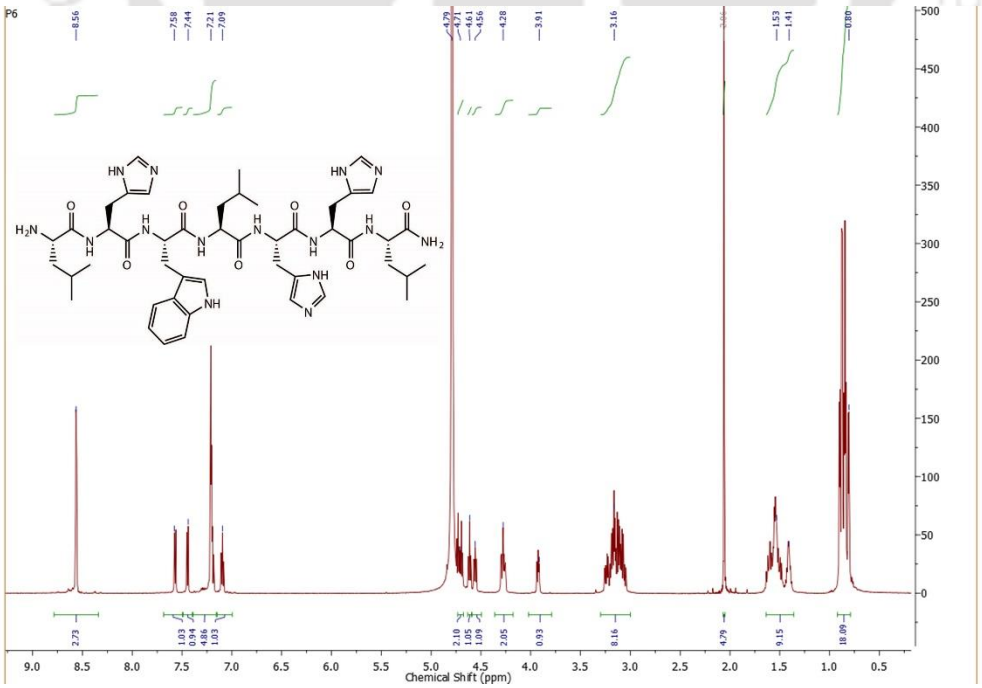

Figure A45: qHNMR of **P6** at a concentration of 15.97 mM in D_2O at room temperature. Acetonitrile was added as an internal calibrant.^{1}H NMR (600 MHz, D_2O) δ 0.78-0.96 (18H, Leu), 1.34-1.65 (9H, Leu), 3.0-3.30 (8H, His and Trp), 3.91, 4.28, 4.56, 4.61, 4.71 (7 αH), 7.21, 7.44, 7.58, 8.56 (11H, Trp and His).

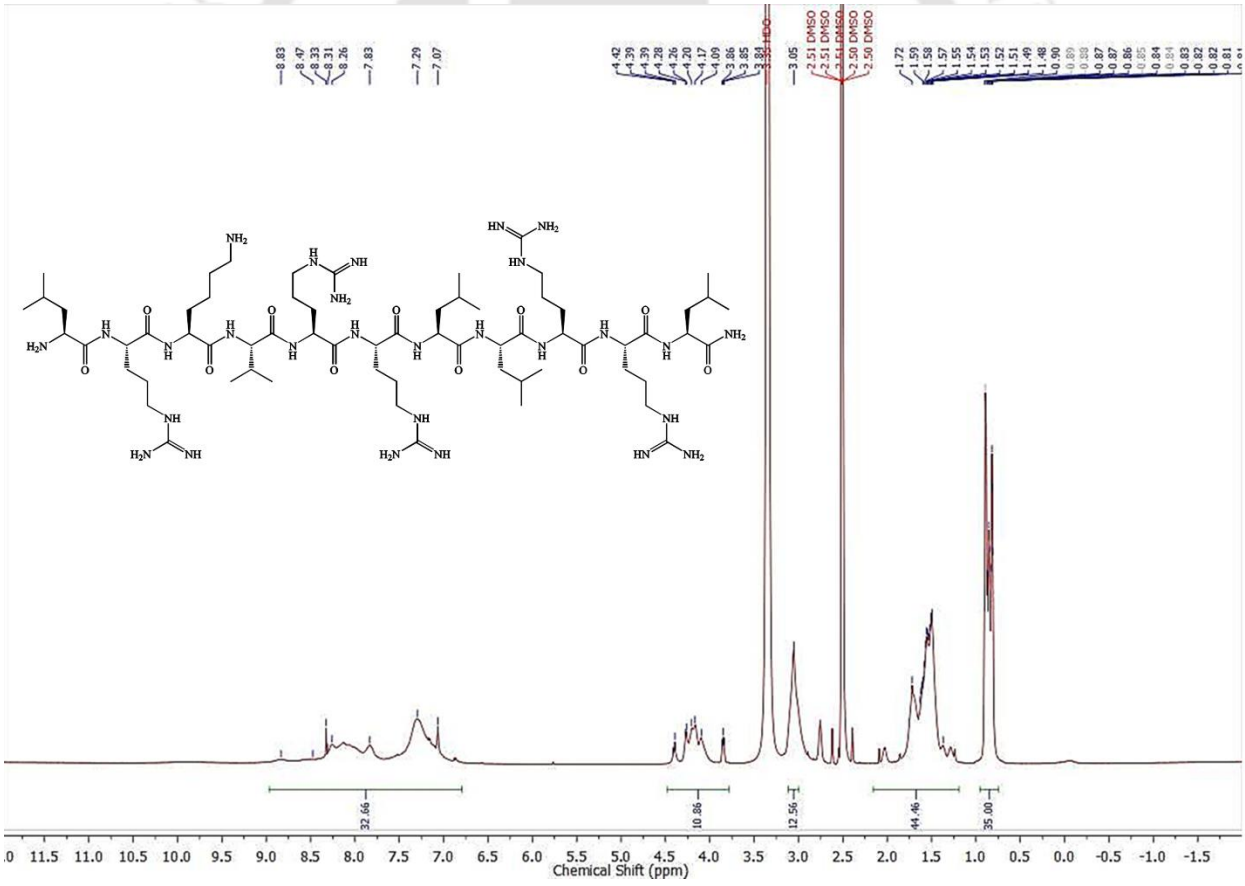

Figure A46: ^{1}HNMR of **AMP21** at a concentration of 10 mM in DMSO-d_6 at room temperature. ^{1}H NMR (600 MHz, DMSO-d_6) δ 0.88-0.94 (m, 35H, Leu, Val), 1.21-1.88 (m,

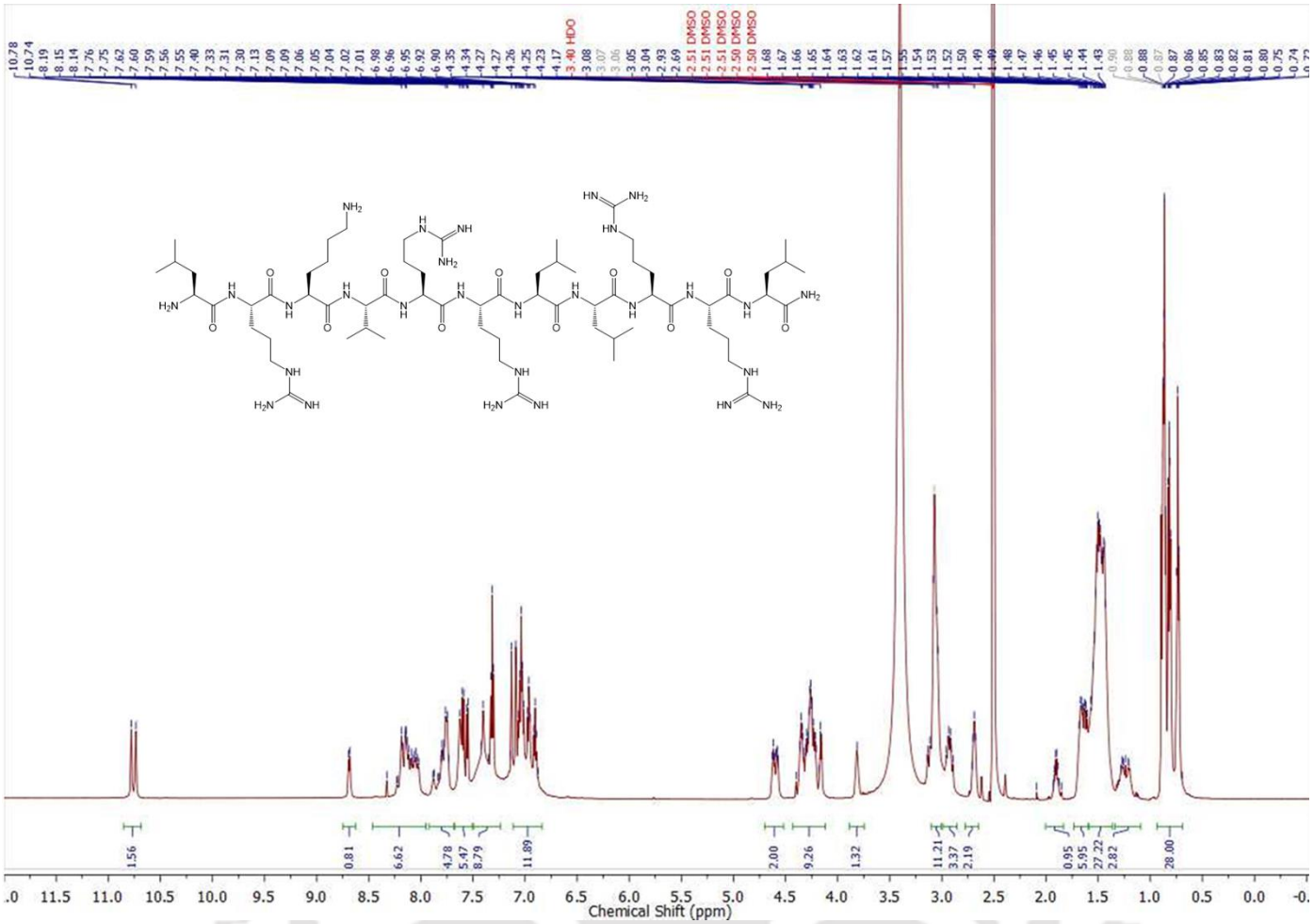

44H, Leu, Lys and Arg), 3.35 (residual water), 2.96-3.04 (m, 12H, Arg, Lys), 4.4-3.8 (11 αH). 6.6- 8.6 (m, 33H, NH and Aromatic proton)

Figure A47: ^{1}HNMR of **AMP22** at a concentration of 10 mM in DMSO-d_6 at room temperature. ^{1}H NMR (600 MHz, DMSO-d_6) δ 0.88-0.94 (m, 28H, Leu, Val), 1.21-1.88 (m, 37H, Leu, Lys and Arg), 3.35 (residual water), 2.6-3.2 (m, 16H, Arg, Lys,Trp), 4.4-4.0 (11 αH). 6.7- 8.75 (m, 38H, NH and Aromatic proton),10.80-10.71 (d, 2H, Indole-NH).

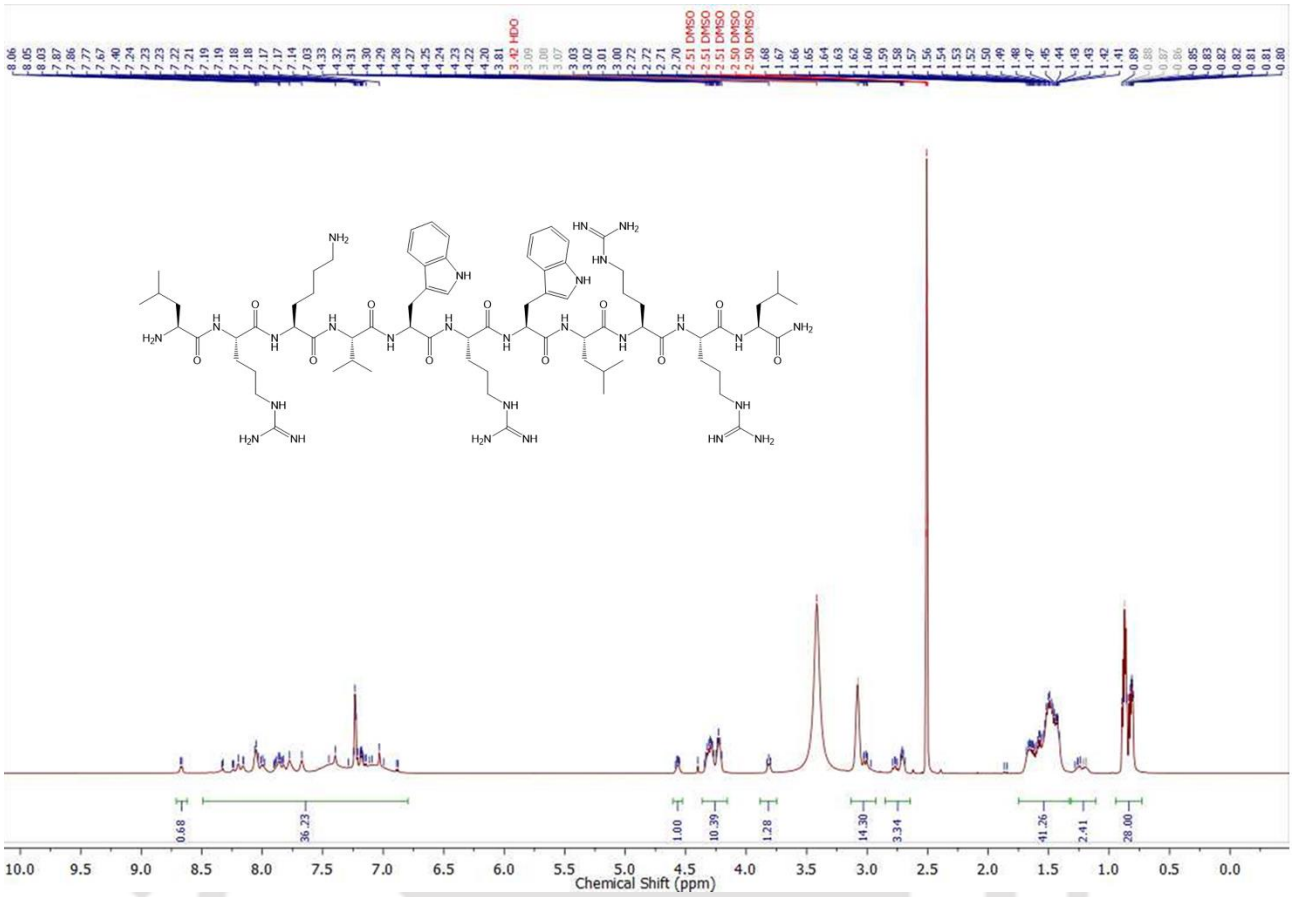

Figure A48: ^{1}HNMR of **AMP23** at a concentration of 10 mM in DMSO-d_6 at room temperature. 1H NMR (600 MHz, DMSO-d_6) δ 0.66-0.94 (m, 28H, Leu, Val), 1.04-1.91 (m, 43H, Leu, Lys and Arg), 3.35 (residual water), 2.56-3.17 (m, 17H, Arg, Lys), 4.05-4.71 (11 αH). 6.57-9.02 (m, 37H, Arg, lys and NH).

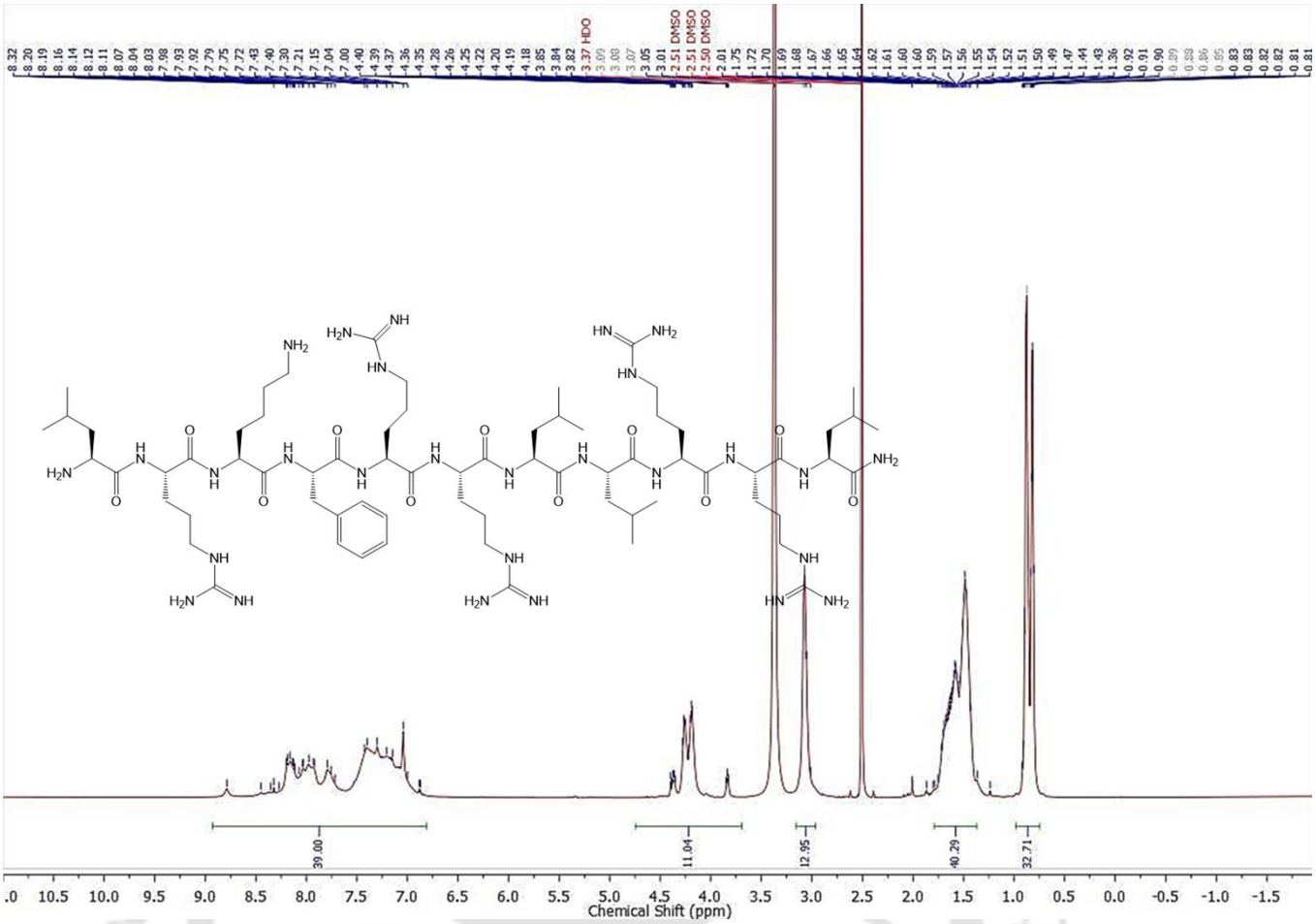

Figure A49: ^{1}HNMR of **AMP24** at a concentration of 10 mM in DMSO-d_6 at room temperature. 1H NMR (600 MHz, DMSO-d_6) δ 0.73-1.06 (m, 32H, Leu), 1.38-1.86 (m, 40H, Leu, Arg), 3.35 (residual water), 2.89-3.2 (m, 13H, Arg), 3.69-4.76 (11 αH). 6.81-8.97 (m, 39H, Arg,NH).

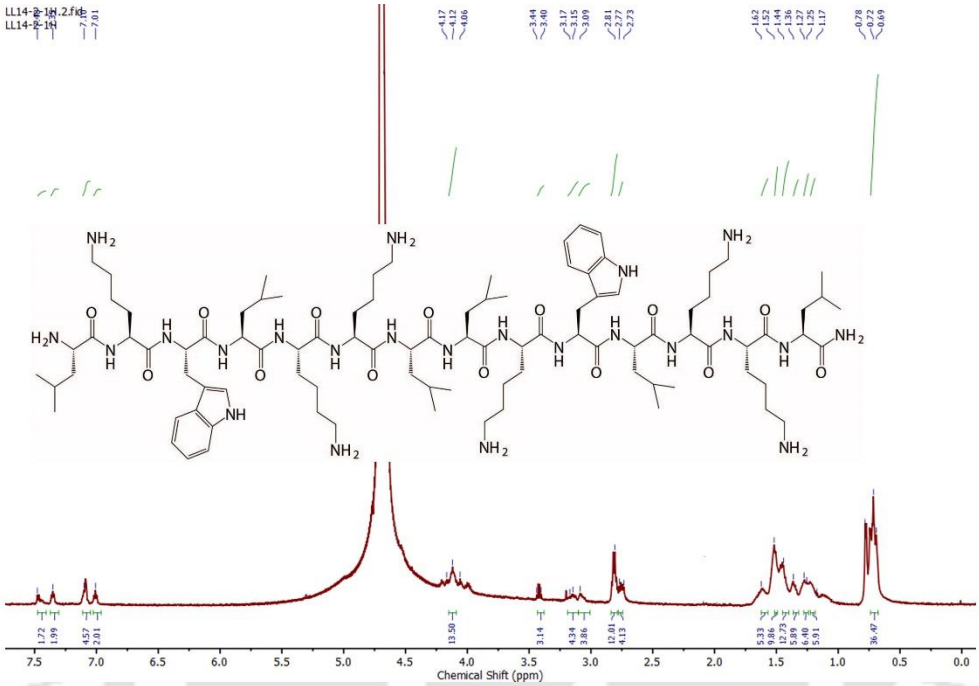

Figure A50: ^{1}H NMR of LL-14 in D_2O at room temperature. ^{1}H NMR (600 MHz, D2O) 0.61-0.78 (m, 36 H, Leu), 1.16-1.69 (m, 44H, Leu and Lys), 2.68-3.21 (32H, m, Lys, Leu, Trp.),3.93-4.27 (14 αH). 6.96-7.52 (10H, Trp.)

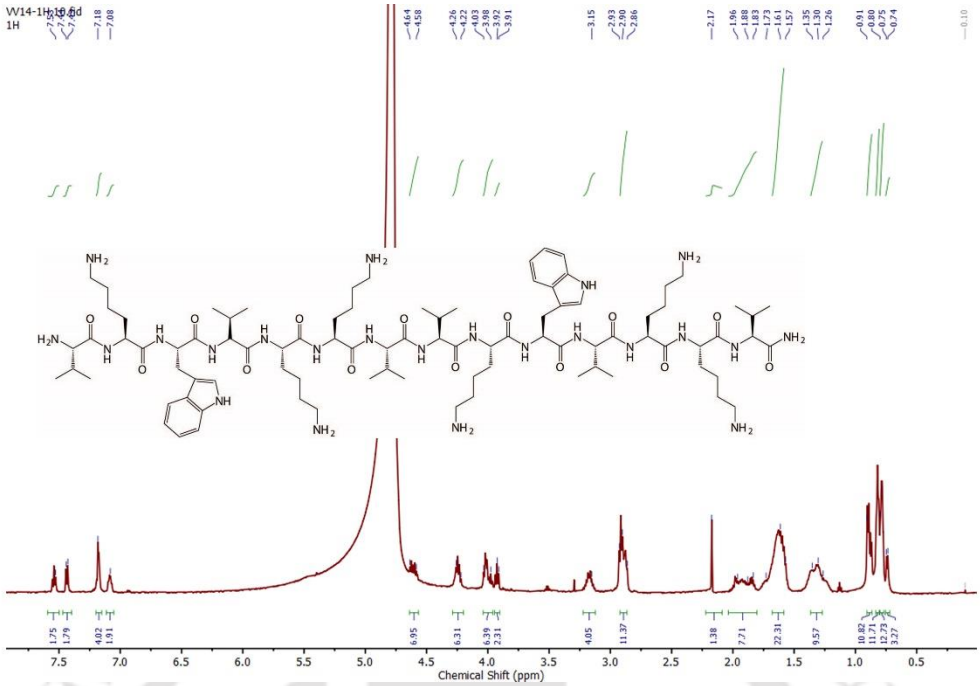

Figure A51: ^{1}H NMR of VV-14 in D_2O at room temperature. ^{1}H NMR (600 MHz, D2O) 0.68-0.95 (m, 36 H, Leu), 1.5-2.01(m, 38H, Leu and Lys), 2.9-3.25 (15H, m, Lys, Leu, Trp.), 3.8-4.7 (Lys, Trp and 14 αH). 6.96-7.7 (10H, Trp.).

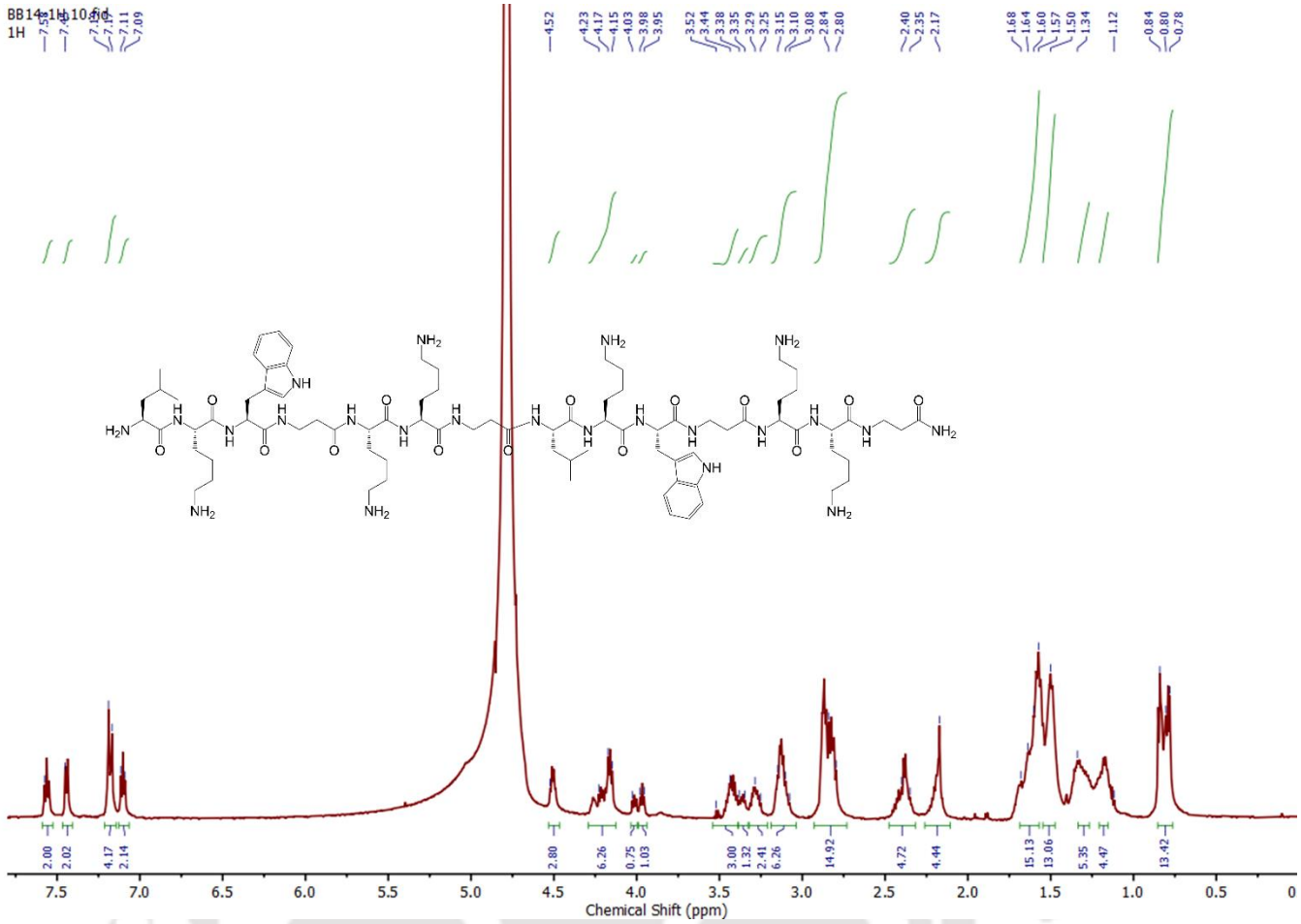

Figure A52: ^{1}H NMR of ββ-14 in D_2O at room temperature. ^{1}H NMR (600 MHz, D2O) 0.68-0.95 (m, 13H, Leu, β ala), 1.1-1.8 (m, 38H, Leu and Lys), 2.2-2.5 (9H, m, Leu, β ala.), 2.8-3.5 (26 H Lys, Trp). 3.9-4.6 (11H, Trp. And 9 αH).7.1-7.7 (10 αH).

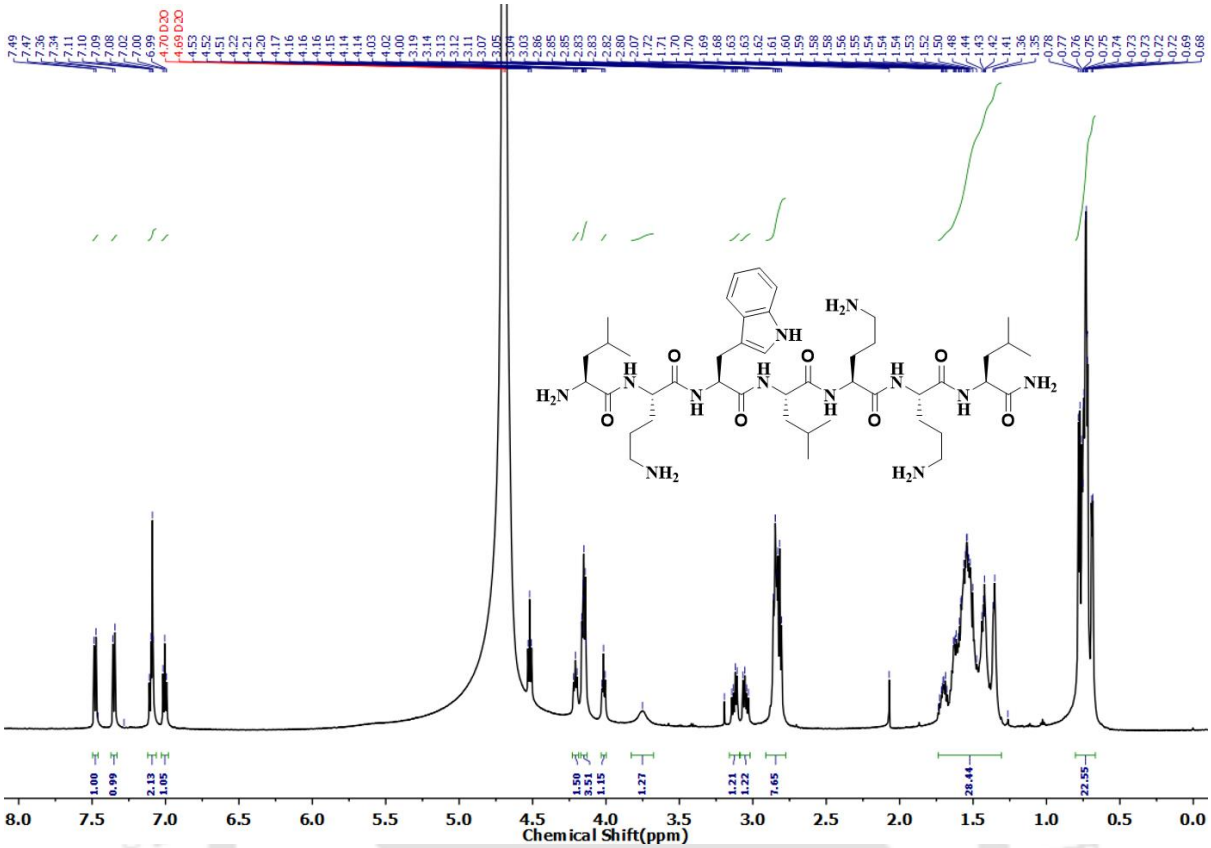

Figure A53: ^{1}H NMR of **P31** in D_2O at room temperature. ^{1}H NMR (600 MHz, D_2O). 0.8-0.96 (22H, Leu),1.19-1.87 (28H, Leu and Orn), 2.9-3.3 (8H, m, Orn and Trp), 3.7-4.7 (7 αH, 1 merged with water signal), 7.1- 7.6 (5H, Trp).

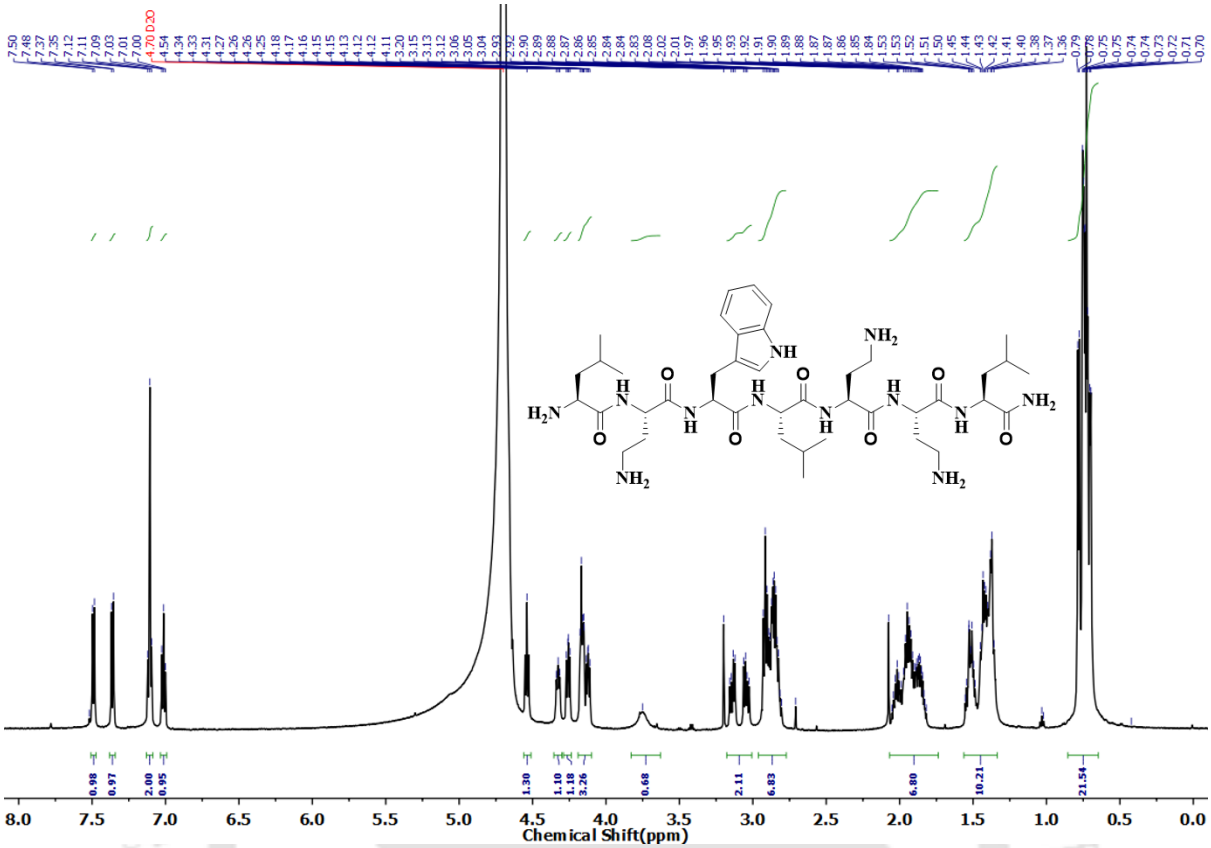

Figure A54: ^{1}H NMR of **P32** in D_2O at room temperature. ^{1}H NMR (600 MHz, D_2O). 0.8-0.96 (22H, Leu),1.19-1.59 (10H, Leu and Dab), 1.79-2.14 (7H, m, Dab), 3.7-4.6 (7 αH, 1 merged with water signal), 6.98- 7.56 (5H, Trp).

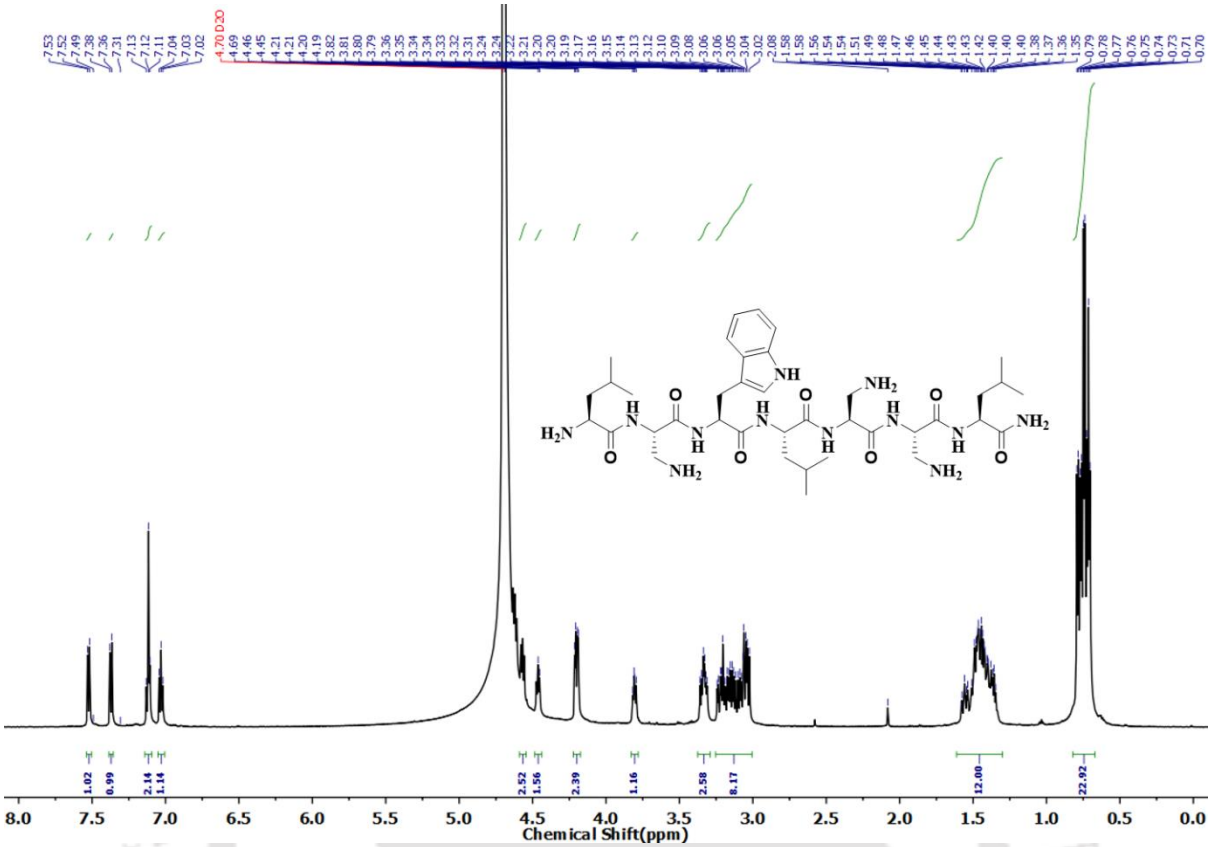

Figure A55: ^{1}H NMR of **P33** in D_2O at room temperature. ^{1}H NMR (600 MHz, D_2O). 0.8-0.96 (22H, Leu),1.29-1.61 (10H, Leu and Dap), 2.99-3.4 (10H, m, Dab and Trp), 3.7-4.6 (7 αH,1 merged with water signal), 6.98- 7.58 (5H, Trp).

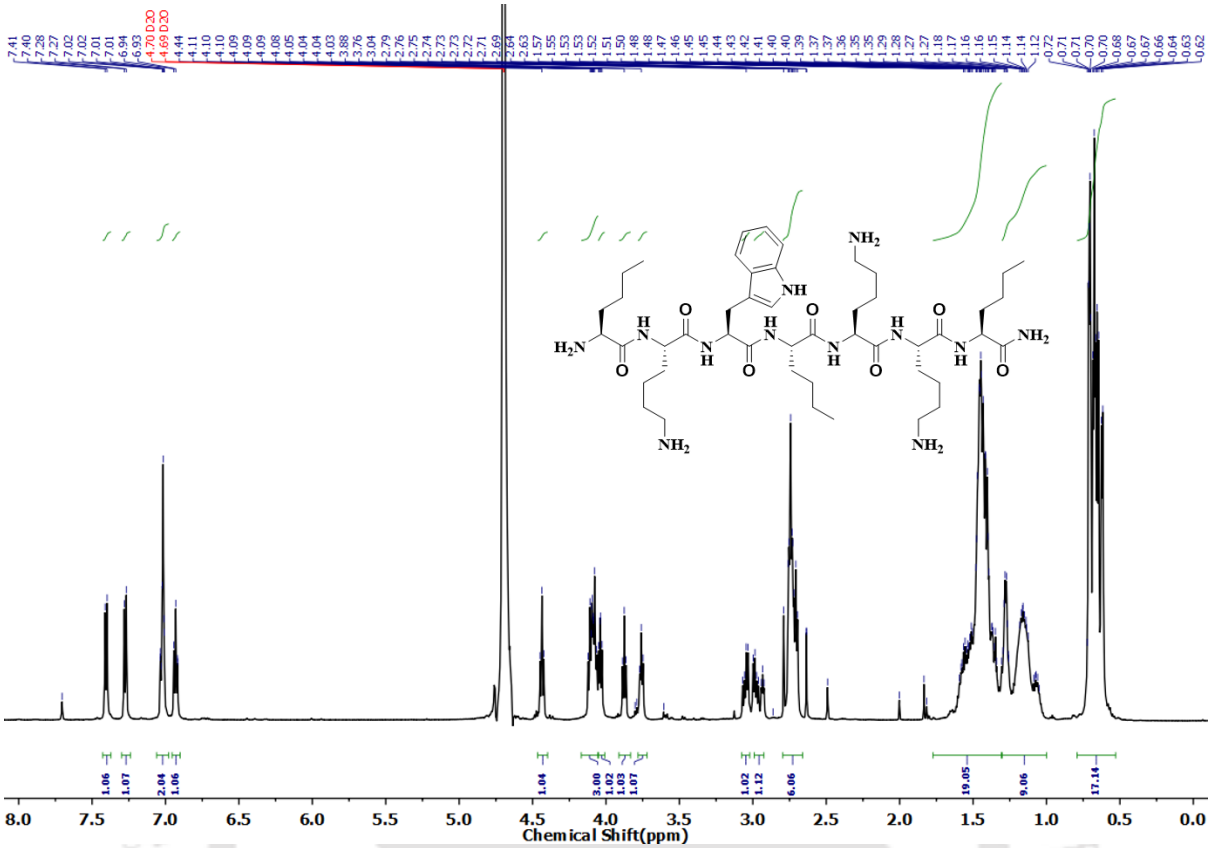

Figure A56: ^{1}H NMR of **P34** in D_2O at room temperature. ^{1}H NMR (600 MHz, D_2O). 0.59-0.74 (17H, Nle, Orn), 1.03-1.60 (28H, Nle and Orn), 2.68-3.07 (8H, m, Orn and Trp), 3.74-4.45 (7 αH), 6.92- 7.41 (5H, Trp).

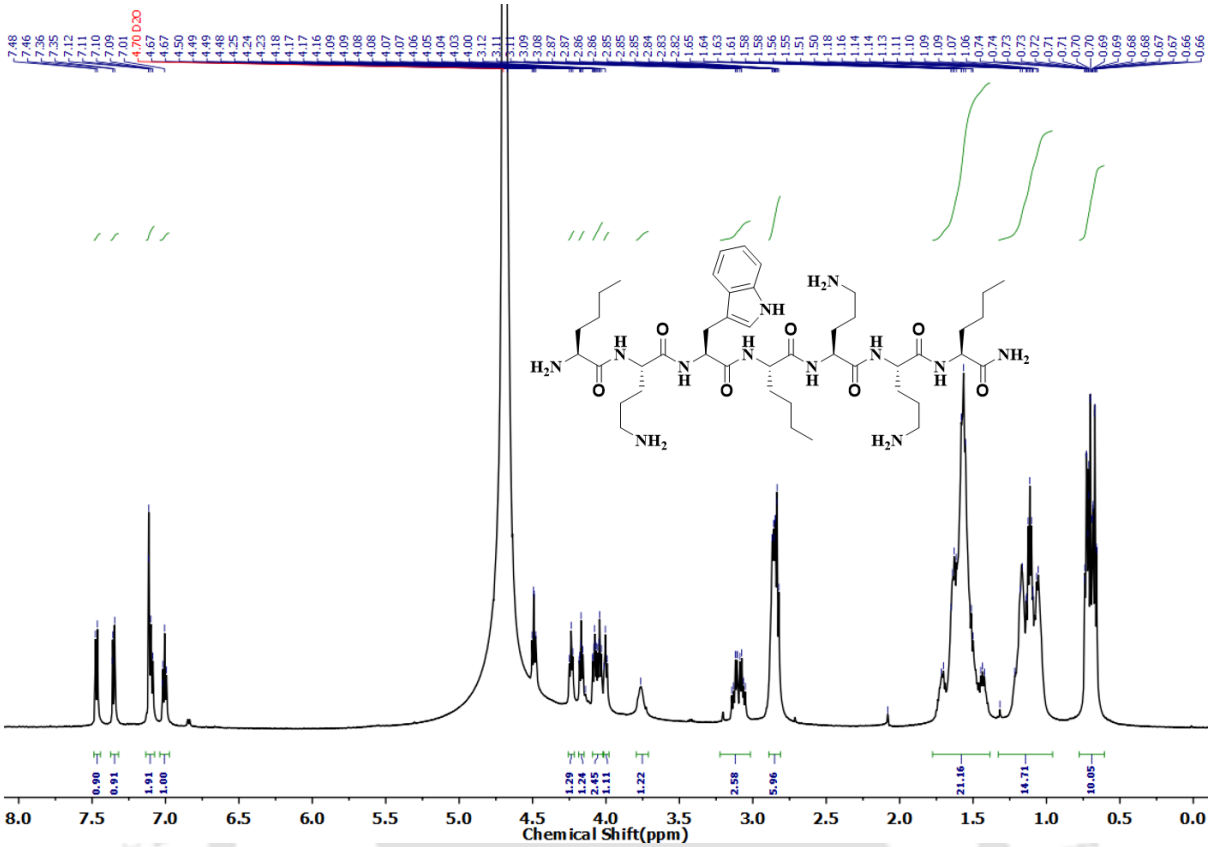

Figure A57: ^{1}H NMR of **P35** in D_2O at room temperature. ^{1}H NMR (600 MHz, D_2O). 0.6-1.28 (24H, Nle, Orn),1.33-1.81 (21H, Nle and Orn), 2.74-3.19 (8H, m, Orn and Trp), 3.67-4.55 (7 αH, 1 merged with water signal), 6.97- 7.52 (5H, Trp).

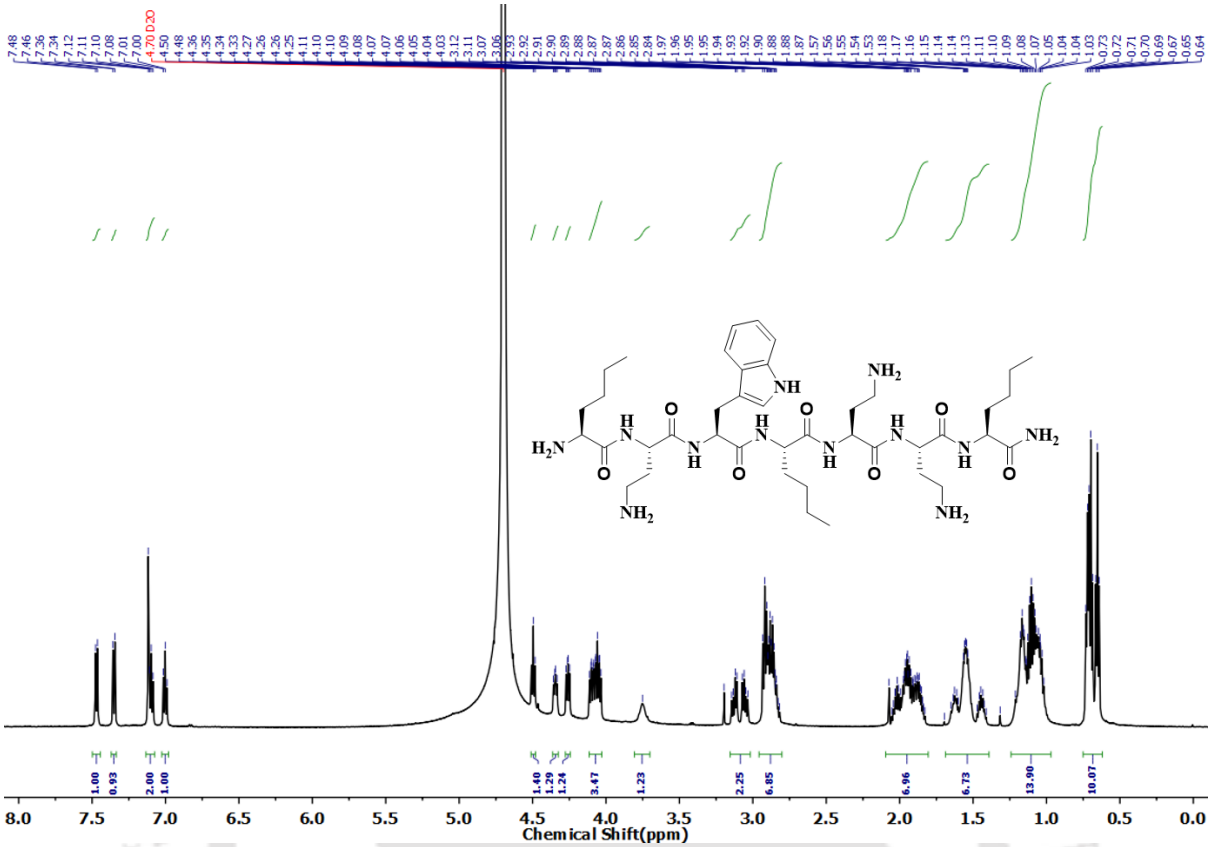

Figure A58: ^{1}H NMR of **P36** in D_2O at room temperature. ^{1}H NMR (600 MHz, D_2O). 0.58-1.31 (23H, Nle, Dab),1.41-2.14 (14H, Nle and Dab), 1.79-2.14 (8H, m, Dab and Trp), 3.7-4.6 (7 αH, 1 merged with water signal), 6.98- 7.56 (5H, Trp).

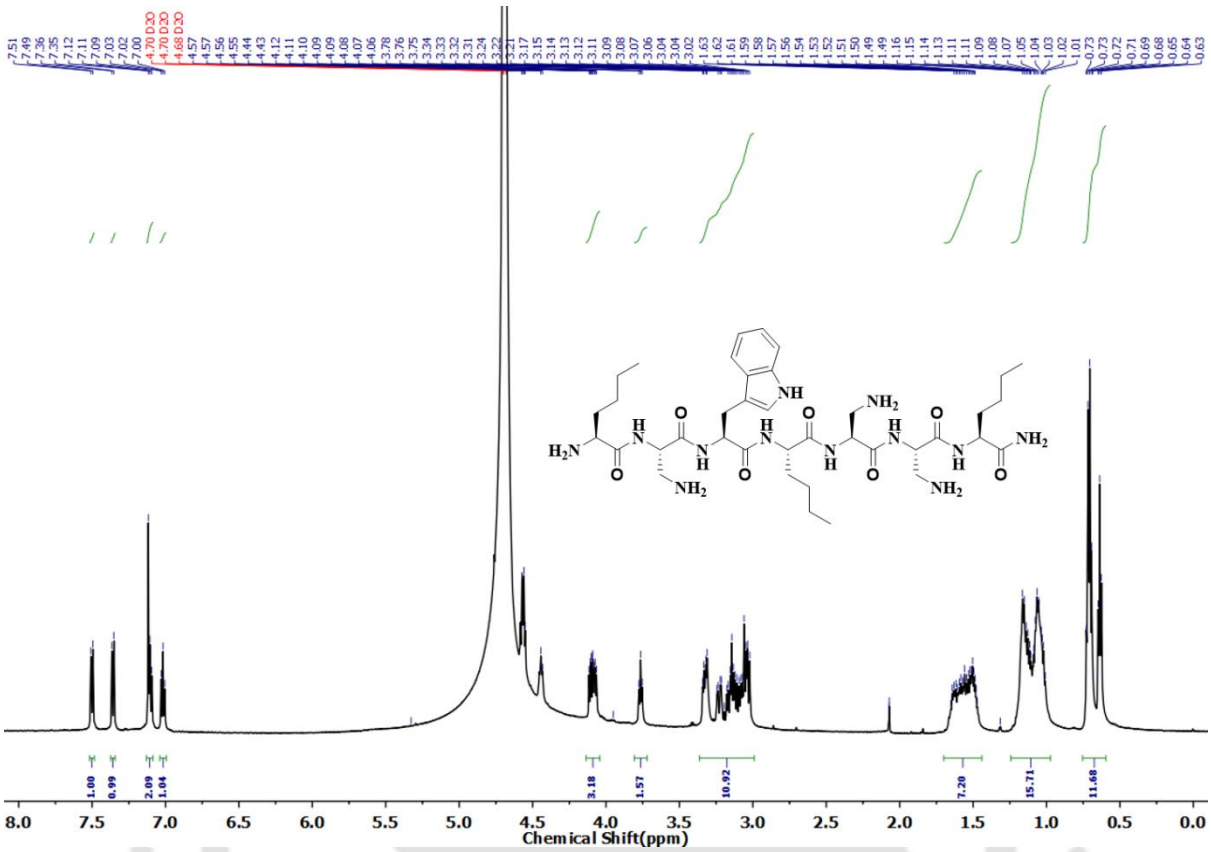

Figure A59: ^{1}H NMR of **P37** in D_2O at room temperature. ^{1}H NMR (600 MHz, D_2O). 0.57-1.24 (28H, Nle, Dap),1.44-1.74 (7H, Nle and Dap), 2.99-3.42 (10H, m, Dap and Trp), 3.7-4.6 (7 αH, 3 merged with water signal), 6.98- 7.58 (5H, Trp).

APPENDIX B

B1. Materials Purchased:

3-(4,5-dimethylthiazol-2-yl)-2,5-diphenyltetrazolium bromide (MTT), Dulbecco's modified Eagle's medium (DMEM), Dimethylsulfoxide (DMSO), NMR solvents, Propidium Iodide (PI), 3,3'- Dipropylthiadicarbocyanine Iodide ($DISC_3$), Polymyxin B and Calcein were purchased from Sigma Aldrich (St. Louis, USA). Protected amino acids, solid phase resins, coupling reagents for solid phase peptide synthesis were obtained from G. L. Biochem, China (Shanghai, China). Dodecylphosphocholine (D38, 98%) were purchased from Cambridge Isotope Laboratories, Inc. (Tewksbury, USA). 1,2-Dioctanoyl-rac-phosphatidylglycerol (D8PG), 1-palmitoyl-2-oleoyl-sn-3-glycero-phosphocholine (POPC), 1-palmitoyl-2-oleoyl-sn-3-glycero-phosphoethanolamine (POPE), 1-palmitoyl-2-oleoyl-sn-3-glycero-phosphatidylglycerol (POPG) and Ergosterol (Erg) were procured from Avanti Polar Lipids (Albaster, AL). Amphotericin B and all bacterial and fungal media components were purchased from Himedia Laboratories Pvt. Ltd. (Mumbai, India).

Bacterial strains *E. coli DH5α*, *P. aeruginosa* (ATCC 27853), *K. pneumoniae* (ATCC13883), *S. aureus* (ATCC 25923) were obtained from ATCC (U.S.A) or MTCC (India). Fungal strains *C. albicans* SC5314 and *C. neoformans var. grubii H99* were gifted by Prof. Kaustuv Sanyal, JNCASR, India to Prof. Anirban Bhunia, Bose Institute.

B2. Instruments Used for Various Studies:

1. NMR: 400, 600,700 MHz Bruker NMR spectrometer
2. HPLC: Thermo Scientific Dionex Ultimate 3000
3. ESI-MS: Agilent-Q-TOF 6500 instrument in electrospray ionization positive mode.
4. FESEM: FESEM Sigma 300 microscope, FESEM Sigma Zeiss Gemini microscope
5. FETEM: JEOL JEM (Model 2100F) at an operating voltage of 200 KV
6. Fluorescence: Fluoromax-4 spectrophotometer.
7. DLS/ Zeta Potential: Zetasizer Nano ZS90 from Malvern using a 632.8 nm He−Ne laser
8. CD: Jasco J-1500 spectropolarimeter.
9. Confocal Microscopy: TCS SP8 confocal microscope (Leica, Wetzlar, Germany)
10. ITC: TA-affinity ITC (TA Instruments, New Castle, USA)

List of Publications

1. **Pandit, G.;** Roy, K.; Agarwal, U.; Chatterjee, S. Self-Assembly Mechanism of a Peptide Based Drug Delivery Vehicle. *ACS Omega*. 2018, *3*, 3143−3155.
2. ***Pandit, G.**; Ilyas, H.; Ghosh, S.; Bidkar, A.P.; Mohid, S.A.; Bhunia, A.; Satpati, P.; Chatterjee, S. Insights into the Mechanism of Antimicrobial Activity of Seven-Residue Peptides. *J. Med. Chem*. **2018**, *61*, 7614-7629.
3. ***Pandit, G.;** Biswas, K.; Ghosh, S.; Debnath, S.; Bidkar, A.P.;Satpati, P.; Bhunia, A.; Chatterjee, S. Rationally Designed Antimicrobial Peptides: Insight into the Mechanism of Eleven Residue Peptides Against Microbial Infections. *Biochim. Biophys. Acta, Biomembr*. **2020**, *1862*, 183177-183193.
4. Roy, K; **Pandit, G.;** Chetia, M.; Sarkar, A. K.; Chowdhuri, S.; Bidkar, A. P.; Chatterjee, S. Peptide hydrogel as platform for sustained release of antimicrobial, antitumor drugs and proteins. *ACS Appl. Bio Mater.* **2020**, *3*, 6251–6262.
5. ***Pandit, G.**; Chowdhury, N.; Mohid, S.A.; Bidkar, A.P.; Bhunia, A.; Chatterjee, S. Effect of Secondary Structure and Side Chain Length of Hydrophobic Amino Acid Residues on the Antimicrobial Activity and Toxicity of 14-Residue-Long de novo AMPs. *ChemMedChem*. **2021**, *16*, 355-367.
6. Debnath, S.; Ghosh, S.; **Pandit, G.;** Satpati, P.; Chatterjee, S. Effect of Differential Geminal Substitution of γ Amino Acid Residues at the (*i* + 2) Position of αγ Turn Segments on the Conformation of Template β-Hairpin Peptides. *J. Org. Chem.* **2021,** *86*, 11310–11323.
7. Ghosh, S.; **Pandit, G.;** Debnath, S.; Chatterjee, S.; Satpati, P. Effect of monovalent salt concentration and peptide secondary structure in peptide-micelle binding. *RSC Adv*., **2021**, 11, 36836–36849.
8. ***Pandit, G.;** Sarkar, T.; Debnath, S.; Satpati, P.; Chatterjee, S. J. A. o., Delineating the Mechanism of Action of a Protease Resistant and Salt Tolerant Synthetic Antimicrobial Peptide against Pseudomonas aeruginosa. *ACS Omega***. 2022**, 7, 15951–15968.

*** Marked Publications are included in this Doctoral dissertation.**